SPIE. SECURITY+ DEFENCE

SPIE. REMOTE SENSING

CONNECTING MINDS.
ADVANCING LIGHT.

2017 TECHNICAL SUMMARIES.

WWW.SPIE.ORG/SD

WWW.SPIE.ORG/RS

Conferences: 11–14 September 2017

DoubleTree Hilton Hotel
Warsaw, Poland

CONNECTING MINDS.
ADVANCING LIGHT.

2017

SPIE. REMOTE SENSING

REMOTE SENSING CO-OPERATING ORGANISATIONS

EARSeL

CENSIS Innovation Centre for Sensor and Imaging Systems

PPTF | Polish Technological Platform on Photonics

MIRPHAB

BARSC

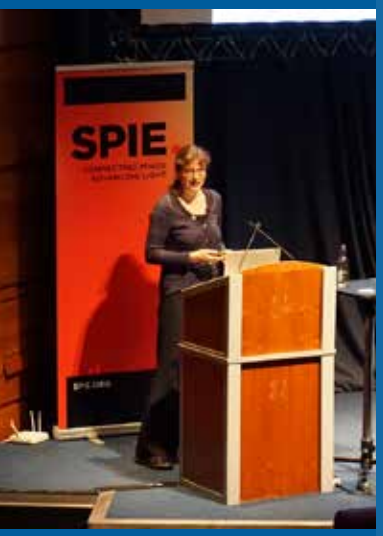

SPIE. SECURITY+ DEFENCE

SECURITY+DEFENCE COOPERATING ORGANISATIONS

CENSIS Innovation Centre for Sensor and Imaging Systems

PPTF | Polish Technological Platform on Photonics

MIRPHAB

Cranfield University

SPIE. REMOTE SENSING

CONFERENCES: 11–14 September 2017
DoubleTree Hilton Hotel
Warsaw, Poland

SYMPOSIUM CHAIR

Klaus Schäfer
Karlsruhe Institute of Technology, Institute of Meteorology and Climate Research (Germany)

SYMPOSIUM CO-CHAIRS

Christopher M. U. Neale
University of Nebraska, Daugherty Water for Food Global Institute (USA)

Stanislaw Lewinski
Space Research Centre, Polish Academy of Sciences (CBK PAN) (Poland)

SPIE Remote Sensing Contents

SPIE. SECURITY+ DEFENCE

CONFERENCES: 11–14 September 2017
EXHIBITION: 12–13 September 2017
DoubleTree Hilton Hotel
Warsaw, Poland

SYMPOSIUM CHAIR

Ric Schleijpen
TNO Defence, Security and Safety (Netherlands)

SYMPOSIUM CO-CHAIRS

Karin Stein
Fraunhofer Institute of Optronics, System Technologies and Image Exploitation IOSB (Germany)

Jan K. Jabczyński
Institute of Optoelectronics, Military University of Technology (Poland)

SPIE Security+Defence Contents

MANAGED BY
SPIE.EUROPE

SPIE Europe Ltd., a subsidiary of SPIE, is a not-for-profit UK-registered company serving SPIE constituents throughout Europe as an advocate and liaison to political and industry associations within the European optics and photonics community.

In addition to providing membership services, SPIE Europe Ltd. organises and manages internationally recognised conferences, education programmes, and technical exhibitions featuring emerging technologies in optics and photonics.

SPIE Europe, 2 Alexandra Gate, Ffordd Pengam, Cardiff, CF24 2SA; Tel: +44 29 2089 4747 • Fax: +44 29 2089 4750
info@spieeurope.org

Conference 10422: Remote Sensing of the Ocean, Sea Ice, Coastal Waters, and Large Water Regions 2017

SPIE. REMOTE SENSING

Monday - Tuesday 11–12 September 2017

Part of Proceedings of SPIE Vol. 10422 Remote Sensing of the Ocean, Sea Ice, Coastal Waters, and Large Water Regions 2017

10422-1, Session 1

Real-time surveillance system for marine environment based on HLIF lidar *(Invited Paper)*

Sergey Babichenko, Ocean Visuals AS (Norway)

The operational monitoring of the risk areas of marine environment requires cost-effective solutions. One of the options is the use of sensor networks based on fixed installations and moving platforms (coastal boats, supply-, cargo-, and passenger vessels). Such network allows to gather environmental data in time and space with direct links to operational activities in the controlled area for further environmental risk assessment.

Among many remote sensing techniques the LiDAR (Light Detection And Ranging) based on Light Induced Fluorescence (LIF) is the tool of direct assessment of water quality variations caused by chemical pollution, colored dissolved organic matter, and phytoplankton composition. The Hyperspectral LIF (HLIF) LiDAR acquires comprehensive LIF spectra and analyses them by spectral pattern recognition technique to detect and classify the substances in water remotely.

Combined use of HLIF LiDARs with Real-Time Data Management System (RTDMS) provides the economically effective solution for the regular monitoring in the controlled area. The HLIF LiDAR is equally effective in icy water and at varied wind, visibility and ambient light conditions. Multiple LiDARs installed on board of moving operational ships constitute the dynamic sensor network for continuous local surveillance. The cloud-based RTDMS serves to handle and visualize the geo-referenced findings of HLIF LiDAR and integrate the information from other cooperative sensors on the multilayer map with back-tracking capability. Flexible shared access to the real-time and historical data allows information delivery to different clients according to their existing control and information systems.

OCEAN VISUALS AS has developed Oil in Water Locator (OWL™) with RTDMS (OWL MAP™) based on HLIF LiDAR technique. This is a novel technical solution for monitoring of marine environment providing continuous unattended operations. OWL™ has been extensively tested on board of various vessels in the North Sea, Norwegian Sea, Barents Sea, Baltic Sea and Caribbean Sea. The presentation describes the technology features and the results of its operational use in 2014-2017.

10422-2, Session 1

Vessel and oil spill early detection using COSMO satellite imagery

Claudio A. Delrieux, Natalia Verónica Revollo Sarmiento, Univ. Nacional del Sur (Argentina)

Oil spillage is among the most common sources of environmental damage in places where coastal wild-life develops natural reservations, like in the Patagonian coast. In addition, furtive fishery activities in national waters are depelleting the food supplies of several species, altering the ecological equilibrium. For this reason, oil spils and vessel detection are among the most required real-time monitoring tasks for environmental and government authorities. In the Patagonian sea platform, with an area above one million square km, human asisted monitoring is unfeasible, and therefore real time remote sensing technologies, for instance based on high revisit rate satellite imagery, is the only operative and economically feasible solution. In this work we describe the theoretical foundations and implementation details of a system specifically designed to take advantage of the SAR imagery delivered by two satellite constellations (the SAR mission, developed by the Argentine Space Agency, and the COSMO mission, developed by the Italian Space Agency), to provide real-time detection of vessels and oil spills.

The core of the system is based on pattern recognition over the statistical parameters of the texture patterns arising in the different conditions being detected. We regarded a resulting satellite SAR image as a product of two different phenomena: the first modeling the backscatter and the second modeling the antena, both being well understood multiplicative processes that can be in turn modelled using Gamma distributions. The product of these two parametric distributions gives rise to the Kappa distribution, with four parameters, some of which lacking a closed formulation for their evaluation. We developed an algorithm for evaluating these four parameters over image windows (ranging from 9x9 to 31x31) with which a feature vector can be created. Then, the pattern recognition system was trained using clips of images containing positive and negative conditions (i.e., vessel, oil, or plain sea surface), collected over a large amount of prior reported contacts that were tagged by experts in the Argentine Space Agency. Distance in the feature space is gauged using the Kullback-Leibler divergence as an estimator of the difference between the statistical parametres in the samples and in the patterns.

The recognition results are above the sensitivity and specificity of other similar systems. Also, the implementation uses entirely royalty-free and open-source platforms, and off-the-shelf hardware, providing the users the possibility to migrate, enlarge, or reproduce the processing capabilities on their own. The system is also interoperable with other software modules that allow for instance to follow the oil fiume according to wind and sea currents, thus providing predictive capabilities.

10422-3, Session 1

Radar and optical remote sensing in offshore domain to detect, characterize and quantify ocean surface oil slicks

Sebastien Angelliaume, Xavier Ceamanos, Françoise Viallefont, Philippe Déliot, ONERA (France); Veronique Miegebielle, Total E&P (France)

One of the objectives of NAOMI (New Advanced Observation Method Integration) research project, partnership between TOTAL and ONERA, is to work on the detection, the characterization and the quantification of offshore hydrocarbon at the sea surface. Search of natural (Seeps) or anthropogenic (Spill) gas or liquid hydrocarbon exhaust, will contribute to:

- The selection of large scale basins and mining domain selection for exploration application

- The detection of oil spill extension and location for environmental application.

This application concerns the detection of oil leakage for regular monitoring of offshore production facilities or in case of incidents occurring on sea surface (spill, boat sewages...). It is important to determine rapidly spill location and extension, but also to predict its drift, in order to inform where interventions teams should take action, and to evaluate the timing of impact areas. For the detection, metocean information as wind and wave improve the quality of the interpretation.

Distinction between natural oil seeps, oil spill and look-alikes such as natural algae may be tricky and requires variety data comparison.

It should be noted that in the offshore domain, the majority of the data used for the detection of hydrocarbons in operational context is SAR sensors. However, the use of optical data is important because the physicochemical properties linked to the optical data make possible the discriminate

between hydrocarbon indices and look-alikes. Moreover, the complementarities of multi-frequency radar data, multi-band optical data and radar / optical data is an important way of improvement in the context of slicks monitoring. In order to work in these fields, an acquisition campaign in Norway during the 2015 NOFO (Norwegian Clean Seas Association for Operating Companies) was led. Images (SAR/Optical) of these exercises, first R&D works and perspectives, related to the emergence of new techniques are presented in this paper.

10422-4, Session 1

Oil spill detection from TerraSAR-X dual-polarized images using artificial neural network

Daeseong Kim, Hyung-Sup Jung, The Univ. of Seoul (Korea, Republic of)

Marine pollution from oil spills not only destroys ecosystems but also causes economic losses by affecting fisheries and the tourism industry. In order to minimize the damage caused by spilled oil, it is important to fast cleanup it after predicting how the oil will spread. In order to predict the spread of oil spill, the remote sensing technique using synthetic aperture radar (SAR) satellite image has been widely used. The SAR image has advantages that it is hardly affected by weather conditions as well as they are obtained at both daytime and nighttime. In previous studies, only the back-scattering value has been generally used for the detection of oil spill. Thus, the detection rate was not relatively high. To overcome the drawback, in this study, we proposed an efficient approach to detect the oil spill. The method applies the artificial neural network (ANN) to SAR image as well as a coherence map extracted from dual-polarized SAR images. TerraSAR-X image of Kerch Strait acquired by HH and VV polarizations were used in this study. Prior to the image processing, the 30m SRTM DEM was used to remove the land of the image. Since the surface of oil spill area is smooth due to the viscosity of the oil, the pulse emitted from the sensor is mostly reflected in the direction of the reflection angle, so that it has a lower back-scattering value than the surrounding pixels. In order to maximize the efficiency of oil spill detection using a back-scattering value, the speckle noise acting as an error factor should be removed first. NL-means filter was applied to single look complex (SLC) image to remove it without smoothing of spatial resolution. In the coherence image generated from the images taken simultaneously using different polarization information, the sea has a high value and the oil spill area has a low value due to the scattering characteristics of the pulse. In order to using the characteristics of SAR image, training sample was set up in all three layers including HH, VV image with speckle noise reduced by applying NL-means filter and coherence image, and ANN was applied to produce probability map of oil spill. Probability map has a value between 0 and 1, and each value means the probability that the pixel is oil spill. In general, the value was 0.4 or less in the case of the sea, and the value was mainly in the range of 0.7 to 0.9 in the oil spill area. Using coherence images generated from different polarizations showed better detection results for relatively thin oil spill areas such as oil slick or oil sheen than using back-scattering information alone. It is expected that if the information about the look-alike of oil spill such as algae, internal wave and rainfall area is provided or if deep-learning technique such as CNN (Convolutional Neural Network) is used, the probability map can be produced with higher accuracy.

10422-5, Session 1

Investigation of excitation efficiency of emission lines of chemical elements in plasma focusing of femtosecond laser pulses on water solutions

Yuliya S. Biryukova, Sergey S. Golik, Anton Borovsky, Far Eastern Federal Univ. (Russian Federation); Dmitriy Y. Proschenko, Maritime State Univ. named after G.I. Nevelskoi (Russian Federation)

The influence of the energy of a femtosecond pulse on the intensity of the emission lines of elements and on the continuous spectrum of a plasma generated on the surface of an aqueous solution by femtosecond pulses (wavelength 800 nm, pulse duration 60 fs, worked from 1 to 5 mJ, time delay of the registration time with respect to the laser pulse was 130 ns,). Time characteristics of the continuous and ruled plasma spectrum for the following elements are obtained: Na, N, Fe, Ca, Mg, Al, Pb, Mn, K, Sr, Ag.

In the tasks of monitoring the atmosphere and the ocean, ecology, there are needs for original remote sensing techniques and direct measurements of the elemental composition of liquid media. In order to cover various tasks, such methods must meet a number of requirements, namely, cover a large number of elements, provide good expressiveness, and have high sensitivity. Finally, the measurements should be sufficiently reproducible for monitoring the ocean in real time. The method of laser spark spectroscopy (LI) satisfies the main above requirements. Considerable attention is paid to the use of femtosecond laser pulses, in order to increase the sensitivity of the LIS method. The detection limit for many elements by the nanosecond LIS method is at the ppm level.

The source of femtosecond laser pulses was a titanium-sapphire laser with a central wavelength of 800 nm, a pulse duration of 45 fs; The pulse duration was controlled by an autocorrelator; In studies to determine the effect of the repetition frequency of laser pulses on the intensity of spectral lines, the energy in the pulse varied from 1 to 5 mJ, and the pulse repetition frequency was 150 Hz. The energy value was varied with the help of the Glan prism. The laser radiation, passing through a mirror system and broadened by a telescope, was focused on the surface of the sample. As a sample, aqueous solutions of chemical elements with an initial concentration of 1.0 g / l were used, which were diluted with distilled water to obtain lower concentrations. Radiation of the plasma with a lens was directed to the entrance slit of the spectrometer. The signal was accumulated by 5000 laser pulses.

10422-6, Session 2

Recognition of bathymetry on the basis of color aerial photographs: Baltic shallow coastal zone studies

Lukasz Cieszynski, West Pomeranian Univ. of Technology (Poland) and Univ. of Szczecin (Poland); Kazimierz Furmanczyk, Univ. of Szczecin (Poland)

In the shallow coastal zone (up to 4 m depth), the quality and accuracy of bathymetry data is insufficient because of the spatial variability of the seabed. For the Baltic polish coast bathymetry data are usually created in profiles based on echo sounding measurements. There are some trial applications of green laser – LIDAR known. It can be a method of shallow areas studies quality improvement. However, this method is still expensive and that is why we have decided to use the RGB digital aerial photographs to create a model for mapping the seabed of the shallow coastal zone.

So far, in the 60's, researchers in the USA (Musgrove, 1969) and Russia (Zdanowicz, 1963) developed the first method of bathymetry determining from aerial panchromatic (black-white) photographs. This method was adapted for the polish

conditions by Furmanczyk in 1975 and in 2014 we returned to his concept using more advanced techniques of recording and image processing.

In our study, we propose to determine the bathymetry in shallow coastal zone of the Baltic Sea by using the digital color vertical aerial photographs (both single and multi-channel spectral). These photos are the high-resolution matrix (10 cm per pixel) containing values of the pixels in the individual spectral bands (RGB). This gives great possibilities to determine the bathymetry in order to analyze the changes in the marine coastal zone. Comparing the digital bathymetry maps - obtained by proposed method - in the following periods, you can develop differential maps, which reflect the movements of sea-bottom sediments. This can be used to indicate the most dynamic parts in the coastal zone.

The model is based on the pixel values and relative depths, measured in-situ in geo-located points (in selected checkpoints for three areas: beach, shoal and depth parts). As a result, the relation of the pixel brightness and sea depth (the algorithm) was defined in two ways: 1) from relation of two or three bands and 2) from ratio of two channels. Using the algorithm, depth calculations for the whole scene were done and high resolution bathymetric map created to obtain three-dimensional bathymetry visualization. However, the algorithm requires numbers of adjustments resulting from, e.g., the phenomenon of vignetting, light propagation in the atmosphere or light reflection from the sea surface. We have developed the algorithm with correction formulas and created a final model in MATLAB. This model enables to determine the bathymetry of the most dynamic areas in the marine coastal zone up to 3-4 meters depth with a relatively good accuracy. In addition, the possibility to take pictures from the drone instead of a plane significantly reduces the cost of the process. We have also tried to adapt our methodology to satellite data processing.

We will present the model and its results for the area of the Polish western Baltic coast.

1. Musgrove R,G., 1969. Photometry for interpretation. Photogrametric Engineering No. 10.

2. Furma?czyk K., 1975. Mo?liwo?ci praktycznego zastosowania metody fotogrametrycznej do okre?lania g??boko?ci w strefie brzegowej morza. Gda?sk.

3. Zdanowicz W.G., 1963. Primienienije aerometodow dlia issledowanija moria. Leningrad.

10422-8, Session 2

Shallow water bathymetry correction using sea bottom classification with multispectral satellite imagery

Yoriko Kazama, Tomonori Yamamoto, Hitachi, Ltd. (Japan)

Bathymetry at shallow water especially shallower than 15m is an important for sea environment. Because the depth of shallow water is changeable by the sediment deposition and the ocean waves, the periodic monitoring at shoe area is needed. Utilization of satellite images are well matched for widely and repeatedly monitoring at sea area.

Sea bottom terrain model using by remote sensing data have been developed. These methods based on the radiative transfer model of the sun irradiance which is affected by the atmosphere, water, and sea bottom. We adopted that general method of the sea depth extraction to the satellite imagery, WorldView-2; which has very fine spatial resolution (50cm/pix) and eight bands at visible to near-infrared wavelengths. From high-spatial resolution satellite images, there is possibility to know the coral reefs and the rock area's detail terrain model which offers important information for the amphibious landing. In addition, the WorldView-2 satellite sensor has the band at near the ultraviolet wavelength that is transmitted through the water. On the other hand, the previous study showed that the estimation error by the satellite imagery was related to the sea bottom materials such as sand, coral reef, sea alga, and rocks. Therefore, in this study, we focused on sea bottom materials, and tried to improve the depth estimation accuracy. First, we classified the sea bottom materials by the SVM method, which used the depth data acquired by multi-beam sonar as supervised data. Then correction values in the depth estimation equation were calculated applying the classification results. As a result, the classification accuracy of sea bottom materials was 93%, and the depth estimation error using the correction by the classification result was within 1.2m.

10422-9, Session 2

Collection and corrections of oblique multiangle hyperspectral bidirectional reflectance imagery of the water surface

Charles R. Bostater Jr., Florida Institute of Technology (United States)

Hyperspectral images of coastal waters in urbanized regions were collected from fixed platform locations. Surf zone imagery, images of shallow bays, lagoons and coastal waters are processed to produce bidirectional reflectance factor (BRF) signatures corrected for changing viewing angles. Angular changes as a function of pixel location within a scene are used to estimate changes in pixel size and ground sampling areas. Diffuse calibration targets collected simultaneously from within the image scene provides the necessary information for calculating BRF signatures of the water surface and shorelines. Automated scanning using a pushbroom hyperspectral sensor allows imagery to be collected on the order of one minute or less for different regions of interest. Imagery is then rectified and georeferenced using ground control points within nadir viewing multispectral imagery via image to image registration techniques. This paper demonstrates the above as well as presenting how spectra can be extracted along different directions in the imagery. The extraction of BRF spectra along track lines allows the application of derivative reflectance spectroscopy for estimating chlorophyll-a, dissolved organic matter and suspended matter concentrations at or near the water surface. Imagery is presented demonstrating the techniques to identify subsurface features and targets within the littoral and surf zones.

10422-10, Session 2

Using remote sensing methods to identify valuable underwater habitats

Meri Koskelainen, SYKE Finnish Environment Institute (Finland); Elina Virtanen, Samuli Korpinen, Markku Viitasalo, Finnish Environment Institute (Finland)

Seagrasses are submerged plants found all over the world from brackish bays to salty continental shelves. Seagrasses create high-productive habitats and are a vital part of the marine ecosystems, providing shelter, nurseries, food, and habitats for other species. Seagrasses can be seen as indicators of environmental changes and ecosystem heath as they are sensitive to water quality.

Accurate and detailed spatial information of seagrasses would be important in assessments of threatened habitats, establishing MPAs and evaluating ecosystem state. However, spatially comprehensive species information is usually lacking and the knowledge of seagrass habitats around the world relies on scarce field observations and models based on inventory records. Because field work is expensive and time consuming, alternative ways of acquiring information of seagrass habitats are needed. Therefore, aerial and satellite images are useful as they are provided in different resolution, times, and prices depending on the purpose of use.

We tested how aerial and high-resolution satellite images could be utilized in finding seagrass habitats in two different environments; in the brackish Finnish coast and in the clear tropical waters of Zanzibar, Tanzania. We did supervised classification to identify seagrasses of pre-processed aerial

and satellite images. For the satellite image of the coast of Zanzibar, we also calculated water column correction. Both ways of the method worked, as the seagrass areas were found, although in the Finnish coast poor water visibility hinders light penetration below 4 meter. In developing countries, where marine inventories are usually non-existent, our methodology of utilizing low-cost images for identifying valuable habitats is the only reasonable way of acquiring marine biodiversity data.

10422-11, Session 3

Grain size mapping in shallow rivers using spectral information: a lab spectroradiometry perspective *(Invited Paper)*

Milad Niroumand-Jadidi, Alfonso Vitti, Univ. degli Studi di Trento (Italy)

Valuable and very promising results have been recently presented regarding the contribution of remote sensing techniques in studying fluvial systems. Every individual attribute of a riverine environment defines the overall spectral signature to be observed by an optical sensor. The upwelling radiance from a river body is then composed of contributions from substrate, water column and surface. In this regard, the spectral characteristic of river bed is influenced not only by the material type but also the roughness of the substrate. Motivated by this assumption, potential of optical imagery for mapping grain size of shallow rivers is examined in this research. Mapping of grain size is of particular importance in studying sediment transportation, morphology and habitat modeling of riverine systems.

The previous studies concerned with grain size mapping are all built upon the texture analysis of exposed bed material using very high resolution (i.e. cm resolution) imagery. However, the application of texture-based techniques are limited to very low altitude sensors (e.g. UAVs) to ensure a sufficient spatial resolution required for grain size mapping and then are not mainly feasible by satellite sensors. Moreover, these techniques are applicable only in the presence of exposed substrates along the river channel. To address these issues, this study examines the effectiveness of spectral information to make distinction among grain sizes for substrates below the water.

To support the objective of this research, sepectroradiometry experiments are performed in controlled condition of lab environment. The spectra are collected over a hydraulic flume in a range of water depths with several grain sizes. A spectral convolution is performed to match the spectra to WorldView-2 spectral bands which is a satellite sensor with spatial resolution appropriate for studying a wide range of rivers. The material type of substrate is considered the same for all the experiments and only the roughness/size of grains is variable. The spectra observed over dry beds revealed that the brightness/ reflectance increases with the grain size across all the spectral bands. To detect this spectral feature, Lyzenga's bathymetry model and also a bottom reflectance retrieval model are examined. Lyzenga's model is applied with simple regression (i.e. single band) which is sensitive to bottom radiance. A water column correction is considered for the approach based on bottom reflectance retrieval. According to the results, both approaches are capable of detecting the spectral feature associated with the grain size which opens up some horizons for mapping this valuable attribute of rivers using remotely sensed data.

10422-13, Session 3

Impact on satellite retrievals of temporal changes in Karenia brevis harmful algal blooms in the West Florida Shelf

Samir Ahmed, Ahmed El-Habashi, The City College of New York (United States); Vincent Lovko, Mote Marine Lab. (United States)

We examine the impact of temporal changes on satellite retrievals of Karenia brevis Harmful Algal blooms (KB HABS) in the West Florida Shelf (WFS). These impacts are compared for retrievals from both VIIRS and MODIS-A using a number of retrieval techniques. The comparisons include our recently developed neural network (NN) technique. The neural network, previously developed by us, was trained on 10,000 data point part of a synthetic data of 20,000 inherent optical properties (IOPs) based on a wide range of IOP parameters for a large variety of natural conditions based on the NOMAD data. The NN then uses as inputs the remote sensing reflectance (Rrs) measurements at 486, 551 and 671 and 488, 555 and 667 nm which are available from VIIRS and MODIS-A respectively, to retrieve phytoplankton absorption at 443 nm in satellite images. This information, when combined with backscatter information has been shown by us to be effective for obtaining retrievals of KB HB HABs in the WFS. Other retrieval algorithms included in the present comparison are the blue/green OCI/ OC3, the Generalized Inherent Optical Property (GIOP) model and the Quasi-Analytical Algorithm, (QAA version 5). The accuracies of VIIRS retrievals using all five techniques were then compared against all the in-situ measurements available over the 2012-2016 period for which concurrent or near concurrent match ups could be obtained with VIIRS retrievals. Analysis of retrieval statistics showed that the NN technique achieved the best accuracies. The analysis highlighted the impact of temporal variabilities on retrieval accuracies. The results showed the importance of having a shorter overlap time window between in-situ measurement and satellite retrieval. Retrievals where the maximum permissible overlap time window was shortened to 15 minutes, exhibited very significantly improved retrieval accuracies over those that were obtained with a 100 minute overlap time window, Retrievals that relaxed the overlap time window between in-situ measurement and satellite retrievals to simply the same day were hopelessly inaccurate by comparison. These results are believed to reflect the impact of temporal variabilities on retrieval accuracies. They underline the time limitations associated with satellite retrievals of inherently variable conditions and a changing scene. The temporal effects associated with KB HABs retrievals in the WFS were also examined by using images from consecutive VIIRS - MODIS-A – VIIRS overpasses overlapping the same parts of the WFS containing KB blooms. The consecutive images, all within an approximately 100 minute period, appear to confirm the changing bloom features. The temporal behavior of the KB blooms in the WFS over short time periods (less than100 minuntes) was further confirmed by a recent set of in-situ field measurements off the coast of Sarasota.

10422-14, Session 3

Trends in phytoplankton phenology in the Mediterranean Sea

Paula Maria Salgado Hernanz, Institut Mediterrani d'Estudis Avançats (Spain); Marie-Fanny Racault, Plymouth Marine Lab. (United Kingdom); Gotzon Basterretxea Oyarzabal, Institut Mediterrani d'Estudis Avançats (Spain)

Phenological indexes provide objective metrics to characterize phytoplankton seasonality and assess its response to environmental change. In this study, we use 16 years (1998-2014) of satellite derived sea surface chlorophyll-a concentration to analyse the spatial and temporal variations

in the phenological indexes of marine phytoplankton in the Mediterranean Sea. We use Level-4 products obtained from the EU Copernicus Marine Environment Monitoring Service (CMEMS) at 8-Day and 1-km resolution. Timing of initiation, peak, termination and duration of phytoplankton growing period were estimated using the long-term chlorophyll median plus 20% pixel-by-pixel threshold criterion and the calculation of the derivative of the cumulative sum of chlorophyll anomalies. The analysis reveals regionally consistent patterns in the shape and timing of the annual cycle of chlorophyll concentration that are consistent with previous information on the Mediterranean Sea. A single peak typically starting between the end of October and mid-November prevails in most of the oceanic areas. Exceptions are the Gulf of Lions and the Adriatic Sea where fall and winter peaks are observed. Peak magnitudes dramatically vary from the oligotrophic areas of the eastern basin (0.2 to 0.5 mg m-3) to the more productive areas of the northern Adriatic Sea (>5 mg m-3). Higher variability is observed in shelf waters where the initiation of the main bloom may significantly vary from that in oceanic waters (i.e. up to 2 months). Furthermore, shelf waters present higher probability (>70%) of displaying a second seasonal phytoplankton bloom. Trends in main bloom duration reveal a consistent increase in the Adriatic Sea and Southern Western basin, including the Alboran and Algerian sub-basins. The peak chlorophyll concentration also increases in the western basin (up 0.03 mg m-3 y-1) while remaining relatively unaffected in the eastern basin. Despite this pattern, some shelf waters of the Gulf of Lions and the Spanish Mediterranean coast have increased their bloom duration but reduced their maximum chlorophyll value during the main phytoplankton growth period.

10422-63, Session 3

Hyperspectral signatures of Indian River Lagoon and Banana River estuarine waters and bottom types

Charles R. Bostater Jr., Florida Institute of Technology (United States)

Hyperspectral signatures and imagery collected during the spring and summer of 2017 and 2016 are presented. Ground sampling distances(GSD) and pixel sizes were sampled from just over a meter and as less than 1.0 mm. A custom pushbroom hyperspectral imager was used to calculate bidirectional reflectance factor (BRF) signatures. Similar signatures of different water types and bottom habitats such as submerged sea grasses, drift algae and algal bloom waters were collected using a high spectral and digital resolution solid state spectrograph. Water was analyzed in the lab using a custom designed 50 cm long path length cuvette in order to calculate hyperspectral signatures of absorption and backscatter coefficients of dissolved organic matter (DOM), chlorophyll-a and related pigments derived from benthic biomass types, sand and mud bottoms The hyperspectral remote sensing data collected from the Banana River and Indian River Lagoon watersheds represents previously unknown signatures to be used in satellite and airborne remote sensing of water in turbid waters along the US Atlantic Ocean coastal region and the Florida littoral zone.

10422-17, Session 4

Experimental study of dual polarized radar return from the sea surface

Irina A. Sergievskaya, Stanislav A. Ermakov, Ivan A. Kapustin, Alexandr A. Molkov, Olga V. Shomina, Institute of Applied Physics of the Russian Academy of Sciences (Russian Federation)

Microwave radars are widely used for remote sensing of the open ocean and coastal areas from ships, aircrafts and satellites. Dual-polarized radars are of particular interest nowadays as perspective tool of ocean remote sensing, which can extend capabilities of retrieval the ocean currents, internal waves, marine slicks etc.

Microwave radar backscattering at moderate and large incidence angles, larger than about 25 degrees, according to conventional models, is determined by resonance (Bragg) surface waves typically of cm-scale wavelength range.

Some recent experiments have indicated, however, the existence of an additional, non Bragg component which contributes to the radar return. This non Bragg component is considered to occur due to wave breaking - strong, with white caps and /or micro breaking and being often interpreted as quasi specular reflection from wave breaking structures and therefore called as a nonpolarized component.

In spite of strong interest to the problem of radar backscattering from strong breaking waves our understanding of characteristics of Bragg and non polarized components and their relative contributions to radar return is still poor. Obviously, characteristics of both the components which are intensity and radar Doppler shifts depend on wind velocity, radar incidence angle, angle between radar look direction and wind velocity, radar wavelength and these dependences are not sufficiently studied in experiment.

This paper presents results of field observations from a Platform on the Black Sea using a new Doppler radar operating HH- and VV-polarizations in three radar bands: X-, C- and S bands in a wide range of azimuth angles and at incidence angles varying from 40 to 70 degrees. Intensity and radar Doppler shifts for Bragg and non Bragg components were retrieved from measured VV and HH intensities and Doppler shifts. It is shown that the intensity of Bragg components depends on azimuth angle and contribution of Bragg components related to the non polarized component at the three bands grows when the radar look is varied from cross wind direction to down or upwind directions. The non polarized component is obtained to be quasi isotropic. The ratio of non polarized and Bragg components decreases with incidence angle and almost does not depend on radar wavelength at incidence angles larger than about 50 degrees. The intensity of non polarized component monotonically decreases with incidence angle while the intensity of Bragg components weakly depends on incidence angle.

Velocity of scatterers , retrieved from radar Doppler shifts grows with incidence angle both for Bragg and non polarized component, but velocities for the latter increases faster and are larger then for Bragg components for all the radar bands. This demonstrates that the non Bragg scattering is associated with structures with larger scales then Bragg waves, thus giving us better understanding of the hydrodynamic nature of radar backscattering

10422-18, Session 4

Imaging of polarized target in underwater environment

Carlos Carrizo, Robert Foster, Ahmed El-Habashi, The City College of New York (United States); Deric J. Gray, U.S. Naval Research Lab. (United States); Alexander Gilerson, The City College of New York (United States)

Imaging of underwater targets is challenging because of the significant attenuation of the propagating light field due to the absorption and scattering by water and suspended/dissolved matter. Some living and manmade objects in water have surfaces which partially polarize the light, whose properties can be used to camouflage or, conversely, to detect such objects. The attenuation of light by the intervening water (so-called veiling light) changes both the intensity and polarization characteristics at each pixel of the image, and does not contain any information about the target but contributes to image degradation and blurring. Its properties need to be understood in order to isolate the true optical signature of the target. The main goal of this study is to retrieve the polarization characteristics of the target from the image in different water environments and illumination conditions by taking into account additionally measured inherent water optical

properties (IOPs).

Measurements were carried out on targets with well-known polarization characteristics in both open ocean (very clear) and coastal (more turbid) waters during recent field campaigns in Curacao (Netherlands), outside the Chesapeake Bay and in New York Bight. The targets were made of polarizers with purposely prearranged orientations and other materials including a highly reflective mirror with known polarization properties (transmission coefficients, polarization efficiency, mirror reflectivity, etc.). Data, in the form of images and videos, was then acquired using a green-band full-Stokes polarimetric video camera. Measurements were collected as a function of the relative solar azimuth angle in different water types and atmospheric conditions. Measurements outside the targets area were compared with collocated and simultaneous measurements acquired by CCNY's hyperspectral underwater polarimeter (i.e.: CCNY-POL) as well as with a modeled image of the target using a coupled atmosphere-ocean vector radiative transfer code combined with a simple imaging model. Analysis of the acquired images show reasonable agreement in Stokes vector components which characterize the intensity and linear polarization effects (I, Q, U) with the measurements by the polarimeter and modeled polarized signals. In addition, Stokes vector components of the veiling light were also estimated and compared with the models. Finally, retrieval of the total attenuation coefficient is attempted from the measurements and compared with the results of the independent measurements of IOPs.

10422-19, Session 4

Characterization of aerosol parameters over ocean from the Ocean Color satellite sensors and AERONET-OC data

Alexander Gilerson, Eder Herrera, Yaron Klein, Robert Foster, The City College of New York (United States)

Data quality of the satellite sensors for ocean monitoring (Ocean Color –OC) like MODIS, VIIRS, MERIS, OLCI sensor on Sentinel-3a is often validated through matchups between normalized water leaving radiances nLw (or remote sensing reflectance Rrs) from satellite data and data from radiometric systems (SeaPRISMs) installed on ocean platforms and which are part of the NASA Aerosol Robotic Network (AERONET) and AERONET-OC networks. While matchups are usually good in open ocean waters, significant discrepancies are observed in coastal areas which are primarily due to the more complex atmospheres near the coast and therefore less accurate atmospheric correction.

Only 10% of the radiometric signal measured by satellites at the top of the atmosphere (TOA) originates from the ocean, the other 90% consists of light scattered by molecules and aerosols in the atmosphere. Thus, satellite-derived water leaving radiances are determined by applying atmospheric correction procedures which include assumptions about the characteristics of atmospheric aerosols. At sea level, SeaPRISM makes direct measurements of nLw from the ocean, as well as observations of sky from which aerosol parameters such as aerosol optical thickness, single scattering albedo, fraction of fine and coarse aerosols, and others are determined.

Using NASA SeaDAS software for OC satellite data processing, characteristics of aerosols used in atmospheric correction models are explicitly retrieved and compared with the ones from AERONET-OC data, thus determining the validity of the aerosol models, evaluating possible errors and reasons for discrepancies and the impact of such discrepancies on the matchups in nLw data. Comparisons are initially presented for the CCNY's Long Island Sound Coastal Observatory (LISCO) AERONET-OC site and then expanded to other AERONET-OC sites with variable water and atmospheric conditions. Results could eventually lead to the improvement of the atmospheric correction models for OC satellite sensors.

10422-20, Session 5

Oil spill characterization thanks to optical airborne imagery during the NOFO campaign 2015 *(Invited Paper)*

Françoise Viallefont, Xavier Ceamanos, Sebastien Angelliaume, ONERA (France); Veronique Miegebielle, Total E&P (France)

One of the objectives of the NAOMI (New Advanced Observation Method Integration) research project, fruit of a partnership between Total and ONERA, is to work on the detection, the quantification and the characterization of offshore hydrocarbon at the sea surface using airborne remote sensing. In this framework, work has been done to characterize the spectral signature of hydrocarbons in lab in order to build a database of oil spectral signatures. The main objective of this database is to provide spectral libraries for data processing algorithms to be applied to airborne VNIR-SWIR hyperspectral images.

A campaign run by the NOFO institute (Norwegian Clean Seas Association for Operating Companies) took place in 2015 to test anti-pollution equipment. During this campaign, several hydrocarbon products, including an oil emulsion, were released into the sea, off the Norwegian coast. The NOFO team allowed the NAOMI project to acquire data over the resulting oil slicks using the SETHI system, which is an airborne remote sensing imaging system developed by ONERA. SETHI integrates a new generation of optoelectronic and radar payloads and can operate over a wide range of frequency bands. SETHI is a pod-based system operating onboard a Falcon 20 Dassault aircraft, which is owned by AvDEF. For these experiments, imaging sensors were constituted by 2 synthetic aperture radar (SAR), working at X and L bands in a full polarimetric mode (HH, HV, VH, VV) and 2 HySpex hyperspectral cameras working in the VNIR (0,4 to 1 μm) and SWIR (1 to 2,5 μm) spectral ranges. Radar and optical acquisitions were acquired successively over the oil slicks along several flight lines with a stadium geometric shape. Optical acquisitions were done along the side of the stadium overpassing the oil slick, whereas the radar sensors were used along the other side to satisfy the off-nadir viewing conditions.

A sample of the oil emulsion that was used during the campaign was sent to our laboratory for analysis. Measurements of its transmission and of its reflectance in the VNIR and SWIR spectral domains have been performed at ONERA with a Perkin Elmer spectroradiometer and a spectrogoniometer. Several samples of the oil emulsion were prepared in order to measure spectral variations according to oil thickness, illumination angle and aging. These measurements have been used to build spectral libraries. Spectral matching techniques, relying on these libraries have been applied to the airborne hyperspectral acquisitions. These data processing approaches enable to characterize the oil emulsion by estimating the properties taken into account to build the spectral library, thus going further than unsupervised spectral indices that are able to detect the presence of oil.

The paper will describe the airborne hyperspectral data, the measurements performed in the laboratory, and the processing of the optical images with spectral indices for oil detection and with spectral matching techniques for oil characterization. Furthermore, the issue of mixed oil-water pixels in the hyperspectral images due to limited spectral resolution will be addressed by estimating the area fraction of each component.

10422-21, Session 5

Revealing the timing of ocean stratification using remotely sensed ocean fronts

Peter I. Miller, Benjamin R Loveday, Plymouth Marine Lab. (United Kingdom)

Stratification is of critical importance to the circulation, mixing and productivity of the ocean, and is expected to be modified by climate change. Stratification is also understood to affect the surface aggregation of pelagic fish and hence the foraging behaviour and distribution of their predators such as seabirds and cetaceans. Hence it would be prudent to monitor the stratification of the global ocean, though this is currently only possible using in situ sampling, profiling buoys or underwater autonomous vehicles. Earth observation (EO) sensors cannot directly detect stratification, but can observe surface features related to the presence of stratification, for example shelf-sea fronts that separate tidally-mixed water from seasonally stratified water. This presentation describes a novel algorithm that accumulates evidence for stratification from a sequence of oceanic front maps, and discusses preliminary results in comparison with in situ data and simulations from 3D hydrodynamic models. In certain regions, this method can reveal the timing of the seasonal onset and breakdown of stratification.

This research is based on the composite front map approach, which is to combine the location, strength and persistence of all fronts detected on EO sea-surface temperature (SST) or ocean colour data over several days into a single map, improving interpretation of dynamic mesoscale structures (Miller, 2009). These techniques are robust and generic, and have been applied to many studies of physical oceanography, and marine animal distribution.

Miller, P.I. (2009) Composite front maps for improved visibility of dynamic sea-surface features on cloudy SeaWiFS and AVHRR data. Journal of Marine Systems, 78(3), 327-336. doi:10.1016/j.jmarsys.2008.11.019

10422-22, Session 5

Identifying pancake ice and computing pancake size distribution in aerial photographs

Fiorigi F. Parmiggiani, Istituto di Scienze dell'Atmosfera e del Clima (Italy); Miguel Moctezuma-Flores, Univ. Nacional Autónoma de México (Mexico)

On the basis of previous studies [1,2], we developed a a processing scheme to provide a rapid measure of pancake ice size distribution from aerial images. The test image used in this study was obtained by the flights which assisted the cruise of a research ship carrying out an extensive study of the autumn sea ice in the Beaufort Sea. The processing scheme is composed of the following steps: i) image enhancement; ii) marker-controlled watershed segmentation; and iii) ice size distribution computation. The results demonstrate the usability of having immediate information on pancake ice size distribution during the field campaigns in the polar regions.

REFERENCES

[1] Zhang, Q. and R. Skjetne, `"Image Processing for Identification of Sea-Ice Floes and the Floe Size Distributions," IEEE Trans. Geosci. and Remote Sensing, 53 (5): 2913--2923, [doi: 10.1109/TGRS.2014.2366640], 2015.

[2] Soh, L.K., C.Tsatsoulis, and B.Holt, "Identifying Ice Floes and Computing Ice Floe Distributions in SAR Images," in

Analysis of SAR Data of the Polar Oceans, 9--34, Springer Berlin Heidelberg, [doi:10.1007/978-3-642-60282-5], 1998.

10422-23, Session 5

Long-term monitoring of sea ice conditions in the Kerch Strait by remote sensing data

Olga Y. Lavrova, Marina I. Mityagina, Tatiana Yu. Bocharova, Space Research Institute (Russian Federation); Andrey G. Kostianoy, P.P. Shirshov Institute of Oceanology (Russian Federation) and S.Yu. Witte Moscow University (Russian Federation)

The results of multi-year satellite monitoring of ice condition in the Kerch Strait connecting the Black and Azov Seas are discussed. The issue gained importance in view of the ongoing construction of the Crimean Bridge across the strait. Our monitoring has been based on the whole variety of available satellite data including visible (Terra/Aqua MODIS, Landsat-5 TM, Landsat-7 ETM+, Landsat-8 OLI and Sentinel-2 A MSI) and radar (ERS-2 SAR, Envisat ASAR, Sentinel -1A, -1B SAR-C) data over past 15 years.

Every year the Azov Sea becomes fully or partially covered by ice during cold season. During severe winters, ice often is carried to the Kerch Strait and even the Black Sea. Since year 2000, the most extensive ice covers over the Kerch Strait were observed in 2003, 2006, 2008, 2010, 2012 and 2014. Tuzla Island and Tuzla Spit are the natural barriers stretching across the strait in its east and central parts. They and north winds force the ice to drift to the Black Sea along the Crimean coast on the west of the Kerch Strait. An analysis of ice drift hydrometeorological conditions is presented.

The ice conditions occurred in 2017 are under special consideration. Everyday satellite monitoring of the Kerch Strait, including the construction area of the Crimean Bridge, has revealed formation and drift features of ice drifting from the Azov Sea through the Kerch Strait and the way it meets the bearings of the technological and main bridges. It was found that even under strong north-east winds, ice does not flow between the bridges' bearings including the widest shipway. At present, it is hard to discern the impacts of the two bridges on floating ice, nevertheless when the construction is over and the technological bridge is gone, by all appearances the main bridge will strongly affect ice conditions in the Kerch Strait. This perspective calls for continual satellite monitoring of the area that is enabled by cutting-edge systems and technologies. We processed and analyzed the satellite data using the toolkit of the See the Sea portal developed at the Space Research Institute RAS.

The study was completed with partial financial support of the Russian Science Foundation, grant #14-17-00555. Basic functionality of the See the Sea portal is implemented with the support of FASO Russia (Theme "Monitoring", state register No. 01.20.0.2.00164).

10422-25, Session 6

Surface circulation in the Western Mediterranean shown by a synergy of satellite-derived datasets

Svetlana Karimova, Univ. de Liège (Belgium)

Satellite oceanography provides a multitude of ways for observing surface circulation of marine basins. The most widely-used technique for extracting surface currents is proposed by satellite altimetry. Studying multiscaling properties of passive microwave, infrared and visible-range imagery is also giving promising results. Finally, synthetic aperture radar (SAR) products also allow extracting information on velocity of surface currents. Certain efforts are being undertaken by the oceanographic community to make a synergetic use of such heterogeneous techniques.

The present study also provides an attempt to bring together the benefits of different approaches for extracting information on surface currents from remotely-derived datasets. As a

region of interest, we use the Western Mediterranean Basin, which is having quite a peculiar pattern of surface circulation due to the inflow of Atlantic water through the Strait of Gibraltar. Despite a great number of oceanographic researches being undertaken in this area, the data provided by satellite observations for the Western Mediterranean is almost unused so far. Thus, the basin-wide surface circulation of this sea is traditionally illustrated by the scheme of Millot (1987).

Among the data analysed, there are different datasets on geostrophic, Ekman and high-resolution currents, based on using satellite altimetry, on an analysis of satellite imagery and, finally, on their synergy. Such datasets are being provided in the framework of different projects by AVISO, GlobCurrent, PEACHI, CLS, LOcean, CTOH, CNES, etc. Since the datasets obtained by different techniques are quite heterogeneous, a methodology for an intercomparison of such datasets was developed and discrepancies revealed were analysed. After the cross-calibration of the datasets, the best available data were merged and a renewed quantitative scheme of the surface circulation for the area of interest was provided for different temporal scales.

Special attention in the study is being paid to the performance of different satellite datasets in manifesting coherent vortical structures, or eddies, of different spatial scales. Being responsible for local extrema in the field of surface currents and having relatively long lifetimes, these structures play a crucial role in horizontal and vertical water transport. Multiple techniques have been proposed for extracting information on the presence of vortical structures and their characteristics from different scalar and vector satellite-derived fields. Among them, there are methods based on front detection, ellipse/circle fitting, analysis vector/streamline geometry, extraction of closed contours, wavelet analysis, observing lagrangian coherent structures, etc.

In this study, we analyse potentials and limitations of different eddy detection techniques as well. As 'ground truth', a dataset of eddy manifestations detected in satellite thermal infrared and SAR imagery of the Western Mediterranean is used. The general preliminary conclusion is that for the region of interest, conventional altimetry-based products, including gridded, along-track, and value-added ones, provide more or less reliable manifestation only of those eddies which exceed approx. 70 km in diameter. Additionally, altimetry-based methods tend to provide similar characteristics for cyclonic and anticyclonic eddies while satellite imagery reveals the dominance of anticyclonic eddies at the spatial scales being under consideration.

10422-26, Session 6

A parallel efficient algorithm for the statistical model of dynamic sea clutter at low grazing angle

Tao Wu, Zhensen Wu, Xidian Univ. (China)

Study of characteristics of sea clutter is very important for signal processing of radar, detection of targets on sea surface and remote sensing. The sea state is complex at Low grazing angle (LGA), and it is difficult with its large irradiation area and a great deal simulation facets. A practical and efficient model to obtain radar clutter of dynamic sea in different sea condition is proposed, basing on the physical mechanism of interaction between electromagnetic wave and sea wave.

The classical analysis method for sea clutter is basing on amplitude and spectrum distribution, taking the clutter as random processing model, which is equivocal in its physical mechanism. To achieve electromagnetic field from sea surface, a modified phase from facets is adding to the semi-deterministic facet scattering model (SDFSM), making the assumption that the phase contributed by facets is from an initial phase and the phase delay of the relative path of each facet. And the backscattering coefficient is calculated by Wu's improved two-scale model since the sea surface is regarded as the small-scale roughness distributed over the slope distribution of the large-scale roughness, while the model can solve the statistical sea backscattering problem less than 5 degree, considering the effects of the surface slopes joint probability density, the shadowing function, the skewness of sea waves and the curvature of the surface on the backscattering from the ocean surface. To reduce the fluctuation, several sea surface samples is required, each sample corresponds to a random seed. The time-varying ensemble average of several samples is obtained to analyze amplitude probability density distribution of radar clutter. And the affection of wind speeds and directions, frequencies and polarization are considered at the same time.

To calculate a wide sea area, such as the size is "2000mx2000m", suitable partitions are adopted. And each partition simulation sea surface is divided into huge amount of small facets, as to Ku-band, the whole ocean area is divided into Nx ? Ny blocks, i.e. 64x64 (4096) sub-partitions. And each partition consists of small facets with subdivision numbers of M in x-axis and N in y-axis, the value of M or N is several thousand or more. We make the assumption that the scattering contribution of each facet is independent, the total field is the superposition of each facet in the receiving direction. Such data characters are very suitable to compute on GPU threads. So we can make the best of GPU resource. We have achieved a speedup of 396-fold for S band and 409-fold for KuX band on the Tesla K20c GPU as compared with Intel(R) Core(TM) CPU.

In this paper, we mainly study the high resolution data, and the radar wavelength is nearly millimeter magnitude, and the time resolution is millisecond, so we may have 10,000 time points, i.e. the same numbers of sea simples, and we analyze the data to achieve the statistical characteristics of two-dimensional dynamics sea clutter, and the Rayleigh distribution-LogNormal distribution-Weibulland distribution K distribution clutter is simulated with method of zero memory nonlinearity(ZMNL) transform and Spherically Invariant Random Process(SIRP).

10422-27, Session 6

Evaluation of Sentinel-2A imagery for regional lake water quality assessments by observing colored dissolve organic matter (CDOM) in freshwater lakes in Västerbotten and Jämtland in northern Sweden

Enass Said Al-Kharusi, Lund Univ. (Sweden)

This study is intended to demonstrate the significant shifts in DOM concentration with space and time within and across inland waters (lakes), which can be acquired by the analysis of DOM concentration using Sentinel-2A imagery. Using a remote sensing method (based on Sentinel-2A data) to evaluate DOM quantity or concentration in freshwater (lakes), optical properties shifts of CDOM of spatial and temporal observations at sites in Västerbotten and Jämtland in Northern Sweden can be understood in terms of the landscape features and hydrological events at those locations. Using Sentinel-2A as a data source for these remote sensing methods can provide an effective approach for estimating CDOM concentrations in water to obtain water quality information regularly, and also could help to accurately estimate the CDOM absorption coefficient (aCDOM) via Sentinel-2A data of the study area. The estimation of (aCDOM) by using Sentinel-2A could help to study DOM in inland waters at global scale by using following equation aCDOM(420)=5.13(B2/B3)-2.67

10422-28, Session 6

Apparent optical properties of the Red Sea from measurements and simulated data

Surya P. Tiwari, King Abdullah Univ of Science and Technology (Saudi Arabia); Burton Harold Jones, King Abdullah Univ. of Science and Technology (Saudi Arabia)

High quality in situ radiometric observations is needed for calibration, validation, and bio-optical algorithm development of ocean color remote sensing, moreover in studying and understanding of ocean optical, biological, and biogeochemical properties. Notably, calibration and validation of ocean color satellite data depend on high quality in situ data. Therefore, to improve our understanding of optical properties of the Red Sea, radiometric field measurements performed during in 2016 oceanographic cruises. The data set measured using the SatlanticTM HyperPro instrument equipped with radiometers, includes downwelling irradiance (Ed), upwelling radiance (Lu), and surface reference irradiance (Es). Profiles of downwelling irradiances were used to calculate diffuse attenuation coefficient, the first optical depth, PAR, and depth of the euphotic zone. Remote sensing reflectance computed from the ratio of upwelling radiance to downwelling irradiance. Derivative analysis performed on the spectral remote sensing reflectance to identify the different phytoplankton pigments based on the various peaks. The results obtain from the observational data analysis will be presented in this paper and discussed for ocean color implications.

10422-29, Session 6

Study on variation in turbidity in Cam Ranh Bay and Thuy Trieu Lagoon, Vietnam

Quang Nguyen Hao, Nha Trang Univ. (Viet Nam)

Turbidity, an indicator of water pollution, is an important water quality parameter directly related to underwater light penetration and thus affects the primary productivity in a water body. This study aims to investigate the variation of turbidity in Cam Ranh Bay and Thuy Trieu Lagoon as well as major factors affecting its spatiotemporal patterns by using remote sensing data. The algorithm for turbidity retrieval was developed based on the correlation between in situ measurements and red band of Landsat 8 OLI with R2 = 0.84, $p < 0.05$, Root Mean Square Error (RMSE) = 0.28 and Scatter Index (SI) = 0.22. Simulating WAves Nearshore (SWAN) model was used to compute bed shear stress, major factor affecting turbidity in shallow waters. In addition, the relationships between turbidity and bed shear stress, rainfall and tidal regime in study area were also analyzed, and found that: (1) During the dry season, turbidity was low in middle of the Bay but high in shallow waters and near coastlines. Resuspension of bed sediment was the major factor controlling turbidity in the time without raining. (2) During the rainy season as well as short time after raining in the dry season, turbidity was high due to the large amount of run-off entering into the study area. (3) Under tidal condition especially the flood tide regime, clear open ocean water entered into the Bay and diluted highly turbid waters resulted in decreasing turbidity. In deep waters, tidal regime combined with rainfall was the significant cause of highly turbid waters.

10422-30, Session 7

Ensuring that the Sentinel-3A altimeter provides climate-quality data

Graham Quartly, Francesco Nencioli, Plymouth Marine Lab. (United Kingdom); Sylvie Labroue, Collecte Localisation Satellites (France); Pierre Femenias, ESRIN (Italy); Remko Scharroo, EUMETSAT (Germany); Saleh Abdalla, European Ctr. for Medium-Range Weather Forecasts (United Kingdom); Pascal Bonnefond, Observatoire de Paris à Meudon (France); Mathilde Cancet, Noveltis SA (France); Marie-laure Frery, Matthias Raynal, Collecte Localisation Satellites (France); Steven Baker, Alan Muir, David Brockley, Univ. College London (United Kingdom); Andrew Shepherd, Univ. of Leeds (United Kingdom); Pablo Garcia, Mònica Roca, isardSAT (Spain); Stéphane Calmant, Lab. d'Etudes en Géophysique et Océanographie Spatiales (France); Jean-Francois Cretaux, Ctr. National d'Études Spatiales (France)

The Sentinel satellites are the backbone of the Copernicus programme to monitor the Earth from space, with the radar altimeter contributing to climate data records on global and regional sea level, wind and wave conditions, river and lake levels, sea-ice thickness and the changing nature of the polar ice sheets. To maintain a high consistency between 4 altimeters spanning 15 years, and a seamless transition with previous missions imposes exacting standards on the instrument monitoring, processing and quality control. With currently just the first mission in orbit, the Sentinel-3 Mission Performance Centre has been developing the methodology appropriate to each of the parameters of interest.

Internal calibrations are used to monitor the evolution and strength of the emitted pulse. Although the signal strength has reduced by almost 1 dB over the first 12 months of operation, this remains well within the design budget; the shape of the pulse including sidelobes remain well within expectation. The strength of altimeter returns from the ocean is related to wind speed, and with the correction for changes in emitted signal, the derived wind speed record now matches that produced by the ECMWF model, with minimal bias and r.m.s. differences commensurate with previous altimeters. The range information, essential for the accurate calculation of sea level, shows the significantly reduced noise level expected for delay Doppler (SAR) processing, with the absolute bias being recorded to within a few centimetres by use of radar transponders, overflights of Lake Issyk-kul and dedicated surveying activities off Corsica.

The recovery of sea-ice thickness requires the careful discrimination between radar echoes from ocean and sea-ice. The initially implemented classification methodology requires improving in order to render its results consistent with those of CryoSat-2. Adaptations are also required to the data collection and processing over the ice shelves of Greenland and Antarctica, because the first year of data showed greater data loss than expected in the ice margins. Plans are being developed to assure the closest possible consistency between Sentinel-3A and its sister satellite, Sentinel-3B due for launch later this year

10422-31, Session 7

Multifrequency radar imagery and characterization of hazardous and noxious substances at sea

Sebastien Angelliaume, ONERA (France); Brent Minchew, British Geological Survey (United Kingdom); Sophie Chataing, Cedre (France); Philippe Martineau, ONERA (France); Veronique Miegebielle, Total E&P (France)

The increase in maritime traffic, particularly the transport of hazardous and noxious substances (HNS), requires advanced methods of identification and characterization in environmental chemical spills. Knowledge about HNS monitoring using radar remote sensing is not as extensive as for oil spills, however any progress on this issue would likely advance the monitoring of both chemical and oil-related incidents. To address the need for HNS monitoring, an experiment was conducted in May 2015 over the Mediterranean Sea during which controlled releases of HNS were imaged by a multifrequency radar system. The aim of this experiment was to establish a procedure for collecting evidence of illegal maritime pollution by noxious liquid substances using airborne radar sensors. In this paper, we demonstrate the ability of radar imagery to detect and characterize chemicals at sea. A Normalized Polarization Difference (NPD) parameter is introduced to quantify both the impact of released product on the ocean surface and the relative concentration of the substance within the spill. We show that radar imagery can provide knowledge of the involved HNS. In particular, one can distinguish a product that

forms a film on the top of the sea surface from another that mixes with seawater, information that is critical for efficient cleanup operations.

10422-33, Session 7

Assessing altimetry close to the coast

Graham Quartly, Francesco Nencioli, Plymouth Marine Lab. (United Kingdom); Daniel Conley, Plymouth Univ. (United Kingdom); Saleh Abdalla, European Ctr. for Medium-Range Weather Forecasts (United Kingdom)

The latest advance in altimetry, SAR processing, promises the potential to recover meaningful data closer to the coast. This is fundamental to increasing the use of altimetry data, as the major societal impacts of sea level rise or increasing wave extremes are most keenly felt at the shoreline. Conventional processing of radar altiimeter returns (waveforms) is significantly affected when the instrument's ~8 km footprint includes returns from land; SAR processing offers a much smaller effective footprint and thus greater resilience to unwanted echoes from land.

We compare currents and wave estimates from the new Sentinel-3A altimeter to records from an HF radar system operating off the northwest coast of Cornwall. The PRIMaRE HF radar system has been operating for many years producing maps of current and wave conditions up to ??70km from the shore. These are being compared to data from the four Sentinel-3A passes through the region to determine at what distance from the shore the satellite values get affected. This will be compared to the performance of conventional processing, in order to demonstrate whether the expected gains from SAR altimetry are being realised.

10422-34, Session 7

Coastline detection with time series of SAR images

Dongyang Ao, Beijing Institute of Technology (China); Octavian Dumitru, Gottfried Schwarz, Mihai P. Datcu, Deutsches Zentrum für Luft- und Raumfahrt e.V. (Germany)

Coastal areas are a special environment in which waves, currents, and sediments are interacting in a complicated way. For maritime remote sensing, coastline detection is a vital task. With continuous coastline detection results from image time series, the actual shoreline, the sea level, and environmental parameters can be observed to support coastal management and disaster warning.

Optical satellite images are commonly being used for coastal monitoring since they are simple to obtain and easy to understand. However, optical images can be severely affected by atmospheric conditions. In contrast, microwave remote sensing is a way to overcome this problem. Synthetic Aperture Radar (SAR) is a day-and-night and all-weather imaging technique with medium and high resolution; it is the most frequently employed imaging tool for coastline extraction. Yet, coastline detection for SAR images is difficult due to image noise and sometimes low contrast between sea and land.

Conventional methods are mainly based on scaled SAR images and image processing approaches. These methods involve a lot of complicated data processing, which is a big challenge for remote sensing time series. Additionally, a number of SAR satellites operating with polarimetric capabilities have been launched in recent years, and many investigations of target characteristics in radar polarization have been performed.

In this paper, SAR polarization information is used to extract coastlines. By calculating a modified correlation of dual-polarimetric SAR images, coastlines can be detected easily and accurately. This method is designed to increase land/sea separation which helps to generate distinguishable coastlines (and coastline maps). For the analysis of image time series, this is a simple and reliable approach to process large datasets.

The coastline detection is processed in three steps. First, we calculate the correlation coefficients of two SAR images of different polarization (e.g., VV and VH). This coefficient differs from the traditional interferometric computation where normalization is needed. Through this modified approach, the separation between sea and land becomes more prominent. Second, we set a threshold to distinguish between sea and land. The threshold setting scheme is based on the statistical distribution of the SAR image characteristics. We use a G0 distribution model and a CFAR method to set up the threshold. Third, we extract the coastline using image edge detectors. To reduce the influence of noise and coastline complexity, we present a simple and effective detector based on a combination of morphology parameters and a Canny operator.

Our study area is the Danube Delta in Romania, which is the largest and best-preserved river delta in Europe. In 1991, the Danube Delta was internationally recognized as a protected area and included on the UNESCO natural Heritage List. The reason for choosing this area is that, during the last years, the Delta has dramatically changed due to decreasing alluvial discharges and, as a consequence, many coastline changes occurred. For a more detailed analysis, we consider a Sentinel-1A SAR dataset consisting of 30 images acquired over 15 months.

The results show that we can assume reliable coastline detection details.

10422-32, Session PS

Assessment of the quality of HY-2A satellite sea surface height data

Qingtao Song, Xuemin Gao, Zhaohui Wang, Yuxin Liu, National Satellite Ocean Application Service (China)

In August 2011, China successfully launched the Ocean II (HY-2A) satellite. HY-2A carries a dual-band radar altimeter with a calibrated microwave radiometer on a precision orbit. The main objective of HY-2A is to observe the elements of marine dynamic environment, including sea surface height field.

The evaluation of HY-2A satellite sea surface data quality is a necessary part of HY-2A satellite sea surface data application. The common method for evaluation is using crossover points of HY-2A and other accurate altimeter data as Jason-2 which is calibrated with many other altimeter. The SLA (sea level anomaly) comparisons show that the number of HY-2A data with low quality is about 12%. It is found in this study the standard deviation of SSH between HY-2A satellite and Jason-2 is 7.0 cm.

The experiment using the HY-2A altimeter data (cycle 18 to 23) in the same time period with the Jason-2 GDR-d data (cycle 143 to 152, 2012 May 26th to 2012 Aug. 18th). HY-2A data provided by NSOAS (National Satellite Ocean Application Service) while Jason-2 GDR-d data download on the website set up by AVISO (Archiving, Validation and Interpretation of Satellite Oceanographic data).The SLA cannot be measured by observation directly, which must be corrected by other correction items as dry troposphere correction, wet troposphere correction, sea state bias, ionospheric correction, solid earth tide, pole tide, ocean tide, inv atmospheric pressure, high frequency fluctuations. All the items should be used as the correction items to filter the altimeter data. The abnormal crossover points are filtered after cubic spline interpolation. The experiment shows that partial cross points of all the cycle 18 to 23 have significantly deviation. The whole data with the deviated cross points in the track will be filtered. For example, the standard derivation of track 017 in cycle 20 for HY-2A is 31.45cm. The drastic fluctuation in the track caused by equipment failure not the changes of marine phenomenon.

The standard derivation of the filtered data (78%) is 7.0cm with Jason-2, while the standard derivation of ERS-1 and T/P is 16cm. The experiment indicates that HY-2A altimeter has the stable and reliable data quality.

10422-35, Session PS

Nonlinear retrieval algorithm for HY-2A spaceborne microwave radiometer

Zhaohui Wang, National Satellite Ocean Application Service (China); Chen Chen, 27th Research institute of China Electronics Technology Group Corporation (China); Qimao Wang, Qingtao Song, National Satellite Ocean Application Service (China)

Spaceborne microwave radiometer is an instrument that measures the electromagnetic waves radiated from the surface or the atmosphere by heat radiation. By observing data by the instrument, retrieved information such as sea surface temperature, sea surface wind speed, atmospheric water vapor content, and cloud liquid water content can be obtained to study the global water cycle and climate change issues. The most commonly used retrieve algorithm is Multiple Linear Regression (MLR) which has the advantages of simple modeling and fast calculation. However the regression method introduced new errors caused by the linear model. So the MLR algorithm does not have the clear physical meaning and high accuracy.

In order to solve the problem that MLR physical meaning not clear and computational complexity of the commonly non-linear retrieve algorithm, the Key Lab of NSOAS (National Satellite Ocean Application Service) developed a useful non-linear algorithm. This non-linear algorithm solved the overdetermined equations constituted by Radiative Transfer Model (RTM) by using the function optimization. The Nelder-Mead method is a kind of direct search algorithm which is comfortably to minimize the function.

RTM established the relationship between brightness temperature observed by instrument and the oceanic and atmospheric parameters, minimize the observed data and the modeling data could find the suitable solution. The non-linear retrieve algorithm retrieve the different parameter used the different channels. For example, using all channels to retrieve sea surface temperature, all channels except C-band to retrieve sea surface wind speed. Such data processing could improve the data resolution without using the low frequency channels.

The simulation experiment without instrumental noise shows that the accuracy of Nelder-Mead method retrieve results is much higher than that of MLR retrieve algorithm. For sea surface temperature, the RMSE of Nelder-Mead is 0.037K and the RMSE of MLR is 0.58K. Compared with MLR algorithm, Our results also indicate that the Nelder-Mead algorithm has definite physical meanings and avoids MLR associated errors.

This non-linear retrieve algorithm based on HY-2A (Haiyang-2A, ocean in Chinese), the satellite platform combined the microwave radiometer, radar altimeter and scatterometer, launched on 2011 which is still on-orbit. The continued China Oceanography Satellite Program contains HY-2B which will launch on 2018, also carry the microwave radiometer, radar altimeter and scatterometer together.

10422-36, Session PS

Ocean subsurface particulate backscatter estimation from CALIPSO spaceborne lidar measurements

Peng Chen, Delu Pan, Tianyu Wang, The Second Institute of Oceanography, SOA (China); Zhihua Mao, The Second Institute of Oceanography (China)

The Cloud-Aerosol Lidar with Orthogonal Polarization (CALIOP)?a primary payload instrument on the Cloud-Aerosol Lidar and Infrared Pathfinder Satellite Observation (CALIPSO)?can produce simultaneous pluses at 532 nm and 1064 nm. The CALIOP lidar was designed to provide the observations necessary for an improved understanding of the impact of clouds and aerosols on the Earth' s radiation budget and climate. Current research shows that the active sensor CALIOP have a potential for quantifying global ocean carbon stocks and ocean subsurface backscatter, due to that the 532 nm laser pulses can penetrate ocean surface, and obtain the backscatter information of subsface water body. In this paper, a method for ocean subsurface particulate backscatter estimation from the CALIPSO satellite was demonstrated. Because the photo multiplier tubes (PMTs) of 532 nm detectors (parallel and perpendicular polarizations) exhibit a non-ideal recovery of the lidar signal after striking a strongly backscattering target, namely transient response. Therefore, when the backscatter signal is received, the transient response of PMT will affect the waveform, the energy of peak signal will spread to the adjacent several bins,which therefore will make the signal intensity more bigger than it should be. Therefore, the effects of the CALIOP receiver's transient response on the attenuated backscatter profile were first removed in order to obtain a reliable attenuated backscatter profile. Hypothesis is based on that land signal have the same response function.So laser signals on land were used to get the transient response function. The results show that different land surfaces have the same transient response function. Then the two-way transmittance of the overlying atmosphere was then estimated as the ratio of the measured ocean surface attenuated backscatter to the theoretical value computed from wind driven wave slope variance to eliminate the effect of aerosol. Finally, particulate backscatter was estimated from the column-integrated depolarization ratio as the ratio of the cross-polarized and co-polarized channels. Statistical results show that the derived particulate backscatter by the new method based on CALIOP agree reasonably well with chlorophyll-a and particulate organic carbon (POC) concentration using MODIS data. It indicates a potential use of space-borne lidar to estimate global primary productivity and particulate carbon stock.

10422-37, Session PS

Laser-induced fluorescence technique for detecting organic matter in East China Sea

Peng Chen, Tianyu Wang, Delu Pan, Haiqing Huang, The Second Institute of Oceanography, SOA (China)

A laser induced fluorescence (LIF) technique for fast diagnosing chromophoric dissolved organic matter (CDOM) in water is discussed. We have developed a new field-portable laser fluorometer for rapid fluorescence measurements. In addtion, the fluorescence spectral characteristics of fluorescent constituents (e.g., CDOM, chlorophyll-a) were analyzed with a spectral deconvolution method of bi-Gaussian peak function. In situ measurements by the LIF technique compared well with values measured by conventional spectrophotometer method in laboratory. A significant correlation (R2 = 0.93) was observed between fluorescence by the technique and absorption by laboratory spectrophotometer. Influence of temperature variation on LIF measurement was investigated in lab and a temperature coefficient was deduced for fluorescence correction. Distributions of CDOM fluorescence measured using this technique in the East China Sea coast were presented. The in situ result demonstrated the utility of the LIF technique for rapid detecting dissolved organic matter.

10422-39, Session PS

Satellite observations of rainfall effect on sea surface salinity in the waters adjacent to Taiwan

Chung-Ru Ho, National Taiwan Ocean Univ. (Taiwan); Po-Chun Hsu, National Taiwan Ocean Univ. (Taiwan) and Atmosphere & Ocean Research Institute, The Univ. of Tokyo (Japan); Chen-Chih Lin, Shih-Jen Huang, National Taiwan Ocean Univ. (Taiwan)

Oceanic salinity plays an important role on Earth's water cycle, ocean circulation, and climate. Changes of ocean salinity may cause the density of water changes and then affect the ocean circulation. The Kuroshio, a western boundary current of the North Pacific, originates from the North Equatorial Current. It flows northward along the eastern coast of Taiwan from the Philippines to Japan and transfers warmer and saltier water from tropical oceans to polar areas and then affects regional climate. The South China Sea (SCS), the largest marginal sea situates at the westernmost side the tropical Pacific. Its water body connects with the East China Sea, the Pacific Ocean, and the Indian Ocean through the Taiwan Strait, the Luzon Strait, and the Strait of Malacca, respectively. Previous studies pointed out that the Kuroshio affects the hydrographic feature and circulation pattern in the SCS. The changes of sea surface salinity (SSS) in the SCS and the Kuroshio region may play an important role on the water exchange between the SCS and the western Pacific. Because the change of SSS is highly related to the variations of evaporation and precipitation, to understand the influence of rainfall on the change of SSS in the waters adjacent to Taiwan may improve our understanding on the waters exchange between the SCS and the western Pacific Ocean. In this study, satellite remote sensing data from the year of 2012 to 2014 are employed. The daily rain rate data obtained from the Special Sensor Microwave Imager (SSM/I), Tropical Rainfall Measuring Mission's Microwave Imager (TRMM/TMI), Advanced Microwave Scanning Radiometer (AMSR) 2, and WindSat Polarimetric Radiometer. The SSS data was derived from the measurements of radiometer instruments onboard the Aquarius satellite. The results show that the average values of SSS in east of Taiwan, east of Luzon and the SCS are 33.75 psu, 34.00 psu, and 32.71 psu, respectively, in the condition of daily rain rate higher than 1 mm/hr. In contrast to the rainfall condition, the average values of SSS are 34.06 psu, 34.24 psu, and 33.05 psu in the three areas, respectively. During the cases of heavy rainfall caused by spiral rain bands of typhoon, the SSS is diluted with an average value of -0.74 psu when the average rain rate is higher than 4 mm/hr. However, the SSS was increased after temporarily decreased during the typhoon cases. A possible reason to explain this phenomenon is that the heavy rainfall caused by the spiral rain bands of typhoon may dilute the sea surface water, but the strong winds can disturb the ocean and uplift the higher salinity of subsurface water to the sea surface.

10422-40, Session PS

Sea surface blended winds based on HY-2A scatterometer and NCEP reanalyzed

Zhaohui Wang, Qingtao Song, Qimao Wang, Yuxin Liu, National Satellite Ocean Application Service (China)

This paper obtains the global coverage rates of HY-2 scatterometer, which is compared with ASCAT, from independent observations and combined observations based on the calculation results of sub-satellite points. Especially in the South China Sea and East China Sea, the improvements of sampling rate by combined observation are discussed. However the current scatterometer cannot satisfy the requirement of actual applications in spatial and temporal resolution. So it is necessary to establish blended winds products from multiple resources to fill the data gap in both spatial and temporal part. Based on the Data of NCEP winds field and scatterometer winds field, the blended winds with resolution of 6h and 0.25°are established using the method of spatial-temporal weighted analysis.

10422-42, Session PS

The artificial object detection and current velocity measurement using SAR ocean surface images

Valery V. Strotov, Boris A. Alpatov, Ryazan State Radio Engineering Univ. (Russian Federation); Maxim D. Ershov, Ryazan State Radio Engineering Univ. (Russian Federation); Vadim S. Muraviev, Ryazan State Radio Engineering Univ. (Russian Federation); Alexander B. Feldman, Ryazan State Radio Engineering Univ. (Russian Federation); Sergey ? Smirnov, Ryazan State Radio Engineering Univ. (Russian Federation)

Processing of synthetic aperture radar (SAR) images is extensively used for control and monitoring of the ocean surface. Image data can be acquired from Earth observation satellites, such as TerraSAR-X, ERS, and COSMO-SkyMed. Due to the fact that water surface covers wide areas, remote sensing is the most appropriate way of getting information about ocean environment for vessel tracking, security purposes, ecological studies and others. Thus, SAR image processing can be used to solve many problems arising in this field of research. This paper discusses some of them including ship detection, oil pollution control and ocean currents mapping. Due to complexity of the problem several specialized algorithm are necessary to develop.

The oil spill detection algorithm consists of the following main steps: image preprocessing, detection of dark areas, parameter extraction and classification. An adaptive filtering and thresholding is performed at the step of dark image areas detection. The window filtering is used to estimate roughness of the surrounding sea surface. The roughness coefficient and a priori information about sea currents velocity allow to detect points with strong local brightness homogeneity. Classification of founded areas is an important step of the algorithm and requires a complex statistical analysis of each segment.

Ship detection is a crucial application for global environmental monitoring and security. It allows to monitor traffic, fisheries and to associate ships with oil discharge. Although ships in the image are clearly visible, the presence of intense noise and clutter makes the problem of its detection much more difficult. The proposed approach consists of the following main steps: prescreening, land masking, image segmentation combined with parameter measurement, ship orientation estimation and object discrimination. Prescreening involves the processing of the original SAR image using a multi-window averaging filter followed by adaptive local thresholding. The collected statistics is used to get approximate object locations based on signal-to-noise local peaks. But the shape of large sized objects in the binary image can be deformed and leads to incorrect ship parameter estimation. Therefore, to restore object mask the image segmentation step is implemented. In this work the modified region growing technique is used as a basis for segmentation due to its speed and computational efficiency. Additionally such parameters as area, average brightness, orientation and bounding box can be estimated at the same step.

The measurement of ocean currents is also important for monitoring many marine processes. To measure the velocity of ocean currents the SSC SAR images that preserve information about the amplitude and phase of the reflected signal are required. It is known that according to Doppler's law the frequency of the reflected signal changes in proportion to the object velocity. The proposed algorithm is based on this law and allows to measure the velocity of surface currents.

The SAR images obtained from TerraSAR-X and ERS-2 satellites are used to estimate efficiency of proposed algorithms. The results show that the developed algorithms can be used in practice in maritime applications.

10422-43, Session PS

Evaluation of HY-2A microwave scatterometer geolocation errors

Robby Chan, Qingtao Song, National Satellite Ocean Application Service (China)

Coastline inflection points can be identified on the basis that the radar backscatter of land and water exhibits a large difference when ocean surface wind speed is relatively low. The longitudes and latitudes of these points from different time periods are fitted to the Global Self-consistent Hierarchical High-resolution Shorelines (GHSSH) map. The comparison results show that the mean geolocation error in cross- and along-track direction is 5.5 km and 7.5 km respectively. Sources of geolocation errors are also analyzed in this paper in order to improve the geolocation accuracy.

10422-44, Session PS

The re-analysis for satellite retrieved chlorophyll-a in East China Sea

Hao Zhengzhou , Delu Pan, Fang Gong, Xianqiang He, The Second Institute of Oceanography, SOA (China); Difeng Wang, Second Institute of Oceanography SOA (China)

Satellite observation is an important way to understanding the variation of marine environments. It is noted that the satellite-retrieved raw ocean color products, such as the chlorophyll, have some missing data on large area where the clouds and heavy aerosols covered or other reasons. In order to monitor their changes and assess their influence on the marine ecosystems or climate, the long-term synchronous and full covered data are needed. The Geostationary Ocean Color Image (GOCI), which is one of sensors onboard COMS Geostationary satellite, observes the East China Sea hourly during the daytime (8 times observation in daytime) and provides nice opportunity to show the diurnal variation of the marine environment which different from the multi-satellite observations during a day. In this study, the hourly remote sensing data of Chlorophyll-a on 2015 in the East China Sea is reconstructed and re-analyzed using the Data Interpolation Empirical Orthogonal Functions (DINEOF) and Optimal Interpolation (OI). The error and variability are examined by some selected valid observations. The results show that the re-analyzed chlorophyll-a products could reveal its tempo-spatial variation features basically and can describe or reappear the Chlorophyll-a distribution characteristics in multi-scale processes.

10422-45, Session PS

Unusual phytoplankton blooms in the southwestern Bay of Bengal: a comparative study

Xiaoyan Chen, Yan Bai, Xianqiang He, The Second Institute of Oceanography, SOA (China); Shaolei Lu, Shujie Yu, The Second Institute of Oceanography (China)

Two unusual phytoplankton bloom events were identified in the southwestern Bay of Bengal from MODIS-derived chlorophyll-a concentration data collected between 2003 and 2015. The occurrence of the unusual phytoplankton bloom in December 2005 (called Bloom 1 in this study) has been reported in the literature to be triggered by multiple forcings, including strong cyclonic eddy, frequent tropical cyclones, and strong wind-induced mixing. Interestingly, the other unusual phytoplankton bloom (called Bloom 2 in this study) was identified in almost the same location in December 2013. Further, it is the strongest bloom during our study period with large area of high Chl-a > 1.0 mg/m3 and shared some similar features with Bloom 1, such as wide coverage and long duration. At the same time, there were also frequent tropical cyclones and a cyclonic eddy. The possible causes of Bloom 2 were examined using time series of multi-satellite datasets, including sea surface height anomalies (SSHA), sea surface temperature (SST), wind stress, together with Argo profile data. We found that the cyclonic eddy might be not yet the dominant factor for Bloom 2 as the eddy was much weaker than that of Bloom 1. Specially, SST in December 2013 was lowest among all the December from 2003 to 2015. That is, the stratification is weakest. Therefore, the weak stratification can be broken easily by mixing induced by tropical cyclones and cyclonic eddies and finally result in the strong bloom. This comparative studies could provide us some insight in understanding the role of eddies and tropical cyclones in phytoplankton dynamics in the Bay of Bengal.

10422-46, Session PS

Multisensor satellite survey of natural oil slicks in the Southeastern Black Sea

Marina I. Mityagina, Olga Y. Lavrova, Space Research Institute (Russian Federation)

Our paper is devoted to the further development and applications of satellite remote sensing technics for identifying and analyzing of spatial and temporal characteristics of sea surface oil-containing slicks caused by natural hydrocarbon seeps including mud volcanoes, natural gas and oil outflows from the sea bottom, and gas hydrates.

The main interest in the study of these phenomena is primarily due to the probable existence of a link between the natural showings of hydrocarbons from the seabed and oil and gas fields presence in the area. This turns these unique phenomena into a kind of oil and gas search criterion. Knowledge of areas of localization of natural manifestations of hydrocarbons is also necessary for the selection of safe places for the construction of underwater engineering structures. On the other hand, the natural manifestations of hydrocarbons are permanent sources of pollution, which should be taken into account when assessing the ecological state of the aquatic areas and when studying the synoptic and climatic changes in the ocean.

The main study area is the eastern part of the Black Sea in the region of the continental slope near the coast of Georgia. Characteristic oil-containing slicks can be frequently seen in sea surface satellite images taken over the Black Sea south-eastern continental slope. The geographical distribution of these slicks is characterized by their persistent locations that correlate with geographical locations of natural hydrocarbon seeps from the sea bottom in this region.

The basic data is high resolution radar imagery obtained by synthetic aperture radars onboard Envisat satellite (till the spring of 2012) and onboard Sentinel-1 satellite (starting from October, 2014). Data in visual and IR bands taken by Envisat MERIS, Terra/Aqua MODIS, by scanning radiometers of Landsat-5, 7, 8 satellites and high resolution optical imagery taken by Sentinel 2a MSI nearly simultaneously with the SAR images is used.

A combined analysis of various satellite data was performed. This multi-sensor approach to the satellite remote sensing survey contributes to a more comprehensive interpretation of the data and helps in developing a better understanding of the sea surface film pollution pattern.

The influence of surface winds and currents on transport, spreading, evolution, and persistence of oil slicks was determined as well as their importance on the trajectory and fate of the released oil. The maps of sea surface oil pollution caused by natural hydrocarbons showings from the sea bottom in the south-eastern of the Black Sea are created. The quantitative assessment of inter-annual, seasonal and spatial variability of natural and oil pollution of the Black is performed.

The work was supported by the Russian Science Foundation under the project # 14-17-00555.

10422-47, Session PS

Longtime variation of phytoplankton in the South China Sea from the perspective of carbon fixation

Teng Li, State Key Lab. of Satellite Ocean Environment Dynamics (China) and State Key Laboratory of Satellite Ocean Environment Dynamics,Second Institute of Oceanography, SOA (China); Yan Bai, Xiaoyan Chen, State Key Laboratory of Satellite Ocean Environment Dynamics,Second Institute of Oceanography, SOA (China); Qiankun Zhu, Fang Gong, Difeng Wang, The Second Institute of Oceanography, SOA (China)

The ocean is a huge carbon pool in the earth, and about half of the anthropogenic emissions of carbon dioxide is absorbed by the ocean each year. By converting inorganic carbon into organic carbon, the photosynthesis process of phytoplankton affords an important way for carbon sequestration in the ocean. It has been reported that marine phytoplankton had declined substantially in the ocean over the past century and phytoplankton concentration in surface waters were estimated to have decreased by about 40% since 1950 possibly in response to ocean warming. Results of majority published researches also indicate that phytoplankton biomass or marine primary production will continue decline over the next century. Furthermore, since phytoplankton come in many shapes and sizes and species, the phytoplankton community structure also changed in the context of climate change. In addition, among the carbon sequestration in the ocean, margin seas may account for about >40% of the whole ocean. The South China Sea (SCS) is one of the largest margin sea and is notable for its shallow mixed layer (<50 m), and the biological activity has strong effected by the water upwelling, the monsoon and the rivers around SCS. Despite these complexities in water exchange, the SCS is an ideal natural laboratory to study the relationship between climate change variability and marine ecosystem response. Satellite remote sensing chlorophyll a concentration, number concentration of pico, nano and micro particles and marine primary production were collected during 1998-2011 to study the long time variation of the marine ecosystem structure in the northern SCS (NSCS). First, the spatial and seasonal distribution of the three parameters mentioned above were studied using climatological monthly mean data (Jan, Apr, Jul and Oct represent winter, spring, summer and autumn respectively). Generally, chlorophyll a concentration and primary production showed the same seasonal trend with the peak values occurred in winter, as well as the proportion of large particle size diameter phytoplankton with diameter between 20 and 50um, namely the micro-phytoplankton. The elevated values were concentrated in the coastal area and areas around islands where persistent nutrient inputs were found and lowest data located in the basin ocean as expected. High values can also be found in the west regions of the Luzon Strait where the upwelling current happened. Second, the longtime variation of the three parameters was analyzed to research the variation of phytoplankton combined with climate change in NSCS. Last, the change rate and time of the three parameter were compared to discuss the adaptive mechanisms of phytoplankton.

10422-49, Session PS

Retrieval of total suspended particulate matter in highly turbid the Hangzhou Bay waters based on geostationary ocean color imager

Jia Liu, Jiahang Liu, Xi'an Institute of Optics and Precision Mechanics, CAS (China); Xianqiang He, The Second Institute of Oceanography, SOA (China); Tieqiao Chen, Xi'an Institute of Optics and Precision Mechanics, CAS (China); Feng Zhu, Yihao Wang, Xi'an Institute of Optics and Precision Mechanics, CAS (China)

Hangzhou Bay waters are often characterized by extremely high total suspended particulate matter (TSM) concentration due to terrestrial inputs, bottom sediment resuspension and human activities. The spatial and temporal variability of TSM directly contributes to the transport of carbon, nutrients, pollutants, and other materials. Therefore, it is essential to maintain and monitor sedimentary environment in coastal waters. Traditional field sampling methods limit observation capability for insufficient spatial and temporal resolution. However, the in-orbit operation of the world's first geostationary satellite ocean color sensor, GOCI, thoroughly changes the situation that it's difficult to synoptically monitor high diurnal dynamics of TSM with hourly observations of covered area. Taking advantage of GOCI high spatiotemporal resolution, we generated TSM maps from GOCI Level-1B data after atmospheric correction based on six TSM empirical algorithms. Validation of GOCI-retrieved normalized water-leaving radiances and TSM concentration was presented in comparison with matched-up in-situ measurements. The mean absolute percentage difference of six TSM regional algorithms was 24.52%, 163.93%, 195.50%, 70.50%, 121.02%, 82.72%, respectively. In addition, the discrepancy reasons were presented, taking more factors such as diversified satellite data, various study area, and different research season into consideration. It's effective and indispensable to monitor and catch diurnal dynamics of TSM in Hangzhou Bay coastal waters, with hourly GOCI observations data and appropriate inversion algorithm.

10422-50, Session PS

Satellite remote sensing of the aquatic pCO2 in the basin of the South China Sea

Hangyu Lu, School of Geography and Marine Sciences, Nanjing University (China); Yan Bai, Xiaoyan Chen, Fang Gong, Qiankun Zhu, Difeng Wang, The Second Institute of Oceanography, SOA (China)

The South China Sea (SCS) is one of the largest marginal seas in the world, and the air-sea CO2 flux in the SCS may contribute significantly to the global air-sea CO2 flux. In the past decade, many researches on the aquatic pCO2 and air-sea CO2 flux mainly in the north SCS were carried out based on the underway measurement of the pCO2, and the results revealed that the SCS is a source of the CO2 as a whole in the annual scale. However, the air-sea CO2 flux is high spatial variability in SCS, for example, the north shelf of the SCS is a CO2 sink while the basin is a source. To monitor the spatial and temporal variations of the air-sea CO2 flux in the SCS, few satellite remote sensing algorithms have been developed to estimate the aquatic pCO2 in the north SCS. However, these algorithms are all the empirical models which depend on the training dataset from the in situ measurement. In this study, we apply the semi-analytical algorithm MeSAA to retrieve the aquatic pCO2 in the SCS basin. The MeSAA algorithm was proposed by the Bai et al. (2016) and was evidenced to be widely applicable to the different marginal seas including the East China Sea and Bering Sea. Based on the underway measured aquatic pCO2 and water temperature, we found that the variation of the pCO2 in the SCS basin is mainly controlled by the temperature. In addition, the increase of the atmosphere pCO2 can also contribute the systematical increase of the aquatic pCO2. Therefore, we established a semi-analytical algorithm for the aquatic PCO2 retrieval in the SCS basin, which considers the thermodynamic effect and air-sea CO2 fluxes. The results showed that the thermodynamic effect in the SCS basin was consistent with the theoretical result with the aquatic pCO2 increasing 4.23% for the 1°C rising of the water temperature. Moreover, the satellite-retrieved aquatic pCO2 match well with the in situ pCO2. Based on the established algorithm, the monthly time-series of the aquatic pCO2 in the SCS basins from 2000 to 2016 were generated from the MODIS datasets from both the Terra and Aqua satellite, and the long-term trends of the aquatic pCO2 in the different parts of the SCS basin were analyzed.

10422-51, Session PS

Measurement errors associated with backscattering measurement in turbid and productive waters

Sayoob Vadakke Chanat, Indian Institute of Technology Madras (India); Palanisamy Shanmugam, Indian Institute of Technology Madras (India)

Backscattering is one of the most important Inherent optical properties that determines the reflected signals received by the remote sensing satellite. The in situ backscattering measurement methods are often impacted by uncertainties due to the influence/inference of absorption by water, phytoplankton and other particulates in water. The backscattering measurement uncertainty can be significant in highly absorbing coastal and inland waters. This work presents a novel method to minimize the absorption introduced errors in the backscattering measurement. This method makes significant improvements over the existing correction procedures. Data generated using Monte Carlo radiative transfer method were used to derive the model parameterizations for the new method and in-situ data collected from different water types were used to assess the performance of the new method.

10422-52, Session PS

On the relationship between sea level anomalies and upper ocean parameters in the Indian Ocean

Venugopal Thandlam, Indian National Ctr. for Ocean Information Services (India)

In the present study, we investigated the relationship between Sea Level Anomalies (SLA) and Upper Ocean parameters in the Indian Ocean spanning 30oS-30oN and 30oE-110oE during the period 1993-2016. The study involves the variability of SLA obtained from Aviso satellite Altimetry data in different spatial and temporal scales in relation with computed Ocean Heat Content (OHC), Dynamic Height (DH) with respect to 300 mts and Thermocline Depth (TD) with respect to 20oC isotherm (D20) obtained from Hadley objective analyzed data (EN 4.2.0) during the study period. The SLA has showcased least coefficient of correlation (R) climatically computed OHC, DH, and TD over central equatorial Indian Ocean, central Bay of Bengal(BoB), western and northern Arabian Sea (AS). Further, the ARGO profile data in the central equatorial Indian Ocean spanning 10oS-5oN also emphasized these results. The TD has highest R with SLA in the south with value 0.95 which further reduced to 0.50 over the equator and increased to 0.82 in the north. The OHC and DH also showed similar results with R values 0.96,0.61,0.93 and 0.96,0.74,0.90 respectively. These results need to be further explored by studying the baroclinic and barotropic process over these regions.

10422-53, Session PS

Tidal strain of landfast sea ice around Campbell Glacier Tongue in East Antarctica analyzed by DDInSAR images

Hyangsun Han, Korea Polar Research Institute (Korea, Republic of); Hoonyol Lee, Kangwon National Univ. (Korea, Republic of)

Landfast sea ice is a type of sea ice that is attached to the coast. Accurate measurement of strain of landfast sea ice is very important because it plays an important role in the variabilities of polynya, marine ecosystem and logistics for research stations near the coast. In this study, we analyzed tidal strain of landfast sea ice near Campbell Glacier Tongue (CGT) in Terra Nova Bay (TNB), East Antarctica and its annual variation using COSMO-SkyMED one-day Interferometric Synthetic Aperture Radar (InSAR) pairs obtained from December 2010 to January 2012. As the landfast sea ice is attached to both the coast and CGT, the tidal strain caused by sea surface tilt and the glacial strain due to the flow of CGT would be mixed in the one-day InSAR signals. The glacial strain caused by the steady flow of CGT (~67 cm/day) is similar to the tidal strain by tide variation in TNB (~60 cm). Therefore, it is very difficult to extract the tidal strain from the one-day InSAR images. If the glacial strain of the landfast sea ice is steady over time, the tidal strain can be observed by Double-Differential InSAR (DDInSAR) technique that differentiates two InSAR images. We generated DDInSAR images from the one-day InSAR images and extracted the vertical tidal displacement of the landfast sea ice around CGT. The DDInSAR-derived tidal displacement was compared with tide variation during the observation predicted by the inverse barometric effect (IBE)-corrected Ross_Inv tide model. For the landfast sea ice near the coast, isolated from CGT by cracks and leads, the linear regression between the DDInSAR-derived tidal displacements and tide variations predicted by the tide model showed high R-squared value. This represents that the tidal strain of the landfast sea ice near the coast is steady throughout the year because it is not affected by the glacial stress. Meanwhile, the R-squared value of the linear regression between the DDInSAR-derived tidal displacements and tide variation predicted by the tide model of the landfast sea ice attached to CGT was less than 0.5, which might be caused by the variation of glacial strain resulting from the change of ice thickness.

10422-54, Session PS

Optical multispectral monitoring of ocean surface

Victor I. Titov, Institute of Applied Physics of the Russian Academy of Sciences (Russian Federation)

The principles of optical multispectral remote sensing of ocean surface from UV to IR are discussed. The mechanism of sea wave visibility taking into account sky radiance and own radiance of sea surface for various angles of incidence is investigated. The deposit of subsurface backscattered radiance to the radiance of sea surface is calculated also. The measured and modeled sky radiance distribution was used in the calculations.

The principles for retrieving of sea roughness characteristics, pollutions of sea surface and near surface winds by its manifestations on waved surface under grazing angles based on the comparison of measured and modeled surface radiance is discussed.

The priciples are verified in natural conditions using developed set of multispectral optical devices. The experiments were conducted simultaneously with the optical set and the buoy equipped with wave-recording gauge and wind sensors placed on various height above sea level.

10422-55, Session PS

Vortex structures in the southeastern part of the Baltic Sea: results of oceanographic experiments and satellite observations

Evgeny V. Krayushkin, Space Research Institute of RAS (Russian Federation); Olga Y. Lavrova, Ksenia R. Nazirova, Space Research Institute (Russian Federation)

In 2014-2016, in summer months oceanographic experiments were held by the Space Research Institute in the southeastern part of the Baltic Sea along the coastline of Kaliningrad Region. The main aim was to provide comprehensive in situ oceanographic data to verify remote sensing data.

During the experiments, ADCP surveys were conducted to

measure current profiles from surface to bottom. In 2014, we managed to detect and describe a complex dynamic vortex structure near Cape Taran. An eddy propagated to the depth of 20 m and had a linear scale of ~ 25 km. This vortex structure was identified using Radarsat-2 images and optical data, obtained by OLI Landsat-8, ETM+ Landsat-7, Modis Terra/Aqua and confirmed by ADCP data. Results of ADCP surveys showed a great amount of different dynamic patterns in the coastal zone of southeastern Baltic Sea.

Along with Euler methods, Lagrangian drifters launched simultaneously with ADCP surveys were also used in the experiments. In total, 4 drifters with GSM remote data transmission link were launched near Cape Taran. The drifters' trajectories revealed a complex picture of coastal dynamics in the near-shore area that could add information to ADCP results. The drifters' trajectories differed completely from one year to another influenced by both complex wind situations in the region and propagation of mesoscale eddies.

During the experiments, CTD-surveys were also conducted along the ADCP tracks to determine the thermohaline structure in the studied area as well as specific distribution of turbidity with the use of optical backscatter sensor. Turbidity is a core parameter for remote sensing data verification as it can be clearly identified from optical images.

A separate part of the research was devoted to the Vistula Lagoon outflow to the Baltic Sea. The experiment showed that Vistula Lagoon waters propagated 5 m deep near the shore and their influence could be tracked as far as Cape Taran on the east and Hel Peninsula on the west.

The work was supported by Russian Science Foundation Grant #14-17-00555.

10422-56, Session PS

The study of long-term sea level variability in the South China Sea based on satellite data

Ying Xu, National Satellite Ocean Application Service (China)

On the basis of the satellite maps of sea level anomaly (MSLA) data and in-situ tidal gauge sea level data, correlation analysis and Empirical Mode Decomposition (EMD) are employed to investigate the applicability of MSLA data, sea level correlation, long-term sea level variability (SLV) trend, sea level rise (SLR) rate and its geographic distribution in the South China Sea (SCS). The findings show that on monthly scale, for Dongfang Station, Haikou Station, Shanwei Station and Zhapo Station, the minimum correlation coefficient between the closest MSLA grid point and tidal station is 0.61. This suggests that the satellite altimeter MSLA data are effective to observe the coastal SLV in the SCS. On monthly scale, sea level variability of Dongfang Station, Haikou station, Shanwei station and Zhapo station is highly correlated with coastal region and uncorrelated/negative correlated with the deep basin portion of the South China Sea and the Luzon Strait region. The consistent of monthly averaged sea level variability among south, west, north part of the SCS is probably due to South China Sea Monsoon Jet and coastal process. On seasonal scale, the above four stations are uncorrelated/negative correlated with the Pacific in summer (from May to September), and highly correlated with the Pacific in winter. This finding is consistent with former research which shows Kuroshio intrudes (Pacific variabililty) the SCS in winter rather than summer. On monthly, seasonal and yearly scale, sea level variability of the internal region of deep basin are negative correlated with coastal region. The empirical mode decomposition (EMD) method is still applied to derive the trend on each MSLA grid point in the entire SCS. According to the 2-D distribution of the trend and rising rate, we found sea level variability is not uniform in the ECS but without distinct flunctuant signature. For the entire SCS, the average sea level rose 90.8 mm between 1993 and 2010, with a rising rate of (5.0 ± 0.4) mm?a-1 which is much faster than global average.The sea level rise rate from Southern Luzon Strait through Huangyan Seamount area to the Xisha Islands area is higher than in other area of the SCS.

10422-57, Session PS

The influence of tide on sea surface temperature in the marginal sea of northwest Pacific Ocean

Shih-Jen Huang, Yun-Chan Tsai, Yao-Tsai Lo, Nan-Jung Kuo, National Taiwan Ocean Univ. (Taiwan)

In this study, the tide gauge data are provided by the website of the University of Hawaii Sea Level Center (http://uhslc.soest.hawaii.edu/datainfo/) and the data of daily sea surface temperature come from the Moderate Resolution Imaging Spectroradiometer (MODIS) product. The dates of spring tide and neap tide are decided by the tide observed data. The daily sea surface temperature of MODIS is used to analyze the influence of tide on sea surface temperature in the marginal sea of Northwestern Pacific. This study also analyzes the sea surface temperature of the locations, including the coastal region, continental region, and open ocean region.

In the marginal sea of Northwest Pacific, the climatology sea surface temperature is found lower in the northwestern region and higher in the southeastern region. In the coastal region, the average sea surface temperature (SST) at spring tide is about 0.36? higher than it at neap tide during winter, but is 0.22?, 0.05?, and 0.23? lower than it at the neap tide during the spring, summer, and autumn, respectively. During winter, the spring tide SST in the southern continental region of the Changjiang estuary is 0.14? lower than it at neap tide. In the eastern continental region of the Changjiang estuary, the SST at spring tide is 0.26? higher than it at neap tide. During spring, the SST at spring tide is about 0.24? lower than it at neap tide both in the southern and eastern continental regions of the Changjiang estuary. The SST at spring tide is 0.41? higher than it at the neap tide both in the southern and eastern continental regions of the Changjiang estuary during the summer season. During autumn, the SST at spring tide is 0.26? lower than it at neap tide both in the southern and eastern continental regions of the Changjiang estuary.

In the rendezvous region of East China Sea and Yellow Sea, during the winter and summer seasons, the SST at spring tide is 0.77? and 0.13?, respectively higher than it at neap tide. Constrictively, in spring and autumn the SST at spring tide of this rendezvous region is 0.44? and 0.01? respectively lower than it at neap tide. In the open ocean region the SST at spring tide is 0.09? higher than it at neap tide during winter, but the SST at spring tide is about 0.16? lower than it at neap tide in the other seasons. Obviously, the convection in the open ocean region is deeper at spring tide than it at neap tide. Since the SST of the deeper water is higher than the surface water during winter, the SST at spring tide becomes higher than it at neap tide. In conclusion, not only the river discharge and topography, but also tides could influence the SST, especially in the open ocean region.

10422-58, Session PS

On possibility of determining wind waves spectra by Snell's window images

Alexandr A. Molkov, Irina A. Sergievskaya, Ivan A. Kapustin, Institute of Applied Physics of the Russian Academy of Sciences (Russian Federation)

The possibility of determining wind waves characteristics by optical images of the sea surface is widely used in scientific oceanological experiments and in solution of remote monitoring problem of natural basins. In this case images can be registered both from air and under water and if the first direction has rather good development then the second direction is poorly developed. The underwater image of a rough surface besides a solar path contains one more informative element - Snell's window. Under conditions of flat surface of some water reservoir its image represents a light circle against the dark background, the angular radius of the borderline of which coincides with the refraction angle

of horizontally located light incident on surface, i. e. with the angle of total internal reflection. The area inside of the circle is formed by the sky diffused light, and outside of it – by the light reversely diffused from the water column, the radiance of which is sufficiently less than the radiance of the light penetrating into the water. When roughness occurs borderlines of the circle are distorted, at that the distortion is more when wave formation is stronger. At that it was experimentally proved that in the image of Snell's window both capillary waves are shown with the length starting from several millimetres and energy bearing waves with the lengths starting from several metres.

On the first approaches of restoration of wind waves frequency spectra by images of Snell's window has been reported at the previous conference. Results of more detailed analysis of image structure, method of restoration not only frequency but also wind waves spatial spectra and results of approbation of these algorithms on data of a natural experiment are represented in this work. The results of testing of the offered method are provided based on natural images registered in expedition on the Black Sea under conditions of different wind and wave environment for clear surface and surface covered by surfactant films. Their verification was carried out by way of comparison with the results of processing the signal from wave meter and scatterometer of K-band working simultaneously with underwater optical system.

The work was supported by the Russian Foundation for Basic Research (Grants no. 16-05-01092, 16-05-00990).

10422-59, Session PS

Satellite observation of the recent changes of chlorophyll in the South China Sea and Bay of Bengal

Shujie Yu, Xiaoyan Chen, Yan Bai, Teng Li, Tianyu Wang, Fang Gong, Qiankun Zhu, The Second Institute of Oceanography, SOA (China)

The South China Sea (SCS) is an almost close marginal sea and is part of the northwest Pacific Ocean. The Bay of Bengal (BOB) is a semi-close marginal sea in the northeast part of the Indian Ocean. Both of them are tropical marginal seas, and share a lot of similar hydrology properties, such as high surface temperature, stable thermocline, deep euphotic zone, etc. Moreover, they are all greatly affected by East Asian monsoon and typhoon. However, there are also several significant differences between them. The current circulation structures in the SCS are more complex with significant season variations. A large amount of fresh water through river inputs is one of the remarkable hydrology characteristic in the BOB. The major rivers include the Ganges, the Brahmaputra, and Irrawaddy River. In addition, the BOB has a large volume of precipitation. Therefore, it is naturally interesting to investigate the different response of the marine ecological properties with the climate changes. In this paper, the MODIS/Aqua monthly averaged record during 2003 and 2014 are used to investigate the spatial and temporal variations of Chlorophyll concentration (Chl-a), Net Primary Production(NPP), Secchi Disk Depth(SDD), Sea Surface Temperature(SST), and Photosynthetically Active Production(PAR)in the SCS and BOB. Climatological data reveal that the SCS has the higher Chl-a, NPP, and water transparency and the BOB has the higher PAR and SST. The South China Sea shows the more significant annual variations of all these parameters. But the differences are not so significant. Linear regression analysis denotes that Chl-a increased in the South China Sea and decreased in the Bay of Bengal. The trends of NPP were similar with Chl-a. SST and SDD increased in both areas, while PAR was on the decline. The rise of SST and/or decline of PAR could lead to the decrease of Chl-a and further result in the increase of SDD, vice versa.

10422-60, Session PS

Damping of surface waves due to oil emulsions in application to ocean remote sensing

Irina A. Sergievskaya, Stanislav A. Ermakov, Tatiana N. Lazareva, Institute of Applied Physics of the Russian Academy of Sciences (Russian Federation)

Detection and identification of oil films with remote sensing methods is a very urgent problem. Applications of different radar and optical methods for detection of biogenic and anthropogenic pollutions based on the effect of strong damping of short wind waves by surface films have been extensively studied last decades. The main disadvantage of these studies, however, was poor knowledge about physical characteristics of films responsible for wave damping effect. Oil pollution can be presented on the sea surface not only in the form of films of a pure oil substance, but also in the form of films of oil and oil products emulsion. According to different authors, oil emulsions on the sea surface are 30-70% of all pollutants. The properties of the emulsion are determined by the conditions of emulsion formation, resistance to destruction, the percentage of water in the oil, by properties of the oil itself, the temperature etc. and are not properly studied. Some of these properties impact on the depression of small-scale waves, for example, viscosity. So these properties determine the possibility of detecting oil pollution on the sea surface and estimating of the pollution characteristics.

In this paper some results of laboratory studies of damping of gravity-capillary waves on the water surface covered by oil emulsion are presented and compared with our previous analysis of characteristics of crude oil and oil derivatives films. The emulsion was manufactured in a dispersant with cooling. A laboratory method for determination of film characteristics is based on measuring the damping coefficient and wavelength of parametrically generated standing waves. Investigations of oil derivatives films were carried out in a wide range of film thicknesses (from some hundredths of a millimetres to a few millimetres) and in a wide range of surface wave frequencies (from 7 to 27 Hz). The selected frequency range corresponds to the operating wavelengths of microwave, from C- to Ka-band radars typically used for the ocean remote sensing. The studied range of film thickness covers thicknesses of routine spills in the ocean.

The study of wave damping on the surface of the bulk oil emulsion at several wavelengths in the specified range is allowed us to eliminate the effect of a film on the surface. The dependence of the viscosity of the oil emulsion on the percentage of water in the emulsion was investigated. An effect of enhanced wave damping due to oil emulsion compared to ordinary oil film is demonstrated. The dependences of wave damping and wavelength on the emulsion layer thickness on the water at fixed wave frequencies demonstrate some significant differences from the crude oil, which was used to create the emulsion. The wave damping due to emulsion oil film was described in the frame of two layer models. Elasticity on the layers boundaries was estimated when tuning the film parameters to fit theory and to the experimental dependencies. Comparison between wave damping due to oil emulsion, crude oil and oil derivatives films have shown some capabilities of distinguishing of oil films from remote sensing measurements of short surface waves.

10422-61, Session PS

Utilization of Multi-channel Ocean LiDAR Data to Classify the Types of Waveform

Tiancheng Huang, Bangyi Tao, The Second Institute of Oceanography, SOA (China); Peng Chen, The Second Institute of Oceanography (China); Yan He, Shanjiang Hu, Shanghai Institute of Optics and Fine Mechanics (China); Gongbo Xu, The Second Surveying and Mapping Institute of Zhejiang Province (China); Jiayong Yu, Shandong Univ. of Science and Technology (China); Congcong Wang, Zhejiang Univ. (China)

Abstract Sea and land waveform classification is a preliminary problem of airborne LiDAR bathymetry. In this paper, a method is proposed, which is based on the features of multi-channel ocean LiDAR waveform data, such as 4 features of the 532 nm green channel(width of first echo waveform , area under normalized curve , skewness and kurtosis), and 2 features of the 1064 nm infrared channel (infrared-green intensity ratio , and width of response waveform). The validation results indicate that overall accuracy and kappa coefficient of our classification method are 99.03% and 0.9805, respectively. The accuracy of the sea and land waveform classification method is good enough for the pratical application , and this method has been applicable to airborne LiDAR bathymetry waveform data processing, which can be used as a basis for correcting the velocity of light in the water medium during the depth calculation procedure and tidal and wave correction.

10422-62, Session PS

Estimation of chlorophyll-a concentration in inland and marine waters using HICO, MODIS, Landsat OLI-8 and OCM-2 sensors

Varunan Theenathayalan, Indian Institute of Technology Madras (India)

Estimation of chlorophyll-a pigment is highly important in mapping the distribution of phytoplankton concentration, detecting and monitoring harmful blooms tracing various ecological changes in a wide range of oceanic and inland waters. The present study is focused on the development of a new algorithm suitable for both inland and marine waters, where chl-a ranges from 0.1 to 1000 mg m-3 and no single algorithm provides accurate estimates of chl-a. Unlike the two/three band ratio algorithms, the present algorithm takes into account different water types defined by different spectral ratios to comprehensively provide estimates of chl-a concentration in most natural waters. For productive and turbid inland waters characterized by a high level of dissolved and detrital matters, the band architecture chosen is not sensitive to these interferences. Results of the algorithm applied to in-situ data and different satellite data (e.g., HICO, OLI, OCM-2, and MODIS-Aqua) are further discussed and its validity in global waters is further discussed.

10423-1, Session 1

ESA Observation Missions *(Invited Paper)*

Jean-Loup Bézy, European Space Research and Technology Ctr. (Netherlands)

No Abstract Available

10423-2, Session 1

AEOLUS mission: the latest preparations before launch

Anders Elfving, Roland Meynart, A. Straume, European Space Research and Technology Ctr. (Netherlands)

The European Space Agency (ESA) is developing a direct detection Doppler Wind Lidar for measuring wind profiles from space. The pulsed UV Lidar instrument, ALADIN, will deliver horizontally projected single line-of-sight wind profiles from its molecular and particle channels. The development of the AEOLUS mission passed a major milestone with the integration of the full instrument and its functional and performance tests in 2016 and a 6-month life test of the spare UV laser transmitter. The satellite has been assembled and is subjected to a full programme of functional and environmental (vibration, acoustic, shock, EMC) tests, following thermal vacuum tests, including instrument performance in vacuum. The Qualification and Acceptance Review of the satellite is expected to be completed in October 2017.

10423-3, Session 1

Earth cloud, aerosol and radiation explorer optical payload development status

Arnaud Hélière, Kotska Wallace, Joao Pereira do Carmo, Alain Lefebvre, European Space Research and Technology Ctr. (Netherlands)

The European Space Agency (ESA) and the Japan Aerospace Exploration Agency (JAXA) are co-operating to develop as part of ESA's Living Planet Programme, the third Earth Explorer Core Mission, EarthCARE, with the fundamental objective of improving the understanding of the processes involving clouds, aerosols and radiation in the Earth's atmosphere.

EarthCARE payload consists of two active and two passive instruments: an ATmospheric LIDar (ATLID), a Cloud Profiling Radar (CPR), a Multi-Spectral Imager (MSI) and a Broad-Band Radiometer (BBR). The four instruments data are processed individually and in a synergetic manner to produce a large range of products, which include vertical profiles of aerosols, liquid water and ice, observations of cloud distribution and vertical motion within clouds, and will allow the retrieval of profiles of atmospheric radiative heating and cooling.

MSI is a seven-band, push-broom scanner used to provide images at 500 m ground sampling distance over a 150 km wide swath, which is offset from nadir pointing and distributed -35 to +115 km in order to minimise sun-glint. The imagery will serve as context information for the quasi-simultaneous along track measurements of the CPR and ATLID, and also provide additional data on cloud types, texture, cloud top temperature and other micro-physical parameters such as cloud phase.

BBR provides an estimate of the outgoing solar reflected and earth emitted thermal fluxes for a 10 km scene. The Optics Unit will measure the top of atmosphere radiance, at the same location, in two wavebands, using three quasi-simultaneous along track views that point nadir, forward and aft of nadir.

BBR performs measurements in a Total Wave and a Short Wave band and provides top of atmosphere radiance data. Long Wave data is estimated by subtraction of SW from TW channel measurements. Measured radiance is filtered by the instrument spectral response. After un-filtering, using correlation with MSI data for improved performance, an estimate of the reflected solar and Earth emitted radiances will be obtained.

Operating in the UV range at 355 nm, ATLID measures atmospheric profiles, in a direction close to the nadir, with a vertical resolution of about 100 m from ground to an altitude of 20 km and of 500 m from 20 km to 40 km altitude. The instrument transmitter emits short laser pulses with a repetition rate of 51 Hz along the horizontal track of the satellite so that several shots can be locally averaged to improve the signal to noise ratio. The ATLID receiver collects the backscattered photons with a 60 cm diameter telescope. Thanks to a high spectral resolution filtering, the lidar is able to separate the relative contribution of aerosol and molecular scattering, which gives access to aerosol optical depth. Co-polarised and cross-polarised components of the Mie scattering contribution are also separated and measured on dedicated channels.

This paper will provide an updated status of the development of the European payload. Tests results of the Multi-Spectral Imager and the Broad-Band Radiometer calibrations campaign will be presented, as well as progress into the Atmospheric Lidar instrument integration and testing.

10423-4, Session 1

Instrument pre-development activities for FLEX

Jean-Loup Bézy, Michael Francois, European Space Research and Technology Ctr. (Netherlands); Enrico Fossati, Lucia Pettinato, Annalisa Capanni, Peter Coppo, Alessio Taiti, Demetrio Labate, Leonardo (Italy); Roland Meynart, European Space Research and Technology Ctr. (Netherlands); Peter Triebel, Zeiss (Germany)

The FLuorescence Imaging Spectrometer (FLORIS) is the payload of the FLuorescence Explorer Mission (FLEX) of the European Space Agency.

The mission objective is to perform quantitative measurements of the solar induced vegetation fluorescence to monitor photosynthetic activity of vegetation.

The instrument operate in a push-broom configuration and is composed of two spectrometers serving the low and high spectral resolution demands of the mission. The spectrometers will measure in a spectral range between 500 and 780 nm and provide thereby high spectral resolution of 0.3 nm in particular at the Oxygen-A and -B bands (FLORIS HR spectrometer), and 2 nm spectral resolution (FLORIS LR spectrometer) to measure the photochemical reflection features between 500 and 600 nm, the Chlorophyll absorption region between 600 and 677 nm, and the red-edge in the region from 697 to 755 nm. FLEX will fly in formation with Sentinel-3 in order to further enhance the spectral coverage from measurements made by the Sentinel-3 instruments OLCI and SLSTR, particularly for cloud screening, proper characterization of the atmospheric state and determination of the surface temperature.

The instrument concept is based on a common fore optics and two modified Offner spectrometers with reflective concave gratings both for the high resolution (HR) and low resolution (LR) spectrometers. In-field spectral separation between HR and LR spectrometers is provided by a double slit assembly that includes two fold mirrors.

In the frame of the instrument pre-development Leonardo Company (I) has built and tested in cleanroom class ISO 8 an elegant breadboard of the instrument consisting of the telescope fore optics and the HR spectrometer.

The tests have been successful and provided already important indications for the procurement and tests of the instrument flight. All the tests will be repeated in the more clean class ISO 5 before summer 2017 to have a better assessment in particular of the straylight performances.

The development of the LR spectrometer is in charge of OHB System AG (D) and is currently in the manufacturing phase. The LR will be integrated in the breadboard and the complete breadboard will be tested again.

The main objectives of the pre-development activity are:

1. anticipate the development of the instrument and provide early risk retirement of critical components

2. evaluate the system performances such as imaging quality parameters, straylight, ghost, polarization sensitivity and environmental influences

3. verify the adequacy of critical tests such as spectral characterisation and straylight

4. define and optimise instrument alignment procedures

5. develop an elegant breadboard model that can be used as a "workbench tool" in the frame of the flight instrument procurement. (e.g. to perform early integration and test at system level of critical sub systems)

6. develop a complete OGSE that might be re-used for the flight instrument characterisation and calibration

The talk will provide a brief overview of the FLEX mission. It will also cover the design and development of the breadboard with emphasis on the results obtained during the tests and the lessons learned.

10423-5, Session 2

Image quality validation of Sentinel 2 Level-1 products: performance status at the beginning of the constellation routine phase

Benjamin Francesconi, Marion Neveu-VanMalle, Thales Alenia Space (France); Bahjat Alhammoud, ARGANS Ltd. (United Kingdom); Catherine Bouzinac, CS Systèmes d'information (France); Sébastien Clerc, ARGANS Ltd. (United Kingdom); Ferran Gascon, ESRIN (Italy)

Sentinel-2 is an Earth Observation mission developed by the European Space Agency (ESA) in the frame of the Copernicus program of the European Commission. The mission is based on a constellation of 2-satellites: Sentinel-2A launched in June 2015 and Sentinel-2B launched in March 2017. It offers an unprecedented combination of systematic global coverage of land and coastal areas, a high revisit of five days at the equator and 2 days at mid-latitudes under the same viewing conditions, high spatial resolution, and a wide field of view for multispectral observations from 13 bands in the visible, near infrared and short wave infrared range of the electromagnetic spectrum.

The mission performances are routinely and closely monitored by the S2 Mission Performance Centre (MPC), including a consortium of Expert Support Laboratories (ESL).

This publication focuses on the Sentinel-2 Level-1 product quality validation activities performed by the MPC. It presents an up-to-date status of the Level-1 mission performances at the beginning of constellation's routine phase and provides details on the methods applied.

Examples of Level-1 performance validations routinely performed cover:

* Level-1 Radiometric Validation:

- Equalization Validation, using on-board sun-diffuser

- Absolute Radiometry Vicarious Validation, using techniques based on: Rayleigh diffusion, Pseudo-invariant Calibration sites, In-siu measurements

- Absolute Radiometry Cross-Mission Validation, based on Pseudo-invariant Calibration sites

- Multi-temporal Relative Radiometry Vicarious Validation, based on Pseudo-invariant Calibration sites

- Inter-band Relative Radiometric Uncertainty Validation

- SNR Validation, based on on-board diffuser and dark measurements

- Pixel Response Validation

- MTF Validation, based on ground edge targets

* Level-1 Geometric Validation, all based on correlation techniques:

- Geolocation Uncertainty Validation

- Multi-spectral Registration Uncertainty Validation

- Uncertainty Validation

- Multi-temporal Registration Uncertainty Validation

Overall, the Sentinel-2 mission is proving very successful in terms of product quality thereby fulfilling the promises of the Copernicus program.

The ESLs in charge of the Level-1 validation activities are:

- Thales Alenia Space, Cannes, France: ESL Level-1 Products Validation Leader

- Argans, Plymouth, UK: ESL Level-1 Products Radiometry Validation

- ONERA, Toulouse, France: ESL Level-1 Products Radiometry Validation

- CSSI, Toulouse, France: ESL Level-1 Products Radiometry & Geometry Validation (also Prime Contractor, ESL Coordinator)

The other entities involved in MPC/CC activities are:

- Argans, Plymouth, France: Technical Manager, Operation Manager, Operator

- Elecnor Deimos, Madrid, Spain: Operator

10423-6, Session 2

The Copernicus Sentinel-4 mission: a geostationary imaging UVN spectrometer for air quality monitoring

Gregory Bazalgette Courrèges-Lacoste, Giorgio Bagnasco, M. Sallusti, G. Bulsa, Ben Veihelmann, European Space Research and Technology Ctr. (Netherlands); Stefan Riedl, David Smith, Ralf Maurer, Airbus Defence and Space (Germany)

Sentinel-4 is an imaging UVN (UV-VIS-NIR) spectrometer, developed by Airbus DS under ESA contract in the frame of the joint EU/ESA COPERNICUS program. The mission objective is the operational monitoring of trace gas concentrations for atmospheric chemistry and climate applications. Sentinel-4 will provide accurate measurements of key atmospheric constituents such as ozone, nitrogen dioxide, sulphur dioxide, methane and aerosols properties.

In the line of UVN spectrometer with space heritage (SCIAMACHY, OMI, GOME & GOME-2) and under development (TROPOMI and Sentinel-5), Sentinel-4 is unique as being the first geostationary UVN mission, together with very similar geostationary Air Quality Monitoring missions over other continent which are being developed in parallel by NASA (TEMPO), JAXA (GMAP-SIA) and KARI (GEMS). The Sentinel-4 space segment will embark on EUMETSAT's Meteosat Third Generation Sounder satellite (MTG-S), sharing the platform with the MTG IRS instrument. For the period of time between 2021 and 2034 Sentinel-4 will provide coverage of Europe and adjacent regions with a repeat cycle of 60 minutes and a spatial resolution of 8x8 km (at reference point in Europe). This spatial coverage is achieved by push-broom continuous E/W scanning of a slit with 4° N/S field-of-view over a E/W field-of-regard of about 11°.

The Sentinel-4 spectrometer will acquire continuous spectra of Earth radiance covering the UV (305-400 nm), VIS (400-500 nm) and NIR (750-775 nm) bands, with a spectral resolution

of 0.5 nm in the UV-VIS and 0.12 nm in the NIR. Additionally, Sentinel-4 will provide a sun irradiance product with an update frequency of 24 hours, which serves for calibration purpose and for determination of Earth reflectance.

Further key design-driving performance include: low sensitivity to polarization (1%); low level of spectral features (0.05% in the UV-VIOS); low straylight; highly challenging geometric and spectral accuracies (scan accuracies, spatial co-registration, spectral stability, etc.).

Regarding its status of development Sentinel-4 is currently in its CDR (end 1016) with a planned delivery of the first flight model in 2019. Sentinel-4 is currently in its unit level –CDR and –FM manufacturing phase. Results are available from unit level breadboards and engineering models which have been built.

10423-7, Session 2

Sentinel-5 Precursor: pre-launch calibration and commissioning phase preparation

Herbert Nett, S. Ekholm, European Space Research and Technology Ctr. (Netherlands); Quintus Kleipool, Antje Ludewig, Koninklijk Nederlands Meteorologisch Instituut (Netherlands); Daniel Ten Bloemendal, Airbus Defence and Space (United Kingdom); Jos Dingjan, Airbus Defence and Space (Netherlands)

Sentinel-5 Precursor (S-5P) will be the first of a series of atmospheric missions to be launched within the European Copernicus Programme. With a planned launch in second half 2017 and a nominal lifetime of 7 years, S-5P will provide global observations of various key species including tropospheric/ stratospheric ozone, NO2, SO2, CO, CH4, CH2O as well as cloud and aerosol distributions. S-5P's single payload instrument TROPOMI (TROPOspheric Monitoring Instrument) covers spectral ranges located in the ultra-violet (UV), UV-visible (UVIS) and near-infrared (NIR), and in the short-wave infrared (SWIR), respectively.

The instrument passed an extensive ground calibration campaign in the period December 2014 - May 2015 during which the radiometric, spectral and spatial sampling performance were characterized and calibration parameters required in routine Level 0 to 1B processing tasks were collected. Later in-depth analyses of the acquired measurement data revealed a sensitivity of the instrument to out-of-band (OOB) radiance, specifically in the NIR band (wavelength range 661 – 786 nm). This band is of key importance for retrievals of aerosol parameters, which in turn are needed for signal path corrections in CH4 processing, the species with the most demanding accuracy requirements. It was concluded that a correction of OOB straylight could be implemented in the Level 1B algorithm, and that corresponding calibration key data could be collected in a second, dedicated calibration campaign.

The original main calibration campaign was conducted at TROPOMI level under environmental conditions (cooled instrument, vacuum operation). The second campaign was performed at satellite level, in a clean room under ambient conditions. Therefore, a new dedicated setup had to be designed to feed the collimated signal of a tunable, monochromatic source to the instrument's telescope input, with the instrument remaining integrated on the satellite.

The presentation will provide an outline of the S5P mission, with focus on Phase E1 preparatory tasks. Results of the recent measurement campaign, aiming at characterizing the instrument's OOB straylight response, will be specifically addressed.

10423-8, Session 2

Sentinel-5 instrument: status of design, performance and development

Tobias Gühne, Corneli Keim, Peter Bartsch, Stefan Weiss, Markus Melf, Wolfgang Seefelder, Airbus Defence and Space (Germany)

The Sentinel-5 instrument is currently under development by a consortium led by Airbus DS in the frame of the ESA Copernicus program. It is a CFI to the MetOp Second Generation, which will provide operational meteorological data for the coming decades.

Mission objective of the Sentinel-5 is to monitor the composition of the Earth atmosphere for Copernicus Atmosphere Services by taking measurements of trace gases and aerosols impacting air quality and climate with high resolution and daily global coverage.

Therefore the Sentinel-5 provides five dispersive spectrometers covering the UVN (270...500 nm), NIR (685 ...773 nm) and SWIR (1590...1675 & 2305...2385 nm) spectral ranges with resolutions ≤1nm. Spatially the Sentinel-5 provides a 108° instantaneous field of view with a resolution of 7 km at Nadir.

In addition the instrument design is driven by:

spatial co-registration bet ween the spectral channels (in the order of 0.1 – 0.3 sampling distances)

accurate knowledge of the spectral response function (in the order of 2%), in particular with respect to insensitivity to inhomogeneous illumination

high radiometric accuracy (3-6%), requiring low polarisation sensitivity, low level of spectral features, level and control of straylight, highly accurate on-ground and in-orbit calibration.

The development program is post PDR and the build-up of the industrial team is finalised. We report on the instrument architecture and design derived from these demanding requirements, the predicted instrument performance, and the status of the development program.

10423-52, Session 2

A multistatic SAR mission concept enhancing Sentinel-1 capability in surface current dynamics retrieval

Valentina Boccia, European Space Agency (Netherlands); Erik De Witte, Josep Roselló, Michel Tossaint, Craig Donlon, Klaus Scipal, European Space Agency (Netherlands); Geoff Burbidge, Airbus Defence and Space (United Kingdom); Harald Johnsen, Norut Tromsø (Norway)

Mesoscale and sub-mesoscale variability of surface currents play an essential role in ocean circulation dynamics, physical-biological coupling, redistribution of heat, salt, and bio-geo-chemical tracers, both in the open ocean and in the shelf/ closed seas. Moreover, interaction between the atmosphere and the ocean complicated circulation patterns determines much of the climate variability on time scales from several hours to decades. Understanding this variability is essential to detect and predict climate conditions and changing. Enhanced knowledge on ocean waters and their motion would contribute directly to improve the ability to model and predict the function and evolution of global ocean ecosystems and the ocean interaction in the Earth climate system which, in turn, would have a direct impact on furthering knowledge on societal issues related to climate change.

However, mesoscale to sub-mesoscale variability of surface currents in the open ocean and in the coastal regions is still not adequately resolved due to the fast decay of mesoscale structures. Indeed, the present array of surface drifters is not able to capture mesoscale dynamics at the time and space scales required by many users, and satellite altimetry data cannot resolve the small scale oceanic circulations.

Therefore, new high-resolution, global observations of total surface current velocity dynamics are required to make further advancement. New ocean observing missions shall require global measurements of the important small-scale forcing, with revisit time sufficiently short to guarantee an adequate sampling of the associated processes.

In this work we propose a new mission concept, referred as StereoSAR, aimed at measuring surface currents at mesoscale (10-50 km) and sub-mesoscale (<10 km) resolution in oceans and coastal areas. It envisages a multi-static configuration based on two passive dual-polarimetric C-band SAR companion satellites flying in formation with Sentinel-1, one in front and one behind at along-track distance of ~275 km, and using Sentinel-1 as illumination source. The Doppler Centroid Anomaly technique is used in order to measure the surface currents.

In the present paper the mission objectives, science drivers and the collected user requirements will be described. Moreover, an overview of the mission concept, mission scenario and operations will be provided. Some issues specific to bistatic SAR missions will be described and solutions offered. Finally, a preliminary performance assessment of the mission concept will be included.

10423-9, Session 3

Overview of EUMETSAT remote sensing products and science activities *(Invited Paper)*

Bojan R. Bojkov, Paul Counet, L. Schueller, EUMETSAT (Germany)

For more than three decades EUMETSAT has been providing the hydro-meteorological user community with satellite data and data products from a combined fleet of geostationary Meteosat satellites and the series of polar orbiting systems (Metop). More recently, EUMETSAT has also started to monitor the marine environment with the scatterometer instruments on the EPS Metop-A/-B missions, with altimeters on the Jason-2/-3 (in partnership with CNES/NASA/NOAA) and with the Copernicus Sentinel-3 missions (in cooperation with ESA). In this paper, highlights of the remote sensing products and science activities of EUMETSAT, including from the EUMETSAT Satellite Application Facilities (SAF) network, will be presented.

10423-10, Session 3

The current EUMETSAT Polar System (EPS) products and services

K. Dieter Klaes, Manfred Lugert, EUMETSAT (Germany)

This Paper provides an overview on the products and services of the EUMETSAT Polar System (EPS), highlighting the scientific aspects. EPS is the European contribution to the Polar Meteorological Satellite Observing System and is part of the Initial Joint Polar System (IJPS) together with NOAA (National Oceanic and Atmospheric Administration). Eight meteorological instruments are embarked on the Metop satellites, which form the space segment of EPS and provide data on the atmospheric state, land and ocean surface, cryosphere and atmospheric composition. There are three Metop satellites in the programme and fly in a sun-synchronous mid morning polar orbit with equator crossing time of 9:30 Local Solar Time (LST) for the descending node. At least 15 years of operations are foreseen to provide measurements from space. Currently two Metop satellites are in orbit (Metop-A launched 2006 and Metop-B in 2012), with the third, Metop-C being prepared for a launch in October 2018.

10423-11, Session 3

The current Meteosat Second Generation (MSG) products and services

Jochen Grandell, Joachim Saalmüller, EUMETSAT (Germany)

EUMETSAT has provided the user community with more than three decades worth of satellite data, starting with the mandatory geostationary missions of first generation Meteosat, and since 2002 the Meteosat Second Generation (MSG) series satellites. In addition to these geostationary satellite systems, EUMETSAT is operating a mandatory Low Earth Orbiting System, the EUMETSAT Polar System (EPS). Furthermore EUMETSAT is operating together with its partners CNES, NOAA and NASA the Jason-2/-3 missions and prepares to start the operations and marine services of the European Commission Copernicus Sentinel-3 mission that has been developed by ESA. The Jason missions are also a part of the Copernicus marine service.

The Meteosat satellites – Meteosat-8, -9, -10 and -11 (currently in in-orbit storage) – operate in a geostationary orbit 36,000 km above the equator at 0°, 9.5 E and 41.5 E to cover Europe, Africa and the Indian Ocean region. MSG data is of unique value to nowcasting of high-impact weather. Meteosat-10 (launched in 2012) is the prime operational geostationary satellite, positioned at 0 degrees and providing full disc imagery every 15 minutes. Meteosat-9 (launched in 2005) provides the Rapid Scanning Service, delivering more frequent images every five minutes over parts of Europe, Africa and adjacent seas. Meteosat-8 (launched in 2002) operates over the Indian Ocean since early 2017. Meteosat-11 was launched in 2015 and is stored in orbit, until required.

The MSG satellites carry a pair of instruments — the Spinning Enhanced Visible and InfraRed Imager (SEVIRI), which observes the Earth in 12 spectral channels and the Geostationary Earth Radiation Budget (GERB) instrument, a visible-infrared radiometer for Earth radiation budget studies.

EUMETSAT products are developed and processed either centrally at the EUMETSAT Headquarters or at the Satellite Application Facilities (SAF) distributed among the Member States.

The presentation will give an overview of the MSG mission and the current status of product development.

10423-12, Session 3

The Copernicus Sentinel-3 Mission, marine products and services

Francois Montagner, European Organisation for the Exploitation of Meteorological Satellites (Germany); Hillary Wilson, EUMETSAT (Germany)

Sentinel-3, was launched from Plesetsk Cosmodrome, in Russia, on 16 February 2016, is a dedicated series of Copernicus satellites for operational remote sensing of the Earth environment. Sentinel-3 satellites are routinely operated by EUMETSAT, and their data are processed jointly by EUMETSAT for the marine part and ESA for the land part.

The mission's main objective at EUMETSAT is in support to the Marine Environment is to determine parameters such as sea-surface topography, sea-surface temperature and ocean colour. It provides two day global coverage Earth observation data (with two satellites) for sea and land applications with real-time products delivered in less than three hours. An overview of the marine products from Sentinel-3 will be given, encompassing Level 1 and Level 2 products from the OLCI (Ocean and Land Colour Imager), SLSTR (Sea and Land Surface Temperature Radiometer), SRAL (SAR Altimeter). The product range also includes Level 2P i.e. Level 2 products with added quality information derived from comparison with other satellites or in situ observations. The portfolio of products will also be broadened to include atmospheric properties.

The Sentinel-3 operational data access services will be also

presented. Those services use complementary technologies, including EUMETCast, and modalities: satellite, internet, etc., to optimise data access for near real time as well as offline or re-processed data products.

The second spacecraft, Sentinel-3b is due to be launched in 2017, working together with S-3A to provide optimal spacio-temporal coverage.

10423-13, Session 4

An overview of the EUMETSAT surface topography missions

Remko Scharroo, Francois Parisot, EUMETSAT (Germany)

During the last year, EUMETSAT's operational commitment to surface topography missions has widened rapidly with the launch of Jason-3 (January 2016) and Sentinel-3A (February 2016). Both missions carry the three prerequisite instrumentations for precise measurements of the ocean and land topography:

• a satellite altimeter, measuring the range between the satellite and the surface to centimetric precision;

• a microwave radiometer, determining the delay of the altimeter radar signal due to humidity in the atmosphere;

• a precise orbit determination package, consisting of GNSS (Global Navigation Satellite System) and DORIS (Doppler Orbitography and Radiopositioning Integrated by Satellite) receivers, as well as a laser retroreflector.

Together, these instrumentations are providing the basics for the measurements of sea level and its spatial and temporal variations due to ocean currents, El Niño, heating and cooling, wind upset, and tides, as well as for measurements of wind speed and significant wave height.

Jason-3 is the follow-on of Jason-2 (launched in June 2008). Now both part of the Copernicus service, Jason-3 took over from Jason-2 as the operational reference altimeter mission in October 2016. While Jason-2 is still in very good shape, it was moved to an orbit such that its ground-track precisely interleaved with that of Jason-3. This creates an near-optimal spatial-temporal coverage of the ocean that can be obtained with just two satellites. It creates repeated observations of all ocean surfaces up to 66º latitude, at intervals of almost 10 days, and a track spacing of about 145 km near the equator. While this is sufficient monitor large-scale ocean phenomena, as well as the larger mesoscale features, a complementary mission is needed to cover the smaller mesoscale, land, in-land waters, and higher latitude surfaces.

Sentinel-3A is the first of a series of ocean observing missions under the umbrella of Copernicus (see the presentation by Montagner and Wilson). For measuring surface topography it carries a Synthetic Aperture Radar Altimeter (SRAL). Together with a denser track pattern of about 100 km at the equator, this mission aims at measuring ocean features of smaller scale, with a revisiting period of 29 days. The SRAL altimeter particularly outperforms other missions in noise level and ability to measure features very near to the coast, as well as measuring elevations of in-land waters and reservoirs, which helps to investigate, monitor, and provide warning for droughts and floods.

Sentinel-3A will be accompanied by Sentinel-3B (launch scheduled for the end of 2017) to be cross-calibrated against each other and then be moved to densify the track pattern further to 50 km. This will allow unprecedented sampling of mesoscale ocean features and will enhance the capabilities for ship routing, fisheries, and forecasting of hurricane intensity and path.

EUMETSAT is currently preparing for the follow-on of the Jason-series of "reference altimeter missions". Sentinel-6 (Jason-CS) of which the first satellite is to be launched in 2020, is in many ways a totally new type of mission, a different platform (similar to CryoSat) and a different altimeter (dissimilar from any of the previous altimeters). Not only will it be the first Synthetic Aperture Radar Altimeter used on one of the reference missions, it will also be the first altimeter that operates in a continuous high-rate pulse mode, 100% of the time. This particular operating mode allows simultaneous production of conventional Low Resolution (LR) mode measurements on-board as well as the processing of SAR echoes (High Resolution, HR, processing) on-ground. This will allow for a smooth transition of the reference missions from conventional to SAR altimetry and secure the Continuity of Service in the establishment of the decades-long global and regional sea level time series from satellite altimetry.

10423-14, Session 4

Introduction to the next generation EUMETSAT Polar System (EPS-SG) observation missions

Peter Schlüssel, European Organisation for the Exploitation of Meteorological Satellites (Germany); Gökahn Kayal, EUMETSAT (Germany)

The EUMETSAT Polar System Second Generation (EPS-SG) will provide operational meteorological measurements from polar orbiting satellites in the mid-morning orbit from 2021 onwards and contribute to the Joint Polar System being set up with NOAA. The Metop Second Generation (Metop-SG) satellites with their instruments, constituting the space segment of EPS-SG, are being developed by ESA with three instruments to be provided by CNES and DLR. The Metop-SG satellites will be arranged as a two satellite constellation (satellites A and B) on the same Sun synchronous, low earth orbit at about 820 km altitude and 09:30 descending equatorial crossing time, providing observations with global coverage. Both satellites will carry instruments providing measurements in support of operational meteorology, climate monitoring, and environmental services, covering oceans, atmosphere, land, and biosphere supporting a variety of application areas. The payload complement of the first satellite consists of atmospheric sounding and optical imaging instruments, while the second one is dedicated to surface scatterometry and micro-wave imaging.

The EPS-SG encompasses observation missions supported by the following instruments:

Satellite A:

• The Infra-red Atmospheric Sounding Interferometer – New Generation (IASI-NG), covering a wide swath of hyper-spectral infra-red soundings in four spectral bands, over the spectral domain from 3.62 to 15.5 μm at a spatial sampling of about 25 km, being developed under the responsibility of CNES;

• The METimage, providing cross-purpose, moderate-resolution optical imaging in 20 spectral channels ranging from 0.443 to 13.345 μm with a spatial sampling of 500 m, being developed under the responsibility of DLR;

• The Micro-Wave Sounder (MWS) allowing for all-weather soundings over a wide swath in the spectral region between 23 and 229 GHz, at a spatial sampling of about 30 km, being developed under the responsibility of ESA;

• The Radio Occultation (RO) receiver, providing high vertical resolution, all-weather soundings by tracking GPS (Global Positioning System) and Galileo satellites, being developed under the responsibility of ESA;

• The Sentinel-5 (S-5) for nadir-viewing ultraviolet, visible, near-infra-red, short-wave-infra-red sounding, providing hyper-spectral sounding with a spectral resolution from 0.05 to 1 nm within the spectral range from 0.27 to 2.4 μm at a spatial sampling of 7 km, being developed for Copernicus under the responsibility of ESA.

• The Multi-viewing Multi-channel Multi-polarisation Imaging mission (3MI), providing moderate resolution aerosol imaging in the spectral region ranging from ultra-violet (0.342 μm) to short-wave infra-red (2.13 μm), at a spatial sampling of 4 km, being developed under the responsibility of ESA.

Satellite B:

• The Scatterometer (SCA), providing back-scattered signals in the 5.355 GHz band at a spatial resolution of 25 km, being

developed under the responsibility of ESA;

• The Micro-Wave Imager (MWI), providing precipitation and cloud imaging in the spectral range from 18.7 to 183 GHz at a footprint size of about 10 km (highest frequency) to 30 km (lowest frequency), being developed under the responsibility of ESA ;

• The Ice Cloud Imager (ICI), providing ice-cloud and water-vapour imaging in the spectral range from 183 to 664 GHz at a footprint size of 16 km, being developed under the responsibility of ESA;

• The Radio Occultation (RO) receiver, providing high vertical resolution, all-weather soundings by tracking GPS (Global Positioning System) and Galileo satellites, being developed under the responsibility of ESA.

In addition, Satellite B embarks an Advanced Data Collection System (ARGOS-4), being developed by CNES.

The ground segment of EPS-SG will provide data with high timeliness through polar receiving stations in Arctic and Antarctic areas for the global data service and a network of distributed receiving stations for the regional data service covering the European and North-Atlantic regions. The targeted timeliness, which is the time span from the measurement to the delivery of calibrated and navigated measurements to the users, is 70 minutes for the global and 30 minutes for the regional service.

10423-15, Session 4

Introduction to the Meteosat Third Generation (MTG) geostationary system

Jochen Grandell, Alexander Schmid, EUMETSAT (Germany)

EUMETSAT has provided the user community with more than three decades worth of satellite data, starting with the mandatory geostationary missions of 1st generation Meteosat, and since 2002 the Meteosat Second Generation (MSG) series satellites. The fourth, and the last satellite in the series, MSG-4 was launched in July 2015 and is stored in orbit, until required. In addition to these geostationary satellite systems, EUMETSAT is operating a mandatory Low Earth Orbiting System, the EUMETSAT Polar System (EPS). The first Metop satellite of the EPS system was launched in October 2006, and the second in September 2012. The third Metop satellite, Metop-C, is currently planned for launch October 2018. Furthermore EUMETSAT is operating together with its partners CNES, NOAA and NASA the Jason-2/-3 missions and prepares to start the operations and marine services of the European Commission Copernicus Sentinel-3 mission that has been developed by ESA.

EUMETSAT is currently developing the future geostationary program. The Meteosat Third Generation (MTG) will host a more advanced 16-channel VIS/IR Flexible Combined Imager as well as a Lightning Imager on its geostationary imaging platform, whereas the sounding platform will host the MTG InfraRed Sounder and the Copernicus Sentinel-4 ultraviolet/near-infrared sounding mission. The launch of the first two satellites MTG-I1 and MTG-S1 hosting the imaging and sounding instruments, respectively, is foreseen in the early 2020s.

EUMETSAT products are developed either centrally at the EUMETSAT Headquarters or at the Satellite Application Facilities (SAF) distributed among the Member States. With the range of new instruments becoming operational in the next decade, and some with very limited heritage in space such as the Lightning Imager or the InfraRed Sounder, it is a challenge for their development, but also for the user community to make best use of these missions early on.

The presentation will give an overview of the MTG system, its observations missions and products.

10423-16, Session 5

The NASA Earth Science Flight Program: an update *(Invited Paper)*

Steven P. Neeck, NASA Headquarters (United States)

NASA's Earth Science Division (ESD) develops a scientific understanding of Earth and its response to natural or human-induced changes. Earth is a system, like the human body, comprised of diverse components interacting in complex ways. Understanding Earth's atmosphere, crust, water, ice, and life as a single, connected system is necessary in order to improve our predictions of climate, weather, and natural hazards. ESD's Flight Program consists of a coordinated series of satellite and airborne missions for long-term global observations of the land surface, biosphere, solid Earth, atmosphere, and oceans. In addition, the Flight Program provides infrastructure for operating these missions, processing their scientific data, and distributing them on a free and open basis to researchers, operational users, and the public. The Flight Program currently has 21 operating Earth observing space missions. There are 22 more missions and instruments planned for launch over the next decade. These comprise missions recommended by the 2007 Earth Science Decadal Survey, missions and selected instruments to assure availability of key climate data sets, operational missions to ensure the sustained land imaging provided by the Landsat system, and small-sized competitively selected orbital missions and instrument missions of opportunity belonging to the Earth Venture (EV) Program. These missions include the recently launched SAGE III on ISS instrument for Ozone and other atmospheric measurements and the Cyclone Global Navigation Satellite System (CYGNSS) microsatellite constellation for observing factors related to tropical cyclone intensification and genesis. Others projects include the Sentinel-6A/B dual satellite altimetry mission; Landsat 9; Pre-Aerosol, Cloud, and ocean Ecosystem (PACE); NASA-ISRO Synthetic Aperture Radar (NISAR); Surface Water and Ocean Topography (SWOT), ICESat-2, Gravity Recovery and Climate Experiment Follow On (GRACE FO), Tropospheric Emissions: Monitoring of Pollution (TEMPO), ECOsystem Spaceborne Thermal Radiometer Experiment on Space Station (ECOSTRESS), the Global Ecosystem Dynamics Investigation (GEDI) Lidar. Recent additions are the Timed-Resolved Observations of Precipitation structure and storm Intensity with a Constellation of Smallsats (TROPICS) nanosat constellation mission, the Multi-angle Imager for Aerosols (MAIA) pollution monitoring instrument, and the recently selected Geostationary Carbon Cycle Observatory (GeoCARB). An overview of plans and current status, including topics related to small satellite enabling activities, will be presented.

10423-17, Session 5

Implementing Earth science flight projects at NASA-JPL

Amit Sen, Steven Bard, Tooraj Kia, Jet Propulsion Lab. (United States)

The Earth Science Flight Projects Office (ESFPO) at the Jet Propulsion Laboratory (JPL) provides programmatic, technical and business management oversight and support to all Earth Science spaceflight projects implemented by JPL. The ESFPO oversees missions in formulation, development and operations, in support of NASA's Earth Science Directorate (ESD), and in coordination with the Earth Systematic Missions Program Office (ESMPO) at the Goddard Space Flight Center (GSFC), and the Earth System Science Pathfinder (ESSP) Program Office at the Langley Space Flight Center. This paper summarizes how the ESFPO provides leadership and guidance to enable mission success on the wide array of JPL-managed Earth Science spaceflight missions and instruments, many with complex international and domestic agency partnerships. An overview of the whole spectrum and various classes of Earth Science missions at JPL, and their current status is also presented.

10423-18, Session 5

Radiation Budget Instrument (RBI): preserving observational continuity of the multi-decadal earth radiation budget climate data record

Kory J. Priestley, Mohan Shankar, Anum R. Barki, NASA Langley Research Ctr. (United States)

The Radiation Budget Instrument (RBI) is one of five instruments hosted aboard the NOAA JPSS-2 spacecraft; a polar-orbiting sun-synchronous satellite in Low Earth Orbit. The primary RBI mission goals and objectives are to measure the reflected sunlight and thermal radiation emitted by the Earth and provide transparent product consistency to the CERES data sets. RBI provides an independent measurement of the broadband reflected solar radiance and Earth's emitted thermal radiance using three spectral bands (Shortwave, Longwave, and Total) which have matched point spread function footprints on Earth. RBI accomplishes this by having three co-aligned telescopes whose fields-of-view, detector time constants, filtering, cross-track scan rates, and sampling rates match the RBI PSF to the heritage CERES PSF.

The Field-of-Regard scanning capability matches CERES and provides cross-track and bi-axial scanning for full Earth disk coverage extending to deep-space as well as enabling solar and lunar calibration verification. RBI has multiple on-orbit calibration sources in order to provide high quality calibrated data products ensuring calibration stability is maintained over the RBI sensor lifetime. To ensure NIST traceable calibration in space the sensor uses a visible calibration target (VCT) and an infrared calibration target (ICT). The VCT is a thermally controlled integrating sphere with Spectralon covering the inner surface and fiber-coupled laser diodes in the UV to IR wavelength region. An Electrical Substitution Radiometer (ESR) monitors long term stability of the sources and degradation of the Spectralon. The radiometric calibration protocol will use a solar calibration target (SCT) with multiple Spectralon diffusers.

10423-19, Session 5

HydroCube Mission concept: P-Band signals of opportunity for remote sensing of snow and root zone soil moisture

Simon Yueh, Jet Propulsion Lab. (United States); Rashmi Shah, Jet Propulsion Lab (United States); Xiaolan Xu, Jet Propulsion Lab. (United States); Kelly Elder, Rocky Mountain Research Station, U.S. Forest Service (United States); Chun Sik Chae, Jet Propulsion Lab. (United States); Steven Margulis, Univ. of California, Los Angeles (United States); Glen E. Liston, Colorado State Univ. (United States); Michael Durand, The Ohio State Univ. (United States); Chris Derksen, Environment and Climate Change Canada (Canada)

We have developed the HydroCube mission concept with a constellation of small (6U) satellites to remotely sense Snow Water Equivalent (SWE) and Root Zone Soil Moisture (RZSM). The satellites will operate at sun-synchronous 3-day repeat polar orbits with a spatial resolution of about 1-3 Km. The mission goals are to improve the estimation of terrestrial water storage and weather forecasts. Root-zone soil moisture and snow water storage in land are critical parameters of the water cycle. The Signals of Opportunity (SoOp) concept, in which passive receivers make use of strong existing satellite transmissions available across most all microwave bands penetrating the Earth's atmosphere (VHF to Ka band), will complement or even become a cost-effective alternate to active technologies. This variety of signals is well suited for land remote sensing. Here we report the analysis of coherent reflection of P-band (360-380 MHz and 250-270 MHz) radio signals from geostationary Mobile Use Objective System (MUOS) communication satellites.

The SWE remote sensing measurement principle using the P-band SoOp is based on the propagation delay (or phase change) of radio signals through the snowpack. The refractive index or dielectric constant of snow is closely related to the snow density. The additional time delay of the reflected signal due to the snowpack with respect to snow-free conditions is directly proportional to the snowpack SWE. To address the ionospheric delay at P-band frequencies, the signals from both MUOS bands (360-380 MHz and 250-270 MHz) can be used. We have conducted an analysis to trade off the spatial resolution for a space-based sensor and measurement accuracy, confirming that the residual effects will have a negligible impact on satellite SoOp SWE observation accuracy and spatial resolution.

Through theoretical modeling analysis, we find that the dual-band MUOS signals have the potential to allow estimation of soil moisture and surface roughness together. At the MUOS frequencies with a wavelength of about a meter, typical surface roughness of natural terrain can be modeled by small perturbation. From the two MUOS frequencies at 260 MHz and 370 MHz, we can retrieve the soil moisture from the reflectivity ratio scaled by wavenumbers using the two P-band frequencies for MUOS. Collocating the P-band measurements with the L-band GPS reflection signal from the NASA Cyclone Global Navigation Satellite System (CYGNSS) mission, we can also estimate the vertical profile of soil moisture. A modeling analysis using layered stratified model has been completed to determine the sensitivity requirements of HydroCube measurements.

For proof-of-concept demonstration, a field campaign has been conducted at the Fraser Experimental Forest in Colorado since February 2016. A tower-based SoOp receiver was installed to observe the coherent reflection from MUOS. Time series of in situ data includes snow depth, snow temperature, soil temperature and soil moisture. Periodic snowpit measurements provide snow density and water equivalence. The data acquired from early 2016 has shown the root-mean-square accuracy of 7.4 mm for retrieving SWE from phase changes observed by the SoOp receiver. Preliminary analysis of the MUOS reflection signals also show good correlation with soil moisture.

10423-20, Session 6

Overview of Japanese Earth observation programs *(Invited Paper)*

Haruhisa Shimoda, Tokai Univ. (Japan)

Five programs, i.e. ASTER, GOSAT, GCOM-W1, GPM and ALOS-2 are going on in Japanese Earth Observation programs. ASTER on EOS-Terra are operating well except SWI channels. ASTER SWI channels have stopped the operation because of a refrigerator failure in 2009. ADEOS2 was failed, but AMSR-E on Aqua was operating until 14, Oct. 2011. AMSR-E has stopped at that time because of the antenna driving mechanism's torque increase. AMSR-E instrument has been on from March 2012 without antenna rotation and antenna rotation has been started from Dec. 2012 with 2rpm. AMSR-E has finally stopped on Dec. 2015. The fuel of TRMM has been exhausted and the height of TRMM is decreasing. TRMM has finally stopped on April 2015. GCOM-W1 was launched on May, 2012.GCOM-W1 carries AMSR2. The orbit is A-train and has higher resolution than AMSR-E. GOSAT was launched on 23, Jan., 2009. GOSAT carries 2 instruments, i.e. a greenhouse gas sensor (TANSO-FTS) and a cloud/aerosol imager (TANSO-CAI). TANSO-FTS is a Fourier transform spectrometer (FTS) and covers 0.76 to 15 ?m region with 0.2 cm-1 resolution. TANSO-CAI is a 5 channel push broom scanner to observe aerosols and clouds. Both sensors are operating well. SMILES was on JEM of ISS. SMILES is a sub-millimeter limb sounding instrument using super conducting mixer and measures stratospheric ozone and related compounds. Unfortunately, SMILES stopped its operation on 21, April, 2010. ALOS was launched on 24, Jan., 2006 and stopped on 22, April, 2011 by power anomaly. ALOS carried three instruments, i.e., PRISM, AVNIR-2 and PALSAR.

PRISM is a 3 line panchromatic push broom scanner with 2.5m IFOV. AVNIR-2 is a 4 channel multi spectral scanner with 10m IFOV. PALSAR is a full polarimetric active phased array SAR. GPM core satellite is a joint project with NASA and carries two instruments. JAXA has developed DPR. DPR has Ka band channel in addition to Ku band channel. NASA has developed GMI which is a microwave imager. GPM core satellite was launched on February 2014 and operating well. ALOS-2 was launched on 24, May 2014. ALOS-2 carries PALSAR-2, which is a L-band SAR. PALSAR-2 has full polarimetric mode as PALSAR. In addition, the spatial resolution of PALSAR-2 is higher than PALSAR. The highest resolution is 3m X 1m. Next generation satellites will be launched in 2017-2019 timeframe. They are GCOM-C1, EarthCare, GOSAT-2 and Advanced Optical Satellite (AOS). GCOM-C1 will carry SGLI. SGLI has polarization channels. GCOM-C1 will be launched on 2017. Another project is EarthCare. It is a joint project with ESA and JAXA is going to provide CPR with NICT. EarthCare will be launched on 2019. GOSAT-2 is a follow on of GOSAT and will carry 2 instruments, i.e. TANSO-FTS2 and TANSO-CAI2. FTS2 is an improved version of FTS on GOSAT, but CAI2 is a 10 channel ultra violet to near infrared imager. GOSAT-2 will be launched on 2019. AOS will carry a panchromatic camera and a multi-spectral camera and will be launched on 2019.

10423-21, Session 6

Prime mission results of the dual-frequency precipitation radar on the global precipitation measurement core spacecraft and the version 5 GPM standard products

Kinji Furukawa, Tomomi Nio, Riko Oki, Takuji Kubota, Japan Aerospace Exploration Agency (Japan); Toshio Iguchi, National Institute of Information and Communications Technology (Japan)

The Dual-frequency Precipitation Radar (DPR) on the Global Precipitation Measurement (GPM) core satellite was developed by Japan Aerospace Exploration Agency (JAXA) and National Institute of Information and Communications Technology (NICT). The GPM is a follow-on mission of the Tropical Rainfall Measuring Mission (TRMM). The objectives of the GPM mission are to observe global precipitation more frequently and accurately than TRMM. The frequent precipitation measurement about every three hours is achieved by some constellation satellites with microwave radiometers (MWRs) or microwave sounders (MWSs), which were developed by various countries. The accurate measurement of precipitation in mid-high latitudes is achieved by the DPR. The GPM core satellite is a joint product of National Aeronautics and Space Administration (NASA), JAXA and NICT. NASA developed the satellite bus and the GPM microwave radiometer (GMI), and JAXA and NICT developed the DPR.

The configuration of precipitation measurement using an active radar and a passive radiometer is similar to TRMM. The major difference is that DPR is used in GPM instead of the precipitation radar (PR) in TRMM. The DPR consists of Ku-band (13.6 GHz) precipitation radar (KuPR) and Ka-band (35.5 GHz) precipitation radar (KaPR). The inclination of the GPM core satellite is 65 degrees, and the flight altitude is about 407 km. The non-sun-synchronous circular orbit is necessary for measuring the diurnal change of rainfall similarly to TRMM.

The objectives of the DPR are

(1) to provide three-dimensional precipitation structure including snowfall over both ocean and land,

(2) to improve the sensitivity and accuracy of precipitation measurement,

(3) to calibrate the estimated precipitation amount by MWRs and MWSs on the constellation satellites.

GPM core observatory was successfully launched by H2A launch vehicle on Feb. 28, 2014. DPR keeps its performances on orbit after launch. GPM products were released to the public on Sep. 2, 2014 and Normal Observation Operation period was started. JAXA is continuing DPR trend monitoring, calibration and validation operations to confirm that DPR keeps its function and performance on orbit. The DPR prime mission period was completed in May 2017. JAXA will start to provide a new version (Version 5) of GPM standard products in April, 2017. Concurrently, existing GPM data are also being reprocessed back to the start of the mission. GPM version 5 products are available from JAXA G-Portal. Various improvements of the DPR algorithm were implemented in the version 5 product. The prime mission results of the GPM/DPR and highlights of the version 5 product will be reported.

10423-22, Session 6

Pre-launch instrument characterisation results and in-orbit verification plan of GCOM-C/SGLI

Tomoyuki Urabe, Shigemasa Ando, Yoshihiko Okamura, Kazuhiro Tanaka, Masaaki Mokuno, Japan Aerospace Exploration Agency (Japan); Takahiro Amano, Koichi Shiratama, NEC Corp. (Japan); Jun Yoshida, NEC Space Technologies Ltd. (Japan)

The Global Change Observation Mission (GCOM) aims to establish and demonstrate a global, long-term satellite-observing system to measure essential geophysical parameters to facilitate understanding the global water circulation and climate change, and eventually contribute to improving future climate projection through a collaborative framework with climate model institutions. GCOM consists of two polar orbiting satellite observing systems, GCOM-W (Water) and GCOM-C (Climate). The first satellite, GCOM-W with Advance Microwave Radiometer -2 (AMSR-2), was already launched in 2012 and is observing continuously. The follower satellite, GCOM-C with Second Generation Global Imager (SGLI), will be launched in Japanese fiscal year 2017. SGLI enables a new generation of operational moderate resolution-imaging capabilities following the legacy of the GLI on ADEOS-II (Advanced Earth Observing Satellite-II) satellite. The SGLI empowers surface and atmospheric measurements related to the carbon cycle and radiation budget, with two radiometers of Visible and Near Infrared Radiometer (VNR) and Infrared Scanning Radiometer (IRS) which perform a wide-band (380nm-12um) optical observation not only with as wide as 1150-1400km FOV but also with as high as 250-500m resolution. Also, polarization and along-track slant view observation are quite characteristic of SGLI, providing the sensor data records for more than 28 standard products and 23 research products including clouds, aerosols, ocean color, vegetation, snow and ice, and other applications. Sensor instrument proto-flight tests including optical characterisation tests such as radiometric and geometric were completed, and satellite system proto-flight tests are on-going including thermal vacuum, vibration and acoustic test. In this paper, the pre-launch phase instrument characterisation of SGLI flight model and status of GCOM-C satellite system flight model along with the overview of them will be described. Especially we focus on the pre-launch geometric and radiometric performance test results and in-orbit verification plan during a commissioning phase lasting approximately 3 months.

10423-23, Session 6

Overview of the Japanese Advanced Optical Satellite: mission objectives, an onboard camera and a satellite system

Hidenori Watarai, Haruyoshi Katayama, Takeo Tadono, Eri Kato, Masakazu Sagisaka, Japan Aerospace Exploration Agency (Japan)

The Japanese “Advanced Optical Satellite” (as the tentative name, hereafter AOS) is an earth observing satellite being

developed to succeed the optical mission of the Advanced Land Observing Satellite (ALOS) operated from 2006 to 2011. Both high Ground Sampling Distance (GSD) and wide swath will be accomplished by an onboard camera which became upsizing and high performance in comparison with ALOS's cameras.

The main objectives of the AOS project are as follows:

1) image the land surface of all over the world with high GSD (0.8m at nadir) and wide swath (70 km) and build a big image database to prepare for natural disasters. By extracting the changes before and after the disaster, the damage situations will be captured as soon as possible.

2) contribute to generate and update geospatial information. AOS has capabilities to take stereo images by the body-pointing of satellite (up to 60 deg for all direction), and be able to process Digital Surface Model (DSM) using them in area of the interests.

This paper introduces the specifications of AOS and the basic design of the onboard camera as well as project status.

10423-24, Session 7

Flight model of HISUI hyperspectral sensor onboard ISS (International Space Station)

Jun Tanii, Japan Space Systems (Japan); Yoshiyuki Ito, NEC Space Technologies Ltd. (Japan); Akira Iwasaki, The Univ. of Tokyo (Japan); Osamu Kashimura, Japan Space Systems (Japan)

Hyper Spectral Sensor of HISUI(Hyper-spectral Imager Suite) is a next-generation Japanese sensor that will be mounted on JEM(Japanese Experiment Module) of ISS(International Space Station) in 2019 as timeframe. HISUI hyperspectral sensor obtains spectral images of 185 bands with the ground sampling distance of 20x30 meter from the visible to shortwave-infrared region . Simultaneously, the development of JEM-EF (External Facility) Payload system for the instrument is being carried out. The system includes the structure, the thermal control system and the electrical system. The sensor is the follow-on mission of the Advanced Spaceborne Thermal Emission and Reflection Radiometer (ASTER) in the visible to shortwave infrared region [1]. The critical design review of the sensor was held in 2014. Integration and tests of flight model of HISUI hyperspectral sensor have been completed in the beginning of 2017. The results of PFT (Proto-Flight Test) of the Instrument flight model, including environment tests, such as acoustic test and thermal vacuum test, are reported in this work.

REFERENCES

[1] Y.Yamaguchi, A.B.Kahle, H.Tsu, T.Kawakami, and M. Pniel, "Overview of Advanced Spaceborne Thermal Emission and Reflection Radiometer (ASTER)," IEEE Trans. Geosci. Remote Sens., Vol.36, No.4, 1998, pp.1062-1071.

[2] A. Iwasaki, N. Ohgi, Jun Tanii, T. Kawashima, and H. Inada, "Hyperspectral imager suite (HISUI): Japanese hyper-multi spectral radiometer" in Proc. IEEE IGARSS, Jul. 2011, pp.1025-1028.

[3] Yoshiyuki Ito, Takahiro Kawashima, Hitomi Inada, Jun Tanii and Akira Iwasaki, "The Instrument Development Status of Hyper Spectral Imager SUIte (HISUI)" Proc SPIE Asia-Pacific Remote Sensing 2012, Oct 2012, pp8528-39

[4] J. Tanii, Y. Ito, and A. Iwasaki, "Instrument development status and performances of hyperspectral imager suite (HISUI) — Onboard data correction" in Proc. IEEE IGARSS, Jul. 2014, pp. 2007 - 2010.

[5] J. Tanii, O. Kashimura Y. Ito, and A. Iwasaki, "Flight model performances of HISUI hyperspectral sensor onboard ISS (International Space Station)" in Proc. SPIE 10000, Sensors, Systems, and Next-Generation Satellites XX, 100000A (October 19, 2016); doi:10.1117/12.2243846

10423-25, Session 7

Observation planning algorithm of a Japanese space-borne sensor: Hyperspectral Imager SUIte (HISUI) onboard International Space Station (ISS) as platform

Kenta Ogawa, Yukiko Konno, Rakuno Gakuen Univ. (Japan); Satoru Yamamoto, Tsuneo Matsunaga, National Institute for Environmental Studies (Japan); Tetsushi Tachikawa, Mako Komoda, Japan Space Systems (Japan)

Hyperspectral Imager Suite (HISUI) is a Japanese future space-borne hyperspectral instrument being developed by Ministry of Economy, Trade, and Industry (METI). ?HISUI will be launched in 2019 or later onboard International Space Station (ISS). HISUI has 185 spectral band?from 0.4 to 2.5 μm with 20 m spatial resolution. HISUI will be delivered to ISS by Dragon /Falcon 9 cargo rocket and will be installed on JEM EF (Japanese Experimental Module Exposed Facility).

To make effective observation plan, HISUI OPS (Observation Planning Subsystem at ground data system) will automatically generate observation schedule of HISUI based on platform orbit, observation target maps, their priorities, and available resources such as instrument operation time, data storage capability and other limitations of HISUI and ISS. To archive HISUI mission, the observations of large area of continental scale is requested for resource exploitation and other spot observations for various objectives, however the swath of HISUI is limited to as small as 20 km. Therefore, years of observations are needed to satisfy the coverage of observation target maps. Making practical scenario of observations through HISUI's life is critical for mission planning and improving efficiency of observations are quite important.

To address these issue, we have developed observation simulator. The simulator's input includes observation target maps and the ISS's orbit, HISUI limitation in observation minutes per orbit, data storage and past MODIS cloud coverage data for period equivalent to HISUI mission life of three years.

Then the outputs of the simulator are coverage map of each day. Areas with cloud free image are accumulated for the observation. The simulation for three year can be finished in about 8 hours by a MacPro.

HISUI OPS is originally developed for HISUI on a sun-synchronous orbit satellite platform and now it is changed to be onboard ISS. The difference of platform is analyzed. Altitude is changed to 370 km ± 40 km, originally from 600 km. High latitude regions will not be observed due to ISS orbit?(≈ 51.6?degree inclination). Observation local time varies because of ISS orbit, which is non-sub-recurrent orbit.

HISUI data will be partially transmitted to ground stations (≈ 10 GB/day). The rest will be recorded in removal media in ISS's pressurized zone and shipped back to Earth by cargo ships once in several months. An advantage of ISS as platform is that we can use conventional low cost and large capacity storage.

The results of simulations indicate that the progress of the observation much depends on data transfer speed between sensor to storage in ISS's pressurized zone. Coverage of priority observation area varies from 73 % (in the case of 7.4 GB/orbit) to 99.5 % (in the case of 51.7 GB/orbit) after 1080 days of observation.

We also checked how the cloud free probability in the afternoon is different from the one in the morning. For this purpose, the MODIS Terra data and the MODIS Aqua data are compared.

The detail of the results of observation simulation will be presented at the time of presentation.

10423-26, Session 7

The development status of the mission instruments of GOSAT-2

Masakatsu Nakajima, Hiroshi Suto, Hiroko Imai, Yukie Yajima, Makiko Hashimoto, Kei Shiomi, Japan Aerospace Exploration Agency (Japan)

The GOSAT was launched in January of 2009 as the first satellite dedicated to the measurements of the greenhouse gases such as carbon dioxide and methane. And the GOSAT has been operated for more than eight years and has obtained a lot of data and has shown the useful results to contribute to the global warming issues.

One of them is the detection of the anthropogenic emission of the carbon dioxide from Mega-City regions. Correlations with a close to 1:1 relationship were found between the anthropogenic carbon dioxide concentrations estimated from GOSAT data ad those estimated using data on inventory in Japan and its surroundings.

On the other hand, GOSAT has encountered a few problems on orbit.

One of them is that the one solar array had stopped to rotate due to the failure of the electronic parts of the control circuit and only one solar array paddle has generated the power that is enough for the complete operation.

The GOSAT-2 is the successor satellite to the GOSAT.

The development of the GOSAT-2 has been continued for more than three years, and currently the proto-flight model of the mission instruments, TANSO-FTS-2 and TANSO-CAI-2, are under manufacturing and test.

TANSO-FTS-2 is the Fourier Transform Spectrometer observing greenhouse gases and TANSO-CAI-2 is the imager observing the aerosols and clouds to compensate the TANSO-FTS-2 data and to grasp the movements of the aerosols such as PM2.5.

These instruments will follow the observation methods of the GOSAT. But some improvements will be carried for the purposes of the estimation of the anthropogenic emission and improvement of the aerosols observation performances.

The critical design had completed in beginning of 2016. The results of the design had met the all requirements. But the gap has emerged between the design and manufacturing results through the manufacturing and test of the test models or the proto-flight models. Especially, the design of the polarization sensitivity of the TANSO-CAI-2 had met the requirement of 3% or less, but the test manufacturing results was over 40%. The root cause of this anomaly was that the thickness of the antireflection coating became thinner toward the edge due to the configuration of the coating of the antireflection coating in the chamber. The coating materials are evaporated from the point source and the lens has the curved surfaces. So the angle between the lens surface and coating material flux is different from part to part and the amount of sediment of the coating materials differ according to the places. Therefore the difference of the thickness according to the place had been taken into account in design of the antireflection coating. And finally we could meet the polarization sensitivity requirements.

In this presentation, the current status of the development of the GOSAT-2 mission instruments including the results of a part of the proto-flight test will be shown as well as the results of the GOSAT on orbit operation.

10423-27, Session 7

Aircraft experiment to demonstrate intelligent pointing system onboard GOSAT-2

Yukie Yajima, Hiroshi Suto, Masakatsu Nakajima, Japan Aerospace Exploration Agency (Japan)

TANSO-FTS-2 on the GOSAT-2 spacecraft, to increases useful data collections in the presence of clouds, will implement the newly pointing system using a high-resolution RGB visible camera and a nadir-looking pointing system with image motion compensation (IMC), named Intelligent Pointing (IP) system.

To demonstrate the IP system, we conducted aircraft experiments with “TSUKUBA model” in Feb, 2017. TSUKUBA model was installed in the aircraft, and fly over the actual cloud area with field of view as ~110m with 7km flight altitude. we will present the experimental results.

10423-28, Session 7

Development status of multi-footprint observation lidar and imager (MOLI) on ISS

Toshiyoshi Kimura, Tadashi Imai, Daisuke Sakaizawa, Jumpei Murooka, Rei Mtsuhashi, Japan Aerospace Exploration Agency (Japan)

IPCC AR5 reports suggests the such biomass estimation error is still large in the global carbon cycle system. To evaluate biomass directly and globally from satellite, L-band SAR is mostly expected instrument considering L-band capability to penetrate forest. Although, there is still issue to measure dense tropical forest region. Because L-band signal is saturated for such target, i.e. over 100 t/ha. To conquer them, combination use of L-band SAR and Lidar is getting expected recently. Forest evaluation from spaceborne Lidar was firstly made using NASA ICESat/GLAS. However, it is known that there are several observational characters to be optimized for forest observations. JAXA studied Multi-footprint Observation Lidar and Imager (MOLI) to conquer the lessens-learned points from them. Additionally, to supress Laser Induced Contamination (LIC) effect, which shorten Laser transmitter’s life is the key technology for high power pulse spaceborne Lidar. We made a life test under vacuum for newly developed 40 mJ power and PRF 150 Hz transmitter. The test is continuing successfully over one year and total number of shot reached 4.5 billion. MOLI is the engineering and mission demonstration Lidar on ISS/JEM towards future operational vegetation Lidar system. Expected launch year of MOLI is around 2019.

10423-29, Session 8

VIIRS pre-launch testing and performance: an overall comparison between S-NPP, JPSS-1 and JPSS-2 instruments *(Invited Paper)*

Hassan Oudrari, Jeffrey McIntire, Science Systems and Applications, Inc. (United States); Xiaoxiong J. Xiong, Kurtis J. Thome, James J. Butler, NASA Goddard Space Flight Ctr. (United States); Thomas Schwarting, Qiang Ji, Science Systems and Applications, Inc. (United States); Jinan Zeng, Fibertek, Inc. (United States)

The Visible-Infrared Imaging Radiometer Suite (VIIRS) is a key sensor on-board the Joint Polar-orbiting Satellite System satellites. The first VIIRS flight unit has been on-orbit for about 5 years on board Suomi-National Polar-orbiting Partnership (S-NPP) mission. The following two units JPSS-1 and JPSS-2 VIIRS are scheduled to launch in the summer of 2017 and early 2022 respectively. This paper will present VIIRS pre-launch radiometric performance for all three instruments, S-NPP, JPSS-1 and JPSS-2, as well as key features and issues observed during testing for each instrument. JPSS-1 VIIRS has successfully completed its sensor and spacecraft level pre-launch calibration and characterization, while JPSS-2 VIIRS has completed its initial pre-launch ambient testing phase at the sensor level. The VIIRS instrument has 22 spectral bands covering wavelengths from visible (0.4 ?m) to long-wave infrared (12.6 ?m), including a day-night band (DNB) that can collect data over a very large radiometric dynamic range. The derived VIIRS SDR products represented by the calibrated

radiance/reflectance and brightness temperature are key inputs to the production of many environmental data records (EDRs) used in research and operational studies and applications. This paper provides an overview of the radiometric performance comparison between SNPP, JPSS-1 and JPSS-2 VIIRS based on the pre-launch testing program, focusing on key radiometric performance metrics, such as sensor signal-to-noise ratios (SNRs), scattered light, relative spectral response (RSR), response versus scan-angle (RVS), and polarization sensitivity. The team collaboration processes and structure used by the sensor vendor and the government team to improve sensor testing procedures and performance assessment approaches as well as lessons learned will also be presented in this paper.

10423-30, Session 8

JPSS-1 OMPS instrument sensor data records

Chunhui C. Pan, Univ. of Maryland, College Park (United States); Fuzhong Weng, Trevor beck, National Oceanic and Atmospheric Administration (United States)

The Ozone Mapping Profiler Suite (OMPS) is an advanced hyper-spectral instruments suite that carries on a long tradition of space borne measurements of ozone beginning in 1970 with the US NASA and NOAA Nimbus 4 satellite. The first OMPS is onboard the Suomi National Polar-orbiting Partnership (Suomi NPP) satellite launched in 2011. The second OMPS will fly on the Joint Polar Satellite System-1 (JPSS-1) to maintain continuity of ozone observations into the late 2020s. The most challenge issue in Suomi NPP OMPS calibration is to correct sensor in-flight spectral variation. Analysis of on-orbit data has demonstrated that OMPS wavelength change exceeded sensor performance requirement. JPSS-1 OMPS likely to have the same issue in its operation. A further calibration of the Suomi NPP OMPS in-flight spectral registration has minimized wavelength-dependent albedo error, allows Sensor Data Records (SDRs) meet OMPS product requirement for most of the channels across all of the IFOVs. The same correction methodology will be applied to the JPSS-1 OMPS. The JPSS-1 OMPS has an extended spectral coverage from 380 nm to 420 nm, allowing a better geo-location calibration via a comparison of OMPS data with Visible Infrared Imaging Radiometer Suite (VIIRS) data; benefiting sensor Out Of Band stray light calibration. The JPSS-1 OMPS uses Reflective Quasi-Volume Diffusers (QVD) instead of alumina diffusers to maintain on-orbit calibration stability, which will minimize sensor spectral features in sensor observed solar data, significantly improves wavelength dependent albedo accuracy by ~ 5% for Nadir Profiler and 10% for Nadir Mapper. Our presentation will demonstrate Suomi NPP OMPS spectral calibration results; address our experience from Suomi NPP OMPS on-orbit SDR calibration that applicable to the JPSS-1 SDR calibration. Examples will be given on the major improvements made to the JPSS-1 OMPS SDR that fully utilize new capabilities of JPSS-1 OMPS to benefits OMPS users.

10423-31, Session 8

First-principle dynamic electro-thermal numerical model of the Radiation Budget Instrument (RBI)

Anum R. Barki, Kory J. Priestley, NASA Langley Research Ctr. (United States); James R. Mahan, Brian Vick, Virginia Polytechnic Institute and State Univ. (United States)

The Radiation Budget Instrument (RBI) is one of five instruments hosted aboard the NOAA JPSS-2 spacecraft; a polar-orbiting sun-synchronous satellite in Low Earth Orbit. The primary RBI mission goals and objectives are to measure the reflected sunlight and thermal radiation emitted by the Earth and provide transparent product consistency to the CERES data sets. RBI provides an independent measurement of the broadband reflected solar radiance and Earth's emitted thermal radiance using three spectral bands (Shortwave, Longwave, and Total) which have matched point spread function footprints on Earth. RBI accomplishes this by having three co-aligned telescopes whose fields-of-view, detector time constants, filtering, cross-track scan rates, and sampling rates match the RBI PSF to the heritage CERES PSF.

High-level, first-principle dynamic electro-thermal models of the RBI radiometric channels and on-board calibration targets have been completed under NASA sponsorship. The RBI Radiometric channels each consist of a cassegrain telescope, containing a unique optical bandpass filter, with dual, single pixel, thermopile detectors.

In order to provide high quality calibrated data products, RBI has multiple on-orbit calibration sources that ensure calibration stability and traceability is maintained over the mission lifetime. To ensure NIST traceable calibration in space, the sensor uses a Visible Calibration Target (VCT) and an Infrared Calibration Target (ICT). The VCT is a thermally controlled integrating sphere with Spectralon covering the inner surface and fiber-coupled laser diodes in the UV to IR wavelength region. An Electrical Substitution Radiometer (ESR) monitors long term stability of the sources and degradation of the Spectralon.

The current manuscript describes the modeling of the RBI instrument comprised of first-principle optical, thermal and electrical numerical modules. Optical characterization of the telescopes and calibration targets is ensured by Monte-Carlo-based ray-traces. Accurate thermal and electrical characterization is assured by transient numerical formulations. This body of research presents the evolution of these models by outlining their development and validation. Validation of the models is accomplished by simulating the ground calibration process of the actual instruments and verifying that the models accurately predict instrument performance. The result of this agreement is a high confidence in the model to predict other aspects of instrument performance.

10423-32, Session 8

Landsat 9 TIRS-2 prelaunch calibration approach

Joel McCorkel, NASA Goddard Space Flight Ctr. (United States)

Landsat-9, the next in the series of Landsat satellites, will have the same complement of two sensors as Landsat-8: The Operational Land Imager (OLI) that covers the reflective solar part of the spectrum in 9 spectral bands and the Thermal Infrared Sensor (TIRS) with two bands in the thermal infrared region. The main changes to the sensors for Landsat-9 will be to increase redundancy in the TIRS instrument, called TIRS-2, to bring it up to a five year design lifetime and fixes for anomalies observed on-orbit on Landsat-8 TIRS: Stray light and scene select mechanism encoder degradation. This work reports on the multi-pronged approach that will be used to ensure that stray light is reduced to required levels and properly characterized. Baffles to reduce stray light were designed and tested at several stages of sensor development. In parallel, optical modeling by NASA and independent teams was used to predict performance of the design changes to hold against test results as well as Landsat 8 TIRS on-orbit performance for model validation. A new subsystem-level test allows a large angular range to be tested to characterize out-of-field stray light that was not available during the first TIRS build. Combined, characterization results from modeling and ambient-, component-, subsystem-, and instrument-level testing will fully characterize TIRS-2 performance.

10423-67, Session PS

An onboard star catalog for satellite angular attitude estimation

Ivan S. Kruzhilov, Andrey M. Tchernetsov, National Research University "MPEI" (Russian Federation); Andrei Zakharov, Moscow State University (Russian

Federation); Svyatoslav Kruzhilov, Moscow Technological Univ./Dept. of Hardware and Software for Computer Systems (Russian Federation)

Accuracy assessment of the satellite remote sensing depends on the angular attitude estimation precision. The 1 arc second error in attitude estimation causes 2.5 meter error in the remote sensing accuracy for the 500 km orbit.

A spacecraft angular attitude requires continual adjustment to counteract torque moment caused by the Sun light pressure, the Earth magnetic field, gravitation and aerodynamic forces. Different kind of momentum wheels, propulsions and sensors help correct torque moment to stabilize spacecraft in the orbit.

Star tracker is the most precise optical sensor for spacecraft angular attitude estimation. They are being used for a variety of satellites from cubesats to big satellites for long-life missions. star tracker consist of an optical system, a photo receiver (usually CCD or CMOS matrix) and a computing block capable executing advanced algorithms. A typical spectral response of a star tracker lies between 400 and 1000 nm

An onboard guide star catalog containing data for star pattern identification is essential for star tracker operating. The total number of stars, the faintest stellar magnitude, completeness and uniformity are the key specifications of a star catalog influencing many characteristic of a star tracker.

An onboard catalog is to be created individually for every type of a star tracker. The steps of creating guide star catalog are: instrumental stellar magnitude estimation with respect to the star tracker spectral response, clasterization of nearby stars, removing of unreliable stars and final star selection.

An iterative algorithm for thinning down the catalog allows reducing appreciably the number of stars in the catalog and improving its uniformity.

The key point of the algorithm is the lower bound evaluation of star number in the FOV (field of view) for every boresight position within a triangle area. The algorithm uses recursive quaternary division of the icosahedron for the celestial sphere tessellation.

The correction methods of stellar aberration and star proper motion are discussed as well.

An onboard star catalog designed in a proper way enhances the reliability and the accuracy of the star tracker.

10423-68, Session PS

An approach for detecting satellite stability

Bai Jie, Chen Fang, Zi Jia Liu, Yi Xuan Sun, Beijing Space Electromechanical Research Institute (China)

The satellite, especially for the remote sensing satellite, must ensure the stability of the mechanical structure, whether through rocket launch or into space environment. The stability of the structure can be judged directly by the final image quality. However, it will be difficulty to figure out which part is in problem if the system worked improperly after launch simulation test and vacuum environment simulation test. Hence another method is improved which is to measure the positions of the main points on the satellite before and after the experiments. The stability of each structural part is obtained by comparing the coordinate values. The points which have significant changes mean relative unstable while the few changes mean more stable. In most cases, the structure is measured by the coordinate measuring machine. Due to the complexity of the satellite, it generally requires a lot of measurement points. Coupled with the measurement error of the equipment itself, it is difficult to select an effective datum to establish the coordinate system, and to have a reasonable assessment of the coordinate change of the measuring points system. Normally, three points are needed to build a reference coordinate system during the measurement. Since these three points have repeated errors in the measurement process, it is likely that position repetitive error of other points will be enlarged after the projection onto the coordinate system, especially for the far points. Based on this, a data analysis method is presented, make the final results has nothing to do with the reference coordinate, which can more reliably react to the stability of the structure.

10423-69, Session PS

Cross comparison of the Collection 6 and Collection 6.1 Terra and Aqua MODIS Bands 1 and 2 using AVHRR N15 and N19

Xuexia Chen, Aisheng Wu, Science Systems and Applications, Inc. (United States); Xiaoxiong J. Xiong, NASA Goddard Space Flight Ctr. (United States); Na Chen, Science Systems and Applications, Inc. (United States)

The MODIS (Moderate Resolution Imaging Spectroradiometer) is a key scientific instrument that was launched into Earth orbit by NASA in 1999 on board the Terra (EOS AM) satellite and in 2002 on board the Aqua (EOS PM) satellite. Terra and Aqua MODIS collect the entire Earth's images every 1 to 2 days in 36 spectral bands. MODIS band 1 (620-670nm) and band 2 (841-876nm) have nadir spatial resolution of 250 m and their measurements are crucial to derive key land surface products. This study evaluates the performance of the Collection-6 (C6, and C6.1) L1B calibrations of both Terra and Aqua MODIS bands 1 and 2 using Simultaneous Nadir Overpass (SNO) data to compare with AVHRR sensors. We examine the relative stability between Terra and Aqua in reference to NOAA 15/19 AVHRR (The Advanced Very High Resolution Radiometer). The comparisons for MODIS to AVHRR are over a fifteen-year period from 2002 to 2017. Results from this study provide a quantitative assessment of Terra and Aqua MODIS bands 1 and 2 calibration stability and the relative differences from the NOAA 15/19 AVHRR sensors.

10423-70, Session PS

Near-infrared imager for spectral and polarization analysis of planetary surfaces

Denis Belyaev, Space Research Institute (Russian Federation); Konstantin B. Yushkov, Sergey P. Anikin, National Univ. of Science and Technology "MISiS" (Russian Federation); Nadezhda Evdokimova, Yury Dobrolenskiy, Oleg Korablev, Space Research Institute (Russian Federation); Vladimir Y. Molchanov, National Univ. of Science and Technology "MISiS" (Russian Federation)

We propose a concept of an imaging near-IR spectrometer for sensing of planetary surfaces. This instrument is intended to analyze mineralogical and, in some cases, petrographic composition of the upper surface layer in the planetary regolith; to identify and monitor OH/H2O bearing minerals and water adsorption in this layer. The scheme of the spectrometer was designed on a basis of an acousto-optic tunable filter (AOTF) that allows imaging of samples in two orthogonal polarization planes simultaneously. Images are registered as a light (e.g. solar one) reflected and scattered from an observed target in the near infrared spectral range. The AOTF's electrical tuning provides fast and flexible spectral scanning of an image through whole the range analyzed – potentially, ten microseconds per a spectral point. Thus, it is possible to explore reflectance spectra of specified areas on a sample and to detect its minerals composition and microstructure variations. In parallel, one can estimate polarization contrast at different wavelengths thanks to the AOTF's birefringence properties.

In this paper we report design and performance of a laboratory prototype for the near-IR spectro-polarimeteric imaging AOTF

system operating in the spectral range from 0.8 to 1.8 μm. Reflectance spectra of some minerals were measured with the spectral resolution of 200 cm-1 (20 nm at 1 μm). When imaging samples the spatial resolution as high as 0.5 mm was reached at the target distance of one meter. It corresponds to 100 by 100 resolving elements on the CCD matrix for each of two polarizations of the reflected light. Such a concept is also being designed for the spectral range from 1.7 to 3.5 μm.

Near-IR imaging spectrometers are optimal for remote and in-situ sensing of planetary surfaces, for discriminating between various minerals, including OH/H2O bearing species (sulfates, silicates, hydroxides and carbonates). One of the applicabilities is the diurnal monitoring of the hydroxyl (OH) absorption line depth in spectra of the lunar surface. Such an experiment may allow estimating diurnal hydration rate on the Moon's surface in order to better understand the hydration mechanism. For Mars it can be renovated spectroscopic studies of surface's minerals and rocks in a vicinity of the spectrometer's sounding. Study of hydrated minerals and other minerals originated from the hydrothermal or aqueous environment is emphasized as well. This subject is currently linked to the search for signs of life on Mars (in the past or in the present). Spectral images in two orthogonal polarizations at different phase angles will help to estimate the polarization contrast and to distinguish grains from several regoliths' species.

Acknowledgements. Co-authors from IKI acknowledge the RSF grant #16-12-10453 for the support in this work.

10423-71, Session PS

Electronic crosstalk impact assessment in the Terra MODIS mid-wave infrared bands

Truman Wilson, Ashish Shrestha, Science Systems and Applications, Inc. (United States); Xiaoxiong J. Xiong, NASA Goddard Space Flight Ctr. (United States)

The Moderate Resolution Imaging Spectroradiometer (MODIS) on board the Terra spacecraft is one of the key instruments in NASA's Earth Observing System. Since 2000, MODIS has collected continuous data in 36 spectral bands ranging in wavelength between 0.4 um and 14.2 um. Since before launch, signal contamination in the form of electronic crosstalk has been observed in many of the MODIS thermal emissive bands, particularly for bands 27-30, a correction for which has been applied to the current Collection 6 algorithm. The mid-wave infrared bands in Terra MODIS, 20-25, also show signs of electronic crosstalk contamination, which can be seen clearly during observations of the Moon. In this paper, we'll present an impact assessment of electronic crosstalk on the mid-wave infrared bands in Terra MODIS. While the contamination levels of the mid-wave bands compared to bands 27-30 are much lower, particularly late in the mission, the impact on the calibrated signal can be clearly observed for some Earth-view scenes. We will also derive correction coefficients from the lunar observations, which can be applied to correct the calibrated radiance in the MODIS Level-1B product. This technique has been highly successful in correcting bands 27-30 in Terra MODIS and band 24 in Aqua MODIS. We will provide an analysis of these results and potential improvements to the MODIS Level-1B product for Terra MODIS.

10423-72, Session PS

Assessment of BRDF effect of Kunlun Mountain glacier on Tibetan Plateau as a potential pseudo-invariant calibration site

Ling Wang, Xiuqing Hu, Lin Chen, China Meteorological Administration (China)

Calibration is a critical step to ensure data quality and to meet the needs of quantitative remote sensing in a broad range of scientific applications. One of the least expensive and increasingly popular methods of on-orbit calibration is the use of pseudo invariant calibration sites (PICS). A spatial homogenous and temporally stable area about 34 km2 in size around the center of Kunlun Mountain (KLM) on Tibetan Plateau (TP) was identified by our previous study, and the spatial and temporal coefficient of variation (CV) related to the first four bands of Moderate Resolution Imaging Spectroradiometer (MODIS) (659 nm, 865 nm, 460 nm and 555 nm) of this region was better than 4%, which is comparable with the CV values of established PICS by the cal/val community. However, the KLM glacier has several advantages over the current established PICS, such as high reflectance and high altitude (>4000 m above sea level). Hence atmospheric effect to the satellite observed top-of-atmosphere (TOA) reflectance can be minimized. In addition to atmospheric effect, the surface bidirectional reflectance distribution function (BRDF) is another major factor must be concerned in the processes of sensor cross-calibration and long-term stability monitoring. The viewing geometries differ from two different sensors or different imaging time. This often implies larger uncertainty due to amplified BRDF effects. To reduce this uncertainty, a good knowledge of the BRDF characteristic should be obtained before applying an effective BRDF correction to the observed TOA reflectance. In this study, the BRDF impacts of KLM glacier on MODIS observed TOA reflectance in the first four bands are examined. The BRDF impact of KLM glacier related to the view zenith angle is studied through using the observations at a fixed solar zenith angle, and the effect related to the sun zenith angle is studied based on the observations collected at the same view angle. Then, two widely used BRDF models are applied to our test data to simulate the variations of TOA reflectance due to the changes in viewing geometry. The first one is Ross-Li model, which consists of two kernel-driven functions combined in a linear equation with coefficients tuned for each surface type. This model has been used to produce the MODIS global BRDF albedo data product. The second one is derived based on in-situ near-surface BRDF measurements for the snow surface in Antarctica. Finally, the accuracy and effectiveness of these two different BRDF models are tested through comparing the simulated TOA reflectance based on the BRDF models with the observed one. Results show that the snow surface BRDF model produces much smaller root mean square error (RMSE) than the kernel-driven BRDF model.

10423-73, Session PS

A global restriction method fused IMU data for spectrum reconstruction of static Fourier transform spectral imager

Chuncheng Zhou, Lingling Ma, Chuanrong Li, Lingli Tang, Yongguang Zhao, Academy of Opto-Electronics, CAS (China)

Static imaging interferometry is an emerging technology increasingly adopted for novel Earth remote sensing instruments. Several static Fourier transform spectral imager has been developed for various scientific applications, such as, LASIS (Large Aperture Static Imaging Spectrometer) developed by Chinese Academy of Sciences, SYSIPHE developed in European cooperation, ALISEO (Aerospace Leap-frog Imaging Stationary Interferometer for Earth Observation) developed by Italian Space Agency. For obtaining a spectral image, a sequence of images are registered, so that the interferogram can be retrieved from all the images of the sequence. The state of the art data process chain is just registering sequence images frame by frame, and doesn't fuse the data of the inertial measurement unit. The registering error of frame by frame could be accumulated up to several pixels, so that the interferogram retrieved from sequence would be distorted and spectral image would be blurred. This paper presents a new data process chain for static Fourier transform spectral imager to conquer this problem.

The precise association of sequence images is the key point

for obtaining a spectral image. Registering sequence images frame by frame ignores the association information of other frames, which leads to miss a global restriction and accumulate registering error. So that, we build upon a pose constraint graph for modeling the association of sequence images. The nodes in the graph represent the unknown platform poses, and the edges express translation constraints between the poses. When available, the data of the inertial measurement unit is used to initialize the pose nodes, otherwise the pose nodes are initialized to unit matrix. A few images among the whole sequence are chosen as keyframes, with an overlap of about three-quarters between two consecutive keyframes. The pairwise association of keyframe by keyframe, keyframe by frame and frame by frame are used to initialize the graph edges. The pose constraint graph forms a global restriction for association of sequence images and eliminates the accumulated error. We optimize the pose constraint graph using the g2o framework, which performs a minimization of a nonlinear error function that can be represented as a graph. Then, we obtain globally optimal platform poses and more precise association of sequence images. Finally, the interferograms are retrieved from all the images of the registered sequence, and the spectrum are computed by a Fourier transformation.

An experiment based on the proposed method is conducted. The sequence images data are acquired from an airborne static Fourier transform spectral imager LASIS developed by Chinese Academy of Sciences. A comparison between the state of the art method and the proposed method is carried out to demonstrate the improvement.

10423-75, Session PS

Assessment of stability of the response versus scan angle for the S-NPP VIIRS reflective solar bands using pseudo-invariant desert and Dome C sites

Aisheng Wu, Science Systems and Applications, Inc. (United States); Xiaoxiong J. Xiong, NASA Goddard Space Flight Ctr. (United States); Changyong Cao, National Environmental Satellite, Data, and Information Service (United States) and National Oceanic and Atmospheric Administration (United States)

The Visible Infrared Imaging Radiometer Suite (VIIRS) on the Suomi NPP (National Polar-orbiting Partnership) satellite has been in operation for five years. VIIRS has 22 bands with a spectral range from 0.4 μm to 12.0 μm. The Earth view swath covers a distance of ~3000 km over scan angles of ± 56.0o off nadir. The on-board calibration of the reflective solar bands (RSB) relies on a solar diffuser (SD) and a solar diffuser stability monitor (SDSM) located at a fixed scan angle. The response versus scan angle (RVS) was characterized prelaunch in ambient conditions and is currently used to determine the on-orbit response for all scan angles relative to the SD scan angle. Since the RVS is vitally important to the quality of calibrated level 1B products, it is important to monitor its on-orbit stability, particularly at the short wavelengths (blue) where the most degradation occurs. In this study, the RVS stability is examined based on reflectance trends collected at various scan angles over the selected pseudo-invariant desert sites in Northern Africa and the Dome C snow site in Antarctica. These trends are corrected by the site dependent BRDF (bi-directional reflectance function) model to reduce seasonally related fluctuations. The BRDF corrected trends are examined so any systematic drifts in the scan angle direction would indicate a potential change in RVS. The results of this study provide useful information on VIIRS RVS on-orbit stability performance.

10423-76, Session PS

Characterization of imaging spectrometers

Valentin Atanassov, Denitsa Borisova, Doyno Petkov, Hristo Lukarski, Space Research and Technology Institute (Bulgaria)

Imaging spectrometers provide high quality data by registering reflected light at high spectral and spatial resolution. At present they are widely recognized as a powerful tool not only for a direct identification of natural scenes but also for an in-depth analysis of their physical and biological components, biochemical processes, the dynamics of their development, etc. To solve successfully these tasks the researchers need spectral data obtained with multispectral and even hyperspectral resolution in ranges which include the ultraviolet (UV), the visible (Vis), the near infrared (NIR), and the short wave infrared (SWIR) regions of the electromagnetic spectrum. As the use of imaging spectrometers in the studies increases, the designers have to deal with strictly requirements towards the parameters and the characteristics of these systems.

The characterization procedures of imaging spectrometers start up with planning and implementing methods for laboratory characterization and foreseen methods for on-board characterization. The characterization methods are critically dependent on the instrument design and construction methods and performance requirements. The on-ground and on-board characterization of the instrument provides coefficients for correction algorithms. The preprocessing of imaging spectrometric data encompasses such procedures. More imaging spectrometer characteristics will be expected to remain constant through instrument life and can be characterized in laboratory condition, while others will be expected to change during the operating mode and these must be characterized on-board.

In the paper are highlight the characteristics which are expected to be considered critical for instruments performance:

- spatial characterization – spatial resolution, FOV (Field of View), IFOV (Instantaneous Field of View), MTF (Modulation Transfer Function);

- spectral characterization - spectral response function, spectral dispersion function, spectral resolution (channel bandwidth FWHM, pixel dispersion, spectral sampling interval;

- radiometric characterization - the dark current levels variation for each pixel, spectral response function, spectral sensitivity, linearity of response function, pixel response nonuniformity, SNR (Signal to Noise Ratio).

The basic steps for characterization of imaging spectrometer are indicated in the flow diagrams. The characterization methods and correspondence correction procedures are determined in detail on the basis of error analyses. The frequency of characterization processes and algorithm update will vary with rate of errors change.

10423-77, Session PS

Removal of instrument artefacts by harmonisation of hyperspectral sensor data from multiple detectors

Tim H. Hultberg, Thomas August, EUMETSAT (Germany)

IASI has 4 different detectors, CrIS has 9, IASI-NG will have 16 and MTG-IRS 25600. There is a clear interest to harmonise the sensor data originating from different detectors, if it can be done be removing the parts of the instrument artefacts, which does not manifest itself in common directions for all detectors.

When IASI spectra are analysed in principal component (PC) score space, differences between the four detectors are clearly observed. These differences are caused by different characteristics and different strengths of the ghost effect among the detectors and although they are small when

analysed in radiance space, they can have a distinct negative impact. Considering that a large part of the operationally disseminated IASI PC scores are dominated by instrument artefacts, the partial removal of instrument artefacts is also of interest for data compression purposes.

The instrument artefacts can be partly removed by projection onto a subspace common to all detectors. We show how the techniques of canonical angles can be used to compute a set of orthogonal vectors capturing only directions which are close to directions found in the signal spaces of all detectors. This principle can also be applied to detectors on-board different satellites, as we demonstrate with the example of IASI-A and IASI-B.

The danger of the method is that a single deficient detector, 'blind' to one or more directions of the atmospheric signal, could potentially 'contaminate' the data from the other detectors. We discuss how to detect and avoid this problem and check it in practice with CrIS data.

10423-78, Session PS

Recent ground-based testing of the NAST-I airborne interferometer

Allen M. Larar, NASA Langley Research Ctr. (United States); Luc Rochette, LR Tech Inc. (Canada); Anna M. Noe, Daniel K. Zhou, Xu Liu, NASA Langley Research Ctr. (United States); Bill Smith, Science Systems and Applications, Inc. (United States)

The NASA Langley Research Center (LaRC) National Airborne Sounder Testbed – Interferometer (NAST-I) is a cross-track scanning Fourier Transform Spectrometer system that is frequently deployed aboard NASA high-altitude aircraft as a key payload in support of validation and airborne science field campaigns. This presentation addresses recent ground-based testing activities focusing on calibration and characterization of system performance and implications toward airborne field campaign flights.

10423-80, Session PS

Development of a computationally efficient algorithm for attitude estimation of a remote sensing satellite

Javad Haghshenas, Amir Labibian, Satellite Research Institute (Iran, Islamic Republic of); Amir Hossein Bahrami, Amirkabir Univ. of Technology (Iran, Islamic Republic of)

Fine pointing and stability accuracies are among the important mission requirements of complex remote sensing satellites in which high resolution cameras are utilized. In order to meet the mentioned requirements, multiple Attitude Determination (AD) sensors and strong processors for data fusion purposes are used. On the other hand, one of the major issues in design of remote sensing satellites is computation load of Attitude Determination and Control Subsystem (ADCS) algorithms. Specifically, the most complex ones are attitude determination (AD) algorithms which are used in different mission modes.

Basic sensor data fusion methods employ all measurements at each sampling time and apply them in AD algorithms at the same time. Therefore, in complex remote sensing satellites which use different AD sensors, the dimension of propagation matrices increase and gain matrix calculation in Extended Kalman Filter (EKF) structure is computationally expensive. Reducing AD computation burden using processors with medium computational load is one of the main goals in this research. Regarding to this matter, fine AD mode of a remote sensing satellite using magnetometer, sun sensor, star tracker and precession gyroscope is implemented via Multiplicative EKF (MEKF) in which quaternion normalization is considered.

Flexible solar panels usually are included in remote sensing satellites and modeling of their dynamics in attitude propagation causes noticeable uncertainties. In order to avoid this problem, instead of using dynamical model, gyro data are directly utilized in the propagation part of the filter. In addition, it decreases computational load in the filter structure.

Measurements of all sensors including magnetometer, sun sensors and star trackers are used in propagation part of EKF. Therefore, filter gain computation using all of the measurements simultaneously and at each sampling time requires inverting a 3n?3n matrix. Since, sampling time of sensors are different, their data are utilized in propagation part individually. Consequently, taking an inverse of a 3n?3n matrix reduces to taking an inverse of a 3?3 matrix. However, regarding to the number of sensors, gain propagation part of EKF is iterated at each sample time. This type of utilization of sensors data in EKF structure is called Murrell's version. In this paper, using an ARM Cortex M4 onboard computer, basic EKF and MEKF are implemented and their performance compared.

Moreover, in order to obtain high accuracies for AD and jitter control in remote sensing satellites, gyro calibration is required. In this paper, the process of gyro calibration and determining main gyro parameters, e.g. scale factor, misalignments matrix and biases, are presented.

10423-81, Session PS

Real-time attitude independent magnetometer calibration method in a high-resolution remote sensing CubeSat

Javad Haghshenas, Amir Labibian, Satellite Research Institute (Iran, Islamic Republic of); Amir Hossein Bahrami, Amirkabir Univ. of Technology (Iran, Islamic Republic of)

One of the major constraints in CubeSats is size constraint. However, nowadays, using modern technology and miniaturization of electronic components/equipment in CubeSats, high imaging accuracies are attainable. In order to meet mass, size and cost requirements in design of satellites, low cost sensors are used in Attitude Determination and Control Subsystem (ADCS). Specifically, magnetometers, gyroscopes and sun sensors are appropriate sensors which can be utilized for Attitude Determination (AD) purposes.

Moreover, in eclipse conditions, only gyros and magnetometer are the sensors whose data are available and can be employed for AD. On the other hand, regarding to the size constraints of CubeSats, magnetic torquers and magnetometers could not be located in sufficient distances from each other. In addition, Electromagnetic Interference (EMI) disturbs magnetometer data and AD of high resolution remote sensing satellites with accuracies better than 1 deg would be practically impossible. Real-time calibration of magnetometers is a practical solution to recover disturbed data and make precise AD possible.

In this paper, a real-time attitude independent magnetometer calibration algorithm is presented. All of the calibration parameters, such as scale factor, bias and misalignment matrix are determined via the mentioned algorithm. Moreover, an Extended Kalman Filter (EKF) which uses gyro and magnetometer measurements are implemented to achieve attitude estimation accuracies better than 1 deg.

Majority of magnetometer calibration systems employ offline methods in which batch estimation algorithms are used. By transposing terms in magnetometer measurement equations, magnetometer calibration would be independent to attitude. This method results to a cost function which is quartic in bias terms. Next, with the centering approach it is converted to a quadratic form and approximate linear solution.

Real-time calibration algorithms usually implemented by two methods: sequential and filtering. Unlike sequential methods, filtering methods can be used to directly determine calibration parameters. In this regard, an EKF structure is implemented in this paper for real-time determination of calibration parameters. These parameters in calibration of magnetometer include scale factor, misalignment matrix and bias as well. The

structure of EKF is kinematic approach in which gyro data are utilized in satellite kinematic model. In this approach, accurate gyro data are employed and uncertainties in determination of moment of inertia matrix and disturbance torques are avoided. In addition, calibrated magnetometer and sun sensor data are utilized as measurements in the EKF.

The simulation results show that using uncalibrated magnetometer data, the accuracy of attitude estimation is approximately 4 deg. However, with real-time calibrated magnetometer data in filter structure, the attitude estimation error is less than 1 deg even in conditions in which satellite is in eclipse and sun sensors data are unavailable.

10423-82, Session PS

Modular design of electrical power subsystem for a remote sensing satellite

Javad Haghshenas, Ehsan Kosari, Satellite Research Institute (Iran, Islamic Republic of); Sajjad Ghazzanfarinia, Satellite Systems Research Institute (Iran, Islamic Republic of); Mahboobeh Hosseingholi, Material and Energy Research Ctr. (Iran, Islamic Republic of)

Power Supply is one of the most important subjects in Remote Sensing satellite. Having an appropriate and adequate power resources, A Remote Sensing satellite may utilize more complex Payloads and also make them more operable in orbit and mission timeline. This paper is deals with a design of electrical power supply subsystem (EPS) of a hypothetical satellite with remote sensing mission in Low Earth Orbits, without any restriction on the type and number of Payloads and only assuming a constraint on the total power consumption of them. EPS design is in a way that can supply the platform consumption to support Mission and Payload(s) requirements beside the power consumption of the payload(s). The design is also modular, as it can be used not only for the hypothetical system, but also for the other systems with similar architecture and even more needs on power and differences in some specifications. Therefore, a modularity scope is assumed in design of this subsystem, in order to support the satellite in the circular orbits with altitude of 500 to 700 km and inclination of 98 degrees, a sun-synchronous orbit, where one can say the design is applicable to a large range of remote sensing satellites. Design process will be started by high level and system requirements analysis, continued by choosing the best approach for design and implementation based on system specification and mission. After EPS sizing, the specifications of elements are defined to get the performance needed during operation phases; the blocks and sub-blocks are introduced and details of their design and performance analysis are presented; and the modularity is verified using calculations for the confined area based on design parameters and evaluated by STK software analysis results. All of the process is coded in MATLAB software and comprehensive graphs are generated to demonstrate the capabilities and performance. The code and graphs are developed in such a way to completely review the design procedure and system efficiency in worst case of power consumption scenario at the beginning and end of satellite life.

10423-33, Session 9

Multiyear on-orbit calibration and performance of S-NPP VIIRS *(Invited Paper)*

Xiaoxiong J. Xiong, NASA Goddard Space Flight Ctr. (United States); Ning Lei, Zhipeng Wang, Vincent Chiang, Science Systems and Applications, Inc. (United States); James J. Butler, NASA Goddard Space Flight Ctr. (United States)

The first Visible Infrared Imaging Radiometer Suite (VIIRS) on-board the Suomi National Polar-orbiting Partnership (S-NPP) has successfully operated for more than 5 years since its launch in October, 2011. The VIIRS observations are made in 22 spectral bands, covering wavelengths from 0.4 to 12.4 microns. 7 of the 22 spectral bands are capable of making measurements in both high and low gains. The VIIRS sensor also includes a day/night band (DNB) that can make observations covering almost 7 orders of magnitude in its dynamic range. Its reflective solar bands (RSB) are calibrated each orbit by a solar diffuser (SD), coupled with a solar diffuser stability monitor (SDSM) to track on-orbit changes in SD reflectance properties. The thermal emissive bands (TEB) are calibrated on a scan-by-scan basis using an on-board blackbody (BB). In addition to the on-board calibrators, regularly scheduled lunar observations are made to support its RSB calibration. We provide in this paper an overview of the S-NPP VIIRS on-orbit calibration activities and methodologies, including latest improvements applied to derive its mission consistent calibration look-up tables (LUTs) in support of sensor level 1B (L1B) data (re)processing performed at the NASA Science Investigator-led Processing Systems (SIPS). We also illustrate instrument multiyear on-orbit performance using examples derived from its OBC and lunar observations. Lessons learned from S-NPP operation and calibration are discussed and considered for future improvements and applications to the upcoming JPSS-1 VIIRS on-orbit calibration.

10423-34, Session 9

SNPP VIIRS reflective solar bands on-orbit calibration using the Moon

Junqiang Sun, Global Science & Technology, Inc. (United States); Menghua Wang, National Oceanic and Atmospheric Administration (United States)

The Visible Infrared Imaging Radiometer Suite (VIIRS) onboard the Suomi National Polar-orbiting Partnership (SNPP) spacecraft has been on orbit for more than five years. It has been scheduled to view the moon approximately monthly since its nadir door open on November 21, 2011. The scheduled lunar observations have been used to monitor the VIIRS reflective solar bands (RSB) on-orbit gain changes. The VIIRS RSB are primarily calibrated by an onboard Solar Diffuser (SD) panel and an accompanying Solar Diffuser Stability Monitor (SDSM). Due to non-uniformity of the SD degradation, the SD/SDSM calibration may have non-negligible errors, especially for the short wavelength bands. Since lunar surface is very stable, the Moon can be used to provide more reliable on-orbit long-term gain changes of the RSB. The RSB calibration coefficients derived from the lunar calibration are generally consistent with those derived from the SD/SDSM calibration, but clear differences in trend are seen, especially for the short wavelength bands.

10423-35, Session 9

Sentinel-2B geometric image quality commissioning phase results and Sentinel2 constellation performances

Florie Languille, Angélique Gaudel-Vacaresse, Bruno Vidal, Renaud Binet, Ctr. National d'Études Spatiales (France); Vincent Poulain, Thales Services (France); Thierry L. Trémas, Ctr. National d'Études Spatiales (France)

In the frame of the Copernicus program of the European Commission, Sentinel-2 is a constellation of 2 satellites on a polar sun-synchronous orbit with a revisit time of 5 days (with both satellites), a high field of view - 290km, 13 spectral bands in visible and shortwave infrared, and high spatial resolution - 10m, 20m and 60m. The Sentinel-2 mission offers a global coverage over terrestrial surfaces. The satellites acquire systematically terrestrial surfaces under the same viewing

conditions in order to have temporal images stacks. The first satellite was launched in June 2015 and the second in March 2017.

In cooperation with the European Space Agency (ESA), the French space agency (CNES) is in charge of the image quality of the project, and so ensured the CAL/VAL commissioning phase during the months following the launch. This cooperation is also extended to routine phase as CNES supports European Space Research Institute (ESRIN) and the Sentinel-2 Mission performance Centre (MPC) for validation in geometric and radiometric image quality aspects, and in Sentinel-2 Global Reference Image (GRI) geolocation performance assessment.

This paper points on geometric image quality on Sentinel-2B commissioning phase. It relates to the methods and the performances obtained, as well as the comparison between S2A and S2B. This deals with geolocation and multispectral registration. A small focus is also done on the Sentinel-2 GRI which is a set of S2A images at 10m resolution covering the whole world with a good and consistent geolocation. This ground reference leads to ensure an accurate multi-temporal registration -on refined Sentinel-2 products over GRI- which is also presented in this paper.

10423-36, Session 9

Near-nadir scan overlap in Earth observations from VIIRS and MODIS

Slawomir Blonski, ERT, Inc. (United States); Changyong Cao, NOAA/NESDIS/STAR (United States)

Satellite multi-detector cross-track scanners, such as MODIS (Moderate Resolution Imaging Spectroradiometer) and VIIRS (Visible-Infrared Imaging Radiometer Suite), require synchronization of optical and orbital characteristics to avoid gaps in Earth coverage between scans. Prelaunch tests have revealed that such scan-to-scan gaps will occur near nadir in VIIRS observations from the future JPSS-1 (Joint Polar Satellite System) and JPSS-2 satellites. Our analysis of VIIRS geolocation products show that the gaps do not occur for the instrument currently on orbit onboard the S-NPP (Suomi National Polar-orbiting Partnership) spacecraft. When the same analysis is applied to the MODIS data products, it reveals that the small, near-nadir gaps exist in MODIS observations from both Aqua and Terra satellites.

For Terra MODIS, the gaps occur between latitudes of 20°S and 50°N, with maximum value of approximately 100 m at 15°N. These gaps appear to be similar to the ones currently predicted for the JPSS-1 and JPSS-2 VIIRS. For Aqua MODIS, the gaps occur every other scan north of the 30°S parallel with the maximum value of approximately 150 m at 15°N. For the other scans, the extent and the maximum value of the gaps are smaller: 5°S to 35°N and ~50 m. While use of the terrain-corrected geolocation data adds some uncertainty to these analyses, the results are very consistent over time: scan-to-scan gaps have existed in MODIS data near nadir since the beginning of the Terra and Aqua missions. Some month-to-month variation in scan overlap can be seen due to satellite orbit precession, but this mostly creates 10-20 m scan overlap differences between the ascending and descending parts of the orbits. The 100-m asymmetry in the overlap between the alternating scans for Aqua MODIS indicates a misalignment of the scan mirror sides. Similar, but smaller (~50 m), difference exists for the S-NPP VIIRS scan overlap indicating a misalignment of the half-angle mirror sides.

A model that uses S-NPP orbit data in ECEF (Earth-centered, Earth fixed) coordinates, as well as the current VIIRS telescope focal length and scan rate, predicts the overlap that agrees very well with the analysis of the geolocation data. For JPSS-1/-2 VIIRS focal length and scan rate, the model predicts scan overlap gaps of more than 100 m. Although magnitude of the MODIS scan overlap gaps (up to 100 m for Terra and 50/150 m for Aqua) is quite small in comparison to the 1-km pixels, it is rather significant for the bands with the 250-m and 500-m pixels. Despite the size of the gaps, it appears that their effects on scientific analyses (e.g., NDVI) have not been reported since launch of the MODIS instruments. Because the gaps currently predicted for the JPSS-1 and -2 VIIRS are similar to the one occurring for MODIS, one can expect that their effects on science data will be similarly negligible. With a shorter telescope focal length and a faster scan rate than for the JPSS-1/-2 VIIRS, the scan overlap gaps are expected to be avoided altogether for VIIRS on the future JPSS-3 and -4 satellites.

10423-37, Session 10

Lunar calibration improvements for the short-wave infrared bands in Aqua and Terra MODIS

Truman Wilson, Amit Angal, Ashish Shrestha, Science Systems and Applications, Inc. (United States); Xiaoxiong J. Xiong, NASA Goddard Space Flight Ctr. (United States)

The Moderate Resolution Imaging Spectroradiometer (MODIS) is one of the key sensors among a suite of remote sensing instruments on-board the Terra and Aqua spacecraft. Since the beginning of each mission, regularly scheduled lunar observations have been used in order to track the on-orbit gain changes of the reflective solar bands. However, for the short-wave infrared bands, 5-7 and 26, the measured signal is contaminated by both electronic crosstalk and an out-of-band response due to transmission through the MODIS filters at undesired wavelengths. These contaminating signals cause significant oscillations in the derived gain from lunar observations for these bands, which limits their use in determining the scan mirror response versus scan angle at these wavelengths. In this paper, we show a strategy for correcting this contaminating signal using both lunar observations and nighttime observations, where the magnitude and the source of the contaminating signal is clear. This approach uses a similar strategy as for the successful correction of bands 27-30 in Terra MODIS Collection 6 in order to derive correction coefficients for the electronic component of the contamination from lunar observations. To determine the magnitude of the optical contamination, nighttime observations are used in order to limit the size of the reflective band signals. The combination of these contamination corrections should greatly improve the lunar calibration result for these bands. We will present the impact of these corrections on the MODIS RSB calibration for these bands.

10423-38, Session 10

Aqua MODIS electronic crosstalk survey from Moon observations

Graziela R. Keller, Zhipeng Wang, Aisheng Wu, Science Systems and Applications, Inc. (United States); Xiaoxiong J. Xiong, NASA Goddard Space Flight Ctr. (United States)

The Moderate Resolution Imaging Spectroradiometers, or MODIS, on board the Terra and Aqua low-orbit satellites, launched on 1999 and 2002, respectively, are cross-track scanners that image the Earth in 16 thermal emissive and 20 reflective solar bands. They are heritage Earth observing sensors that require very accurate and stable calibration and carry a suite of on-board calibrators used to derive the calibration coefficients on-orbit and to assess sensor stability. These measurements are complemented by Moon observations during scheduled lunar roll maneuvers, when the Moon is viewed through the space view port. A sector rotation operation causes the images to be stored in the earth view data sector instead, where the Moon appears in several consecutive scans, co-registered in all bands. The images of the lunar disk registered by the consecutive scans overlap, making it possible to create images of the entire Moon using single detectors.

Signatures of electronic crosstalk contamination between detectors from bands belonging to the same focal plane

assembly are clearly seen in Aqua MODIS single detector Moon images from bands 20 to 30 (3.66 – 9.88 and 1.36 – 1.39 microns), obtained during these scheduled lunar events. Electronic crosstalk can potentially impact the Level 1B products, causing image artifacts such as striping. The severity of such artifacts will depend not only on the absolute value of the signal leak and how it compares to the flux levels in the receiving image, but also on the ability of the calibration coefficients in absorbing the contamination. When the sending and receiving bands are close enough in wavelength that their images show similar patterns, the calibration will lessen the impact on the product more than when bands displaying contrasting images contaminate one another. The latter is the case of the receiving band 24, which is a thermal emissive band, contaminated with signal coming from band 26, a reflective solar band. Band 24 L1B images display bright detector 1 strips that were characterized, described, and corrected by us in Keller et al. 2017.

In the present paper, we map the crosstalk signatures in single detector Moon images from bands 20 to 30, back to their respective sending bands and detectors. This is done by determining the displacement between the lunar disk in the receiving band single detector images and the crosstalk ghosts, in both the track and the along-scan directions. The displacement in the track direction is related to the distance between the sending and the receiving detectors and the displacement in the along-scan direction corresponds to the distance between the sending and receiving bands in the focal plane assembly. Here, we assume that the electronic crosstalk contamination is proportional to the signal of the sending band/detector combination and we derive linear crosstalk coefficients for all the bands/detectors concerned, from the single detector lunar images, for the entire mission. These are then applied in the correction of L1A Earth and calibration data, which can then be used to generate new calibration coefficients and corrected L1B images. Finally, we assess the impact the contaminations have on the L1B product.

10423-39, Session 10

Crosstalk effect and its mitigation in MODIS and VIIRS thermal emissive bands

Junqiang Sun, National Oceanic and Atmospheric Administration (United States) and Global Science and Technology, Inc. (United States); Menghua Wang, National Oceanic and Atmospheric Administration (United States)

It has been found that there is severe electronic noise in the Terra Moderate Resolution Imaging Spectroradiometer (MODIS) bands 27-30 which corresponds to wavelengths ranging between 6.7 ?m to 9.73 ?m. The cause for the issue has been identified to be crosstalk, which is significantly amplified since 2010 due to severe degradation in the electronic circuitry. The crosstalk effect causes unexpected discontinuity/change in the calibration coefficients and induces strong striping artifacts in the earth view (EV) images. Also it is noticed, that there are large long-term drifts in the EV brightness temperature (BT) in these bands. An algorithm using a linear approximation derived from on-orbit lunar observations has been developed to correct the crosstalk effect for them. It was demonstrated that the crosstalk correction can remarkably minimize the discontinuity/change in the calibration coefficients, substantially reduce the striping in the EV images, and significantly remove the long-term drift in the EV BT in all these bands. In this paper, we present the recent progresses in the crosstalk effect analysis and its mitigation. In addition, we will show that besides these four bands, the TEBs in Aqua MODIS and Suomi National Polar-orbiting Partnership (SNPP) Visible Infrared Imaging Radiometer Suite also have significant crosstalk contaminations. Further, it will be demonstrated that the crosstalk correction algorithm we developed can be successfully applied to all the contaminated TEBs to significantly reduce the crosstalk effects and substantially improve both the image quality and the radiometric accuracy of Level-1B (L1B) products for the bands.

10423-40, Session 10

Suomi NPP VIIRS solar diffuser screen transmittance model and its applications

Ning Lei, Science Systems and Applications, Inc. (United States); Xiaoxiong J. Xiong, NASA Goddard Space Flight Ctr. (United States); Jeff McIntire, Science Systems and Applications (United States)

The Visible Infrared Imaging Radiometer Suite (VIIRS) on the Suomi National Polar-orbiting Partnership satellite calibrates its reflective solar bands through observations of a sunlit solar diffuser (SD) panel. Sunlight goes through a perforated plate, denoted as the SD screen, before strikes the SD. It is critical to know whether the prelaunch measured SD screen transmittance is correct right after the measurement. During the measurement, misalignment of the SD panel and the apparatus could lead to significant errors in the given transmittance. We develop a mathematical model to describe the transmittance as a function of the angles that the incident light makes with the SD screen, and apply the model to fit the prelaunch measured transmittance. The fit results reveal that the measured transmittance does not follow the model unless the size of the hole on the SD screen is significantly different from the design value. We attribute the reason to be the orientation alignment errors for the SD panel and the apparatus during the prelaunch measurement. We model the alignment errors and apply our transmittance model to fit the prelaunch transmittance to retrieve the “true” transmittance. To use the model correctly, we examine the effect of the finite source size on the transmittance. We further examine the difference between the product of the retrieved transmittance and the prelaunch SD BRDF value and the one measured from on-orbit data to determine whether the prelaunch SD BRDF value is correct.

10423-41, Session 10

The positional dependence of the SNPP VIIRS SD BRDF degradation factor

Ning Lei, Science Systems and Applications, Inc. (United States); Xuexia Chen, Tiejun Chang, Science Systems and Applications (United States); Xiaoxiong Xiong, NASA Goddard Space Flight Center (United States)

The Earth-observing Visible Infrared Imaging Radiometer Suite (VIIRS) on the Suomi National Polar-orbiting Partnership satellite regularly performs on-orbit radiometric calibration of its reflective solar bands primarily through observations of an onboard sunlit solar diffuser (SD). The on-orbit change of the SD bidirectional reflectance distribution function (BRDF) value is determined by the onboard solar diffuser stability monitor. It has been observed that the BRDF value decreases over time. The decrease is quantified by a numerical factor denoted as the BRDF degradation factor. We showed previously that the degradation factor is solar angle and detection direction dependent. In this study, we determine the positional dependence of the SD BRDF degradation factor and access its impact on calibration quality.

10423-42, Session 11

Assessment of MODIS reflective solar bands calibration stability

Xiaoxiong J. Xiong, NASA Goddard Space Flight Ctr. (United States); Amit Angal, Dan Link, Aisheng Wu, Science Systems and Applications, Inc. (United States)

This paper provides an assessment of MODIS reflective solar bands (RSB) calibration stability over both short- and long-term timescales. The MODIS RSB, with center wavelengths varying from 0.41 to 2.2 micron, are calibrated by an on-board

solar diffuser (SD) and a solar diffuser stability monitor (SDSM). The SD calibration can be performed each orbit but only during a short period when the SD is fully illuminated as the spacecraft moves across its day/nighttime terminator. In addition to SD/SDSM calibration system, the MODIS instrument carries a unique spectroradiometric calibration assembly (SRCA), which is equipped with internal light sources (e.g., lamps within an integration sphere) that can support on-orbit radiometric stability monitoring. Since their respective launches, Terra and Aqua MODIS continue to operate for over 17 and 15 years and it is not surprising that their detector gains (or responses) have experienced changes. These changes are spectral-band dependent with the largest changes occurring at the shortest wavelengths. On a regular basis, MODIS RSB detector gains are calibrated using on-board SD/SDSM and lunar observations. Calibration look-up tables (LUTs) are derived and updated to support generation of consistent Level 1B (L1B) data products. In this study, we carefully select and analyze data collected from the on-board SD and SRCA to evaluate MODIS RSB short-term calibration stability. Using L1B data collected over pseudo-invariant calibration targets, we also assess the RSB long-term calibration stability.

10423-43, Session 11

The use of deep convective clouds to uniformly intercalibrate the next generation of geostationary reflected solar imagers

David R. Doelling, NASA Langley Research Ctr. (United States); Rajendra Bhatt, Benjamin R. Scarino, Arun Gopalan, Science Systems and Applications, Inc. (United States)

The CERES project has been providing shortwave and longwave fluxes for climate monitoring and studies over the last 17 years. The CERES instrument is on multiple platforms including the Terra, Aqua, NPP and the future JPSS-1 satellites. The satellites also contain the MODIS and VIIRS imagers. The associated imager cloud retrievals are used to select the scene conditions needed to convert the CERES radiances into fluxes. CERES also utilizes geostationary imager radiances to retrieve both clouds and derived broadband fluxes. The next generation of geostationary imagers will have many reflected solar channels similar to the VIIRS imager. The next generation of geostationary imagers have the potential for MODIS quality cloud retrievals from geostationary satellites. In order to derive a consistent cloud and flux product designed for climate studies, the geostationary, MODIS and VIIRS imagers must be uniformly calibrated both in time and space.

The CERES calibration team currently calibrates the geostationary imager constellation using all-sky ocean and deep convective cloud (DCC) ray-matching techniques and also uses invariant Earth DCC and desert targets. DCC are successfully used to calibrate visible imager radiances for wavelengths less than 1 μm. For wavelengths greater than 1 μm, the DCC reflectance is also a function of the DCC micro-physics. Lately, the CERES team has been refining the DCC calibration algorithm to the shortwave infrared (SWIR) bands for MODIS and VIIRS as well as the next generation geostationary Himawari-8 imager. The DCC clouds have the advantage of being located at the top of troposphere, where the impact of water vapor absorption is minimal. Since DCC are located over every satellite domain, they can be used to uniformly calibrate all sensor used by CERES by using either invariant Earth target or ray-matching inter-calibration algorithms. Results from the DCC calibration techniques applicable to the next generation geostationary imagers will be highlighted at the conference.

10423-44, Session 11

A comparison of validation and vicarious calibration of high and medium resolution satellite-borne sensors using RadCalNet

Andrew C. Banks, Samuel E. Hunt, Javier Gorroño, Tracy Scanlon, Emma R Woolliams, Nigel P Fox, National Physical Lab. (United Kingdom)

The Radiometric Calibration Network (RadCalNet, www.radcalnet.org) routinely brings together data from several instrumented ground sites to provide users with top-of-atmosphere reflectance data. These data are provided on cloud free days between 09:00 and 15:00 local time and between 400 nm and 1000 nm at a 10 nm spectral resolution, although the range can extend up to 2500 nm depending on available instrumentation. The data represents the nadir view of the ground and covers an area on the ground of between 50 m and 1 km. The smaller spatial coverage sites cannot be utilized effectively for the vicarious calibration of medium resolution sensors (> 250 m spatial resolution), due to the limited number of pixels available over each site. However, the RadCalNet data from the 1km spatial coverage site of Railroad Valley (RRV) in Nevada is potentially applicable to vicariously calibrate medium as well as high resolution sensors (≤ 30 m).

It is proposed here that a high and medium resolution sensor are utilised to compare and cross-validate the vicarious calibration using RadCalNet-RRV, in particular assessing the differences in the calibration coefficients at the same wavelengths. Essentially, this means viewing the RadCalNet site with a high resolution sensor that has previously been assessed in detail against RadCalNet, determining the associated calibration coefficients, then viewing the same site under near-simultaneous conditions with the medium resolution sensor and comparing calibrations.

The methodology can be seen in more detail in Figure 1. From this flow diagram it is evident that as part of the implementation of the method a major effort has been made in focusing on the differences between the high and medium resolution sensors in terms of spectral, spatial and temporal data acquisition characteristics. For both sensors it was important to derive an uncertainty analysis for each of these procedural steps and differences in order to allow an accurate comparison. This uncertainty analysis includes uncertainty contributors such as those associated with the satellite-borne sensors themselves, where pre-flight calibration and level-1 top-of-atmosphere uncertainties are included at a per-pixel level. The uncertainty evaluation also then goes on to include other contributors such as temporal differences between overpasses, different viewing angles, and calculation of the spectral band adjustment factors.

In the case study presented here, results are shown for the Sentinel-2 MultiSpectral Instrument (S2-MSI) as the high resolution sensor, having been assessed extensively against RadCalNet in previous work, and the Sentinel-3 Ocean and Land Colour Instrument (S3-OLCI) as the medium resolution sensor. The initial results show the potential for RadCalNet to be used to validate and vicariously calibrate data from both high and medium resolution sensors. Furthermore, the cross-validation between high and medium resolution sensors gives further information regarding the potential for RadCalNet to provide an accurate vicarious calibration of medium resolution sensors like OLCI. These implications are discussed in the context of the design of RadCalNet and terrestrial vicarious calibration sites in general.

10423-45, Session 11

Ground comparisons at RadCalNet sites to determine the equivalence of sites within the network

Tracy Scanlon, Claire L. Greenwell, National Physical Lab. (United Kingdom); Jeffrey S. Czapla-Myers, Nikolaus J. Anderson, College of Optical Sciences, The Univ. of Arizona (United States); Teresa M. Goodman, National Physical Lab. (United Kingdom); Kurtis J. Thome, NASA Goddard Space Flight Ctr. (United States); Emma Wolliams, National Physical Lab. (United Kingdom); Geiland Porrovecchio, Petr Lindu?ka, Marek ?míd, Czech Metrology Institute (Czech Republic); Nigel Fox, National Physical Lab. (United Kingdom)

The Radiometric Calibration Network (RadCalNet, www.radcalnet.org) routinely brings together data from several instrumented ground sites to provide users with TOA reflectance data. These data are provided on cloud free days between 09:00 and 15:00 between 400 and 1000 nm (and up to 2500 nm depending on available instrumentation) at a 10 nm spectral resolution at nadir.

In order to ensure that the different sites operating within RadCalNet are consistent, core metrological principles are applied through peer review of uncertainty analysis and through comparisons. Comparisons of instrumentation measuring ground radiance at each of the sites is being undertaken throughout 2017. The comparisons consist of viewing the ground with the site instrumentation and a travelling transfer radiometer (TR) or spectrometer and comparing the radiance results. These comparisons may be extended to TOA reflectance in the future, however this requires many assumptions and data processing which will introduce additional uncertainties which will affect the accuracy of the comparisons.

The TR(s) utilised for the comparison must be able to measure the target (which may be the ground or an artificial target such as a tarpaulin or reference Lambertian panel) at the same time as the instrument under test. In addition, the TR(s) must have a better performance (higher stability, lower uncertainty) than the instrument under test and be able to provide information in the same spectral regions as the instrument under test.

In addition to practical considerations, set of criteria on the instrument design have been defined by the University of Arizona (UOA) and NASA GSFC: Signal to noise ratio (SNR) should be > 1000, linearity error should be < 0.25 %, spatial stray light should be < 1 %, long-term (months) repeatability variation should be < 2 %, dark current variation should be < 0.001 x expected signal and spectral stray light should be < 0.5 %. It is particularly important that adherence to these criteria can be demonstrated as the use of the instrument in the field environment will result in additional uncertainties between even coincident measurements.

Two TRs have been developed for use with RadCalNet: the Multispectral Transfer Radiometer (MuSTR) designed and built by CMI for NPL and the CaTSSITTR instrument designed and built by the University of Arizona, with one of the two instruments built now owned by NASA GSFC. This presentation will discuss the design of each instrument and comparison results from the laboratory and at RadCalNet sites.

MuSTR consists of a handheld dust-proof enclosure with two array spectrometers, two entrance optics, and a tablet computer for data acquisition and post processing. One spectrometer covers the spectral range 280 nm to 900 nm (0.5 nm resolution) while a second spectrometer (NIR) covers 800 nm to 1700 nm (2 nm resolution).

CaTSSITTR is a filter radiometer with 7 channels in the visible range matching the channels of the radiometers currently deployed at the Railroad Valley RadCalNet site. The instrument is provided with a tripod and is operated using an iPod touch.

Comparisons of these instruments has been undertaken in the laboratory and in a field environment. Both have been tested at the Railroad Valley site to allow comparison to the in-situ radiometers.

10423-46, Session 11

Assessment of polarization correction impact on the calibration of Terra MODIS reflective solar bands

Aisheng Wu, Amit Angal, Xu Geng, Science Systems and Applications, Inc. (United States); Xiaoxiong J. Xiong, NASA Goddard Space Flight Ctr. (United States)

The Moderate-Resolution Imaging Spectroradiometer (MODIS), launched in 1999 on Terra and 2002 on Aqua spacecraft respectively, is a scanning radiometer that covers a wavelength range from 0.4 μm to 14.4 μm and scans the Earth over an angular range from -55o to +55o. After a few years in the Terra mission, it became extremely challenging to characterize the changes in the sensor gain and response versus scan angle (RVS) at short wavelengths due to significant degradation and increased polarization sensitivity. To better characterize the system-level degradation, the MODIS Characterization Support Team (MCST) developed an enhanced approach in Collection-6 (C6) L1B algorithm by supplementing the on-board calibration data with the Earth-scene response trends at various scan angles obtained from the pseudo-invariant desert sites. However, the trends at short wavelengths experienced significant impact due to the increased polarization sensitivity, especially at the end of scan. In this study, a polarization correction algorithm developed by MCST is applied to the Terra MODIS RSB response trends obtained from the desert sites. The trends after polarization correction are used to derive the gain and RVS based on the existing MODIS C6 calibration algorithm. Impact of the polarization correction is examined for gain, RVS and their fitting uncertainties over the entire mission. The results of this study provide useful information on how to further improve accuracy and stability of the calibrated L1B product.

10423-47, Session 12

Microsat camera with high resolution and wide FoV

Roland Geyl, Safran Reosc (France)

Safran Reosc is European leader in high performance optics for advanced earth observation, science and wheather forecast applications. Safran Electronics & Defense hold decades of experience in optronics instrument development for defense applications as well as advance image processing solutions. The market of earth observation with microsats is still in a maturation phase and is still lacking high performance camera equipment for professional applications on-board nano-micro-minisatellites. Safran is now developing such space camera offering 6° wide field of view and 10-m class high resolution adapted to variety of civil applications. We offer this 'SPOT-1 in a shoe-box' camera with multi/hyperspectral and image processing capability to the microsat community as an advanced, high performance, modular COTS product.

10423-48, Session 12

Sentinel-5/UVNS: Instrument:

The principle ability of a slit homogenizer to reduce scene contrast for earth observation spectrometer

Christian Meister, Corneli Keim, Juan Irizar, Martin Bauer, Airbus Defence and Space (Germany)

SENTINEL 5 is an earth observation spectrometer system that is operating in nadir looking push broom mode from a low earth orbit. While having a wide across-track field of view (2670 km) it covers approximately 7 km at Nadir in flight direction during one dwell. Although any spatial information

along track within the exposure time is lost, a high contrast in the scene may lead to disturbance of the Instrument Spectral Response Function (ISRF). In order to reduce the scene contrast along track, two mirrors are introduced, in between which the light is prolonged.

The mirrors have a narrow distance forcing the light to be reflected several times along track (i.e. in spectral direction). The entrance length across track however is wide enough to let light pass unchanged.

This concept is known as Slit Homogenizer (SH). The entrance of the two mirrors is placed on the focal plane of the preceding optics. The exit of the SH represents the image plane of the subsequent spectrometer.

Ignoring any diffraction or interference the SH would homogenize scenes nearly perfect providing its dimension fulfill certain conditions.

If the spectral resolution is sufficiently small, say less than 1 nm the coherent length may easily be larger than the maximal optical path difference (OPD) inside the SH. So interference may not be ignored per se. On the other hand diffraction or mirror imperfection may smooth the interference effects.

This article assess to which extend diffraction and interference impact the ability of the SH to homogenize scenes with the aim to establish a more simple analytical model. It is used to evaluate quantitatively the homogenizing ability of the device. To this end rather few simplification and approximations on optics and the SH are assumed.

Some parameters in the discussed example are taken from Sentinel 5 project but the model and its application is not limited to.

10423-49, Session 12

An innovation approach to construct an additional VIIRS moderate resolution spectral band centered at 630 nm, and a discussion of the potential application of that band to detect certain coastal processes

Bruce Guenther, Stellar Solutions Inc. (United States)

The Visible/Infrared Imaging Radiometer Suite (VIIRS) is the NOAA operational follow-on to the Moderate Resolution Imaging Spectrometer on NASA's Earth Observing System. VIIRS operates on the Joint Polar-orbiting Satellite System which is the now current NOAA low-earth orbit operational Meteorological Satellite system. The VIIRS has Moderate (750 m nadir resolution) and Imaging (375 m nadir resolution) bands, as well as a band with large dynamic range that operates as a 750 m resolution, full swath imaging band in both day and night viewing conditions. This presentation will look at one specific M-band centered at 680 nm and one I-band centered at 640 nm which are nested spectrally, but for which the I-band has an 80 nm bandwidth and the M-band has a 20 nm bandwidth. We will show that an additional band of 60 nm (centered at 630 nm) may be synthesized from these two bands because the trailing edges of the spectral response of these two bands are nearly identical. The synthetic band will have lower radiometric accuracy and is considered most useful for diagnostic rather than specific quantitative objectives. Potential guidelines for the use of this synthetic band are provided also. A coarse uncertainty budget is shown that provides the uncertainty sources unique to the synthetic band, which are in addition to the uncertainties of the input bands. The concept of constructing a synthetic spectral band in this manner is considered an appropriate remote sensing concept only in the context of spectro-radiometric calibration approaches when tunable laser-source, absolute detector based calibrations are provided due to the enhanced calibrations with this class of standard devices. Traditional radiometric calibrations using integrating spheres are not considered sufficiently precise or sufficiently accurate to support computations of this nature.

This may be thought of as a solution looking for a problem. Then we will show the results of an investigation into applying this solution to the detection of Harmful Algal Blooms (HAB). Laboratory results from the literature are introduced showing that species common to HAB in the Florida USA Gulf Coast have an absorption feature centered near 630 nm. This species is Karenia brevis which is the most common algae in West Florida shelf HABs. HAB outbreaks observed within the 6-year VIIRS dataset will be investigated using this synthesized band to assess the usefulness of this band as another tool for the study of coastal processes.

10423-50, Session 12

Local or global? How to choose the training set for principal component compression of hyperspectral satellite measurements. A hybrid approach.

Tim H. Hultberg, Thomas August, Flavia Lenti, EUMETSAT (Germany)

Principal Component (PC) compression is the method of choice to achieve band-width reduction for dissemination of hyper spectral (HS) satellite measurements and will become increasingly important with the advent of future HS missions (such as IASI-NG and MTG-IRS) with ever higher data-rates. It is a linear transformation defined by a truncated set of the leading eigenvectors of the covariance of the measurements as well as the mean of the measurements. We discuss the strategy for generation of the eigenvectors, based on the operational experience made with IASI.

To compute the covariance and mean, a so-called training set of measurements is needed, which ideally should include all relevant spectral features. For the dissemination of IASI PC scores a global static training set consisting of a large sample of measured spectra covering all seasons and all regions is used. This training set was updated once after the start of the dissemination of IASI PC scores in April 2010 by adding spectra from the 2010 Russian wildfires, in which spectral features not captured by the previous training set were identified.

An alternative approach, which has sometimes been proposed, is to compute the eigenvectors on the fly from a local training set, for example consisting of all measurements in the current processing granule. It might naively be thought that this local approach would improve the compression rate by reducing the number of PC scores needed to represent the measurements within each granule. This false belief is apparently confirmed, if the reconstruction scores (root mean square of the reconstruction residuals) is used as the sole criteria for choosing the number of PC scores to retain, which would overlook the fact that the decrease in reconstruction score (for the same number of PCs) is achieved only by the retention of an increased amount of random noise.

We demonstrate that the local eigenvectors retain a higher amount of noise and a lower amount of atmospheric signal than global eigenvectors. Local eigenvectors do not increase the compression rate, but increase the amount of atmospheric loss and should be avoided. Only extremely rare situations, resulting in spectra with features which have not been observed previously, can lead to problems for the global approach. To cope with such situations we investigate a hybrid approach, which first apply the global eigenvectors and then apply local compression to the residuals in order to identify and disseminate any directions in the local signal, which are orthogonal to the subspace spanned by the global eigenvectors.

10423-51, Session 12

Mechanical monolithic compact sensors for real-time linear and angular broadband low-frequency monitoring and control of spacecrafts and satellites

Fabrizio Barone, Gerardo Giordano, Univ. degli Studi di Salerno (Italy)

In this paper we describe the characteristics and performances of a new and compact monolithic sensor designed for low frequency motion measurement of spacecrafts and satellites, whose mechanics is based on the UNISA Folded Pendulum.

The new implementations of the UNISA Folded Pendulum, a mechanical seismometer/accelerometer, whose mechanical configuration, optimized for low frequency characterization of sites (including underground sites) and structures as inertial linear and angular sensor (seismometer) appear to be suitable for this purpose. In fact, this mechanical architecture allows the design and implementation of very large band monolithic linear and angular sensors (10^-7 Hz ÷ 10^2 Hz) monolithic linear and angular sensors, whose sensitivities are defined for the most common applications by the noise introduced by their readouts (e.g. < 10^-9 m/sqrt(Hz) for linear sensors and < 10^-9 rad/sqrt(Hz) for angular sensors with commercial LVDT readouts).

These unique features, coupled other relevant properties like scalability, compactness (<10 cm side), lightness (<250 g), high directivity, frequency tunability (typical resonance frequencies in the band 10^-1 Hz ÷ 10^2 Hz), very high immunity to environmental noises and low cost make this class of sensors very effective for the implementation of uniaxial (horizontal and/or vertical) and triaxial seismometers and accelerometers for ground, space and underwater applications, including UHV and cryogenics ones.

In this paper we introduce and discuss the general methodology used to extend the application of ground-based folded pendulums to space, also in total absence of gravity in connection with the improvements performed on the new version of monolithic sensors, still keeping all their peculiar features and characteristics.

References

[1] Barone, F., Giordano, G., Mechanical Accelerometers, J. Webster (ed.), Wiley Encyclopedia of Electrical and Electronics Engineering. John Wiley & Sons, Inc., doi: 10.1002/047134608X.W8280 (2015).

[2] Barone, F., Giordano, G., Acernese, F., and Romano, R., Watt's linkage based large band low frequency sensors for scientific applications, Nucl Instrum. and Meth. A, doi: 10.1016/j.nima.2015.11.015 (2015).

[3] Acernese, F., De Rosa, R., Giordano, G., Romano, R., and Barone, F., Low frequency seismic characterization of underground sites with tunable mechanical monolithic sensors, Proc. SPIE 9435, SPIE, Bellingham, 94352Q, ISBN: 9781628415384, doi: 10.1117/12.2083362 (2015).

[4] Barone, F., Giordano, G., Low frequency folded pendulum with high mechanical quality factor, and seismic sensor utilizing such a folded pendulum, International application published under the patent cooperation treaty (PCT), WO 2011/004413 A3 (2011), Patent Numbers: IT 1394612 (Italy), EP 2452169 (Europe), JP 5409912 (Japan), RU 2518587 (Russia), AU 2010269796 (Australia), US 8,950,263 (USA), Canada pending.

[5] Barone, F., Giordano, G., Acernese, F., Low frequency folded pendulum with high mechanical quality factor in vertical configuration, and vertical seismic sensor utilizing such a folded pendulum, International application under the patent cooperation treaty (PCT) WO 2012/147112 (2012), Patent Number: IT 1405600 (Italy), EP2643711 (Europe), AU 201247104 (Australia), US 9,256,000 (USA), JP 5981530 (Japan), RU 2589944 (Russia), 9256000 (USA), Canada pending.

[6] Barone, F., Giordano, G., Acernese, F., Method for the measurement of angular and/or linear displacements utilizing one or more folded pendula, International application under the patent cooperation treaty (PCT) WO 2016/020947 (2016), Patent Number: IT 1425605 (Italy), Europe, Japan, USA, Canada pending.

10423-53, Session 13

Multiangle spectropolarimetric imagers for aerosol

Giacomo Mariani, John C. Pearson, Kevin Burke, David J. Diner, Jet Propulsion Lab. (United States)

Aerosols influence Earth's climate and water cycles by scattering and absorbing sunlight and affecting the albedo of underlying surfaces. Over the past 15 years, passive remote sensing has experienced considerable technological developments towards characterizing atmospheric aerosols. Multispectral [1], multiangle [2], and polarimetric [3] techniques can measure aerosol properties in complex clouds/surrounding surfaces. This work combines together multispectral, multiangle, and polarimetric capabilities into a push-broom camera that modulates the polarization of incoming light. The multispectral capability is achieved by narrowband filters integrated into a butcher-block assembly atop a silicon complementary metal-oxide semiconductor (CMOS) detector array. The filter assembly includes wire-grid polarizers for the polarimetric bands. The multiangle feature is driven by a programmable actuator with high flexibility in the multi-angle observing modes. The polarimetric component is performed by a pair of photoelastic modulators sandwiched between two achromatic quarter wave plates. The imagers are sensitive to light in the ultra-violet/near-infrared and short-wave infrared regions. Detectors and read-out circuits are designed at JPL with outsourced fabrication. The presentation will be focused on detector architecture and testing to space-qualify the imagers. Such class of remote-sensing imagers will help prioritize air quality guidelines, and aid research into the biological mechanism for aerosols toxicity.

References:

1. Chu D.A., Kaufman Y.J., Ichoku C., Remer L.A., Tanré D., Holben B.N. Validation of MODIS aerosol optical depth retrieval over land. Geophys. Res. Lett. 29, 10.1029/GL013205 (2002).

2. Veefkind J.P., Leeuw G., Durkee P.A. Retrieval of aerosol optical depth over land using two-angle view satellite radiometry during TARFOX. Geophys. Res. Lett. 25, 3135-3138 (1998).

3. Cairns B., Travis L.D., Russell E.E. The Research Scanning Polarimeter: Calibration and groundbased measurements. Proc. SPIE 3754, 186-196 (1999).

10423-54, Session 13

Characterisation results of the CMOS visnir detector for metimage instrument

Jérôme Pratlong, e2v technologies plc (United Kingdom); Michel Breart De Boisanger, Airbus (France); Michael Skegg, Airbus Defence and Space (Germany); Robert Simpson, Steve Bowring, e2v technologies plc (United Kingdom); Victor Benitez Casma, Deutsches Zentrum für Luft- und Raumfahrt e.V. (Germany); Natalie krzizok, e2v technologies plc (United Kingdom)

The CMOS VISNIR Detector presents several technical challenges. First, the pixel is very big 250?m square using 4T technology. This brings a first constraint from a manufacturing point of view since in CMOS process there are limitations in terms of minimum and maximum active density. Definitely, such pixel size was violating the maximum density rule and the technique used to overcome this issue will be explained. Large pixel have trade-off between lag performance due to the use of large photodiode and maximum conversion factor achievable at sense node (usually large transfer gate or multi-transfer gate are used increasing the local capacitance). To be successful two main approaches have been used one was to reduce the transit time (modulation of the electrical field) for electrons to go from the far end of the photodiode to the transfer gate; the second was to optimise the conversion factor by minimising the parasitic capacitance at sense node and adding column

amplification. These techniques will be discussed and silicon results will show their good impact on the lag and conversion factor trade-off and performance.

The dark current was also a concern for such large pixel and its degradation with proton. The measurements will be shown pre-radiation revealing very low values at room temperature and the doubling factor will be discussed and how it helps to understand the quality of the photodiode processing. The dark current degradation with proton has been modelled and this will also be reported.

In order to optimise the noise floor from the pixel the source follower sizing has been especially considered in relation with the conversion gain. This will be demonstrated and silicon results will show good correlation.

Finally this CMOS detector needed additional process steps one was an ARC and a second one was black coating in between the multi-spectral bands. Etalon effects minimised by custom ARC and reflectivity measurements will be presented.

The overall silicon performance of the detector will be reported: photon transfer curve, conversion gain, linearity, noise, dark current and QE.

10423-55, Session 13

Dark current at low operating temperatures in InAs/GaSb type-II superlattice infrared detectors

Volker Daumer, Johannes Schmidt, Frank Rutz, Andreas Wörl, Tim O. Stadelmann, Raphael Müller, Vera Gramich, Robert Rehm, Fraunhofer-Institut für Angewandte Festkörperphysik (Germany)

In recent years, InAs/GaSb type-II superlattice (T2SL) infrared detectors reached market maturity and start now replacing HgCdTe detectors in first applications. Similar to HgCdTe, they offer a broad flexibility to tailor the bandgap from mid wavelength infrared (MWIR, 3-5 μm) up to the long (LWIR, 8-12 μm) or even very-long wavelength infrared regime (VLWIR, >12μm) when grown lattice-matched on GaSb substrates. The effective bandgap can be engineered by selecting the appropriate thickness for the alternating InAs and GaSb layers during the molecular epitaxial growth process with excellent homogeneity over the whole GaSb substrate, which is already available up to 6 inch in diameter. This offers the possibility to design heterojunction devices including unipolar barriers with higher bandgap to reduce the dark current. Quantum efficiency and responsivity are comparable to HgCdTe. Due to the much larger effective electron mass in InAs/GaSb T2SLs tunneling current contributions to the dark current are considerably less pronounced compared to HgCdTe at low operating temperatures. Therefore, this new material system which offers comparable or even better performance and benefits from a matured III/V process technology, is a good candidate for future space applications.

Fraunhofer IAF played a vital role in the development of III-As/Sb T2SLs right from the start. We have demonstrated mono- and bi-spectral focal plane arrays up to 640?512 pixels for the MWIR and LWIR, respectively. We have characterized our T2SL detectors down to low temperatures (below 40K) with promising trends regarding the dark current. For MWIR detectors the resolution limit of the measurement setup with a dark current density of 2?10-10A/cm? has almost been reached at 77K. This paper will report on these measurements and compare them with published HgCdTe data.

10423-56, Session 13

Environmental evaluation of the ULIS Pico1024 microbolometer

Thierry Dartois, Thales Alenia Space (France); Ilias G. Manolis, Jean-Loup Bézy, Roland Meynart, European Space Research and Technology Ctr. (Netherlands); Christel-Loïc Tisse, ULIS (France)

In the framework of potential future thermal infra-red (TIR) radiometry missions, suitable for the monitoring of Land Surface Temperature on Earth, ESA is currently conducting studies to investigate the feasibility of different instrument concepts and their relevant options as well as breadboarding activities in order to retire any associated technological risks. Among the options being investigated is a small class mission, with moderate radiometric performances based on commercial off-the-self micro-bolometer detectors.

The latest generation of microbolometer arrays now available offer large formats and small pixel sizes. Small pixels are favourable for keeping the instrument size within reasonable limit while addressing the same swath. A major concern however, in using commercial microbolometers in space is their ability to sustain the radiation environment of space but also the harsh mechanical environments. COTS microbolometers are potentially susceptible to SEE (single even effects) because of the use of commercial CMOS technology/libraries and no implementation of specific design rules (i.e. space tailored rad hardened). In the past, and in the context of their national program, CNES has performed a space evaluation of COTS microbolometer arrays of 640x480 with 25 ?m pitch. Despite successful gamma irradiations and vibration tests; degradation of the ROIC has been evidenced during the heavy ions tests, which makes the full qualification of COTS microbolometers for future space programmes mandatory. Similar tests have been performed on an even earlier device (384x288 with a pitch of 35 ?m) under the ESA EarthCARE programme.

ESA is now running an activity with the objective to validate a third-generation COTS microbolometer offered by ULIS (France) against the relevant environment for a candidate TIR space mission. The micro-bolometer selected is the Pico1024E, which offers 1024x768 pixels of size 17 ?m square. The validation is done against heavy ion irradiation, ionizing and non-ionizing irradiation (hence, gamma and protons), as well as random vibration and shock tests. Ageing tests are included and synergetic effects are also investigated. The detector performances are tested before, after and during any test sequence. We will be reporting on the results of this activity.

10423-57, Session 13

Measuring Te inclusion uniformity over large areas for CdTe/CZT imaging and spectrometry sensors

Joseph G. Bolke, Kathryn O'Brien, Peter Wall, Mike Spicer, 5N Plus Semiconductors, LLC (United States); Guillaume Gelinas, Regroupment Quebecois sur les materiaux de pointe (Canada); Jean-Nicolas Beaudry, 5N Plus Inc. (Canada); Brock Alexander, 5N Plus Semiconductors, LLC (United States)

CdTe and CZT are promising materials for gamma and x-ray imaging applications in industry, homeland security, defense, space, medical and astrophysics. This is due to their high stopping power and their availability in the market place. There remain challenges in spectroscopic uniformity over large detector areas (50~75mm) due to a combination of material purity, handling, growth process, grown in defects, doping/compensation, metal contacts/surface states, among others. In this study, we looked at improving the source material, compounding processes, and crystal growth to improve detector performance. We report on the electrical and spectroscopic performance of CdTe crystals that can be used for hard x-ray imaging and spectroscopy applications.

In this investigation, we measured impurities in the Cd and Te source materials, the compound CdTe, poly and single crystals of CdTe and the crystallographic structure of single crystal materials. The impact of these various factors has yet to be explored at the large substrate level required for devices with higher resolution both spatially and spectroscopically. We were able to grow single crystals as large as 75mm in diameter and map the uniformity of the crystal structure using

X-ray topography and defect revealing etches. Additionally, IR imaging was used to spatially characterize three-dimensional defects such as Te inclusions. We correlated these bulk crystallographic defects to individual pixelated device performance to by patterning and depositing gold and/or platinum contacts to form pixelated devices on substrates 10mmx10mmx1mm or as large as 50mmx50mmx2mm.

We report on the degree of impairment that of each of these observed defects contribute to charge transport and spectroscopic uniformity. In order to test these large devices we developed automated electrical testing to measure resistivities >1x109 Ohm-cm, Hecht fit mobility-lifetime >2.2x10-3cm2/V using ohmic contacts. Inhomogeneities were further investigated with TEM to look at the interface between the metal and CdTe crystal.

This work brings together the optimization of the upstream processes from raw feed materials to crystal growth and detector fabrication to enable manufacturing of remote sensors that image hard x-rays from transient phenomena in astrophysics. 5N Semiconductors wishes to thank the Air Force Research Laboratory for their support for this R&D effort.

10423-58, Session 14

Multispectral imaging photometer-polarimeter for Aerosol-UA space mission

Ivan I. Syniavskyi, Yuriy S. Ivanov, Georgii Koshman, The National Academy of Sciences of Ukraine (Ukraine); Gennadi P. Milinevsky, The National Academy of Sciences of Ukraine (Ukraine) and Taras Shevchenko National Univ. of Kyiv (Ukraine); Mikhail Sosonkin, The National Academy of Sciences of Ukraine (Ukraine)

The state-of–art of the wide angle field-of-view multispectral imaging polarimeter (MSIP) for Ukrainian space project Aerosol-UA is discussed [1, 2]. The polarimeter MSIP will serve for study of the terrestrial atmospheric aerosol spatial distribution and microphysics to quantify the aerosol contribution to the climate change. The aerosol remote sensing concept of the project is based on precise orbital measurements by the scanning polarimeter ScanPol accompanied by the wide-angle multispectral imager photometer-polarimeter MSIP.

MSIP consists of five optical channels (cameras) with 60°x60° FOV across and along satellite path at the Earth surface. Three channels are polarized and two channels are photometric. Polarizing channel measure Stokes parameter I, Q, and U with central wavelength 410, 555 and 865 nm and with the spectral FWHM 20 nm. Two photometric channels of the MSIP will serve to obtain image in eight spectral wavebands to retrieve the aerosol optical depth. The central wavelengths for the first photometric channel are 410, 443, 470, and 490 nm with FWHM 20 nm and for the second one are 555, 670, 865 and 910 nm with FWHM 20–40 nm.

Optical layout of the MSIP channels was constructed according to the prototype described in [3, 4]. The each channel consists of: wide angle FOV input lens, collimator, sectoral polarizer (in the polarizing mode) or sectoral filter (in the photometric mode), prism-splitter system, camera lens and image detector. Collimator performs several functions: partial correction of field aberrations, builds the pupil and collimation of the light. In the pupil plane the sectoral polarizer or the sectoral filter are placed. The sectoral polarizer consists of polarizing components with axis orientation 0°, 45°, 90°and 135°. The special prism-splitter system allows to obtain four image at the detector simultaneously. Thus we perform simultaneous four polarizing or photometric measurements. The detector consists of 1024x1024 pixels with pixel size 15μ. One of the special features of MSIP concept is the polarization calibration using ScanPol data in the same field-of-view. We expect that the polarization accuracy of MSIP should be better than ~1%. The computed optical and construction design of the MSIP has been developed and optical components and mechanics are under assembly.

[1] Milinevsky G, Yatskiv Ya, Degtyaryov O, et al. (2016) New satellite project “Aerosol-UA”: remote sensing of aerosols in the terrestrial atmosphere. Acta Astronautica 123: 292–300.

[2] Milinevsky G, Yatskiv Ya, Degtyaryov O, et al. (2015) Remote sensing of aerosol in the terrestrial atmosphere from space: new missions. Advances in Astronomy and Space Physics 5: 11–16.

[3] Sinyavski? I, Ivanov Yu, Vil’machenko A. (2013) Concept of the construction of the optical setup of a panoramic Stokes polarimeter for small telescopes. Journal of Optical Technology. 9:545-548.

[4] Syniavskyi I., Ivanov Yu. (2014) Four-channel imaging Stokes polarimeter for small telescopes. Contrib. Astron. Obs. Skalnate Pleso. 43:253-255.

10423-59, Session 14

Optical concept of imaging space-borne spectrometer for ozone monitoring

Yury Dobrolenskiy, Space Research Institute (Russian Federation); Yurii Ivanov, Main Astronomical Observatory of the National Academy of Sciences of Ukraine (Ukraine); Ilia Dziuban, Space Research Institute (Russian Federation); Dmitry Ionov, Saint Petersburg State Univ. (Russian Federation); Oleg Korablev, Space Research Institute (Russian Federation); Ivan I. Syniavskyi, Main Astronomical Observatory of the National Academy of Sciences of Ukraine (Ukraine); Nikita Vyazovetskiy, Space Research Institute (Russian Federation)

A preliminary optical design of an imaging spectrometer to monitor terrestrial atmospheric ozone (ozonometer) from near-Earth orbit will be presented. The instrument is being developed for Russian space program Ionozond-2025. The instrument would supplement the existing ozone mapping spectrometers as well as those planned for the future, and would contribute to validation of the remote sensing ozone data. The instrument is an imaging spectrometer with a wide field of view across flying trajectory (100°), providing a swath of ~2000 km from the Ionozond-2025 700 km and 98° inclination orbit. The spectral range is from 300 to 800 nm, allowing ozone measurements in the Huggins band (300 – 360 nm), nitrogen dioxide NO2 in the 400 – 500 nm range, oxygen absorption at 760 nm, and possibly the oxygen dimer O4 throughout the visible range. The spectrometer includes two channels: UV channel (300 – 400 nm) and VIS channel (400 – 800 nm).

The spectral resolution will be ~0.3 nm in UV channel and ~0.5 nm in VIS channel. The spatial resolution is 0.5° for both channels, which gives pixel size on the surface ~7 km. The spectrometer employs plane diffraction grating with refractive collimator and camera lenses. To eliminate polarization effects a scrambler is put prior to the entrance slit. The entrance reflective telescope providing 100-degrees field of view has the same design for both channels.

Acknowledgements. We acknowledge FSF #16-12-10453 for the support in of this work.

10423-60, Session 14

Modeling and design of a tunable spatial heterodyne spectrometer for broadband spectral line studies

Nirmal K., Sridharan Rengaswamy, S. Sriram, Jayant Murthy, Indian Institute of Astrophysics (India)

Spatial Heterodyne Spectroscopy (SHS) is a relatively novel interferometric technique similar to Fourier transform spectroscopy and shares design similarities with a Michelson Interferometer. An Imaging detector is used at the output

of a SHS to record the spatially heterodyned interference pattern. The spectrum of the source is obtained by Fourier transforming the recorded interferogram. The merits of the SHS -its design, including the lack of moving parts, compactness, high throughput, high SNR and instantaneous spectral measurements - makes it suitable for space as well as ground observatories. The small bandwidth limitation of the SHS can be overcome by building it in tunable configuration (Tunable Spatial Heterodyne Spectrometer(TSHS)). In this paper, we describe the modeling and design of a TSHS to study diffused, faint and extended, emission line targets such as comets, airglow, planetary auroras and inter stellar medium. The instrument has been designed with a resolving power above 54000 covering a wavelength range from 350 nm to 700 nm. It is compact and rugged compared with other instrument having the similar configurations.

10423-61, Session 14

Influence of high-resolution satellites attitude parameters on image quality

Walid A. Wahballah, Taher M. Bazan, Fawzy El-Tohamy, Egyptian Armed Forces (Egypt); Mahmoud Fathy, Benha Univ. (Egypt)

One of the important functions of the satellite attitude control system is to provide the required pointing accuracy and attitude stability for optical remote sensing satellites to achieve good image quality. Although offering noise reduction and increased sensitivity, time delay and integration (TDI) charge coupled devices (CCDs) utilized in high-resolution satellites (HRS) are prone to introduce large amounts of pixel smear due to the instability of the line of sight. During on-orbit imaging, as a result of the Earth's rotation and the satellite platform instability, the moving direction of the TDI-CCD linear array and the imaging direction of the camera become different. The speed of the image moving on the image plane (focal plane) represents the image motion velocity whereas the angle between the two directions is known as the drift angle (?). The drift angle occurs due to the rotation of the earth around its axis during satellite imaging; affecting the geometric accuracy and, consequently, causing image quality degradation. Therefore, the image motion velocity vector and the drift angle are two important factors used in the assessment of the image quality of TDI-CCD based optical remote sensing satellites.

A Model for estimating the image motion velocity and the drift angle in HRS is derived. The six satellite attitude control parameters represented in the derived model are the (roll angle ?, pitch angle ?, yaw angle ?, roll angular velocity ??, pitch angular velocity ?? and yaw angular velocity ??). The influence of these attitude parameters on the image quality is analyzed by establishing a relationship between the image motion velocity vector, drift angle and the six satellite attitude parameters. The influence of the satellite attitude parameters on the image quality is assessed by the presented model in terms of MTF in both cross- and along-track. Three different cases representing the effect of pointing accuracy (?, ?, ?) bias are cosidered using four different sets of pointing accuracy typical values, while the satellite attitude stability parameters are ideal. In the same manner, the influence of satellite attitude stability (??, ??, ??) on image quality is also analysed for ideal pointing accuracy parameters.

The results reveal that cross-track image quality is influenced seriously by the yaw angle bias and the roll angular velocity bias, while along-track image quality is influenced only by the pitch angular velocity bias.

10423-62, Session 15

Smear effect on high-resolution satellites image quality

Walid A. Wahballah, Taher M. Bazan, Fawzy EL-Tohamy, Egyptian Armed Forces (Egypt); Mahmoud Fathy, Benha Univ. (Egypt)

The image quality of high-resolution remote sensing satellites (HRRSS) is influenced by several issues including optics, detector, and satellite attitude and vibration aspects. Although offering noise reduction and increased sensitivity, time delay and integration (TDI) charge coupled devices (CCDs) utilized in HRRSS are prone to introduce large amounts of pixel smear due to these aspects. If careful analysis is not performed during the design phase, the amount of pixel smear may be significant and, hence, will reduce the modulation transfer function (MTF); causing image quality degradation.

The overall impact of clocking smear, velocity mismatch smear and satellite platform vibration on the MTF is analyzed and studied thoroughly taking into consideration the effects of the optical system and detector parameters. Clocking smear can be classified as internal smear within TDI CCDs; representing the pixel smear error due to the clocking scheme adopted to clock out the charge from each TDI step to the next one during the imaging process. Velocity mismatch smear occurs during the on-orbit imaging process and results from the relative motion between the satellite sensor and the Earth targets. In an ideal imaging scenario, the velocity of charge transfer must be synchronized with the image velocity on the focal plane so that the photon generated charge packets are always synchronized with the image. In practical, there is always a drift between the two speeds and a compensation mechanism should be adopted to minimize such drift. Furthermore, during off-nadir imaging, the image velocity will change and leads to an asynchronization between the image velocity and the rate of charge packet transfer in the TDI-CCD. This asynchronization will not only change the spatial resolution of the imaged object, but also leads to deterioration in the quality of the produced images. Another important source of smear is the sinusoidal vibration smear due to satellite platform vibration during imaging. Such vibration results from the changing speed of the momentum wheel, solar array flutter or any moving mechanisms in the satellite.

A Model for estimating the image motion velocity is derived. The influence of the above-mentioned issues on MTF is investigated by using Matlab simulation. Furthermore, the analysis is performed for cross-track and along-track imaging; examining different satellite attitude angles, TDI steps, low and high-frequency sinusoidal vibration frequencies and amplitudes. Through the presented results, there is a trade-off between the image quality and mutual HRRSS factors particularly low-frequency vibration parameters, TDI-CCD steps, and satellite attitude.

The analysis showed that the effect of high-frequency vibration on image quality is negligible in comparison to low-frequency vibration. Furthermore, low-frequency vibration parameters play an important role in the level of image quality. More than 41 % reduction in the MTF occurs if the low frequency vibration amplitude increases from 10 ?m to 20 ?m. From the presented study, the velocity mismatch error and low frequency vibration are the most influencing factors that cause degradation in the image quality.

10423-63, Session 15

High efficient optical remote sensing images acquisition for nanosatellite framework

Feng Li, China Academy of Space Technology (China); Lei Xin, Qian Xuesen Lab. of Space Technology (China); Yang Liu, China Academy of Space Technology (China); Jie Fu, Yuhong Liu, Lanzhou Jiaotong Univ. (China); Yi Guo, Western Sydney Univ. (Australia)

Nano-satellite (NanoSat) usually refers to satellites less than 10 kg and has the practical function and specific purposes. It is more difficult and challenging to implement NanoSat based optical Earth observation missions than conventional satellites because of the limitation of volume, weight and power consumption. In general, an image compression unit

is a necessary onboard module to save data transmission bandwidth and disk space. Let us review the whole image compression procedure. First, a scene is projected to CCD or CMOS sensors arrays. The CCD or CMOS sensors work as A/D converters. Then the compression technique is used to get rid of redundant information of those captured images. Here is the question, why not acquire the compressed information while image acquisition based on the idea of compressive sensing (CS)? CS theory has been a hot research area in recent years. It combines the procedures of sampling and compression so that the measurement based on CS is already compressed. CS has been applied in many research areas such as MRI, radio astronomy, SAR imaging and etc.. However, there are few applications for CS to replace the traditional image compression. In this paper, a new image acquisition framework is proposed for NanoSat. A new type of sensing matrix is proposed by combining image acquisition and image compression. It includes two separate sensing modules: one is the traditional CS sensing matrix; the other is the downsampling module. Both the downsampling matrix and the traditional CS sensing matrix can be regarded as a brand new sensing matrix. A downsampling matrix is included in the framework, there are two reasons to do so: one the on hand, the downsampled data will be regarded as an extra constraint in the CS reconstruction algorithm, which will greatly reduce the solution space to improve the quality of reconstructed images. On the other hand, the downsample thumbnail can also be regarded as a bonus to provide quick view without any iterative reconstruction computation.

The entire process of image acquisition and compression unit can be integrated in the photo detector array chip, that is, the output data of the chip is already compressed. That is to say, extra image compression unit is no longer needed; therefore, the power, volume, and weight of the common onboard image compression units consumed can be largely saved. The advantages of the proposed framework are: the image acquisition and image compression are combined into a single step; it can be easily built in CMOS architecture; quick view can be provided without reconstruction in the framework; Given a certain compression ratio, the reconstructed image quality is much better than those CS based methods. The framework holds promise to be widely used in the future.

10423-64, Session 15

The design of visualization telemetry system based on camera module of the commercial smartphone

Chao Wang, Zhao Ye, Bin Wu, Huan Yin, Qipeng Cao, Jun Zhu, Aerospace DongFangHong Satellite Co., Ltd. (China)

Satellite telemetry is the vital indicators to estimate the performance of the satellite. The telemetry data, the threshold range and the variation tendency collected during the whole operational life of the satellite, can guide and evaluate the subsequent design of the satellite in the future. The rotational parts on the satellite (e.g. solar arrays, antennas and oscillating mirrors) affect collecting the solar energy and the other functions of the satellite. Visualization telemetries (pictures, video) are captured to interpret the status of the satellite qualitatively in real time as an important supplement for troubleshooting. The mature technology of commercial off-the-shelf (COTS) products have obvious advantages in terms of the design of construction, electronics, interfaces and image processing. Also considering the weight, power consumption, and cost, it can be directly used in our application or can be adopted for secondary development. In this paper, characteristic simulations of solar arrays radiation in orbit are presented, and a suitable camera module of certain commercial smartphone is adopted after the precise calculation and the product selection process. Considering the advantages of the COTS devices, which can solve both the fundamental and complicated satellite problems, this technique proposed is innovative to the project implementation in the future.

10423-65, Session 15

SRS-lidar for 13C/12C isotops measurements environmental and food

Alexsandr S. Grishkanich, ITMO Univ. (Russian Federation); Yan Chubchenko, D.I. Mendeleyev Institute for Metrology (Russian Federation); Valentin V. Elizarov, Aleksandr P. Zhevlakov, ITMO Univ. (Russian Federation); Leonid Konopelko, D.I. Mendeleyev Institute for Metrology (Russian Federation)

Research isotopic composition of carbon, provide important information for the study of the genesis of oil, gas, native S, and the well to determine the ripeness of the fruit. The separation of carbon isotopes in nature is called isotope-exchange reactions leading to preferential accumulation of the heavy isotope C13 in carbonates, and biological processes, in t. Ch. Photosynthesis, resulting in the light isotope C12 is enriched with organic matter of plant and animal origin. We developed Raman lidar for measurements of the isotopic composition of CO2 and CH4 mixtures. 12CO2 and 13CO2 mixture of isotopes was prepared with a molar CO2 magnitude of 1000 ppm. The isotope ratio in the mixture was measured by the analyzer isotopic composition on PICARRO G2131-I The intracavity cavity ring down spectroscopy (CRDS) was used to measure the radiation damping time in the cell (cuvette) with three highly reflective mirrors with multiple passes of light between them. Use CRDS analyzer has a measurement accuracy of 0.05 ‰. High accuracy is achieved by using the optical path about 17 km long. According to the measurement results was obtained ratio of 12CO2 to 13CO2 equal to 46.1 %. Standard deviation was 0.7%. Stokes shift 12CO2 molecules was found to be 1388 cm-1, a molecule 13CO2 -1370 cm-1. In turn, the Stokes shift is a mixture of isotopes Stokes shift 12CO2 1388 cm-1. CO2 isotopes have Stokes shifts are located close to each other. The sensitivity of the Raman method is inversely proportional to the fourth power of the wavelength dispersion. We developed lidar with selectivity at ? / ?? = ? / ?? >> 1000, which allows to solve the Stokes shift of the measured isotope 12CO2 and 13CO2, equal to ? = 2 cm-1 at wavelengths shorter than 2.0 micron (?> 5000 cm-1) with 5 ppm sensitivity.

10423-66, Session 15

Optical system design of the coded aperture superresolution imager

Linlin Pei, Academy of Opto-Electronics, CAS (China)

The super-resolution imager based on the coded aperture is a novelty technology. It breaks the constraints of conventional optical imager in techniques and principles. Compared to the conventional optical imager, the spatial resolution of the imager using the coded aperture technology can be increased 1-fold. Therefore, this kind of technology can be used in the finalized imager by installing a robust coded aperture to improve the resolution of the imager. Compared to conventional remote sensing cameras, to obtain the same performance and indicators, the super-resolution imager based on the coded aperture can be designed based on the spectrum of super-resolution encoder plate imaging optical more simple and smaller. In this paper, we study and analysis the principle of the super-resolution spectrum based on the coded aperture. To prove the advantages of the super-resolution imager sufficiently, we design a complete optical system based on the principle of the super-resolution imager. We design the optical system which can be built in the laboratory. It can be simpler when it will be used outside. Its focal length is 90mm. It is a coaxial optical path, and the total length is 538.5mm. At 56lp / mm, the MTF value is close to the diffraction limit. The image quality is good. Then we do experiments to verify the theory. The spatial resolution of the optical system is increased 1-fold than the conventional system.

10423-79, Session 15

Onboard TDI stage estimation and calibration using SNR analysis

Javad Haghshenas, Satellite Research Institute (Iran, Islamic Republic of)

Electro-Optical design of a push-broom space camera for a Low Earth Orbit (LEO) remote sensing satellite is performed based on the noise analysis of TDI sensors for very high GSDs and low light level missions. It is well demonstrated that the CCD TDI mode of operation provides increased photosensitivity relative to a linear CCD array, without the sacrifice of spatial resolution. However, for satellite imaging, in order to utilize the advantages which the TDI mode of operation offers, attention should be given to the parameters which affect the image quality of TDI sensors such as jitters, vibrations, noises and etc. A predefined TDI stages may not properly satisfy image quality requirement of the satellite camera. Furthermore, in order to use the whole dynamic range of the sensor, imager must be capable to set the TDI stages in every shots based on the affecting parameters. This paper deals with the optimal estimation and setting the stages based on tradeoffs among MTF, noises and SNR. On-board SNR estimation is simulated using the atmosphere analysis based on the MODTRAN algorithm in PcModWin software. According to the noises models, we have proposed a formulation to estimate TDI stages in such a way to satisfy the system SNR requirement. On the other hand, MTF requirement must be satisfy in the same manner. A proper combination of both parameters will guaranty the full dynamic range usage along with the high SNR and image quality.

10424-26, Session PS

Clouds effect on the atmospheric total column carbon dioxide retrieval by space orbiting Argus 1000 microspectrometer: introductory study

Naif Alsalem, Catherine Tsouvaltsidis, York Univ. (Canada); Caroline Roberts, Thoth Technology Inc., (Canada); Brendan Quine, York Univ. (Canada)

Carbon Dioxide (CO2) is one of the most important greenhouse gases after water vapor (H2O) which plays significant role in the climate process. Accurate space-based measurement of CO2 is of great significance in inferring the location of CO2 sources and sinks. Uncertainties in greenhouse gases (GHG) retrieval process must be minimized to accurately infer the actual amount of the atmospheric species. Clouds pose a large uncertainty in CO2 space-based retrieval process leading, mostly, to an underestimation in the CO2 absorption amount above the cloud layer provided that photons do not perform multiple paths. In this paper, three different cases of data collected over cloudy and clear skies by Argus 1000 micro-spectrometer were analyzed. Findings show that the CO2 absorption in the absence of clouds is approximately 4.5% higher than when clouds are present.

10424-27, Session PS

Cluster analysis algorithms for RS and WWLLN data processing

Nikolay V. Baranovskiy, National Research Tomsk Polytechnic Univ. (Russian Federation); Svetlana Y. Karanina, Marina Y. Belikova, Nina A. Kocheeva, Gorno-Altaisk State Univ. (Russian Federation); Ksenia S. Yankovich, ITMO Univ. (Russian Federation); Alena V. Glebova, Gorno-Altaisk State Univ. (Russian Federation)

Determination of convective cells in the clouds characterized by high lightning activity is an urgent task. On the one hand, research requires information on the atmospheric parameters and the microphysical properties of the clouds for these purposes. On the other hand we need information on lightning discharges. In the first case, as a rule, satellite images of cloud cover in the infrared range and satellite thematic products are used. In the second case, data from lightning discharge location systems can be used. The algorithms for clustering are used to identify single-cell and multi-cell storms from data on lightning discharges.

The choice of the clustering algorithm is influenced by such properties of the initial data as the dimensionality of the feature space and the presence of a complex structure of the resulting clusters. As a rule, three variables (geographic coordinates and time) are essential for the clustering of data on lightning discharges. The Euclidean distance and the condition for lightning to belong to the same cluster are used as a proximity measure. The condition is chosen, as a rule, from the physical conditions for the existence of thunderstorms: average lifetime of thunderstorm cell and mean area.

Despite the fact that the problem of cluster analysis of lightning discharges does not initially looks complicated and natural for solving it, the choice of a “typical” algorithm based on any known approach depends mainly on the researcher’s preferences. However, the results of clustering and the conclusions based on these results can essentially depend on the chosen proximity measures (conditions for lightning of one convective cell), the algorithm and the set of input parameters for it.

The article is devoted to a comparison of the results of the data grouping on lightning discharges of the WWLL Network. The results are obtained using clustering algorithms based on different methods: hierarchical agglomerative (Ward, single, complete), k-means (k-medoids) and density (dbscan). Internal clustering validation index - Average Silhouette width (asw) was selected as a formal comparison criterion. It is widely used to estimate the number of clusters and to select the proper clustering algorithm. The construction of grouping solutions with selected clustering algorithms with quality assessment was performed using the Nbclust and fpc cluster analysis packages developed in the R language.

The computational experiment showed that for the proximity measure given by the average lifetime (30 minutes) and the average width (30-50 km) of the thunder cell, the best lightning grouping can be obtained using the Ward hierarchy algorithms and the complete), as well as the dbscan algorithm. The lowest quality of clustering among the considered clustering algorithms was obtained in a hierarchical single algorithm.

The results of the comparative analysis should be taken into account when selecting and improving methods for analyzing the space-time relationship between the electrically active clouds zones, the microphysical parameters of the clouds, and the meteorological parameters of the atmosphere.

This work is implemented at financial support of Russian Foundation for Basic Research and administration of Tomsk region. The grant N 16-41-700831.

10424-28, Session PS

Regional problems of forest fire danger assessment in Jewish Autonomous Region using GIS and RS technologies

Nikolay V. Baranovskiy, National Research Tomsk Polytechnic Univ. (Russian Federation); Rita M. Kogan, Anna M. Zubareva, Vladimir A. Glagolev, Institute for Complex Analysis of Regional Problems (Russian Federation)

Main factors of forest fire danger are the characteristics of the vegetation, climate and weather conditions, as well as the level of anthropogenic load on controlled forested area. Forest fire danger in the Far East of the Russian Federation has its own characteristics in each region. Remote sensing (RS) and geographic information systems (GIS) are used to evaluate and spatial analysis of forest fire danger data. The aim of the study is to examine the nature of forest fire danger of Jewish Autonomous Region using RS and GIS to improve the fire service organizations.

GIS “EAO Pozhary – JAR Fires” was created in order to address this goal in MapInfo Professional software. GIS consists of three subsystems:

- Data collection and processing subsystem of RS monitoring of objects;

- Electronic maps (general geographic or topographic layers);

- Attribute Database for each fire.

Information about the vegetation fire location and its state can be obtained from satellite imagery from the TERRA satellite. RS Subsystem uses MODIS information in 36 spectral channels with a resolution of 250, 500, 1000 m per pixel. Information are shared on NASA site (http://rapidfire.sci.gsfc.nasa.gov). MOD14 (Thermal Anomalies - Fires and Biomass Burning) algorithm is used to recognize the images. Russian mirror of this site is presented on the website ISDM-Rosleskhoz (http://aviales.ru), that hosts the data of satellite monitoring of vegetation fires throughout the Russian Federation.

The required map material has been created in the form of a complex electronic maps “Rastitelnost EAO - Plant formations JAR”, “EAO Relief – JAR Relief”, “Hydrographia EAO –

Hydrography JAR", "Dorozhnaya set EAO - Road network JAR". This set of maps forms topographic base, supplemented with boundaries.

Databases include 15 main characteristics of the fire incident (burning area, initial date, end date, day of week, detector, fire number, forestry, local forestry, quarter number, vegetation characteristics, fire rating class, angle, elevation, height of the top edge, slope exposition.

Meteorological data is provided by the Internet service: Russian Hydrometeorological Center (http://meteoinfo.ru); Space Research Institute (http://meteo.infospace.ru); Scientific-Production Center "MEP-maker» (http://gismeteo.ru). Meteorological elements include daily measurements of daily air temperature and dew point temperature, wind speed and direction in the 13-15 hours of the day, the daily amount of rain from 9 am to 9 of the previous day in the afternoon of the day, as well as forecasts of public weather to advance to 3 days.

Using of the developed GIS in forestry enables spatial data analysis. The analysis results can be used in the design and implementation of prescribed fire within the boundaries of natural taxonomic units, to monitor changes in the forest fund, to determine the level and mode of protection of forests against fire, depending on their economic and ecological importance, to more accurately reflect the size of the area to organize and use permanent network of barriers and supporting strips to control burn-prevention and launch counter fell to extinguish fires.

This work is partly implemented at financial support of Russian Foundation for Basic Research and administration of Tomsk region. The grant N 16-41-700831.

10424-29, Session PS

Convective initiation algorithm of Geo-KOMPSAT-2A (GK-2A) Advanced Meteorological Imager (AMI)

Eun-Bin Park, Korea Aerospace Research Institute (Korea, Republic of); Hye-Sil Kim, National Meteorological Satellite Ctr. (Korea, Republic of); Sung-Rae Chung, National Satellite Meteorological Ctr. (Korea, Republic of); Sun-Hee Woo, Korea Aerospace Research Institute (Korea, Republic of)

Geo-KOMPSAT-2A (GK-2A), which is scheduled to be launched in 2018, is a next geostationary satellite of South Korea, following to Communication, Ocean and Meteorological Satellite (COMS). Advanced Meteorological Imager (AMI) on the GK-2A can scan the Earth with high resolution of both time and spatial. Furthermore, image-processing system of the GK-2A ground system will produce the level 1B images in 2 minutes. Convective Initiation (CI) algorithm can get more accurate weather forecast for heavy rainfall, thunderstorm and lightning through the high resolution of time and spatial data of the GK-2A AMI. Since the convective clouds are usually caused by rapid developing clouds in unstable atmosphere, they can be detected by the temperature differences more than two of consecutive images. The CI algorithm of GK-2A AMI has four steps. Convective cloud masking is the first step in the CI algorithm, which extract mature cloud area using infrared channels. The next step is grouping cloud pixels using region growing method for immature cloud area. And then, the clustered area (the immature cloud area) will be tested in overlapping detection step in sequential images. The last step of the CI algorithm is "Interest field tests" for each cloud object which can cause severe weather. The CI algorithm was tested by Himawari-8 Advanced Himawari Imager (AHI) data similar with the GK-2A AMI and validated with lightning data and radar observed in ground.

10424-30, Session PS

Evaluation of ground-based particulate matter in association with measurements from space

Makiko Nakata, Akihito Yoshida, Itaru Sano, Kindai Univ. (Japan); Sonoyo Mukai, The Kyoto College of Graduate Studies for Informatics (Japan)

Concerns about air pollution caused by fine particulate matter (PM2.5) and its effect on human health are increasing. High PM2.5 concentrations cause a spike in the mortality rate of patients suffering from heart and lung diseases. Particulate matter is also responsible for most visibility problems. Based on the known health effects, both short-term (24-hour) and long-term (annual) guidelines are needed for PM2.5. The Japanese environmental quality standard for PM2.5 was ratified on 2009. Environmental quality standards for other air pollutants, including sulfur dioxide, nitrogen dioxide, carbon monoxide, photochemical oxidants, and suspended particulate matter (defined as airborne particles with a diameter smaller than or equal to 10 ?m), were ratified in the 1970s. The air pollution levels experienced during the recent period of rapid economic growth have been reduced. Concentrations of these air pollutants are observed by an atmospheric environmental regional observation system with stations all over Japan. Japanese air pollutants, except for PM2.5 and photochemical oxidants, have all reached the environmental standards.

Air pollution from PM2.5 is widely thought to be caused by pollutants that come from overseas. Certainly, trans-national air pollutants have been observed to cause high concentrations of PM2.5 in Japan. It is natural to consider that the possible polymerization of domestic and trans-national pollutants intensifies air pollution. In this study, the concentration of PM2.5 sampled near the surface was analyzed in detail to clarify the state and the causes of this observed change. It has been shown that the atmospheric aerosol optical thickness (AOT) correlates with a direct effect on the Earth radiation budget, and the values of AOT can be readily obtained from ground- and space-based measurements at the global scale. Accordingly, a linkage analysis of PM2.5 concentrations with AOT would provide a way to infer the characteristics and global distribution of PM2.5. Further, the environmental influences of PM2.5 could be examined based on these results. In this study, PM2.5 concentrations were measured using ground samplers in Japan and the aerosol properties, such as size and composition, were determined. AOT observations from satellites and ground photometers were then correlated with the observed PM2.5 aerosol properties, taking into consideration various geographical and weather conditions.

10424-31, Session PS

Role of near ultraviolet wavelength measurements in the detection and retrieval of absorbing aerosols from space

Sonoyo Mukai, Toshiyuki Fujito, The Kyoto College of Graduate Studies for Informatics (Japan); Makiko Nakata, Itaru Sano, Kindai Univ. (Japan)

Aerosol remote sensing by ultraviolet (UV) wavelength is established by a Total Ozone Mapping Spectrometer (TOMS) mounted on the long-life satellite Nimbus-7 and continues to make observations using an Ozone monitoring instrument (OMI) located on the Aura satellite. For example, TOMS demonstrated that UV radiation (0.331 and 0.360 ?m) could easily detect absorbing particles such as mineral dust or smoke aerosols. TOMS-AI (absorbing aerosol index) has been used to identify the absorbing aerosols from space.

For an upcoming mission, JAXA/GCOM-C will have the polarization sensor SGLI boarded in December 2017. The SGLI has multi (19)-channels including near UV (0.380 ?m) and

violet (0.412 ?m) wavelengths. This work intends to examine the role of near UV data in the detection of absorbing aerosols similar to TOMS-AI played. In practice, the measurements by GLI mounted on the short Japanese mission JAXA/ADEOS-2, whose data archive period was just 8 months from April to October in 2003, are available for simulation of SGLI data because ADEOS-2/GLI is involved near UV and violet channels. First of all, the ratio of data at 0.412 ?m to that at 0.380 ?m is examined as an indicator to detect absorbing aerosols on a global scale during of the entire ADEOS-2 era. The results are validated with the TOMS-AI, Terra/MODIS products, ground measurements, and numerical model simulations (SPRINTARS). It is notable that the data assimilation between various kinds of products upgrades the accuracy of each product itself. Aerosol retrieval is then achieved with both radiance and polarization by GLI and POLDER-2, respectively, on board the ADEOS-2 satellite.

It is noted that our research group has developed an efficient algorithm for aerosol retrieval in hazy episodes (dense concentrations of atmospheric aerosols). Dust storms or biomass burning plumes due to large forest fires pose serious environmental hazards merged with the increased emissions of anthropogenic aerosols associated with economic growth, yet their aerosol characteristics are poorly understood. It can be said that at least this work is an attempt to grasp the biomass burning plumes from the satellite.

10424-32, Session PS

Study of different operational modes of the IAP 2-port-DOAS instrument for investigation of atmospheric trace gases during CINDI-2 campaign

Alexander N. Borovski, Alexander Elokhov, Oleg V. Postylyakov, A.M. Obukhov Institute of Atmospheric Physics (Russian Federation); Ilya I. Bruchkouski, Belarusian State Univ. (Belarus)

An instrument for measuring atmospheric trace gases by DOAS method using scattered solar radiation was developed in A.M.Obukhov IAP RAS (see Proc. SPIE, 2016, Vol. 10035, 100353C-9). The instrument layout is based on the lab Shamrock 303i spectrograph supplemented by 2-port radiation input system employing optical fiber. Optical ports may be used with a telescope with fixed field of view or with a scanning MAX-DOAS unit. MAX-DOAS unit port will be used for investigation of gas contents and profiles in the low troposphere.

In September 2016 the IAP instrument participates in the CINDI-2 campaign, held in the Netherlands. CINDI 2 (Cabauw Intercomparison of Nitrogen Dioxide Measuring Instruments -2) involves about 40 instruments quasi-synchronously performing DOAS measurements of NO2 and other gases.

During the campaign the instrument ports had telescopes A and B with similar field of view about 0.5°. Telescope A was always directed to the zenith. Telescope B was directed at 5° elevation angle. Two gratings were installed in the spectrometer. They provide different spectral resolution (FWHM ~0.4 and 0.8 nm respectively) and spectral window width (~70 and ~140 nm respectively). During CINDI-2 campaign we performed test measurements of NO2 and HCHO spectra in UV and visible wavelength ranges to investigate instrument stability and retrieval errors of gas contents. Two used gratings may provide the following spectral intervals in dependence of grid and grid positions:

grating #1:

a. 424 – 490 nm (NO2 retrieval)

b. 397 – 464 nm (NO2 retrieval in small visible region)

c. 313 – 382 nm (NO2, HCHO and O3 retrieval in UV region)

grating #2:

d. 389 – 532 nm (NO2 retrieval in 425-490 nm)

During CINDI-2 campaign we test our instrument with 4 operation modes:

- Mode Vis – the instrument is locked at position a.
- Mode UV-2Vis – the instrument scans of grid positions a, b, c.
- Mode UV – the instrument is locked at position c.
- Mode 2UV-2Vis– the instrument scans of grid positions a, b, c, d.

Errors typical for these four modes are estimated based on comparison of our results with median results of all CINDI-2 instruments.

10424-33, Session PS

Cloud aerosol interactions by multiple scenarios approach

Jonatan J. da Silva, Univ. de São Paulo (Brazil) and Univ. Federal do Oeste da Bahia (Brazil); Fábio J. S. Lopes, Eduardo Landulfo, Instituto de Pesquisas Energéticas e Nucleares (Brazil)

Aerosols can play an important role on cloud formation and ice condensation nuclei. Clouds, in turn, can affect the radiation budget by scattering and absorbing solar radiation. This study shows a set of measurements and analysis in remote sensing, in distinct scenarios of cloud cover during diurnals measurements using lidar, visible all-sky camera and solar photometry. This study will show some preliminary results of a field experimental campaign conducted during the winter/dry season at SPU LALINET station at São Paulo – Brazil using several remote sensing instruments, i.e., an elastic lidar, a visible all-sky camera and the sunphotomenter from AERONET. In this approach, information of cloud cover, cloud pixel identification, e. g., Red/Blue Difference, Red/Blue Ratio, Normalized Red/Blue Ratio, Saturation and Intensity should be retrieved from all-sky camera and used to extract the correlation between aerosol optical depth (AOD) from AERONET.

10424-34, Session PS

Atmospheric synchronous correction of GF-2 satellite multispectral image

Dongdong Fan, Aerospace DongFangHong Satellite Co., Ltd. (China); Fuqiang Bian, Aerospace DongFangHong Satellite Co., Ltd. (Qatar)

GF-2 as China's first sub-meter spatial resolution remote sensing satellite provides high-quality remote sensing products in the aspect of resource exploration, environmental monitoring, crop yield estimation, disaster prevention and mitigation, which play an important role in the macroeconomic decisions. Atmospheric correction is the necessary part in the data preprocessing of the quantitative high resolution remote sensing, which can eliminate the signal interference in the radiation path caused by atmospheric scattering and absorption, and reducting apparent reflectance into real reflectance of the surface targets.

Aiming at the problem that current research lack of atmospheric date which are synchronization and region matching of the surface observation image, this research utilize the MODIS Level 1B synchronous data to simulate synchronized atmospheric condition, and write programs to implementation process of aerosol retrieval and atmospheric correction, then generate a lookup table of the remote sensing image based on the radioactive transfer model of 6S (second simulation of a satellite signal in the solar spectrum) to correct the atmospheric effect of multi-spectral image from GF-2 satellite PMS-1 payload.

According to the correction results, this paper analyzes the pixel histogram of the reflectance spectrum of the 4 spectral bands of PMS-1, and evaluates the correction results of different spectral bands. Then conducted a comparison experiment on the same GF-2 image based on the QUAC. According to the different targets respectively statistics the average value of NDVI, implement a comparative study of NDVI from two

different results. The degree of influence was discussed by whether to adopt synchronous atmospheric date.Research shows that the correction adopt synchronous atmospheric date significantly improves vegetation extraction ability of the GF-2 remote sensing data. NDVI increased in the vegetation-coverd areas , vegetation and non-vegetation area are more obviously distincted. After the correction of QUAC process, there are still exist the spectrum distortion in the complex light condition surface, the correction did not fully meet the purpose of correcting atmospheric radiation interference. Finally, the prospect of the synchronous atmospheric correction is discussed.

10424-35, Session PS

Selection of optical model of stereophotography experiment for determination the cloud base height as a problem of testing of statistical hypotheses

Alexey I. Chulichkov, M.V. Lomonosov Moscow State Univ. (Russian Federation); Oleg V. Postylyakov, A.M. Obukhov Institute of Atmospheric Physics (Russian Federation); Stanislav V. Nikitin, M.V. Lomonosov Moscow State Univ. (Russian Federation)

For the reconstruction of some geometrical characteristics of clouds a method was developed based on taking pictures of the sky by a pair of digital photo cameras and subsequent processing of the obtained sequence of stereo frames to obtain the height of the cloud base. The method of the morphological analysis of images is used to determine the relative shift of the coordinates of some fragment of cloud. The shift is used to estimate the cloud base height and cloud speed.

Since in practice the positioning of the cameras enough precise to solve the stated problem can't be provided, we proposed an approach to adjusting the relative position of the optical axis of one (adjustable) of two cameras relative to another (reference) using photographs of specially selected test objects. As test objects for the calibration we used the starry sky. Frames of cloudy sky with the adjustable camera, using parameters estimated by the photographing the starry sky, were converted to mean that it would be in the perfect adjustment of its characteristics relative to the reference camera. We developed three models of distortion of photo camera glasses. The simplest one neglect the distortion, and use affine transformation to adjust the position of one camera to the position of another one. Two more complicated models take into account radial distortion of 3rd and 3rd&5th order accordingly.

We developed a method for determination of the optical model of camera gasses which should be used for different field of view of cameras. Using our experimental setup we tested it in application to experimental observations of starry sky and in the problem of the determination of cloud bottom.

10424-1, Session 1

Maritime aerosol network optical depth measurements and comparison with satellite retrievals from various different sensors *(Invited Paper)*

Alexander Smirnov, NASA Goddard Space Flight Ctr. (United States) and Science Systems and Applications, Inc. (United States); Maksym Petrenko, NASA Goddard Space Flight Ctr. (United States) and ADNET Systems, Inc. (United States); Charles Ichoku, Brent Holben, NASA Goddard Space Flight Ctr. (United States)

The paper reports on the current status of the Maritime Aerosol Network (MAN) which is a component of the Aerosol Robotic Network (AERONET). A public domain web-based data archive dedicated to MAN activity can be found at http://aeronet.gsfc.nasa.gov/new_web/maritime_aerosol_network.html (Smirnov et al. 2009). MAN deploys handheld sunphotometers and utilizes the calibration procedure and data processing traceable to AERONET. Since 2006 over 350 cruises were completed and data archive consists of more than 5500 measurement days. MAN represents an important strategic sampling initiative and ship-borne data acquisition complements island-based AERONET measurements. Data are easily accessible in the web-based public data archive and stimulate research and international collaboration in various scientific areas.

Building upon the AERONET network the use of mobile sun-photometers in the MAN project has led to substantially increased coverage over the oceans, and its data archive (2006-2016) provides a basis for evaluation and inter-comparison of aerosol optical depth (AOD) retrievals from various spaceborne sensors. In this work, we analyze collocated MAN, MODIS Terra, MODIS Aqua, MISR, POLDER, SeaWIFS, OMI, CALIOP, and VIIRS spaceborne aerosol products using a modified version of the Multi-Sensor Aerosol Products Sampling System (MAPSS) framework (Petrenko et al., 2012). Data product versions used in this paper are as follows: MAN - version 2, MODIS (Terra and Aqua) - collections 5.1 and 6, MISR – version 22, POLDER - versions J and K, SeaWIFS - version 4, OMI - version 3, CALIOP – versions 3 through 3.30, and VIIRS – version 1. Because of different spatio-temporal characteristics of the analyzed products, the number of MAN data points collocated with spaceborne retrievals varied between ~1500 matchups for MODIS to 39 for CALIOP (as of August 2016). Despite these unavoidable sampling biases, latitudinal dependencies of AOD differences for all satellite sensors, except for MODIS Aqua, showed positive biases against ground truth (i.e. MAN) in the southern latitudes (>50º S) and substantial scatter in the Northern Atlantic "dust belt" (5º-15º N). MODIS Aqua differences (against MAN) are almost evenly distributed around zero as a function of latitude and Collection 6 performs better overall. Our analysis did not intend to determine how many retrievals are within claimed uncertainty boundaries but rather show where bias exist and corrections are needed. The frequency of occurrences histogram of all considered AOD differences (SAT-MAN) indicates that vast majority are positive. Only two of them (SeaWIFS and CALIOP) are biased negative with median differences of -0.01 and -0.03 correspondingly. We foresee continuation of our effort in data collection and further comparison with aerosol models and satellite retrievals.

References

Smirnov, A., B.N.Holben, I.Slutsker, et al. Maritime Aerosol Network as a component of Aerosol Robotic Network, J. Geophys. Res., 114, D06204, doi:10.1029/2008JD011257, 2009.

Petrenko, M., C.Ichoku, and G.Leptoukh, Multi-sensor Aerosol Products Sampling System (MAPSS), Atm. Meas. Tech., 5, 913-926, doi:10.5194/amt-5-913-2012, 2012.

10424-2, Session 1

An effective method for retrieval of three kinds of aerosol properties focusing on a coming GCOM-C1 / SGLI in December of 2017

Itaru Sano, Kindai Univ. (Japan); Sonoyo Mukai, The Kyoto College of Graduate Studies for Informatics (Japan); Makiko Nakata, Kindai Univ. (Japan)

The Japanese space agency has a plan to launch new Earth observing satellites. The first satellite was successfully launched in May of 2012 to aim to understand the water cycle of the Earth, so called the water version of global change observation mission satellite (GCOM-W1). The second satellite is developed to measure physical variables of atmosphere, land and ocean, called GCOM-Climate (GCOM-C1). The GCOM-C1 boards the second generation global imager (SGLI) observing the Earth's reflectance from near UV to thermal infrared wavelengths.

This work intends to describe an algorithm to retrieve aerosol properties to be provided from SGLI measurements.

One of specific feature of SGLI is the polarimetric optics for the Earth's atmosphere and surface system. This is designed to measure the aerosol information over land. The first polarization dataset was successfully collected by the polarization directionality of the Earth's reflectance (POLDER) on advanced earth observing satellite-1 (ADEOS-1). The POLDER provided us with three components (I, Q, and U) of Stokes vector from measurements of three different polarization angles (0-60-120 degrees). The SGLI also gives us (I, Q, and U) components available for aerosol retrieval at two wavelengths (674 and 869 nm). Our procedure also simultaneously uses the observations at near UV channel as well as polarization measurements to detect the absorbing aerosols.

Modern aerosol retrieval procedure, such as the GRASP, provides us with great aerosol information as well as surface properties. However this inversion system still takes a lot of computing time compared to the conventional look-up table approach. Polarimetric information of SGLI will be collected with high spatial resolution (1 km x 1 km). Accordingly we have chosen the look-up table method for faster processing of entire SGLI dataset in near real time under the premise to the high precision and efficiency improvement. Then it is possible to estimate three kinds of aerosols properties as aerosol optical thickness, size information, and single scattering albedo.

10424-3, Session 1

Deriving aerosol parameters from in-situ spectrometer measurements for validation of remote sensing products

Sebastian Riedel, Joanna Janas, Peter Gege, Deutsches Zentrum für Luft- und Raumfahrt e.V. (Germany)

Atmospheric correction is important for the application of quantitative evaluation methods in optically complex coastal and inland waters. In particular when applying bio-optical models, atmospheric correction is the limiting factor in the results accuracy.

The most critical parameter for atmospheric correction is the aerosol, especially for turbid and spatially inhomogeneous coastal and inland waters. For validation of atmospheric correction accurate aerosol parameters, measured very close to a number of matchup locations are required. Therefor it is often necessary to measure aerosol parameters during field campaigns on a boat. Aerosol parameters are usually derived from stationary, self-aligning sunphotometers at fixed locations or from mobile handheld sunphotometers at a number of test sites during field campaigns. The spatial coverage of ground based sunphotometers is often insufficient for validation purposes, and targeting the sun with the required accuracy below 1° with a handheld device on a boat can be challenging. To be more flexible during field campaigns, we are developing a method which allows the derivation of aerosol parameters from measurements with any spectrometer with suitable spectral range and resolution. While sunphotometers measure the radiance from the direction of the sun, this method uses a pair of downwelling irradiance and sky radiance measurements. Since no accurate alignment is necessary, the data can be acquired fast and reliable at almost any place during a wide range of weather conditions. In contrast to sunphotometers, spectrometers are commonly used by researchers in aquatic optics or limnology, which greatly extends the number of potential users.

For our studies we used an Ibsen Freedom VIS spectrometer with a spectral range of 350-850 nm and a spectral resolution of approx. 1.5 nm. We developed a model for sky reflectance and sky radiance spectra based on the analytic model of Gregg and Carder for downwelling irradiances (W. W. Gregg and K. L. Carder, "A simple spectral solar irradiance model for cloudless maritime atmospheres," Limnol. Oceanogr. 35 , 1657 – 1675 (1990)). Aerosol is parameterized in this model in terms of a turbidity coefficient (aerosol optical depth at 550 nm) representing concentration, and an Ångström exponent characterizing the wavelength dependency of scattering. These two aerosol parameters are derived by inverse modelling. For validation we used data from sunphotometers of the Aerosol Robotic Network (AERONET) and from handheld devices (SolarLight Microtops).

10424-4, Session 1

South-East Asia cirrus cloud and aerosols radiative effect assessment by ground-based NASA MPLNET lidar network data and CALIPSO satellite measurements

Simone Lolli, NASA Goddard Space Flight Ctr. (United States) and Instituto di Metodologie per l'Analisi Ambientale, CNR (Italy); James R. Campbell, U.S. Naval Research Lab. (United States); Jasper R. Lewis, Ellsworth J. Welton, NASA Goddard Space Flight Ctr. (United States); Yu Gu, Univ. of California, Los Angeles (United States); Jared Marquis, Univ. of North Dakota (United States)

Thin cirrus clouds are the only genus that are capable of cooling and warming the system earth-atmosphere during daytime. South-East Asia, one of the most vulnerable regions of the world to climate change that has known both a strong economic and population growth in the last few years, shows a cirrus cloud relative frequency up to 70%. The purpose of this study is to assess the radiative effects of the cirrus clouds in a region delimited by 55N to 11S in latitude and 70E to 150E in longitude with a spatial resolution of 5 degrees. The radiative effect is assessed inputting the atmospheric profile of the cloud optical properties retrieved from CALIOP, the lidar onboard CALIPSO satellite and from three MPLNET ground-based permanent observational sites as Singapore, Omkoi (Thailand) and Penang (Malaysia), into the 4-stream Fu-liou-Gu radiative transfer model.

10424-5, Session 1

First tests of a multiwavelength mini-DIAL system for the automatic detection of greenhouse gases

Michela Gelfusa, Stefano Parracino, Michele Lungaroni, Emmanuele Peluso, Univ. degli Studi di Roma "Tor Vergata" (Italy); Andrea Murari, Consorzio RFX-Association EURATOM-ENEA (Italy); Jean Francois Ciparisse, Andrea Malizia, Riccardo Rossi, Univ. degli Studi di Roma "Tor Vergata" (Italy); Piergiorgio Ventura, Ctr. Tecnico Logistico Interforze NBC (Italy); Pasqualino Gaudio, Univ. degli Studi di Roma "Tor Vergata" (Italy)

Considering the increase of atmospheric pollution levels in our cities, due to emissions from vehicles and domestic heating, and the growing threat of terrorism, it is necessary to develop instrumentation and gather know-how for the automatic detection and measurement of dangerous substances as quickly and far away as possible.

The Multi-Wavelength DIAL, an extension of conventional DIAL technique, is one of the most powerful remote sensing methods for the remote sensing of multiple substances and seems to be a promising solution compared to existing alternatives.

In this paper, first in-field tests of a smart and fully automated Multi-Wavelength mini-DIAL will be presented and discussed in details. The recently developed system, based on a CO2 laser source operating in IR-C band, has the potential of giving an early warning, whenever something strange is found in the atmosphere, followed by identification and simultaneous concentration measurement of many chemical species, ranging from the most important Greenhouse Gases (GHG) to other

harmful Volatile Organic Compounds (VOCs).

Preliminary studies, regarding the fingerprint of the investigated substances, have been carried out by cross-referencing database of IR spectra, obtained using in-cell measurements, and typical Mixing Ratios in the examined region, extrapolated from the literature. Preliminary experiments in atmosphere have been performed into a suburban and moderately-busy area of Rome. Moreover, to optimize the automatic detection of the harmful species to be recognized an advanced multivariate statistical method has been developed and tested.

10424-6, Session 1

Fast radiative transfer model from IR to UV for remote sensing applications

Xu Liu, NASA Langley Research Ctr. (United States); Q. Yang, W. Wu, Science Systems and Applications, Inc. (United States); Daniel K. Zhou, Allen M. Larar, NASA Langley Research Ctr. (United States)

Fast and accurate radiative transfer model is the key for satellite data analysis, numerical weather prediction, and observation system simulation experiments for climate study applications. We have developed a Principal Component-based radiative transfer model (PCRTM) which can simulate radiative transfer in the cloudy atmosphere from far IR to visible and UV spectral regions quickly and accurately. Multi-scattering of multiple layers of clouds/aerosols is included in the model. A hybrid stream discrete multiple scattering scheme is used to minimizing the number calculation need. The computation speed is 3 to 4 orders of magnitude faster than the medium speed correlated-k option MODTRAN5 and LBLRTM. The PCRTM calculated radiance spectra agree with the Modtran and LBLRTM within 0.02%. Application of this model to various hyperspectral instrument will be shown and discuss.

10424-7, Session 2

Detection and retrieval of single and multilayer clouds in an artificial neural network approach

Sunny Sun-Mack, Science Systems and Applications, Inc. (United States) and NASA Goddard Space Flight Ctr. (United States); Patrick Minnis, William L. Smith Jr., NASA Langley Research Ctr. (United States); Gang Hong, Science Systems and Applications, Inc. (United States) and NASA Langley Research Ctr. (United States); Yan Chen, Science Systems and Applications, Inc. (United States) and NASA Langley Research Ctr. (United States)

Satellite remote sensing is essential for monitoring clouds on regional and larger scales. Because clouds affect radiation, precipitation, atmospheric heating, and visibility, it is critical to understand and model those variables that cloud vertical structure be characterized as well as the bulk microphysics of the cloudy column. Most retrievals of cloud properties from satellites rely on interpretation of the observed radiances as emanating from a single plane-parallel layer. A physical model is employed to convert the radiances into several parameters, such as cloud top height (CTH), optical depth (COD), and particle size (CER), which are assumed to represent the average for the observed cloud. Yet, many cloud systems consist of one or more cloud layers, each having its own average properties. Determining the layers of the cloud system and their average properties is a daunting challenge for passive remote sensing. A variety of multispectral techniques have been employed to detect multilayer systems with varying degrees of success. Fewer methods have gone to the next step and attempt to retrieve the properties of the bottom and top layers. These various methods have been only mildly successful. Much of the difficulty in addressing this challenge has been the ambiguity of the signals used in the methods. Determining whether the observed scene is composed of a thin cirrus over a water cloud or thick cirrus contiguous with underlying layers of ice and water clouds is often difficult because of similarities in the observed radiance values. Recently, artificial neural network algorithms employing two or more infrared channels have been developed to detect thin and thick ice clouds and estimate CTH and COD regardless of the underlying background, clear or cloudy. They are based on training with CALIPSO and/or Cloudsat (CC) data matched with multispectral radiances from various satellites. The CC lidar and radar profiles provide the vertical structure, CODs, and CER values that serve as output for a neural network (NN) algorithm that employs various combinations of multispectral infrared radiances. By applying the trained NN to MODIS data, it is possible to estimate the height and optical properties of the upper-layer clouds. It may also be possible to determine whether the cloud is mostly contiguous in the vertical or whether it comprises well-separated distinct layers. Knowing the properties of the upper part of the cloud and its layering status, it should be possible to determine the properties of the lower layer using a multilayer retrieval model. This paper explores the potential of this approach for better defining and monitoring multilayer cloud systems.

10424-8, Session 2

A Meteosat Bayesian Cloud Fractional Cover Climate Data Record: evaluation, homogeneity assessment and intercomparison with existing climate data records

Jedrzej S. Bojanowski, Institute of Geodesy and Cartography (Poland); Reto Stöckli, Anke Duguay-Tetzlaff, MeteoSwiss (Switzerland); Stephan Finkensieper, Deutscher Wetterdienst (Germany)

A cloud fractional cover dataset covering 1991-2015 derived from Meteosat First Generation (MFG) and Meteosat Second Generation (MSG) has been recently produced by the EUMETSAT's Satellite Application Facility for Climate Monitoring. The dataset optimally exploits the limited information from only two channels (broad band visible and thermal infrared) acquired by older geostationary sensors. The underlying algorithm employs a cyclic generation of clear sky background fields, uses continuous cloud scores and runs a Bayesian cloud fraction estimation using concurrent information on cloud state and variability. The algorithm depends on well characterized IR radiances and VIS reflectances from the Meteosat Fundamental Climate Data Record (FCDR) provided by EUMETSAT. The evaluation of both Level-2 (instantaneous) and Level-3 (daily and monthly means) data has been performed using two reference datasets: ground-based observation (SYNOP) and retrievals from an active satellite instrument (CALIPSO/CALIOP). Inter-comparisons have employed concurrent state-of-the-art satellite-based datasets derived from geostationary and polar orbiting passive visible and infrared imaging sensors (MODIS, PATMOS-x, CLARA-A2, CLAAS-2 and CC4CL-AVHRR). Averaged over all reference sites, Meteosat CFC complies with requirements for accuracy and precision (defined by EUMETSAT and reflecting GCOS requirements) as compared to SYNOP. We conclude the Meteosat CFC corresponds to CFC measured at WMO SYNOP sites, and it is thus useful to extend in both space and time century-long ground-based climate observations. We also emphasize that Meteosat CFC is the longest currently available high temporal (sub-daily) and high spatial (0.05x0.05 deg) resolution satellite-derived CFC climatology. The current time span of 25 years (1991–2015) will be extended back to 1983 once the underlying inter-calibrated FCDR becomes available for MFG-2 and MFG-3.

10424-9, Session 2

Macrophysical properties of continental cumulus clouds from active and passive remote sensing

Evgueni I. Kassianov, Pacific Northwest National Lab. (United States); Erin A. Riley, Jessica M. Kleiss, Lewis & Clark (United States); Charles N. Long, Univ. of Colorado Boulder (United States); Laura Riihimaki, Donna Flynn, Connor Flynn, Larry K. Berg, Pacific Northwest National Lab. (United States)

Cumulus clouds exhibit extreme variability and have relatively small (~1 km) horizontal and vertical sizes, thus they represent a great challenge for the remote sensing. The conventional retrievals of their properties rely heavily on the ground-based active remote sensing. However, the corresponding measurements are commonly zenith pointing with a very narrow field of view (FOV). Therefore, the cloud properties provided by these measurements may not be representative of a larger surrounding area. Long-term integrated measurements at the U.S. Department of Energy (DOE) Atmospheric Radiation Measurement (ARM) program's Southern Great Plains (SGP) site in Oklahoma provide a unique opportunity to assess the representativeness of cloud properties obtained from the narrow-FOV observations. For our assessment, we use the narrow-FOV ARM Active Remotely Sensed Clouds Locations (ARSCL) and large-FOV Total Sky Imager (TSI) cloud products for selected days with single-layer cumulus clouds from the existing multi-year climatology (2005-2008). We start our assessment with obtaining information about cloud field inhomogeneity from statistical analysis of the spatial distribution of cloud cover over a 160-degree FOV TSI images. Then we apply the obtained information to segregate the selected days into different groups with various degrees of cloud field inhomogeneity. Finally, we compare TSI- and ASCRL-based cloud macro-physical properties for the segregated groups. In our presentation, we will discuss initial results of our assessment and highlight their importance for evaluation of model predictions.

10424-10, Session 2

Cloud cover forecast from a ground-based all sky infrared thermal camera

Sylvain Cros, Olivier Liandrat, Antonin Braun, Reuniwatt (France); Laurent Saint-Antonin, Jacques Decroix, IRT Antoine de Saint Exupéry (France); Nicolas Schmutz, Reuniwatt (France)

Obtaining in real-time and forecasting the cloud pattern of the sky vault within 30 min. is useful for various application such as solar energy systems managements, air traffic or free space optical communication with a satellite.

Forecast models using camera in visible spectrum faces several challenges. The image segmentation algorithm (differencing cloudy and cloud free pixels) must take into account diurnal variations of cloud illumination due to solar zenith angle, as well as sensor saturation near the Sun. Lack of information concerning cloud thickness involves strong hypothesis on radiation attenuation factor. Determination of cloud shadow map around a given site requires cloud base altitude that is eventually retrievable by stereoscopy using several cameras.

In this work, we present Sky Insight, a sky imager using thermal infrared vision. It has the advantages to observe the radiance emitted by the sky vault in the 8-14 μm spectra. This atmospheric window permits to obtain a good contrast between cloud and clear sky. In addition, radiance does not depend on sunlight reflected by clouds and no saturation occurs around the sun. Finally, thermal infrared radiance can be signature of cloud physical properties such as cloud optical depth and cloud base height.

We propose to assess the benefits of Sky Insight for very short-term solar irradiance forecast, by comparing it to a sky imager with a sensor in the visible spectra. A 1- year of collocated observations taken in Saint-Leu (Reunion Island in Indian Ocean) including visible and infrared images of the sky acquired every 30 seconds and global horizontal irradiance every minute was used as dataset for the comparison. We implemented and assessed a proven forecast algorithm on the visible sky imager and adapted the same on Sky Insight. We determined the benefits brought separately by different feature. In particular, at first we used the enhanced cloud segmentation allowed by Sky Insight, and in a second case, we add the possibility to obtain the cloud optical depth, where a visible camera permits to have a 3-class values of cloud attenuation.

Forecasts were compared with GHI measurement. A test on the whole year determined that at 5 and 10 minutes time horizon, Sky Insight enabled a relative RMSE decrease of 25 % using the cloud segmentation and up to 45 % by adding the retrieved cloud optical depth. A feasibility study is finally outlined considering cloud height base would be available thanks to Sky Insight.

10424-12, Session 2

Smart air quality net

Matthias Budde, Till Riedel, Michael Beigl, Karlsruhe Institut für Technologie (Germany); Klaus Schäfer, Stefan Emeis, Karlsruher Institut für Technologie (Germany); Josef Cyrys, Jürgen Schnelle-Kreis, Helmholtz Zentrum München GmbH (Germany); Andreas Philipp, Univ. Augsburg (Germany); Volker Ziegler, GRIMM Aerosol Technik GmbH & Co. KG (Germany); Hans Grimm, Aerosol Akademie e.V. (Germany); Thomas Gratza, Umweltamt, Stadt Augsburg (Germany)

Air quality and the associated subjective and health-related quality of life are among the important topics of our time. However, it is very difficult for many cities to take measures that to accommodate today's needs concerning e.g. mobility, housing and work, because a consistent data base with fine-granular data and information on causal chains is missing. This has the potential to change, as today, both large-scale basic data as well as new promising measuring approaches are becoming available.

Project "SmartAQnet", funded by the Federal Ministry of Traffic and Infrastructure, is based on a pragmatic, data driven approach, which for the first time combines existing data sets with a networked mobile measurement strategy. By connecting open data, such as weather data or development plans, remote sensing of influencing factors, and new mobile measurement approaches, such as participatory with ultra-low sensor technology, "scientific scouts" (prototypes of small air quality sensors) and demand-oriented measurements by light weight UAVs, a novel measuring and analysis concept is created within the model region of Augsburg. In addition to novel analytics, a prototypical technology stack is planned which, through modern analytics methods and Big Data and IoT technologies, enables application in a scalable way.

10424-13, Session 2

Generalization of optical, energy and excess-noise parameters to compare capabilities of lidar with PMT/APD/SiPM

Ravil R. Agishev, Kazan State Power Engineering Univ. (Russian Federation); Adolfo Comerón, Univ. Politècnica de Catalunya (Spain)

Further developments of the methodology for comparative analysis of the capabilities of different lidar systems [1],[2], from micro-lidars to systems employing high peak-power lasers, using different receiving systems are conducted.

Following the dimensionless parameterization approach and in order to simplify the prediction of capabilities and system comparison, to improve its clarity and to expand its applicability, we propose specific ways to generalize optical, energetic and excess-noise parameters inherent to lidar atmospheric monitoring, taking into account their possible high scale variability. The generalized approach is adapted to compare lidars with PMT/APD/SiPM detectors. Examples of the proposed approach in different conditions and applications are discussed.

[1] Adolfo Comerón, Ravil R. Agishev "Dimensionless parameters for lidar performance characterization", Proceedings of SPIE vol. 9242, pp. 92420U-1 – 92420U-10, 2014

[2] Ravil Agishev, Adolfo Comerón, Alex Gilerson, "About the potential of lidars with different photodetectors under daytime sky radiation", 27th International Laser Radar Conference (ILRC 27), EPJ Web of Conferences, 119 (2016) 25009, doi: 10.1051/epjconf/201611925009, doi: 10.1117/12.2068743

10424-14, Session 3

Determination of aerosol optical properties for retrieval of water-leaving radiance at Roodeplaat Dam relating to calibration and validation of Sentinel 2 and 3

Zimbini Faniso, CSIR National Laser Ctr. (South Africa) and Univ. of Fort Hare (South Africa); Derek J. Griffith, Council for Scientific and Industrial Research (South Africa); Mark Metthews, CyanoLakes (Pty) Ltd. (South Africa); Jeremy Kravitz, CyanoLakes (Pty) Ltd. (South Africa) and Univ. of Cape Town (South Africa)

Remote sensing of inland water quality is a particularly challenging satellite Earth observation EO application. This arises because inland water bodies are small and optically complex targets that are generally dark compared to surrounding land. Inland water bodies are source supplies of water hence they need an observation. The spatial distribution of water changes over time and that leads to issues in different sectors like agriculture, environmental and ecological. Signal reaching the satellite is usually dominated by light scattered in the atmosphere. Aerosols are strongly variable atmospheric constituents, they play a major role in generating this unwanted signal which must be quantified and removed before any conclusions about water state that can be reached. The light will be scattered in different bands, the study will consciously analyse at visible and near infrared where it will be easy to distinguish the atmospheric noise types. A field campaign has been executed at Roodeplaat dam near Pretoria relating to calibration and validation (calval) of the recently launched Sentinel 2 and Sentinel 3 satellites. In situ measurements are taken at Roodeplaat dam simultaneously with the satellite overpass. The Atmospheric Radiative transfer modelling (RTM) for the atmosphere is required for satellite retrievals of surface radiant quantities for analysing the data. Aerosol models for radiative transfer have been evaluated and refined to improve retrieval accuracy of water-leaving radiance at Roodeplaat dam. A retrieval algorithm for water-leaving radiance Lw and remote-sensing reflectance Rrs has been developed to analyse the sensitivity of the retrieval to aerosol optical properties. Sensitivities, as well as proposals for enhanced retrieval methods, are presented.

10424-15, Session 3

Use of the fragmentary spectrum registration method for Raman spectroscopy

Alexander V. Fadeyev, Vitold E. Pozhar, Scientific and Technological Ctr. for Unique Instrumentation (Russian Federation)

In this paper the possibilities of the new analytical method, named fragmentary spectrum registration (FSR), for work with Raman spectra are analyzed.

FSR was developed by authors of this paper as a specialized technique of spectral analysis, which can be effectively used by spectrometers with ability of fast random spectral access (RSA). Use of FSR-method in the measurement systems based on acousto-optical (AO) spectrometers - spectrometers based on acousto-optical tunable filters (AOTF's) – allows significantly reducing the measurement time or the error of measurement results for such important practical tasks such as rapid analysis of multi-component gaseous mixtures for air pollution detection.

FSR-method is closely linked to the possibility of RSA-spectrometers to provide fast random spectral access when addressing into any spectral point takes equally small time (comparable with the transit time of acoustic wave through AOTF crystal (microseconds) for AO spectrometers). For efficient use of RSA-property AO spectrometers need to determine the selection algorithm in order to register the spectrum in optimal way, i.e. only in those spectral points that are needed for specific practical task. The FSR fundamental principal is the use of only a few selected spectral points, which is sufficient for a complete determination of the substances. FSR is based on the method of differential optical absorption spectroscopy (DOAS), which analyzes a series of narrow spectral regions that are characteristic for analyzed components (substances).

Due to the use of RSA-spectrometers it is sufficient to use only the limited set of pre-selected spectral points for a complete determination of substances. It can give a substantial (up to 100 times) reduction of detection interval in comparison with the record time of total spectrum. Selection of the most informative spectral points is performed by specialized procedure based on the criteria of minimizing both measurement time and error of measurement results. In addition to FSR-method the procedure of qualitative analysis based on statistical independent component analysis method (ICA) was developed. It allows estimating the loss of important information during the spectral selection procedure and enables to expand the potential of the method to construct adaptive measurement systems based on RSA-spectrometers.

FSR-method was developed for work with absorption spectra, but obtained results allow us to make an assumption about its applicability and effectiveness for work with sparse line spectra of a different nature. In this paper the possibilities of FSR-method for work with Raman spectra which are similar to the absorption spectra (narrow lines on a solid background) are analyzed. Nowadays there are numerous examples of practical use of Raman spectra, in particular, the Raman spectroscopy has become a de facto standard method of identification of samples in a condensed phase.

Numerical simulations have been carried out using specially developed software that allows simulating mixture spectra and using FSR-algorithm for selecting the most informative points for the given constraints of time and accuracy. The results of numerical simulation of FSR-method with Raman spectra are presented. Spectral database of Raman spectra created by Scientific and Technological Centre for Unique Instrumentation of the Russian Academy of Sciences (STC UI of RAS) was used during numerical simulations. Obtained results confirm the assumption of applicability of FSR-method to work with Raman spectra. The use of FSR-method the more effective the more sparse structure the analyzed spectra have.

This work was supported in part by the Russian Foundation for Basic Research project 16-29-11802.

10424-16, Session 3

Freezing level and bright band height over the Indian Ocean

Rajasri Sen Jaiswal, Sonia R. Fredrick, Rasheed Mohammed, Sona College of Technology (India)

The freezing level height (HFL) and the radar bright band height (BBH) are the two important parameters pertaining to cloud physics and precipitation study. The present paper investigates these two parameters over the Indian Ocean over the latitudinal range 36S-8N and the longitudinal range 45E-110E. For this purpose, the freezing level height and radar bright band height data have been obtained from the data product 2A23 of the precipitation radar (PR) onboard the Tropical Rainfall Measuring Mission satellite (TRMM). The period of study is 1999-2002; 2007-2008.

The authors have made an attempt to investigate the latitudinal variations of the HFL and the BBH over the Indian Ocean; and the monthly and yearly variations of these parameters. The study shows that in individual months, the longitudinally averaged HFL and the BBH shows very strong correlations with the latitude, more significant correlations being with the HFL than with the BBH. The HFL also shows excellent correlations with the latitude at a fixed longitude. However, at a fixed longitude, the BBH at times, shows, but not always, correlations with the latitude.

At a particular location over the Indian Ocean, the HFLmx/min occurs mostly in the same month throughout the period of study. However, at a particular location, the maximum BBH does not occur in the same month, so also the minimum BBH.

The author further makes an attempt to find out whether the BBHmx or the BBHmin always occurs at the same location over the Indian Ocean. The study shows that the BBHmin mostly occurs around 35S, while the location of the BBHmx shows strong seasonal dependence.

The study also shows that over the Indian Ocean, both in the northern and the southern hemisphere, as the latitude increases, the % of times BBH>HFL also increases.

10424-17, Session 4

Improving consistency of CERES ERB record measured by scanneres on Terra/Aqua/NPP-S satellites

Z. Peter Szewczyk, Science Systems and Applications, Inc. (United States); Dale R Walikainen, Susan Thomas, Natividad M Smith, Science Systems and Applications (United States); Kory J Priestley, NASA LaRC (United States)

A CERES (Clouds and the Earth's Radiant Energy System) scanning radiometer is designed to measure accurately the solar radiation reflected, and thermal radiation emitted by the Earth. Two CERES instruments (FM1 and FM2) aboard the Terra spacecraft have been in operation since 2000, out of the two (FM3 and FM4) aboard the Aqua spacecraft (launched 2002) only FM3 has still been fully operational since 2005, and one scanner (FM5) aboard the NPP-S was launched in 2012. There are four CERES scanners on three different platforms collecting science data without any disruptions, and maintaining the continuity and consistency of this dataset have been in the focus of the instrument group. Currently, a new edition of an instantaneous CERES science data product, referred to as the ERBE-like or ES8s for the continuity with Earth budget missions before CERES instruments, is being considered to further improve the consistency of the ERB dataset over all four instruments. Since this product lays foundation for other products, it is important to maintain the high accuracy of 1% and 0.5% for shortwave and longwave fluxes, respectively, as specified in the mission objectives.

In the early stage of the Terra and Aqua mission (until 2005), one of the instruments on each platform operated in the RAPS (Rotational Azimuth Plane Scan) mode that caused increased throughput degradation as opposed to the other instrument operating in the XT (cross-track) mode. A certain strategy to model this degradation was devised and implemented in the current editions of the Terra and Aqua ES8s; however most recent analyses and FM5 data show the need for further improvements. It is sufficient for this work justification to state that the difference between FM2 and FM1 shows to be 0.5% in the shortwave channel, the difference between FM5 and FM3 is about 2%, and 1% for FM1 and FM5 in the same channel. In order to eliminate the existing inconsistencies between instruments, a comprehensive validation approach is taken that examines modeling techniques for quantifying the RAPS mode degradation, and its effect on setting scanners on the same radiometric scale. The RAPS degradation correct modeling is particularly important for the Aqua mission, in which the instrument (FM3) that was in the RAPS mode is used for SW measurements since the XT scanner (FM4) has failed in May 2005.

The full paper describes a comparison technique that is used to quantify the differences in scanners measurements, shows the required changes to the numerical models of spectral response functions (SRFs) to reduce these differences. It also verifies the validity of the previous work of setting Terra and Aqua instruments on the same radiometric scale, and its effect on existing differences between FM5 on NPP-S and FM1 and FM3 on the Terra and Aqua satellites, respectively.

10424-18, Session 4

Joint use of weather radars, satellites and rain gauge for precipitation monitoring

Andrea Antonini, Lab. per la Meteorologia e la Modellistica Ambientale (Italy); Samantha Melani, Alessandro Mazza, Alberto Ortolani, Lab. per la Meteorologia e la Modellistica Ambientale (Italy) and Istituto di Biometeorologia (Italy)

Intense precipitation phenomena occurring over the Tyrrhenian area between Tuscany, Corse Sardinia, and Liguria very often cause floods with considerable socio-economic damages. The need of monitoring such events has led to the implementation of an observing weather radar network: it firstly started with an S-band radar in Corse, three C-band radars in Liguria, Tuscany and Sardinia. Recently, the implementation of an X–band network of three radars in Tuscany and two further C-band radars in Sardinia completed the network. This work shows how this network can be used for the characterization of weather events, following their development and dynamics and providing some information about their possible evolution. Furthermore, the use of meteorological satellites observations can upscale the area of interest to the mesoscale level, and provide an enlarged temporal overview. For instance, the Meteosat Second Generation satellites provide useful information about the air mass distribution, convective phenomena occurrence and microphysics in the observed scene, by combining different spectral channels. Finally, ground-based observations are meaningful for assessing the observing capabilities of other instruments and for characterizing the effects on soil surface. For some selected case studies, the different observing instruments were compared and a methodology to integrate them synergically is presented and tested. The elaboration processes are well-defined and structured to optimize the integration of the heterogeneous sensors in order to amplify the effectiveness of the measurements.

A first case study (9th April 2016) is related to a cyclogenesis event (as confirmed by satellite imagery), characterized by a low-pressure vortex located between Corse and Cote d'Azur and by a series of precipitation fronts in the Tyrrhenian area approaching the Italian coasts. The second case study (19th May 2016) is characterized by a strong precipitation event in the northern part of Italy that partially involves Liguria and Tuscany areas when moving in the south direction. This event is also characterized by convection activity as observed by satellites and a great number of lightning. Precipitation measured by the rain gauge network reaches peaks of more than 70 mm in 6 hours, which is not in absolute a huge value for the area, but it is related to a strong precipitation event as witnessed by local journals and reports. Finally, a third case study (6th March 2017) is an investigation of a weather system coming from the Tyrrhenian sea and propagating easterly, that

causes a series of strong rainfall events in Tuscany from the coast to the inner regions.

Weather radars correctly detect the rainfall systems and their motion in all the case studies. Clearly, the higher spatial resolution of X-band radars allows detecting the different precipitation areas with great spatial details, while C- and S-band radars can detect phenomena at higher distances. Satellites images have lower spatial resolutions, but especially thanks to the RSS (Rapid Scan Service) they can help to detect the growing or dissipating stage of the whole phenomena. Moreover the ground-based network confirms its relevance in improving the identification of the precipitation intensity and in reducing the number of false alarms.

10424-19, Session 4

Development of multi-sensor global cloud and radiance composites for earth radiation budget monitoring from DSCOVR

Konstantin V. Khlopenkov, David P. Duda, Mandana Thieman, Patrick Minnis, Science Systems and Applications, Inc. (United States); Wenying Su, Kristopher M. Bedka, NASA Langley Research Ctr. (United States)

The Deep Space Climate Observatory (DSCOVR) enables analysis of the daytime Earth radiation budget via the onboard Earth Polychromatic Imaging Camera (EPIC) and National Institute of Standards and Technology Advanced Radiometer (NISTAR). EPIC delivers adequate spatial resolution imagery but only in visible and NIR bands, while NISTAR measures the top-of-atmosphere (TOA) whole-disk radiance in shortwave and longwave broadband windows. Accurate calculation of albedo and outgoing longwave flux requires a high-resolution scene identification such as the radiance observations and cloud properties retrievals from low earth orbit (LEO, including NASA Terra and Aqua MODIS, Suomi-NPP VIIRS, and NOAA AVHRR) and geosynchronous (GEO, including GOES east and west, METEOSAT, INSAT-3D, MTSAT-2, and Himawari-8) satellite imagers. The cloud properties are derived using the Clouds and the Earth's Radiant Energy System (CERES) mission Cloud Subsystem group algorithms. These properties have to be co-located with EPIC pixels to provide the scene identification and to select anisotropic directional models (ADMs), which are then used to adjust the NISTAR-measured radiance and subsequently obtain the global daytime shortwave and longwave fluxes.

This work presents an algorithm for optimal merging of selected radiance and cloud property parameters derived from multiple satellite imagers to obtain seamless global hourly composites at 5-km resolution. Selection of satellite data for each 5-km pixel is based on an aggregated rating that incorporates five parameters: nominal satellite resolution, pixel time relative to the EPIC time, viewing zenith angle, distance from day/night terminator, and probability of sun glint. To provide a smoother transition in the merged output, in regions where candidate pixel data from two satellite sources have comparable aggregated rating, the selection decision is defined by the cumulative function of the normal distribution so that abrupt changes in the visual appearance of the composite data are avoided. Higher spatial accuracy in the composite product is achieved by using the inverse mapping with gradient search during reprojection and bicubic interpolation for pixel resampling.

For accurate spatial matching between EPIC measurements and the high-resolution cloud properties in the global composite, the composite data are subsequently remapped into the EPIC-view domain by using geolocation information supplied in EPIC Level 1B data. This step includes convolution of the composite pixels with the EPIC point spread function (PSF) defined with a half-pixel accuracy. Within every EPIC footprint, the PSF-weighted average value of each radiance and cloud property parameter is computed for each cloud phase based on the cloud mask from the global composite. The obtained values are then stored within five data subsets (clear-sky, water cloud, ice cloud, total cloud, and no retrieval) for each pixel in EPIC domain.

Spatial variability and continuity of the global composite data have been analyzed to assess the performance of the merging criteria. The proposed algorithm has demonstrated contiguous global coverage for any requested time of day with a temporal lag of under 2 hours in over 94% of the globe, which makes it useful for many climate applications.

10424-20, Session 4

Detecting of convective overshooting cloud tops using Himawari-8 images and machine learning approaches

Miae Kim, Junghee Lee, Juhyun Lee, Jungho Im, Minso Shin, Ulsan National Institute of Science and Technology (Korea, Republic of)

As severe convective clouds such as thunderstorm develop, overshooting top clouds sometimes form at the very top of the clouds, penetrating through cloud top or even into the lower stratosphere due to strong updraft. It is known that convective clouds accompanied by OTs can cause severe weather conditions such as lightning, large hail, strong winds, and heavy rainfall more frequently, influencing ground and aviation operation. Since water vapor as a major greenhouse gas is transported by overshooting clouds from troposphere into stratosphere, it can also affect the global climate change. Therefore, the detection and monitoring of OTs are needed to predict the degree of severity of convective clouds with correlation of the occurrence of severe weather events. Himawari-8 images were used as main input data to detect OTs with machine learning approaches such as random forest and logistic regression for binary classification of OT and nonOT (i.e. anvil clouds and non convective clouds) class and class probability. Reference regions for the two classes were constructed from August 2015 to August 2016 with MODIS and Himawari-8 visible images based on manual interpretation of human experts. Based on the reference regions, a total of 15 input variables?brightness temperature (TB), its standard deviation at five moving window sizes (MWSs), the difference of OT center and surrounding anvil clouds at 5 MWSs, and four split window differences? were extracted from multiple channels of Himawari-8 infrared images. The constructed dataset were randomly separated into training dataset (80%) and testing dataset (20%) for the use of developing classification model and evaluating the performance of the model, respectively. The developed OT classification algorithms were applied to the different dates of Himawari-8 images for hindcast validation. Probability of detection (POD) and false alarm ratio (FAR) were calculated for the prediction results for quantitative evaluation. The results produced promising prediction performances of over 85% of POD and less than 20% of FAR, which outperformed or were comparable to the previous studies.

10424-21, Session 4

Estimating PM2.5 spatial and temporal variation in Hong Kong with GTWR model and MODIS AOD retrieval

Xin Li, Shandong Agricultural Univ. (China) and The Hong Kong Polytechnic Univ. (Hong Kong, China); Yongjun Feng, Shandong Agricultural Univ. (China); Hongyu Liang, The Hong Kong Polytechnic Univ. (Hong Kong, China)

The particular matter with aerodynamic diameter ≤ 2.5 ?m (PM2.5) influences air visibility and human health significantly. Many environmental epidemiologic studies have demonstrated an association between PM2.5 and mortality, respiratory disease and cardiovascular disease. Since the ground-based

PM2.5 measurements are limited by the number of stations and are costly to maintain, it can hardly satisfy the requirement of PM2.5 monitoring in large and global scale. The aerosol of depth (AOD) retrieved from the remote sensing visible bands is most sensitive to the particular matter 0.1-2 ?m. Their correlation coefficient ranges from 0.2 to 0.8. Therefore, PM2.5 estimation based on satellite AOD data becomes a popular way by expanding ground monitoring to a large area. Most recent PM2.5 prediction models are global regression models of which coefficients are constants in space and time. In order to capture the spatial and temporal heterogeneity of PM2.5, a geographically and temporally weighted regression (GTWR) model based on AOD data was developed. The MODerate resolution Imaging Spectroradiometer (MODIS) data was used for AOD retrieval. MODIS has two types of AOD products at 10 km and 3 km spatial resolution which are retrieved based on Dark Target aerosol algorithm. However, AOD product at rough resolution might introduce some error and cannot satisfy air pollution application in Hong Kong. Therefore, a AOD product with 500 m spatial resolution was produced using a simplified aerosol retrieval algorithm (SARA) which directly used the radiance transfer model (RTM) for AOD estimation instead of using look-up table (LUR). The SARA retrieved AOD at 500 m resolution was validated with Aerosol Robotic Network (AERONET) AOD data showing a good agreement with R2 of 0.921 and RMSE of 0.059. In order to improve the accuracy of the model, some meteorological (temperature, pressure, relative humidity, wind speed and wind direction) and land use (NDVI, road length) factors were added into the model. The PM2.5 concentration estimation from GTWR model were validated with ground PM2.5 measurements and compared with the estimation from geographically weighted regression (GWR), temporally weighted regression (TWR) and ordinary least squares (OLS). The result shows that the GTWR shows better prediction accuracy for PM2.5 concentrations than OLS, GWR, and TWR since it incorporates both spatial and temporal nonstationarity. Compared with OLS, GWR, and TWR models, the R2 value of GTWR was improved from 0.598, 0.655, 0.778 to 0.792. The RMSE of GTWR was improved from 15.885, 14.723, 11.817 ?g/m3 to 11.463 ?g/m3. At last, the GTWR model was applied to estimate PM2.5 concentration of Hong Kong in 2013. According to the averaged PM2.5 concentration distributions in 2013, the districts with high population and traffic have higher PM2.5 concentration than districts with low population and traffic. Therefore, the GTWR model may provide a more accurate way to predict PM2.5 spatio-temporal variation, which is significant for the atmosphere environment protection and relative epidemiologic research.

10424-22, Session 4

Preliminary comparisons of HCHO integral contents in ABL estimated during clear sky and overcast by DOAS technique

Oleg V. Postylyakov, Alexander N. Borovski, A.M. Obukhov Institute of Atmospheric Physics (Russian Federation); Victor A. Ivanov, V.E. Zuev Institute of Atmospheric Optics (Russian Federation)

Spectral measurements of scattered solar radiation are used to determine the vertical column density (VCD) of absorbing gases in the atmosphere by DOAS technique. VCD is obtained by two consecutive steps. At the first step the slant column density (SCD) of a gas is obtained. SCD is the weighted average of vertical distribution of the gas in the atmosphere. The weighting function depending on height is determined by the scattering and absorbing properties of the atmosphere and may be accurately estimated using a radiative transfer model if optical state of the atmosphere is known. This weighting function is also called the layer air mass factor (AMF). At the second step we may transform SCD to VCD if we may calculate the layer AMF and have information on the relative vertical distribution of the gas.

The simples and more popular atmospheric state to which such a method is usually applied is the clear sky conditions. In this case the main variable factor which influence on the atmospheric state in UV and visible wavelengths, used for determination of NO2, HCHO and some other gases, is aerosol. In our previous works (see Proc. SPIE, 2015, Vol. 9680, 96804O-10) we proposed an algorithm for converting SCD to VCD in overcast and investigated related errors for HCHO retrieval depending on the level of available information on clouds.

Spectral measurements of scattered solar radiation are performed at Zvenigorod Scientific Station (ZSS, 55°41'49"N, 36°46'29"E) located in 38 km west from Moscow Ring Road by MAX-DOAS instrument since 2008. This location of the observational station allows evaluating the background levels of formaldehyde in the troposphere and the levels that are associated with pollution from Moscow. Basing on ZSS data we processed separately observations obtained in clear sky conditions and in overcast. Classification of observations as "clear sky", "cloudy", "undefined" was based on meteorology date corrected by several indexes inferred from measured spectral radiances (see Proc. SPIE, 2016, Vol. 10035, 100353A-8).

The first preliminary results of statistical parameters of HCHO variability obtained using "clear sky" and "cloudy" dataset are presented and compared. Effects of parameters of the "cloudy" algorithm in the result are also under investigation.

10424-23, Session 4

First experiments on high-detailed mapping of tropospheric NO2 using GSA hyperspectral imager on board Resurs-P satellite aimed to natural resource investigation

Oleg V. Postylyakov, Alexander N. Borovski, A.M. Obukhov Institute of Atmospheric Physics (Russian Federation); Aleksandr A. Makarenkov, Ryazan State Radio Engineering Univ. (Russian Federation)

Tropospheric nitrogen dioxide is routinely retrieved by OMI/Aura and GOME-2/MetOp-A&B with typical spatial resolution of 13x24 km and 40x80 km, respectively. Expected to launch in 2017 TROPOMI/Sentinel-5P will have resolution of 3.5x7 km.

A series of Russian satellite Resurs-P operate since 2013 in sun-synchronous orbit. Three Resurs-P satellites are operating now and two more are expected to launch until 2020. A hyperspectral imager GSA is mounted on its board, which resolves more than 230 spectral bands from 400 nm to 1000 nm. It takes image of area of 30-km width and of several hundreds km length with 30 m resolution. The main goal of the instrument is natural resource investigation.

The instrument has spectral resolution up to 3 nm at 430-490 nm spectral region which is used for the retrieval of NO2. GSA resolution is worse than those what is usually used for NO2 oriented satellite. We investigate opportunity to retrieve tropospheric NO2 based on GSA images of highly polluted regions of China. The developed algorithm shows the spatial resolution of about 2 km what exceed other available now satellite instrument and considered as a target for future GEO instruments. So it provide the interesting tool for NO2 investigations.

The algorithm and the first experimental results will be presented.

10424-24, Session 4

Mesoscale atmospheric eddies over the Black Sea and the Caspian Sea on synthetic aperture radar and optical images

Andrei Y. Ivanov, Nadezda Terleeva, P.P. Shirshov

Institute of Oceanology (Russian Federation)

The paper presents results of studies of mesoscale cyclonic eddies and local cyclones, atmospheric events from time to time taken place over the Black Sea and the Caspian Sea, using Radarsat-2 Sentinel-1A and Sentinel-1B synthetic aperture radars (SAR) and optical images of the Aqua, Terra and Suomi NPP satellites. It is worth mention that they leave pronounced footprints on the sea surface, which look similar to those of local cyclones. A number of case studies based only on simultaneous analysis of SAR and optical images demonstrate SAR capability to provide detailed information on the near surface wind field associated with these atmospheric cyclonic eddies. The SAR images, together with optical accompanying meteorological measurements, re-analysis and optical images with associated cloud patterns, show the well-marked cyclonic spirals of the. Several types of cyclonic eddy were discovered and studied, among them are: winter coastal, summer offshore, ambient cyclonic eddies, as well as quasitropical cyclones. For Black Sea and Caspian Sea eddies statistics of their frequency, life-time and intensity, as well as information on diurnal and seasonal cycles, are presented. By analysis of SAR and optical images it is established that these atmospheric mesoscale cyclonic eddies have various spatial and temporal parameters from hundred kilometers and a day to typical parameters of synoptic cyclones that moving over the seas. Centers of mesoscale atmospheric cyclonic eddies are scattered occasionally over the sea basins. Over the Black Sea they move occasionally, but mostly in the north/north-easterly direction, whereas over the Caspian Sea they move in the east and west directions. Ambient cyclones vary from common large scale extratropical cyclones to secondary mesoscale eddies associated with coastal mountains influence and barotrophic/baloclinic instability of the marine atmosphere. Most frequently mesoscale cyclones appeared on satellite images in the east part of the Black Sea and in the northern part of the Caspian Sea. It is also shown that their generation and evolution are characterized by seasonal and diurnal cycles, respectively. By analysis of satellite images the general characteristics of the cyclones, their time-life, and evolution can be obtained. Usually they are small having 50-200 km in diameter and lifetime of about a day, but in some cases deepened and can lead to a sharp deterioration of the local and regional weather. Based on interpretation results, characteristic scales and formation mechanism can be defined. General characteristics of these mesoscale atmospheric cyclonic eddies and their evolution and physical formation mechanisms are also discussed. These atmospheric cyclonic eddies will be further characterized with the help of high-resolution regional modeling, for example, like the Weather Research and Forecasting model (WRF). Finally it is concluded that use of SAR and optical images together with other remote sensing data such as microwave radiometers and scatterometers in studies of particular cases and events can significantly improve our knowledge about mesoscale local cyclogenesis.

10425-20, Session PS

The design method of Fresnel CGH for real-time control of phase wavefront aberrations

Polina Malinina, Sergey B. Odinokov, Michael Kovalev, Vladimir I. Bobrinev, Bauman Moscow State Technical Univ. (Russian Federation); Vladimir Y. Venediktov, Saint Petersburg Electrotechnical Univ. "LETI" (Russian Federation)

We propose a method to create a Fresnel CGH for holographic wavefront sensor, that can replace the modern and widely-common in Adaptive Optics systems Shack-Hartmann sensor. It is found to be the optimal way to construct such type device. Computer modeling and experimental results of the proposal are presented using a reflective liquid crystal on silicon (LCoS SLM) modulator Holoeye Pluto. In addition some theoretical and practical study with multiplexing of computer generated holograms are examined.

10425-1, Session 1

Comparison of integrated optical turbulence over the sea in different coastal regions in the world

Detlev Sprung, Erik Sucher, Christian Eisele, Dirk P. Seiffer, Fraunhofer-Institut für Optronik, Systemtechnik und Bildauswertung (Germany); Alexander M. J. van Eijk, TNO Defence, Security and Safety (Netherlands)

Electro-optical and laser systems are presently deployed in naval operations around the world. The performance these systems is negatively affected by optical turbulence in the atmosphere, quantified by the parameter Cn2. The strength of the integrated optical turbulence Cn2 was investigated for several coastal locations in different climatic conditions: False Bay (South Africa), the Baltic Sea (Bay of Eckernförde, Germany), the Mediterranean Sea (Crete, Greece), the Gulf of Mexico (Dauphin Island, Alabama, US), and Chesapeake Bay (Virginia, US). The over-water, near-surface turbulence was characterized along paths that typically spanned 8 – 16 km, using large aperture scintillometers and high speed cameras monitoring halogen lamps. The sequences of camera pictures were analyzed using the angle-of arrival technique. The dependency of Cn2 on the air-sea surface temperature difference and other meteorological conditions is discussed, and the results for the five geographic regions are compared and discussed in terms of environmental conditions and climate.

10425-3, Session 1

Meteorological measurements to characterize atmospheric turbulence variation

Robert Gignilliat, U.S. Naval Research Lab. (United States); Rebekah F. Wilson, Thomas M. Taczak, Applied Technology, Inc. (United States)

IR propagation through the atmosphere is strongly affected by atmospheric turbulence. To correctly model IR propagation, this turbulence must be well characterized and understood. To that end, this paper presents propagation measurements including detailed meteorological measurements that have been made along a 16 km propagation path. Variation in these meteorological parameters, specifically air temperature, will be studied to determine their effect on optimal measurement parameters and practices. Additionally, Cn2 measurements were taken in the MWIR band. A preliminary comparison of these results to modeled results from IRBLEM (IR Boundary Layer Effects Model) will be presented. The goal of these comparisons is to determine optimum measurement practices and determine the variation in Cn2 given the measured variation in meteorological parameters along the propagation path. Significant work has been done by others to measure and model turbulence and the effects on IR propagation. This paper hopes to contribute to that work by providing an especially well-characterized experimental location along with MWIR Cn2 measurements.

10425-5, Session 1

Temporally resolved refractive index structure parameter measurement

Markus Henriksson, Robin Forsling, FOI-Swedish Defence Research Agency (Sweden)

The refractive index structure parameter is the most common measure of optical turbulence. It is defined as a statistical quantity for the Kolmogorov spectrum energy cascade of turbulent eddies of different sizes. As such it is formally assumed to be constant in time and space. However, the large scale variation with the diurnal cycle, with altitude or with terrain characteristics is well known. The ensemble average in the definition of the refractive index structure parameter is thus assumed to be applied over a restricted region in space and time. The question of how large volume is needed to determine the refractive index structure parameter and on how short temporal scales it can vary has not received significant attention. To study the temporal variation we have used two independent measurement systems to measure the path-averaged refractive index structure parameter over a 171 m path at 1 m above ground with higher than 1 Hz temporal resolution. One measurement system uses the differential angle-of-arrival of an array of LEDs. The other system measures the scintillation of a single path laser beam using a photon counting system, with time correlation of picosecond pulses for simultaneous measurement of signal and background and with temporal autocorrelation-based variance determination to separate turbulence related scintillations from shot noise. The data shows excellent agreement between the two measurement systems on second level temporal variation, giving confidence in that the measured values show true variation of the refractive index structure parameter. Large scale variation of up to two orders of magnitude can be coupled to solar insolation on this partly cloudy day. High frequency variations that are consistent between the systems used show factor two changes at time scales below one second.

10425-8, Session 1

Characterizing the Discoloration of EBT3 Films in Solar UV A+B Measurement using Red LED

Ahmad Fairuz Omar, Ummi Shuhada Osman, Kok Chooi Tan, Univ. Sains Malaysia (Malaysia)

The development of mobile optical instrument for solar ultraviolet (UV) radiation online monitoring is an essential indicator nowadays for health risk prevention. To develop it, an experiment using Gafchromic EBT3 film need to be done to study the trend of Solar UV radiation dose emitted by Sun and the ability of that film to absorb Solar UV radiation. Gafchromic EBT3 film is a type of film that has an ability to measure UV

radiation, apart from its main usage for X-ray radiation. 50 pieces of Gafchromic EBT3 films were prepared with the dimension of 2 cm x 3 cm, exposed directly under the Sun for 25 minutes. Every 30 seconds, a film was taken from the exposure session. Color of the films changed from light green to dark green, depending on the exposure time, irradiance level and condition of the sky. Then those films were analysed using the absorbance spectroscopic technique and the absorbance spectra graphs were plotted for both peak wavelengths of 582.64 nm and 634.23 nm. The value of R? and RMSE for both peak wavelengths were calculated. For 582.64 nm, R? and RMSE values are 0.9811 and 0.241148, while for 634.23 nm, R? and RMSE values are 0.9511 and 0.15941. Between both peak wavelength, 634.23 nm gives high value of R? and low value of RMSE, so that red LED that have the wavelength around that peak value was chosen as the response light source to the instrument detector. Those values also show a high correlation between UV radiation dose and color changes of Gafchromic EBT3 films. The absorption of Solar UV radiation on the films increase with the exposed dose. This shows that Gafchromic EBT3 film has it ability as a dosage absorption tool of UV radiation in this mobile optical instrument.

10425-2, Session 2

Electro-optical propagation measurements during the MINOTAUROS experiment in the Cretan Sea

Christian Eisele, Erik Sucher, Norbert Wendelstein, Karin U. Stein, Fraunhofer-Institut für Optronik, Systemtechnik und Bildauswertung (Germany)

We will report on measurements performed during the MINOTAUROS (Maritime INvestigations On Targets & Atmosphere Under Reduction of Optical Signatures) experiment in late summer of 2016. The field trial has been organized by NATO RTO Task Group SET-211 on Naval Platform Protection in the EO/IR Domain with strong support of the Hellenic Navy.

This includes measurements of turbulence using a boundary layer scintillometer on a slant path (d = 8 km) across the entry of Souda Bay (Crete). These will be compared to values obtained by the angle of arrival method. Additionally the turbulence has been characterized using a sonic anemometer at one end of the propagation path. Refraction effects have been measured using a 14 km path from Drapanos to Gerani. Two meteorological buoys along the path were used to gather information about the atmospheric conditions. An overview and a first analysis of the results will be presented.

10425-4, Session 2

Inhomogeneity of optical turbulence over False Bay (South Africa)

Carmen Ullwer, Detlev Sprung, Fraunhofer-Institut für Optronik, Systemtechnik und Bildauswertung (Germany); Willie Gunter, Institute for Maritime Technology (South Africa); Alexander M. J. van Eijk, TNO Defence, Security and Safety (Netherlands); Karin U. Stein, Fraunhofer-Institut für Optronik, Systemtechnik und Bildauswertung (Germany)

Atmospheric turbulence impacts on the propagation of electro-optical radiation. Typical manifestations of optical turbulence are scintillation (intensity fluctuations), beam wander and (for laser systems) reduction of beam quality. For longer propagation channels, it is important to characterize the vertical and horizontal distribution (inhomogeneity) of the optical turbulence. In the framework of the First European South African Transmission ExpeRiment (FESTER) optical turbulence was measured between June 2015 and February 2016 over a 2 km over-water link over False Bay. The link ran from the Institute of Maritime Technology (IMT) at Simons Town to the lighthouse at Roman Rock island. Three Boundary layer scintillometers (BLS900) allowed assessing the vertical distribution of optical turbulence at three different heights between 7 and 14 m above the water surface. The expected decrease with Cn2 with height is not always found. These results are analyzed in terms of the meteorological scenario, and a comparison is made with a fourth optical link providing optical turbulence data over a 8.7 km path from IMT to Kalk Bay, roughly 36° shifted to the three 2 km paths. The results are related to the inhomogeneous meteorological conditions over the Bay as assessed with the numerical weather prediction tool WRF.

10425-6, Session 2

Characterization of underwater optical turbulence on the example of the Rayleigh-Benard water tank

Szymon Gladysz, Rui Barros, Fraunhofer-Institut für Optronik, Systemtechnik und Bildauswertung (Germany); Andrey V. Kanaev, Weilin W. Hou, U.S. Naval Research Lab. (United States)

Laser beam propagation underwater is becoming an important research topic because of high demand for its potential applications. Namely, ability to image underwater at long distances is highly desired for scientific and military purposes, including submarine awareness, diver visibility, and mine detection. Optical communication in the ocean can provide covert data transmission with much higher rates than that available with acoustic techniques, and it is now desired for certain military and scientific applications that involve sending large quantities of data. However, extending the laser light propagation range underwater leads to significant beam distortions due to optical underwater turbulence. Experiments show that the magnitude of the distortions that are caused by water temperature and salinity fluctuations can significantly exceed the magnitude of the beam distortions due to atmospheric turbulence.

In this paper we will discuss the joint IOSB-NRL experiment whose goal was to test techniques for characterization of underwater optical turbulence. The methods such as differential motion measurement from an LED array, modulation transfer function measurement, and wavefront sensing, have all been tested in a controlled environment using the Rayleigh-Benard water tank with dimensions 5m by 0.5m by 0.5m. The paper presents comparison of results and recommendations for future use of the proposed measurement methods.

10425-7, Session 2

Long-term experiment VERTURM (vertical turbulence measurements): comparison of measurements and modeling of the vertical distribution of optical turbulence in the surface layer

Detlev Sprung, Peter Grossmann, Erik Sucher, Fraunhofer-Institut für Optronik, Systemtechnik und Bildauswertung (Germany); Alexander M. J. van Eijk, TNO Defence, Security and Safety (Netherlands); Karin U. Stein, Fraunhofer-Institut für Optronik, Systemtechnik und Bildauswertung (Germany)

Atmospheric turbulence (quantified by refractive structure function parameter Cn?) can significantly reduce the performance of electro-optical systems, especially when the optical path includes the near-surface environment. For a proper description of slant optical paths, it is necessary to characterize the vertical profile of turbulence. The long-term experiment VerTurM (Vertical Turbulence Measurements) in a rural region in North-West Germany provided 7 years of

near-continuous measurements of the vertical profile of Cn2 in and above the atmospheric surface layer, up to 64 m. A micrometeorological model driven by the vertical gradients of standard meteorological parameters (wind, temperature and humidity) was developed to generate the vertical distribution of Cn2 in the surface layer. The agreement between the simulation and the measurements is discussed in terms of atmospheric stability. The diurnal cycle of the vertical profiles of optical turbulence will be presented and discussed.

10425-9, Session 2

Seasonal ionospheric scintillation analysis during increasing Solar activity at mid-latitude

Wasiu Akande Ahmed, Falin Wu, BeiHang Univ. (China); Ganiyu I. Agbaje, African Regional Ctr. for Space Science and Technology Education (Nigeria); Ednofri Ednofri, Dessi Marlia, Yan Zhao, BeiHang Univ. (China)

Ionospheric scintillation occurs when there is significant fluctuation in phase or amplitude of GNSS signals as it travels from the transmitter (satellite) to the receiver due to ionospheric layer effects. It could cause degradation of GNSS signal tracking in terms of accuracy and reliability [1-3]. Monitoring of ionospheric parameters is of great importance as it affects and contributes to the errors encountered by radio signals. Therefore, it requires constant measurements to avoid disastrous situation for space agencies, parastatals and departments that employ GNSS applications in their daily operations.

The research objective is to have a better understanding of the behaviour of ionospheric scintillation at mid-latitude being an important factor that threatens the performance of satellite communication, navigation system and military operations. This paper describes seasonal ionospheric scintillation monitoring. The seasonal variations of amplitude and phase scintillation have been studied and the correlation between them.

The solar cycle activity demonstrates the frequent changes in the levels of solar radiation and number of sunspots. These changes may cause adverse effects in the atmosphere, Earth surface and particularly space. Studies have shown that the occurrence of ionospheric scintillation depends on 11-year solar cycle, season, local time and latitudinal location. Strong phase scintillation may lead to loss of phase lock and frequent cycle slips while amplitude scintillation could degrade carrier phase measurements and pseudo-range [4, 5]. Thus, there is the need to pay more attention and hence the mid-latitude investigation of ionospheric effect of scintillation was conducted during the increasing solar activity from 2011-2015.

Ionospheric scintillation data were obtained from Shenzhen North Station, Beijing Changping North Station Branch, Beijing North Station and Beijing Miyun ground Station. The data was collected from January 2011 to December 2015. At some points, there was absence of data due to software problem or system failure. Amplitude scintillation was computed by ( ) index produced using GISTM Model [6]. In this experiment, index range are assumed and classified as 0.2≤ <0.3 (Weak), 0.3≤ <0.4 (Moderate), ≥ 0.4 (Strong) and <0.2 (Negligible). While on the other hand carrier phase generated by GISTM describes phase scintillation which is measured in radian. The sixth order high-pass and low-pass Butterworth filters were used to detrend the carrier phase measurements and signal intensity respectively [7].

Ionospheric scintillation could be analyzed on diurnal, monthly, seasonally and annual basis. In this scenario, seasonal analysis was adopted. There are four seasons which existed in China, i.e., Spring, Summer, Autumn and Winter. The relationship between amplitude and phase scintillation are expressed in this research during each of these seasons (solar maximum). In essence, it complies with theoretical prediction by National Aeronautics and Space Administration (NASA).

The results show that the weak amplitude scintillation was witnessed as against phase scintillation which on the other hand was high. Phase scintillation was gradually enhanced from 2011 to 2012 and later declined till 2014. The seasonal events temporal density characteristics comply with solar cycle prediction as such there was ascending trend from 2011 to 2013 and then scintillation parameters declined significantly afterwards.

References

[1] L. Pan, P. Yin , “Analysis of Polar Ionospheric Scintillation Characteristics Based on GPS Data”, Lectures Notes in Electrical Engineering 303, vol. I, DOI:10.1007/978-3-642-54737-92, 2014.

[2] P. Theerapatpaiboon, P. Supnithi, N. Leelaruji and N. Hemmakorn, “The Analysis of Ionospheric Scintillation on the Global Positioning System (GPS) at Bangkok”, SICE-ICASE International Joint Conference 2006, Oct. 18-2 1, 2006, Busan, Korea

[3] Y. Norsuzila, et al, “Mitigate the GPS Ionospheric Scintillation during

Solar Flare”, IEEE Control and System Graduate Research Colloquium (ICSGRC), 2012.

[4] W. A. Ahmed, et al, “Ionospheric Behaviour Analysis over Thailand using Radio Occultation Technique”, Int. J. of Eng. Research and Applications, 5(11), pp.01-07, 2015.

[5] S. Aramesh, M. Abdullah, A. M. Hesbi, Y. Zhou, “Observation of GPS Ionospheric Scintillation at UKM, Malaysia”, Proceeding of the 2011 IEEE International Conference on Space Science and Communication (IconSpace) 12-13 July 2011.

[6] Y. Zhou, “Ionospheric scintillations at Guilin detected by GPS ground-based and radio occultation observations”, Advances in Space Research 47(6), pp.945-965, 2011.

[7] A. J. Van Dierendonck, “Satellite Navigation Science and Technology for Africa. GPS Ionospheric Scintillation & TEC Monitor (GISTM) user’s manual (GSV4004B)”, Abdus Salam International Centre for Theoretical Physics, Italy, pp1-52, 2009.

10425-10, Session 3

Preliminary results from the Stereo-SCIDAR at the VLT Observatory: extraction of reference atmospheric turbulence profiles for E-ELT adaptive optics instrument performance simulations *(Invited Paper)*

Marc S. Sarazin, European Southern Observatory (Germany); James Osborn, Durham Univ. (United Kingdom); Arlette Chacon, Frédéric J. Dérie, European Southern Observatory (Germany); Julien Milli, European Southern Observatory (Chile); Miska Le Louarn, European Southern Observatory (Germany); Julio Navarrete, European Southern Observatory (Chile); Richard R. W. Wilson, Durham Univ. (United Kingdom)

The Stereo-SCIDAR (Scintillation Detection and Ranging) atmospheric turbulence profiler, built for ESO by Durham University, operates at the focus of one of the four VLTI auxiliary telescopes (AT) at the VLT Paranal Observatory. It is composed of 2 low noise detectors attached to a rotator stage conjugated to a plane situated 3 km below ground. Each camera records the short exposure pupil image of one of the observed binary. The output parameters are updated every 2mn and converted back to zenith. The optical turbulence is expressed in terms of index of refraction structure coefficient (Cn2dH, m+1/3) integrated within the vertical resolution slab (200 to 300m depending on binary separation) and the wavefront velocity in m/s. The wavefront coherence time (s) and isoplanatic angle (arcsec) are computed from the combined turbulence and velocity vertical profiles. A set of reference profiles is proposed, based on the data collected during more than 20 nights of operation, as input for the various models developped by the E-ELT instruments Consortia. Grouping criteria are compared based on either altitude distribution or principal component analysis.

10425-11, Session 3

Local optical turbulence at and in the vicinity of the GREGOR solar telescope at the Teide Observatory, Tenerife

Oskar F. von der Lühe, Thomas Berkefeld, Kiepenheuer-Institut für Sonnenphysik (Germany); Detlev Sprung, Erik Sucher, Karin U. Stein, Fraunhofer-Institut für Optronik, Systemtechnik und Bildauswertung (Germany)

The image quality of ground-based solar telescopes depends on the amount of turbulence in the Earth's atmosphere, which is strongest in layers close to the ground during daytime. Local optical turbulence affects the performance of adaptive optical systems and reduces the spatial resolution of solar observations. Increased turbulence which is caused by solar irradiation of the infrastructure close to the telescope and obstructions to a free airflow are major concerns, but difficult to detect and to monitor. We have conducted measurements of optical turbulence at the GREGOR solar telescope (Teide Observatory, Tenerife, Canary Islands) to assess quantitatively the influence of the infrastructure on the image quality.

The strength of optical turbulence is determined by the structure function parameter of the refractive index Cn2. We have measured the temporal behavior of the free flow optical turbulence about 30m above ground using a laser scintillometer between the towers of the Vacuum Tower Telescope and of GREOR. Local measurements of Cn2 were taken on the observing platform of GREGOR using three ultrasonic anemometers. Two anemometers are located at the north and south ends of the telescope building, a third one was be placed close to the telescope main mirror cell. Air temperature, pressure, humidity as well as wind speed and direction were measured along with refractive index measurements. An image quality indicator based on an estimate of the Fried parameter r0 was recorded whenever the adaptive optics system GAOS at the GREGOR telescope was operating. Recordings of the net solar radiation were obtained from the GONG experiment which is located a few 100 m from GREGOR. All data were taken between May 2015 and March 2016.

We investigate the relation between optical turbulence, solar irradiance and meteorological parameters. Under almost all conditions, optical turbulence nearby the telescope is stronger than free flow turbulence. We note significant dependencies of the strength and the horizontal gradient of Cn2 on wind direction. The moderate influence on image quality indicates that there is only a thin layer with strong turbulence just above the telescope.

10425-12, Session 3

The turbulence study in the astronomical observatory in the North Caucasus

Vladimir P. Lukin, Viktor V. Nosov, Eugenii V. Nosov, Andrey V. Torgaev, V.E. Zuev Institute of Atmospheric Optics (Russian Federation)

In the Special Astrophysical Observatory (SAO) continued pilot studies and research astroclimate coherent turbulence, similar to those given by us to the CAO in October 2012. To this end, under the dome of the Big Telescope Alt-azimuthal (BTA) has been measured astroclimate parameters. Measurements made throughout the volume of the dome of the specialized facilities BTA using ultrasonic weather station AMC-03 is fastened to the structure of the rotating telescope and dome. Also construction of temperature measurements of the telescope and the dome (and their size) used a thermometer and a laser rangefinder. Along with the state of the atmosphere measurements dome of the telescope is controlled ultrasonic meteosystems Meteo-2, mounted on 20-meter meteorological mast at the telescope site. Meteo-2 was used for the registration of long-term observations of atmospheric turbulence parameters for the expedition in order to clarify the conditions of the emergence of coherent areas of turbulence over the observatory territory. As a result of field research in 2016 following major scientific results obtained for the studied geographic region SAO:

1) reported the presence of a coherent area of turbulence observatory, which improves image quality,

2) The influence of the type of underlying surface wind speed and direction in the mode of occurrence of coherent turbulence, the cause of which is mountainous terrain and uneven heating of the underlying surface,

3) the results of measurements restored experimental painting movements of air streams in the dome space BTA, confirmed the presence of coherent vortex structures,

4) data on the BTA dome measurements obtained in an expedition in 2016, and confirmed in agreement with the results of further numerical calculations based on the Navier-Stokes equations with the appropriate boundary conditions.

10425-13, Session 4

Nightglow studies at Onera for nightvision applications *(Invited Paper)*

Pierre Simoneau, Sophie Derelle, Joel R. Deschamps, Stephane Langlois, Didier Henry, ONERA (France)

Since September 2010, we work in the characterization and modeling the nightglow radiation in the SWIR band for nightglow applications. In this presentation we show radiance measurements, images in clear and cloudy sky conditions and we present the characterization methods implemented for radiometric calibration of our instruments.

10425-14, Session 4

Shortwave infrared for night vision applications at Fraunhofer IOSB

Uwe Adomeit, Jürgen Krieg, Fraunhofer-Institut für Optronik, Systemtechnik und Bildauswertung (Germany)

"Nightglow" is an illumination phenomenon created by luminance processes in the higher earth atmosphere. It covers the spectral range from the ultraviolet up to the thermal infrared, but its maximum is found in the shortwave infrared (SWIR). Although known for a long time the advent of high sensitive SWIR detectors in the last decade enables todays use for night vision applications.

In 2013 Fraunhofer IOSB started its assessment of SWIR for night vision applications. The approach was twofold. Continuous measurements were started to get an understanding of the highly variable illumination levels created by the nightglow under different environmental conditions. Future goal here is the standardization of the SWIR illumination levels corresponding to the defined visual full moon, quarter moon, starlight and overcast starlight ones. Additionally, performance assessment of SWIR detectors in comparison to the visual image intensifiers respectively low light focal plane array detectors were conducted in the laboratory as well as in the field.

The paper gives history and status of IOSBs assessment of SWIR for night vision applications. It explains the ideas behind the illumination characterization, the conducted measurements and the inherent problem of artificial stray light. For sensor assessment it presents recent work on the influence of the spectral coverage (e. g. broadband versus atmospheric window only) on system performance for different environmental conditions.

10425-15, Session 4

Experimental study on spectral absorbance of fog as a function of temperature, liquid water content and particle size

Aki P. Mäyrä, Eero Hietala, Matti H. Kutila, Pasi Pyykönen, Mikko Tiihonen, Tuomas Jokela, VTT Technical Research Ctr. of Finland Ltd. (Finland)

The ECSEL joint undertaking RobustSENSE [1] focuses on technologies and solutions for automated driving in adverse weather conditions. One of the main technology challenges is to improve laser scanner performance in fog where the existing 905 nm lidars reliability degrades below tolerances. This report briefly summarizes the results of experimental fog absorbance measurements, which were conducted in icing tunnel test laboratories located in VTT's premises. The content of the presentation will focus on spectral absorbance at low visibility artificial fog in near infrared band.

VTT Icing Wind Tunnel is assembled inside a large temperature controlled room with minimum temperature of -25C. The test section part has cross section of 700x700mm. Wind speed, liquid water content and droplet size can be controlled. In the RobustSENSE icing tunnel test campaign, the aim was to understand performance of a potential new lidar sensor when using short infrared band (1000 - 1700 nm) instead of currently used visible band (850 - 1000 nm). The measured scenarios included several foggy environments with known pre-set parameters for wind, temperature, liquid water content (LWC) and droplet median volume diameter (MVD). In total 63 scenarios were measured during the campaign. Most fogs[2] have LWC ranging from 0.01 to 0.4 g m^-3 and in the test campaign the used range was 0,1-0,8 g m^-3. Typical radius [3] values for fog range from 1-20 um and in the test campaign region from 10 um to 17,5 um was used. Measured temperatures were -5,0 and +5 degrees Celsius.

The measurement set-up consisted of a collimated white light halogen source and VIS-NIR spectrograph which were placed on opposite sides of the measurement test section. The measured spectra clearly indicate that, in the measured wavelength band ranging from 400 nm to 1600 nm, the fog attenuation is wavelength dependent and that absorbance spectrum slopes can be either increasing or slightly decreasing. In the presentation, the measured spectral absorbance will be presented as a function of the temperature, liquid water content and particle size.

[1] "RobustSENSE project.", < https://www.robustsense.eu/>.

[2] Kim, I. I., Mcarthur, B., Korevaar, E., Street, R., Diego, S., "Comparison of laser beam propagation at 785 nm and 1550 nm in fog and haze for optical wireless communications," Proc. SPIE - Int. Soc. Opt. Eng. 4214, 26–37 (2001).

[3] Gultepe, I., Ardif, R. T., Ichaelides, S. C. M., Ermak, J. C., Ott, A. B., Endix, J. B., "Fog Research: A Review of Past Achievements and Future Perspectives," Pure Appl. Geophys. 164, 1121–1159 (2007).

10425-16, Session 4

Aerosol optical properties inferred from in-situ and path-averaged measurements

Sven A. van Binsbergen, TNO Defence, Security and Safety (Netherlands); Peter Grossmann, Fraunhofer-Institut für Optronik, Systemtechnik und Bildauswertung (Germany); Faith J. February, Institute for Maritime Technology (South Africa); Leo H. Cohen, Alexander M. J. van Eijk, TNO Defence, Security and Safety (Netherlands); Karin U. Stein, Fraunhofer-Institut für Optronik, Systemtechnik und Bildauswertung (Germany)

Atmospheric aerosols adversely affect the propagation of electro-optical radiation through scattering and absorption processes. Consequently, knowledge of the aerosol concentration and composition is required to predict the performance of electro-optical sensor systems in the operational theatre. A study is reported of aerosol properties over the False Bay area, near Cape Town in South Africa. Aerosol properties were measured by in-situ optical particle counters and a transmissometer, operating at 7 wavelengths between the visible and far-infrared, set up for a 7.8 km over-water path. The transmissometer receiver was collocated with the optical particle counters. The aerosol properties are discussed in terms of meteorological scenario (wind speed, wind direction, etc), and the path-averaged results are compared to the in-situ measurements. The results are also compared to a test trial that took place in Meppen, Germany.

10425-17, Session 4

The upper atmosphere layer height changes as a precursor of the Padang earthquake on 30 September 2009

Ednofri Ednofri, Falin Wu, Wasiu Akande Ahmed, Yan Zhao, BeiHang Univ. (China)

Effects of the earthquake in addition resulted in fatalities also caused material losses are not few in number, then efforts to increase knowledge about earthquakes and mitigation requires serious attention. This research aims to determine the altitude changes that occur in the upper layers of the atmosphere before the earthquake in Padang Indonesia on September 30, 2009 with magnitude 7.6 strength. To obtain information altitude changes that occur in the upper atmosphere associated with earthquake precursors, this research used use an all-sky imager (ASI) mounted on Kototabang (0.2oS, 100.3oE, -10.4o magnetic latitude) Indonesia, to detect the propagation of atmospheric gravity waves (AGW) in the form of a two-dimensional image, the apparent height of the F layer (h'F) obtained from ionosonde Frequency Modulated Continuous Wave (FMCW) installed at the same location and occurrence of magnetic storms (Dst index) were obtained from the World Data Center for Geomagnetism, Kyoto. We analyzed the occurrence of AGW in ASI images and h'F in ionosonde FMCW from 7 days before and after the earthquake. During the 7 days of observations made before the quake, only obtained a four-daynight sky in bright conditions, namely on 24, 25, 26 and 28 September 2009. While the observations of 7 days after the earthquake can not be done, because the instruments were damaged by the earthquake. From the equation obtained, Padang earthquake preparation zone radius is 1,853.5 km, while the distance from the epicenter to the equipment ionosonde FMCW Kototabang is 77 km. It found that there was unusual evening in h'F variation on September 24 and 29, 2009, i.e., six and one days before the earthquake. A positive h'F deviation on 24 and 29 September 2009 are with a maximum value of 42 and 31.5, respectively. For both these dates, the maximum h'F value reached 234 km and 261 km at 00:30 LT and 20:30 LT with the median value of 192 km and 229.5 km, respectively. The increase in h'F on 24 September 2009 before the middle of the night likely was caused by encouragement from AGW happened a few minutes earlier. The emergence of the AGW on September 24, 2009 observed at wavelength of OH bands (~86km). At a wavelength of 557.7 nm (~95km) and 630 nm (200-300km) at about the same time also observed as plasma bubbles. While the increase in h'F on 29 September 2009, suspected to be caused by the emergence of the AGW a few minutes earlier, though it cannot be proven because ASI does not operate due to rainy weather over Kototabang. The h'F improvement was caused by AGW resulting from the epicenter after the influence of magnetic storm eliminated. For Dst index during the month of September 2009, there is nothing worth under -50 nT, this means a change of altitude h'F is not caused by the influence of magnetic storm. The results of this research are expected to be a reference to enrich the knowledge of the relationship between the variation of the upper atmosphere as a precursor to the occurrence of an earthquake.

10425-18, Session 5

Dynamic adaptive control algorithm based on the realization of Kalman filter

Vladimir P. Lukin, Lidia N. Lavrinova, Vitalii V. Lavrinov, V.E. Zuev Institute of Atmospheric Optics (Russian Federation)

Any dynamic system is characterized in that each element for the time and the position in the phase space is a function of time and position in the phase space of its other components, and is described by a state vector, ie, a set of parameters describing the state of the system at some point in time. Statistical description of the time system status during underlies the realization of Kalman filter, ie, Kalman filter describes the dynamics of the state vector of the system through the probability density distribution of its components at any given time.

Digital Kalman filter gets its name in honor of the Hungarian mathematician R.E. Kalman, who proposed it. Then, this filter has been modified for continuous time model, scientists from the University of South Carolina, R.S. Bucy. In fact, the Kalman filter is a special case of a more general, non-linear filter developed somewhat earlier Soviet mathematician R.L. Stratonovich. Therefore, the full name should be Stratonovich filter - Kalman - Bucy. Use of the Kalman filter to reduce the influence of the time delay in the system of adaptive optics (AO) was first proposed in the 2002 Year and experimentally implemented in 2006 at the stand ONERA companies in order to reduce noise resulting from natural vibration measuring system AO.

Synthesis of a statistically-optimal control algorithm of the system AO based on the implementation of the Kalman filter involves building a model of the evolution of this system. The main parameters responsible for the evolution of the system, in this case will be the wind speed and the structural characteristics of the refractive index. Knowing them allows to calculate the altitude dependence fluctuation parameters of a light wave propagating in the atmosphere, and therefore to evaluate the distortions caused by turbulence. And for this you need to build a numerical model of atmospheric turbulence and wind speed characteristic of the optical system's location, as well as to improve the existing adaptive mirror control algorithm. When considering policy options to increase the efficiency of the adaptive system in a Big solar vacuum telescope, from our point of view, it must be assumed that the input aperture of the light field AO system evolve randomly. Under the evolution of phase fluctuations refers to the process of gradual quantitative changes wave-front fluctuations that result in qualitative changes. The evolution of the transformation phase fluctuations or turbulent irregularities in time is characterized by speed, which includes the transfer of turbulent wind speed irregularities as well as small-scale fluctuations in wind speed present in the real atmosphere. Slowly evolving aberration telescope leveled using a differential approach to the measurement of S-H WFS at a speed of calculation.

10425-19, Session 5

Experimental demonstration of holographic wavefront sensor, based on diffuse Fourier holography

Vyacheslav V. Orlov, ITMO Univ. (Russian Federation); Vladimir Y. Venediktov, Saint Petersburg Electrotechnical Univ. "LETI" (Russian Federation)

Holographic wavefront sensors provide very fast and computation-lacking means of measurement of wavefront distortions, e.g. by direct evaluation of amplitudes of Zernike polynomials (modes) in the wavefront expansion. Earlier variants of such devices were based on the straight-forward use of the overlapped Fresnel holograms; however, the use of such devices is severely tantalized by the cross-modulation noise, arising from the holograms' overlapping. The Fourier holography with the record by the diffuse-scattered beams opens the way to creation of similar devices with the much lower noise level. We present the results of first experimental testing of the method.

10425-21, Session 6

Measurement of the spatial distribution of atmospheric turbulence characteristics: evaluation of SCINDAR on a mosaic of urban surfaces

Khanh-Lin Nguyen, Clélia Robert, J. M. Cohard, Jean-Pierre Lagouarde, ONERA (France); Michael P. Irvine, AngioDynamics (United Kingdom); Jean-Marc Conan, Laurent M. Mugnier, ONERA (France)

The observation of the exchange of water and heat between the ground and the atmosphere in complex environments remains a challenge for the atmospheric and hydrology sciences. The infrared scintillometry developed in the 1980s is now a proven method for measuring sensible heat fluxes over a mosaic of surfaces. However, it only provides an integrated measurement. More recently, developments in adaptive optics, in particular to correct images in astrophysics, have led to the emergence of tomographic scintillometry techniques that allow restoring the turbulence profile along the atmospheric column. The turbulence profiler SCINDAR, developed at ONERA, was adapted in the framework of the ASCOETscs project (CNRS Innovative Instrumentation), to propose a new instrument able of measuring the spatial distribution of the intensity of atmospheric turbulence (Cn?) along a horizontal line of sight close to the surface, and to derive the heat fluxes. The Cn? profiler SCINDAR - equipped with a 4 micrometers Shack-Hartmann infrared wavefront sensor, and coupled to a 35-cm-diameter telescope - has a high spatio-temporal resolution. The images of a double source, for the 5x5 sub-pupils, are recorded at 140 Hz and allow rebuilding the Cn? profile from the inter-correlations of scintillation indices and wavefront angles.

Two experiments of urban scintillometry, along a line of sight of 4.2 km, 40 m above a composite urban-forest ground, located between ONERA Châtillon and the solar tower of the Observatory of Meudon were performed in autumn 2015 and in summer 2016. The objective of these campaigns was to compare the distributed Cn? measurements of SCINDAR to the measurement of three scintillometers - configured to observe three different portions of the optical path - and with local measurements of Cn? obtained by eddy-covariance systems and a micro-thermal sensor. The SCINDAR data are currently being analyzed, and provide already horizontal Cn? profiles with a few hundred meters resolution. These Cn? distributed values are estimated with small error bars and the non-uniformity of the Cn? is shown to be consistent with the differences in height of observations and coverage along the optical path, and with respect, temporally, to the diurnal cycle, with the averaged Cn? from scintillometers. These experimental results will be presented and analyzed after recalling the principle of the SCINDAR instrument.

10425-22, Session 6

Experimental studies of the correlation of wave-front aberrations of coherent radiation source and an extended luminous object

Vladimir P. Lukin, Nina N. Botygina, Oleg N. Emaleev, V.E. Zuev Institute of Atmospheric Optics (Russian Federation)

This experiment was motivated by the search for an answer to the question about the possibility of effective use of incoherent sources as reference. In the experiment were compared to

fluctuations in the image shake for coherent radiation source for an extended incoherent. Simultaneous measurements of the wave-front aberrations were carried out in the urban atmospheric turbulence on the horizontal track length of 104 meters at a height of 10 m above the underlying surface.

As a luminous object was used a metal disc 12 mm in diameter with holes in which the ends of optical fibers were fixed glowing. Measurements were made with different configurations of luminous points on the disk surface. Coherent laser light is also discharged into the atmosphere through the hole in the disk. Parameter coherent source Fresnel is 0.0021, for incoherent source - 0.0102. Adjustable output power laser modules allows you to choose the desired brightness of the luminous dots to provide the same conditions for registration of images of coherent and incoherent sources. The diameter of the wave-front sensor input aperture is 98.6 mm, the diameter of sub-apertures - 22.05 mm (input sub-aperture Fresnel parameter is 6.9).

The results show a high correlation between the fluctuations of components of the mode decomposition for coherent radiation, and for the incoherent extended source of radiation. This means that a non-coherent source can be used effectively as a reference in a number of applications.

10425-23, Session 6

Modelling of propagation and scintillation of a laser beam through atmospheric turbulence

Fedor V. Shugaev, Ludmila S. Shtemenko, Olga I. Dokukina, Oxana A. Nikolaeva, Dmitri Y. Cherkasov, Natalia A. Suhareva, M.V. Lomonosov Moscow State Univ. (Russian Federation)

The investigation was fulfilled on the basis of the Navier-Stokes equations for viscous heat-conducting gas. The Helmholtz decomposition of the velocity field into a potential part and a solenoidal one was used. We considered initial vorticity to be small. So the results refer only to weak turbulence. The solution has been represented in the form of power series over the initial vorticity, the coefficients being multiple integrals. In such a manner the system of the Navier-Stokes equations was reduced to a parabolic system with constant coefficient at high derivatives. The first terms of the series are the main ones that determine the properties of acoustic radiation at small vorticity. We modelled turbulence with the aid of an ensemble of vortical structures (vortical rings). Two problems have been considered : (i) density oscillations (and therefore the oscillations of the refractive index) in the case of a single vortex ring; (ii) oscillations in the case of an ensemble of vortex rings (ten in number). We considered vortex rings with helicity, too. The calculations were fulfilled for a wide range of vortex sizes (radii from 0.1 mm to several cm). As shown, density oscillations arise. High-frequency oscillations are modulated by a low-frequency signal. The value of the high frequency remains constant during the whole process excluding its final stage. The amplitude of the low-frequency oscillations grows with time as compared to the high-frequency ones. The low frequency lies within the spectrum of atmospheric turbulent fluctuations, if the radius of the vortex ring is equal to several cm. The value of the high frequency oscillations corresponds satisfactorily to experimental data (Shugaev, F.V.; Shtemenko, L.S. Propagation and Reflection of Shock Waves. Pp. 174-176. World Scientific Publishing: Singapore; N.Y.; London; Hong Kong; 1998).

The results of the calculations may be used for the modelling of the Gaussian beam propagation through turbulence (including beam distortion, scintillation, beam wandering). A method is set forth which describes the propagation of non-paraxial beams. The method admits generalization to the case of inhomogeneous medium.

10425-24, Session 6

Wave-optic analysis with phase screen method using Non-Kolmogorov atmospheric turbulence

Fehmiye Yildiz, TOBB Univ. of Economics and Technology (Turkey) and Roketsan A.S. (Turkey); Hamza Kurt, TOBB Univ. of Economics and Technology (Turkey)

An optical wave propagating in atmosphere is affected by temporarily changing of the refractive index. This phenomenon is called atmospheric turbulence. Atmospheric turbulence causes different variation for the propagating laser beam including beam wandering, beam spreading, the scintillation and image jitter. All these effects are the parameter which reduce the performance of system. There are many models proposed for atmospheric turbulence description. However, turbulence power spectrum models can be generally classified by the two types: Kolmogorov models and non-Kolmogorov models. The Kolmogorov spectrum is with the power law value of 11/3, whereas the non-Kolmogorov power spectrum uses a generalized exponent and a generalized amplitude factor instead of constant standard exponent value. Its power law value is in the range between three and five depending on applications. Besides, there are many spectra which have specific inner and outer scales like Tatarskii, von Karman, Kolmogorov and generalized modified spectra. In this study, we perform wave optic analyzes which are beam spreading, mean irradiance and strehl ratio numerically and analytically. We create a Non-Kolmogorov turbulence model which is based on geometrical optics approximation. We do some derivations for it. And the simulation of laser beam propagation through Non-Kolmogorov turbulence is made with spatially varying 3-D phase screens, using phase screen method, which represent the turbulence effect numerically. Using MATLAB we obtain 1-D beam cross section and 3-D beam images after turbulence. We compare numeric simulations results to analytic results within strong and weak atmospheric turbulence conditions. We perform all these calculations at different wavelengths such as 1064nm, 1310nm, 1550nm and 3000nm. We examine how beam spreading change in these circumstances. And we evaluate how the mean irradiance of Gaussian beam changes with respect to different operating frequencies and strong and weak atmospheric turbulence. We declare that this work provides crucial insight for understanding the behavior of Gaussian beam propagation in Non-Kolmogorov atmospheric turbulence for various applications such as free space optical communication systems, LIDAR-LADAR applications and directed energy weapon systems.

We show that Gaussian beam profile is stable when beam propagates in vacuum medium, but the mean irradiance is reducing dramatically when it passes at long distances through the turbulence atmosphere. And also the stronger turbulence atmosphere parameter, the worst Gaussian beam cross section is. The numerical simulations indicate that different wavelengths response divergently to variable atmospheric conditions. Also we report that short-term spreading is more critical than long-term spreading to Non-Kolmogorov turbulence inner and outer scale. And the more phase screen number, the more similar the simulation medium is with real medium. Therefore we optimize the phase screen number. And we demonstrate that the numerical simulations are compatible with analytical derivations.

10425-25, Session 6

Beam wander of focused electromagnetic multi-Gaussian Schell-model beams propagation in anisotropic turbulence

Mingjian Cheng, Xidian University (China); Lixin Guo, Qingqing Huang, Jiangting Li, Xidian Univ. (China)

The propagation behavior of electromagnetic partially

polarized beams through atmospheric turbulence has recently been extensively investigated based on the unified theory of coherence and polarization. Theoretical and experimental investigations show that an electromagnetic partially polarized beam characterized by its polarization properties shows a significant advantage over fully coherent or polarized ones in lowering the turbulence-induced scintillation effect. This approach has potential applications in remote sensing, tracking, optical imaging, and free-space optical (FSO) communications. Beam wander is an important effect of the turbulence as the scintillation that determines the transmission performance of the beams through atmospheric turbulence, and it can be represented statistically by the variance in transverse displacement. Several researchers have studied beam wander effects and the related concept of beam spreading of electromagnetic partially polarized beam propagation through an isotropic turbulent atmosphere, and this scenario considers different beams with different shapes, including electromagnetic Gaussian-Schell model (GSM) beams, electromagnetic partially coherent flat-topped beams, and electromagnetic GSM vortex beams. A novel beam called Multi-GSM (MGSM) beam, whose far field intensity distribution has a flat-topped profile (although its source intensity can be a Gaussian shape), was introduced by Korotkova. MGSM beams can now be easily generated in an optical laboratory and applied to study their focusing properties experimentally. Previous research indicates that partially coherent or polarized beams with a special intensity profile can further mitigate the negative influence of turbulence. The unique characteristics of such beams contributed to extensive studies on the propagation properties of MGSM beams in an isotropic turbulent atmosphere, such as spectral density, degree of coherence, scintillation, quality M2 factor, and polarization transverse distribution. To the best of our knowledge, the beam wander of focused electromagnetic MGSM beams in non-Kolmogorov anisotropic turbulence has yet to be reported. Our purpose is to investigate how non-Kolmogorov anisotropic turbulence and source parameters influence the propagation properties of focused electromagnetic MGSM beams in non-Kolmogorov anisotropic turbulent atmosphere.

In this paper, we have quantitatively investigated the effects of turbulence on the beam spreading and beam wander of focused electromagnetic MGSM beams propagation through a non-Kolmogorov anisotropic turbulent atmosphere. The influence of the source parameters of focused electromagnetic MGSM beams (i.e., beam order, beam width, wavelength, polarization, spatial correlation length, and phase curvature parameter) and the parameters of non-Kolmogorov anisotropic atmospheric turbulence (i.e., anisotropy coefficient, the turbulence structure parameter, power spectrum index, and inner scale), and propagation distance were considered. Compared with isotropic turbulence, anisotropic turbulence with greater value of anisotropy coefficient produces less effect on the beam spreading and beam wander of focused electromagnetic MGSM beams. Numerical results also indicate that we could expand the long-term beam width of focused electromagnetic MGSM beams in the turbulence atmosphere to decrease beam wander via suitable options of the source parameters based on the turbulence strength. Focused electromagnetic MGSM beams could better mitigate the turbulence effects than GSM beams and could be adopted as the light source to lower the intensity scintillation and beam wander in FSO communication. The turbulence effects on the beam wander strengthened as the spatial correlation length, phase curvature parameter, and power spectrum index increased. Focused electromagnetic MGSM beams with larger beam width and wavelength were less sensitive to atmospheric turbulence, which would mitigate the beam wander effects of the turbulence. The values of the turbulence structure parameter, inner scale and propagation distance had significant effects on the beam wander, where a peak phenomenon of the beam wander existed as they increased. These results indicate that focused electromagnetic MGSM beams could be a better light source to mitigate the turbulence effects on remote sensing, tracking, optical imaging and FSO communication through turbulent atmosphere channels with several adjustable parameters.

10426-5, Session PS

HimSAR: A Scientific Toolbox for Snowpack Parameters Estimation

Surendar Manickam, Friedrich-Alexander-Univ. Erlangen-Nürnberg (Germany); Arun Bharathi Pugazhenthi, Shaunak De, Arnab Muhuri, Abhishek Maity, Priya Jothi, Rajesh Jeyakrishnan, Avik Bhattacharya, Gulab Singh, Gopalan Venkataraman, Indian Institute of Technology Bombay (India); . Snehmani, Snow and Avalanche Study Establishment (India)

In this paper, we present HimSAR: a toolbox for snowpack parameter estimation from Synthetic Aperture Radar (SAR) data. Implementations of recently developed algorithms for the estimation of snow wetness, snow density, and snow surface dielectric constant are the main components in the toolbox. The main objective of this toolbox is to make accessible state of the art polarimetric techniques for cryosphere applications.

HimSAR is an anglicized portmanteau of the Devanagari word ??? (him) meaning snow and SAR. This toolbox contains algorithms for snowpack parameters estimation from dual and full polSAR data obtained from ALOS PALSAR/ALOS-2, RADARSAT-2 and TerraSAR-X radar sensors. Additionally, it also provides the conventional SAR processing algorithms, and commonly used PolSAR decomposition techniques.

This software is written in Qt, a modern cross-platform framework in C++, allowing it to be run on a variety of system environments: Windows, Linux and Mac. The toolbox being a Graphical User Interface (GUI) based application enables user to select, set, experiment parameter values and run the software. The HimSAR application acts as a complimentary toolbox to the existing open-source SAR package like PolSARpro and commercial ones like ENVI etc. The software is licensed under the 'Apache License 2.0' with the source code made freely available to the public.

In-house developed snow wetness [1] snow density [2], snow surface dielectric constant [3] and snow cover map [4] algorithms are the main contributions to this toolbox. Polarimetric SAR data is used to derive the generalized surface and volume scattering parameters over the snow cover area. These parameters are then inverted as a snow surface and volume dielectric constants. These snow surface and volume dielectric constants are then used for the estimation of snowpack

wetness and density. Adaptive Generalized Unitary (AGU) transformation based optimum degree of polarization proposed in [5] are used for the estimation snow surface dielectric constant. Polarization fraction based snow cover mapping approach is proposed in [5]. Apart from these other existing snowpack parameter estimation algorithms proposed are also included in this toolbox.

References

[1] M Surendar, A Bhattacharya, G Singh, Y Yamaguchi, and G Venkataraman, "Development of a snow wetness inversion algorithm using polarimetric scattering power decomposition model," International Journal of Applied Earth Observation and Geoinformation, vol. 42, pp. 65– 75, 2015.

[2] M Surendar, A Bhattacharya, G Singh, and G Venkataraman, "Estimation of snow density using fullpolarimetric synthetic aperture radar (sar) data," Physics and Chemistry of the Earth, Parts A/B/C, vol. 83, pp. 156–165, 2015.

[3] S. Manickam, A. Bhattacharya, G. Singh, and Y. Yamaguchi, "Estimation of snow surface dielectric constant from polarimetric sar data," IEEE Journal of Selected Topics in Applied Earth Observations and Remote Sensing, vol. PP, no. 99, pp. 1–8, 2016.

[4] G. Singh, G. Venkataraman, Y. Yamaguchi, and S. E. Park, "Capability assessment of fully polarimetric alospalsar data for discriminating wet snow from other scattering types in mountainous regions," IEEE Transactions on Geoscience and Remote Sensing, vol. 52, no. 2, pp. 1177–1196, Feb 2014.

[5] A. Bhattacharya, G. Singh, S. Manickam, and Y. Yamaguchi, "An adaptive general four-component scattering power decomposition with unitary transformation of coherency matrix (AG4U)," IEEE Geoscience and Remote Sensing Letters, vol. 12, no. 10, pp. 2110–2114, Oct 2015.

10426-9, Session PS

Correlation between land cover and ground vulnerability in Alexandria City (Egypt) using time series SAR interferometry and optical Earth observation data

Tarek A. Seleem, Suez Canal Univ. (Egypt); Vyronas Stergiopoulos, Harokopio Univ. of Athens (Greece); Penelope Kourkouli, GAMMA Remote Sensing Research and Consulting AG (Switzerland); Theodora Perrou, Issaak Parcharidis, Harokopio Univ. of Athens (Greece)

The main scope of this study is to investigate the potential correlation between land cover and ground vulnerability over Alexandria city, Egypt. Two different datasets for generating ground deformation and land cover maps were used. Hence, two different approaches were followed, a PSI approach for surface displacement mapping and a supervised classification algorithm for land cover/use mapping. In the current analysis, two main data stacks were used for generating ground deformation and land cover maps, respectively. The two methodologies applied in this study are a) the PSI approach for surface deformation mapping and b) a supervised classification algorithm for land cover/use mapping. For the PSI analysis, a dataset of 40 Single Look Complex (SLC) Advanced Synthetic Aperture Radar (ASAR) scenes, acquired from the European Space Agency Environmental Satellite (ENVISAT), was used. The scenes acquired in descending orbit covering the period between 2003 and 2010. For the supervised classification an ASTER image acquired from the Terra satellite dated 13/10/2010, was used.

The interferometric results show a gradual qualitative and quantitative differentiation of ground deformation from East to West of Alexandria government. We selected three regions of interest in order to compare the obtained interferometric results with the different land cover types. The ground deformation may be resulted due to different geomorphic and geologic factors encompassing the proximity to the active deltaic plain of the Nile River, the expansion of the urban network within arid regions of recent deposits, the effects due to urban density increasing, and finally the combination of the above mentioned parameters.

10426-19, Session PS

Building damage mapping of 2016 Kumamoto, Japan, earthquake using ALOS-2/PALSAR-2 interferometric coherence

Tomohisa Konishi, Yuzo Suga, Hiroshima Institute of Technology (Japan)

The 2016 Kumamoto earthquake sequence started with a Mj (Japan Meteorological Agency magnitude) 6.5 event on

April 14, and culminated in a Mj 7.3 event on April 16. Rapid damage assessment after natural disasters is crucial to a fast crisis response, e.g. to support rescue, first aid, medical and emergency supplies as necessary and reconstruction operations in the crisis area. Remote sensing techniques are useful to obtain damage information because of their wide area acquisition, non-contact, low cost, and rapid response capabilities. Very high resolution optical satellite images provide useful information for damage assessment. However, it is difficult to identify the damaged buildings in case of the less intact roof. On the other hand, Synthetic Aperture Radar (SAR) interferometric analysis has a great potential due primarily to its phase difference. In this study, we demonstrated the applicability of interferometric coherence from SAR images for detection of building damages and liquefactions caused by the earthquake. In general, L-band SAR interferometry is advantageous for detecting ground displacements, even in vegetated areas, due to its high coherence, compared with C- or X-band SAR interferometry. The Japanese ALOS-2 was launched on 24 May 2014. ALOS-2 has aboard L-band SAR called PALSAR-2. Three PALSAR-2 data acquired on November 30, 2015, March 7, 2016 and April 18, 2016 were used, the former two were acquired before the earthquake occurrence and the third was acquired two days after the main shock. The interferometric coherence was calculated within several moving window pixels from multi-temporal PALSAR-2 images. Then, the interferometric coherence images were ortho-rectified using 10 m mesh Digital Elevation Model (DEM) generated by the Geospatial Information Authority of Japan (GSI). For damage assessment, normalized difference (ND) interferometric coherence was calculated using pre-disaster and co-disaster SAR image pairs. The ND shows high value in damaged areas compared to undamaged areas. For validation process, we adopted assumption map of collapsed ratio calculated by the National research Institute for Earth science and Disaster resilience, Japan (NIED). The validation map shows three ranking, which were more than 50 collapsed buildings, more than 20 collapsed buildings and more than 10 collapsed buildings within 250 ? 250 m2 area. The ND interferometric coherence over several windows depended on the collapsed ratio. The averaged ND interferometric coherence within more than 50, more than 20, more than 10 collapsed buildings and no collapsed building were 0.14, 0.09, 0.06 and 0.01, respectively. In addition, the ND interferometric coherence image showed liquefaction as a high value in urban areas. The distribution pattern was in good agreement with a liquefaction map referred to literatures. Two major results were obtained from the study. The first is the verification of the effectiveness of interferometric coherence information for detecting the building damage areas induced by the earthquake. The second result also proves that the liquefaction distribution pattern can be extracted by the interferometric coherence. The results indicate the possibility of rapid damage mapping after the earthquake for fast crisis response using SAR interferometric coherence.

10426-20, Session PS

Persistent scaterer interferometry synthetic aperture radar technique for monitoring of land subsidence of Gangotari(Himalayan) Region, India

Harikesh Singh, Central Univ. of Jharkhand (India)

This research aims to provide a strategic technique for detecting Land subsidence of a Himalayan region nearby Gangotri region by integrating geo-spatial technique with the city plan. With the integration of this technology, it would enable us in detecting Land subsidence of any area. Land subsidence is one of the major geological hazard in urban construction region. For this research, PSInSAR technique will be used for getting land subsidence. PSInSAR is being used since past decade and it has helped in detecting land subsidence. PSInSAR technique allows efficient planning by providing accurate data about land subsidence and predicting urban growth of a city. The major application of PSInSAR technique is the analysis monitoring of land subsidence of specific areas. PSInSAR technique is also known as advanced technique of DInSAR. DInSAR is used for detcecting small scale movement of earth surface but in case of PSInSAR, It detects large scale subsidence of land surface.

In this paper we will use PSInSAR technique for detecting land subsidence of Urban area. For completing this paper, we used param super facility computing. In this research we used time series of nearby Gangotari glacier region. This technique consumes much time. This research comprises of satellite images like ENVISAT images and SRTM data which help in broader aspects of urban land subsidence. ENVISAT images will be acquired during 2004 to 2007 will be used for detecting land subsidence. For completing this technique this paper we used many geospatial tools such as DORIS, STaMPS, MATLAB etc. The purpose of this article is providing scientific basis for urbanization over the study area.

10426-22, Session PS

Advanced subsidence monitoring using persistent scatterer interferometry for Jharia Coal Field, Dhanbad, India

Shailaja Thapa, R. S. Chatterjee, Indian Institute of Remote Sensing (India); Dheeraj Kumar II, Indian School of Mines (India); K. B. Singh III, Central Institute of Mining and Fuel Research (India); Vivek K. Sengar, Indian Institute of Remote Sensing (India)

This paper presents a spatio-temporal dynamics of surface subsidence over an urban area due to coal mining using Persistent Scatterer Interferometry (PS-InSAR) techniques. In the past few years Differential Interferometric Synthetic Aperture Radar (D-InSAR) technique has emerged as a very useful remote sensing technique for measuring land subsidence. It plays a vital role in in-situ subsidence prediction of coal mining area. However, there are some limitations in conventional D-InSAR techniques viz. atmospheric decorrelation, temporal decorrelation and spatial decorrelation, which can be overcome up to a certain extent by using multi-interferogram framework approach. There are many techniques which have been developed utilizing multi-interferogram framework concept like PS-InSAR developed by Ferretti et al., 1999, Interferometric Point Targets Analysis (IPTA) developed by GAMMA Remote Sensing, Spatio-Temporal Unwrapping Network (STUN) proposed by Kampes et al, Small Baseline Subset (SBAS) algorithm proposed by Berardino et al 2001; 2002 and Coherent Pixels Techniques (CPT) developed by O. Mora et al (2003) etc.

The PS-InSAR comprises of number of SAR datasets, it only concentrates over the pixels which remain coherent over the long periods of time. Persistent scatterer interferometry makes deformation measurement of the permanent scattering location of the targeted ground surface. Mainly, these permanent scatterer are man-made features like metallic bridges, dams, antennae on the roofs of buildings, etc. apart from man-made features some permanent scatterer may comprise of prominent stable natural targets like rocks. The results obtained from PS-InSAR technique gives a more precise measurement of surface deformation history. In this study total eight Advanced Land Observing Satellite (ALOS-1) Phased array L-band synthetic aperture radar (PALSAR) scenes acquired with ascending nodes, covering the time period from 2007 to 2010 have been utilized to produce ground deformation map using PS-InSAR technique for Jharia coal fields, Dhanbad. The ALOS-1 scenes were acquired in fine beam single polarization (FBS) mode and, HH polarization was used for the study. The Synthetic Aperture Radar (SAR) data sets were selected in such a manner that it overcomes the temporal decorrelation problem.

In India, Jharia Coal Fields (JCF), Dhanbad is one of the most important resource of fossil fuel. This coal field has undergone extensive exploitation since beginning of mining, which resulted in formation of underground voids manifested on the surface as cracks, fissures and subsidence. Thus, PS-InSAR is one of the advance space borne technique, which helps to

identify the persistent land surface movement. It gives more precise measurement than any other techniques.

The results obtained from PS-InSAR techniques were analyzed over an urban areas in Jharia coal field (JCF), Dhanbad. The area undergoing deformation was delineated using PS-InSAR technique in Jharia coal fields. The Persistent Scatterer interferometry technique results were validated using mining plan provided by mining authorities. The results demonstrate that PS-InSAR can be used as a potential tool to highlight the subsidence prone areas depending upon the spatial and temporal coherency of SAR data. Also, it is one of the potential tool which can be used to monitor time series deformation history in the coal mining area thus it helps to reduce the socio-economic losses caused due to subsidence.

10426-23, Session PS

The effect of precipitation on measuring sea surface salinity from space

Xuchen Jin, Delu Pan, Xianqiang He, Difeng Wang, Qiankun Zhu, Fang Gong, The Second Institute of Oceanography, SOA (China)

The sea surface salinity (SSS) can be measured from space by using L-band (1.4Ghz) microwave radiometers. The L-band has been chosen for its sensitivity of brightness temperature to the change of salinity. However, SSS remote sensing is still challenging due to the sensitivity of brightness temperature to SSS remains low: for the vertical polarization, the sensitivity is about 0.4 to 0.8 K/psu with different incident angle and sea surface temperature; for horizontal polarization, the sensitivity is about 0.2 to 0.6 K/psu. It means that we have to make radiometric measurements with accuracy better than 1K even for the best sensitivity of brightness temperature to SSS. Therefore, in order to retrieve SSS, the measured brightness temperature at the top of atmosphere (TOA) needs to be corrected for many sources of error. One main geophysical source of error comes from atmosphere. Currently, the atmospheric effect at L-band is usually corrected by absorption and emission model, which estimate the radiation absorbed and emitted by atmosphere. However, the radiation scattered by precipitation is neglected in absorption and emission models, which might significant under heavy precipitation. In this paper, a vector radiative transfer model for coupled atmosphere and ocean systems with a rough surface is developed to simulate the brightness temperature at the TOA under different precipitations. The model is based on the adding-doubling method, which includes oceanic emission and reflection, atmospheric absorption and scattering. For the ocean system with a rough surface, an empirical emission model established by Gabarro and the isotropic Cox-Munk wave model considering shadowing effect are used to simulate the emission and reflection of sea surface. For the atmospheric attenuation, it is divided into two parts: For the rain layer, a Marshall-Palmer distribution is used and the scattering properties of the hydrometeors are calculated by Mie theory (the scattering hydrometeors are assumed to be spherical). For the other atmosphere layers, which are assumed to be clear sky, Liebe's millimeter wave propagation model (MPM93) is used to calculate the absorption coefficients of oxygen, water vapor, and cloud droplets. To simulate the change of brightness temperature caused by different rain rate (0-50 mm/hr), we assume a 26-layer precipitation structure corresponding to NCEP FNL data. Our radiative transfer simulations showed that the brightness temperature at TOA can be influenced significantly by the heavy precipitation. Thus, in the case of heavy precipitation, the current absorption and emission model is not accurate enough to correct atmospheric effect, and a radiative transfer model which consider the effect of radiation scattering should be used.

10426-24, Session PS

Creating soil moisture maps based on radar satellite imagery

Volodymyr Hnatushenko, EOS Data Analytics (Ukraine) and Dnipropetrovsk National Univ. (Ukraine); Igor Garkusha, EOS Data Analytics (Ukraine); Volodymyr Vasyliev, EOS Data Analytics (Ukraine) and Dnipropetrovsk National Univ. (Ukraine)

The presented work is related to a study of mapping soil moisture basing on radar data from Sentinel-1 and a test of adequacy of the models constructed on the basis of data obtained from alternative sources. Radar space imagery of territories in certain bands of the electromagnetic spectrum has a number of advantages in comparison with multispectral satellite imagery, as well as certain disadvantages. An undoubted advantage is its weatherproof capability and independence of the time of the day. A certain number of problems can be solved with the use of radar imagery data. One of them is mapping soil moisture. Radar signals are reflected from the ground differently, depending on its properties. In radar images obtained, for example, in the C-band of the electromagnetic spectrum, soils saturated with moisture usually appear in dark tones. Although, at first glance, the problem of constructing moisture maps basing on radar data seems intuitively clear, its implementation on the basis of the Sentinel-1 data on an industrial scale and in the public domain is not yet available. In the process of mapping, for verification of the results, measurements of soil moisture obtained from logs of the network of climate stations NOAA US Climate Reference Network (USCRN) were used. This network covers almost the entire territory of the United States. In addition, other supplementary cartographic materials were used, such as maps of soil types and ready moisture maps. The paper presents a comparison of the effect of the use of certain methods of roughening the quality of radar data on the result of mapping moisture. Regression models were constructed showing dependence of backscatter coefficient values Sigma0 for calibrated radar data of different spatial resolution obtained at different times on soil moisture values. The obtained soil moisture maps of the territories of research, as well as the conceptual solutions about automation of operations of constructing such digital maps, are presented. The comparative assessment of the time required for processing a given set of radar scenes with the developed tools and with the ESA SNAP product was carried out. Next ways of development of the proposed technique for mapping moisture basing on the Sentinel-1 data are described.

10426-25, Session PS

A comparative study of change detection of land use/land cover classification using multisensor and mutitemporal data

Punithraj G., Pruthviraj U., Amba Shetty, National Institute of Technology Karnataka, Surathkal (India)

Use of optical remote sensing data is limited due to the cloud cover in tropical areas, microwave remote sensing data is considered as one of the solution. The objective of the study is to compare the change detection over tropical region using optical, synthetic aperture radar (SAR) and fusion of both images. In this present study, 2 sets of data are used one from ENVISAT and sentinel-1 which are SAR data and other from LandSAT-7 which is optical data of the period 2006 and 2016 over the coastal areas of Karnataka, India. As a part of analysis use of speckle filters such as Lee, Forst, Gama and local Sigma has been explored. The optical and SAR data was georectified and supervised classification is carried out. Finally accuracy assessment of the classified map is carried out using kappa statistics. The change of land forms spatially and temporally was estimated under three scenarios. The present study gives the unique application of fusion SAR data with optical data in Change detection studies.

10426-26, Session PS

Sea surface wind retrievals from SAR using theoretical backscattering model

Xiaomin Ye, National Satellite Ocean Application Service (China)

Sea surface wind speeds can be retrieved from normalized radar cross section (NRCS) of SAR images by using a Geophysical Model Function (GMF) and outside wind directions. GMF relates NRCS to sea surface winds with parameters of frequency, polarization, sensor/sea-surface geometry (i.e. the azimuth, wind direction and the incident angle of radar wave). For wind retrieval, we must choose a suitable established GMF for the SAR frequency and polarization, or else it will not work if the frequency and polarization of SAR are not the same as that of GMF. The composite radar backscattering theoretical model is combined by two-scale backscatter model and geometric optics model. The two-scale backscatter theory is described as the short waves of which wavelengths are comparable to the incident electromagnetic wave on the ocean surface are tilted by long wave and the electromagnetic back scattering the Bragg scattering. The theoretical backscattering model can simulate the radar backscattering from oceanic surface at any microwave frequency and polarization.

In this study, we retrieve sea surface wind speeds from SAR images (both RARDASAT-2 at C-band and COSMO-SkyMed at X-band) using theoretical backscattering model. The simultaneous wind directions of Advanced Scatterometer (ASCAT) onboard European Metop-A/B satellites are used as the input of winds retrievals. The sea surface wind retrieval results are evaluated by simultaneous wind speed measured by ASCAT. Sea surface wind speeds are retrieved from 46 SAR images at C-band of RARDARSAT-2 by using the composite microwave backscattering model, the mean of RMSEs compared with sea surface wind speeds of ASCAT is 1.5 m/s. Sea surface wind speeds are also retrieved from 2 SAR images at X-band of COSMO by using this composite model with the RMSE of 1.6 m/s compared with ASCAT. The results of wind speeds retrievals show that the improved backscattering model of oceanic rainfall (i.e. the composite microwave backscattering model) can be applied in sea surface wind field retrieval for SAR images at both C-band and X-band.

10426-27, Session PS

Influence of different DEMs on the quality of the InSAR results – case study over Bankya and Mirovo areas

Hristo Nikolov, Space Research and Technology Institute (Bulgaria); Mila Atanasova, National Institute of Geophysics, Geodesy and Geography (Bulgaria)

One of the key input parameters in obtaining end products from SAR data is the DEM used during their processing. This holds true especially when persistent scatterers InSAR method should be applied for example to study slow moving landslides or subsidence. Since nowadays most of the raw SAR data are of space borne origin for their correct processing to high precision products for relatively small areas with centimeter accuracy a DEM taking into account the particularities of the local topography is needed. Most of the DEMs used by the SAR processing software such as SRTM or ASTER are obtained by the same type of instrument and present some disagreements with height information acquired by leveling measurements or other geodetic means. This was the motivation for initiating this research – to prove the need of creating and using local DEM in SAR data processing at small scale and to check what the magnitude of the discrepancy between final InSAR products is in both cases where SRTM/ASTER and local DEM has been used. In addition investigated were two scenarios for SAR data processing – one with small baseline between image pairs and one having large baseline image pairs – in order to find out in which case local DEM has bigger impact.

In course of this study two reference areas were considered – Bankya village near Sofia (SW region of Bulgaria) and Mirovo salt extraction site (NE region of Bulgaria). The reason those areas were selected lies in the high number of landslides registered and monitored by the competent authorities in the mentioned locations. The significance of the results obtained is witnessed by the fact that both sites we used have been included as reference sites for Bulgaria in the PanGeo EU funded project dealing with delivering information regarding ground instability geohazard as areas prone to subsidence of natural and manmade origin. In the said project largest part of the information has been extracted from Envisat SAR data, but now this information could be supplemented by adding such from Sentinel-1 derived by us.

10426-16, Session JS2

Investigating ground instabilities in Indonesia through SAR Interferometry

Fabio Bovenga, Alberto Refice, Antonella Belmonte, CNR ISSIA (Italy); Raffaele Nutricato, Davide O. Nitti, Maria T. Chiaradia, Univ. degli Studi di Bari Aldo Moro (Italy); Athanassis Ganas, National Observatory of Athens (Greece); Paolo Manunta, Collaborative Space Ltd. (Ireland); . Elizar, . Darusman , Syiah Kuala Univ. (Indonesia); Philippe Bally, ESRIN (Italy)

Indonesia is periodically affected by severe volcanic eruptions and earthquakes, which are geologically coupled to the convergence of the Australian tectonic plate beneath the Sunda Plate. SAR interferometry (InSAR) can be used to support studying and modeling of terrain movements such as tectonic motions associated with faults. Multi-temporal InSAR (MTI) techniques provide both mean displacement maps and displacement time series over selected, stable objects on the Earth surface. The study of tectonic phenomena requires large-scale spatial analysis that poses challenges in MTI processing. A reliable modelling needs additional information coming e.g. from geodetic data, such as those provided by GNSS networks.

This work is aimed at performing an analysis of ground displacements over Indonesian sites through MTI techniques. Test sites have been selected according to the availability of archived SAR data, GNSS networks, and geological data. Based on the existence of i) onshore active faults, ii) undergoing deformation as from GPS data, iii) foreseen good interferometric coherence, iv) availability of SAR imagery, two stacks of COSMO-SkyMed data, both acquired in stripmap mode between 2011 and 2015, have been selected, one on the capital Banda Aceh (descending geometry, mean incident angle of 32.2°) and a second one on the city of Yogyakarta (ascending geometry, mean incident angle of 29.3°). Geological maps of the Banda Aceh and Yogyakarta test sites are available, and several GNSS stations from the Continuously Operating Reference Stations (CORS) Indonesian network are found to be located in the areas of interest: 24 in Banda Aceh and 36 in Yogyakarta. For each station, horizontal velocity values and displacement time series are available.

Sentinel-1 data are also available, even though their number is quite limited because of the reduced acquisition frequency on the area. Both the SPINUA and the StaMPS algorithms have been used to process the data. The former is well suited for scarcely urbanized areas and high resolution local scale analysis, while the latter has been proven effective for studying both volcanic deformations and fault slips. This processing strategy also allows us to cross-validate MTI results.

Integration of Java and Aceh province observations from SAR satellites with ground-based GNSS observations has been attempted, with the aim of producing a uniform product, improving on the existing, low-resolution global strain rate map (http://gsrm.unavco.org/) derived from GNSS alone. The work describes the MTI processing adopted, and the procedure developed to integrate the MTI deformation maps with the records derived from GNSS observations where possible. The ground deformations undergoing on the area of interest are then modelled according to the available products and

information.

ACKNOWLEDGMENTS

Work supported by ESA project titled “Integrating SAR interferometry and GNSS for studying tectonic processes in Indonesia” (contract 4000114611/15/F/MOS), ESA ITT AO/1-7864/14/F/MOS, Alcantara Study reference 14-P16 “Alcantara Study Enhanced Tectonic Characterization for Indonesia”.

10426-17, Session JS2

KydroSAT: a Ku/Ka band synthetic aperture radar space mission concept for high-resolution mapping of hydrometeorological parameters

Saverio Mori, Frank S. Marzano, Sapienza Univ. di Roma (Italy) and Univ. degli Studi dell’Aquila (Italy); Nazzareno Pierdicca, Sapienza Univ. di Roma (Italy); Ornella Bombaci, Domenico Giancristoforo, Thales Alenia Space (Italy); Giovanni Macelloni, Consiglio Nazionale delle Ricerche (Italy); Juha Lemmetyinem, Finnish Meteorological Institute (Finland); Davide Giudici, ARESYS s.r.l. (Italy); Armen Poghosyan, Skolkovo Institute of Science and Technology (Russian Federation)

Several spaceborne X-band synthetic aperture radars (SARs) are nowadays operational, representing a well-established tool for Earth remote sensing at very high spatial resolution (order of meters up to tens of meters). Consolidated civil applications include flood area detection and monitoring, earthquake analysis, digital elevation modelling, land use monitoring and classification. Until now, the exploitation of SAR for hydrological cycle modelling and numerical weather forecast has not been pursued, mainly due to the use of relatively low microwave frequency bands, such as L, S and X. However, there are scientific and experimental evidences that: i) atmospheric precipitation in liquid and ice phase can affect SAR imagery at X band and beyond and its intensity can be retrieved (e.g., Marzano et al., 2010; Marzano et al., 2012; Pulvirenti et al., 2014), ii) snow areal extent and mass (water-equivalent) can be detected and estimated by using SAR measurements at X band and beyond (e.g., Rott et al., 2010; Montomoli et al., 2016; Cui et al., 2016). In this respect, spaceborne SARs cannot be always considered “all weather” sensors and the use of higher frequencies can be also exploited to retrieve atmospheric water content both within clouds and near the surface.

Within the frame of H2020 COMPET-2-2017 call, the KydroSAT mission concept has been proposed. KydroSAT foresees a high-performance miniaturised SAR at Ku and Ka band, named KydroSAR, specifically devoted to mapping, detecting and estimating atmospheric precipitation and surface snow. The KydroSAR instrument is a dual-frequency lightweight fully-digital SAR whose baseline includes dual-polarization capability, large variable swath (between 50 and 150 km), high orbit duty cycle (>75%) and flexible ground resolution (between 5 and 150 m), depending on the scan/observation mode. The overall KydroSAT mission concept is based on the formation of two near-polar low-Earth-orbit minisatellites (less than 400 kg), named KydroSats and both carrying a KydroSAR payload, in order to extend the swath up to 150-300 km. These 2 KydroSats are part of an along-track convoy with X-band SAR COSMO-SkyMed and L-bad SAR SAOCOM platforms. In this way, the same Earth scene would be observed at L, X, Ku and Ka bands, representing a unique opportunity to improve high-resolution atmospheric and cryospheric products, but also useful for other applications.

In order to demonstrate the validity of the KydroSAT concept, in this work we will simulate the SAR response at L, X, Ku and Ka bands of a same scene, using the SAR forward model described in Mori et al. (2017). Both realistic 3D scenes, generated by high-resolution Cloud Resolving Models (e.g., SAM) and simplified scenarios, easier to be interpreted, will be considered. Numerical results will be discussed in order to exploit the synergic approach of the KydroSAT convoy approach and to evaluate new quantitative retrievals of rain cloud parameters, such as columnar water content and precipitation rate. Using cryospheric synthetic scenarios (Montomoli et al., 2016), numerical simulations will be also used to show the capabilities of KydroSAT for snow areal extent and mass (water equivalent) monitoring.

10426-18, Session JS2

Extraction of damaged area caused by debris flows in Hiroshima using COSMO-SkyMed images

Tomohisa Konishi, Yuzo Suga, Hiroshima Institute of Technology (Japan)

A heavy rain occurred in Hiroshima city on 20 August 2014. 107 debris flows and 59 shallow slides were induced by the heavy rain. Rapid damage assessment after natural disasters is crucial for initiating effective emergency response actions. Remote sensing techniques play an important role in obtaining damage information because of their wide area and revisit observation, non-contact, low cost, and high resolution imaging. Very high resolution optical satellite images provide useful information for a damage assessment, although the target acquisition depends on the weather (cloud cover) and acquisition time (sun light) condition. In contrast, Synthetic Aperture Radar (SAR) has great potential due primarily to its all-weather day-and-night imaging capabilities. Extraction of damage area for debris flows using SAR images is a challenging task, although there are a lot of literatures for landslide monitoring using differential interferometric SAR (DInSAR). It is rare on the research for the damaged area caused by debris flows utilizing SAR images.

The Italian constellation of satellites COSMO-SkyMed provides high-resolution image with short revisit time. COSMO-SkyMed image is suited for detecting damaged area in terms of the resolution because the debris flows are narrow width along the valleys. In addition, the short revisit time capability is suited for the interferometric coherence analysis because it depends on temporal baseline. In this study, we examine an extraction of damaged area induced by debris flows using multi-temporal COSMO-SkyMed images. Three COSMO-SkyMed images were used acquired on 6 August, 10 August and 22 August, 2014. There were one pre-disaster pair and two co-disaster pairs. The extraction methods are interferometric coherence, intensity correlation and normalized sigma nought index (NDSI) using COSMO-SkyMed image pair. These methods have been used for the assessment of building damage caused by earthquake.

The Single Look Complex data of COSMO-SkyMed were co-registered each other for calculating interferometric coherence. The interferometric coherences were calculated within several moving windows. Then, interferometric coherence images were ortho-rectified using 10 m gridded Digital Elevation Model (DEM) generated by the Geospatial Information Authority of Japan (GSI). On the other hand, the Multi Look Intensity data of COSMO-SkyMed were ortho-rectified using the DEM. Then, the intensity correlation and NDSI were calculated within several moving windows. For damage assessment, normalized difference (ND) was calculated by each interferometric coherence, intensity correlation and NDSI using pre-disaster and co-disaster image pairs. The ND value increases when the land surface was changed by a disaster.

Comparing with aerial photograph after the disaster and the official announcement, ND of NDSIs increased in the discharged sediment area occurred by the debris flows in the study area. As the false positive region, a playground at the Bairin elementary school was detected because there were many cars as a temporary parking for rescue.

In conclusion, ND of NDSIs showed good capability for extraction of damaged area induced by the debris flows at a rapid response phase.

10426-1, Session 1

Deformation vector measurement by means of ground based Interferometric radar system

Alberto Michelini, Francesco Coppi, IDS GeoRadar (Italy)

Ground Based Interferometric Radar (GBInRad) is a class of terrestrial remote sensing imaging system, based on microwave interferometric techniques. The principal application of GBInRad system is deformation monitoring, since respect to other techniques they can provide remote sensing, high sensitivity to small deformations, long range of measurements, imaging capability and fast scan time.

The main limitation of standard GBInRad system is their capability of detecting movements only along the Line of Sight (LoS) of the sensor, although actual targets may show deformations in any direction of space; this represents an important limitation with respect to other techniques able to estimate the full 3D deformation vector.

Without considering integration between GBInRad and other measurement system, to obtain actual 3D displacement vector it is therefore necessary to apply some measurement strategy or some geometrical assumptions on the deformation direction. For example, if the 3D deformation direction is known a priori, the measured LoS deformation can be back-projected onto a 3D total deformation rate.

If the displacement direction is not known a priori, combining together LoS displacement measured from different spatial positions, it is possible to reconstruct the actual 3D displacement vector of monitored targets.

In this paper are introduced and analysed the various aspect of the displacement vector measurement with multiple GBInRad system that work both in a monostatic and in a bistatic configuration.

In the monostatic configuration every system transmits and receives the signal independently from the others; this approach requires multiple GBInRad system deployed to monitoring the same scenario and therefore its main limitations lie in the costs, power consumption and maintenance.

A possible cost-effective evolution of the monostatic configuration is to exploit GBInRad system in a multiple bistatic configuration; a multiple bistatic Radar is a system in which a transmitter operates together with multiple receivers located in different positions in space; these systems are widely employed, for example, in military applications as receivers are passive and hence undetectable. The main difficulty in the exploitation of a bistatic Radar system is that it requires an accurate time and phase synchronization of the Radio Frequency (RF) signal between transmitter and receivers.

In the past has been presented a multiple bistatic GBInRad system designed for very short range operation; in this system the synchronization between the transmitter radar unit and the remote receivers were obtained connecting them through coaxial cables. This architecture restricts considerably the system operative ranges and performances.

A first proposed solution that could overcome those limitations is to substitute the coaxial cables with a transceiver located far away from the transmitter radar unit. A second solution is to endow the bistatic GBInRad system with GPS disciplined oscillators that allow the RF signal time and phase remote synchronization.

In this paper are presented the system analysis, the deformation vector measurement and the sources of errors for the proposed solutions.

10426-2, Session 1

Using multitemporal interferometry and Sentinel-1 data to monitor ground instability hazards related to open-cast mining operations

Janusz Wasowski, Istituto di Ricerca per Protezione Idrogeologica (Italy); Fabio Bovenga, CNR ISSIA (Italy); Davide O. Nitti, Raffaele Nutricato, Khalid Tijani, GAP S.r.l. (Italy); Alberto Morea, Univ. degli Studi di Bari Aldo Moro (Italy); Maria T. Chiaradia, Politecnico di Bari (Italy)

Surface mining represents the predominant mineral and coal exploitation method in Europe and worldwide. Different mining methods can be involved, but most often: open-cast (open-pit) mining; terrace mining; contour strip mining; quarrying. Although surface mining is considered safer than underground mining, ground instability hazards represent an ever-present concern and important problem limiting the mining operations (e.g., slope instability in high wall open-cast mines and quarries). However, given the often large extent of areas affected by surface mining and life span of mines (tens of years), long-term monitoring via traditional in-situ methods is typically impractical (economically and technically).

Here we focus on the use of an advanced multi-temporal interferomery (MTI) and Sentinel-1 imagery for mapping and monitoring of ground instabilities in open-cast mines and adjacent areas. Open-cast mines represent a good target for MTI, because they are i) often very large (from few to tens of km2); ii) free of or covered by sparse vegetation; iii) require long-term regular monitoring, which can now rely on free of charge Sentinel-1 data from the European Space Agency.

However, a cursory review of the recent literature (international journals) suggests that in comparison to applications to underground mines, MTI has been relatively little exploited to investigate ground instabilities related to surface mining. One reason for this is that some portions of open-cast mines can lack measurable radar targets due to rapid changes of ground surface caused by intense mining operations (e.g., overburden stripping, waste material damping). We argue that this limitation can now be mitigated by the higher frequency and regularity of acquisitions provided by Sentinel-1 (nominally every 6 days since October 2016).

To illustrate the potential of MTI for detecting and monitoring ground instabilities induced by surface mining, we present case study example of the Belchatow mine (Poland), one of the largest brown coal open-cast operations in Europe (about 12 km long and 3 km wide). The Belchatow open-cast mine reaches the depth of 310 m and has been affected by a number of slope failures in the last few decades. The failures disrupted the mining operations, destroyed in part the mining machinery and resulted in high economic losses. In this study we assess the recent and current stability conditions in the mine area by exploiting several tens of medium resolution (~20 m) images acquired by Sentinel-1 since October 2014. Despite the local lack of information (areas affected by intensive surface disturbance due to ongoing mining operations), the MTI results provided a valuable synoptic overview of the ground instability/stability condition within and outside the active mine. Although it is not simple to provide short-term forewarning of the impeding slope failure on the basis of the surface displacement time series alone, our experience indicate that long-term, high frequency MTI measurements offer the following benefits: i) better anticipation of risk of failure over large areas and more rational design of ground-based monitoring networks; ii) better planning for maintenance and management of open-cast mines.

10426-3, Session 1

Sentinel-1 interferometric coherence assessment for land cover and vegetation mapping (SInCohMap)

Fernando Vicente-Guijalba, DARES Technology (Spain); Zbigniew Bochenek, Katarzyna Dabrowska-Zielinska, Institute of Geodesy and Cartography (Poland); Javier Duro, DARES Technology (Spain); Marcus Engdahl, ESRIN (Italy); Alexander Jacob, EURAC (Italy); Agata Hoscilo, Institute of Geodesy and Cartography (Poland); Marco Lavalle, Jet Propulsion Lab. (United States); Carlos López-Martínez, Univ. Politècnica de Catalunya (Spain); Juan M. Lopez-Sanchez, Univ. de Alicante (Spain); Jordi J. Mallorquí Franquet, Univ. Politècnica de Catalunya (Spain); Eric Pottier, Univ. de Rennes 1 (France); Claudia Notarnicola, Ruth Sonnenschein, EURAC (Italy); Dariusz Ziólkowski, Institute of Geodesy and Cartography (Poland)

In this abstract new ESA SEOM project SInCohMap is presented, which has just started in January 2017.

The main objective of this research is to develop, analyze and validate novel methodologies for land cover and vegetation mapping using time series of Sentinel-1 data and in particular by exploiting the temporal evolution of the interferometric coherence. Further, the project aims at quantifying the impact and possible benefit of using Sentinel-1 InSAR (Interferometric Synthetic Aperture Radar) data relative to traditional land cover and vegetation mapping using optical data (especially Sentinel-2) and traditional intensity-based SAR (Synthetic Aperture Radar) approaches.

The main addressed classes are: forests, agricultural areas (e.g. Crops), artificial surfaces (e.g. urban), water bodies, scrub and herbaceous vegetation, open or bare land with little to no vegetation and Wetlands.

We have setup three different reference test areas with very accurate ground truth data for performing quantitative assessment and validation in Spain, Italy and Poland.

In order to scientifically evaluate the performance of different methodologies for land cover and vegetation mapping a round robin is organized. Participants will get access to pre-processed datasets over the three study areas together with some access for relevant training data for classification purposes. Further participants will also get access to processing facilities via a private cloud platform hosted at EURAC Research. The kickoff for this round robin will be in September 2017 and it will stay active for 4-6 month.

10426-6, Session 2

Soil moisture products comparison between SMAP, SMOS, ASCAT, ERA and ISMN: an error characterization through extended quadruple collocation technique

Fabio Fascetti, Nazzareno Pierdicca, Sapienza Univ. di Roma (Italy); Luca Pulvirenti, CIMA Research Foundation (Italy); Raffaele Crapolicchio, Serco SpA (Italy)

The role of soil moisture as a key variable for the characterization of the global climate is widely recognized within the international scientific community. Indeed, soil moisture content (SMC) represents an essential variable for a large number of disciplines, influencing several geophysical processes, as the water and carbon cycle. In situ probes can directly measure SMC, but they are generally very sparse, so that the spatial variation cannot be retrieved. Microwave remote sensing represents a very useful tool to monitor such parameter at different spatial and temporal scales, including both active and passive observations, depending on the sensor mode of operation, with different swath widths and temporal and spatial resolutions. Microwave scatterometers (active sensors) and radiometers (passive sensors) can be used to monitor the radar backscattering and the surface emission, respectively. These quantities are sensitive to common parameters that include not only the soil permittivity, but also vegetation conditions and roughness. Then, a validation of remotely sensed data is of extreme importance for a better exploitation of the data.

In this work, a comparison study was performed among different remotely sensed surface soil moisture datasets, including the L-band Soil Moisture and Ocean Salinity (SMOS) radiometer, the C-band Advanced Scatterometer (ASCAT) onboard METOP and the Soil Moisture Active and Passive (SMAP) satellite developed by NASA. These satellite retrievals were compared with the simulations of the ERA-Interim model produced by the European Centre of Medium Range Weather Forecasts (ECMWF) and with ground measurements available in the frame of the International Soil Moisture Network (ISMN). The reprocessed L2 SMOS SMC products, produced by the version 6.20 of the ground processor, and the SMAP passive L2 moisture products version 4 were used. As for ASCAT, since each data represents a soil moisture relative index between 0 and 100% (i.e., driest and wettest conditions), the retrievals were converted into volumetric soil moisture using the porosity map available from the Global Land Data Assimilation System website. All the data were collocated in time and in space over the SMOS grid in the period from April 2015 to July, 2016.

The Triple Collocation (TC) technique is often adopted to validate soil moisture retrievals derived from different sensors, allowing to estimate the error standard deviations of three systems measuring the same target parameter. Several extensions of this method were proposed in order to evaluate the performances of more than three systems and to soften the TC hypothesis. In particular, a novel Extended Quadruple Collocation (E-QC) was developed and used in order to consider the possibility of an error cross-correlation between soil moisture products, identifying automatically the couple of error cross-correlated systems. The method was able to correctly retrieve the error of each system and identified the presence of error cross-correlation between the satellite products, even if such sensors work with different algorithms and operation principles.

10426-7, Session 2

Monitoring by forward scatter radar techniques: an improved second-order analytical model

Marta Tecla Falconi, Davide Comite, Alessandro Galli, Frank S. Marzano, Debora Pastina, Pierfrancesco Lombardo, Sapienza Univ. di Roma (Italy)

A closed-form model for the forward scatter radar (FSR) received signal based on a second- order phase approximation is introduced in this work to provide an improved analytical model for active microwave monitoring. The traffic control of city airspace is one of the most challenging objectives not only for population safety but also, as recently emerged, for population security. The service provided by ground-based controllers has been hindered by an ever increasing diffusion of unmanned aerial vehicles (UAVs), in particular drones. These air targets have usually reduced radar cross-section (RCS) and therefore may result invisible to common monostatic and bistatic radars. A viable alternative is the FSR, a specific class of bistatic systems with a bistatic angle close to 180°. The typical FSR configuration comprises a target crossing the baseline (BL) between transmitter (Tx) and receiver (Rx) while following arbitrary trajectories. Differently from the monostatic case, the signal received results from the interference between the direct signal (i.e. signal received directly from the transmitter) and the signal scattered from the target. The forward scatter signature, named forward scatter cross-section (FS-CS), is related to the electrical dimensions

of the involved target along with the target-Tx and target-Rx distances. The peculiar capability to detect low-observable targets is related to the enhancement of the FS-CS that, under certain conditions, might be several dBs higher than the backscatter RCS. Looking at the physical counterpart, the improvements in the detection are associated to the effect of strengthening of the electromagnetic (EM) field focused on the opposite direction with respect to the impinging angle. In order to design proper signal processing strategies able to exploit such advantageous features, a key role is undoubtedly played by an accurate electromagnetic modeling of the forward scattering (FS) phenomenon. A simple but comprehensive EM modeling for the FSR has been proposed by the Authors in [1], referring to a standard diffraction problem. In that analysis, two canonical approximations were assumed: (i) a paraxial approximation; (ii) a first-order Taylor's approximation on the phase expansion of the re- irradiated field. In the present work, the model in [1] is further generalized, both by removing the paraxial approximation and by including the second-order term of the phase expansion in the relevant scattering problem. The effects of the different approximations are discussed referring to different study cases; a phase error analysis is provided to characterize the limits of validity of the proposed analytical model as well as to quantify the improvements introduced in comparison with the previous approximation. Furthermore, this novel analytical model is compared with a reference full-wave numerical solution of the scattering problem obtained by using EM CAD tools. The results show that, particularly in near-field conditions, this improved approach is a useful tool for the development of more accurate signal processing techniques and FSR system design.

[1] M. T. Falconi, D. Comite, A. Galli, D. Pastina, P. Lombardo, and F. S. Marzano, "Forward Scatter Radar for air surveillance: Characterizing the target-receiver transition from far-field to near-field regions," Remote Sensing, 9(1), 50, 2017.

10426-8, Session 2

Spatiotemporal hazard mapping of a flood event "migration" in a transboundary river basin as an operational tool in flood risk management

Theodora Perrou, Asterios Papastergios, Issaak Parcharidis, Harokopio Univ. of Athens (Greece); Marco Chini, Luxembourg Institute of Science and Technology (Luxembourg)

Flood disaster is one of the heaviest disasters in the world. It is necessary to monitor and evaluate the flood disaster in order to mitigate the consequences. Rapidly obtaining the flood extent is a basis for monitoring and evaluating the flood disaster. As floods do not recognize borders, transboundary flood risk management is imperative in shared river basins, involving both Governments and their citizens as borders and risk are involved respectively. The transboundary cooperation is intended to widen the knowledge/information sharing, to enlarge the established available strategies and to find better and more cost effective solutions. Disaster management is highly dependent on early information and requires data from the whole river basin. Based on the hypothesis that the flood events over the same area with same magnitude have almost identical evolution it is crucial to develop a repository, database of historical flood events on their spatial extension. This tool, in the case of extended transboundary river basins, could constitute an operational warning system for the downstream area. The utility of the SAR images for flood mapping, providing high quality flood maps, was demonstrated by several literature studies and the use of SAR data is presently well-established in operational services for inundation management, especially during emergency phase. In addition, the operational capabilities have been significantly improved by newly available satellite constellation, such as the Copernicus Sentinel- 1A/B mission, which is able to provide systematic acquisitions with a revisit time of 3-4 days. The present study deals with the monitoring of a transboundary flood event in Evros River basin. Evros River system is the second largest river in Eastern Europe after the Danube; it belongs to the Evros prefecture, located in southern part of Greece. Evros has a total length of about 515km, flowing through Bulgaria Greece and Turkey. The river drains a catchment of 52,900km2 with a high socioeconomic and environmental importance. The objective of the study is to create the "migration story" of the flooded areas on the basis of the evolution in time for the events occurred in the seven-month period from October 2014 through April 2015. The study uses time series of SAR images from Sentinel-1A/B, acquired on interferometric wide swath mode and in two different polarizations, VV and VH. Once flood extent maps are obtained, making use of SAR-based automatic algorithms, they will be imported as polygons in a GIS-system and will be classified according to their temporal evolution. The results of this study can be considered as the first step of a flood maps record obtained in a transboundary river basin which can be used as an operational tool particularly if incorporated and compared with other flood events of past years and combined with exposure inputs. Considering that Sentinel-1 data have a great advantage of being open access and have extensive coverage, the results of this study offers important information towards exploring the possibilities of the use of such Earth Observation data to map other significant transboundary flood events in a very cost-effective and sustainable way.

10426-11, Session 2

Weather radar performance monitoring using a metallic-grid ground-scatterer

Marta Tecla Falconi, Sapienza Univ. di Roma (Italy); Mario Montopoli, Istituto di Scienze dell'Atmosfera e del Clima (Italy); Frank Silvio Marzano, Sapienza Univ. di Roma (Italy); Luca Baldini, Istituto di Scienze dell'Atmosfera e del Clima (Italy)

The use of ground return signals is investigated for monitoring of the system calibration for a polarimetric C-band radar. To this aim, a peculiar permanent single scatterer (PSS) consisting of a big metallic roof with a hemisphere-like shape is considered. Calibration is one of the most critical aspects in the modern weather radar community due to the sensible effect on the quantitative radar retrievals of precipitation and also on the hydrometeors classification. Calibration techniques used routinely or at scheduled maintenance include measures of antenna gain, standard targets and solar radiation [1]. Calibration through standard targets, such as suspended spheres, can be very cumbersome and not always applicable. In this respect, permanent scatterers, such as the ground clutter around the radar, allows to have a constant monitoring in space and time of the whole radar system [2]. The main issue is to detect and characterize such permanent scatterers. We have focused our efforts to characterize the feasibility of using the single permanent scatterers methodology for polarimetric weather radar calibration to investigate their optimal exploitation and characterization.

In this analysis we have considered the coherent C-band Doppler dual polarization Polar 55C located 20 km South-East of Rome (Italy) and installed at a height of 102 m. We define a permanent single scatterer (PSS) as an object that, although with considerable size, partially occupies the pulse volume of the radar within the beam. This definition is clearly different from a typical object, observed by a meteorological radar, that is a weather distributed scatterer (WDS) which likely fills the beam completely. For this study we take in consideration a PSS located in the near field of the radar, named "Vela di Calatrava", that is a periodic structure of metallic grids devised as a swimming stadium for an ideal City of the Sports in Rome, Tor Vergata. Preliminary results from the actual data have been considered for the monitoring of both reflectivity (Zhh) and differential reflectivity (Zdr), highlighting that the signal returns from the PSS are very stable for the Zhh in time even in presence of heavy precipitation. In terms of Zdr, the stability of the echoes is actually higher than needed for an accurate calibration whereas PSS-derived median values

are in agreement with a well- known technique of absolute calibration, obtained considering the vertical measurements in ice or light rain. The PSS has been also tested for the check of antenna de-pointing. The experimental observations, carried out using radar data, are confirmed by the EM numerical results obtained with a full-wave commercial tool. Future analysis should be devoted to develop an automatic method to select and classify various PSSs with peculiar characteristics similar to those here considered.

[1] V. Chandrasekar, L. Baldini, N. Bharadwaj, and P. Smith, "Calibration procedures for global precipitation-measurements ground-validation radars," Radio Science Bulletin, 355, 45–73, 2015.

[2] M.T. Falconi, M. Montopoli, and F.S. Marzano, "Bayesian statistical analysis of ground-clutter for the relative calibration of dual polarization weather radars," European Journal of Remote Sensing, 49, 933– 953, 2016.

10426-13, Session JS

Application of Sentinel 1 VH and VV and Sentinel-2 for soil moisture studies

Katarzyna Dabrowska-Zielinska, Maria Budzynska, Radoslaw Gurdak, Jan Musial, Alicja Malinska, Martyna Gatkowska, Maciej Bartold, Institute of Geodesy and Cartography (Poland)

The objectives of the study were to determine the spatial soil moisture under grasslands of Biebrza wetlands ecosystem in north-eastern Poland applying Sentinel-1 IWS data registered in VH and VV polarization. During the satellite acquisition, the ground truth data applied for the study included various biophysical parameters measured at test site during satellite overpasses. These were: volumetric soil moisture (SM, [%]) measured using TRIME FM, Leaf Area Index (LAI) measured using LAI-2000 Plant Canopy Analyzer, wet and dry biomass, height and type of vegetation habitat. Measurements were carried out at the areas of different wetlands communities. The data from Terra MODIS, Sentinel-2 have been collected at the same time of Sentinel-1. The wetland vegetation differed , there were reeds, sedge-moss, sedges, grass-herbs, and grass. Soil moisture during two years of measurements differed – from 30 % during the drought season in 2015 to 95%. It has been examined the impact of vegetation and soil moisture on radar signal under changing soil moisture and vegetation growth conditions. Vegetation biomass has been characterised by measured in-situ LAI and by vegetation indices calculated from Sentinel-2 and Terra MODIS data. The impact of soil moisture and LAI on backscattering coefficient (?°) calculated from Sentinel-1 data showed that LAI dominates the influence on ?° when soil moisture is low. The analysis have been done to estimate the threshold of the soil moisture values which dominate the backscatter. It was examined that the difference of sigma polarisation of VH and VV characterises LAI and may replace vegetation descriptor. The model has been developed characterising the vegetation by the difference between VH and VV polarisation. Finally the model for soil moisture has been elaborated applying only Sentinel1 data. The developed model has been used for mapping spatial and temporal distribution of soil moisture over Biebrza wetland habitat types. The study was carried out at Biebrza Wetland test site, which is located in North-East Poland. The Wetland was designated as wetland site of international importance in the NATURA 2000 Network and since 1995 has been under the protection of the RAMSAR Convention on Wetlands. Information about soil moisture is very important for monitoring changing conditions which could provide to dangerous change of wetlands into mineral soils and release of methane.

10426-14, Session JS

Application of multifrequency SAR data and neural networks for Mediterranean forests characterization

Emanuele Santi, Simone Pettinato, Simonetta Paloscia, Istituto di Fisica Applicata "Nello Carrara" (Italy); Fabio Maselli, Marta Chiesi, Istituto di Biometeorologia (Italy); Gherardo Chirici, Univ. degli Studi di Firenze (Italy); Andrea Garzelli, Univ. degli Studi di Siena (Italy)

The aim of this research was to assess the sensitivity of multi-frequency SAR data to forest characteristics and to exploit the SAR backscatter capabilities for classifying forest types and estimating forest biomass - expressed as Woody Volume (WV m3/ha) - in Mediterranean areas.

In this study, we investigated the use of multi-frequency SAR images from different sensors (ALOS/PALSAR, ENVISAT/ASAR, and Cosmo-SkyMed) for the estimation of major forest characteristics in two test areas in Central Italy (San Rossore and Molise), where detailed ground measurements and Airborne Laser Scanning (ALS) data were available. These areas are representative of different environmental conditions, i.e. a coastal plain mostly covered by evergreen conifers and a hilly land covered by deciduous broadleaves. Time-series of SAR images from ALOS/PALSAR (L band), ENVISAT/ASAR (C band) and Cosmo-SkyMed (X band) were acquired on these areas between 2009 and 2010.

A preliminary discrimination of the main land cover classes and forest types was carried out by exploiting the synergy among various frequencies (L, C and X bands). After a pre-processing of the available SAR images by applying a multi-look approach, SAR data were used for discriminating forest from non-forest land covers and separating broadleaved from coniferous forest types. The classification has then been performed by applying to the SAR images, in different configurations of polarizations and frequencies, a new method based on a quadratic Bayesian classifier, which is able to overcome the limits of ground-truth classes that contain not homogenous targets (i.e. non-forest class). The best classification accuracy was obtained by considering the joint use of L and X bands (80.06% pixels correctly classified).

Subsequently, a retrieval algorithm based on ANN techniques was implemented for estimating WV from the multi-polarization SAR data at L and C bands. Two different approaches to the retrieval were followed and compared in this study. In the first approach the training was based on experimental data only: two different ANN, one for each test area, were implemented. Each ANN was trained with a subset of the experimental data available for the corresponding test area and then validated on the remaining part of the dataset. In the second approach, a single ANN, able to work on both areas, was implemented. In this case, the representativeness of the training set was addressed by combining WV derived from LiDAR data with data simulated obtained from an updated implementation of the water cloud model with gaps (Santoro et al. 2006; Fransson and Israelsson, 1999).

The overall accuracy of both approaches is summarized by a correlation R= 0.92-0.97 and RMSE = 25-30 m3/ha on both areas. A final independent validation was then carried out on some forest plots, outside the area covered by LIDAR, for which conventional WV measurements were available. In this case, the algorithm resulted in R= 0.86 and RMSE ≈77 m3/ha.

The obtained result demonstrated the capabilities of multi-frequency SAR data, combined with ANN techniques, for predicting the WV of Mediterranean areas independently of the forest types and of their climatic and orographic conditions.

References

Fransson J.E.S., Israelsson H., (1999), Estimation of stem volume in boreal forests using ERS-1 C- and JERS-1 L-band SAR data. Int. J. Remote Sens., 20, 123-137.

Santoro M., Eriksson L., Askne, J., Schmullius C., Assessment of stand-wise stem volume retrieval in boreal forest from JERS-1 L-band SAR backscatter. Int. J. Remote Sens. 2006, 27, 3425-3454.

Conference 10427: Image and Signal Processing for Remote Sensing

SPIE. REMOTE SENSING

Monday - Wednesday 11–13 September 2017

Part of Proceedings of SPIE Vol. 10427 Image and Signal Processing for Remote Sensing XXIII

10427-1, Session 1

Bulk processing of the Landsat MSS/TM/ETM+ archive of the European Space Agency: an insight into the level 1 MSS processing

Sebastien Saunier, Telespazio France SAS (France); Amy Northrop, Telespazio VEGA UK Ltd (United Kingdom); Luca Galli, Riccardo Ferrara, Stefano Mica, Advanced Computer Systems (ACS) (Italy); Samatha Lavender, Telespazio VEGA UK Ltd (United Kingdom); Roberto Biasutti, Philippe Goryl, Ferran Gascon, ESA/ESRIN (Italy)

Whilst recent years have witnessed the development and exploitation of operational Earth Observation (EO) satellite constellation data, the valorisation of historical archives has been a challenge. The European Space Agency (ESA) Landsat Multi Spectral Scanner (MSS) products cover Greenland, Iceland, Continental Europe and North Africa and expect to represent an archive of over 600,000 processed Level 1 (L1) scenes to join the 1 million ESA Landsat Thematic Mapper (TM) and Enhanced Thematic Mapper Plus (ETM+) products already available.

The ESA Landsat processing baseline has been significantly updated to account for MSS data ageing and to accommodate for remote sensing techniques used during the past.

ESA began acquiring MSS data in 1975 and it is known that the old data can be degraded including accuracy lost and missing data. For these reasons, the content of the product format has been reviewed and significantly updated to make products fit for user purposes. This paper presents the new MSS product format including the updated metadata parameters for error traceability and the specification of the Quality Assurance Band (BQA) engineered to allow the best pixel selection and also the application of image restoration schemes.

Due to quantification, the radiometric sensitivity of MSS data is reduced; the ground calibration performs well for scenes observed in mid latitude regions but shows strong limitations in the polar and sub-tropical regions. This paper therefore describes the processing approach that has been adopted in order to adjust sensor minimum and maximum radiance depending on the area of the scene in order to reduce saturation introduced at L1 processing.

Some past data suffers from corrupted/missing data telemetry (ephemeris, attitude and gyro information) as well as several gaps in the coverage of the supporting data (orbital data). In most cases, these issues prevent the production of accurate L1 orthorectified scenes or in the worst case the production of systematic corrected L1 data. To overcome this issue, besides standard scene-based processing, the geometric processing improves the localisation of a scene by using information from other scenes; distortion parameters are modelled by using weighted least square fitting. This innovative approach, allowing the generation of L1T (Standard Terrain Correction) products even where there are no Ground Control Points (GCPs) in the scene, is also discussed in this paper.

For the benefits of the community, ESA is now able to maximize the number of L1 MSS products that can be potentially generated from the raw Level 0 (L0) data and the highest possible data quality is reached. Also, by improving product format, processing and adding a pixel based quality band, the old MSS archive becomes interoperable with recent data from on-going missions by way of assuring product quality on a pixel basis.

10427-2, Session 1

Fast and accurate denoising method applied to very high resolution optical remote sensing images

Antoine Masse, Ctr. National d'Études Spatiales (France); Sebastien Lefevre, Univ. de Bretagne-Sud (France); Renaud Binet, Stéphanie Artigues, Pierre Lassalle, Gwendoline Blanchet, Simon J. Baillarin, Ctr. National d'Études Spatiales (France)

Restoration of Very High Resolution (VHR) optical Remote Sensing Image (RSI) is critical and leads to the problem of removing instrumental noise while keeping integrity of relevant information. Improving denoising in an image processing chain imply increasing image quality and improving performance of all following tasks operated by experts (photo-interpretation, annotation, cartography) or by algorithms (land cover, land use, change detection, 3D reconstruction). Instrumental noise is known and follows a Poisson distribution which is converted to additional Gaussian noise with Anscombe transform.

In a context of large industrial VHR image production, the selected denoising method should optimized 3 objectives: (1) accuracy and robustness with relevant information and saliency conservation, (2) rapidity due to huge amount of data acquired and/or archived and (3) flexibility with adaptation to image content. Very recent research in image processing leads to a fast and accurate algorithm called Non Local Bayes (NLB) [Buades, 2013] that we propose to adapt, optimize and improve for VHR RSI. This method is well suited for mass production thanks to its best tradeoff between accuracy and computation complexity compared to other state-of-the-art methods. NLB is based on a simple principle: similar structures in image have similar noise distribution and thus can be denoised with the same noise estimation. Non Local Bayes operates as follow: for each pixel of the image, (1) similar patches are found around the pixel and (2) a Bayesian estimation of the denoised pixel is computed. Non Local Bayes algorithm is iterative; previous iteration is used to improve the search of similar patches for the next one. Due to Gaussian hypothesis and by application of Large Number law, treatments could be restrained to local searches and all the similar patches around a pixel could be denoised in the same time.

In this article, we will describe in details algorithm operations and performances. We will also propose improvements and optimizations to decrease computation complexity while keeping high denoising accuracy. Finally, we will show and explain denoising results on various typical real areas: land, water; urban, airport, etc.

10427-3, Session 1

Sen2Cor for Sentinel-2

Magdalena Main-Knorn, Bringfried Pflug, Deutsches Zentrum für Luft- und Raumfahrt e.V. (Germany); Jerome Louis, Vincent Debaecker, Telespazio France SAS (France); Uwe Müller-Wilm, Telespazio VEGA Deutschland GmbH (Germany); Ferran Gascon, European Space Agency (Italy)

In the frame of the Copernicus programme, ESA has developed and launched the Sentinel-2 optical imaging mission that delivers optical data products designed to feed downstream services mainly related to land monitoring, emergency management and security. The Sentinel-2 mission is the constellation of two polar orbiting satellites Sentinel-2A and Sentinel-2B, each one equipped with an optical imaging sensor MSI (Multi-Spectral Instrument). The MSI aims at measuring reflected radiance in 13 spectral bands spanning from the

Visible and Near Infrared (VNIR) to the Short Wave Infra-Red (SWIR) spectral range. Sentinel-2A was launched on June 23rd, 2015 and Sentinel-2B followed on March 7th, 2017. With the beginning of the operational phase the constellation of both satellites will enable image acquisition over the same area every 5 days or less.

To use unique potential of the Sentinel-2 data for quantitative land applications and ensure the highest quality of scientific exploitation, accurate correction of satellite images for atmospheric effects is required. Therefore the atmospheric correction processor Sen2Cor was developed by Telespazio VEGA Deutschland GmbH on behalf of ESA. Sen2Cor is a Level-2A processor which main purpose is to correct single-date Sentinel-2 Level-1C Top-Of-Atmosphere (TOA) products from the effects of the atmosphere in order to deliver a Level-2A Bottom-Of-Atmosphere (BOA) reflectance product. Additional outputs are an Aerosol Optical Thickness (AOT) map, a Water Vapour (WV) map and a Scene Classification (SC) map with Quality Indicators for cloud and snow probabilities. Sen2Cor outputs are provided for spatial resolutions 60m, 20m and 10m.

Telespazio France and DLR have teamed up in order to provide the calibration and validation of the Sen2Cor processor. Calibration and Validation datasets cover different atmospheric conditions and different latitudes in order to cover various solar angles and seasons, as well are representative for all continents, different topography and land cover types like cropland, forest, grass, sparsely vegetated land, urban, coastal, desert and snow. Level-2A BOA, AOT and WV outputs are calibrated and validated using ground-based data of automatic operating stations and data of reference campaigns. Scene classification is validated by the visual inspection of test datasets and cross-sensor comparison, supplemented by meteorological data, when available.

This presentation provides an overview over the Sentinel-2 data, processor and products. It presents some processing examples of Sen2Cor applied to Sentinel-2 data, provides up-to-date information about the Sen2Cor release status and recent validation results at the time of the SPIE Remote Sensing 2017.

10427-5, Session 1

Stray light simulation tool for GOCI ISRD (inter-slot radiometric discrepancy)

Ki-Beom Ahn, Seong-Ick Cho, Eunsong Oh, Korea Institute of Ocean Science & Technology (Korea, Republic of) and Yonsei Univ. (Korea, Republic of); Young-Je Park, Korea Institute of Ocean Science & Technology (Korea, Republic of); Sug-Whan Kim, Yonsei Univ. (Korea, Republic of)

Geostationary Ocean Color Imager (GOCI) is the world's first geostationary satellite for ocean color remote sensing mission. It observes coastal and ocean region around the Korean Peninsula, Japan, and East China with a spatial resolution of 500 meters.

GOCI uses step-stare imaging technique by the implementation of 2D detector array (1413 x 1430) and 2-axis pointing mechanism. It enables multiple image acquisitions for the same location of FOR (Field Of Regard) at sixty-minute intervals during daytime (8 images per day in nominal operation). Because GOCI IFOV is about a sixteenth of GOCI FOR, an image acquisition and processing sequence for GOCI FOR consists 16 (4 x 4) slot image acquisitions which correspond to GOCI IFOV and image processing to combine 16 slot images into one image for GOCI FOR.

Inter Solar Radiometric Discrepancy (ISRD) of GOCI means the radiance (i.e. digital count) discrepancy in the overlapped area between adjacent slot images. This is mainly derived by the difference of solar zenith angle by the gap of acquisition time between slots with overlapped area. Due to the boustrophedonic pattern of GOCI slot image acquisition sequence, maximum difference of acquisition time is about 12 minutes. After the normalization processing in terms of solar zenith angle for the reduction of ISRD, early in GOCI on-orbit operation, systematic residual ISRD about 3% discrepancy was observed for B6 (680nm) and B8 (865nm), where optical ghost/straylight in the southern part of a slot image was found to cause ISRD in the overlapped area between southern part of upper slot and northern part of lower slot.

For the qualitative and quantitative analyses of ISRD and the development of ISRD correction algorithm, end-to-end ISRD simulation tool based on ray tracing technique is developed. This also can be used for ISRD analysis of GOCI-II which is planned to be launched in late 2018. In this paper, we present the verification result of end-to-end ISRD simulation tool by comparing with pre-flight straylight/ghost test results, and development status of correction algorithm of systematic ISRD induced by straylight/ghost.

10427-6, Session 2

Resolution enhancement of DEM using photometric stereo method in time-varying shadowed region

SungHyun Moon, Han-Lim Choi, KAIST (Korea, Republic of)

Information gathered by satellites around the Earth, orbiter of planets or moon, and space explorer can be used in many fields such as monitoring the global environment, selecting landing sites for a planet and lunar exploration, astronomical observation. Among them, Digital Elevation Model (DEM), which is a 3D map of the ground, is built by observing the surface. It can be used to observe the unknown terrestrial area and changes of the Earth, as well as exploring planets, moons, and asteroids. It is an essential element that must be executed first in space exploration. Unlike the global environment, which is relatively easy to acquire data for constructing DEM, it is costly to send an out-of-earth orbiter or explorer. Furthermore, the limit of space and power constraints that can be mounted on the probe has been decided. So, the number and types of sensors are limited. Generally, DEM can be obtained by using a photogrammetry technique that estimates triangulation using a stereo image pair obtained from a stereo imaging sensor mounted on a orbiter, direct measurement of altitude using a laser altimeter mounted on a orbiter, and a method to obtain DEM with improved resolution by fusion of image and altimeter information making use of the spatial resolution of image better than spatial resolution of DEM.

In order to enhance the spatial resolution of DEM using image resolution, shape from shading (SfS) is obtained from the pixel information of an image, then used to improve the resolution of DEM generated by pair images and laser altimeter is used. [1] At this time, in order to construct SfS using a single image, we need multiple constraints and surface reflectance parameters, albedo on the ground surface. When improving the resolution of the DEM on the Moon or the surface of the Mars using SfS, the reflection model such as lunar-Lambertian reflectance [2] and the Hapke model [3, 4] on the surface is presumed.

In this paper, an algorithm is proposed for constructing DEM from image data with varying shadows according to a position of light source. At this time, the Sun is considered as a dominant light source in the solar system. First, orthorectification is applied to images with different shadows according to the direction of sunlight using an existing DEM made of stereo image pair or laser altimeter. This process can create ortho-images that look straight down on the surface and camera position is adjusted based on DEM. After that, a photometric stereo technique can be used to acquire more accurate surface normal information of the target area. The surface normal can be obtained from various images even when the albedo information of the area is unknown using a photometric stereo method. Finally, it is possible to acquire more precise DEM by using the photometric stereo based surface normal which has higher spatial resolution than the existing DEM altitude information and altitude information by optimization function to minimize cost.

For the validation of the proposed method, a down-sampled DEM is generated from the original DEM and a down-sampled

image set is created according to the resolution of the original DEM. Then, the difference in pixels between the generated DEM according to the proposed method and the original DEM is calculated for performance evaluation.

Reference

[1] Intelligent Robotics Group, NASA Ames Research Center, "The Ames Stereo Pipeline (Version 2.5.3)," 23 August 2016, https://byss.arc.nasa.gov/stereopipeline/binaries/asp_book-2.5.3.pdf (23 August 2016).

[2] Alfred S McEwen, "Photometric functions for photoclinometry and other applications," Icarus, 92(2): 298_311 (1991).

[3] Bruce Hapke, "Bidirectional reflectance spectroscopy: 6. Effects of porosity," Icarus, 195(2):918_926 (2008).

[4] J Fernando, F Schmidt, X Ceamanos, P Pinet, S Douté, and Y Daydou, "Surface reflectance of Mars observed by CRISM/MRO: 2. Estimation of surface photometric properties in Gusev Crater and Meridiani Planum," Journal of Geophysical Research: Planets, 118(3):534_559 (2013).

10427-7, Session 2

Benefits of haze removal for modulation-based pansharpening

Simone Lolli, Instituto di Metodologie per l'Analisi Ambientale (Italy); Luciano Alparone, Univ. degli Studi di Firenze (Italy); Andrea Garzelli, Univ. degli Studi di Siena (Italy); Gemine Vivone, Univ. degli Studi di Salerno (Italy)

Among remote sensing image fusion applications, multispectral (MS) pansharpening has received considerable attention over the last quarter of century. Pansharpening techniques take advantage of the complementary characteristics of spatial and spectral resolutions of MS and panchromatic (P) data, in order to synthesize a unique product that exhibits as many spectral bands as the original MS image, each with same spatial resolution as the P image.

After the MS bands have been interpolated and co-registered to P, spatial details are extracted from P and added to the MS bands according to the injection model. The latter rules the combination of the low-pass MS image with the spatial detail extracted from P. Such a model is stated between each of the re-sampled MS bands and a low-pass version of the P image having same spatial frequency content as the MS bands.

Although several models have been introduced, the most popular are: i) the projection model, which may be derived from the Gram-Schmidt (GS) orthogonalization procedure, representing the basis of the GS spectral sharpening and of the context-based decision (CBD); ii) the multiplicative or modulation model, which is the basis of such techniques as HPM, Brovey, SVR, Zhang's UNB pansharp, SFIM and AWLP.

The pioneering paper that introduced SFIM firstly gave an interpretation of the multiplicative injection model in terms of the radiative transfer model ruling the acquisition of an MS image. Accordingly, the kth MS band interpolated at the pixel scale of P represents a low spatial resolution spectral radiance, that is, a radiance with a spectral diversity. P represents the high spatial resolution solar irradiance, which bears no spectral information, but only spatial and radiometric information. Thus, its lowpass-filtered version, PL, having the same spatial frequency content as the interpolated MS bands, is a low-resolution irradiance and conveys radiometric information at the spatial resolution of MS. Ultimately, a high resolution MS (HRMS) is synthesized at each pixel as low resolution MS (LRMS) divided by PL and multiplied by P. Since the ratio of spectral radiance to solar irradiance is an estimate of spectral reflectance, when the ratio between LRMS and PL is multiplied by P, a low-resolution reflectance is multiplied by a high resolution irradiance.

So far, very few authors have ever considered the path radiance of the kth band, which is an energy scattered by the atmosphere that reaches the aperture of the instrument without being reflected by the Earth's surface. Thus, the path radiance of each band, which appears as a haze in a color composite display of the MS bands, should be estimated and removed before the modulation is accomplished and re-inserted after the sharpening.

In this paper, several methods for estimating the path radiance, one empirical, another statistical and a third based on modelling the atmosphere (Fu-Liou-Gu), are compared in terms of benefits on the quality of fusion, both CS and MRA. Experiments on true MS images show that the advantages are more consistent in terms of spectral quality (colors) and are especially significant on vegetated areas.

10427-8, Session 2

The effect of denoising on superresolution of hyperspectral images

Armin Eskandari Nasab, Shahid Bahonar Univ. of Kerman (Iran, Islamic Republic of); Azam Karami, Shahid Bahonar Univ. of Kerman (Iran, Islamic Republic of) and Univ. Antwerpen (Belgium)

Hyperspectral images (HSI) are usually affected by different type of noises such as Gaussian and non-Gaussian in addition, the spatial resolution of HSI in comparison with spectral resolution is not significant. These noises have bad effects on classification accuracy, spectral unmixing and superresolution of HSI. In this paper a new method based on shearlet transform (ST) [1] and Bayesian Sparse (BS) representation [2] is introduced in order to decrease the noise effect and increase the spatial resolution of the HSI simultaneously. The proposed method (ST-BS) creates HSI with high spatial and spectral resolutions. In this method first, ST is applied to the existing low resolution HSI (LRHSI) for denoising after that BS is used in order to increase the spatial resolution of HSI. This algorithm is applied to two real datasets. First dataset is Pavia University. The images were acquired by the ROSIS-03 hyperspectral sensor. In this dataset, existing HSI are considered as ground truth. Then, LRHSI are created using the low-pass filter with downsampling factor four. After that, 4-band multispectral images (MSI) are generated by filtering HSI with IKONOS-like reflectance spectral responses for fusing with LRHSI in order to increase spatial resolution of LRHSI. Finally, Gaussian noise and non-Gaussian noise (Poisson) are randomly added to 30 bands of LRHSI for investigating about the effect of denoising on superresolution of HSI. Second dataset "Shiraz" is taken above Shiraz city in Iran, and obtained by two instruments, the Hyperion instrument and the ALI instrument, the Gaussian and Poisson noises are added to the LRHSI. Then ST-BS is applied to the noisy LRHSI and MSI. Obtained results show an improvement in peak signal to noise ratio (PSNR) and also a reduction in root mean square error (RMSE) and dimensionless global error (ERGAS) for ST-BS in comparison the two state-of-the-art fusion methods: coupled non-negative matrix factorization (CNMF) and spectral unmixing sparse coding (SUSC).

[1] A. Karami, R. Heylen, and P. Scheunders, "Band-specific shearlet-based hyperspectral image noise reduction", IEEE Transactions on Geoscience and Remote Sensing, vol. 53, no. 9, pp. 5054–5066, 2015.

[2] Q.Wei, J. Bioucas-Dias, N. Dobigeon, J. Y. Tourneret, "Hyperspectral and multispectral image fusion based on a sparse representation", IEEE Transactions on Geoscience and Remote Sensing ,53, pp.3658-3668, 2015.

10427-9, Session 2

New developments in super-resolution for GaoFen-4

Feng Li, Lei Xin, Qian Xuesen Lab. of Space Technology (China); Jie Fu, Yuhong Liu, Lanzhou Jiaotong Univ. (China); Zhijia Liu, DFH Satellite Co., Ltd. (China)

One of the shortcomings of geostationary-orbit based earth

observing satellite is the limitation of spatial resolution, however, the pursuit of high resolution is never cease for the human being. In this paper, the application of super resolution (SR, restoring a high spatial resolution image from a series of low resolution images of the same scene) techniques to GaoFen(GF)-4, which is the most advanced geostationary-orbit earth observing satellite in China, remote sensing images is investigated and tested. This is the first experiment of applying super resolution to a sequence of low resolution images captured by GF-4 within a short time period. SR has been a hot research area for decades, but one of the barriers of applying SR in remote sensing community is the time slot between those low resolution (LR) images acquisition. GF-4 has the unique advantage of capturing a sequence of LR of the same region in minutes, i.e. working as a staring camera from the point view of SR.

In this paper, we use Maximum a Posteriori (MAP) to solve the ill- conditioned problem of SR. In general, a probability density function of the data or a sparse prior is needed in MAP. For nature images, smooth features can show the sparsity in the wavelet domain, this can explain why the wavelet transform is widely used in image compression community. However, wavelet transform can only provide well sparse representation for features along horizontal, vertical and diagonal. Remote sensing images include various objects with complex features, it is very hard to use the wavelet transform to dig the sparsity for remote sensing images. Human eyes are very sensitive to curves or edges, and the curvelet transform can show the superiority in well sparse representing curves or edges features. Therefore, both the wavelet transform and the curvelet transform are used to setup a sparse prior for remote sensing images.

By combining several images of both the BeiJing and DunHuang regions captured by GF-4 at different time points within a short period, the use of a super resolution reconstruction technique improves spatial resolution both visually and numerically as shown in our experiments. Experimental tests show that lots of detail cannot be observed in the captured LR images, but can be seen in the super resolved high resolution (HR) images. To help the evaluation, Google Earth image can also be referenced. Moreover, our experimental tests also show that the higher the temporal resolution, the better the HR images can be resolved. The study illustrates that the application for SR to geostationary-orbit based earth observation data is very feasible and worthwhile, and it holds the potential application for all other geostationary-orbit based earth observing systems.

10427-10, Session 2

Superresolution mapping of satellite images to estimate the water spread area of reservoirs using multi-objective genetic algorithm

Heltin Genitha C., Indhumathi Muthiah, St. Joseph's College of Engineering (India)

Many researchers have developed algorithm for generating the super resolved maps from the remotely sensed satellite images with heterogeneous class components. Each algorithm has its own advantages and limitations. Slow rate of convergence, low accuracy, local optimum solution are some of the issues in the super resolution mapping algorithms. Many researchers used per-pixel classification techniques (maximum likelihood, minimum distance classifier etc.,) in which each pixel is assigned to a single class. If the pixel contains mixed class components, some information will be lost. Some researchers used sub-pixel classification techniques (Linear Spectral Unmixing, Fuzzy c means etc.,) which predicts the fraction of class components within a pixel. But, it fails to locate the position of the class components within a pixel. To overcome these problems, super resolution mapping algorithm was developed which predicts the location of class components within a pixel.

In this paper, a new soft classification algorithm (New Fuzzy Cluster Centroid for Unsupervised Classification Algorithm) and super resolution mapping algorithm (Multi-objective Genetic Algorithm) was developed and demonstrated. Super Resolution Mapping consists of two steps. The first step is the generation of proportion images from the satellite image using the soft classification algorithm, New Fuzzy Cluster Centroid (NFCC) for Unsupervised Classification Algorithm. The proportion images contains the proportion or percentage of class components within a pixel. The second step is the generation of super resolved map from the proportion images using super resolution mapping algorithm, multi-objective genetic algorithm.

In NFCC, a new objective function is formulated which increases the stability of the algorithm and reduces the number of iterations for image classification. In genetic algorithm, multiple objectives and the concept of elitism used which improves the performance of the super resolution mapping. The fitness function of genetic algorithm is the maximization of spatial dependence and spatial attraction. Thus, genetic algorithm considers the spatial attraction between the pixels and also the spatial dependence between the sub-pixels.

Experiments are carried out with the use of multi-date Landsat OLI image of the drinking water reservoir, Puzhal of Chennai City. The super resolved map is generated for the water spread area of the reservoir. From the super resolved map, water spread area of the reservoir is accurately estimated. The water-spread area estimated using super resolution mapping approach can be used as an input to estimate the volume at different water levels of the reservoirs. This super resolution mapping approach gives minimum error when compared to other sub-pixel, per-pixel approaches. Genetic algorithm represents a simple, robust, and efficient technique, and results suggest that it is a useful tool for vegetation mapping, land cover mapping, water mapping etc., from remotely sensed imagery at the sub-pixel scale.

10427-11, Session 3

Aggregation of Sentinel-2 time series classifications as a solution for multitemporal analysis

Stanislaw Lewinski, Artur Nowakowski, Marcin Rybicki, Ewa Kukawska, Radoslaw Malinowski, Michal Krupi?ski, Space Research Ctr. (Poland)

Sentinel-2 Global Land Cover project (S2GLC) aims at developing procedures and providing recommendations for deriving land cover classifications on a global scale from the imagery of Sentinle-2 constellation. By assuring high temporal resolution the Sentinel-2 dataset allows revision of existing and development of new solutions for multitemporal image analysis.

The study described here is a part of the S2GLC research project that presents a method for combining results of land cover classification performed on individual Sentinel-2 images acquired at different time periods. The general aim of this methods is to derive a map that represents the most reliable land cover information.

The study starts with a pre-processing part consisting of an atmospheric correction and a cloud mask derivation as obligatory procedures for a multitemporal data analysis. This is followed by supervised classification of Sentinel-2 images with Boosting, Random Forest and Support Vector Machine algorithms and classification features (i.e. spectral, statistical, structural and multitemporal). The number and acquisition dates of the classified images are based on the user selection and should reflect different conditions met in the landscape and assure better differentiation of classes when multitemporal observations are combined. However, the final selection is also strongly dependent on the amount and distribution of cloud-covered areas within an individual satellite scene.

The goal of this analysis, which is under development, is to elaborate the most efficient and reliable aggregation method. Important aspect of the aggregation relates to the method of assigning a class label to a given pixel in the resulting land

cover map. In our work we examine such factors as the number of occurrence of a certain land cover class within a time series, the level of fitting of a classified pixel to the training data of a given class (prediction score resulting from a classifier) and a combination of both factors. Due to the global approach of the project our methods are being tested on study areas located in various parts of the globe representing different landscape and climate conditions and characterised by various combination of land cover types and degree of cloudiness.

The initial results show that the mapping accuracy resulting from our aggregation method outperform accuracies of individual classifications within the time series. They also show that besides the class aggregation strategy itself the availability of cloud free images and the quality of a cloud mask and alignment of images from a time series are critical.

10427-12, Session 3

Semi-autonomous remote sensing time series generation tool

Dinesh Kumar Babu, Christof Kaufmann, Marco Schmidt, Hochschule Bochum (Germany); Thorsten Dhams, Christopher Conrad, Julius-Maximilians-Univ. Würzburg (Germany)

With the increasing focus in remote sensing applications such as crop monitoring and ecology change detection, the requirement for daily high resolution data for the generation of various biophysical parameters is growing rapidly. The current satellite architecture is not capable of providing high spatial as well as high temporal data for these applications. Remote sensing time series generation by data fusion methods seems to be an interesting alternative in fulfilling the data needs of many remote sensing applications. Using various data fusion methods, generation of time series of synthetic high quality remote sensing data is very much possible and is proved. But remote sensing time series generation process is a complicated process. It is a multi step process, which involves variety of tools, applications and data from multiple satellites. The process begins with the downloading of different satellite data from their respective servers, pre-processing the different satellite data to be compatible for data fusion, performing data fusion, measuring the accuracy of the generated data and finally using the synthetic data to derive biophysical parameters. Because of the complexity in the time series generation, there are some major difficulties a user has to overcome in order to generate the data he needs for his remote sensing applications. It begins with the handling of huge amount of data a user must handle for the time series generation, secondly the user should possess specific skills and knowledge to use various tools and lastly the user is required to constantly provide information as parameters to perform the time series generation. This shows that a lot of human interaction is required to perform this process. To make it simple, a single tool which performs all the above mentioned processes autonomously will be a great benefit.

In this paper a framework of a Geo Information System based tool is presented for autonomous time series generation. The main objective of our work is to create a powerful tool which eliminates all the above mentioned difficulties and enable the users to generate remote sensing time series with ease. This tool will make the complete process so simple that the generation of remote sensing time series will be comparable to downloading satellite data from the server and using it directly in remote sensing application. To achieve this objective, a study was conducted to assess the feasibility of having such a tool. From the outcome of the study two frameworks are created, one performs all the pre-processing steps on multiple satellite data using the functionalities from GDAL and the other performs data fusion to generate the time series using the functionalities from GDAL and OPENCV. Later they are combined to perform both the processes in one go. Our framework is capable of handling multiple data formats which includes most of the known geo data formats currently available. This tool also includes lot of generic functionalities which is suitable for various remote sensing applications. A detailed description on the capabilities of this framework and its various advantages are explained in this paper.

10427-13, Session 3

A theoretical Gaussian framework for anomalous change detection in hyperspectral images

Nicola Acito, Accademia Navale (Italy); Marco Diani, Accademia Navale (Italy); Giovanni Corsini, Univ. di Pisa (Italy)

Exploitation of temporal series of hyperspectral images is a relatively new discipline that has a wide variety of possible applications in fields like remote sensing, area surveillance, defense and security, search and rescue and so on. In this work, we discuss how images taken at two different times can be processed to detect changes caused by insertion, deletion or displacement of small objects in the monitored scene. This problem is known in the literature as anomalous change detection (ACD) and it can be viewed as the extension, to the multitemporal case, of the well-known anomaly detection problem in a single image. In fact, in both cases, the hyperspectral images are processed blindly in an unsupervised manner and without a-priori knowledge about the target spectrum.

We introduce the ACD problem using an approach based on the statistical decision theory and we derive a common framework including different ACD approaches. Particularly, we clearly define the observation space, the data statistical distribution conditioned to the two competing hypotheses and the procedure followed to come with the solution. The proposed overview places emphasis on techniques based on the multivariate Gaussian model that allows a formal presentation of the ACD problem and the rigorous derivation of the possible solutions in a way that is both mathematically more tractable and easier to interpret. The unification of different approaches under a single rigorous statistical scheme provide both a tutorial overview of ACD techniques, and a useful instrument for researchers already familiar with the ACD problem.

We also discuss practical problems related to the application of the detectors in the real world. We focus on the problems of radiometric and geometric correction. These aspects are mainly due to physical constraints associated to the acquisition process. In fact, when the emitted or reflected electro-magnetic energy is acquired by an airborne or spaceborne sensor, the collected energy differ from the energy emitted or reflected from the same portion of the scene observed at a different time. This is due to variation in atmospheric conditions, sun's azimuth and elevation, presence of aerosols. Thus, to make multi-temporal images radiometrically comparable, the radiometric distortions have to be compensated. Geometric correction is concerned with the correspondence between homologous pixels of the multitemporal images, so that pixels of each image refer to same portion of the scene. In the case of aerial or satellite images, this operation is performed by transforming the geodetic or UTM coordinates available of each pixel to image coordinates. Nevertheless, perfect registration of the images is very difficult to achieve because of the unavoidable onboard instrumentation errors. Thus, a residual mis-registration error (RMRE) inevitably remains and causes performance degradation of pixel-based ACD algorithms. In this work, we describe the whole ACD data processing chain that includes the atmospheric and RMRE compensation strategies and, specifically, we show how the recalled ACD algorithms can be adapted to include such strategies.

Real freely available data are exploited to test and compare the presented methods, highlighting advantages and drawbacks of each approach.

10427-14, Session 3

Change detection analysis using information theoretic measures on SAR images

Debanshu Ratha, Avik Bhattacharya, Indian Institute of Technology Bombay (India); Alejandro C. Frery, Univ. Federal de Alagoas (Brazil)

The usefulness of Synthetic Aperture Radar (SAR) lies in its all-weather acquisition capability. Hence, change detection is an important application of SAR. The short revisit time of the satellites acquiring SAR images makes it a powerful tool in regard to various applications. Change detection is the comparison of at least two images of the same scene acquired at di?erent times. Change detection methodologies may use as input only pixel intensities or local statistics (i.e. within a neighborhood), but all rely on co-registered images. In this paper we have used two statistics in the context of change detection in mono-polarized Synthetic Aperture Radar (SAR) imagery. The data used in this study is a multi-temporal pair of HH channel intensity RADARSAT-2 images of an agricultural scene in Winnipeg, Manitoba which was acquired on 7th and 31st of July 2012. One of the statistics is derived from a stochastic distance viz., Hellinger distance, and the other is based on the Shannon entropy which gives a measure of randomness. We have assumed the established Gamma model for the HH channel intensity data with mean and number of looks as the two free parameters. E?cient measures for identifying relevant changes are always sought after. The wealth of knowledge about the statistical properties of SAR data can be used for this task. In particular, the methodology of statistical hypothesis tests is useful to assess the null hypothesis that there was no change under the model assumed; data are transformed into estimates, which are compared through a test statistic rather than directly. At the same time these hypothesis tests to have a practical utility, require a judicious choice of sample size, and a level of significance for thresholding. In this study we have assumed the Gamma model for the HH channel intensity data with mean and number of looks as free parameters. Instead of relying on the validity of the asymptotic distribution of test statistics (i.e. an implicit assumption for using p-values and levels of significance), in this work we use the test statistics as direct quantifiers of change. A simple k-means clustering with k = 2 is applied on these quantifiers which segregates change and no-change regions. The two information theoretic measures chosen provide substantive evidence for change detection. The corresponding change maps are studied together to understand the complementary nature of the selected statistics. It is inferred that these two statistics may be used in tandem for better change detection analysis in SAR imagery.

10427-15, Session 3

Change detection approach using co-occurrence matrix on multitemporal SAR imagery

Na Li, Tianhui Satellite Ctr. of China (China); Fang Liu, Xiangchenyang Su, National Univ. of Defense Technology (China)

Change detection (CD), using multi-temporal remote sensing images acquired over the same geographical areas, has great significance for a large number of applications, urban planning, environment monitoring and maritime surveillance for instance. Due to the characteristics of SAR sensors being advantageous over the optical sensors in terms of the insensitiveness to the atmospheric conditions and day-and-night, the use of SAR sensors in CD is highly attractive from the operational viewpoint. However, the presence of the intrinsic speckle and geometry distortions make any automatic analysis difficult.

In terms of the change detections for medium-/ high-resolution SAR images, a generally accepted procedure is: first compare the two images using acquired on the same geographical area at different times to obtain a temporal change feature; then take an automatic thresholding technique to the change feature to obtain the change detection (CD) map. An effective temporal change detector has great significance in change detection process.

For multi-temporal SAR images, the changes are usually connected to the modification of the terrestrial surface resulting in the backscattering variation and textual variation. Therefore, inspired by the properties, a change detection method based on the co-occurrence matrix is proposed. The procedure of the proposed approach is as follows:

Step1: The spatial FCM clustering technique is applied to two SAR images separately with a certain number of clusters involved. The obtained number of classes corresponds to the specific levels of the backscattering where each pixel belongs to either backscattering level in a membership degree.

Step2: The co-occurrence matrix is calculated in a local neighborhood. For a pair of pixels from the two SAR images in the same coordinates, since each pixel belongs to the obtained number of backscattering levels in a membership degree respectively, a co-occurrence matrix can be computed by combining the membership values of the pair of pixels in a conjunctive way. From the resulting matrix, the temporal change feature can be extracted since the upper and the lower triangular elements off the diagonal represent the positive change and negative change respectively.

Step3: Kittler-Illingworth (K&I) minimum error thresholding algorithm is applied to the temporal change feature to acquire the final change detection map.

Experiments are carried on a subset of a multi-temporal TerraSAR-X image acquired in Stripmap mode with spatial resolution about 3 m. Qualitative and quantitative results confirm the effectiveness of the co-occurrence matrix technique in detecting the changes.

10427-16, Session 4

Uncertainty analysis of in-flight spectral calibration for hyperspectral imaging spectrometers

Huijie Zhao, Ruonan Geng, Guorui Jia, BeiHang Univ. (China); Daming Wang, China Aero Geophysical Survey & Remote Sensing Center for Land and Resource (China)

Hyperspectral imaging instrument performance, especially spectral response parameters, may change when the sensors work in space due to vibrations, temperature and pressure changes compared with the laboratory status. In order to derive valid information from imaging data, accurate spectral calibration accompanied by uncertainty analysis to the data must be made. At present, the laboratory spectral calibration methods and corresponding uncertainty analyses have been available. Automatic methods for the estimation of in-flight spectral calibration parameters (spectral response function, band-center and bandwidth) at atmospheric absorption regions from high spectral resolution imaging spectrometers have been raised. However, the uncertainty of the in-flight spectral calibration products has not been calculated.

The purpose of this work is to present a process to estimate the uncertainties of in-flight spectral calibration parameters by analyzing the sources of uncertainty and calculating their sensitivity coefficients. The calibration algorithm is based on the atmospheric absorption features. In this method, the band-center and bandwidth determinations are made by correlating the in-flight sensor measured radiance with reference radiance. The latter is calculated by convolving MODTRAN data with spectral response functions fitting with Gaussian. The most accurate spectral calibration parameters can be obtained when the measured data matches the reference data. In the above procedure, the uncertainty analysis is conducted separately for three factors: (a) the radiance calculated from imaging data; (b) the reference data; (c) the deviation between the

above two items. The first uncertainty is calculated according to radiometric calibration process. In the second item, the influence of land surface reflectance, atmospheric parameters, geometric model and other factors on the simulation results is considered. In addition, the accuracy of fitting spectral response function with Gaussian is tested by using covariance matrix and comparing the results of different models. For the third item, an appropriate matching model is chosen to calculate the deviation between measured and reference data, then the deviation is propagated to result. To obtain the final uncertainty, contributions due to every element must be propagated through this process.

Analyses have been made using above process for the Hyperion data. To increase the signal-to-noise ratio, the spatial averaging of the data is made and the band with the most significant absorption feature is chosen. The results show that the shift of band-center in the oxygen absorption (about 762nm), compared with the value measured in the lab, is less than 0.9nm with uncertainties ranging from 0.072nm to 0.09nm related to spatial distribution along the across-track direction of the image, the change of bandwidth is less than 1nm with uncertainties ranging from 0.085nm to 0.2nm, that verify the validity of the in-flight spectral calibration process.

Following this approach, the impact of the quality of image data, the spectral selection, the parameters used for the reference spectrum and the shape of spectral response function can be linked to the uncertainty in the in-flight spectral calibration products.

10427-17, Session 4

Evaluation of dimensionality reduction techniques in hyperspectral imagery and their application for the classification of terrestrial ecosystems

Edurne Ibarrola-Ulzurrun, Francisco Javier Marcello-Ruiz, Univ. de Las Palmas de Gran Canaria (Spain); Consuelo Gonzalo-Martín, Univ. Politécnica de Madrid (Spain)

Hyperspectral imagery has significantly contributed to the progress of remote sensing studies. The hyperspectral imagery is formed by a several narrow and continuous bands covering different regions of the electromagnetic spectrum, such as spectral bands of the visible, near infrared and far infrared. Hyperspectral imagery provides extremely higher spectral resolution than high spatial resolution multispectral imagery, improving the detection capability of terrestrial objects. The greatest difficulty found in the hyperspectral processing is the high dimensionality of these data, which brings out the 'Hughes' phenomenon. This phenomenon implies that the size of training set required for a given classification increases exponentially with the number of spectral bands. Therefore, the dimensionality of the hyperspectral data is an important drawback when applying traditional classification or pattern recognition approaches to this hyperspectral imagery. In our context, the dimensionality reduction is necessary to obtain accurate thematic maps of natural protected areas. Dimensionality reduction can be divided into the feature-selection algorithms and feature-extraction algorithms. We focus the study in feature-extraction algorithms like Principal Component Analysis (PCA), Minimum Noise Fraction (MNF) and Independent Component Analysis (ICA), which are algorithms that use mathematical procedure to transform a number of possibly correlated bands into a new set of uncorrelated variables. After a review of the state-of-art, it has been observed a lack of a comparative study on the techniques used in the hyperspectral imagery dimensionality reduction. In this context, our first objective was to perform a comparative assessment of the traditional techniques of dimensionality reduction (PCA, MNF and ICA) to evaluate their performance in the classification of high spatial resolution imagery of the CASI (Compact Airborne Spectrographic Imager) sensor. In our field campaign, the CASI sensor was configured to provide 72 bands covering a spectral range from 380 to 1050 nm and with 0.5 meters of spatial resolution. The study area chosen for carrying out the analysis was the Teide National Park in Canary Islands (Spain). It is a complex vulnerable heterogeneous ecosystems characterized by its small and mixed vegetation. In order to evaluate the dimensionality reduction techniques, a sufficient number of training samples were selected during a field campaign to include in the classification approach. We used a robust classification approach like the Support Vector Machine (SVM) algorithm, which is an efficient alternative for the hyperspectral imagery classification. Then, confusion matrices showed the Overall Accuracy and Kappa Coefficient of each classification after applying the PCA, MFN and ICA techniques. On the other hand, previous studies have used some bands from a single dimensionality reduction technique to obtain suitable classification maps. In this context, our second objective was to obtain the most accurate classification map using a suitable fusion of a selection of those transformed bands having more information and separability from each dimensionality reduction technique.

10427-18, Session 4

Classification of hyperspectral images using unsupervised support vector machine

Sayyed Ashkan Adibi, Mohammad Hassani, Shahid Bahonar Univ. of Kerman (Iran, Islamic Republic of); Azam Karami, Shahid Bahonar Univ. of Kerman (Iran, Islamic Republic of) and Univ. Antwerpen (Belgium)

Recently hyperspectral classification is highly considered in many practical applications such as communication systems, geology, agriculture, military applications, and etc. Two main types of classification algorithms are supervised and unsupervised methods. One of the popular supervised algorithms in the classification of hyperspectral images (HSI) is support vector machine (SVM) technique. Classification using SVM requires the ground truth of HSI. The majority of supervised algorithms such as SVM randomly consider some pixels for training and remaining pixels for testing. However, in some application, the ground truth doesn't exist therefore in this paper we introduce a novel unsupervised classifier for HSI by using image segmentation and spectral unmixing. In contrast with supervised methods, our method does not require prior training for processing data, while this algorithm uses the reflectance properties of HSI. Generally, hyperspectral datasets have high spectral and low spatial resolutions. Therefore, it contains mixed pixels which means that the value of each pixel is composed of some pure pixels (endmembers). So in our proposed method, first of all, the number of classes is considered equal to number of endmembers and it is approximated using hyperspectral signal subspace identification by minimum error (HySime). Second, the endmember matrix is obtained using Lloyd's algorithm. Third, fully constraint least square unmixing (FCLSU) is applied and the abundance fraction matrices are calculated. Fourth, the abundance values for each pixel are sorted. If the difference between first and second values are greater than a threshold, the mentioned pixel is labeled with the endmember number of higher value. If this assumption is not valid the pixel is considered as an unclassified pixel. Finally, the initial classification map is constructed. Fifth, training samples are selected from the initial classification map. If each pixel has the same eight neighboring (vertical, horizontal and diagonal) labels, it is a good candidate for train samples. Ten percent of proper candidate pixels are randomly selected as final training data and the remaining pixels are considered as test data. In fact, a virtual ground-truth is created at this step. Sixth, SVM is applied to the virtual ground truth and HSI. After applying SVM, the classification map is obtained, this map is considered as an initial ground-truth again. Then the algorithm is iteratively repeated from step five for five times. Indeed, the initial ground- truth is updated in each iteration. Finally, the classification map is obtained.

In order to validate the efficiency of the proposed algorithm, two real HSI datasets are used. The obtained classification

results are compared with some state-of-the-art algorithms and the classification accuracy of the proposed method is close to the supervised algorithms.

10427-19, Session 4

Nearest neighbor-density-based clustering methods for large hyperspectral images

Claude Cariou, Kacem Chehdi, Univ. de Rennes 1 (France)

We address the problem of hyperspectral image partitioning using nearest neighbor - density-based (NN-DB) clustering methods. Unsupervised classification, or clustering, is an important tool for image interpretation when no reference (ground truth) data is available. However, despite the vast literature in this field, this is still a difficult task for which no definitive solution has been found yet, especially for large size images.

NN-DB methods are able to cluster data objects without specifying the number of clusters to be found. Among the NN-DB approaches are deterministic methods, e.g. ModeSeek [1], knnClust [2], and GWENN [3]. These methods require as input the kNN graph, i.e. the set of distances of objects to their NNs, as well as their indices. As such, they only need to specify the number of neighbors k around each object in the representation space. Recently, a new NN-DB clustering method, called Density Peak Clustering (DPC) [4], has been proposed and received much attention from the data scientists' community. kNN versions of DPC have been proposed since and shown their efficiency for a wide range of applications. NN-DB clustering methods are specifically well adapted to non-convex clusters as often observed in high dimensional data, and especially for hyperspectral images. However, they still suffer from the difficulty of obtaining the kNN graph due to the quadratic complexity with respect to the number of pixels. In [3], a multiresolution (MR) scheme has been proposed to bypass the computation of the full kNN graph over the image, by restricting the NN search to ascendants of the cluster modes found at each lower level of the Discrete Wavelet Transform approximation coefficients.

The present work extends the method presented in [3] on two aspects. Firstly, we introduce the generalization to 'variable k' NN graphs, by computing a maximal number of NNs for each object in the data set. This approach allows to find automatically a number of clusters consistent with the data set, and to tackle the problem of unbalanced clusters which can dramatically limit the performances of clustering methods. Secondly, we set up a modified NN search procedure within the MR scheme, in order to insure the stability of the number of clusters found from the coarsest to the finest spatial resolution. We show how these extensions are easily adapted to four NN-DB methods (ModeSeek, knnClust, knn-DPC, and GWENN).

Experiments are conducted to assess the reliability and compare the four NN-DB methods for clustering pixels in hyperspectral images. Using the AVIRIS Salinas image (512 ? 217 pixels, 204 spectral bands) and its reference map, we show that NN-DB methods can outperform classical clustering methods such as k-means and FCM, by more than 10% on overall accuracy, without providing the number of classes. Among the NN-DB methods, we show that GWENN provides the best classification accuracy. Another experiment is performed on a very large image acquired by our AISA Eagle hyperspectral imaging sensor (8192?960 pixels, 62 spectral bands), still showing the efficiency of GWENN in terms of both clustering quality (measured by the CVR index [5]) and speed.

References

[1] R. P. W. Duin, A. L. N. Fred, M. Loog, and E. Pekalska, "Mode seeking clustering by knn and mean shift

evaluated." in SSPR/SPR, ser. Lecture Notes in Computer Science, vol. 7626., Springer, 2012, pp. 51–59.

[2] T. N. Tran, R. Wehrens, and L. M. C. Buydens, "knn-kernel density-based clustering for high-dimensional multivariate data," Computational Statistics & Data Analysis, vol. 51, no. 2, pp. 513–525, Nov. 2006.

[3] C. Cariou and K. Chehdi, "A new k-nearest neighbor density-based clustering method and its application to hyperspectral images," in Proc. IEEE Intern. Geoscience and Remote Sensing Symposium, Beijing, China, 2016, pp. 6161–6164.

[4] A. Rodriguez and A. Laio, "Clustering by fast search and find of density peaks," Science, vol. 344, no. 6191, pp. 1492–1496, 2014.

[5] G. Ver Steeg, A. Galstyan, F. Sha, and S. DeDeo, "Demystifying information-theoretic clustering," in Proc. International Conference on Machine Learning, Beijing, China, 2014, pp. 19–27.

10427-20, Session 4

Maximum auto-mutual-information factor analysis

Allan A. Nielsen, Technical Univ. of Denmark (Denmark)

Based on the information theoretical measure mutual information derived from entropy and Kullback-Leibler divergence, an alternative to maximum autocorrelation factor analysis is sketched.

1. INTRODUCTION

In signal and image processing principal component analysis [1] (PCA) is often used for dimensionality reduction and feature extraction in pre-processing steps to for example classication.

In remote sensing image analysis PCA is often replaced by maximum autocorrelation factor [2] (MAF) or minimum noise fraction [3] (MNF) analysis. This is done because MAF and MNF analyses incorporate spatial information in the orthogonalization of the multivariate data which is conceptually more satisfactory and which typically gives better results.

In this contribution, autocorrelation between the multivariate data and a spatially shifted version of the same data in the MAF analysis is replaced by the information theoretical, entropy and Kullback-Leibler divergence based measure mutual information [4-8]. This potentially gives a more detailed decomposition of the data. Also, the orthogonality between already found components and components of higher order requested in the MAF analysis is replaced by a requirement of minimum mutual information between components. These ideas resulting in maximum auto-mutual-information analysis are in turn based on [9-11]. The sketched methods are used on the well-known AVIRIS [12] (https://aviris.jpl.nasa.gov/) Indian Pines data.

REFERENCES

[1] Hotelling, H., "Analysis of a complex of statistical variables into principal components," Journal of Educational Psychology 24, 417-441 (1933).

[2] Switzer, P. and Green, A. A., "Min/max autocorrelation factors for multivariate spatial imagery," Tech. Rep. 6, Department of Statistics, Stanford University (1984).

[3] Green, A. A., Berman, M., Switzer, P., and Craig, M. D., "A transformation for ordering multispectral data in terms of image quality with implications for noise removal," IEEE Transactions on Geoscience and Remote Sensing 26, 65-74 (Jan. 1988).

[4] Shannon, C. E., "A mathematical theory of communication," Bell System Technical Journal 27(3), 379-423 and 623-656 (1948).

[5] Hyvärinen, A., Karhunen, J., and Oja, E., Independent Component Analysis, J. Wiley (2001).

[6] Mackay, D. J. C., Information Theory, Inference and Learning Algorithms, Cambridge University Press (2003).

[7] Bishop, C. M., Pattern Recognition and Machine Learning, Springer (2007).

[8] Canty, M. J., Image Analysis, Classication and Change Detection in Remote Sensing. With Algorithms for ENVI/IDL and Python, Taylor & Francis, CRC Press, third ed. (2014).

[9] Yin, X., "Canonical correlation analysis based on information

theory," Journal of Multivariate Analysis 91, 161-176 (2004).

[10] Karasuyama, M. and Sugiyama, M., "Canonical dependency analysis based on squared-loss mutual information," Neural Networks 34, 46-55 (2012).

[11] Vestergaard, J. S. and Nielsen, A. A., "Canonical information analysis," ISPRS Journal of Photogrammetry and Remote Sensing 101, 1-9 (2015). http://www.imm.dtu.dk/pubdb/p.php?6270, Matlab code at https://github.com/schackv/cia.

[12] Vane, G., Green, R. O., Chrien, T. G., Enmark, H. T., Hansen, E. G., and Porter, W. M., "The airborne/infrared imaging spectrometer (AVIRIS)," Remote Sensing of Environment 44, 127-143 (1993).

10427-21, Session 5

Hyperspectral image classification using nonsubsampled shearlet transform

Mohamad Reza Soleimanzadeh, Azam Karami, Shahid Bahonar Univ. of Kerman (Iran, Islamic Republic of)

In this paper a new supervised method for classification of Hyperspectral Images (HSI) based on 2D Non-Subsampled Shearlet Transform (NSST) and Minimum Noise Fraction (MNF) is introduced.

Recently some methods based on Wavelet Transform for HSI classification have been introduced. But wavelets are known to successfully represent 1D signals with high sparsity. However, 2D wavelet representation is not highly sparse. In recent years, multidirectional representations based on contourlets, curvelets, and etc. have been introduced in order to efficiently handle the geometrical features of multidimensional signals. The shearlet transformation was introduced and shown that it has a superior directional selectivity which makes it an optimal sparse representation of images. In this paper a special type of discrete shearlet transform is applied, called Non-Subsampled Shearlet Transform (NSST). The implementation of the NSST contains two steps: the application of Non-Subsampled Pyramid (NSP) filter banks and Non-Subsampled Shearing (NSS) filter banks. A non-subsampled filter bank has no downsampling or upsampling, and hence it is shift-invariant. In fact, NSP filter banks create a multiscale decomposition of the original image into high-frequency subbands and low-frequency subbands which are of the same size as the original image.

In this paper, HSI are considered as a 3D dataset: two spatial dimensions and one spectral dimension. NSST is applied to each spectral bands of HSI. After that, because the NSST coefficients at any level of decomposition retain the same size of the original signal even though the number of subbands grows as more and more levels of decomposition applied. The MNF is applied to all NSST coefficient subbands in order to reduce the dimensionality reduction. MNF sorts the informative bands based on signal to noise ratio (SNR). The bands with high SNR are preserved. Finally, the Support Vector Machine (SVM) classifier is used in order to classify the image based on these extracted features.

In order to validate the efficiency of the proposed algorithm, two real HSI datasets (Pavia and Indian) are used. The obtained classification results are compared with popular supervised classification algorithms: Generalized Composite Kernel (GCK), Multi-Hypothesis Prediction (MH-SVM) and Spatial-Aware Dictionary Learning (SADL). Obtained results shows that the proposed method has reached the highest classification accuracy.

10427-22, Session 5

Blind estimation of blur in hyperspectral images

Mo Zhang, Benoit Vozel, Kacem Chehdi, Univ. de Rennes 1 (France); Mykhail Leontievich Uss, Sergey K. Abramov, Vladimir V. Lukin, National Aerospace Univ. (Ukraine)

The spectral channels of hyperspectral images acquired by remote sensing systems are generally degraded by noise and can be sometimes degraded by blurs due to lens imperfections, chromatic aberration, atmospheric or air turbulence or even sensor drift after the system deployment. We address the blind restoration of these degraded channels component-wise. By blind, we mean absolutely no knowledge neither of the blur point spread function nor the original latent channel. Our contribution in this work is to propose a new sequential mono-component blind method for effectively estimating the blur point spread function in the first step, and deburring in the second step the corresponding blurred channel by means of the previously accurately estimated blur kernel.

Indeed, the quality of the blur kernel estimation plays a crucial role in any alternate or sequential restoration method efficiency. A general idea is that edges in an degraded channel provide relevant information for estimating the blur kernel. But it occurs that not all of them are fully helpful. Just salient edges with large gradient values have good influence and contribute to improving accuracy estimation. Tiny edges, small tiny details (rich textures) happen to deteriorate the estimation efficiency. Thus, selecting appropriate structures in a degraded channel for supporting the blur estimation reveals itself of key importance. Following this idea [1,2], we propose as the first step an alternate estimation of both the blur kernel and the intermediate latent channel.

Given the current intermediate latent image, blur kernel estimation is achieved through efficient detection, selection and use of its sufficiently salient edges. To separate main useful or salient structures from fine-scale damaging details, textures and possibly noise, the optimization of a suitable energy functional is carried out. Next, retained structures are enhanced via shock filtering and salient edges are selected. Finally, blur kernel estimation is performed with imposing sparsity prior.

Given the current blur kernel estimate, the intermediate latent image estimation is in turn updated by employing a low rank prior for improving the current estimate.

Compared to [2], several modifications are beneficially introduced with a minimum of a priori knowledge. Four gradient directions and corresponding adaptive regularization terms are considered and a different selection of final salient edges (through thresholding adequately their cumulative distributions) is preferred. Besides, we enforce the gradients of the current unknown latent channel to be sufficiently close to those of its low rank approximation, instead to those of previously selected salient edges. The latter approximation is obtained by minimizing the Frobenius norm to its current k-Nearest-Neighbor patch-based estimation.

To prove higher efficiency of the proposed method, we compare it against the original method it is based on and four recent representative edge-sparsifying regularized methods [3-7]. Our attention is mainly paid to the objective analysis of the blur filter error estimation accuracy (via l1-norm, l2-norm).

The tests are performed on a synthetic hyperspectral image, degraded with various synthetic blurs (out-of-focus, Gaussian, motion, arbitrary), without and with noise components. Conclusions, practical recommendations and perspectives are drawn from the results experimentally obtained and analyzed.

REFERENCES

[1] J. Pan, R. Liu, Z. Su, X. Gu, "Kernel estimation from salient structure for robust motion deblurring," Signal Processing: Image Communication, Vol. 28, Issue 9, pp. 1156-1170, October 2013.

[2] J. Pan, R. Liu, Z. Su and G. Liu, "Motion blur kernel estimation via salient edges and low rank prior," 2014 IEEE International Conference on Multimedia and Expo (ICME), Chengdu, pp. 1-6, 2014.

[3] M. S. C. Almeida and L. B. Almeida, "Blind and Semi-Blind Deblurring of Natural Images," IEEE Trans. Image Process., vol. 19, no. 1, pp. 36–52, Jan. 2010.

[4] D. Krishnan, T. Tay, and R. Fergus, "Blind deconvolution using a normalized sparsity measure," IEEE Conference on Computer Vision and Pattern Recognition (CVPR), Providence, RI, pp. 233–240, 2011.

[5] F. Sroubek and P. Milanfar, "Robust Multichannel Blind Deconvolution via Fast Alternating Minimization," IEEE Trans.

Image Process., vol. 21, no. 4, pp. 1687–1700, Apr. 2012.

[6] M. S. C. Almeida and M. A. T. Figueiredo, “Blind image deblurring with unknown boundaries using the alternating direction method of multipliers,” IEEE Int. Conf. Image Process., ICIP 2013 - Proc., pp. 582–585, 2013.

[7] M. S. C. Almeida and M. A. T. Figueiredo, “Parameter Estimation for Blind and Non-Blind Deblurring Using Residual Whiteness Measures,” IEEE Trans. Image Process., vol. 22, no. 7, pp. 2751–2763, Jul. 2013.

10427-23, Session 5

Hyperspectral image denoising and anomaly detection based on low-rank and sparse representations

Lina Zhuang, Instituto Superior Técnico, Univ. de Lisboa (Portugal); Lianru Gao, Bing Zhang, Institute of Remote Sensing and Digital Earth (China); José M. Bioucas-Dias, Instituto Superior Técnico (Portugal) and Instituto de Telecomunicações (Portugal) and Univ. de Lisboa (Portugal)

The very high spectral resolution of Hyperspectral Images (HSIs) enables the identification of materials with subtle differences and the extraction subpixel information. However, the increasing of spectral resolution often implies an increasing in the noise linked with the image formation process. This degradation mechanism limits the quality of extracted information and its potential applications. Since HSIs represent natural scenes and their spectral channels are highly correlated, they are characterized by a high level of self-similarity and are well approximated by low-rank representations. These characteristic underlies the state-of-the-art in HSI denoising. However, in presence of rare pixels, the denoising performance of those methods is not optimal and, in addition, it may compromise the future detection of those pixels. To address these hurdles, we introduce RhyDe (Robust hyperspectral Denoising), a powerful HSI denoiser, which implements explicit low-rank representation, promotes self-similarity, and, by using a form of collaborative sparsity, preserves rare pixels.

1. Problem formulation: Assume that the dataset contains a small number of spectral/spatial outliers in unknown positions, we adopt the observation model

Y = X+S+N,

which assumes that the observed data matrix Y is the sum of matrix X, representing the signal component, with matrix S representing the rare pixels, and N, representing the noise and modeling errors. Given Y, our objective is the estimation of X and S, by exploiting the fact that X is low-rank and self-similar and S is columnwise sparse.

An usual assumption in HSIs is that the columns (spectral vectors) of matrix X live in a low-dimensional subspace that may be estimated from the observed data Y with good approximation. Thus, we write X=EZ, with E holding an orthogonal basis for the signal subspace. Hence, the observation model may be written as

Y = EZ+S+N.

We propose to estimate the matrix Z and the sparse matrix S representing outliers by solving the optimization in Fig. 1. We solve this optimization with CSALSA algorithm.

In addition, we also introduce an anomaly detection method, which is a spin-off of the denoiser algorithm and is derived from the estimate of outlier matrix S. If Euclidean norm of i-th column of outlier matrix is larger than a threshold, then i-th pixel is calssified as an anomalous pixel.

2. Experiments:

A semi-real hyperspectral dataset (Fig. 2) was simulated by adding Gaussian independent noise and anomaly pixels in clean Pavia University data. The denoising performance of RhyDe is compared with those of BM4D (M. Maggioni, 2013), NAILRMA (W. He, 2015), and FastHyDe (L. Zhuang, 2016). We can see that the RhyDe yields uniformly the best performance from Table 1. The quality of reconstructed spectra may also be inferred from Fig. 3.

The proposed anomaly detector is compared with the state-of-the-art. Receiver operating characteristic (ROC) curve plotting the detection rate against false alarm rate is usually adopted to illustrate the performance of a detector. Here we report the minimum false alarm rates when the detectors reach 100% detection rates in Fig. 4. The detection based on RhyDe yields almost uniformly the best detection results.

10427-25, Session 5

A method to correct the smile effect based on the combination correction of radiometric and spectrum

Chuncheng Zhou, Chuanrong Li, Lingli Tang, Yongguang Zhao, Academy of Opto-Electronics, CAS (China)

The hyperspectral imageries obtained from dispersive imaging spectrometer often contain significant cross-track spectral curvature nonlinearity disturbances, known as the smile/frown effect, which is due to the change of dispersion angle with field position. The smile effect must be corrected because the across-track wavelength shift from center wavelength alters the pixel spectra and reduces the application effect of classification and target recognition. There are several methods to correct the smile effect which don’t take into account the fact that the smile effect is woven together with the sensor radiation characteristic, just processing spectra distortion to correct the smile effect would renewably lead to radiometric distortion of the radiometric correction image. This paper presents a new method to deal with this problem.

Firstly, it is analyzed that the CCD relative radiometric correction model with these conditions of the inconsistent radiation characteristic of CCD array and the dispersion angle changing with field position. Secondly, the relative radiometric and spectra laboratory calibration of the dispersive imaging spectrometer is carried out and the relative radiometric calibration data and the actual center wavelength of each detector are obtained. Then, the interpolation approximation of relative radiometric calibration data at actual center wavelength is taken into the CCD relative radiometric correction model, and radiation calibration coefficients considered spectra distortion effect are obtained. Finally, hyperspectral images would be corrected by the relative radiometric correction model and the operation of interpolation approximation at corrected center wavelength.

An experiment based on the proposed method is conducted. Hyperspectral images are acquired from an UAV airborne Offner Spectral Imager which has a spectral coverage of 0.395-1.028?m. The band of corrected image at 760nm, the absorption peak of O2, has become consistent which shows that the smile effect is effectively removed, and meanwhile the radiometric correction result is finely reserved.

At last we have conducted quantitative evaluation by the spectral characteristics analysis on the same line, which demonstrate the effectiveness of the proposed method.

10427-26, Session 6

Convolutional neural networks for estimating spatially distributed evapotranspiration

Angel M. García-Pedrero, Consuelo Gonzalo-Martín, Univ. Politécnica de Madrid (Spain); Mario F. Lillo-Saavedra, Univ. de Concepción (Chile); Dionisio Rodriguéz-Esparragón, Univ. de Las Palmas de Gran Canaria (Spain); Ernestina Menasalvas, Univ. Politécnica de Madrid (Spain)

Efficient water management in agriculture requires an accurate estimation of evapotranspiration (ET).

The estimation of ET at the land surface is fundamental in the determination of the exchanges of energy and mass among hydrosphere, atmosphere and biosphere in order to understand the state of agricultural areas. Even though local measures can be used to estimate the components of the energy balance, these values can not be extended to large areas due to the heterogeneity and complexity of land surfaces; and the dynamic nature of heat processes.

Nowadays, there are available several balance energy surface models (e.g. SEBAL, METRIC) that provide a daily ET estimation (ETd) spatially and temporarily distributed for different crops, over wide areas. These models use sensed imagery gathered from aircraft and satellite platforms, in particular, they need infrared thermal spectral band to estimate sensible heat flux from the surface temperature. However, this spectral band is not available for most current operational remote sensors, which limits the precision of the estimations to the coarsest resolution (e.g., the thermal band of Landsat 7 has a resolution of 60 m), as well as the temporality to the dates of the available images.

Even though the good results provided by machine learning (ML) methods in many different areas, few works have applied these approaches for forecasting distributed ETd on space and time where aforementioned information is missing. However, these methods do not exploit the land surface characteristics and the relationships among land covers producing estimation errors.

Recently deep learning-based methods have demonstrated excellent performance on different artificial-intelligence tasks, in particular Convolutional Neural Networks (CNNs) have been used for solving image processing issues. CNNs are biological-inspired variants of feed-forward neural networks, where each layer is a non-linear feature detector performing local processing of contiguous features within each layer. This leads to higher conceptual representation as information moves up to the output layer. In this context, a CNN is able to generate patterns from an image in a hierarchical manner similar to that of the visual cortex. In this regard, CNNs are able to exploit contextual information similarly as a human vision does (i.e. cognitive process).

In this work, we have developed and evaluated a methodology that provides spatial distributed estimation of ETd by means of CNNs. The inputs to the training phase of these models will be the images containing spectral bands and indexes (such as NDVI and LAI), and the values of reference evapotranspiration (ETr) registered through a meteorological station. Several training experiments with different input datasets has been carried out to select the best model. After the training of the CNNs, the performance of these models have been evaluated by comparing the values of ETd provided by them with the obtained by using METRIC.

10427-27, Session 6

An approach to conifer stem location and modeling in high density airborne lidar data

Aravind Harikumar, Francesca Bovolo, Fondazione Bruno Kessler (Italy); Lorenzo Bruzzone, Univ. degli Studi di Trento (Italy)

Inventorying at the individual tree level is very important for accurate forest modeling, management and ecosystem studies. High density multi-return airborne Light Detection and Ranging (LiDAR) systems acquire both internal and external geometric detail about the individual tree crowns. Among the forest parameters, the stem position and its diameter at breast height (DBH) are the most relevant ones for accurate biomass, and forest growth estimation. Techniques that analyze 2D structural information extracted from the 3D point cloud [1] assume that the local maxima in Canopy Height Models (CHMs) correspond to the tree-tops, which in turn are used to calculate the stem location. Three dimensional (3D) point based methods [2] and voxel based [3] techniques provide improved performance over their 2D counterparts. However it is important to develop methods that can accurately locate tree stem along the vertical canopy, and estimate DBH.

In this paper, we propose a method to locate and model the stem by analyzing the empty volume within the 3D point cloud for individual conifers. The laser beams do not penetrate the opaque wood, i.e., stem and branches, and hence no point samples exist within the stem volume. Thus an empty volume exists within the tree point cloud. The proposed method assumes that a high density point cloud associated with individual trees is extracted using any state-of-the-art 3D crown delineation algorithm [4]. Then, the method relies on the fact that conifer branches grow linearly outward from the stem in a direction nearly perpendicular to it. Therefore, the stem position can be estimated with the knowledge of approximate direction and slope vectors of the branches (i.e., the knowledge of the branch skeletal structure). We derive these vectors using a previously proposed internal crown structure model [5]. The branch tips are first identified using a crown boundary detection algorithm, and the LiDAR points associated with individual branches (i.e., branch clusters) are identified using a region growing technique. For each branch cluster, the point farthest from the respective branch tip along the main direction is identified. These points are the most proximal ones to the stem, and have a high probability to be formed due to laser reflections from the stem or branch-stem junctions. The conifer stem is located within the lattice defined by these points. Under the assumption that conifer stem can be closely modelled using a cone shape. We fit a cone to the lattice of points likely to envelop the stem such that no LiDAR point falls within the cone. In most airborne LIDAR data acquisitions, the upper half of the tree is sampled highly (thus, stem lattice is modeled better) than the lower half. Accordingly, stem-lattice cone parameters are estimated from upper half crown points only. The parameters of this cone are used to estimate the DBH, and tree height.

The experiments were performed on a set of twenty conifers consisting of trees from five dominant European conifer species, for which the height and the DBH were known. The obtained results prove the method to be accurate.

References:

[1] Hyyppä, J., Kelle, O., Lehikoinen, M., Inkinen, M., 2001. A segmentation-based method to retrieve stem volume estimates from 3-D tree height models produced by laser scanners. IEEE Transactions on Geoscience and remote Sensing, vol. 39, no. 5, pp. 969-975, May. 2001.

[2] Reitberger J, Krzystek P, Stilla U. Combined tree segmentation and stem detection using full waveform lidar data. International Archives of Photogrammetry, Remote Sensing and Spatial Information Sciences, vol. 36, pp. 332-337, Sep. 2007.

[3] Lamprecht S, Stoffels J, Dotzler S, Haß E, Udelhoven T. aTrunk—An ALS-Based Trunk Detection Algorithm. Remote Sensing. vol. 7, no. 8, pp. 9975-999, Aug. 2015.

[4] J. Reitberger, M. Heurich, P. Krzystek, and U. Stilla, "Single tree detection in forest areas with high-density lidar data," International Archives of Photogrammetry, Remote Sensing and Spatial Information Sciences, vol. 36, no. 3, pp. 139–144, Sep. 2007.

[5] A. Harikumar, F. Bovolo, L. Bruzzone. An Internal Crown Geometric Model for Conifer Species Classification with High Density LiDAR Data, IEEE Transactions on Geoscience and Remote Sensing, in press 2017.

10427-28, Session 6

Comparative study of building footprint estimation methods from LiDAR point clouds.

Esteban Rozas, Univ. of Santiago de Compostela (Spain); Francisco Fernández Rivera, José Carlos Cabaleiro Domínguez, David L. Vilariño, Tomás Fernández Pena, Univ. de Santiago de Compostela (Spain)

Building detection and characterization is one of the most active research areas in the remote sensing community. 3D-building reconstruction or urban planning are examples of important applications that benefit of accuracy building footprint estimation.

The extraction of building footprints is usually performed from aerial photograph or satellite images. However, automatic approaches have to deal with shadows and relief displacements. Airborne LiDAR technology represents an alternative to those conventional methods to estimate building footprints. Nevertheless, the irregular space distribution of the LiDAR points are an important issue affecting the accuracy of the boundary and area estimations.

Building footprint extraction usually starts from processing steps like segmentation and classification of points to decide which points belong to buildings. Then, the building footprint is estimated from the boundary points. In this paper, we have carried out a study of accuracy in the estimation of the footprint of buildings from LiDAR points. The analysis focuses on the processing steps following the object recognition, assuming that the labelling of building points have been previously performed. Then, we perform an in-depth analysis of the influence of the point density over the accuracy of the building area estimation.

The most popular methods to extract the outline of objects from irregularly distributed data points have been considered. These methods are based on the extraction of the convex and concave hull, the exterior outline, and the Voronoi surround. Using the mentioned methods, the outline of a building is extracted and, then, smoothed to eliminate small angles in order to reduce the outline distortion. Finally, the Gauss method is used to compute the object area.

The comparison of the approaches to estimate the outline of buildings is based on the accuracy measured from the symmetric difference between the automatic boundary estimation and the corresponding ground truth. This ground truth consists of a dataset from the OpenTopography database, containing eight buildings with different shape, size, and point density, and whose boundaries have been manually estimated.

The influence of the point density in the accuracy has been analysed by reducing the point density of the LiDAR point datasets in a half from the previous point count. The density reduction has been performed based on the frequency of the sensing process. If the points are sensed every t ms, the point density is lowered to a half by removing all points except one in intervals of t/2 ms. This approach is recursively repeated to produce different versions with scaled point density.

The experimental results show that the error sources of the building area estimation are mainly the building shape (quantified from the corresponding circularity), the point density, and the number of points of the buildings. There are other secondary sources of error, hard to quantify, as the point distribution. Regardless of these factors, we show that the concave hull-based method ended up being the most accurate approach.

10427-30, Session 6

Semi-automatic tree detection from images of unmanned aerial vehicle using object-based image analysis method

Serdar Selim, Namik Kemal Sonmez, Mesut Coslu, Isin Onur, Akdeniz Üniv. (Turkey)

In 21st century, global environmental problems constitute important rate of pressures on natural resources. Protection and management of these natural resources is important in terms of sustainable development. Ecological values have priority for creating a sustainable society. In this scope; detecting, researching and managing the natural structure spatially create the agenda of ecological researches in recent years. Detecting the green texture fast, low cost and with high accuracy are becoming widespread in the direction of developments in remote sensing techniques. Effective techniques are being developed in many applications like data obtaining, processing, analyzing etc. In this context, object based classification is a commonly used image analysis method in recent years. This method is not only based on spectral information in high-resolution images, but also segmenting objects using their texture, shape and dimensions then classifying them by creating a set of rules. Unmanned Aerial Vehicles (UAVs) have advantages over other sensor platforms in obtaining image data with high spatial resolution, low cost, repeatable measurement capability and flight ability in cloudy weather.

The aim of this study is detection of trees with low cost, fast and reliably with object based image analysis method by using high resolution UAV data. The study consists of three basic process steps. In the first stage, high resolution aerial photographs were obtained with UAV. Aerial photographs with approximately 1 cm spatial resolution were obtained from 30 m. flight height with 80% front overlap and 80% side overlap. Orthorectification, mosaicing, georeferencing and filtering processes were performed to the obtained photographs in order to make them ready for the analysis. Orthoimage in three spectral bands (RGB) and Digital Surface Model (DSM) were generated by processing the aerial images. Rotation and translation errors were corrected with the help of ground control points in the obtained images. The second phase of the study constitutes the most important process steps of object based classification: They are segmentation and classification. In this phase various parameters such as scale, shape and integrity were used to obtain the best result. Furthermore accuracy assessments were performed with field observations and ground control points. In the classification process step, specified set of rules applied to segmentation result objects thus trees and other classes were determined in the study area. The generating of the rule sets was performed using the height information obtained from DSM and spectral data collected from orthoimages. Accuracy analysis was performed at the last stage of the study. The number of trees determined in the classification result is compared with the known number of the trees in the field. As the result of comparison, tree numbers and crown widths were found to be consistent. This study tests and implements a method that produces data at low cost, fast and high accuracy which can be used in ecological studies and specially in determination of tree density.

10427-31, Session 7

Land cover classification using deep learning convolutional neural networks with spectral curves

Junghee Lee, Jungho Im, Daehyeon Han, Ulsan National Institute of Science and Technology (Korea, Republic of)

Land cover classification is one of the major research endeavors in the field of remote sensing since it provides a basis for documenting changes over time. So far, numerous classification methods have been developed. During the recent decade, machine learning techniques such as decision trees, support vector machines, and random forest have been successfully introduced in remote sensing classification. Deep learning, a branch of artificial neural networks, has recently gained popularity in computer science and other disciplines since it significantly improves the well-known limitations of typical neural networks. Deep learning can abstract features from numerous training data at a high level based on a series of combinations of non-linear transformation, which has been proved powerful in many areas. Various deep learning algorithms have been proposed and, in this study, we focused on convolutional neural networks, which are motivated by the organization of animal visual cortex. Since convolutional neural networks contain feature-extraction steps unlike other classification algorithms, it does not require any pre-processing steps from input images. Several studies have used deep convolutional neural networks for land cover classification, but all of them focused on extracting spatial features. In this study, we aimed to use deep convolutional neural networks for land cover classification through the convolution of spectral curve images. We evaluated our approach using Landsat 8

time series data collected over two study sites, Gunsan-si, South Korea and Las Vegas, United States. Both study sites contain heterogeneous land cover composition, but they have different climatic and topographic characteristics. FLAASH in ENVI software was used for atmospheric correction of Landsat 8 images. Based on visual interpretation of high-resolution Google Earth images, we extracted training samples per land cover class. Multi-temporal spectral curve images were then extracted from Landsat 8 reflectance images. The convolutional neural networks were developed with four layers whose filter size was a 3x3 window. The approach proposed in this study was compared with the traditional machine learning algorithms—support vector machines, decision trees, and random forest. Results showed that the multi-temporal spectral curve-based approach produced better performance than the single-date spectral curve-based approach and the other classification algorithms. Factors that influenced the spectral curve-based classification results were carefully discussed.

10427-32, Session 7

Increasing the UAV data value by an OBIA methodology

Consuelo Gonzalo-Martín, Univ. Politécnica de Madrid (Spain); Mario F. Lillo-Saavedra, Univ. de Concepción (Chile); Angel M. García-Pedrero, Univ. Politécnica de Madrid (Spain); Dionisio Rodriguéz-Esparragón, Univ. de Las Palmas de Gran Canaria (Spain); Alejandro Rodriguez-Gonzalez, Univ. Politécnica de Madrid (Spain)

Recently, there has been a noteworthy increment of using images registered by unmanned aerial vehicles (UAV) in different remote sensing applications; most of them are in an experimental stage. Sensors boarded on UAVs has lower operational costs and complexity than other remote sensing platforms, quicker turnaround times, as well as, higher spatial resolution. Concerning this last aspect, it has to pay attention on the limitations of classical algorithms based on pixels, when they are applied to high resolution images. It is well known that they provoke undesirable effects, as for example, the "salt-and-pepper" effect. In this sense, in this study, it is investigated the capability of an OBIA methodology developed "ad-hoc" for data registered by a Parrot Sequoia multispectral sensor board on a eBee SQ agricultural drone, for a particular task: the automatic generation of a digital terrain model in an agricultural area, starting from digital elevation model (DEM) and multispectral images (four bands, Green, Red-edge and NIR) generated from data registered by the eBee SQ UAV. The first step of the methodology is a segmentation step carried out by a super-pixel algorithm (SLIC). A set of spectral indices (NDVI, NDRE, GNDVI and GRVI) have been used to characterised the superpixels. Context and elevation information is used to merge the superpixels in a bottom up approach at the same time that objects that does not correspond to terrain are eliminated. The final product is the automatic procedure to generate Digital Terrain Model of the analysed area.

10427-33, Session 7

Object-based image analysis for cadastral mapping using satellite images

Divyani Kohli, Faculty of Geo-Information Science and Earth Observation, ITC (Netherlands); Sophie Crommelinck, Rohan Bennett, Mila Koeva, Univ. Twente (Netherlands); Christiaan Lemmen, Kadaster International (Netherlands)

Estimates suggest that only 30% of the world's population has documented and recognized land rights. Cadastres form a core ingredient of any land administration system. Cadastral maps comprise of the extent, ownership and sometimes, value, of land which are essential for recording and updating land records. Mapping cadastral/parcel boundaries using traditional, field surveys often proves to be time, cost and labour intensive. Alternate approaches, specifically, remote sensing based methods that could provide low-cost and up-to-date solutions for rapid creation and upgrading of cadastral maps, are thus being investigated. Although, (semi)-automatic methods for detecting parcel boundaries are increasingly being explored, creating approaches that are both automated and transferable between contexts remains a challenge: the diversity of morphologies of parcel boundaries both within and across country contexts presents a major challenge. Object-based image analysis (OBIA) methods appear highly promising as these mimic the human interpretation process of identifying features. The objective is to find the most suitable approach for extracting visible parcel boundaries using very high resolution (VHR) satellite images. To do so, two segmentation approaches were applied: i) Multi-resolution segmentation (MRS) at two spatial levels, using a texture layer in addition to the image layers and ii) Segmentation using Estimation of Scale Parameters (ESP) tool. A pan-sharpened and orthorectified WorldView-2 image from the year 2010, with 0.5 m spatial resolution, of Amhara region in Ethiopia was used.

Results were compared with a reference cadastral map obtained from the field and accuracy assessment was carried out in terms of detection and localization quality for the two segmentation approaches. The detection quality in terms of error of commission and omission for MRS was 75% and 38.5% whereas for ESP, the errors were 66.1% and 58.2% respectively. The ESP approach achieved better results in terms of detection of additional boundaries whereas there is high percentage of missed boundaries. The MRS, on the other hand, results in lower number of missed boundaries. This could be due to over segmentation which also resulted in high error of commission for MRS. The localization quality, which implies accuracy of boundaries in a geometric sense, is similar for both methods with low percentages, i.e. between 12.3% and 16.1%, of true positive localized within 20 cm and 40 cm distance from the reference layer. This is due to the low overall accuracy but could also be attributed to the quality of reference data. The localization quality within 41 to 200 cm distance increases to 70.9% and 72.9% for ESP and MRS respectively, which shows the potential for improvement in future work.

Our results demonstrate the potential of OBIA for detecting visible cadastral boundaries but also shows that a balance between high completeness and correctness is hard to achieve: a low error of commission often comes with a high error of omission. Future work will focus on optimizing the results and finding the optimal trade-off in terms of detection and localization quality. Additionally, future work will focus on determining the quality of the reference data with regard to the application case.

10427-34, Session 7

Integrating support vector machines and random forests to classify crops in time series of Worldview-2 images

Azar Zafari, Raúl Zurita-Milla, Emma Izquierdo-Verdiguier, Univ. Twente (Netherlands)

Crop maps are essential inputs for the agricultural planning done at various governmental and agribusinesses agencies. Remote sensing offers timely and cost efficient technologies to identify and map crop types over large areas. Among all the plethora of classification methods, Random Forest (RF) and Support Vector Machine (SVM) are widely used in crop classification problems because of their proven performance. In this work, we study the synergic use of these two classifiers by introducing the use of a random forest-based kernel (RFK) in an SVM classifier. A time series of multispectral WorldView-2 images over Mali, West Africa in 2014 was used to develop a case study to illustrate the use of RFK. Ground truth containing five crop classes (Cotton, maize, millet, peanut, and sorghum) was collected at 45 farms to train and test the classifiers. RF, SVM with the standard Radial Basis Function (RBF) kernel, and SVM-RFK were trained and tested over 10 random training and test subsets generated from the ground data. Results show that

the newly proposed SVM-RFK classifier outperforms both RF and SVM-RBF. The overall accuracies based on spectral bands are of 66, 65 and 63% respectively. Adding vegetation indices to the analysis improves the classification accuracy for SVM-RFK, RF, and SVM-RBF to 70%, 68%, and 65%, respectively. The newly proposed RF-based kernel is therefore promising, and has the potential to become a good alternative to RF and SVM for the classification of remotely sensed images.

10427-35, Session 7

On the interest of the spectral bands in the automatic selection of high quality MODIS data through spatial pattern identification

Cristina Domingo-Marimon, Lluís Pesquer, CREAF (Spain); Natalia Gómez, María Teresa Jiménez, Univ. Autònoma de Barcelona (Spain); Xavier Pons, Dept. Geografia. Univ. Autònoma de Barcelona (Spain)

MODIS (MODerate resolution Imaging Spectroradiometer) surface reflectance data is, among other medium spatial resolution multispectral imagery, the one that is distributed with the most complete quality ancillary data set.

Such amount of quality information is essential for automatically selecting the highest quality MODIS daily images, using, for instance, a geostatistical analysis of spatial pattern images based on variogram tools. However, this automatic selection certainly could depend on the spectral information of each MODIS band. This work studies the influence of MODIS spectral bands on the automatic identification of high quality daily images. In particular, it studies the effect of each spectral band pattern on the variogram analysis and it aims at the identification of the most suitable spectral band (or band combination) for the spatially characterization of a given geographical region. The analysis consists in testing the influence of each of the reflectance bands (1, 2, 3, 4, 6 and 7; spectral range from 620 nm to 2155 nm) and the first component of the Principal Component Analysis for each of the MODIS MOD09GA Daily Surface Reflectance product at 500 m spatial resolution, corresponding to the year 2009 (365 images). The study region selected, Catalonia, northeast Iberian Peninsula in southwest of Europe, covers an area of 32000 km2. Specifically, the combination of the MODIS quality data set information and the variogram analysis of reflectance data allows the detection of different types of anomalies in the variability among the pixels of a given image that are identified through its correspondence with the fitted variogram parameters: nugget, sill and range. Consequently, snow pixels apparently misidentified in the MODIS quality mask increase the value of sill while bow-tie effect images' distortion increases the range on the fitted variograms.

The results are threefold: first, the variogram analysis is reaffirmed as an extremely useful technique for automatically selecting remote sensing high quality images, second, the role of the spectral bands on the spatial pattern variability of the variogram is confirmed, and third, the analysis highlights the potential of high computational effort needed for huge processing, computing the variogram analysis of a big set of images composed of 6 spectral bands per 365 scenes (384391 pixels each). Indeed, bands corresponding to the visible spectrum (bands 1, 3 and 4) and confident with the reality of a more constant true color composition landscape present smaller variogram variability. On the other hand, bands related to sensitivity to large seasonal variability in the phenology and water content of this Mediterranean study area, such as the near infrared and shortwave infrared (bands 2, 6 and 7), present high spatial pattern variability of the variogram, a behavior that may introduce false variability to the analysis.

Therefore, it is crucial to select the appropriate spectral band in order to, not only optimize but substantially improve the automatic selection of remote sensing images using geostatistical analysis based on variogram tools. Using information in the visible region appears to be an advantage when applying these methodologies.

10427-43, Session PS

Application of asymmetric mapping and selective filtering (AM and SF) method to Cosmo/SkyMed images by implementation of a selective blocks approach for ship detection optimization in SEASAFE framework

Davide Loreggia, INAF - Osservatorio Astronomico di Torino (Italy); Francesco Tataranni, INNOVA Consorzio per l'Informatica e la Telematica (Italy); Paolo Trivero, Walter Biamino, Lorenza Di Matteo, Univ. degli Studi del Piemonte Orientale Amedeo Avogadro (Italy)

Ship detection in SAR images has been studied from a long time and many methods have been discussed to deal with different targets and to get the best characterization of sea objects, as in harbor, in coastal, and in open ocean region.

Currently an efficient and widely utilized method is the 2D-CA technique, generalizing to 2D case the standard CFAR detection algorithm used in many detectors. This method consists in comparing the intensity value of each pixels with the mean value of the background and to take out, as potential target, those pixels that have an intensity above a fixed threshold.

The azimuth ambiguity (AA) is an artefact, or ghost, of the detection procedure due to the overlapping of the Doppler shifted SAR echoes returning from the secondary lobes of the antenna azimuth pattern (AAP) on the echo due to the main lobe and it is a consequence of the finite duration of the radar signal (Pulse Repetition Frequency - PRF).

Typically, the AA is weak with respect to the main signal (central lobe echo) and can be very difficult to detect in high contrast images (or part of an image). Despite this, if a very high reflectivity target has generated the SAR echo and the secondary lobes ghost signal overlap a very low contrast image area, e.g. the sea surface, the AA becomes a critical issue being easily confused with a different target.

The AA is one of the main sources of false alarm in ship detection and its identification plays an important role in the optimization of ship detection procedures. To our aid, AAs occurs at a well-defined position with respect to the source generated them, both along the azimuth and the range.

Many methods to face with this problem were proposed and presented in recent literature. After a review of different approach to this problem, we present the implementation of a procedure to adapt an asymmetric Wiener filtering (AWF) methodology, aimed to detect and discard ghost signal due to azimuth ambiguities in SAR images, to the case for X-band Cosmo Sky Med (CSK) images by implementing a selective blocks approach.

The application of the described method to the Cosmo SkyMed images is not trivial because of the very poor sampling of the AAP released. This leak of information required to generate a synthesized profile of the Azimuth Antenna Pattern. Moreover, we considered DGM_B (spectro-detected) images and not SLC/SCS as commonly found in literature. This approach revealed to be correct; preliminary results are satisfactory.

Another important issue was the definition of the filtering thresholds for the binary images that are needed to select the areas where are the AAs and that must be substitute in the input image. The solution was to adopt a blocks approach so that the original image is divided in blocks (same number of columns but different rows) and the normalization and the filter calculation is repeated over each block.

This work has been realized in the framework of the SEASAFE (Slick Emissions And Ship Automatic Features Extraction) program aimed to develop an automatic system for oil spills detection, ship detection and wind estimate from C-, L-, and X-band SAR images, based on a statistical methodology and able to operate in real time.

10427-52, Session PS

Target detection with compressive sensing hyperspectral images

Yaniv Oiknine, Daniel Gedalin, Isaac Y. August, Dan G. Blumberg, Stanley R. Rotman, Adrian Stern, Ben-Gurion Univ. of the Negev (Israel)

During the past years several compressive spectral imaging techniques were developed. With these techniques an optically compressed version of the spectral datacube is captured. Consequently the information about the object and targets is captured in a lower dimensional space. A question that rises is whether the reduction of the captured space affects the target detection performance. The answer to this question depends on the compressive spectral imaging technique employed. In most compressive spectral imaging techniques, the target detection performance is deteriorated. We show that with our recently introduced technique, dubbed Compressive Sensing Miniature Ultra-Spectral Imaging (CS-MUSI) [1-2], target detection with similar detection and false detection rates, compared to conventional hyperspectral cameras, is accomplished [3].

[1] Y. August, Y. Oiknine, M. Abuleil, I. Abdulhalim, and A. Stern, "Miniature Compressive Ultra-spectral Imaging System Utilizing a Single Liquid Crystal Phase Retarder," Scientific Reports 6, 23524 (2016).

[2] Y. Oiknine, I. August, and A. Stern, "Along-track scanning using a liquid crystal compressive hyperspectral imager," Optics Express 24, 8446-8457 (2016).

[3] D. Gedalin, Y. Oiknine, I. August, D. G. Blumberg, S. R. Rotman, and A. Stern, "Performance of target detection algorithm in compressive sensing miniature ultraspectral imaging compressed sensing system", Optical Engineering, 56(4), 041312 (2017).

10427-53, Session PS

Image focusing in the remote sensing problem

Andrei Sushchenko, Far Eastern Federal Univ. (Russian Federation); Igor V. Prokhorov, Institute for Applied Mathematics (Russian Federation) and Far Eastern Federal Univ. (Russian Federation)

Authors study a problem of reconstruction seabed surface based on signal of side-scan-sonar(SSS). The propagation of acoustic waves occurs in the semispace

$G={rin mathbb{R}^3:r_3>-l}$

with inhomogeneous boundary $partial G={yinmathbb{R}^3:y_3=-l}$. Signal propagation in a fluctuating ocean is described by the radiative transfer equation with corresponding initial and boundary conditions[1]. The BC sets of diffusion reflection on $partial G$ with the coefficient $sigma_d$. The source and receiver are located at the same vehicle which moving along path $r=V t$ with constant velocity V, where $V=(0,V,0)$. Thus, authors formulated an inverse problem for determination $sigma_d$ based on signal emitted and received by SSS. Using an assumptions of single-scattering approximation and point-view source authors deduce an a formula for the function $sigma_ d$ which described inhomogeneous boundary $partial G$ [2]:

begin{equation}

label{I_gamma}

I(t)= frac{1}{pi}frac{1}{Delta}frac{1}{2sinbeta}

int limits^{Delta/2}_{-Delta/2}

intlimits^{epsilon}_{-epsilon}

sigma_d(y_1, y_2)

frac{ c I^2 J_i exp (-mu c (t-t_i)) }{ y_1(t-t')|V t'- y |^2 |y -V t||k_2V-c|} dk_2 dt' + I_G(t).

end{equation}

Here, $I(t)$ denotes received signal of SSS, $Delta$ is pulse time-interval and t_i is the median of one, $beta$ is angle of width of directivity pattern, I is altitude, the coefficients mu and c corresponds to attenuation and sound speed. $I_G(t)$ corresponds to volume scattering signal. $V t$ and $V t'$ denote points of receiver and source, correspondingly.

$epsilon=sin{beta} sqrt{1-k_3^2}$

and

$k_3={2Ic(t-t')}/(c^2-V^2)$.

The first integral corresponds to non-impulse source and integrated over pulse time-interval whereas the second one to the width of directivity pattern of the receiving antenna. In paper [3] for solving the inverse problem authors use assumptions such as impulse source and narrow-beam antenna. That approach fetch to objects defocusing on the boundary $partial G$.

In this paper, for determination the function $sigma_d$ authors solve the integral Eq.1 using by discretization method. On the first stage, they make a rectangular grid on $partial G$. In each rectangular $sigma_d$ is set as constant. Hence, the inverse problem is reduced to SLE with sparse matrix which solving by iterative method.

Thus, authors construct the algorithm for focusing objects on the inhomogeneous boundary based on the signal of SSS.

[1] I.V. Prokhorov, A.A. Sushchenko, Studying the Problem of Acoustic Sounding of the Seabed Using Methods of Radiative Transfer Theory, Acoustical Physics, v. 61(3), 368--375 (2015).

[2] I. Prokhorov, A. Sushchenko, Analysis of the impact of volume scattering and radiation pattern on the side-scan sonar images, Proceedings of Meetings on Acoustics, v. 24, 005007 (2015).

[3] E.O. Kovalenko, A.A. Sushchenko, I.V. Prokhorov, textit{Processing of the information from side-scan sonar}, Proceedings of SPIE, v. 10035, 100352C (2016).

10427-54, Session PS

Implementing and validating of pan-sharpeninig algorithms in open-source software

Paúl Pesántez-Cobos, Univ. de Cuenca (Ecuador); Fulgencio Cánovas-García, Univ. Politécnica de Cartagena (Spain); Francisco Alonso-Sarría, Instituto Univ. del Agua y del Medio Ambiente (Spain)

Several approaches have been used in remote sensing to integrate images with different spectral and spatial resolution in order to obtain fused enhanced images. Such techniques have been mostly implemented on proprietary software, which limits the access to them and show also some delay in the adoption of novel statistical tools. On the other hand, in academia, programs with scripting capacity, such as MatLab, Octave or R, are used to implement new techniques to manipulate raster layers.

The objective of this research is three-fold. First, to implement in R three image fusion techniques: High Pass Filter, Principal Component Analysis and Gram-Schmidt; two, the application of these techniques to merge multispectral and panchromatic images from four satellite platforms (QuickBird, IKONOS, Landsat-7 and Landsat-8) and an airborne platform (Project Natmur-08); third, to evaluate the results using a visual comparison and two indices: universal image quality index (Q index) and the ERGAS index (both spatial and spectral), that we also implemented in R. This way, the five algorithms have been made available to the scientific community.

The application of fusion techniques in both R and proprietary software produce equivalent results. Qualitative evaluation reports better results in images with a larger spatial ratio. Landsat-7 and Landsat-8 suffered the greater color distortions using the three fusion methods; in the case of Landsat-7 the distortion was smaller with the HPF method, whereas in the Landsat-8 image it was GS the method with best results. In the QuickBird, IKONOS and Natmur-08 images the results

were better. The application of the indices implemented in this research revealed better spectral scores (Q index and spectral ERGAS) with the HPF fusion in the QuickBird, IKONOS and Landsat-7 images, followed by the GS fusion; whereas in the case of Landsat-8 and Natmur-08 images, the results were much evener. Regarding the ERGAS spatial index, the ACP fusion methods presented a better result for the QuickBird, IKONOS, Landsat-7 and Natmur-08 images, followed closely by the GS method. Only in the case of the Landsat-8 image, the GS method presented the best results. On the other hand, whereas in the evaluation of spectral components HPF results were better and ACP results worse, the opposite results occurred with the spatial components.

Better quantitative results were obtained in Landsat-7 and Landsat-8 with the three fusion methods compared to the QuickBird, IKONOS and Natmur-08 images. This contrasts with the qualitative evaluation reflecting the importance of splitting the two evaluation approaches (qualitative and quantitative), something that has also been reported in previous research.

Significant disagreement may arise when different methodologies are used to asses the quality of an image fusion. Although in this research the results are grouped for the five images used, they indicate that there is greater consistency when an independent evaluation is carried out for each image, not only because of the different characteristics of the sensors, but also because of the different atmospherics conditions or peculiarities of the different study areas, for example.

10427-55, Session PS

Deep convolutional neural networks for airport detection in remote sensing images

Ümit Budak, Bitlis Eren Üniv. (Turkey); Abdulkadir ?ENGÜR, Fırat University Electrical and electronics engineering (Turkey); U?ur HALICI, Middle East Technical University (Turkey)

The first stage of the proposed method aims to locate various candidate airport regions in the input RSI. For this stage, methodology proposed in [5] is applied, where Budak et al. developed an efficient candidate airport region extraction method by improving the Line Segment Detection (LSD) algorithm given in [13]. In the second stage, a popular deep CNN architecture [9] is employed for verification purposes. For this stage the AlexNet architecture was used, which consists of five layers of CNN and three fully-connected layers for largescale image classification [9].

Extensive experiments based on accuracy, sensitivity, and specificity values were conducted in order to evaluate the performance of the proposed scheme. Several experiments were also conducted to compare the performance of the proposed method with previously proposed methods. Experimental results showed that the deep CNN outperforms the previously proposed methods.

10427-56, Session PS

Verification of the test stand for microbolometer camera in accredited laboratory

Michal Krupi?ski, Jaroslaw Barela, Krzysztof Chmielewski, Mariusz Kastek, Wojskowa Akademia Techniczna im. Jaroslawa Dabrowskiego (Poland)

Micro-bolometer belongs to the group of thermal detectors and consist of temperature sensitive resistor which is exposed to measured radiation flux. Bolometer array employs a pixel structure prepared in silicon technology. The detecting area is defined by a size of thin membrane, usually made of amorphous silicon (a-Si) or vanadium oxide (VOx). FPAs are made of a multitude of detector elements (for example 384 x 288), where each individual detector has different responsivity and offset due to detector-to-detector spread in the FPA fabrication process, and additionally can change with sensor operating temperature, biasing voltage variation or temperature of the observed scene. The difference in responsivity and offset among detectors (which is called non-uniformity) additionally with its high sensitivity, produces fixed pattern noise (FPN) on produced image. Fixed pattern noise degrades parameters of infrared cameras like sensitivity or NEDT. Additionally it degrades image quality, radiometric accuracy and temperature resolution.

In order to objectively compare the two infrared cameras ones must measure and compare their parameters on a laboratory test stand. One of the basic parameters for the evaluation of a designed camera is NEDT. In order to examine the NEDT, parameters such as sensitivity and pixels noise must be measured. To do so, ones should register the output signal from the camera in response to the radiation of black bodies at two different temperatures. The article presets an application and measuring stand for determining the parameters of microbolometers camera. Prepared measurements were compared with the result of the measurements in the Institute of Optoelectronics, MUT on a MST test stand by CI SYSTEM. This test stand consists of IR collimator, IR standard source, rotating wheel with test patterns, a computer with a video grabber card and specialized software. The parameters of thermals cameras were measure according to norms and method described in literature.

10427-57, Session PS

A high resolution imaging algorithm for synthetic aperture interferometric radiometers in near-field

Tao Zheng, Fei Hu, Feng He, Xiaohui Peng, Hao Hu, Huazhong Univ. of Science and Technology (China)

Synthetic aperture interferometric radiometers (SAIR), which are fully passive radiation signal receiver working in millimeter wave band most of the time, have been proved powerful instruments for high spatial resolution observation of planetary surfaces. Recently, it is being introduced to human security applications, because human body and prohibited items are quite different in the brightness temperature map and passive mode eliminates security concerns about the damage of radiation to human body. However, the most important problem we face is that the contours and details of prohibited items are blurry in rebuild image by the traditional inversion method, such as inverse fourier transformation method, near-field focusing algorithm (NFA) and moore-penrose method, which makes it difficult to identify prohibited items.

The relationship between visibility function (V) and brightness temperature (T) is no longer fourier transformation in near-field. And the brightness temperature image inversion problem will become more difficult without a doubt. In this study, in order to solve the blurry contour problem in rebuild image, a regularization model based on G-matrix model (V=GT) is proposed by introducing a penalty function. In image processing, the contour can be regarded as a line of marks where the brightness temperature changes sharply. So, the gradient filed of the brightness temperature map is reasonable to quantify the contours. Therefore, the penalty function is represented as a function of gradient of the image. For keeping the contour feature, the penalty function must meet the following two rules: 1) in no contour area, the function shows the characteristic of smooth and isotropic; 2) in contour area, the function is smooth in the gradient direction and rough in gradient orthogonal direction.

At last, an appropriate penalty function has been found. Then according to the regularization model, we can obtain the optimal brightness temperature estimation by iterative method. However, at this point, the question arises on the optimum value of the regularization parameter. The regularization parameter controls the tradeoff between the image noise and sharpening degree. Usually, the regularization parameter is small enough empirically to keep the contour in the image.

Simulation for SAIR is performed to validate the contour enhancement imaging method. A complex scene consisting of many small area with different shape and brightness temperature value corresponding to different prohibited items is created. The different results are displayed with the increase of regularization parameter. And the reconstructed image by proposed method is compared with the results by inverse fourier transformation method, near-field focusing algorithm and moore-penrose method. The proposed method show better image quality.

10427-59, Session PS

The laboratory demonstration and signal processing of the ISAL

Si Gao, Zenghui Zhang, Shanghai Jiao Tong Univ. (China); XianWen Xu, Shanghai Aerospace Electronics Equipment Institute (China); Wenxian Yu, Shanghai Jiao Tong Univ. (China)

An inverse synthetic aperture imaging ladar(ISAL) combines the inverse synthetic aperture technique with coherent laser radar to achieve high resolution, well-focused images. It overcomes the constraint by the diffraction limit of the conventional telescope aperture imaging ladar and improves the imaging quality in terms of azimuth resolution compared to the conventional microwave radar. However, it will introduce many new problems. Similar as ISAR imaging process, the range migration will result in errors both in the envelope and the phase history of the echo. Because the phase error is corresponding to radar wavelength, it is more serious for ISAL than microwave ISAR. The platform vibration in centimeters degree can be ignored for microwave radar, while it can destroy the Doppler phase and then destroy the cross-range focusing for ISAL. The phase errors are also caused by the atmosphere turbulence. In addition, the phase error is usually a high order function of azimuth time and is difficult to be modeled in advance. Thus, the high order phase errors should be compensated by special digital signal processing technique to achieve well-focused images.

This paper presents a coherent inverse synthetic-aperture imaging ladar(ISAL)system to obtain high resolution images. A balanced coherent optics system in laboratory is built with binary phase coded modulation transmit waveform which is different from conventional chirp. A whole digital signal processing solution is proposed both quality phase gradient autofocus(QPGA) algorithm and cubic phase function(CPF) algorithm.

In the complex image domain, each range bin contains many scatterers distributed, i.e. probably including more than one dominant scatterer while no dominant scatterer exists in another range bin. When the least-brightest scatterer in a particular range gate turns out to be of higher intensity as compared to the maximum brightest scatterer of another range gate, the conventional PGA algorithm will be in trouble to deal with the following interferences. Thus, the QPGA is used for our ISAL system. Considering the that the QPGA algorithm have no ability to compensate the linear phase error(even introducing the new linear phase errors), we utilize first order polynomial fitting of the phase gradient to remove the linear phase temporarily for minimizing the effects of linear phase error in phase error estimation. The CPF algorithm is further used to compensate phase error caused by regular mechanical vibration finely.

Some high resolution well-focused ISAL images with retro-reflecting targets at slant range 3 meters away are shown to validate the concepts. The whole digital signal processing technique is used to successfully estimate and remove the pulse-to-pulse phase errors, which proving the robustness of this technique to compensate for unmodeled platform vibration. These images are well focused despite the weak return from circulator power induced backscatter and diffuse surface. It demonstrates that high resolution images can be achieved and the influences from vibrations of platform involving targets and radar can be automatically compensated by the distinctive laboratory system and digital signal process.

10427-60, Session PS

Ground-based automated radiometric calibration system in Baotou site, China

Ning Wang, Chuanrong Li, Lingling Ma, Yaokai Liu, Fanrong Meng, Yongguang Zhao, Academy of Opto-Electronics, CAS (China); Bo Pang, Academy of Opto-Electronics (China); Yonggang Qian, Wei Li, Lingli Tang, Academy of Opto-Electronics, CAS (China); Dongjin Wang, Univ. of Science and Technology of China (China)

As the improvement of temporal, spatial, spectral resolution of the satellite sensor, remote sensing technique becomes a more and more important way to understand the status and changing in both local and global scale. Remotely sensed data has been widely used in environment change, land cover and land use, forest and agricultural application, human activities and healthy and so on. Among all these quantitative researches and applications, how to accurately calibrate the remotely sensed data is one of the primary problems. During the past several decades of years, there are many radiometric calibration methods, including pre-launch laboratory-based, post-launch onboard-based, post-launch vicarious, have been developed. As an important post launch method, vicarious calibration can monitor the change of sensor's performance. Moreover, for the instruments and models used in vicarious calibration can be traced to SI, this method can also build a bridge between the metrology standards and the remote sensor. There is no denying that vicarious calibration method has some drawbacks. The expensive on personal and cost limits the frequency of the in situ experiment. Besides, when using the field instrument, such as the spectrometer, sunphotometer and so on, the personal operations may also introduce some errors in the measurement. These factors leads to the difficulties in improving the accuracy of radiometric calibration.

Just to overcome the mentioned problems, Committee on Earth Observation Satellites (CEOS) Working Group on Calibration & Validation (WGCV) Infrared Visible Optical Sensors (IVOS) subgroup has proposed an Automated Radiometric Calibration Network (RadCalNet) project in 2014. The rationale for this project is to provide reference top-of-atmosphere (TOA) reflectance spectra over several instrumented sites for the radiometric calibration and radiometric monitoring of optical sensors onboard Earth Observation satellites. Baotou site, which is managed by Academy of Opto-Electronics, CAS, is one of the four demonstration sites of RadCalNet. The superiority characteristics of Baotou site is the combination of various natural scenes and artificial targets. The main targets for automated radiometric calibration is a three-gray-level permanent targets, which are paved by gravels with different reflectance, nominally 8%, 20% and 60%, respectively. The targets is distributed as a chess box. Each single target has a size of 48m?48m. To perform the automated calibration, the site is equipped with automated sunphotometer (CIMEL CE 318) and meteorological station to observe the basic atmospheric parameters. Besides, in each target, an automated spectrum measurement instrument is developed to obtain the surface reflected radiance spectra every 2 minutes with a spectrum resolution of 2nm. According to the requirement of RadCalNet interface, a surface reflectance spectrum retrieval method has been developed to generate the standard input files to RadCalNet. Then the TOA reflectance spectra can be derived from the input files. In order to solve the problem of adjacent effect due to the limited size of targets, an adjacent-effect-correction method has also been proposed. Now, the whole automated radiometric calibration system has provided products nearly one year. The results of the demonstration satellites, including Landsat 8, Sentinal-2A, show that the overall accuracy can be within 5%.

10427-61, Session PS

Adaptive RANSAC approach for building roof planes extraction from lidar point cloud

Aluir P. Dal Poz, Michelle Sayuri Yano, Univ. Estadual Paulista "Júlio de Mesquita Filho" (Brazil)

Building extraction methods are important in the context of capturing and updating spatial data for applications that involve urban areas. For example, accurate and reliable building roof boundaries are useful in applications that involve real estate, large-scale mapping, and risk management. However, automated building roof extraction has remained a challenging task, mainly due to the varying building roof configurations, the varying neighborhood contexts, and noise in the input data. This paper proposes a method for extraction of buildings roof planes from Light Detection and Ranging (LiDAR) data. The proposed method is based on two main steps: the extraction of building roof boundaries; and the extraction of roof planes within regions delimited by the building roof boundaries previously extracted. The first step aims at avoiding the exhaustive search for planar roof faces throughout the LiDAR point cloud, which in turn helps to reduce the computational effort and to increase the reliability of the roof plane extraction process. The extraction of polylines that represent building roof boundaries from LiDAR data is accomplished as follows. First, the original LiDAR point cloud is submitted to the progressive filtering algorithm for getting ground and non-ground points. These two sets of points allow the generation of a Digital Surface Model (MDS) and a Digital Terrain Model (MDT). Second, a normalized Digital Surface Model (nDSM) is computed by subtracting the MDT from the MDS. Third, taking into account that building roof points are found at certain height above the ground, points below a height threshold (e.g., 2.5 m) are eliminated from the nDSM. Fourth, the Axelsson classification algorithm is applied to the resulting nDSM to classify the aboveground objects into two classes: vegetation and building roofs. Next, the region-growing algorithm is applied to building roof points to group them into roof segments, taking into account the proximity criterion. Finally, the convex hull algorithm is used for computing polylines that represent boundaries of building roofs. The second step consists in extracting roof planes within regions delimited by the building roof boundaries previously extracted. We use the RANdom SAmple Consensus (RANSAC) algorithm to detect roof plane points, tanking into account two parameters for checking the consistence of LiDAR building points with candidate planes: the distance between LiDAR building points and candidate planes; and the angle between the gradient vectors at LiDAR building points and the candidate planes' normal vector. Each LiDAR building point is classified as consistent if computed parameters are below corresponding thresholds, which are automatically determined by thresholding histograms constructed for both parameters. As the RANSAC algorithm can generate fragmented results, a post-processing is accomplished to merge planes that are approximately collinear and spatially close. The proposed method has been evaluated by using a LiDAR point cloud at approximately 8 pts./m2 density. The results obtained in the experimental evaluation showed that the method works properly in the task of extracting building roof planes. The evaluation of the obtained results has been carried out using the completeness and correctness quality parameters, and both are around 93% in average.

10427-62, Session PS

Supervised classification of remotely sensed images using Bayesian network models and Kruskal algorithm

Radja Kheddam, Youcef Boudissa, Aichouche Belhadj-Aissa, Univ. des Sciences et de la Technologie Houari Boumediene (Algeria)

One of the most investigated problems in remote sensing is image classification which is used with the purpose of detecting land use and land cover in several practical applications, such as, land inventory, vegetation monitoring, management of natural resources, etc. Classification approaches are many; they can be based on a theoretical mathematical concept, such as probability theory, evidence theory, possibility theory, etc., as they can be inspired by a natural phenomenon observed in the real world, such as neural stimulation, genetic selection, immune response, swarm intelligence, etc. Based on Bayes theory and the probability foundations, Bayesian networks (BNs) are modern classifiers and become the vehicle of choice in many artificial intelligence applications. BNs are graphical models that encode probabilistic relationships among variables of interest. They have not only advantages of probabilistic models as the factorization of the joint probability distribution of the variables, but also, they provide additional benefits from their graphical representation which encodes dependencies among all variables and then handles situations where some data entries are missing. The aim of this work is to present and compare the performances of three Bayesian networks widely used for multispectral image supervised classification. Developed networks structures are constructed due to Kruskal algorithm which allows the determination of the maximum weight spanning tree by using the mutual information between the attributes. These structures provide the reduction of unnecessary redundancy that can improve the classification result. We started by the Bayesian naive classifier (BNC), which assumes that there is no dependency, between the pixel attributes to classify. The BNC seems as the exact opposite of the classical probabilistic classifier which takes into account by its covariance matrix of all existing correlations between the variables. Thereafter and to relax the strong assumption of independence between the attributes imposed by the BNC, we tested the tree augmented naïve Bayes classifier (TANC) where each feature variable has at most one feature variable as parent, and the forest augmented naïve Bayes classifier (FANC) where each attribute forms an arbitrary graph rather than just a tree. Performances of the three classifiers are evaluated using two multispectral images. The first one represents a north-eastern part of Algiers acquired by the Algerian satellite Alsat-2A (2010) and the second one covers the region of Moffett Field located at the extreme west of the United States of America, acquired by the American Airborne AVIRIS (1997). The aim of choosing these two images is to evaluate the structure classifier complexity according to the number of attributes (04 and 10 spectral bands for the two images respectively). Obtained results are quantitatively compared with state-of-the art competitor, namely, the SVM (support vector machines). Classified images by TANC and FANC achieved higher accuracies (especially when the number of attributes increases) than other classifiers including SVM in terms of the overall accuracy and kappa coefficient. It is concluded that the choice of attributes dependencies significantly contributes to the discrimination of subjects on the ground. Thus, Bayesian networks appear as powerful tool for multispectral and hyperspectral image classification.

10427-64, Session PS

Progressive sample processing of band selection for hyperspectral imagery

Keng-Hao Liu, Hung-Chang Chien, National Sun Yat-Sen Univ. (Taiwan); Shih-Yu Chen, National Yunlin Univ. of Science and Technology (Taiwan)

Remote sensing imaging has been used in various applications including geology, agriculture, mineral mapping, land cover classification, chemical defense, law enforcement and military defense. Nowadays, the most popular remote sensed image system in remote sensing community is hyperspectral imaging (HSI). Among all the topics of hyperspectral image processing, Band selection (BS) is one of the most important topics. The objective of BS is to find a set of representative bands that can represent the whole image with lower inter-band redundancy. Then the subsequent processing such as image analysis, compression, or storage can be carried on.

Many types of BS algorithms have been proposed in the recent years. However, most of them belong to "Off-line" methods. It means that the algorithms can only be implemented on the collected data. Those off-line methods are sometime useless since many HSI applications are timeliness, particular in disaster prevention and target detection. To tackle this issue, a new concept, called Progressive Sample Processing (PSP), was proposed recently. The core concept of PSP is that it is an "On-line" framework where the specific algorithm can process the currently collected data during the data transmission under band-interleaved-by-pixel/sample (BIS/BIP) protocol. In other words, it progressively processes the data and can show/update the temporary results through the pixel transmission.

This paper proposes a new BS method that integrates a sparse-based BS method into PSP, called PSP-BS. In PSP-BS, the BS can be carried out by updating BS result recursively pixel by pixel in the same way that a Kalman filter does for updating data information in a recursive fashion. More specifically, we use the self-sparse model to select the representative bands where the orthogonal matching pursuit (OMP) is used to solve the regression problem. In order to perform more efficiently, we adopt two least-square updating procedures to avoid duplicate computation when receiving new pixels. The experiments conducted on two real hyperspectral datasets show that the PSP-BS can progressively output the BS status with reasonable computing time. In addition, we design several pixel sampling methods and compare their convergence properties during BIP/BIS transmission. The experiments also show that using appropriate pixel sampling method will accelerate the algorithm and achieve higher BS consistency. Compared to traditional BS methods, the newly developed PSP-BS algorithms have potential to fulfill real-time applications. We are convinced that such achievements can push ahead with the progress of the related researches in remote sensing community.

10427-65, Session PS

Evaluation of feature extraction and descriptor calculation methods for automatic georeferencing of Philippines' first microsatellite imagery

Jerine A. Amado-Dasallas, Benjamin Joseph D. Jiao, Julius Noah H. Sempio, McGuillis Kim F. Ramos, Romer Kristi D. Aranas, Ayin M. Tamondong, Mark Edwin A. Tupas, PHL-Microsat, Univ. of the Philippines Diliman (Philippines)

This work focuses in the evaluation of FAST feature detection, SIFT descriptor extraction, and improvement of matching methods using RANSAC applied to automatic georeferencing of incoming DIWATA-1 Spaceborne Multispectral Imager and High Precision Telescope images. Group A of the SMI and HPT images are same scene images of varying bands, specifically near-infrared, red, blue, and green. Group B are five scenes captured sequentially. After the automatic georeferencing, the images of Group A are stacked while images of Group B are stitched. Two images are matched. The first, the master image, contains the correct geographic information to be transferred to the second, slave image. Features from Accelerated Segment Test (FAST) algorithm detects corners or keypoints in an image. These robustly detected keypoints have well-defined positions. FAST is a high-speed corner detection method introduced by Rosten and Drummond (2006). Unlike other feature detection methods, it allows the use of feature points in real-time without compromising the feature quality. This was done by using machine learning to classify patches in the image as corners or non-corners. Even in the change of perspective and feature types, this method is repeatable. The interest points or keypoints extracted serves as tie points between the master image and slave image.

Before the images can be matched, descriptors need to be assigned to their keypoints. The descriptors are computed using the Scale-Invariant Feature Transform (SIFT) descriptor extractor, a popular method introduced by Lowe (1999, 2004). A corner or a keypoint's SIFT descriptor is a 3-D elementary feature vector. The pixel location and the gradient orientation forms the 3D spatial orientation histogram with 36 bins covering 360o. For the OpenCV implementation used in this study, a 16x16 neighbourhood around the keypoint is taken which is then divided into 16 sub-blocks of 4x4 size. For each sub-block, 8 bin orientation histogram is created so that a total of 128 bin values are available represented by a vector, forming the descriptor. Finally, the vector is normalized to cancel the effect of contrast change, making the descriptor invariant to changes in illumination.

Keypoints are matched based from their descriptor vector. Nearest-neighbor matching is employed based on a metric distance between the descriptors. The metrics include Euclidean, Minkowski, and city block, among others. The closest are returned. From previous test by Kouyama et al. (2017), rough matching outputs not only the correct matches but also the faulty matches. The latter work incorporates a geometric restriction to the keypoints to improve the matching. In this work, we applied a simplified version of the learning method. RANSAC was used to eliminate fall-out matches and ensure accuracy of the feature points. This method identifies if a point fits the transformation function and returns inlier matches. The transformation matrix was solved by Affine, Projective, and Polynomial model. The DIWATA-1 images were also matched with other satellite images to test the sensor-invariance of the FAST-SIFT combination. Accuracy of the automatic georeferencing method were determined by calculating the RMSE of interest points, selected randomly, between the master image and transformed slave image.

10427-66, Session PS

Subaperture analysis to measure directivity and isotropy in pol-CSAR

Fei-Teng Xue, Univ. of Chinese Academy of Sciences (China); Yun Lin, Institute of Electronics, Chinese Academy of Sciences (China); Bingchen Zhang, Institute of Electronics, Chinese Academy of Sciences (China); Wenjie Shen, Yue Zhao, Univ. of Chinese Academy of Sciences (China); Wen Hong, Institute of Electronics, Chinese Academy of Sciences (China)

Polarimetric synthetic aperture radar (pol-SAR) polarimetry obtains polarimetric scattering of interesting targets when platform takes a straight, circle or other flight track. The scattering properties of interesting targets are usually considered as invariant in azimuth. In some new SAR system, such as wide-angle SAR and circular SAR (CSAR), targets are illuminated longer and look angle changes a lot. Some targets have different physical shape in different look angle. Thus complex targets can no longer be considered as having invariant scattering properties in azimuth. In fact, angle information provided by new SAR system should be considered as useful and can help to describe scattering properties of interesting targets. With enough angle information, precise description of complex target is now possible to achieve. Directivity and isotropy are important features when angle information is available. In this paper, sub-aperture analysis and polarimetric entropy are used to measure directivity and isotropy. Targets are classified into three classes based on measurement. One is targets with strong directivity. This means targets have strong scattering only in one direction. One is isotropic targets. This means targets have one certain scattering mechanism in several or all directions. One is targets with neither strong directivity nor isotropy. This means targets have random scattering mechanisms in any directions. In our method, pol-CSAR data is divided into sub-apertures in order to achieve scattering properties in different look angle. Target vector is extended into this multi-aperture situation. Covariance matrix in multi-aperture situation can then be calculated. Polarimetric entropy in multi-aperture situation can be calculated by eigen-decomposition of the covariance matrix. When targets have strong directivity, scattering power in that direction is high, which causes low value of polarimetric entropy in multi-aperture situation. Therefor polarimetric

entropy in multi-aperture situation can measure directivity. Isotropic targets have similar polarimetric entropy in sub-apertures that have same certain scattering mechanism. The values are usually low. In other sub-apertures, the polarimetric entropy is different and usually high. Calculate the polarimetric entropy of all sub-apertures and find the pattern raised above can identify isotropic targets. Useful information of targets with strong directivity is mainly from sub-apertures in strong scattering direction. For targets with strong directivity, coherent integrate sub-apertures in strong scattering direction instead of all sub-apertures. For isotropic targets, sub-apertures with same scattering mechanism may not neighbor, so coherent integration is not suitable. Incoherent integration is a better choice. For targets with neither directivity nor isotropy, coherent integrate all sub-apertures. Targets with strong directivity are enforced and isotropic targets become more distinct by this method. The effectiveness of the method is demonstrated on polarimetric CSAR(pol-CSAR) data, acquired by the Institute of Electronics airborne CSAR system at P-band

10427-67, Session PS

Small real time detection satellites for MDA using hyperspectral images

Daiki Nakaya, Hiroki Yanagida, Happy Science (Japan); Shin Satori, Happy Science (Japan); Tomonori Ito, Yusuke Takeuchi, Hokkaido Satellite Co., Ltd. (Japan)

Hyperspectral Images are now used in the field of agriculture, cosmetics, and space exploring. Behind this fact, there is a result of efforts to contrive miniaturization and decreasing in costs. This paper describes low-cost and small hyperspectral camera (HSC) under development and a method of utilizing it. Real Time Detection System for MDA is that government agencies put those cameras in small satellites and use them for MDA (Maritime Domain Awareness). MDA is required for national defense and disaster prevention especially in Japan. We assume early detection of unidentified floating objects to find out disguised fishing ships and submarines. For the analysis, there is one of the famous anomaly detections called Reed-Xiaoli Detector (RXD). RXD is considered as the inverse operation of principal component analysis (PCA). The preliminary experiment had done with a small helicopter instead of a satellite. Consequently, all objects including a person who put on a life jacket, a ship, and a buoy are recognized. In regards to HSC, it was successful to invent a small-size and light hyperspectral camera. It is of course possible to load on a satellite. In addition to that, the imaging performance satisfied the requirement as the mission equipment. MDHU makes it possible to process the large-volume data like hyperspectral data in the satellite. In MDHU, hyperspectral data is collected by the Backside Irradiation-type CMOS Image Sensor and transferred rapidly by FPGA and memorized into SSD at last. Then, the data is sent to the onboard computer (OBC) of the satellite by Space Wire/RMAP and downlinked into a ground station by laser communication. For the data transmission, laser communication is used. The experiment of the laser communication was successful when the distance between the transmitter and the receiver was 15km. In addition, total dose experiments of the CMOS sensor, SH2, and SSD were performed in Komazawa branch of Tokyo Metropolitan Industrial Technology Research Institute. As the result of the total dose experiment, there was no sign of deterioration of the CMOS sensor at 22.5krad (corresponds to 7.5 years in polar orbit). On the other hand, there is concern that SSD and FPGA may be out of order because of the current destruction by the dose effect in 7.1 years and in 8.4years respectively. The SH2 and the SSD are durable enough to fly through space. By employing 10 or more this satellites, Japan can perform MDA for Japanese territorial sea in real time.

10427-68, Session PS

Remote sensing applied to terrestrial laser scanner surveys, case study walls paintings of the Sant Miquel chapel

Juan Manuel Corso Sarmiento, Josep Roca Cladera, Felipe Buill Pozuelo, Univ. Politècnica de Catalunya (Spain)

This article proposes a methodology to optimize Terrestrial Laser Scanning (TLS) survey as 2D and 2.5D images, as layers or information, using Remote Sensing operations to find pathologies or representative elements of the heritage site. These processes were carried out on the mural paintings of the Sant Miguel del Real Monasterio de Pedralbes (about the year 1300).

In these paintings, three processes have been carried out: analysis of deformations, processes of digital illumination and classification of materials. The analysis of deformations allows to identify spalling and cracks of wall paintings. The processes of digital lighting allow to see the relief of the surface, emphasizing the techniques used in the elaboration of the murals, as it is the use of compass, rule, among others. The base object classification of the paintings allows a preliminary distinction between materials, in this case study, the fresco and secco painting techniques are identified, being indispensable a chemical study to concretize this classification, identifying the limitations of this technique given the historical complexity of the paintings.

All this to guarantee the ideal conditions for its conservation and safeguard the perdurability of the murals paintings.

10427-69, Session PS

Unsupervised hyperspectral image classification using spectral unmixing and spatial filtering

Mohammad Hoshyar Moghadam, Shahid Bahonar Univ. of Kerman (Iran, Islamic Republic of); Azam Karami, Shahid Bahonar Univ. of Kerman (Iran, Islamic Republic of) and Univ. Antwerpen (Belgium)

Hyperspectral Image Classification using Spectral Unmixing and Spatial Filtering

Recently hyperspectral classification has gained particular attention in many practical applications such as weather forecasting, geology, agriculture and etc. Two main types of classification algorithms are supervised and unsupervised methods. In supervised classification, the ground truth of HSI is required. Many supervised algorithms randomly select some pixels for training and remaining pixels for testing. However in some applications, the ground truth is not available. Therefore in this paper we introduce a new unsupervised classifier for HSI by using spectral unmixing. In contrast with supervised methods, our method does not require any training set for classifiaction, while this algorithm uses the reflectance properties of HSI. Hyperspectral dataset has high spectral and low spatial resolutions. Therefore, it includes mixed pixels which means that the value of each pixel is composed of some pure pixels (endmembers). So in our proposed method, first the number of endmembers is approximated using hyperspectral signal subspace identification by minimum error. Second, the endmember matrix is calculated using vertex component analysis. Third, fully constraint least square unmixing is applied and the abundance fraction matrices are extracted. Forth, hyperspectral images are usually affected by different type of noises due to sensor limitations. Therefore, in order to reduce the noise effect and improve the classification accuracy, a spatial filtering is then applied to the abundance maps. Fifth, the abundance maps are clustered with K-means algorithm. In K-means clustering, we should fix the number of clusters. In the proposed method, the number of clusters and the number of endmembers are not similar. Because the endmembers are the

chemical species which exist in HSI, such as water, vegetation and etc. A cluster can contain a single or mixture of different endmembers, therefore the cluster number is usually higher than the endmember number. The number of the clusters can be automatically defined by some algorithms such as Krzanowski and Lai's method. Finally, the classification map is calculated.

In order to validate the efficiency of the proposed algorithm, real HSI datasets are used. The obtained classification results are compared with some state-of-the-art classification algorithms.

10427-70, Session PS

A modified four components decomposition method using C band PolSAR DATA

Houda Latrache, Mounira Ouarzeddine, Univ. des Sciences et de la Technologie Houari Boumediene (Algeria)

Polarimetric target decomposition is a useful technique for POLSAR information extraction. The main purpose of target decomposition is to decompose the polarimetric data (scattering matrix, covariance or coherency matrix) into sum of scattering mechanisms, each one corresponding to a certain physical meaning. Many decomposition algorithms have been proposed, these approaches show good application potential for terrain classification and natural disaster evaluations. Incoherent decompositions can be classified as two main categories, eigenvalue-eigenvector based and model-based methods. Models-based decompositions are the most used, because they are directly related to the physical scattering mechanisms. The most commonly used are Freeman and Yamaguchi methods. Freeman decomposition divides the covariance matrix into three types of scattering components: volume scattering obtained by the vegetation canopy, double bounce scattering from buildings and artificial structures, odd-bounce components from Bragg surface scattering. Yamaguchi add a helix scattering components to Freeman decomposition, in order to establish a four component scattering model. Helix scattering can characterize the scattering from complex structure in build up areas. However, these decomposition methods adopting fixed scattering model are not adaptive to the directional scattering features. These models caused scattering mechanisms ambiguity. The orientation angle also affects the decomposition results because it increases the HV component, which causes the overestimation of volume scattering in urban regions.

This paper intends to enhance the decomposition results in build up areas which suffer from scattering ambiguity. For that, we propose to modify the Yamaguchi four components decomposition method with the extended volume model .Where we introduce the correlation between the circular components RR and LL to the Yamaguchi decomposition scheme, in order to affect to every pixel of the image its appropriate volume model. The correlation coefficient between the two circulars components RR and LL is not affected by the orientation angle; since the circular polarization components are roll invariant. This parameter was chosen because it gave high values in case of artificial structures such us build up area, and it gave low values in forest area. The correlation between RR and LL can be used to distinguish the urban from the forest area, because this coefficient is directly related to the urban structures. In the modified method, the volume scattering model is selected adaptively using the correlation coefficient. To test the performance of the proposed method, two PolSAR images acquired in C-band by RADARSAT-2 satellite over the El Hamiz city in Algeria and San Francisco Bay were used.

The results were compared with the original Yamaguchi and the modified Yamaguchi four components with a stochastic distance (Y4OSD) methods, it is shown that the proposed decomposition overcomes the scattering mechanism ambiguity between forest and oriented built-up areas, since it identifies successfully the oriented buildings as double or odd bounce, while keeping the volume scattering dominant for the forest.

To evaluate the results, we selected small patches in build up and vegetation areas from the obtained results. The scattering contribution of each scattering components was extracted in order to highlight the enhancement of the decomposition results using the proposed method.

10427-72, Session PS

Analysis of the SNR and Sensing Ability of Different Sensor Types in a LIDAR System

Gyudong Choi, Bongki Mheen, Hong Seok Seo, Munhyun Han, Electronics and Telecommunications Research Institute (Korea, Republic of)

LIDAR systems use sensors to detect reflected signals. The performance of sensors affects the performance of LIDAR systems. The number and size of the sensors also determine the FOV (field of view) and resolution of the systems.

The resolution of the array type sensor is determined according to the number of arrays. In this type of sensor, there are limitations to increasing the number of arrays, such as complexity, cost, and size. Another type of sensors use multiple single channel. A single channel detects a point where is indicated by a laser point. This type of sensor requires several pairs of sending and receiving modules to improve resolution. Therefore, there is a problem of size to be applied to a high-resolution system.

In this paper, we present a method to overcome these limitations and improve the performance of the LIDAR system. ETRI developed a kind of scanning LIDAR system which called STUD (static unitary detection) LIDAR system. It has been developed to solve the problems of the above-mentioned other type sensors. The STUD LIDAR system can use a variety of sensors without any limitation on the size and the number of sensors unlike other LIDAR systems so, the LIDAR system is an optimal system to perform this research. We analyze the performance according to the type of sensor and propose a sensor type that can improve the sensing performance.

10427-73, Session PS

Estimating the number of endmembers in hyperspectral imagery using accumulated convex hull vertex and similarity measure

Kang-Pei Wu, Hong-Chao Teng, Tungnan Univ. (Taiwan); Jee-Cheng Wu, National Ilan Univ. (Taiwan)

The key to successful spectral un-mixing is indicating number of endmembers and their corresponding spectral signatures. Nevertheless, correctly estimate the number of endmembers without a priori knowledge is a very hard task because pixels in a hyperspectral image are always contain a mixture of the several reflected spectra. Currently, Noise Whitened Harsanyi, Farrand, and Chang (NWHFC) and hyperspectral signal subspace identification by minimum error (HySime) are two well-known eigenvalue-based methods for estimating the number of endmembers. However, in practice, because NWHFC requires fixing the false-alarm probability and HySime needs estimate noise of each spectral band, the two methods may be computationally very expensive.

In this paper, assuming endmembers in a hyperspectral image can be modeled by convex geometry. We propose a three-stage process to estimate the number of endmembers. At the first stage, an anomaly algorithm is used to remove outlier pixel vector. At second stage, based on the fact that all the observed pixel vectors lie in a convex hull, a successive endmember extraction algorithm (EEA) is used to obtain accumulated vertex at different dimensional convex hulls. At the third stage, the processing includes two steps. In step 1, remove duplicate vertex. In step 2, based on the predefined angle, remove

similarity vertex using spectral angle mapper (SAM) measures.

Finally, the proposed method is applied to synthetic hyperspectral data and real AVIRIS and HYDICE hyperspectral data for estimating the number of endmembers. The results demonstrate that the proposed method can be used to estimate more reasonable and precise number of endmembers than the two published methods.

10427-74, Session PS

Research of generalized wavelet transformations of Haar correctness in remote sensing of the Earth

Maretta Kazaryan, Financial Univ. under the Government of the Russian Federation (Russian Federation); Mihail Shakhramanyan, Researching Institute "AEROCOSMOS" (Russian Federation); Roumen Nedkov, Space Research and Technology Institute (Bulgaria); Andrey Richter, Researching Institute "AEROCOSMOS" (Russian Federation); Denitsa Borisova, Nataliya Stankova, Iva Ivanova, Mariana Zaharinova, Space Research and Technology Institute (Bulgaria)

In this paper, Haar's generalized wavelet functions are applied to the problem of ecological monitoring by the method of remote sensing of the Earth. We study generalized Haar wavelet series and suggest the use of Tikhonov's regularization method for investigating them for correctness. In the solution of this problem, an important role is played by classes of functions that were introduced and described in detail by I.M. Sobol for studying multidimensional quadrature formulas and it contains functions with rapidly convergent series of wavelet Haar.

A theorem on the stability and uniform convergence of the regularized summation function of the generalized wavelet-Haar series of a function from this class with approximate coefficients is proved.

The article also examines the problem of using orthogonal transformations in Earth remote sensing technologies for environmental monitoring. Remote sensing of the Earth allows to receive from spacecrafts information of medium, high spatial resolution and to conduct hyperspectral measurements. Spacecrafts have tens or hundreds of spectral channels. To process the images, the device of discrete orthogonal transforms, and namely, wavelet transforms, was used.

The aim of the work is to apply the regularization method in one of the problems associated with remote sensing of the Earth and subsequently to process the satellite images through discrete orthogonal transformations, in particular, generalized Haar wavelet transforms.

General methods of research. In this paper, Tikhonov's regularization method, the elements of mathematical analysis, the theory of discrete orthogonal transformations, and methods for decoding of satellite images are used.

Scientific novelty. The task of processing of archival satellite snapshots (images), in particular, signal filtering, was investigated from the point of view of an incorrectly posed problem. The regularization parameters for discrete orthogonal transformations were determined. The article deals with the solution of the problem associated with increase of the efficiency of the appliance of digital images filtration methods for storing and further processing of images, stored in image archives.

The results of the experiment are given where, using the example of the problem of Wiener filtering of space images that are located in the database, the Tikhonov regularization method for generalized wavelet-Haar series is confirmed and their comparison with Fourier and Walsh transforms is also represented.

The errors of the noise-filtered signal reconstruction with regularization and without regularization are obtained. From these estimates it follows that the signal reconstructed with the help of the Tikhonov regularization method is closer to the original signal than the signal reconstructed without the use of the regularization method. The experiment was carried out with considering the features of space images during their modeling.

10427-76, Session PS

Multisource data fusion for documenting archeological sites

Vladimir A. Knyaz, GosNIIAS (Russian Federation); Alexander G. Chibunichev, Moscow State Univ. of Geodesy and Cartography (Russian Federation); Denis V. Zhuravlev, State Historical Museum (Russian Federation)

The quality of archeological sites documenting is of great importance for cultural heritage preserving and investigating. The progress in developing new techniques and systems for data acquisition and processing creates a great basis for achieving a new quality of archeological sites documenting and visualization. Possibility of using huge amount of data of different types and of different nature is some kind of challenge for developing new approaches and algorithms of information retrieving and understanding.

Archeological data has some specific features which have to be taken into account when acquiring, processing and managing. First of all it is a needed to gather as full as possible information about findings providing no loss of information and no damage to artifacts. So the most powerful and convenient means which satisfy this requirement is remote sensing technologies.

A novel approach to archeological data acquiring and fusion is presented. It combines a set of photogrammetric techniques for obtaining geometrical and visual information at different scales and detailing and new approach for archeological data analysis, fusion and presenting. The whole archeological site is concerned as an unified cluster containing a set of objects which have relations between each other of different level of correlation. So when acquiring data it is important to take into account all information about every artifact such as position in reference coordinate system, orientation, relative position in a group of artifacts, level of cultural layer etc.

So a set of data acquisition techniques is developed for capturing different types of information. At the most common level aerial imaging by UAV-based digital camera is performed for obtaining 3D model of the whole archeological site. A geodetic support performed by standard techniques and satellite imagery are used for accurate geo-referencing. The UAV imagery is processed by original software which implements original technique for photorealistic 3D reconstruction of the site. At the next level of data acquisition 3D scanning techniques are used for generating accurate 3D models of artifacts and detailed 3D models of environment. Also a set of high resolution color images is acquired for photorealistic presentation of the 3D models. To provide accurate positioning of finding relatively reference coordinate system special coded targets are used. This approach allows to combine all data in unified archeological information model with the possibility of expanding with the new sets and new types of data.

Several novel techniques are developed for automation of registration procedure, for shape and texture analysis of found artifacts. The automation for registration of multi-scale data is based on using coded targets which allow automatically to detect and identify the reference points for transformation into one reference coordinate system. Also an technique for automated registration based on detection given shapes in multi-scale data is evaluated.

The proposed approach is applied for documenting of Bosporus archeological expedition of Russian State Historical Museum. The results of its evaluation on real data approve the accuracy of developed algorithms and demonstrate high visual quality of produced 3D models.

10427-77, Session PS

Ensemble learning for spatio-temporal rice area mapping using Landsat 8 satellite data

Jayantrao D. Mohite, Tata Consultancy Services Ltd. (India); Suryakant Sawant, Indian Institute of Technology Bombay (India); Gajanan Kothawade, Savitribai Phule Pune Univ. (India); Srinivasu Pappula, Tata Consultancy Services Ltd. (India)

Rice is one of the major food sources for many regions of the world especially in the monsoon Asia and accounts for more than 11% of the global cropland. Accurate, on-time and early information on spatial distribution of rice would be useful for stakeholders (cultivators, fertilizer/pesticide manufacturers and agricultural extension agencies) to effectively plan supply of inputs, market activities also government agencies can plan and formulate policies regarding food security. Methods of manual surveying for developing spatio-temporal crop datasets are very costly and time consuming as compared to information generated through remote sensing. Researchers have reported the use of satellite based remote sensing time series observations effective for rice area mapping. However, it is difficult to utilize time series based methods for the early season crop acerage estimation. The key contribution of this work is rice area mapping using ensemble learning method on remote sensing observations for year 2014 to 2017. Cloud free post-monsoon cropping season (locally called Rabi season spanning between January to May) is considered for rice area mapping in major rice growing region, Barddhaman district of West Bengal, India. In this study we have attempted to use early season single date images to provide crop acreage estimates. Literature suggests Land Surface Water Index (LSWI) is higher than Normalized Difference Vegetation Index (NDVI) for rice than non-rice areas during rice transplanting period; images considered for the study are within 10-15 days after transplanting of rice. The indices such as NDVI, LSWI and Tasseled Crop Transformation components (TCT) viz. Brightness (BR), Greenness (GR), and Wetness (WT) were estimated for Landsat 8 sensor observations. Slope estimated from ASTER DEM has been used as one of the features along with estimated vegetation indices for mapping rice areas. Initially individual machine learning algorithms such as Random Forest (RF), Support Vector Machine (SVM) and Naive Bayes (NB) were used for rice area classification. Stratified random sampling has been used for accuracy assessment of the classified map. Results depicts that RF performs best with average classification accuracy of 88.48% followed by SVM (84.67%) and NB (78.11%). Further, we have also carried out model ensemble where the predictions from any two models have been stacked (referred as Model Stacking) in each iteration and given as an input to the Gradient Boosting Machine (GBM) for further training. This way, the performance of three different models ensembles viz. RF-SVM, RF-NB and SVM-NB was compared. It has been observed that model ensemble of RF and SVM performs best among all ensemble models with average classification accuracy of 89.21% (Improvement of 0.8183% than individual RF model).

10427-78, Session PS

Multispectral image enhancement processing for microsat-borne imager

Jianying Sun, Zheng Tan, Qunbo Lv, Linlin Pei, Academy of Opto-Electronics, CAS (China)

With the rapid development of remote sensing imaging technology, the micro satellite, one kind of tiny spacecraft, appears during the past few years. A good many studies contribute to dwarfing satellites for imaging purpose, including SkyBox, Shanghai Engineering Center for Microsatellites, and so forth. Generally speaking, micro satellites weigh less than 100 kilograms, even less than 50 kilograms, which are slightly larger or smaller than the common miniature refrigerators. However, the optical system design is hard to be perfect due to the satellite room and weight limitation. In most cases, the unprocessed data captured by the imager on the microsatellite cannot meet the application need. Spatial resolution is the key problem. As for remote sensing applications, the higher spatial resolution of images we gain, the wider fields we can apply them. Consequently, how to utilize super resolution (SR) and image fusion to enhance the quality of imagery deserves studying.

With an ideal sensor, we would have high-resolution color images. Unfortunately, due to spatial decimation, we only have sequent multi-frame multispectral (MS) images and panchromatic images without ideal spatial resolution. SR reconstruction is a capable way to enhance the spatial resolution of panchromatic data, whilst image sharpening is a feasible way to enhance MS imagery's quality.

Our team, the Key Laboratory of Computational Optical Imaging Technology, Academy Opto-Electronics, is devoted to designing high-performance microsat-borne imagers and high-efficiency image processing algorithms. Recently, Shanghai Engineering Centre for Microsatellites launched an experimental science microsatellite. The carried imager, designed by our team, could provide MS data and panchromatic data simultaneously.

This paper proposed a strategy to realize microsat-borne MS image's enhancement without high-resolution panchromatic image. The only tested data are a serious of same-resolution panchromatic images and MS images. We combined SR technique and a hybrid image sharpening algorithm to achieve the results. Specifically speaking, the strategy utilizes the redundancy of successive information to achieve SR in panchromatic images. Then we fuse the panchromatic image and multispectral image via PCA transformation and wavelet fusion, aiming at enhancing the spatial resolution and reducing the spectral distortion. The experiments designed for the microsat-borne sensors, illustrate that the proposed strategy is feasible and performs well under real on-orbit microsatellite platform. On the aeronautic or astronautic platform, we can easily obtain the multi-frame MS image and the corresponding panchromatic image with the same resolution. Therefore, the proposed strategy can be widely used in remote sensing field.

10427-79, Session PS

Evaluation of different image processing methods in the context of an image registration framework

Stefan Brüstle, Fraunhofer-Institut für Optronik, Systemtechnik und Bildauswertung (Germany)

Imagery acquired by airborne sensors is used to address many different tasks in various fields of application. Many of those tasks require the imagery to be georeferenced, i.e. providing a relation between the image coordinate of an image pixel and the real world coordinate of the location on the earth's surphase it represents. The georeference of airborne imagery is usually implemented via GPS and INS sensors on board the sensor platform, but potential problems such as transmission problems, jamming or temporal sensor malfunction together with a potentially poor knowledge of ground elevation can render location information accuracy less than sufficient for a given task.

We established an image registration framework which has the capability to improve the georeference of an image in such cases by matching it with a reference image with a satisfying georeference accuracy, i.e. an image covering the same area at a similar resolution. This is achieved by a four steps workflow in which an object extraction step is followed by a contour extraction step, which is then followed by a contour point reduction step and finally by a contour matching step. This approach has proven to be both feasible and robust to appearance unsimilarity between the image and the reference image. As each step of the workflow has well defined interfaces for both their input and output, we can easily exchange the methods implementing the operation to be performed with

the respective steps. This allows us to to easily and efficiently evaluate different existing methods for these operations.

The scope of this work is the evaluation of the performance of several methods for each of the four steps within the context of our image registration framework. For the object extraction step we compare several road network extraction methods and a contour line extraction method based on Geodetic Active Contours against each other. We further compare several contour point reduction methods, and in addition to that we compare different Hausdorff distances as the distance measure is crucial to the contour matching step.

10427-80, Session PS

A new inversion algorithm for volume height estimation based on the fusion between CAPON and LS in a multi-baseline SAR application

Hichem Mahgoun, Mounira Ouarzeddine, Univ. des Sciences et de la Technologie Houari Boumediene (Algeria)

This work treats a new inversion algorithm used to retrieve the volume back scattering signal. This is achieved by combining two spectral estimation algorithms, CAPON (Multiple Signal Classification) and LS (Least Square). The fixed objective is the estimation of the Biomass of forested area with high resolution capabilities. This work is also an extension of a previous validated algorithm related to the fusion between DFT (Discrete Fourier Transform) and LS.

The CAPON inversion is a non parametric estimation algorithm used in this paper to estimate the volume backscatter. For this purpose, it needs the computation of the covariance matrix of the measured coherence signals in a multi-baseline configuration. This method presents many limitations, because it doesn't correctly estimate the volume backscatter with the needed accuracy, and this will result in a medium DSM quality.

The LS inversion is a parametric estimation algorithm, it can achieve very high resolution capabilities, and these performances are related to the algorithm that uses maximum likelihood criterion to estimate the backscattering signal. This algorithm is limited to be used for point like scattering mechanisms, and is not suited for distributed ones, as the volume backscattering signal.

In this work we propose a new inversion algorithm based on the fusion between the robustness of the CAPON inversion, and high resolution capabilities of the LS inversion for a better estimation of the volume backscattering signal. The proposed approach uses a uniformly distributed model of the backscatter signal over the elevation axis.

The inversion algorithm is tested on forested area (Västerbotten), with multi-baseline data set acquired in L-band (BioSAR-2008 project). Results are promising with the proposed algorithm. We used LIDAR (Laser Imaging Detection And Ranging) image as datasets for validation of the results.

10427-81, Session PS

High efficient optical remote sensing images acquisition for nanosatellite reconstruction algorithms

Yang Liu, CAST-Xi'an Institute of Space Radio Technology (China); Feng Li, Lei Xin, Qian Xuesen Lab. of Space Technology (China); Jie Fu, Lanzhou Jiaotong Univ. (China); Puming Huang, CAST-Xi'an Institute of Space Radio Technology (China)

It is very difficult and challenging to implement Nano-satellite (NanoSat) based optical Earth observation missions, because of the limitation of volume, weight and power consumption. In general, an image compression unit is a necessary onboard module to save data transmission bandwidth and disk space for spacecraft based remote Earth observation. Here, we propose a new High efficient optical remote sensing images acquisition framework for Nano-satellites without extra image compression unit. The image acquisition and image compression can be combined into a single step, and it can be easily built in CMOS architecture. In the theory of compressed sensing (CS), the construction of classical sensing matrix for all sparse signals has to satisfy the Restricted Isometry Property (RIP) strictly, which limits applying CS in practical in image compression. For remote sensing images, we know some inherent characteristics such as non-negative, smoothness and etc.. Therefore, a sensing matrix is not necessary to follow RIP strictly. A novel sensing matrix is proposed, which consists of two parts: the standard Nyquist sampling matrix for thumbnails and the conventional CS sampling matrix that randomly obtains measurements in the Noiselet transform domain. In this paper, we focus on the reconstruction algorithms based on the novel sensing matrix.

Given the incomplete measurements with the sensing matrix, a Split Bregman based algorithms is investigated to solve the above optimization problem. Meanwhile, a novel deep convolutional neural network (CNN) based reconstruction algorithms will also be investigated with those measurements through the new framework. Since most of sun-synchronous based satellites fly around the earth 90 minutes and the revisit cycle is also short, lots of previously captured remote sensing images of the same place are available in advance. This drives us to reconstruct remote sensing images through a deep learning approach with those measurements from the new framework. Unlike traditional CNN based applications for target recognition or segmentation, the input for CNN is not images but measurements from the new sensing matrix. While the output of the new CNN based method is the original images, thus we use a fully-connected layer to increase the dimensionality of the inputs at the beginning and then put the outputs of the first layer into the following convolutional layers to recover images. It is well known that the training procedure to the network costs long time, luckily, the training step can be done only once off line. Our experiments will show that the novel network closely approximates the conventional CS reconstruction algorithms with hundreds of times faster in terms of computational effort. Those reconstructed algorithms make the high efficient optical remote sensing images acquisition framework useful in practice for NanoSat.

10427-82, Session PS

Content based multilabel image retrieval with deep features

Xavier Giro, Michele Compri, Univ. Politècnica de Catalunya (Spain); Begüm Demir, Univ. degli Studi di Trento (Italy)

Recent advances in satellite technology has led to an increased volume of remote sensing (RS) image archives, from which retrieving useful information is challenging. Therefore, one important research area in remote sensing (RS) is the content-based retrieval of RS images (CBIR). The performance of the CBIR systems relies on the capability of the RS image features in modeling the content of the images as well as the considered retrieval algorithm that assesses the similarity among the features. Using supervised classification methods in the context of CBIR by training the classifier with the already annotated images has attracted attention in RS. However, existing supervised CBIR systems in the RS literature assume that each training image is categorized by only a single label that is associated to the most significant content of the image. However, RS images usually have complex content, i.e., there are usually several regions within each image related to multiple land-cover classes. Thus, available supervised CBIR systems are not capable of accurately characterizing and exploiting the high level semantic content of RS images for retrieval problems. To overcome these problems and to effectively characterize the high-level semantic content of RS images in supervised CBIR problems, we investigate effectiveness of different deep learning architectures in the

framework of multi-label remote sensing image retrieval. It is worth noting that deep learning architectures such as CNNs have recently attracted great attention in RS due to its effective and accurate feature learning. However, according to our knowledge this is the first work that deals with adaptation of CNN models to multi-label RS image retrieval problems. This is achieved based on a two-steps strategy. In the first step, a Convolutional Neural Network (CNN) pre-trained for image classification with the ImageNet dataset is used off-the- shelf as a feature extractor. In particular, three popular architectures are explored: 1) VGG16; 2) Inception V3; and 3) ResNet50. VGG16 is a CNN characterized by 16 convolutional layers of stacked 3x3 filters, with intermediate max pooling layers and 3 fully connected layers at the end. Inception V3 is an improved version of the former GoogleNet, which contains more layers but less parameters, by removing fully connected layers and using a global average pooling from the last convolutional layer. ResNet50 is even deeper thanks to the introduction of residual layers, that allow data to flow by skipping the convolutional blocks. In the second step of our research, we modify these three off-the- shelf models by fine-tuning their parameters with a subset of RS images and their multi-label information. Experiments carried out on an archive of aerial images show that fine-tuning CNN architectures with annotated images with multi-labels significantly improve the retrieval accuracy with respect to the standard CBIR methods. We find that fine-tuning using with a multi-class approach achieves better results than considering each label as an independent class. Due to the space constraints, the detailed information on each step of the proposed method will be given in the full version of the paper.

10427-83, Session PS

Effects of the modulation transfer function of high spatial resolution remote sensing imaging system on localization errors in land use patches

Jiehai Cheng, Feng-yuan Wei, Zhanliang Yuan, Huazhu Xue, Henan Polytechnic Univ. (China)

The Modulation Transfer Function (MTF) of high spatial resolution remote sensing imaging system can influence the edge sharpness of the images and can obscure the edges of land use patches. This paper examines the effects of the MTF on localization errors, discrepancies between delineated land use patches and the corresponding reference data. We generated a series of synthetic images and applied the MTF to each, in order to determine the relationship between the MTF and any localization errors in the land use patches. Experimental results show that localization errors in the patches are less than 1% as the MTF values are greater than 0.35 and rapidly increase when the MTF values are less than 0.25. The spectral separability between land use patches and patch size can determine the degree of localization error. The larger the spectral separability and patch size, the smaller the localization error. The MTF values and the corresponding localization errors in the patches obey an approximately logarithmic relationship. This logarithmic correspondence was validated using real remote sensing images. This study could be used as a reference by other researchers and promotes the establishment of a comprehensive image quality equation for assessing the application performance of a given image with known quality parameters.

10427-84, Session PS

Output MSE and PSNR prediction in DCT-based lossy compression of remote sensing images

Ruslan A. Kozhemiakin, Sergey K. Abramov, Vladimir V. Lukin, National Aerospace Univ. (Ukraine); Benoit Vozel, Kacem Chehdi, Univ. de Rennes 1 (France)

Lossy compression of acquired images is a typical operation in remote sensing (RS) applications used for data transferring, storage and dissemination. In lossy compression, one should also keep in mind quality of compressed images since the increase of compression ratio (CR) most often inevitably leads to worse quality. The recommendations concerning possible level of distortions are that their influence should be as low as to avoid essential decrease of accuracy of RS data classification [1] or they have to be less than noise intensity [2].

Control and providing of a desired level of distortions according to a chosen metric is problematic [3,4] even for compressing single-band images or multichannel images in component-wise manner. A fixed CR can correspond to considerably different mean square error (MSE) of introduced distortions and, respectively PSNR. Because of this, people often use iterative procedures for providing a desired value of a metric [5] and this often takes considerable and unpredictable time.

An interesting solution to the aforementioned problem has been proposed in [4] where the authors have designed a method for prediction of PSNR of introduced losses for JPEG based on the use of Laplacian approximation of AC DCT coefficients determined for all possible positions of blocks for a given image. We propose a way to accelerate prediction (without loss of accuracy) using a limited number of 8x8 pixel blocks for which 2D DCT has to be performed with further analysis of DCT coefficient quantization errors [6]. At the first stage, design and analysis has been done for uniform quantization of DCT coefficients. We also show that fast prediction of MSE and PSNR is possible for other than JPEG DCT based coders as AGU [7] and ADCT [8]. We carry out analysis for test images typical for remote sensing applications and introduce correcting factors for MSE and PSNR calculation for AGU and ADCT. This allows getting more accurate prediction of MSE and PSNR.

Besides, analysis is carried out for the case of non-uniform quantization of DCT coefficients that is applied in conventional version of JPEG and in modifications of other DCT-based coders called AGU-M and ADCT-M. Larger values of MSE are observed for more complex structure images and the difference in MSE values can reach several times. For the same scaling factor, JPEG produces MSE of distortions that is about 5...10% larger than for the coders AGU and ADCT. The errors of PSNR prediction are usually smaller than 0.5 dB. It is also possible to easily solve an inverse task, i.e. to determine QS or SF to provide a desired MSE or PSNR.

REFERENCES

[1] Blanes I., Magli E., Serra-Sagrista J. A tutorial on image compression for optical space imaging systems. IEEE Geoscience and Remote Sensing Magazine. 2014;2(3):8–26.

[2] Aiazzi B., Alparone L., Barducci A., Baronti S., Pippi I. Estimating noise and information of multispectral imagery. Journal of Optical Engineering. 2002;41:656–668.

[3] H. Jiang, K. Yang, T. Liu, Y. Zhang, “Quality Prediction of DWT-Based Compression for Remote Sensing Image Using Multiscale and Multilevel Differences Assessment Metric”, Mathematical Problems in Engineering, Volume 2014, Article ID 593213, 15 p., 2014.

[4] J. Minguillon, J. Pujol, “JPEG Standard Uniform Quantization Error Modeling with Applications to Sequential and Progressive Operation Modes,” Electron. Imaging, vol. 10(2), pp. 475-485, 2001.

[5] A. Zemliachenko, N. Ponomarenko, V. Lukin, K. Egiazarian, J. Astola, “Still Image/Video Frame Lossy Compression Providing a Desired Visual Quality”, Multidimensional Systems and Signal Processing, 22 p. June 2015.

[6] R. Kozhemiakin, V. Lukin, B. Vozel, “Image Quality Prediction for DCT-based Compression”, 14th International Conference CADSM 2017, pp 225-228, 21-25 February, Polyana-Svalyava (Zakarpattya), Ukraine, 2017

[7] N.N. Ponomarenko, V.V. Lukin, K.Egiazarian, J. Astola, “DCT Based High Quality Image Compression,” Proceedings of 14th Scandinavian Conference on Image Analysis, Joensuu, Finland, pp. 1177-1185, June 2005.

[8] N. Ponomarenko, V. Lukin, K. Egiazarian, J. Astola, “ADCT: A new high quality DCT based coder for lossy image compression, “ CD ROM Proceedings of LNLA, 6 p., 2008.

10427-85, Session PS

Vehicle detection in UAV remotely sensed images

Mohamed Salah Ismail, Mohammed Abdel-Megeed Salem, German University in Cairo (Egypt)

Traffic monitoring and management is of the crucial tasks of modern cities governments. Day by day increases the complexity of traffic monitoring, and hence increases the need for novel solutions. In this paper, experimental work is introduced for vehicle detection in parking lots, where few centimeter resolution images captured by unmanned aerial vehicle are used. The images are first thresholded in HSV color space and then converted YC_b C_r color space for detecting the regions where the cars should be found. Bag of Words (BoW) uses SURF technique and K-mean clustering to extract features from the data set provided for training the SVM. SVM are used to produce a linear classifier which enables the classification of new datasets into either one of the learned classes. The results show that the accuracy of classification is more than 82% when appropriate number of training images is used.

The proposed system follows the typical modules of the pattern recognition architecture, e.g. sensing, preprocessing, feature extraction, training and classification. Fig.1, illustrates the proposed method. It shows the training and the testing phases. The inputs are remote sensed colored images in RGB space acquired using a UAV. The images are then transformed to HSV and color spaces. In the training phase, the images used are for vehicles and non-vehicles. The SURF is used for interest-points extraction to build the feature vector of the image. The feature vectors as well as the actual classification are fed to the support vector machines (SVM) for training. The testing could be carried out after completing the training. First each pixel in the input image is examined to extract the region of interest (ROI).The feature extraction is done as in the training phase. The extracted features are classified using the support vector machines.

10427-36, Session 8

Analysis of signal-dependent sensor noise on JPEG 2000-compressed Sentinel-2 multi-spectral images

Mykhail Leontievich Uss, National Aerospace Univ. (Ukraine); Benoit Vozel, Univ. de Rennes 1 (France); Vladimir V. Lukin, National Aerospace Univ. (Ukraine); Kacem Chehdi, Univ. de Rennes 1 (France)

The Sentinel-2A satellite acquires multi-spectral data with 13 bands covering visible, near infrared and short wave infrared part of the spectrum [1]. The application range of these data includes but is not limited to risk management, land use, forest monitoring, water management, soil protection, urban mapping.

An important characteristic of a remote sensing sensor is its signal-to-noise ratio (SNR) influencing quality of products derived from the original data. SNR is related to the sensor noise parameters, knowledge of which is needed for performing data filtering, spectral unmixing, or classification. Sensor noise parameters are determined during pre-flight sensor calibration and later controlled during in-flight calibration process. However, freely distributed Sentinel-2A data lack detailed information on the sensor noise properties.

Alternatively, sensor noise properties can be analyzed directly from the noisy data by blind noise parameter estimators [2]. For Sentinel-2A, application of existing blind noise parameter estimators is problematic. First, images are distributed being compressed with JPEG 2000 coder. Image compression modifies noise both in the sense of its statistics and spatial correlation width [3]. The strength of filtering effect is data-dependent [4], i.e., may locally vary over image area depending on such factors as local SNR, image texture roughness and anisotropy, presence of small-sized objects or edges [5, 6]. Apart from this, noise for optical sensors inherently depends on image intensity [2]. This makes noise model of compressed data multivariate, the kind of problem state-of-the-art noise parameter estimators cannot deal with. Second, noise parameter estimators of multichannel data work under assumption that all bands are represented at the same spatial grid [7]. This is not the case for Sentinel-2A image data: bands have different spatial resolution (10, 20, 60m) and non-negligible inter-band misregistration.

In the paper, we overcome the above mentioned difficulties by special preprocessing of Sentinel-2 data that allows applying previously proposed noise parameter estimator vcNI+fBm [8]. For a reference band, the preprocessing includes selection of bands with the same or finer spatial resolution, band mutual registration, interpolation to the reference band grid, and point spread function adjustment. Application of vcNI+fBm to multichannel image thus pre-processed provides individual noise parameter estimates, variance and spatial correlation width, that are further analyzed as a bivariate function of local SNR and image intensity.

In the experimental part of the paper, we analyze noise parameters of ten Sentinel-2 granules. Analysis reveals that influence of both image intensity and local SNR on noise variance is significant. For a fixed SNR, noise model agrees with mixture of additive and scaled Poisson noises. The model parameters fall into distinctive groups (presumably due to image intensity scaling with a finite set of scaling factors). For low SNR, noise variance decreases approximately by a factor of 2 as compared to high SNR due to JPEG 2000 compression. We have also analyzed noise spatial correlation width and found it consistent with image compression influence.

Sentinel-2A noise models obtained in this paper could be useful for end-users and researchers working in a variety of remote sensing applications.

[1] F. Spoto, O. Sy, P. Laberinti, P. Martimort, V. Fernandez, O. Colin, et al., “Overview Of Sentinel-2,” in 2012 IEEE International Geoscience and Remote Sensing Symposium, 2012, pp. 1707-1710.

[2] M. L. Uss, B. Vozel, V. V. Lukin, and K. Chehdi, “Local Signal-Dependent Noise Variance Estimation From Hyperspectral Textural Images,” IEEE J. Sel. Topics Signal Process., vol. 5, pp. 469-486, 2011.

[3] A. N. Zemliachenko, R. A. Kozhemiakin, M. L. Uss, S. K. Abramov, N. N. Ponomarenko, V. V. Lukin, et al., “Lossy compression of hyperspectral images based on noise parameters estimation and variance stabilizing transform,” Journal of Applied Remote Sensing, vol. 8, pp. 083571-083571, 2014.

[4] V. V. Lukin, S. S. Krivenko, M. S. Zriakhov, N. N. Ponomarenko, S. K. Abramov, A. Kaarna, et al., “Lossy compression of images corrupted by mixed Poisson and additive Gaussian noise,” in 2009 International Workshop on Local and Non-Local Approximation in Image Processing, 2009, pp. 33-40.

[5] P. Chatterjee and P. Milanfar, “Practical Bounds on Image Denoising: From Estimation to Information,” Image Processing, IEEE Transactions on, vol. 20, pp. 1221-1233, 2011.

[6] M. Uss, A. Rubel, V. Lukin, B. Vozel, and K. Chehdi, “Lower bound on image filtering mean squared error in the presence of spatially correlated noise,” in Microwaves, Radar and Remote Sensing Symposium (MRRS), 2014 IEEE, 2014, pp. 10-13.

[7] G. Lianru, D. Qian, Z. Bing, Y. Wei, and W. Yuanfeng, “A Comparative Study on Linear Regression-Based Noise Estimation for Hyperspectral Imagery,” IEEE J. Sel. Topics Appl. Earth Observ. in Remote Sens., vol. 6, pp. 488-498, 2013.

[8] M. L. Uss, B. Vozel, V. V. Lukin, and K. Chehdi, “Maximum likelihood estimation of spatially correlated signal-dependent noise in hyperspectral images,” Optical Engineering, vol. 51, pp. 111712-1-111712-11, 2012.

10427-37, Session 8

Using the time shift in single pushbroom datatakes to detect ships and their heading

Katharina A. M. Willburger, Kurt Schwenk, Deutsches Zentrum für Luft- und Raumfahrt e.V. (Germany)

In the recent years, the detection and monitoring of ships from remote sensing data has become an essential task for the improvement of maritime security. The comprehensive variety of application scenarios includes among others piracy, illegal fishery, ocean dumping and ships carrying refugees.

While techniques using data from synthetic aperture radar (SAR) sensors are widely common, there is only few literature discussing algorithms based on imagery of optical camera systems. In fact, optical sensors are dependent on day light and convenient weather conditions. However, they also offer several advantages, not at least due to their availability and lower processing effort.

An automatic ship detection algorithm for optical pushbroom imagery has been developed. It makes use of the special detector assembly of most of those scanners, which allows apart from the detection of a ship and its position also the calculation of its heading out of a single acquisition.

Pushbroom scanners onboard of earth observation satellites usually consist of more than one CCD detector line for recording the reflection in their channels. The mounting geometry of such a scanner together with the movement of the spacecraft causes a small time shift in the acquisition of different channels acquired by different CCD lines. During the process of coregistration, this time shift is mostly eliminated, yielding superimposed images with static areas and objects being congruent. But, if an object was moving during acquisition, its position within channels corresponding to different CCD lines will be displaced.

The Jenaoptronik camera JSS-56 carried onboard of the RapidEye satellites comprises 5 separate CCD detector lines, one for each spectral channel from the visible to the near infrared region. The maximal time shift exists between the blue and red channel, where the blue band is acquired about 3 seconds earlier than the red one. The effect of the time shift on rapidly moving objects is striking. For instance, in a RapidEye RGB composite, one and the same airplane appears at three different positions, colored blue, green and red respectively. Since ships move considerably slower, the effect is reduced, but still clearly visible due to a significant cluster of red pixels in the direction of movement.

The proposed algorithm for the automatic detection of moving ships was developed with RapidEye imagery. It consists mainly of three steps: the creation of a land-watermask, the object extraction by means of connected-component labeling in the binary image and the examination of each single object. The latter step is build up by several spectral and geometric filters, making heavy use of the displacement caused by multiple CCD lines as stated above, finally yielding a set of moving ships. At last, the direction of movement is calculated and converted into geographic coordinates.

In this article, an overview of existing ship detection methods for optical imagery will be given. The algorithm described above and its theoretical background will be explained in detail. The performance in terms of accuracy, detection rate and false alarms will be examined thoroughly and results will be presented.

10427-38, Session 8

Comparison of different detection methods for persistent multiple hypothesis tracking in wide area motion imagery

Christine Hartung, Raphael Spraul, Tobias Schuchert, Fraunhofer-Institut für Optronik, Systemtechnik und Bildauswertung (Germany)

Wide area motion imagery (WAMI) sensors, a relatively new class of airborne multicamera sensors, provide large images (~ 100 megapixel) at typical framerates of 1-2 Hz, allowing for continuous monitoring of large urban areas. Each image can cover a geographic region of up to several square kilometers and contain thousands of individually discernible vehicles. Reliable vehicle detection and tracking in this imagery is an important prerequisite for surveillance tasks, but remains challenging due to low frame rate and small object size (~ 10x20 pixel).

Most WAMI tracking approaches are detection-based and rely on moving object detections generated by frame differencing or background subtraction methods. These detection methods fail when objects slow down or stop. Recent approaches for persistent tracking, i.e. tracking vehicles even if they become stationary, compensate for missing motion detections by combining a detection-based tracker with a second tracker based on appearance or local context [1, 2]. In order to avoid the additional complexity introduced by combining two trackers, we propose an alternative framework that requires only a single tracker and enables persistent tracking in WAMI data by recovering missing motion detections with a classifier-based detector. The tracker is based on multiple hypothesis tracking (MHT) and processes input detections independently of whether they were generated by motion detection or with the classifier, providing a systematic solution to the data association problem. We adapt the MHT approach to the specific context of WAMI tracking by integrating an appearance-based similarity measure, merge handling, and vehicle-collision tests, and finally extend the processing pipeline by a clutter handling module. We quantitatively evaluate the tracking performance on a 1408 x 1408 pixel region of interest of the publicly available WPAFB 2009 dataset. The chosen sequence comprises 1025 frames and 410 ground truth tracks; we use the common metrics recall, precision, f-score (harmonic mean of recall and precision), track swaps, track breaks, and multiple object tracking accuracy (MOTA). A comparison to other persistent WAMI trackers demonstrates state of the art performance of the proposed approach.

Furthermore, we analyze in detail the impact of different object detection methods and detector settings on the quality of the output tracking results. For this purpose, we choose four different motion-based detection methods to generate the input detections: Three-frame differencing with neighborhood consideration, median background subtraction (median BG) with neighborhood consideration, median BG with gradient magnitude thresholding, and median BG with gradient magnitude suppression. All four approaches showed promising results in a study by Sommer et al. [3], but vary in detection performance (measured by precision, recall, and f-score) and computation time. As detector parameters can be adjusted to achieve different precision and recall performance, we combine each detection method with three different representative detector settings that yield (1) high precision and low recall, (2) high recall and low precision, and (3) best f-score, i.e. best overall detection performance. Using the evaluation sequence described above, we compare the tracking performance achieved with the different sets of input detections in order to quantify the sensitivity of the tracker to different types of detector errors (false positives, false negatives), and thus derive recommendations for detector and parameter choice.

[1] J. Prokaj et al., “Persistent tracking for wide area aerial surveillance,” 2014.

[2] B. Chen et al., “Exploring local context for multi-target tracking in wide area aerial surveillance,” 2016.

[3] L. W. Sommer, M. Teutsch, T. Schuchert, and J. Beyerer, “A survey on moving object detection for wide area motion imagery,” 2016.

10427-39, Session 8

Ship detection leveraging deep neural networks in WorldView-2 images

Tomonori Yamamoto, Yoriko Kazama, Hitachi, Ltd. (Japan)

Recently, the resolution of the satellite images is getting finer and finer. In 2009, WorldView-2 achieved the 50cm at panchromatic mode, and WorldView-4, launched in 2016, supports the resolution of 31cm. Such high-resolution satellites are recognized as the effective tools for monitoring the terrestrial objects especially in surveillance and defense. For these purposes, extracting target objects from the satellite images has been one of the most important tasks of IMINT.

However, the interpretation of high-resolution satellite images has been so difficult that skilled interpreters must have checked the satellite images manually because of the following issues. One is the requirement of the high detection accuracy rate. Regarding the interpretation operation, there are too many satellite images and too vast areas to look through, so it is difficult to re-check the same satellite image after finished interpreting and missed the target; therefore, infinitely zero missing rate is required to introduce automatic target extraction techniques. The other is the variety of the target, i.e. there are so many kinds of ships, such as boat, cruise ship, cargo ship, aircraft carrier, and so on. Furthermore, there are similar appearance objects throughout the image because satellite imagery is the bird's-eye view photograph; therefore, it is often difficult even for the skilled interpreters to distinguish what object the pixels really compose.

Conventionally, fully customized machine learning has been applied to extract the target objects; however, it requires the thorough feature analyses for each target. On the other hands, recently deep learning is becoming more common and revealed as the most powerful feature extraction tool.

In this paper, we explore the feasibility of object extraction leveraging deep learning with high- resolution satellite images, especially focusing on "ship" detection. Deep learning enables us to extract target object features automatically as long as the data preparation is enough. As for the high-resolution satellite images, it is generally difficult to prepare a plenty of training data, but we managed to gather a certain amount of training data.

We calculated the detection accuracy using the WorldView-2 images. First, we collected the training images labelled as "ship" and "not ship". After preparing the training data, we defined the deep convolutional neural network models to judge whether ships are existing or not, and trained them with about 50,000 images for each label. Subsequently, we scanned the evaluation image and extracted the images predicted as "ship" by the neural networks. The range of ship size was assumed from 20 to 200m, while the convolutional neural networks could accept fixed size images, so detection size and resolution were in the trade-off relationship. We scanned with plural size of scan windows and leveraged the neural networks trained with resolution-adjusted pan-sharpened images to detect the ships ranging widely in size. Finally, we identified the location of individual ships using another deep neural network for segmentation. Experimental result shows the detection accuracy is over 90%, which proves the effectiveness of the deep learning based object detection.

10427-40, Session 8

A novel class sensitive hashing technique for large-scale content-based remote sensing image retrieval

Thomas Reato, Begüm Demir, Lorenzo Bruzzone, Univ. degli Studi di Trento (Italy)

During the last decade, a huge number of earth observation satellites have been launched, leading to massive remote sensing (RS) data archives. Such archives require scalable and accurate methods for the quick access to RS data. In view of that, content based image retrieval (CBIR) has recently attracted great attention in the RS community [1]. To accomplish an accurate and scalable image search and retrieval in large RS data archives, hashing-based CBIR methods have been recently introduced in RS [1]. Hashing methods map high-dimensional image features into compact binary hash codes based on hash functions that can be defined by using either unlabeled images (i.e., unsupervised hashing) or a set of annotated training images (i.e., supervised hashing) [1]. Generally, supervised hashing methods achieve higher retrieval accuracy than unsupervised methods, since they provide more distinctive hash functions (and thus more distinctive hash codes). These methods describe each image by a single hash code attained by applying hash functions to global image descriptors. Moreover, they do not model possible primitives (such as different land-cover classes) present in the images. This is an important limitation as RS images generally contain several regions that may be associated to different land-cover classes and represent complex semantic content. Ignoring this in hashing-based CBIR may lead to inaccurate retrieval results, especially under complex RS image retrieval tasks.

In this paper, we focus our attention on supervised hashing in RS CBIR problems. To overcome the limitations of the literature supervised hashing methods, we introduce a novel technique that aims at accurately modeling primitives (different land-cover classes) in the definition of the hashing functions. To this end, the proposed technique is defined based on a three-steps algorithm: 1) characterization of each image with descriptors of primitive classes; 2) transformation of descriptors into primitive class-sensitive multi-hash codes; and 3) assessment of the similarities between the multi-hash codes of the query image and those of each image in the archive to retrieve images similar to the query image. The first step is achieved by: i) segmenting images in the archive into a set of regions; and ii) associating region descriptors with primitive classes present in the images. To define a correspondence between the regions of an image and the primitive classes, we propose a novel strategy that estimate the probability of each land-cover class to be present at each region. This is done by exploiting the softmax function [4] in conjunction with the information contained in the training set. We consider that all the regions belonging to the specific primitive class with a probability higher than a given threshold are highly representative of that class. Thus, the average value of the descriptors of these regions is used to characterize that primitive class. Then, in the second step supervised hashing is applied to the descriptors of each primitive class independently from each other by properly adapting it to supervised multi-hash codes generation problems. To this end, we consider the kernel-based supervised locality sensitive hashing (KSLSH) method presented in [2]. Differently from the standard way of using the training samples within the KSLSH, we exploit the primitive class descriptors of the training images to define the hash functions related to each primitive class. It is worth noting that any kind of supervised hashing method available in the literature can be used with the proposed method. The first two-steps of the proposed method, unlike the standard supervised hashing methods, allow one to represent each image by a set of primitive class sensitive descriptors and their hash codes. Then, in the third step a multi-hash-code-matching scheme is introduced for retrieving images based on the similarities of multi-hash codes. Due to the space constraints, the detailed information on each step of the proposed method will be given in the full version of the paper.

In the experiments, we assessed the effectiveness of the proposed primitive class sensitive hashing technique with: 1) the standard hashing method (which does not evaluate the primitives present in the images during hashing) [1] and 2) the multi-label SVM [3]. Experimental results show that the proposed technique provides 9% higher retrieval accuracy with respect to the standard hashing method, while keeping the same retrieval time. Moreover, it results in similar accuracies with respect to the multi-label SVM with significantly reduced retrieval time (which is of two order of magnitude). Detailed results will be presented in the full paper.

REFERENCES

[1] B. Demir, L. Bruzzone "Hashing based scalable remote

sensing image search and retrieval in large archives", IEEE Transactions on Geoscience and Remote Sensing, vol. 54, no.2, pp. 892-904, 2016.

[2] W. Liu, J. Wang, R. Ji, Y. G. Jiang, and S-F. Chang, "Supervised hashing with kernels", Conference on Computer Vision and Pattern Recognition, pp. 2074-2081, Rhode Island, USA, 2012.

[3] M. R. Boutell, J. Luo, X. Shen, and C. M. Brown, "Learning multi-label scene classification," Pattern Recognition, vol. 37, no. 9, pp. 1757 – 1771, 2004.

[4] E. Alpaydin, Introduction to Machine Learning (Adaptive Computation and Machine Learning). The MIT Press, 2004.

10427-41, Session 9

A filtering framework for SAR data based on nongaussian statistics and pixel clustering

Anca Cristea, Anthony P. Doulgeris, Torbjørn Eltoft, UiT The Arctic Univ. of Norway (Norway)

We present a filtering framework based on a new statistical model for Single-Look complex SAR data – the SNIG (Scaled Normal-Inverse Gaussian). The model is based on the assumption of a geometric Brownian motion with drift. The associated compound random variable is expressed as X=?Z+√Z N, where N is a zero-mean Gaussian with variance ?2 (a measure of diffuse scattering), ? is the drift (a measure of coherent scattering), and the latent variable Z is an Inverse Gaussian with unit mean and shape parameter ? (a measure of texture). The model is applied to the real and imaginary parts of complex SAR data, separately. Parameter estimation is performed using an Expectation-Maximization scheme adapted to compound probability distributions, more specifically the family of hyperbolic distributions.

Furthermore, the real and imaginary parts of a single SAR image are considered as mixtures of SNIGs. Separation of the mixture components (classes) is conducted using a Stochastic Expectation-Maximization algorithm: at each iteration, every pixel is associated to one class prior to class parameter estimation. After convergence, all the pixels are clusterered into the final classes using a MAP decision rule. Model parameters are associated to each pixel according to its class, thus producing parametric images of the entire scene.

A closed-form MAP filter is designed to deliver an estimate of the texture Z and uses as input the parametric images together with the original Single-Look intensity values. The result is a despeckled image with preserved texture details.

The framework is tested on RADARSAT-2 data, HV polarization, representing an image of ocean water and icebergs off the coast of the Hopen Island (Svalbard archipelago). The method is applied to areas of the image containing individual icebergs surrounded by water. For each of the areas, a prior estimation is conducted on large patches of water (5000 pixels), in order to extract parameters for the corresponding class. Clustering is then performed on the entire area, assuming three classes and constraining the parameters of the water class to the previous estimation. The water class is found to be a zero-mean Gaussian, but the iceberg classes are non-Gaussian and have non-zero means. Post-clustering, the iceberg pixels are recovered into the two remaining classes. The parametric images obtained for the real and imaginary parts are then used as inputs for the filter.

Post-processing, the ocean background is smoothed, while the iceberg margins are not affected. The iceberg contrast-to-noise ratio (CNR) is improved compared to the Single-Look Intensity, increasing from a value of 11 to a value of 30, and the iceberg signal-to-noise ratio (SNR) is doubled compared to the same reference. We conclude that the detectability of the icebergs versus the ocean background is improved, thus demonstrating the potential of this method for iceberg detection.

10427-42, Session 9

Computational efficient unsupervised coastline detection from single-polarization 1-look SAR images of complex coastal environments

Andrea Garzelli, Claudia Zoppetti, Univ. degli Studi di Siena (Italy)

Coastline detection in synthetic aperture radar (SAR) images is crucial in many application fields, from coastal erosion monitoring to navigation, from damage assessment to security planning for port facilities.

The backscattering difference between land and sea is not always documented in SAR imagery, due to the severe speckle noise, especially in 1-look data with high spatial resolution, high sea state, or complex coastal environments.

First solutions have been proposed starting from edge-based segmentation [Lee and Jurkevich IEEE TGARS, 1990], also within a two-step procedure [Mason and Davenport, IEEE TGARS 1996].

More recent solutions have adopted level set segmentation either in a hierarchical scheme, also for multi-polarization images [Liu et al., IEEE JSTARS 2016], or by following a semi-supervised approach [Silveira and Heleno, IEEE GRSL 2009]. Other solutions need more than one SAR image, specifically a stack of at least three Stripmap CSK images, to extract the coastline [Baselice and Ferraioli, IEEE GRSL 2013].

This paper presents an unsupervised, computationally efficient solution to extract the coastline acquired by only one single-polarization 1-look SAR image. The method processes the original Spotlight CSK image at 1m resolution (0.5m pixel spacing) first at reduced spatial resolution (4m), and then at full spatial resolution. A preliminary segmentation is performed by jointly clustering the local variation coefficient and a radiometrically transformed version of the amplitude image. Prior knowledge for shape analysis of the resulting sea-candidate regions and accurate correction of possible focalization errors produce an accurate sea segmentation at reduced spatial resolution. Standard morphological operators are applied to this aim. Low-amplitude land regions which may be very close to the coastline are then accurately detected and processed to avoid possible errors. The final coastline extraction is performed in a computational efficient way by resorting to the original spatial resolution of the SAR image.

Extensive tests on Spotlight COSMO-SkyMed images of complex coastal environments and objective assessment will demonstrate the validity of the proposed procedure which is compared to state-of-the-art methods through visual results and with an objective evaluation of the distance between the detected and the true, manually selected, coastline.

10427-44, Session 9

Classification of RISAT-1 data using SVM with hybrid polarimetric descriptor

Varsha A. Turkar, Vidyalankar Institute of Technology (India); Shaunak De, Indian Institute of Technology Bombay (India); Anup K. Das, Space Applications Ctr. (India)

In recent years, interest has increased on compact and hybrid polarimetric SAR data analysis for various applications mainly due to its advantages like wide swath, low PRF, higher incident angle range coverage and less data rate over fully polarimetric SAR [1-2]. Using simulated hybrid polarimetric data from Convair-580 and Radarsat-2, they were able to successfully undertake various studies like land-use change, crop classification, soil moisture estimation, ship detection and sea-ice classification. The work carried out so far using compact or hybrid polarimetric SAR data has been based on simulated hybrid-polarimetric data from fully polarimetric airborne or spaceborne SAR systems. With its launch in April

2012, RISAT-1 became the first spaceborne hybrid PolSAR system. It carries a C-band hybrid polarimetric radar supporting right circular transmit and coherent linear receive mode (CTLR) in addition to other standard modes [3]. Although several theoretical studies have been shown with simulated data, very few works have emerged which examine the effects and capabilities of actual Hybrid PolSAR systems, with their inherent antenna construction and calibration difficulties. In this paper, we have examined the backscattering coefficient (?0) for discrimination of various land features using both linear and hybrid polarimetric RISAT-1 data. Further, we have analyzed the classification accuracy obtained using various approaches to the classification problem. For this study, the test site chosen is the metropolis of Mumbai, India. The area consists of built-up dense urban settlements, moderately dense deciduous forest, mangroves, wetlands, bare-land, grasslands and water. RISAT-1 data has been acquired on two successive days over Mumbai test site. The linear HH/HV dual polarization data at incidence angle of 49.3? and RH/RV hybrid mode data at 35.9? have been acquired on 14th and 15th November 2012 respectively. Ground-truth parameters in terms of soil moisture, vegetation height and biomass, etc., were collected synchronous with both the satellite passes. The CPR is used as an indicator of the degree of surface roughness whose order of magnitude is comparable with radar imaging wavelength. The SPAN is an indicator of the backscattered power and tends to be high for targets like urban structures etc. Together the SPAN and the CPR help to distinguish various classes by accounting for both their total power and structure of the targets. All bands are normalized before the application of the SVM classifier. The classification effectiveness of RISAT-1 linear dual polarization mode (HH and HV mode) was also evaluated. RISAT-1 HH/HV image was acquired just one day before the RH/RV dataset was acquired. An overall classification accuracy of 91.61% and 92.84% was achieved when the SVM classifier was applied on the 3 components of the m-? or m-?, SPAN and CPR was applied. It is observed that the classification accuracy is also dependent on multilook factor. The overall accuracy increases almost by 12% when multilook factor is changed from 3:3 to 8:8. The performance of hybrid polarimetric (RH, RV) data in terms of classification accuracy is better than dual polarization (HH, HV) data. The classification accuracy increases by combining three components (surface, double and volume) of m-? or m-? along with CPR and SPAN for RISAT-1.

[1] R.K. Raney, “Hybrid-polarity SAR architecture”, IEEE Trans. Geosci. Remote Sens., 45(11):3397 –3404, Nov. 2007.

[2] R.K. Raney, T.S. Cahill, G.W. Patterson and D.B.J. Bussey, “The m-? decomposition of hybrid dual-polarimetric radar data with application to lunar craters”, Journal of Geo-physical Research, vol. 117, EOOH21, pp.1 - 8, 2012

[3] Tapan Misra, S. S. Rana, N. M. Desai, D. B. Dave, Rajeevjyoti, R. K. Arora, C. V. N. Rao, B. V. Bakori, R. Neelakantan and J. G. Vachchani, “Synthetic Aperture Radar payload on-board RISAT-1: configuration, technology and performance”, Current Science, vol. 104, 4,pp. 446 - 461, 2013

10427-45, Session 9

An automatic unsupervised maritime target detection method based on generative adversarial network using medium-low resolution SAR images

Qian Song, Ding Tao, Fudan Univ. (China)

Maritime target detection in medium-low resolution wide-swath Synthetic Aperture Radar (SAR) images is a challenging task due to complicated marine environments and limited target information. Most ship-like targets are represented only by tens-to-hundreds pixels and easily confused with each other. For many marine applications, accurate target detection is a key process and can provide important information to an extended target recognition stage. Until now, various constant false alarm rate (CFAR) based detection algorithms have been proposed based on statistical modeling of the background sea surface, but result in unstable performance due to the capture effect and complex sea clutter variations. Thus, a discrimination step is commonly applied to reduce false alarm rate. Recent years, convolutional neural network (CNN) with ability to learn the geometrical information of images, has attracted lots of attentions in target classification and recognition fields, which can be potentially used as an effective discriminator in medium-low resolution SAR images.

In this work, a coarse-level CFAR detection process is applied firstly to select all region-of-interests (ROI), with a goal of maximize the detection rate. Next, in order to utilize both the statistical and geometrical information, we propose an unsupervised algorithm using generative adversarial network (GAN) to discriminate targets from the look-alikes. GAN consists of a generative model and discriminative model: generative model aims at generating as real as the trained images given a distribution sampled from input space; discriminative model is to distinguish whether the input image is generated or real. Both models are trained simultaneously, and compete with each other. It can capture a mapping from feature space into SAR image space automatically. The background clutter excluding ROIs and their statistical features are utilized as training sets for GAN.

The main benefits of our proposed method are three-fold: first, the statistical information and GAN are tightly combined, thus can obtain a more robust performance in the discrimination stage; second, no extra labeled data from other sources is needed for training the network; third, after GAN is trained on one of a series of SAR images, the weights can be served as initial values to the others, or applied to other SAR images directly. Preliminary results show that our new detection method can achieve comparable performances with other traditional schemes.

REFERENCE

[1] Y. Cui, G. Zhou, J. Yang, and Y. Yamaguchi, “On the iterative censoring for target detection in SAR images,” IEEE Geoscience and Remote Sensing Letters, vol. 8, no. 4, pp. 641–645, Jul. 2011.

[2] J. Martín-De-Nicolás, D. Mata-Moya, M.P. Jarabo-Amores, et al., “High-order neural network-based ship detection algorithms applied to SAR imagery,” European Conference on Synthetic Aperture Radar. VDE, no. 555-558, 2012.

[3] J. Martín-De-Nicolás, D. Mata-Moya, M.P. Jarabo-Amores, et al., “Neural network based solutions for ship detection in SAR images,” IEEE International Conference on Digital Signal Processing, no. 1-6, 2013.

[4] I. J. Goodfellow, J. Pouget-Abadie, M. Mirza, et al., “Generative Adversarial Nets,” Advances in Neural Information Processing Systems, vol. 3, no. 2672-2680, 2014.

[5] M. Mirza, S. Osindero, “Conditional Generative Adversarial Nets,” Computer Science, no. 2672-2680, 2014.

[6] C. Bentes, D. Velotto, and S. Lehner, “Target classification in oceanographic SAR images with deep neural networks: Architecture and initial results,” 2015 IEEE International Geoscience and Remote Sensing Symposium (IGARSS), Jul. 2015.

[7] C. Bentes, A. Frost, D. Velotto, and B. Tings, “Ship-Iceberg Discrimination with Convolutional Neural Networks in High Resolution SAR Images,” Proceedings of EUSAR 2016: 11th European Conference on Synthetic Aperture Radar, Jun. 2016.

[8] C. P. Schwegmann, W. Kleynhans, B. P. Salmon, L. W. Mdakane, and R. G. V. Meyer, “Very deep learning for ship discrimination in Synthetic Aperture Radar imagery,” 2016 IEEE International Geoscience and Remote Sensing Symposium (IGARSS), Jul. 2016 .

[9] C. P. Schwegmann, W. Kleynhans, and B. P. Salmon, “Synthetic Aperture Radar Ship Detection Using Haar-Like Features,” IEEE Geoscience and Remote Sensing Letters, vol. 14, no. 2, pp. 154-158, Feb. 2017.

10427-46, Session JS1

Time domain SAR raw data simulation using CST and image focusing of 3-D objects

Adnan Saeed, Olaf Hellwich, Technische Univ. Berlin (Germany)

This paper presents the use of a general purpose electromagnetic simulator, CST, to simulate realistic synthetic aperture radar (SAR) raw data of three-dimensional objects. Raw data is later focused in MATLAB using range-doppler algorithm. Within CST Microwave Studio a replica of TerraSAR-X chirp signal is incident upon a modeled Corner Reflector (CR) whose design and material properties are identical to that of the real one. Defining mesh and other appropriate settings reflected wave is measured at several distant points within a line parallel to the viewing direction. This is analogous to an array antenna and is synthesized to create a long aperture for SAR processing. The time domain solver in CST is based on the solution of differential form of Maxwell's equations. Exported data from CST is arranged into a 2-d matrix of axis range and azimuth. Hilbert transform is applied to convert the real signal to complex data with phase information. Range compression, range cell migration correction (RCMC), and azimuth compression are applied in the time domain to obtain the final SAR image. This simulation can provide valuable information to clarify which real world objects cause images suitable for high accuracy identification in the SAR images.

10427-47, Session JS1

L1 regularization recovered SAR images based interferometric SAR imaging via complex approximated message passing

Chenyang Wu, Hui Bi, Institute of Electronics, Chinese Academy of Sciences (China) and Univ. of Chinese Academy of Sciences (China); Bingchen Zhang, Yun Lin, Wen Hong, Institute of Electronics, Chinese Academy of Sciences (China)

This paper presents an interferometric synthetic aperture radar (InSAR) imaging method based on L1 regularization recovered SAR images via complex approximated message passing (CAMP). The contributions of the presented method are as follows. Compared to conventional matched filtering (MF) results, the recovered images of the presented method have higher phase difference accuracy. While the presented method can reduce the computational cost efficiently by decoupling the azimuth-range couple compared with conventional L1 regularization technique.

In sparse signal processing based SAR imaging, due to the couple of range and azimuth in raw data, conventional L1 regularization method needs to transfer the two-dimensional (2-D) echo data matrix into a vector to reconstruct the surveillance region, which produces significant computational cost. While the presented azimuth-range decouple based L1 regularization SAR imaging method solve this problem well by introducing an echo simulator to decouple the azimuth-range couple.In the presented method, we first construct the 2-D SAR imaging model based on the imaging geometry and the relationship between considered scene and platform, then construct the echo simulator based on chirp scaling algorithm to achieve azimuth-range decouple, finally use CAMP iterative recovery algorithm to solve the Lasso optimization problem, and hence achieve the sparse and non-sparse images of the considered scene. The presented method makes large-scale sparse reconstruction of surveillance region become possible.

Since the presented CAMP based method can suppress the sidelobes and clutter efficiently in the recovered results which will be used to the InSAR image formation, thus the achieved interferogram has higher phase difference accuracy compared with MF obtained one. InSAR technique exploits the slightly phase difference of two or more SAR images to extract the height information or surface deformation of the focused target. Therefore, accurate phase difference is essential for InSAR image formation. Due to the fact that typical L1 regularization recovery algorithms, e.g., iterative thresholding algorithm (ITA), could not obtain accurate phase difference, thus some applications such as InSAR processing could not be used directly via their recovered images. As an iterative recovery algorithm for L1 regularization, CAMP can not only obtain the sparse estimation of considered scene as other regularization recovery algorithms, but also a non-sparse solution with preserved background information. With the help of its characteristic, CAMP recovered reconstructed images can be used to InSAR processing, which show better performance in height accuracy estimation than MF recovered results.

Experiments carried out on simulated and real data confirmed the validity of the presented approach, and the feasibility of the CAMP recovered images being used for InSAR processing with higher height estimation accuracy.

10427-48, Session JS1

An automatic technique for the probabilistic detection of subglacial lakes in radar sounder data acquired in Antarctica

Ana-Maria Ilisei, Mahdi Khodadadzadeh, Lorenzo Bruzzone, Univ. degli Studi di Trento (Italy)

The presence of Antarctic subglacial lakes increases the ice flow speed and facilitates the sliding of the ice masses towards the borders of the continent, consequently rising the sea level. This has motivated the growing interest in the detection and classification of lakes at the base of the ice sheet. Indeed, over the past half century, several types of instruments and techniques allowed the identification of hundreds of subglacial lakes under the Antarctic ice sheet, as reported in the most recent subglacial lake inventory (SLI) [1]. Among such instruments, radar sounders (RS) have shown a great potential for the large scale analysis of the subglacial environment [1]. RSs mounted on airborne platforms emit low-frequency electromagnetic waves that penetrate the ice sheet and are reflected by subsurface interfaces. The reflected waves are recorded by the RS receiver in 2D images of the ice sheet cross-section, called radargrams. The detection of subglacial lakes in radargrams has been mainly manually carried out [2], [3], with limited automatic contributions [4]. However, the manual approaches to the analysis of radargrams limit the objective and effective detection and classification of subglacial lakes. Moreover, the manual analysis does not allow the joint and effective use of multiple features that can be associated to the presence of lakes. This becomes critical when considering the expected growth in RS data from both airborne and potentially future spaceborne RS missions for Earth observation.

In this paper, we propose an automatic technique for the probabilistic detection of subglacial lakes in RS data. The aim of the proposed technique is to provide a soft output for the lake detection, i.e., an estimate of the probability of subglacial lake detection. This is in contrast to the available manual and automatic techniques which provide a hard decision in the classification or detection of lakes, e.g., [3], [4], [5]. To this aim, we propose a technique made up of two main steps, i.e., i) extraction of multiple features for the characterization of the basal interface; and ii) automatic probabilistic detection of lakes via multivariate classification. The first step, which is the core of the method, aims at extracting features of the basal interface that can be used by an automatic classifier for the discrimination between lake and bedrock radar returns. We extract two types of features, i.e., a) structural features, which model the geometry, radar coherency and strength of basal returns; and b) statistical features, which model the statistical behaviour of the radar signals at the basal interface. In particular, the structural features are extracted by taking into account previous observations regarding the difference between lake and bedrock radar reflections. For instance, in

[6] it has been proven that, compared to the bedrock, water reflected radar waveforms show steeper rising and trailing edges, narrower main lobe and greater peak power. Moreover, compared to bedrock waveforms, lake waveforms show greater radar coherency in the azimuth direction [2], [3]. Considering the above-mentioned properties, we propose to extract features that locally capture both the range and the azimuth characteristics of the basal interface. Thus, we consider sequences of basal waveforms to which we fit two separate planes: one plane to the raising edge sequence, and one plane to the trailing edge sequence. The coefficients of each fitted plane are then used to extract three angular structural features characterizing the analyzed edge steepness and its orientation. This amounts to a total of six structural features for each sequence of waveforms. The second type of extracted features models the local statistical properties of the basal interface in terms of variance, skewness and kurtosis of sequences of waveforms. Note that the extraction of both types of features, i.e., structural and statistical, represents the main contribution of this work with respect to the available related literature, e.g., [4], [5]. It is also worth mentioning that the choice of the range extent of the basal waveforms and the length of the sequence are driven by the data resolution and expected minimum lake dimension in the azimuth direction. Then, in the second step of the technique, all nine extracted features are normalized and given in input to an automatic classifier for the final probabilistic lake detection. Here, we use the Support Vector Machine classifier extended with Platt's algorithm [7] in order to enable the probabilistic classification of the basal interface, although other probabilistic classifiers could be used, e.g., [8].

We applied the proposed automatic technique to a subset of radargrams acquired by the MultiChannel Coherent Radar Depth Sounder [9]. The analysed dataset has been acquired in 2013, after the generation of the latest SLI in 2012 [1], over about 3000 km in the East Antarctic ice sheet. Experimental results show that by hardening the probabilistic output (i.e., output probabilities less (more) than 50% indicate lake (bedrock) returns) we obtained overall and average classification accuracies of 95.72% and 92.92%, respectively. Interestingly, the proposed method provided a high probability of presence of lakes at locations which are not reported in the Antarctic SLI. Thus, the proposed technique for the probabilistic detection of subglacial lakes can be a helpful tool for the glaciologic community for better analyzing the surveying region and possibly updating the current SLI.

Further details about related works, the proposed method and quantitative and qualitative results obtained on the investigated dataset will be provided in the full paper.

References:

1. REFERENCES

[1] A. Wright and M. Siegert, "A fourth inventory of Antarctic subglacial lakes," Antarctic Science, vol. 24, no. 06, pp. 659–664, 2012.

[2] S. Urbini, L. Cafarella, I. Tabacco, J. Baskaradas, M. Serafini, and A. Zirizzotti, "RES signatures of ice bottom near to Dome C (Antarctica)," IEEE Transactions on Geoscience and Remote Sensing, vol. 53, no. 3, pp. 1558–1564, 2015.

[3] S. Popov and V. Masolov, "Forty-seven new subglacial lakes in the 0-110? E sector of East Antarctica," Journal of Glaciology, vol. 53, no. 181, pp. 289–297, 2007.

[4] S. Carter, D. Blankenship, M. Peters, D. Young, J. Holt, and D. Morse, "Radar-based subglacial lake classification in Antarctica," Geochemistry, Geophysics, Geosystems, vol. 8, no. 3, 2007.

[5] C. Gifford and A. Agah, "Subglacial water presence classification from polar radar data," Engineering Applications of Artificial Intelligence, vol. 25, no. 4, pp. 853–868, 2012.

[6] G. Oswald and S. Gogineni, "Recovery of subglacial water extent from Greenland radar survey data," Journal of Glaciology, vol. 54, no. 184, pp. 94–106, 2008.

[7] J. Platt, "Probabilistic Outputs for Support Vector Machines and Comparisons to Regularized Likelihood Methods," inAdvances in large margin classifiers. 1999, pp. 61–74, MIT Press.

[8] D. Bohning, "Multinomial logistic regression algorithm," Ann. Inst. Stat. Math., vol. 44, no. 1, pp. 197–200, 1992.

[9] F. Rodriguez-Morales, S. Gogineni, C. Leuschen, J. Paden, J. Li, C. Lewis, B. Panzer, D. Gomez-Garcia Alvestegui, A. Patel, K. Byers, R. Crowe, K. Player, R. Hale, E. Arnold, L. Smith, C. Gifford, D. Braaten, and C. Panton, "Advanced multifrequency radar instrumentation for polar research," IEEE Transactions on Geoscience and Remote Sensing, vol. 52, no. 5, pp. 2824–2842, 2014.

10427-49, Session JS1

Improved signal processing algorithm for a practical WAS-GMTI system

Yong Li, He Yan, Nanjing Univ. of Aeronautics and Astronautics (China)

A WAS-GMTI (Wide-area Surveillance, Ground Moving Target Detection) mode is now an essential mode for the most airborne reconnaissance radar systems which can provide the information of the moving targets on a very wide area to realize traffic monitoring and battlefield surveillance.

Since different WAS-GMTI systems have different system parameters and scan mode, therefore signal processing algorithm of the WAS-GMTI mode should be carefully designed according to the feature of the radar system. For our three-channel X-band radar system, a simple and effective algorithm is designed and tested by the real data. The simple construction of the algorithm makes it easy for hardware implementation and real-time processing.

The algorithm can be divided into four stages: pre-processing, clutter suppression, CFAR (Constant False Alarm Rate) detection and parameter estimation.

The first step of pre-processing is to perform DC component removing and I/Q balancing of the data, which is followed by the range compression.

The second procedure is the clutter suppression. We take full advantage of the azimuth phase of the real data to realize an accurate estimation of the steering vector and the Doppler centroid. Note that the reconstructed spatial steering vector includes the fixed channel error which is beneficial to clutter suppression. Combing with the estimated spatial steering vector, the extended factored STAP algorithm is selected to suppress clutter in the real WAS-GMTI data processing.

The next step is CFAR detection. The three-step cell-averaging CFAR detector we apply to process the real data of our system shows a good performance to minimize the number of false alarms.

The main object for parameter estimation is to estimate the azimuth angle of the detected targets. The estimation errors are within 0.1 degree which meets the requirement of our WAS-GMTI system.

To observe the effect of the proposed algorithm, the real data processing results are shown after each stage. Moreover, some of the moving target positioning results of five successive scan periods are presented to demonstrate that the proposed algorithm can obtain a satisfactory performance in real application.

In sum, the core idea of the proposed algorithm is that the Doppler centroid corresponds to the antenna look direction. Therefore, the spatial steering vector can be obtained from the estimated Doppler centroid. Besides, the fixed channel error can be calculated and calibrated before parameter estimation, which makes it robust for real environment processing.

10427-50, Session JS1

Design, deployment and localization of bidirectional corner reflectors for TerraSAR-X

Adnan Saeed, Olaf Hellwich V, Technische Univ. Berlin (Germany)

This paper reports on the use of a distinctively designed

and deployed bi-directional trihedral corner reflector pair. The reflector is adjustable having two degrees of freedom in azimuth and elevation directions with one end of the pair firmly attached together. Oppositely faced and precisely oriented renders it visible in ascending and descending satellite orbital pass. Lightweight Aluminum and assemble able design makes it easy to be manufactured and transported

to the rooftops. Moreover, the design is simulated using a general purpose electromagnetic simulation software, CST and the Radar Cross Section is measured and verified. The installed reflectors were identified and localized in the acquired TerraSAR-X image data.

10427-51, Session JS2

Automatic identification of nonreflective subsurface targets in radar sounder data based on morphological profile

Mahdi Khodadadzadeh, Ana-Maria Ilisei, Lorenzo Bruzzone, Univ. degli Studi di Trento (Italy)

The analysis of the ice sheet subsurface is crucial for understanding the Earth climate changes, whereas the analysis of the subsurface of other planetary bodies (e.g., the poles of Mars, the moons of Jupiter) is fundamental for better understanding their formation and possible habitat. During the past decades, the development and use of radar sounder (RS) instruments to assist such investigations has received increasing attention. For example, the airborne Multichannel Coherent Radar Depth Sounder (MCoRDS) [1] and the spaceborne Shallow Radar sounder (SHARAD) [2] are two RS instruments that are successfully applied to the analysis of the ice sheets of the Earth and the subsurface of Mars, respectively. A RS is an active instrument that transmits low-frequency electromagnetic waves vertically towards the ice and measures the power of the waves reflected by the subsurface dielectric or mechanical discontinuities. Such measurements are recorded in two dimensional images called radargrams. The radargram horizontal axis is the distance along the acquisition track and the vertical axis shows the subsurface vertical profile as a function of depth. Thus, the radargrams show the subsurface cross-section.

Recently, the visual interpretation of radargrams has revealed that in addition to the common targets, i.e., layers of ice, the underlying basal interface and the thermal noise region at the bottom of the radargrams (that appears below the basal interface), there are other interesting non-reflective targets which frequently appear in the subsurface of the ice sheets of the Earth and also the south pole of Mars. Such targets are characterized by the absence of reflections. In the Antarctic and Greenland ice sheets, this target is called echo-free zone (EFZ). The EFZ can be hundreds of meters thick and is located just above the bedrock [3]. The literature shows that there are different possible causes for the presence of the EFZ in radargrams, e.g., elevated basal temperature, deformed ice, stagnant ice, increased layer roughness [3]. At the south pole of Mars, these non-reflective targets are called reflection-free zones (RFZs) and are located hundreds of meters below the surface [4,5]. A recent study argued that the RFZs are composed of massive deposits of CO2 ice [4]. The scientific importance of such non-reflective subsurface targets and their presence in wide areas covered by RS acquisitions call for the development of efficient automatic techniques designed specifically for their identification in radargrams.

In this paper, we propose a technique for the automatic identification of non-reflective subsurface targets in radar sounder data. The accurate automatic discrimination of the non-reflective targets in radargrams is a challenging task mainly because of their similarities to the thermal noise region. Regarding the EFZ, in [6], the authors proved the existence of such similarities in terms of power, statistical distributions and texture in RS data acquired in Antarctica. Moreover, they showed that the EFZ and the thermal noise regions can also be located at similar depths at different azimuth coordinates. For these reasons, the method proposed in [6] has classified the EFZ target together with the thermal noise as a unique class, preventing the possibility to accurately identify and perform detailed analysis of the EFZ. On the other hand, regarding the planetary RS data, the RFZ has been only manually detected [4]. This represents a strong limitation to the large-scale analysis of RFZs considering the huge amount of RS data acquired on Mars. The aim of our technique is thus the automatic discrimination of the non-reflective targets from the other subsurface targets, i.e., thermal noise, layers and bedrock, present in radargrams. To achieve this goal, we propose a supervised classification system which classifies the radargrams into three classes, i.e., non-reflective targets, thermal noise, and high reflections due to subsurface layers and bedrock. For such classification system, feature extraction is the central and most challenging task. The high reflections class is characterized by its power (or amplitude) value, and thus the main contribution of our method is the extraction of features to discriminate between the non-reflective targets and the thermal noise classes. Such features are extracted by taking into account an important observation, i.e., differently from the thermal noise region, the low backscattering values of the non-reflective targets are enclosed between the high backscattering reflections of ice internal layers and the bedrock. Therefore, the non-reflective targets and the thermal noise regions are characterized by distinct structures. In this work, we capture this structural information by applying morphological closing operation. In our problem, the radargram non-reflective regions appear darker than the surrounding high backscattering regions and in mathematical morphology, closing operation is well suited to isolate such dark regions. Thus, for feature extraction, a morphological profile (MP) is constructed based on the repeatedly application of the closing operation to the original radargram with a structuring element (SE) of increasing size [7]. Note that by doing so, the obtained MP feature set is highly redundant. In order to reduce its redundancy, we use the principal component analysis which retains 99.9% of the variance and simultaneously reduces the initial high dimensionality of the MP feature set. The extracted morphological features are then stacked with the original radargram and given as input to a support vector machine classifier [8], which performs the final supervised classification to identify the non-reflective targets.

We applied the proposed technique to two data sets containing non-reflective targets, i.e., i) a portion of the data set used in [6] which was acquired by MCoRDS [1] over about 200 km in central Antarctica; and ii) a SHARAD [2] data set composed of radargrams acquired on 10 orbits over the south pole of Mars. For the SHARAD data, we manually generated the corresponding reference maps of the subsurface classes, considering the RFZ class as reported in [4]. MPs were built using a squared SE with size increasing in the range {5, 100}, with a stepwise increment of 5. These values are chosen based on the data resolution and expected dimension of the non-reflective regions. For the classification, we used the same scheme of randomly selecting training and test samples reported in [6]. We obtained overall (average) classification accuracies of 98.34% (99.13%) and 98.67% (89.17%), for the Antarctica and Mars data set, respectively. These results and also the qualitative analysis of the obtained classification maps indicate that the proposed method can accurately identify the non-reflective targets in RS data. Most importantly, the proposed method can be effectively applied on large RS data sets in order to estimate the volume and the 3-D structure of the non-reflective targets.

Further details about related works, the proposed method and quantitative and qualitative results obtained on the investigated dataset will be provided in the full paper.

REFERENCES

[1] P. Gogineni. (2012) CReSIS radar depth sounder data. [Online]. Available: http://data.cresis.ku.edu/

[2] R. Seu, R. J. Phillips et al., “SHARAD sounding radar on the Mars Reconnaissance Orbiter,” Journal of Geophysical Research: Planets, vol. 112, no. E5, 2007.

[3] R. Drews, O. Eisen et al., “Layer disturbances and the radio-echo free zone in ice sheets,” The Cryosphere, vol. 3, pp. 195–203, 2009.

[4] R. J. Phillips et al., “Massive CO2 ice deposits sequestered in the south polar layered deposits of Mars,” Science, vol. 332, no. 6031, pp. 838–841, 2011.

[5] N. Putzig, R. Phillips et al., "Low radar reflectivity in planum australe points to past episodes of martian atmospheric collapse," in Lunar and Planetary Science Conference, vol. 46, 2015, p. 2586.

[6] A.-M. Ilisei and L. Bruzzone, "A system for the automatic classification of ice sheet subsurface targets in radar sounder data," IEEE Transactions on Geoscience and Remote Sensing, vol. 53, no. 6, pp. 3260–3277, 2015.

[7] M. Pesaresi and J. A. Benediktsson, "A new approach for the morphological segmentation of high-resolution satellite imagery," IEEE Transactions on Geoscience and Remote Sensing, vol. 39, no. 2, pp. 309–320, Feb 2001.

[8] C. Cortes and V. Vapnik, "Support-vector networks," Machine Learning, vol. 20, no. 3, pp. 273–297, Sep. 1995.

10428-1, Session 1

Change classification in SAR time series: a functional approach

Markus Boldt, Antje Thiele, Karsten Schulz, Fraunhofer-Institut für Optronik, Systemtechnik und Bildauswertung (Germany); Stefan Hinz, Karlsruher Institut für Technologie (Germany)

Change detection represents a broad field of research in remote sensing using Synthetic Aperture Radar, consisting of many different approaches for several applications. Besides the simple recognition of change areas, which delivers information about the location and the time, the analysis of type, category or class of the change areas is at least as important.

Classical strategies for remote sensing change classification require training datasets, which are more or less comprehensive and uneconomical. Moreover, the analyst needs a certain degree of expert knowledge with respect to the available data and the different classes of change regions contained in the specific scenery. The quality of the classification result depends on how accurate and representative the training sample selection for each class is accomplished. Moreover, this selection has to be done under the condition that the particular class actually exists in the dataset.

In this study, a framework for change classification using Synthetic Aperture Radar imagery is introduced, which overcomes the limits mentioned before. To ensure practical relevance, a sparse dataset is considered, containing only a time series of Single Look Complex images.

In detail, the test dataset, showing the area of Stuttgart (GER) airport and its surroundings, comprises 15 High Resolution SpotLight TerraSAR-X and TanDEM-X images, acquired over the period of one year (11/2013 to 11/2014). Due to this long period of time and the scenery containing heterogeneous types of high activity regions, different change categories could be covered in the data, which makes this set well suited for our study.

The proposed method mainly consists of three parts: Feature extraction, categorization and classification. First, the so called high activity change objects, being part of areas which are changing very frequently over time, provide the basis for the analysis.

Second, for the classification of the categorized change objects, an innovative self-checking procedure is introduced, consisting of the two major aspects 'fore-' (FP) and 'backprojection' (BP). The input of these steps is an initial, manually selected class catalogue. Within the FP, it is tested whether a pre-defined class actually exists in the categorized data or not. The BP is an iterative optimization step with the aim to improve the formulation of the manually selected classes. The result of this self-checking procedure is an optimized version of the initial class catalogue, matching best to the data driven reality. Consequently, no detailed expert knowledge is required for the definition of the class scheme. Moreover, the image interpreter is supported to produce a class description that is more meaningful with respect to the available dataset.

As third step, the resulting class scheme is applied on the categorized changes. Since real world examples of high activity regions or classes (e.g. parking places, construction sites) might contain a mixture of different change categories, Fuzzy logic is used to model this kind of uncertainty. In this paper, we focus on the description of the classification step of the proposed framework for change classification.

10428-2, Session 1

Generating high-accuracy urban distribution map for short-term change monitoring based on convolutional neural network by utilizing SAR imagery

Shota Iino, Riho Ito, Kento Doi, Tomoyuki Imaizumi, Shuhei Hikosaka, PASCO Corp. (Japan)

In the developing countries, urban areas are expanding rapidly. For example, Manila has constant attention of economic activities and motivating urban migration from different parts of the Philippines and area of continuous urban development, and for Jakarta in Indonesia more than 80 reclamation projects have been continued, coastal developments have been carried out for developing urban areas and flood management. With the rapid developments, short term monitoring of urban changes is important for various purposes such as marketing, updating development plans and predicting future growth of the cities. Monitoring of urban change will also contribute to predict the economic growth of each country. For short-term monitoring, constant observation and generation of high-accuracy urban distribution map without noise disturbance are key issues. If the accuracy of urban distribution map is not enough, it is very difficult to distinguish between actual changes and misclassification for small urban changes. The periodic imagery acquisitions by TerraSAR-X and ALOS-2 (dual-polarization) SAR satellites of Indonesia and Philippines, are highly suitable for day or night, and regardless of atmospheric weather condition observations for this type of study.

The current study highlights the methodology of generating high-accuracy urban distribution maps derived from SAR satellite imagery based on Convolutional Neural Network (CNN), which showed the outstanding results for image classification. To increase accuracy, several improvements on SAR polarization combinations and the procedure of image denoising of SAR satellite imagery, dataset construction and CNN model structure design were performed. As an additional data, Digital Surface Model (DSM), which are useful to distinguish land cover, were added to improve the accuracy. For polarization combinations, several patterns of polarization were compared. For image denoising of SAR imagery, different filters such as median filter and non-local means filter were tested. For the dataset construction, different sizes of cropped images were compared. In CNN model design, it is required to consider CNN model structure matched with the characteristics of the data. As SAR imagery and DSM have different characteristics, suitable CNN model for the data was designed.

From the obtained result, high-accuracy urban distribution map satisfying the quality for short-term monitoring was generated. For evaluation, urban changes were extracted by taking the difference of urban distribution maps. The change analysis with time series of imageries revealed the locations of urban change areas in each city for short term. Changes of urban distribution maps along the coast of Manila bay and Jakarta bay was observed. The results were validated by comparing with development plans in each country. Finally, analysis of the urban changes with several open data such as census data and economic statistics data was attempted to link urban change with economic growth of each country and further analysis will be conducted as future work of the present study.

10428-3, Session 1

Simulation of TanDEM-X interferograms for urban change detection

Amelie Welte, Karlsruher Institut für Technologie (Germany) and Fraunhofer-Institut für Optronik (Germany); Horst Hammer, Fraunhofer-Institut für Optronik, Systemtechnik und Bildauswertung (Germany); Antje Thiele, Fraunhofer-Institut für Optronik, Systemtechnik und Bildauswertung (Germany) and Karlsruher Institut für Technologie (Germany); Stefan Hinz, Karlsruher Institut für Technologie (Germany)

SAR amplitude change detection applications for spaceborne images have been researched for many years, and with the advent of the new generation of high resolution SAR satellites such as TerraSAR-X and COSMO-Skymed they have become feasible also for urban areas. In contrast to this, the interferometric phase that can be obtained from repeat-pass acquisitions has not been widely used for classical urban change detection. This is mainly due to the long revisit times of e.g. 11 days for TerraSAR-X which for all but the most arid areas causes significant decorrelation of the phase values.

The launch of TanDEM-X and the possibility to create single-pass interferograms in high resolution from space has changed this significantly. Using Tandem-X interferograms recorded at different times, urban change detection can be performed by exploiting the interferometric phase at building locations. The information contained in the interferograms is quite different from that contained in the amplitude images and thus requires different strategies for change detection.

In this paper, we first describe the appearance of buildings in interferometric phase images. For this analysis, we focus on larger buildings with empty surroundings, in order to show clearly the main features of such signatures. These include the layover area, the shadow area behind the buildings, and, for flat-roofed buildings mainly oriented in range direction, the roof heights.

The phase ramp in front of the buildings, also known as front porch, is a very distinct feature of any building with vertical walls. Its location can be determined in interferometric phase images in a stable and concise way by correlating the image with a line segment of the correct slope, which can be determined directly from the interferometric acquisition geometry, the range pixel size and the wavelength of the system. Shadow areas can be detected by their distinct statistics. Since these areas show no return signal, the main contribution to the phase is the additive noise of the system, which is assumed to be normally distributed in real and imaginary part, leading to a uniform distribution of the phase values. For larger flat-roofed buildings, which are oriented in range direction, the layover and shadow areas often are not very distinct. Thus, for these buildings, also the height information contained in the interferometric phase is used to detect the roof areas.

The interferometric change detection proposed in this paper mainly consists of a comparison of the layover, shadow and roof area masks extracted from the two interferometric phase images. However, since larger buildings usually feature distinct layover and shadow areas, also the combined evaluation of these features shows promising results, especially in cases where the buildings are not isolated, and thus the detections are mixed with features from nearby buildings. Some strategies to overcome this difficulty are presented and results are shown both on simulated and real data sets of a test area in Clichy-sous-Bois near Paris (France).

10428-4, Session 1

Sensor data fusion for textured reconstruction and virtual representation of alpine scenes

Gisela Häufel, Dimitri Bulatov, Peter Solbrig, Fraunhofer-Institut für Optronik, Systemtechnik und Bildauswertung (Germany)

The concept of remote sensing is to provide information about a wide-range area without making physical contact with this area. However, because of large processing times and computational resources, such a large area can often be only coarsely covered. Fortunately, the number and quality of additional sources of information for remote sensing tasks increases, which can provide a closer and more detailed insight of relevant subsections of such an area. For example, additionally to satellite imagery, images and videos taken by drones provide more up-to-date data at a higher resolution. Moreover, geographical information can be achieved using GPS-devices and important vector data is downloadable from the Internet. Thus, there is an increasing number of applications (virtual tourism, automatic navigation, hazard assessment, etc.) for which such a concept of sensor data fusion is strongly needed.

In our previous research, we extracted from UAV imagery important 3D objects, their positions in the scenery, and, if needed and available, their textures. In total, there were four object types: Building, tree regions (high vegetation), grass (low vegetation) and background. To achieve a more realistic visualization of the terrain, four object types are clearly not sufficient. Thus, more sophisticated classification and reconstruction algorithms must be applied to extract further object types: Mounds, rifts, single water bodies and others.

In this work, we present a reconstruction of an extremely interesting yet challenging dataset: An Alpine region in Southern Germany. A particular challenge of this work is that rock faces including overhangs are present in the input airborne laser point cloud. The overhangs exhibit a 3D surface, that is, in the ground surface itself, there is more than one value of z for a point (x,y). The first important contribution of this work will be thus identification and reconstruction of overhangs from point clouds. The proposed procedure comprises four steps: Point cloud preparation, filtering out vegetation, mesh generation and texturing.

Further issues addressed in this paper concern extraction of roads, mounds and trees from sensor data. Mounds are detected by several measures such as elevation, planarity, stripeness and NDVI, reconstructed using the method of L1 splines, and textured by the orthophoto. A distinction is made between large forest regions and important regions where individual tree detection is performed by the watershed algorithm the single trees are modeled using a commercial software. Finally, vector data for roads can be retrieved from airborne sensor data as well as GPS-device tracks. We pursue geo-specific reconstruction by assigning texture and width to roads of several pre-determined types.

For visualization and simulation of the area, we made use of the simulation system Virtual Battlespace 3 (VBS3). In its development tool, the elevation map and the orthophoto (texture) build up the map frame. The previously extracted 3D-objects are imported into the map frame. Unfortunately, because the resolution of the ground elevation map must often be reduced, especially in Alpine areas few automatic and interactive corrections must be undertaken in order to attach the 3D objects to the ground. Nevertheless, its extensive library of object types like trees, vehicles, animals etc. and a powerful mission editor tool justify the utilization of VBS3 for a visually-appealing, realistic representation of the scene as well as for simulation of rapid response scenarios.

10428-5, Session 1

Building rooftop classification using random forests for large-scale PV deployment

Dan Assouline, Nahid Mohajeri, Jean-Louis Scartezzini, Ecole Polytechnique Fédérale de Lausanne (Switzerland)

Large-scale solar photovoltaic (PV) deployment on the existing building rooftops has proven to be one of the most efficient and viable sources of renewable energy in urban areas. As it usually requires a potential analysis over the area of interest, a crucial step is to estimate (i) the area available for PV installation over rooftops, (ii) the geometric properties of the roofs including roof shape, slope (tilt) and aspect (azimuth), and (iii) the potential of solar radiation over the roofs. A significant number of studies have presented methodologies to estimate the available rooftop area for PV installation as well as the solar radiation potential over the roofs. Very few studies, however, explore the large-scale estimation of the geometric properties of the roofs. In this paper, we introduce a multi-layer machine learning methodology to classify 6 roof types/shapes, 9 aspect (azimuth) classes and 5 slope (tilt) classes for all building rooftops in Switzerland, using widely available GIS data. We train Random Forests (RF), an ensemble learning algorithm, to build the classifiers. We use (2 ? 2) [m2] LiDAR data (considering buildings and vegetation) to extract several rooftop features, and a generalized footprint polygon data to localize buildings.

The following processing steps are performed. The LiDAR data is first up-sampled to a resolution of (0.5 ? 0.5) [m2] and split into computationally manageable pieces. Python codes are then used to automate the process of extracting useful information from the LiDAR data while overlapping with the building footprint polygons. This includes frequencies of aspect and slope raster cell values for various bin configurations as well as the associated descriptive statistics (e.g. mean, mode and maximum bins). We also gather simple geometric information from the building polygons in the form of the number of vertices and the iso-perimetric quotient. Raster frequencies and statistics as well as geometric variables are then used as input features for the roof, aspect, and slope classifiers. A 6-fold cross validation is performed in the training stage of each RF model for parameter tuning. The accuracy matrices as well as the Out-of-Bag errors are then provided to measure the classification performance of the models. The roof classifier is trained and tested with 1252 labeled roofs from three different urban areas, namely Baden, Luzern, and Winterthur in Switzerland. The model is split into two steps: the first one classifies clusters of buildings between Flat, Single-building (rectangle footprint), and Multi-building (non-rectangle footprint) using the geometric features. The second step further classifies separately the single-building and multi-building roof shapes into 5 predefined types using both geometric and raster aspect and slope features. The results for the overall roof type classification show an average accuracy of 67%. The aspect and slope classifiers are trained and tested in a single step, with 11449 labeled roofs in the Zurich periphery area. The results for aspect and slope classification show different accuracies depending on the classes: while some classes are well identified, other under-represented classes remain challenging to detect.

10428-6, Session 1

3D building reconstruction in a remote sensing application workflow

Merlin Becker, Fraunhofer-Institut für Optronik, Systemtechnik und Bildauswertung (Germany); Irmgard Runkel, GEOSYSTEMS GmbH (Germany); Wolfgang Middelmann, Fraunhofer-Institut für Optronik, Systemtechnik und Bildauswertung (Germany); Nayeli S Espinosa, Fraunhofer-Institut für Optronik (Germany)

3D building reconstruction provides a high-end data product which assists situational awareness, conducting operations and training in simulated environments. The objective of our investigations is to assess existing commercial software for a high performance remote sensing data evaluation workflow. During the last decade software manufacturers have recognized the 3D building reconstruction as a topic. In addition, their differences to the current research topics need to be assessed. Therefore, use cases were developed and test scenarios performed. In this paper, we describe the assessment of commercial software from Agisoft Photoscan Professional and Tridicon BuildingFinder and obtained results regarding robustness, extensibility, applicability and computational performance. A comparison of the used algorithm and systems was made using several RGB-data-sets from various measurement campaigns. Furthermore, the applicability of the functionality and result to a remote sensing context was examined by connecting the system to our ground control station. The workflow will be included in a modern reconnaissance system. This system consists of an aircraft, the Stemme S-10. The sensor payload consists of an airborne laser scanner (ALS) Riegl VQ580 combined with four high resolution industrial cameras from SVS-Vistek with 16 megapixel resolution. Two cameras (RGB and near-infrared) point to NADIR; other two cameras have a slanted view to provide additional information, e.g. building texture data. All visual sensors are synchronized with the GPS/INS module to provide information for direct georeferencing and co-registration.

10428-7, Session 2

Amaro-autonomous real-time detection of moving maritime objects: introducing a flight experiment for an on-board ship detection system

Kurt Schwenk, Katharina A. M. Willburger, Sebastian Pless, Deutsches Zentrum für Luft- und Raumfahrt e.V. (Germany)

Motivated by politics and economy, the monitoring of the world wide ship traffic is a field of high topicality. To detect illegal activities like piracy, illegal fishery, ocean dumping and refugee transportation is of great value. The analysis of satellite images on the ground delivers a great contribution to situation awareness. However, for many applications the up-to-dateness of the data is crucial. With ground based processing, the time between image acquisition and delivery of the data to the end user is in the range of several hours. The highest influence to the duration of ground based processing is the delay caused by the transmission of the large amount of image data from the satellite to the processing centre on the ground. One expensive solution to this issue is the usage of data relay satellites systems like EDRS. Another approach is to analyse the image data directly on-board of the satellite. Since the product data (e.g. ship position, heading, velocity, characteristics) is very small compared to the input image data, real-time connections provided by satellite telecommunication services like Iridium or Orbcomm can be used to send small packets of information directly to the end user without significant delay.

The AMARO (Autonomous real-time detection of moving maritime objects) project at DLR is a feasibility study of an on-board ship detection system involving a real-time low bandwidth communication. The operation of a prototype on-board ship detection system will be demonstrated on an airborne platform. In this article the scope, aim and design of a flight experiment for an on-board ship detection system scheduled for end of 2017 is presented.

First, the scope and the constraints of the experiment are explained in detail. The main goal is to demonstrate the operability of an automatic ship detection system of maritime objects on board of an airplane. For data acquisition the optical high resolution DLR MACS-MARE camera (VIS/NIR) is used. The system will be able to send product data, like position, size and a small image of the ship directly to the userâ€™s smart-phone by email.

The time between the acquisition of the image data and the delivery of the product data to the end-user is aimed to be less than three minutes. For communication, the SMS-like Iridium Short Burst Data (SBD) Service was chosen, providing a message size of around 300 Bytes. Under optimal sending/receiving conditions, messages can be transmitted bidirectional every 20 seconds.

Due to the very small data bandwidth, not all product data may be transmittable at once, for instance, when flying over busy ships traffic zones. Therefore the system offers two services: a query and a push service. With the query service the end user can explicitly request data of a defined location and fixed time period by posting queries in an SQL-like language. With the push service, events can be predefined and messages are received automatically, if and when the event occurs.

Finally, the hardware set-up, details of the ship detection algorithms and the current status of the experiment is presented.

10428-8, Session 2

Evaluation of automatic cloud removal method for high elevation areas in Landsat 8 OLI images to improve environmental indexes computation

César Alvarez, Univ. do Porto (Portugal) and Univ. Politécnica Salesiana (Ecuador); Ana C. Teodoro, Univ. do Porto (Portugal); Alfonso Tierra, Univ. de las Fuerzas Armadas-ESPE (Ecuador)

Quito, Capital from Ecuador, is the second highest capital around the world with 2800 meters in altitude, crossing by equatorial line, located at the middle of Andes Region presenting high cloud frequency during all year, where Landsat 8 images have a high probability to have a big percentage of clouds. The objective of this work was to implement a method that allowed to remove clouds at high elevation areas, like Quito city, in order to obtain better results in the computation of environmental indexes like Normalized Difference Vegetation Index (NDVI). Data from Landsat 8 (six Landsat-8 OLI L1T scenes - Path 10 Row 60) were considered and compared with other products like MODIS MOD13Q1. The new Landsat-8 OLI bands 9 and Quality Assessment (QA) have an important development in the study of clouds removal. The algorithm considered to improve clouds removal was the Automatic Cloud Removal Method which considers a linear regression between bands 1-7 and band 9, where the linear regression that have a good R2 coefficient and the correspondent slope is used to remove clouds, having demonstrating good results in removing clouds in areas with low altitudes, like Sidney, Australia [1, 2]. This method tries to obtain a clean pixel data considering that each digital number (DN) recorded at each OLI spectral band i, i=1-7, is a result to have a clean pixel data plus contamination data at location (u,v). Contaminated data is included cloud effect [1]. The model can be expressed as (1):

DN(u,v)=x_i^f (u,v)+x_i^c (u,v) i=1,2,3,4,5,6,7 (1)

Where x_i^f (u,v) is the clean free pixel cloud from each band from 1 – 7, x_i^c (u,v) is the cirrus cloud pixel from each band from 1 – 7. Band 9 behaves to have an opportunity to obtain cirrus cloud pixel from each band and it is the main objective of this algorithm. The results applying this algorithm over Quito shows that we obtain good R2 coefficients but low slope values. However, considering slope values similar to those were considered in [2], the algorithm works better and an improvement in high elevation areas in visible. All the procedure was implemented in R Studio with Raster Package. Concluding, this modified algorithm can improve the computation of environmental indexes considering the comparison with other data like MODIS and the same Landsat 8 data without removal clouds. This work is a valuable contribution for the study of environmental indexes in high elevation areas very affected by clouds through remote sensing data.

[1] Ji, C. Y. Haze reduction from the visible bands of LANDSAT TM and ETM+ images over a shallow water reef environment. Remote Sens. Environ. 2008, 112, 1773–1783.

[2] Xu, M.; Jia, X.; Pickering, M. Automatic cloud removal for Landsat 8 OLI images using cirrus band. Int. Geosci. Remote Sens. Symp. 2014, 2511–2514.

10428-9, Session 2

A combined use of multispectral and SAR images for ship detection and characterization through object based image analysis

Martina Aiello, Marco Gianinetto, Politecnico di Milano (Italy)

Marine routes represent a huge portion of commercial and human trades, therefore surveillance, security and environmental protection themes are gaining increasing importance. Ship detection from satellite imagery is a well-known application. However, in the last years ship detection has prompted a renewed interest for a continuous monitoring of illegal activities, since it is able to overcome the limits imposed by terrestrial means of monitoring, which require a considerable amount of resources.

This paper describes an automatic Object Based Image Analysis (OBIA) approach to detect various types of vessels in different sea environments. The combined use of high and medium resolution optical images (WorldView-2, QuickBird, GeoEye-1, Sentinel-2) and SAR images (COSMO-SkyMed), which characterizes this work, allows for a regular observation unrestricted by lighting and atmospheric conditions and complementarity in terms of geographic coverage and geometric detail. Moreover, the necessity to detect vessels made of different materials (e.g. wooden or metallic) makes the mutual use of the two acquisition systems particularly significant in terms of detection results, as the use of a single technology may lead to missed identification or misclassification. Optical images are first pre-processed through radiometric calibration, atmospheric correction and Minimum Noise Fraction transform. The method developed adopts a region growing algorithm to segment the image in homogeneous objects, which are then classified through a decision tree algorithm based on spectral (i.e. intensity) and geometrical properties (i.e. area, length to width ratio). Then, a spatial analysis retrieves the vessels' position, length and heading parameters. The image processing chain is optimized to reduce the overall computational time through a chessboard subdivision prior image segmentation. Thus, the input image is divided into smaller tiles and only those including potential vessels are retained for further processing. The selection is made according to the skewness (i.e. symmetry) of the pixels intensity distribution for the selected image component. Image tiles with a Gaussian distribution (i.e. symmetrical) are expected to include only sea, while tiles with asymmetrical distributions are candidates for containing vessels. Processing of SAR images requires an additional step preceding the object based analysis; vessels candidates are detected using amplitude data and a Constant False Alarm Rate (CFAR) algorithm. This method selects the brighter pixels over the background by means of an adaptive threshold defined according to a Gaussian modelling of the sea statistics.

Validation is carried out by comparing the retrieved parameters (vessels' position, length and heading) with the information provided by the Automatic Identification System (AIS), when available, or with manual measurement when AIS data are not available. The estimation of length shows R2=0.87 and estimation of heading R2=0.95, computed as the average of R2 values obtained for both optical and radar images.

Together with length, position and heading, vessels parametric characterization is refined by associating to each detected ship a speed range, determined from AIS speed data of existing vessels comparable for dimension.

10428-10, Session 2

Normalization of time-series satellite reflectance data to a standard sun-target-sensor geometry using a semi-empirical model

Yongguang Zhao, Chuanrong Li, Lingling Ma, Lingli Tang, Ning Wang, Chuncheng Zhou, Yonggang Qian, Academy of Opto-Electronics, CAS (China) and Key Lab. of Quantitative Remote Sensing Information Technology, CAS (China)

Time series of satellite reflectance data have been widely used to characterize environmental phenomena, describe trends in vegetation dynamics and study climate change. However, several sensors with wide spatial coverage and high observation frequency are usually designed to have large field of view (FOV), which cause variations in the sun-target-sensor geometry in time-series reflectance data. Due to the anisotropic characteristics of surfaces, variations in the sun-target-sensor geometry can cause apparent change in reflectance even if the surface properties remain constant, and the variability in time-series reflectance data has the same order of magnitude as the signal related to actual changes in vegetation. Therefore, surface reflectance derived from multi-temporal remote sensing data should be normalized to a common illumination and viewing angles in order to monitor ecosystems and track vegetation dynamics on regional or global scales.

Semiempirical kernel driven BRDF models are widely used for correcting and studying bidirectional effects of a wide variety of land covers. These models are formulated as a linear combination of three terms made up of an isotropic component and two anisotropic kernels, weighted by coefficients.In the past, various investigators have employed the semiempirical kernel driven BRDF models (Roujean, Ross-Li, etc.) to normalize remote sensing data to a standard sun-target-sensor geometry. To obtain the bidirectional information of land surface, these approaches used multiple measurements of the same pixel at different times. One measurement for the time interval that is free from directional effects can be provided by these approaches. However, detailed multiangle measurements at desired spatial and temporal resolutions are often not available. In this study, on the basis of semiempirical kernel-driven BRDF model, a new semi-empirical model was proposed to normalize the sun-target-sensor geometry of remote sensing image. To account for the seasonality of land surface bidirectional reflectance, the polynomial function of vegetation index was used as the coefficients of volume-scatter kernel and surface scatter kernel in the semiempirical kernel-driven BRDF model. Multi-angle observation data acquired at different dates was used to derive the coefficients of the model which were applied to normalize the sun-target-sensor geometry of time-series satellite reflectance data.

To evaluate the proposed model, bidirectional reflectance under different canopy growth conditions simulated by Discrete Anisotropic Radiative Transfer (DART) model were used. The semi-empirical model was first fitted by using all simulated bidirectional reflectance. Experimental result showed a good fit between the bidirectional reflectance estimated by the proposed model and the simulated value. Then, MODIS time-series reflectance data was normalized to a common sun-target-sensor geometry by the proposed model. The experimental results showed the proposed model yielded good fits between the observed and estimated values. The noise-like fluctuations in time-series reflectance data was also reduced after the sun-target-sensor normalization process. The results indicate that the proposed model is capable of normalizing satellite data to a standard sun-target-sensor geometry. In addition, this approach was also compared with a nonlinear temporal angular model (NTAM). In the test, the proposed model yielded better fits between the observed and estimated values.

10428-11, Session 3

Analysis of economic values of land use and land cover changes in crisis territories by satellite data: models of socio-economy and population dynamics in war

Yuriy V. Kostyuchenko, Maxim Yuschenko, Dmytro Movchan, Ivan Kopachevsky, Ctr. for Aerospace Research of the Earth (Ukraine)

In the conflicts and crises the accurate, timely and adequate information acquiring is a daunting challenge. Decision making in the conflict should be based on the all available and accessible information to be correct, adequate, useful and executable. Lack of reliable data, their correct spatial and temporal distribution and dynamics is the main problem of conflict analysis and security management. Usually data set includes maps, GIS, satellite data, regional and local archives, complex of existing statistics, surveys and population census, etc.

This paper aimed to demonstrate how the methods of collecting, filtering, regularization of multi-sources data can be integrated using the models to identify reliable indicators of the socio-economic and socio-ecological security, and the conflict dynamics.

Correct estimation of economic and population dynamics is the important issue of risks assessment and threat analysis during the conflicts. At the same time this is the complicated problem through the lach of reliable data.

Problem of remote sensing data harnessing for decision making in conflict territories is considered. Approach for analysis of socio-economic and demographic parameters with a limited set of data and deep uncertainty is described.

Number of interlinked techniques to estimate a population dynamics and economy in crisis territories are proposed. Stochastic method to assessment of population dynamics in urban and rural areas using multi-source data and modeling of socio-economic parameters using remote sensing data is proposed.

Adaptive Markov's chain based method to study of land-use changes using satellite data is proposed. Proposed approach is applied to analysis of socio-economic situation in Donbas (East Ukraine) territory of conflict in 2014-2015.

Land-use and land-cover patterns for different periods were mapped using the Landsat and MODIS data . The land-use classification scheme includes the following categories: (1) urban or built-up land, (2) barren land, (3) cropland, (4) horticulture farms, (5) livestock farms, (6) forest, and (7) water. It was demonstrated, that during the period 2014-2015 was not detected drastic changes in land-use structure of study area. Heterogeneously distributed decreasing of horticulture farms (4-6%), livestock farms (5-6%), croplands (3-4%), and increasing of barren land (6-7%) have been observed.

Way to analyze land-cover productivity variations using satellite data is proposed. Algorithm is based on analysis of time-series of vegetation (NDVI) and water (NDWI) spectral reflectance indices distributions derived from Landsat 5 and 8. Drastic changes of crop area dynamics and its productivity has been detected. General decreasing of crop productivity was assessed up to 80%.

Set of indirect indicators, such as night light intensity, is also considered. Multi-source data integration algorithm based on Kolmogorov optimization equation is proposed. Using the approach proposed, basing on the data utilized, the local and regional GDP, local population, and its dynamics are estimated.

Conclusions on limitations and advantages of the described integrated approach in risk management and conflict control are proposed and discussed. Role of the remote sensing data in the complex of multi-source data in the tasks of socio-ecological and domestic security is also discussed.

10428-12, Session 3

UAV remote sensing hazard damage assessment in Funing tornado disaster

Qi H. Wen, Wei Wang, Donghua Pan, Ping Wang, Tong Tang, National Disaster Reduction Ctr. of China (China)

On June 23th, 2016, a huge Tornado Disaster occurred in Funing County and Sheyang County, Yancheng City, Jiangxi Province, which brought a huge loss of personal life and property. Municipal administration, infrastracuture and social economic industries suffered serious damage. An UAV group was sent there after one day to acquire disaster area images; After image p reprocessing, 27 UAV images of 0.15 meter resolution were acquired. The damage assessment target mainly included 2 kind of bodies of disaster-affected, and the results were finally verified by reported disaster condition information from local government.

Firstly, building damage resulted in the main economic loss, so background data of buildings was preferentially prepared. High resolution pre-disaster remote sensing images were grab and downloaded from Google Earth. The contour of each building within tornado affected region was extracted by visual interpretation and the attribute of building structure and building function was also labeled. The raster data and vector data were references for comparison with post-disaster images.

Then, post-disaster UAV images were compared with pre-disaster images to define damage grade of each building. The damage condition was divided into four damage grades: completely collapsed, seriously damaged, generally damaged and basically well. Each building was assigned one damage grade according to its damage condition by referring to interpretation keys, and the damage grade was labeled in background vector data. Damage condition of buildings was counted in the village as a unit in order to assess the damage grade of each village within disaster affected region.

Finally, remote sensing assessment results were verified by reported disaster information from local government. A comprehensive disaster condition index(CDCI) was formulated as the assessment index. The number of death, number of injured, number of resettled, number of collapsed and damaged buildings are weighted averaged as CDCI. Death, injury and resettlement were mainly caused by building damage so these indicators can also partly reflect the building damage condition. CDCI of each county within disaster affected region was calculated and damage grade was divided by threshold value. This result was compared with remote sensing assessment result, and they matched each other very well.

NDRCC also assessed damage condition of power facilities such as telegraph pole, electric power tower from UAV images, which also help to judge the damage grade of each county. The assessment results were incorporated into tornado disaster assessment report and put in the Government of Jiangxi Province.

10428-13, Session 3

The use of UAVs for monitoring land degradation

Kyriacos Themistocleous, Cyprus Univ. of Technology (Cyprus)

Land degradation is one of the causes of desertification of drylands in the Mediterranean. UAVs can be used to monitor and document the various variables that cause desertification in drylands, including overgrazing, aridity, vegetation loss, etc. This paper examines the use of UAVs and accompanying sensors to monitor overgrazing, vegetation stress and aridity in the study area. UAV images can be used to generate digital elevation models (DEMs) to examine the changes in microtopography as well as ortho-photos were used to detect changes in vegetation patterns. The combined data of the digital elevation models and the orthophotos can be used to identify the mechanisms for desertification in the study area.

10428-14, Session 3

ERATOSTHENES: excellence research Centre for Earth surveillance and space-based monitoring of the environment, the EXCELSIOR Horizon 2020 teaming project

Diofantos G. Hadjimitsis, Cyprus Univ. of Technology (Cyprus); Charalambos C. Kontoes, National Observatory of Athens (Greece); Gunter Schreier, Deutsches Zentrum für Luft- und Raumfahrt e.V. (Germany); Albert Ansmann, Leibniz Institut für Troposphärenforschung (Germany); Georgios Komodromos, Ministry of Transport, Communications and Works (Cyprus); Kyriacos Themistocleous, Rodanthi-Elisavet Mamouri , Silas C. Michaelides, Argyro Nisantzi, Christiana Papoutsa, Kyriacos Neocleous, Christodoulos Mettas, Marios Tzouvaras, Evagoras Evagorou, Andreas Christofe, George Melillos, Cyprus Univ. of Technology (Cyprus); Ioannis Papoutsis, National Observatory of Athens (Greece)

The aim of this paper is to present our strategy and vision to upgrade the existing ERATOSTHENES Research Centre (ERC) established within the Cyprus University of Technology (CUT) into a sustainable, viable and autonomous Centre of Excellence (CoE) for Earth Surveillance and Space-Based Monitoring of the Environment, which will provide the highest quality of related services both on the National, European and International levels. The EXCELSIOR Project is a Horizon 2020 Teaming project which addresses a specific challenge defined by the work program – namely, the reduction of substantial disparities in the European Union by supporting research and innovation activities and systems in low performing countries. It also aims at establishing long-term and strategic partnerships between the Teaming partners, thus reducing internal research and innovation disparities within European Research and Innovation landscape. The proposed CoE envisions the upgrading of the existing ERC into an inspiring environment for conducting basic and applied research and innovation in the areas of the integrated use of remote sensing and space-based techniques for monitoring the environment. Environment has been recognized by the Smart Specialization Strategy of Cyprus as the first horizontal priority for future growth of the island. The foreseen upgrade will regard the expansion of this vision to systematic monitoring of environment using earth observation, space and ground based integrated technologies. Such an approach will lead to the systematic monitoring of all three domains of the Environment (Air, Land, Water). Five partners have united to upgrade the existing ERC into a CoE, with the common vision to become a world-class innovation, research and education centre, actively contributing to the European Research Area (ERA). More specifically, the Teaming project is a team effort between the Cyprus University of Technology (CUT, acting as the coordinator), the German Aerospace Centre (DLR), the National Observatory of Athens (NOA), the German Leibniz Institute for Tropospheric Research (TROPOS) and the Cyprus' Department of Electronic Communications of the Ministry of Transport, Communications and Works (DEC-MTCW).

10428-15, Session 3

Characterization of satellite-derived surface solar irradiance products: SASSCAL stations

Naveen R. Shahi, Univ. of the Witwatersrand (South Africa)

Accurate satellite measurements and derived data products of surface solar irradiance (SSI) for all sky conditions over Africa is vital for understanding the surface radiative balance uncertainty and robustness analyses of the region. Large number of insitu observations of SSI is provided through SASSCAL Weather stations in Angola, Botswana, Namibia, South Africa and Zambia which are providing hourly measurements of SSI, utilizing these datasets a cross validation and characterization of SSI is done over measurement locations. Cloud and the Earth's Radiant Energy System (CERES) parameterized SSI at 1.0° equal angle region and Spinning Enhanced Visible and Infrared Imager (SEVIRI) on Meteosat Second Generation (MSG)(SEVERI/MSG-10) at 0° longitude, covering 60°S-60°N and 60°W-60°E, at 0.05° latitude-longitude derived SSI measurement for period of two years [2015-2016] are validated. Thereafter, this will be further extended forward and backward time slots with available data observations. This Study focus on the uncertainty analysis of the satellite derived SSI under all atmospheric conditions for the year 2015-16 at particular measurement sites and which will be further utilized in trend-bias estimation of how much radiative flux is getting pumped into African subcontinent. Characterization of current available satellite SSI product will be integrated with multi angle imaging spectroradiometer-high resolution [MISR-HR] derived broadband albedo product in empirical estimation of Net surface shortwave radiation over southern Africa.

10428-16, Session 4

Spectral discrimination of macrophyte species among different seasons in a tropical wetland using in-situ hyperspectral remote sensing

Ridhi Saluja, J. K. Garg, Guru Gobind Singh Indraprastha Univ. (India)

Introduction: Wetlands, one of the most productive ecosystems on Earth perform multitude ecological functions and provide expansive ecological services. Despite of their ecological and economic values, wetlands have experienced significant degradation. Techniques for discriminating macrophyte species in wetland ecosystems are critical for rapid wetland assessment and proactive management. Remote sensing can help monitor the spread and effects of invasive species in wetland ecosystems and thus determine species and locations to target for conversation. However, there is a major problem in mapping macrophyte species due to similar responses in broadband multispectral remote sensing imagery, resulting in misclassification and misinterpretation. In this study an attempt has been made to evaluate the potential of narrowband spectroradiometer data in discriminating wetland macrophytes during different seasons.

Objectives of the research: 1) whether macrophyte species could be discriminated based on in-situ spectral reflectance, 2) which species and season is most influential in affecting discriminability and 3) to determine the corresponding best separable wavebands while comparing the discriminative performance of LSD and SDA technique.

Hypothesis: The null hypothesis, that there was no significant difference in the mean reflectance of wetland macrophytes, was tested using various statistical methods.

Methodology: Spectral characteristics of dominant wetland macrophyte species, including Eichhornia crassipes, Salvinia natans, Phragmites karka, Cyperus alopecuroides, Typha sp., Hydrilla verticillata and Vallisneria spiralis, were measured in the seasons of summer, monsoon and winter by SVC GER 1500 portable spectroradiometer over the 400- to 900-nm spectral range at 1.5nm interval, at the Bhindawas Wetland in the state of Haryana, India. Hyperspectral observations were pre-processed and averaged reflectance values were subjected to statistical tests. Initially, one-way ANOVA and non-parametric Kruskal-Wallis H test were performed for identification of wavebands that exhibited significant differences ($p<0.05$) in the spectral reflectance across species. Factor analysis/ PCA method of band selection procedure is also validated against existing methods of band selection. Two procedures were tested to determine the optimum bands for discriminating macrophyte species: least significant difference (LSD) and stepwise discriminant analysis (SDA).

Results and Conclusion: Statistical analysis revealed that the most influential wavelengths for discrimination were distributed along the spectral profile from the visible to the near-infrared regions. The results suggest that hyperspectral data can be used discriminate wetland macrophyte species working as an effective tool for advanced mapping and monitoring of wetlands.

10428-17, Session 4

Explicit area-based accuracy assessment for mangrove tree crown delineation using geographic object-based image analysis (GEOBIA)

Muhammad Kamal, Univ. Gadjah Mada (Indonesia); Kasper Johansen, The Univ. of Queensland (Australia)

Effective mangrove management requires spatially explicit information of mangrove tree crown map as a basis for ecosystem diversity study and health assessment. Accuracy assessment is an integral part of any mapping activities to measure the effectiveness of the classification approach and evaluate the information accuracy of the maps. In addition to the thematic accuracy, the accuracy assessment of geographic object-based image analysis (GEOBIA) also requires assessment of the geometric accuracy (shape, symmetry and location) of the created image objects from image segmentation procedure. In this study we used an explicit area-based accuracy assessment to measure the degree of similarity between the results of the classification and reference data from different aspects, including overall quality (OQ), user's accuracy (UA), producer's accuracy (PA) and overall accuracy (OA). We developed a rule set to delineate the mangrove tree crown using WorldView-2 pan-sharpened image (50cm pixel size) and compare the result with the reference map. We visually delineate the mangrove tree crowns boundaries form a very high-spatial resolution aerial photograph (7.5cm pixel size) as a reference to assess the thematic and geometric mapping accuracy of the GEOBIA approach. Ten random points with a 10 m radius circular buffer were created to calculate the area-based accuracy assessment. The circular buffer was used for practical reasons to create the area samples, and the number of points and buffer radius were chosen with regard to the size of the objects on the map being assessed. The resulting circular polygons were used to clip both the classified image objects and reference map for area comparisons. In this case, the area-based accuracy assessment resulted 64% and 68% for the OQ and OA, respectively. The overall quality of the calculation results shows the class-related area accuracy; which is the area of correctly classified as tree crowns was 64% out of the total area of tree crowns. On the other hand, the overall accuracy of 68% was calculated as the percentage of all correctly classified classes (tree crowns and canopy gaps) in comparison to the total class area (an entire image). Overall, the area-based accuracy assessment was simple to implement and easy to interpret. More importantly, it shows explicitly the error variations of object boundary delineation with colour coded polygons (i.e. it shows explicitly if there is omission or commission for a certain category).

10428-18, Session 4

Ecological analysis of desertification processes in semiarid land in Algeria using satellite data

Ahmed Zegrar, Mohamed Ghabi, Assia Saad, Ctr. National des Techniques Spatiales (Algeria)

Desertification, a phenomenon of loss of productivity of the land is both a matter of Environment and Development (Cornet, 2002). It is linked to the anthropogenic action and to climate variability but also to changes in biodiversity, in particular the Maghreb (Hobbs et al., 1995). The desertification of the steppe areas of North Africa (Algeria, Morocco and Tunisia) is considered of special concern by the specialists in these regions. Desertification, Climate Change and the erosion of biodiversity are the central issues for the development of arid, semi-arid. In this region, the combination of two factors, climatic and anthropogenic, has fostered a deterioration of the vegetation cover, soil erosion and the scarcity of water resources. The climate of this region is characterized by periods of recurring droughts since the 1970s. The anthropogenic pressure is the result of a combination of factors among which the strong demographic growth, the intensification and extension of production systems agro-pastoral or still further the concentration of a growing livestock on smaller spaces. In this study, the criteria for classification and identification of physical parameters for spatial ecological analysis of vegetation in the steppe region to determine the degradation and vulnerability vegetation formations and how to conduct to phenomenon of desertification. So we use some satellite data in different dates (LANDSAT) in order to determine the ecological of steppe formation and changes in land cover, sand moving and forest deterioration. The application of classification and some arithmetic combination with NDVI and MSAVI2 through specific processes was used to characterize the main steppe formations. An ecological analysis of plant communities and impact of sand move describe the nature of the desertification phenomenon and allow us to determine the impact of factors of climate and entropic activity in the Algerian steppe.

10428-20, Session 4

Impacts of post-disaster recovery on land surface temperature after the 2004 Indian tsunami: a case study of Banda Aceh, Indonesia

Saumi Syahreza, Muhammad Syukri Surbakti, Syiah Kuala Univ. (Indonesia); Kok Chooi Tan, Hwee San Lim, Mohamad Zubir Mat Jafri, Univ. Sains Malaysia (Malaysia)

Aceh had been the focus of an unprecedented international rehabilitation effort in response to the giant Sumatra-Andaman earthquake (Mw 9.3) and tsunami disaster on December 26, 2004. During this period, most researchers have contributed to better understanding what happened in the past, and what going to happen in the future. This paper relates to the environment assessment as consequences of disaster recovery and post-recovery periods and reconstructions by assessing the impacts of land use/land cover change (LULC) on land surface temperature (LST). Land cover classification and LST retrieved and estimated utilizing visible and thermal infrared data based on satellite open data (Landsat-5 TM + Landsat 8 OLI) within the period 2004 to 2015. The surface temperature-vegetation index space of LULC was established to investigate the impacts of land changes over LST sensitivity. The result demonstrated that the post-disaster recovery and reconstruction has had a significant impact to the LULC in Banda Aceh and its fringes. Dramatic LULC in Banda Aceh significantly increases the LST, the temporal trend of pixels migrated from the dense vegetation-low temperature condition to the less dense vegetation-high temperature condition.

10428-21, Session 4

Determination of spatial erosion risk distribution for management and planning in Yeka Ankorucha catchment using ‘RUSLE’ model, GIS and RS, Addis Ababa, Ethiopia

Zebene Worku Woldegeorgis, Ministry of Water, Irrigation and Electricity (Ethiopia)

The use of RS and GIS techniques integrating with RUSLE makes soil erosion estimation and its spatial distribution feasible with reasonable costs and better accuracy in larger area. Such methods provide significantly better results than using traditional methods of measuring and calculating Erosion related biophysical data on the field. Human activities such as urbanization and industrialization and the respective land use change within a basin is one of the contributing factors, which cause deterioration of river water quality through its potential effect on erosion. Sediment yield in the form of suspended solid in the river water body, which is transported to the downstream area, occurs as a sign of lowering of the water quality. Hence, the aim of this study was to determine potential soil loss using the Revised Universal Soil Loss Equation (RUSLE) model in Geographical Information Systems (GIS) environment within selected catchment of Awash River Basin. RUSLE was used to estimate potential soil losses by utilizing information on rainfall erosivity (R) using interpolation of rainfall data, soil erodibility (K) using soil map, vegetation cover (C) using satellite images, topography (LS) using DEM and conservation practices (P) using data collected by GPS for the conservation actions made in the area .The results indicated that the rate of potential soil loss in Yeka Ankorucha catchment, Ethiopia ranged from very low to sever. The area covered by low to moderate potential soil loss was about 51%, whereas moderate to soil loss potential covered about 49% of the study area.

10428-63, Session 4

Application of SAR data for seasonal monitoring of floating reed islands dynamic in Srebarna Lake

Iva Ivanova, Roumen Nedkov, Denitsa Borisova, Space Research and Technology Institute (Bulgaria)

The aim of this paper is seasonal monitoring of floating reed islands dynamic in Srebarna Lake (Bulgaria) using SAR data. Srebarna Lake is a part of Natura 2000 European ecological network. The floating reed islands are unique habitats for Europe. They are presented only in Srebarna Lake and the Danube Delta and they are important for different waterbird species breeding, some of which are endangered species. In order to preserve and manage the resources of these wetlands their inventory and monitoring, together with their surroundings is very important. In order to study the seasonal dynamic of floating reed islands (such as absolute and relative movement) only opportunities which provide high-tech methods based on space remote sensing were used. Sensors with suitable parameters for data registration for this type of unsystematic landscape units were used. SAR data (Synthetic Aperture) are a powerful high-tech tool for ground objects monitoring. SAR data images are privileged to register data at any time of the day or night and in adverse weather conditions, which are the main limiting factor in optical images. For this study data from the ?uropean Space Agency (ESA) satellites from the Copernicus missions “Sentinel-1-A” and “Sentinel-2-A” were used. The “Sentinel-1-A” (C-band with wavelength of ~5,6 cm) is a Synthetic Aperture Radar (SAR) of the sensor. The “Sentinel-2-?” Multi-Spectral Instrument (MSI) registers data in optical bands with different resolutions. Seasonal monitoring of floating reed islands using SAR data was performed - winter - when the water in the lake is frozen, then a relative movement of these islands was observed, spring - melting snow cover

and rising water level in the Danube River and Srebarna Lake were observed, and in the late autumn, when the water level is low. Obtained results give a quantitative assessment of the ecological dynamics of these types of habitats in Srebarna Lake. They show the movement of the islands through the seasons in the period of one year, the changes in their shape and size. Studying the dynamics of the floating reed islands is essential for monitoring of these specific habitats for nesting of endangered bird species. Seasonal monitoring of the floating reed islands dynamic is very important for their preservation as a specific habitat.

10428-49, Session PS

The multiscale classification system and grid encoding mode of ecological land in China

Jing Wang, Wuhan Univ. (China); Aixia Liu, China Land Surveying and Planning Institute (China); Yifan Lin, Peking Univ. (China)

Optimization of national land use spatial pattern and protection of natural ecological system and environment are two critical tasks for ecological civilization construction in China. Ecological land can provide goods and services that have direct or indirect benefic to eco-environment and human welfare. In recent years, the research on ecological land has become a hot spot in the field of land changes and ecosystem management in China. In the study, a multi-scale classification scheme of ecological land was developed for land management based on combination of the land-use classification and the ecological function zoning in China, including eco-zone, eco-region, eco-district, land ecosystem, and ecological land-use type. The geographical spatial unit leads toward greater homogeneity from macro to micro scale. The term “ecological land-use type” is the smallest one which has a homogeneous landscape with specific vegetation, physical environment, climate, and disturbance characteristics (both natural and human), being important to maintain the key ecological processes in land ecosystem. Ecological land-use type was categorized into major-functional and multi-functional ecological land-use type according to its ecological function attributes and production function attributes based on the land use classification system by the Ministry of Land and Resources. Major-functional ecological land-use type was defined as one kind of land-use type mainly providing ecological goods and function attributes, such as river, lake, swampland, reed and shoaly land, glacier and snow, while multi-functional not only providing ecological goods and function attributes but also productive goods and function attributes, such as arable land, forestry land, and grassland. Furthermore, the multi-level grid encoding mode was proposed for modern management of ecological land and data update under cadastral encoding. The multi-level irregular grid encoding from coarse to fine included eco-zone, eco-region, eco-district, cadastral area, land ecosystem, land ownership type, ecological land-use type, and parcel. Besides, the suggestions on ecosystem management were proposed to provide supports for integrated management of natural resources in China.

10428-50, Session PS

Demarcation of mineral rich zones in areas adjoining to a copper prospect in Rajasthan, India using ASTER, DEM (ALOS) and spaceborne gravity data

Vivek K. Sengar, Prashant Kumar Champati Ray, Shovan Lal Chattoraj, Indian Institute of Remote Sensing (India); A. S. Venkatesh, Indian Institute of Technology (Indian School of Mines) (India); R. Sajeev, Purnima Konwar, Geological Survey of India (GSI) (India); Shailaja Thapa, Indian Institute of Remote Sensing (India)

The objective of this work is to identify the potential zones for detailed mineral exploration studies in areas adjoining to a copper prospect using Remotely Sensed data sets. In this study visualization of ASTER data has been enhanced to highlight the mineral-rich areas using various remote sensing techniques such as colour composites and band ratios. VNIR region of ASTER is significant to detect iron oxides while, clay minerals, carbonates and chlorites have characteristic absorption in the SWIR wavelength region. Therefore, an attempt has been made to target the mineral abundant regions through ASTER data processing. Height based information was extracted using high-resolution ALOS-DEM to analyse the topographical controls in the region considering the fact that mineral deposits often found associated with geological structures and geomorphological units. Gravity data was used to generate gravity anomaly map which gives clues about subsurface density differences. In this context, base metal ores may show anomalous (high) gravity values in comparison to the non-mineralised areas. Outputs from all the data sets were analysed and correlated with the geological map and available literature. Final validation of results has been done through proper ground checks and laboratory analysis of rock samples collected from the litho-units present in the study area. Based on this study some new areas have been successfully demarcated which may be potential for base metal exploration.

10428-51, Session PS

Image object-based water body types identification in coastal area

Jian Chen, The Second Institute of Oceanography (China); Jianyu Chen, The Second Institute of Oceanography, SOA (China); Peng Chen, Zengzhou Hao, The Second Institute of Oceanography (China)

For object-based recognition for water body types, aiming at the special characteristics in coastal zone, relevant researches have been carried out by adding spatial semantic features to the extraction process. Through analyzing the spectral and texture features of water, the rule set for extracting water objects is established and specific implementation is based on the segments, adjacent water segments merged together in order to acquiring a new water object. Then utilizing high level features (such as topological relationship and contextual relevance) existed in those water objects to achieve the subdivision for water objects. The water bodies are subdivided into coastal waters, aquaculture ponds and inland water bodies respectively. The water body types’ recognition method proposed in this paper gets rid of the traditional object-based classifications based on statistical law. Using prior knowledge to construct knowledge rules with spatial semantic information makes spatial distribution characteristics in coastal zone can be effectively improving the accuracy of type identification.

10428-53, Session PS

PI2GIS: processing image to geographical information systems, a learning tool for QGIS

Rui Correia, Ana C. Teodoro, Lia Duarte, Univ. do Porto (Portugal)

To perform an accurate interpretation of remote sensing images, it is necessary to extract information using different image processing techniques. Nowadays, it became usual to use image processing plugins to add new capabilities/functionalities for Geographical Information System (GIS) software. The aim of this work is to develop an open source application to automatically process and classify remote sensing images from a set of satellite input data. The application is integrated in a GIS software (QGIS), automating several image processing steps. It is quick, efficient and easy to use. Furthermore, the use of QGIS for this purpose is justified since it is easy and quick to develop new plugins, using Python

language. This plugin is inspired by the Semi-Automatic Classification Plugin (SCP) developed by Luca Congedo [1]. SCP allows the supervised classification of remote sensing images, the calculation of vegetation indices such as NDVI (Normalized Difference Vegetation Index) and EVI (Enhanced Vegetation Index) and other image operations. When analysing SCP, it was realised that a set of operations, that are very useful in teaching classes of remote sensing and image processing, were lacking, such as the visualization of histograms, the application of filters, different image corrections, unsupervised classification, several environmental indices, etc.. The new set of operations included in the PI2GIS plugin can be divided into four groups: pre-processing, processing, classification and classification analysis. In pre-processing group, it is intended to correct any distortion considering radiometric corrections and prepare the multispectral bands to be processed. Firstly, it is possible to create one histogram per band, and apply enhancement procedures to improve image contrast. Secondly, it is possible apply different types of filters (low pass, high pass, median, contour). Finally, the bands are converted from Digital Numbers (DN) to radiance and after to reflectance and therefore one atmospheric correction algorithm must to be chosen. The goal of the processing group is to do a colour composite followed by pan–sharpening process to improve multispectral image resolution previously created. It is also possible to calculate different type of environmental indices with special focus on NDVI, EVI, NDWI (Normalized Difference Water Index) and SMI (Soil Moisture Index). Finally, the coordinate system can be selected and the created colour composite image is projected, with the support of EPSG, which is also an innovation regarding the SCP. In the classification group, the plugin add new supervised classification algorithms non-existent in SCP and the introduction of the unsupervised classification algorithms (has the advantage of do not requiring the definition of training classes before running the algorithm since each class is defined according it´s spectral properties) is also an innovation. The main goal of the fourth group, classification analysis, is to report the statistics of the classification. This plugin performs a report of the classification by providing the percentage and area of each element on the image. The application is tested with data from Landsat 8 OLI and Sentinel 2A from a North area of Portugal.

[1] Congedo, L. (2016). Semi-Automatic Classification Plugin Documentation. DOI: http://dx.doi.org/10.13140/RG.2.2.29474.02242/1

10428-54, Session PS

Mapping impervious surfaces in the Xiangjiang River basin based on remote sensing spectral indices: a case study in Chang-Zhu-Tan region

Xiaoping Zhang, Ying Lv, School of Land and Tourism, Luoyang Normal Univ. (China); Huaguo Zhang, Fang Gong, State Key Laboratory of Satellite Ocean Environment Dynamics, Second Institute of Oceanography (China); Yongxin Zhang, Luoyang Normal Univ. (China); Chaokui Li, Hunan Univ. (China)

The Xiangjiang River is commonly referred as Mother River by people living in Hunan Province for the favorable living conditions it provides, such as fertile lands, rich water for irrigation and drinking purposes. However, increased impervious surfaces pose significant threats to the hydrologic cycle of the Xiangjiang River basin (~86791 km2 in Hunan Province) as a consequence of urbanization. Quantifying the percentage of imperviousness within the Xiangjiang River basin is important to pollution control and watershed management. Yet, few studies explored the use of multisource remote sensing imagery to map impervious surfaces in the Xiangjiang River basin. Over the last few decades, both per-pixel and sub-pixel analyses have been employed for analyzing impervious surface changes in the urban areas with different degrees of success. These methods are always considered as complicated, computationally intensive, and sometimes subjective, especially when applied to a large geographic area (e.g., >1000 km2). When compared with per-pixel and sub-pixel image analyses, spectral indices have apparent advantages due to their easy implementation and convenience in practical applications for mapping watershed impervious surfaces. In this paper, normalized difference built-up index (NDBI), normalized difference impervious surface index (NDISI), and normalized difference vegetation index (NDVI), enhanced built-up and bareness index (EBBI) as well as biophysical composition index (BCI) were respectively used to estimate the impervious surfaces in a local area of the research region, and conduct a comparative analyses among these indices. Specifically, the Defense Meteorological Satellite Program/Operational Linescan System (DMSP/OLS) nighttime stable light data (NTL) was added to extract impervious surfaces, and the mid-infrared band 1 (MIR1) in the NDBI and NDISI was replaced by the NTL data respectively. And then, the optimum spectral index was chosen to map the percentage of impervious surfaces for the total Xiangjiang River basin. The results show that the spectral index of BCI was more effective at discriminating urban areas and bare land and at increasing the estimation of large-scale impervious surfaces, and that the DMSP/OLS NTL data can improve the impervious surface extraction based on spectral indices. The calculated percentage of imperviousness in the Xiangjiang River basin was ~10%.

10428-55, Session PS

Satellite infrared imagery for thermal plume contamination monitoring in coastal ecosystem of Cernavoda NPP

Maria A. Zoran, National Institute of Research and Development for Optoelectronics (Romania); Liviu-Florin V. Zoran, Univ. Politehnica of Bucharest (Romania); Adrian I. Dida, Transilvania Univ. of Brasov (Romania)

The main environmental issues affecting the broad acceptability of NPP (Nuclear Power Plant) are the emission of radioactive materials, the generation of radioactive and heat waste, and the potential for nuclear accidents. Thermal pollution is associated with an increase in ambient temperature arising at both regional and local scales. Heat dissipation from the prevalent use of nuclear power is considered the main source of thermal pollution with negative effects on the atmospheric and aquatic environment, as well as on human health and ecosystems. Satellite remote sensing is an important tool for spatio-temporal analysis and surveillance of NPP environment, thermal heat waste of waters being a major concern in many coastal ecosystems involving nuclear power plants, as sharp changes in water temperature can significantly affect the distribution and physiology of aquatic biota and contribute to global warming. As a test case the adopted methodology was applied for 700x2 MW Cernavoda nuclear power plant (NPP) located in the South-Eastern part of Romania, which discharges warm water affecting coastal ecology. The thermal plume signatures in the NPP hydrological system have been investigated during 1990-2016 years based on TIR (Thermal Infrared) spectral bands of NOAA AVHRR, Landsat TM/ETM, and MODIS Terra/Aqua time series satellite data. If NOAA AVHRR data proved the general pattern and extension of the thermal plume signature in Danube river and Black Sea coastal areas, Landsat TM/ETM and MODIS data used for WST (Water Surface Temperature) change detection, mapping and monitoring provided enhanced information about the plume shape, dimension and direction of dispersion in these waters. Thermal discharge from two nuclear reactors cooling is dissipated as waste heat in Danube-Black -Sea Channel and Danube River. If during the winter thermal plume is localized to an area of a few km of NPP, the temperature difference between the plume and non-plume areas being about 1.7 oC, during summer and fall, is a larger thermal plume up to 5- 10 km far along Danube Black Sea Channel, the temperature change being of about 1.3 oC.

Thermal effluent from the Cernavoda nuclear power plant disperses mainly on the Danube – Black Sea Channel surface

around the outlet due to its higher water temperature than the ambient coastal water, and affects the biota around the power plant. Therefore the quantitative prediction of the dispersion of thermal effluent from the power plant is very important for the successful environmental assessment and management associated with the construction of new UNIT 3 and UNIT 4 reactors for power plant, planned to be operational around 2018 year. Based on these results we suggest that there is an urgent need to protect the health of

Danube river-Black Sea coastal ecosystem from the severe thermal impact by the large quantity of warm water discharged from the Cernavoda nuclear power plant, especially during summer time and under heat waves periods.

10428-56, Session PS

Impact factors on expansion of built-up areas in Zhejiang Province, China

Dong Liu, Nanjing Institute of Geography and Limnology (China); Qiankun Zhu, The Second Institute of Oceanography, SOA (China); Yan Li, Nanjing Univ. (China)

Built-up areas are the results of human activities. Not only are they the real reflection of human and society activities, but also one of the most important input parameters for the simulation of biogeochemical cycle. Therefore, it is very necessary to map the distribution of built-up areas and monitor their changes using new technologies and methods at high tempo-spatial resolution. By combining technologies of Geographic Information System (GIS) and Remote Sensing (RS), this study mainly explored the expansions and driving factors of built-up areas at the beginning of the 21st century in Zhejiang Province, China. Firstly, it briefly introduced the mapping processes of Land Use and Land Cover (LULC) based on the method which combined object-oriented method and binary decision tree. Based on in-situ data from different sources, the final mapping results were verified through confusion matrix method. The kappa coefficient of built-up areas mapping were 93.05%, 92.22%, 91.97% for 2000, 2005, and 2010 respectively. The mapping results were good and met the required accuracy. Then, it analyzed the expansion features of built-up areas in Zhejiang from 2000 to 2005 and 2005 to 2010. In addition to these, potential driving factors on the expansion of built-up areas were also discussed, which contained physical geographical factors, such as railways, highways, rivers, urban centers, elevation, slop, etc.

Results revealed that the expansions of built-up areas in Zhejiang from 2000 to 2005 and from 2005 to 2010 were very significant and showed high levels of spatial heterogeneity. Economy development accelerated the expansion of built-up areas. With total gross domestic product (GDP) in 2000 accounting for 57.8% in Zhejiang, Hangzhou, Shaoxing, Ningbo, and Jinhua developed more early than others. Expansions of built-up areas in these cities were greater from 2000 to 2005. However, counties with significant expansions of built-up areas sprawled out from 2005 to 2010 because of the comprehensive development of social economic overall the Zhejiang Province. Univariate Moran's I of increased built-up areas per county from 2000 to 2005 and from 2005 to 2010 was 0.7506 and 0.2899 respectively. Therefore, neighboring counties in Zhejiang have the similar change trend for increased built-up areas, and that was more obvious from 2000 to 2005. Moreover, from 2000 to 2005 increases of built-up areas in Zhejiang were influenced more by natural conditions, geographic location and topography, which gradually diminished with the economy development.

Except above, increased built-up areas with distance to railways, highways, rivers, and urban centers could be fitted with power function (y = a?xb), with minimum R2 of 0.9507 for urban centers from 2000 to 2005; the increased permillages of built-up areas to mean elevation and mean slop could be fitted with exponential functions (y = a?exp(b?x)), with minimum R2 of 0.6657 for mean slop from 2005 to 2010. Besides, government policy could also impact expansion of built-up areas. In a nutshell, a series of findings were obtained through this study about the spatial features and driving factors of built-up areas evolution in Zhejiang from 2000 to 2010. However, due to the limited data, we did not explore the effects of government policy which might also be an important factor on determining expansions of built-up area.

10428-57, Session PS

Analysis of ozone observation at atmospheric monitoring network station using Brewer ozone spectrophotometer

Kok Chooi Tan, Univ. Sains Malaysia (Malaysia); Mou Leong Tan, National Univ. of Singapore (Singapore); Hwee San Lim, Mohamad Zubir Mat Jafri, Univ. Sains Malaysia (Malaysia)

Ozone (O3) is unique among pollutants because it is not emitted directly into the air, and its results from complex chemical reactions in the atmosphere. O3 can bring different effects for all the living on earth (either harm or protect), depending on where O3 resides. This is the main reason why O3 is such a serious environmental problem that is difficult to control and predict. The objective of this paper is to analyze the variations of total column O3 measured by Brewer O3 spectrophotometer over Global Atmosphere Watch Station (GAW) regional station, which is located at southwest of Peninsular Malaysia, Petaling Jaya. Total column O3 observations in Petaling Jaya are studied for the period January 2008 to December 2008. Ozone shows seasonal variation with maximum (276.8 DU in May 2008) during pre-monsoon season and minimum (246.8 DU in January 2008) during northeast monsoon season. In addition, the monthly O3 maps for the year of 2008 were obtained from the NASA-operated Giovanni portal to overview the distribution of total column O3 in Peninsular Malaysia. For the upcoming studies, validation of ground measurements with satellite O3 data and study of tropospheric O3 over the study area is recommended.

10428-58, Session PS

Peculiarities of use of ECOC and AdaBoost based classifiers for thematic processing of hyperspectral data

Alexander Dementev, Yegor V. Dmitriev, Institute of Numerical Mathematics (Russian Federation); Vladimir V. Kozoderov, M.V. Lomonosov Moscow State Univ. (Russian Federation); Vladimir Egorov, Institute of Numerical Mathematics (Russian Federation)

Hyperspectral images, obtained with the help of airborne or space survey instruments, enable to solve new, more complex tasks of monitoring natural and man-made objects. The presence of a large number of survey channels allows to use subtle differences in the spectral characteristics of objects and, to make a more detailed classification than in the case of using standard multispectral data. The supervised learning algorithms currently used for recognizing objects from multispectral and hyperspectral images are usually based on standard approaches of various complexity: metric classifiers, k-nearest neighbors algorithm, Bayesian classifiers, the support vector machine. When processing hyperspectral images and allocating the spectral radiances of the classified objects as a feature space, the use of redundant spectral channels leads to the problem of the curse of dimensionality. Various methods developed for optimizing the feature space (Feature Extraction, Band Selection) serve to overcome the problem of curse of dimensionality and improve the accuracy of classification of the objects under study and the computational efficiency.

When solving the classification problem, there are well and poorly discriminated objects and the result of optimization of feature space strongly depends on the proportion of these objects in a particular task. The approach of constructing

multiclass recognition methods based on the integration of binary classifiers allows selecting optimal spectral channels for each binary classifier and to avoid the above described problem. For this purpose we use methods of constructing classifying algorithms based on the theory of self-correcting codes (Error-Correcting Output Codes - ECOC) and algorithms for improving classifiers performance, by combining them into a committee (Adaptive Boosting - AdaBoost). Both these methods build a complex algorithm based on the standard ones by forming a composition of binary classifiers according to the code matrix (ECOC) or setting the algorithm of adaptive boosting (AdaBoost). However, time-consuming algorithms are required for the classifier training purpose.

This technique is tested on a test area, which is located on the territory of Savvatievskoe forestry (Tver region, Russia). The ground-based information on the species and age composition of forest stands on the test area is the standard forest inventory tables and maps. The most part of the test area is covered by the forest stands of different ages mainly of the pine and birch species. Aspen and spruce stands are also sparsely present. The technique of the effective use of areas with mixed species composition of stands for the construction of the training data set is presented. Examples of recognition of species and age composition of stands according to aerial hyperspectral survey using the airborne instrumentation produces by NPO Lepton (Zelenograd, Moscow) are given. The data of ground-based measurements (maps and tabular data of forest inventory) are used to obtain numerical estimates of classification accuracy. The comparison of results of recognition of some forest inventory parameters of forest stands retrieved is presented using the proposed and common-used approaches.

10428-59, Session PS

Effects of aerosol phase function and other atmospheric parameters in radiometric calibration of hyperspectral visible/NIR satellite instruments above test sites of different altitudes

Oleg V. Postylyakov, Alexander N. Borovski, A.M. Obukhov Institute of Atmospheric Physics (Russian Federation)

To solve the problem of radiometric calibration of space-based hyperspectral remote sensing instruments an approach based on comparison of the results of shots of a test site with calculations of a radiative transport model is employed. The radiative transfer calculations in such an approach are based on measurements of atmospheric and surface optical characteristics performed from the test site. However, measurements of atmospheric characteristics have limitations on accuracy, and some of the characteristics can not be measured. We investigate how accuracy of ground-based atmospheric measurements and model assumptions influence on accuracy of the radiometric calibration. The aerosol phase function is one of atmospheric parameters usually inferred from models. The contribution of variability of atmosphere in the total error budget of radiance calculation depends on the altitude of the test site. We compared expected accuracy of radiance calculation for a site at the see level and Kislovodsk High Mountain Station (KHMS) of A.M. Obukhov Institute of Atmospheric Physics located at Caucasus Mountains at 2070 m.a.s.l., 43.7N 42.7E. The station situated above the atmospheric boundary layer, so typical aerosol optical depth at 550 nm are 0.03-0.1 (versus 0.2-1.5 at the sea level). Pressure, and consequently the optical thickness of the Rayleigh scattering, is 80% of the pressure at sea level. Optical depth of water vapour is typically about 30% of the thickness at sea level. As the radiation transfer models require knowledge of the vertical distributions of atmospheric characteristics, but ground-based measurements give mainly their total contents, radiance modelling error are less in the mountains where optical depths are less than at the sea level. The report compares atmospheric-related radiometric errors for KHMS and sea-level test site for spectral range 400-1000 nm.

10428-60, Session PS

Characterisation of macrophyte phenology in the Doñana marshland using MODIS NDVI time series from 2000 to 2015

Victor F. Rodriguez-Galiano, Angel Fernandez-Carrillo, Esperanza Sanchez-Rodriguez, Univ. de Sevilla (Spain)

The study of the interaction between vegetation development and climate factors is paramount for the management of protected natural areas. Data provided by remote-sensing satellites and derivative products, such as vegetation indices, permit the extraction of basic information regarding the functioning of vegetation masses and their interaction with certain environmental factors.

This paper carries out an approach regarding the behaviour of radiation intercepted by aquatic macrophytes present in the Doñana National Park marshland, represented by the plant association Bolboschoenetum maritimi, and its relationship with variations in precipitation. Based on NDVI (Normalised Difference Vegetation Index) time series from MODIS, the seasonal and year-on-year dynamics of these vegetation masses were studied over a 16-year period (2000–2015). The time series used correspond to composites formed by the maximum NDVI value for each 16-day period. The vegetation study was carried out by deriving different indicators for seasonal dynamics, which helped to understand its basic functional characteristics: i) NDVI-I, annual average of NDVI; ii) RREL, difference between the maximum and minimum annual NDVI divided by NDVI-I; iii) MAX, maximum annual NDVI; iv) MIN, minimum annual NDVI; v) MMAX, month when MAX occurred; vi) MMIN, month when MIN occurred. Afterwards, different regression analyses were performed between precipitation and the indicators derived from the NDVI time series.

No direct relationships could be established between the raw NDVI time series and precipitation. However, the regression analyses performed between precipitation and the seasonal dynamics values yielded meaningful information. The obtained results indicated that the examined association has a strong dependence on the marshland's flooding processes, requiring a minimum precipitation volume of approximately 350 mm/year for proper flooding and vegetation development, which was scarce during years of drought. The strong correlation found between precipitation and the seasonal nature of the vegetation masses ($r2=0.70$; $p<0.05$), measured via RREL, marked the important influence that rainfall variations have in the phenology of Bolboschoenetum maritimi. Other indicators where precipitation showed significant relationships were MAX and MIN ($r2=0.43$ and $r2=0.61$; $p<0.05$ and $p<0.05$, respectively), enhancing the extremes of both with increased precipitation volume. The differences found in vegetation behaviour across the marshland's different areas is due to differences in elevation which, despite being on the order of decimetres, produce significant variations in the hydroperiod between areas of higher and lower elevation.

The results demonstrated the need to maintain the marshland's flooding regime in its natural state, in order to preserve the ecosystems present therein.

10428-61, Session PS

High-resolution Earth observation data and spatial analysis for burn severity evaluation and post-fire effects assessment in the Island of Chios, Greece

George Athanasakis, Emmanouil Psomiadis, Andromachi Chatziantoniou, Agricultural Univ. of Athens (Greece)

Fire is an important ecosystem process that significantly impacts terrestrial, aquatic, and atmospheric systems throughout the world. Wildfires are one of the most dangerous

causes of natural disasters phenomena and only over the past few decades, have received significant attention. Wildfires are the most visible and devastating consequences regarding environmental damage and, secondly, human losses. Many species of plants depend on the effects of fire on growth and reproduction. Wildfires can cause various post-fire hazardous phenomena such as floods and landslides in the burned area.

The area under study is located on Chios island at the eastern part of the Aegean Sea. The western part of the island suffered many wildfire events the last decades. In the summer of 2016 on July 25th, a devastating wildfire occurred in the southwestern part of the island started from the village Vessa. The fire has destroyed a precious pine tree forest, the only one on the island, many cultivations of mastic, around the villages of Mesta, Olympoi and Vessa and wide areas of vineyards, forest, shrublands, and grasslands. A large part of this area has also burned recently during the summer of 2012.

Fire severity, defined as the degree to which a site has been changed. Variation in burn severity and fire interval leads to a mosaic of vegetation age and cover classes across the landscape. Therefore, estimates of burn severity are important for understanding the effects of fire on post-fire vegetation succession.

Remote Sensing techniques provide effective and cost-profitable tools for monitoring and mapping of wildfire events evolution and the post-fire damages and reinstatement assessment. Multispectral satellite data have become a useful tool utilized in the mapping of typical Mediterranean area fire consequences. In particular, spectral bands such as near infrared, mid-infrared and thermal infrared are very sensitive to burn magnitude changes and can reliably detect burnt areas, burn severity and vegetation changes.

In the present study, Landsat 8 (OLI) Earth Observation (EO) data have been utilized. They consisted of surface reflectance products projected to the ground range using an Earth ellipsoid model of UTM WGS84 and acquired through the USGS EarthExplorer (EE) platform. The data acquired in three-time points, pre and post fire at 13th of July and at 15th of September, respectively and six months later on January 21st of 2017. The processing steps were made to prepare the data by applying a water mask, a radiometric calibration and an atmospheric correction using FLAASH, in ENVI software (v.5,3).

Spectral indices, such as the normalized burn ratio (NBR), Burn Area Index (BAI) and Normalized Burn Ratio Thermal (NBRT), were implemented. These indices, which combine and extract useful information from several spectral bands, were chosen based on a literature search of burn severity studies to investigate fire-induced vegetation changes, including burn severity and regeneration.

Finally, the Normalized Burn Ratio (NBR) index of pre and post-fire images was used in a difference change detection procedure which calculates the Differenced Normalized Burn Ratio ?NBR. This change detection product measures the absolute change in the NBR, mapping that way the fire severity due to the wildland fire.

Overall, the objectives of this study were to a) assess and compare the suitability of three remote sensing indices for fire mapping, b) estimate the fire severity using the differenced Normalized Burnt Ratio, ????, and c) evaluate the vegetation recovery in comparison with burn severity map

A total burned area of 45,9 km2 was calculated, and both burned severity map and vegetation recovery map were created and evaluated.

10428-62, Session PS

A geospatial database model for the management of remote sensing datasets at multiple spectral, spatial and temporal scales

Gabriela Ifimov, J. Pablo Arroyo-Mora, National Research Council Canada (Canada); Grace Pigeau, Queen's University (Canada); Raymond J. Soffer, George Leblanc, National Research Council Canada (Canada)

Data management represents an important part of the remote sensing field where data access to multi-temporal, multi-resolution, and multi-sensor type of datasets is paramount for the traceability and integrity of final data products. Geospatial databases have been shown to be an efficient way to store, mine, and analyze remote sensing data - all while minimizing redundancy. For example, geospatial database engines (e.g. ArcGIS) or data management and storage systems are common tools used to create these geospatial databases. Since 2011, the Hyperspectral and Aeromagnetic group, at the National Research Council Canada, has acquired more than 1000 airborne hyperspectral images along with their associated metadata variables, and ground spectral measurements (e.g. calibration/validation) and their associated metadata. Subsequently, there has been a need for the development of a multi-source geospatial database that integrates the acquired data, leading to an optimization of data management and, ultimately, to a more efficient data processing and analysis.

The main objective of this work was to develop and implement a geospatial database model for the management of very diverse datasets encompassing lab spectroscopy, field spectroscopy (in-situ measurement for calibration and validation purposes), airborne hyperspectral imagery and ancillary data (e.g. photos, atmospheric conditions). For this purpose we used a relational database management system (RDBMS) in ArcGIS and SQL server. We compiled, standardized, and integrated the different datasets into a relational database, where logical associations between different types of information could be linked through a variety of variables (e.g. location, date, instrument). For in-situ spectroscopy data (350 nm – 2500 nm), each target spectral signature (from the raw input values to the reflectance output) is stored in an ENVI spectral library format and linked with tables containing complementary data such as time of collection, GPS location, solar zenith and azimuth angle and target, field and sky photos. In terms of the airborne hyperspectral data, two sensors, CASI (360-900 nm) and SASI (870-2500 nm), have been used. Moreover, different configurations have been employed for the CASI (72, 199, 288 spectral bands), which had to be considered when integrating these data into the geospatial database. A major challenge of the hyperspectral imagery is that multiple data levels are produce when processing the data from raw (digital number) through geocorrected reflectance. In addition, data products from the airborne data are included in the geospatial database where both field spectroscopy and airborne datasets are linked spatially and temporarily.

We demonstrate the utility of our geospatial database model integrating the different datasets with an example of a study on the assessment of the spatial and spectral variability of field measurements for the calibration and validation of airborne imagery. Remote sensing data at multiple spectral, spatial, and temporal scales is inherently complex; therefore, our work provides a valuable model to deal with such complexity.

10428-64, Session PS

Analysis of changes in crop farming in the Dudh Koshi (Nepal) driven by climate changes

Marco Gianinetto, Francesco Polinelli, Federico Frassy, Martina Aiello, Francesco Rota Nodari, Andrea Soncini, Daniele Bocchiola, Politecnico di Milano (Italy)

Nepal is located in an area characterized by sub-tropical climate, but its climate ranges from sub-tropical to artic because of the highly variable topography. Despite Nepal is among the richest countries for water availability (snow, rivers, springs, lakes, and groundwater), however only 72% of people have access to clean water and only the 24% of the cultivated land is provided with an irrigation system. Although the majority of the population relies on a subsistence farming system and many people suffer of malnutrition, however no historic georeferenced information about crop fields is

available.

In this context, future climate changes may have a strong impact on crop yields and, consequently, on food security for the Nepalese population. Thus, studies on past land cover changes and forecast of future land cover changes are very useful. This paper describes the spatial evolution of the farmed areas in Dudh Koshi basin during the last four decades by analysing the farming of its four main crops (maize, rice, wheat and millet) and tries to outline a future scenario. The study area covers the districts of Solukhumbu, Okhaldunga and Kothang, located in the hilly and mountainous region of Nepal.

A Landsat time series made of images collected from 1975 (Landsat-1/MSS) to 2010 (Landsat-8/OLI) is classified with a rule-based expert system implemented with a decision tree algorithm. Input variables are topographic parameters and NDVI values. Since all the cereals farmed in the study area have a very similar NDVI dynamics from sowing to harvesting, the classification scheme uses a multi-temporal approach to map each crop in the period of its maximum vigour. The thematic maps produced are aggregated into statistics for the three districts and results are compared with global data made available by the International Centre for Integrated Mountain Development (ICIMOD) and correlated with climatic time series (temperature and rainfall) from the Department of Hydrology and Meteorology (DHM). The observed dynamics of land cover changes is highly correlated with both the demographic dynamics and with climatic data.

Based on the thematic maps computed for the period 1975-2010, future simulations (until 2100) show an overall increase of cropland in the Dudh Koshi basin, with maize being the main cereal farmed. This expansion of the cultivated areas seems driven by the future demographic growth. Moreover, the forecasted scenario highlights an increase of the altitude being farmed, with significant intensification of cultivated lands in the mountainous region of the Solukhumbu district. This prediction is consistent with the climate changes expected in the study area.

10428-65, Session PS

Spatial indices and dynamics of forest land in the municipality of Ain Fezza, northern Algeria

Driss Haddouche, Univ. Abou Bekr Belkaid Tlemcen (Algeria)

This study takes into worthiness the degradation characteristic of the forest environment by the analysis of a diachronic evolution, which well translate the environmental response to the anthropic pressions and to the climatic changes. To make it into achievement, we have focused-on a methodological approach based on a spatial-temporal analysis that allowed us to evaluate the environmental changes in the study area (Municipality of Ain Fezza, wilaya of Tlemcen), in particular the diachronic evolution of green cover. The data used are satellite images taken by the TM sensor of Landsat 5 (1984) and the ETM + sensor of Landsat 8 (2016) with a spatial resolution of 30 m and a Digital Elevation Model (DEM) with the same spatial resolution. Different improvement treatments (colored compositions and filters) and specific (supervised classifications) were performed on these bi-dates data.

The informatics treatments of optical satellites images with bi-dates [1984-2016] have made into evidence and with efficient practice the generalized degradation of the green cover, where the socio-economical impact is marqued by the reduction rate of natural resources and the diminution of the forest areas. In this side and for example, the « degraded hills » class is high increasing, due to different anthropic incredulous actions (over grazing, forest fire, package, expansion of stone-pit ...etc), is noticed.

10428-66, Session PS

Remote sensing data and hydrogeophysical parameters as a guide for sustainable development in the northwestern coast of Egypt

Ibrahim Salaheldin Khedr, Osama Abdel-Raouf, National Water Research Ctr. (Egypt)

Spatial models are important for detecting and planning development principles especially in the future projects of development areas.

Using some proposed weighted factor to select the suitable areas that achieve most positive parameters, Raster analysis, Buffer zones and If /or equation are the most process steps of the model. This paper aims to study the integration between the remote sensing data and hydrogeophysical parameters to develop the most spatial model helping in the master plan of the sustainable development in the study area.

Calibration of the model was done through 10 field truth sites (Aqurecy assessments). These sites were chosen to cover different conditions of the study area.

The out puts of the model in the form of detailed maps comprises different parameters indicated that the total current land use area which reaches about 88242 feddan can be extend to 234370 feddan. An area of about 146126 feddan can be added to current used areas in future development projects.

10428-67, Session PS

A GIS-based approach to habitat suitability of wild water buffalo (Bubalus arnee) on the Rapti floodplain of Chitwan National Park

Shankar Tripathi, Agriculture and Forestry Univ. (Nepal)

Wild Water Buffalo is listed as an endangered on the IUCN Red list of threatened species and Appendix III of CITES and protected by Nepal's National Park and Wildlife Conservation Act (1973) in its Appendix I. In Nepal, its population is restricted only in the KTWR. Diseases and parasites (transmitted by domestic livestock), rapid and complete inundation of the (KTWR) during the monsoon and frequent changes in river courses almost every year and competition for food and water between wild buffalo and domestic stock are also serious threats (IUCN 2004). It is necessary to search alternate place where the habitat is suitable for sustainable conservation of the Wild Water Buffalo in Nepal. The research entitled "A GIS-Based Approach to Habitat Suitability of Wild Water Buffalo (Bubalus arnee) on Rapti Floodplain of Chitwan National Park". The objective of research was to analyze the habitat suitability of Wild Water Buffalo in CNP. Topographic map required for habitat analysis were collected from NGIIP. Line plot method was used for vegetation analysis. 10m*10m and 1m*1m plot was used to determine tall grass species, average height and grass species density. Four factor suitability criteria (i.e. proximity to river, distance from settlement, grassland cover, and grassland type) were used in suitability analysis. ArcGIS software was used for geospatial analysis. Different function of GIS (buffering, clipping, overlay and other) was used in data processing and analysis. Bombax ceiba was the dominance tree with highest IVI value 112.70 with Trewia nudiflora and others. Saccharum bengalense was the dominance tall grass species with highest RD value 33.04 with Phragmites karka, Narenga prophyrokoma and others. The integration of all four factors shown that the 20% of study area was most suitable for Wild Water Buffalo, whereas 56% and 24% were suitable and moderately suitable respectively.

10428-22, Session 5

Estimating the accuracy of vectors derived from open data

Konstantinos G. Nikolakopoulos, George Dimitropoulos, Univ. of Patras (Greece)

Many geological applications like mapping, open quarry monitoring or even the study of tectonic structures, require a high resolution and a very accurate representation of the surface in order to minimize errors. High resolution satellite images or airphotos can provide the necessary basemap for such applications. Nevertheless these kinds of images are quite expensive and hard to get access to. Google Earth is easily accessible to the public, but the question that arises is, if those images can be as reliable as the original satellite images and if they can be used in their place for geological applications. The purpose of this study was to investigate Google Earth images reliability, measure their accuracy and find out if they can provide valid results and finally if they can be used for geological applications. The region that was investigated is Markopoulo quarry in Attiki Peninsula Greece. Images were taken using Google Earth, one for each direction (North, South, East, and West) from 2004 to 2015. All the images were of the same magnification and same image quality. Subsequently, those images were georeferenced with the use of ArcGIS software. The georeference procedure was executed again using Erdas Imagine software for comparison purposes. A quickbird satellite image over the same area was orthorectified in Leica Photogrammetry Suite. From the orthorectified Quickbird image and the Google Earth images the road network was digitized and the derived vectors were compared in ARCGIS. The comparison showed remarkably low deviation which leads us to the conclusion that Google Earth images can be used as alternative basemap in many applications.

10428-23, Session 5

Coastal areas mapping using UAV photogrammetry

Konstantinos G. Nikolakopoulos, Dimitrios Kozarski, Stefanos Kogkas, Univ. of Patras (Greece)

The coastal areas in the Patras Gulf suffer degradation due to the sea action and other natural and human-induced causes. Changes in beaches, ports, and other man made constructions need to be assessed, both after severe events and on a regular basis, to build models that can predict the evolution in the future. Thus, reliable spatial data acquisition is a critical process for the identification of the coastline and the broader coastal zones for geologists and other scientists involved in the study of coastal morphology. High resolution satellite data, airphotos and airborne Lidar provided in the past the necessary data for the coastline monitoring. High-resolution digital surface models (DSMs) and orthophoto maps had become a necessity in order to map with accuracy all the variations in costal environments. Recently, unmanned aerial vehicles (UAV) photogrammetry offers an alternative solution to the acquisition of high accuracy spatial data along the coastline. This paper presents the use of UAV to map the coastline in Rio area Western Greece. Multiple photogrammetric aerial campaigns were performed. A small commercial UAV (DJI Phantom 3 Advance) was used to acquire thousands of images with spatial resolutions better than 5 cm. Different photogrammetric software's were used to orientate the images, extract point clouds, build a digital surface model and produce orthoimage mosaics. In order to achieve the best positional accuracy signalised ground control points were measured with a differential GNSS receiver. The results of this coastal monitoring programme proved that UAVs can replace many of the conventional surveys, with considerable gains in the cost of the data acquisition and without any loss in the accuracy.

10428-24, Session 5

Tunable compact mechanical monolithic sensors for linear and angular large band low-frequency monitoring and characterization of sites and structures

Fabrizio Barone, Gerardo Giordano, Fausto Acernese, Rocco Romano, Univ. degli Studi di Salerno (Italy)

Among the different mechanical architectures present in literature, the Watt's linkage is one of the most promising ones for the implementation of a new class of mechanical accelerometers (horizontal, vertical and angular). In this paper, we present monolithic implementations of uniaxial linear and angular mechanical seismometers and accelerometers based on the UNISA Folded Pendulum mechanical configuration, optimized for low frequency characterization of sites (including underground sites) and structures as inertial linear sensor (seismometer) and/or angular sensor (tiltmeter). This mechanical architecture allows the design and implementation of very large band compact monolithic sensors (10^-7Hz ÷ 10^2 Hz), whose sensitivities for the most common applications are defined by the noise introduced by their readouts (e.g. < 10^-12 m/sqrt(Hz) linear sensitivity and < 10^-10 rad/sqrt(Hz) angular sensitivity with classical LVDT readouts. These unique features, coupled other relevant properties like scalability, compactness, lightness, high directivity, frequency tunability (typical resonance frequencies in the band 10^-1 Hz ÷ 10^2 Hz), very high immunity to environmental noises and low cost make this class of sensors very effective for the implementation of uniaxial (horizontal and/or vertical) and triaxial seismometers (velocimeters and/or accelerometers) and tiltmeters for ground, space and underwater applications, including UHV and cryogenics ones. Typical applications of this class of monolithic sensors are in the field of earthquake engineering, seismology, geophysics, civil engineering, characterization of sites (including underground sites), structures (e.g. buildings, bridges, historical monuments), and, in general, in all applications requiring large band-low frequency performances coupled with high sensitivities and compactness.

References

[1] Barone, F., Giordano, G., Mechanical Accelerometers, J. Webster (ed.), Wiley Encyclopedia of Electrical and Electronics Engineering. John Wiley & Sons, Inc., doi: 10.1002/047134608X.W8280 (2015).

[2] Barone, F., Giordano, G., Acernese, F., and Romano, R., Watt's linkage based large band low frequency sensors for scientific applications, Nucl Instrum. and Meth. A, doi: 10.1016/j.nima.2015.11.015 (2015).

[3] Acernese, F., De Rosa, R., Giordano, G., Romano, R., and Barone, F., Low frequency seismic characterization of underground sites with tunable mechanical monolithic sensors, Proc. SPIE 9435, SPIE, Bellingham, 94352Q, ISBN: 9781628415384, doi: 10.1117/12.2083362 (2015).

[4] Barone, F., Giordano, G., Low frequency folded pendulum with high mechanical quality factor, and seismic sensor utilizing such a folded pendulum, International application published under the patent cooperation treaty (PCT), WO 2011/004413 A3 (2011), Patent Numbers: IT 1394612 (Italy), EP 2452169 (Europe), JP 5409912 (Japan), RU 2518587 (Russia), AU 2010269796 (Australia), US 8,950,263 (USA), Canada pending.

[5] Barone, F., Giordano, G., Acernese, F., Low frequency folded pendulum with high mechanical quality factor in vertical configuration, and vertical seismic sensor utilizing such a folded pendulum, International application under the patent cooperation treaty (PCT) WO 2012/147112 (2012), Patent Number: IT 1405600 (Italy), EP2643711 (Europe), AU 201247104 (Australia), US 9,256,000 (USA), JP 5981530 (Japan), RU 2589944 (Russia), 9256000 (USA), Canada pending.

[6] Barone, F., Giordano, G., Acernese, F., Method for the measurement of angular and/or linear displacements utilizing one or more folded pendula, International application under the patent cooperation treaty (PCT) WO 2016/020947 (2016), Patent Number: IT 1425605 (Italy), Europe, Japan, USA, Canada pending.

10428-25, Session 5

Monitoring ground deformation of cultural heritage sites using UAVs and geodetic techniques: the case study of Choirokoitia, JPI PROTHEGO project

Kyriacos Themistocleous, Chris Danezis, Evangelos Mendonidis, Efstathia Lymperopoulou, Cyprus Univ. of Technology (Cyprus)

This paper presents the integrated methods using UAVs and geodetic techniques to monitor ground deformation within the Choirokoitia UNESCO World Heritage Site in Cyprus. The Neolithic settlement of Choirokoitia, occupied from the 7th to the 4th millennium B.C., is one of the most important prehistoric sites in the eastern Mediterranean. The study is conducted under the PROTHEGO (PROTection of European Cultural HEritage from GeO-hazards) project, which is a collaborative research project funded in the framework of the Joint Programming Initiative on Cultural Heritage and Global Change (JPICH) – Heritage Plus in 2015–2018 (www.prothego.eu) and through the Cyprus Research Promotion Foundation. PROTHEGO aims to make an innovative contribution towards the analysis of geo-hazards in areas of cultural heritage, and uses novel space technology based on radar interferometry to retrieve information on ground stability and motion in the 400+ UNESCO's World Heritage List monuments and sites of Europe. The field measurements collected at the Choirokoitia site will be later compared with SAR data to verify micro-movements in the area to monitor potential geo-hazards. The site is located on a steep hill, which makes it vulnerable to rock falls and landslides.

10428-42, Session 5

Petroleum exploration in Africa from space

Marco Gianinetto, Federico Frassy, Martina Aiello, Francesco Rota Nodari, Politecnico di Milano (Italy)

Hydrocarbons are nonrenewable resources but they are the cheaper and easier energy we have access today and will remain the main source of energy for this century. However, their exploration is still extremely high-risk, very expensive and time consuming. In this context, satellite technologies for Earth observation can play a fundamental by making hydrocarbon exploration more efficient, less expensive, less risky and, above all, much more eco-friendly.

Complementary to traditional geophysical methods such as gravity and magnetic (grav-mag) surveys, satellite Earth observation can be used to detect long-term biochemical and geochemical environmental alterations produced by invisible small fluxes of light hydrocarbons migrating from the underground deposits to the surface. These effects are known as microseepage.

Recently, several studies demonstrated that multispectral sensors are able to map some of the phenomena involved in the microseepage, such as: i) the reduction engaged by microbial activity from ferric to ferrous oxide in ferric oxide rich soils, ii) the anomalous formation of carbonate cements such as calcite, or iii) the alteration of illitic clays into kaolinite by sulphuric acid. For vegetated areas, the effects of microseepage are much more diversified and can be summarized as stress-related symptoms caused by the long-term exposition of plants to volatile hydrocarbons. However, many of the past studies described laboratory experiments to detect hydrocarbons, oil polluted soils, or reported some case histories where remote sensing was used to detect microseepage signals over small geographic areas.

This paper shows how satellite remote sensing can support hydrocarbon exploration on very wide new venture areas. The first case study analyzes Block 5A inside the Muglad Basin, located in a hard accessible area of South Sudan affected by civil war. The analysis shows some microseepage signals that follow the known petroleum system and some signals in the less explored western part of the block. Even if the Muglad sedimentary basin is older (Cretaceous) than the sedimentary basins of Lake Turkana and Lake Albert (Tertiary) already studied in past with this technology, the microseepage detected signals seems similar. Thus, promising for hydrocarbon exploration.

The second case study analyzes Block PT5–C and the three known oilfields Pande, Temane, and Inhassoro located in Mozambique. Here, the microseepage analysis points out a group of signals in northern of the Inhassoro oilfield and in the south-western of the Temane oilfield. Moreover, the analysis of satellite data shows signs nearby the known Pande oilfield, though not on top of it, and some microseepage contiguous to the proposed prospects Tafula and Corvo, according to Sasol (2016).

Satellite Earth observation is a powerful technology for detecting active petroleum systems through the analysis of microseepage signals. It can support hydrocarbon exploration in remote or hardly accessible areas and without the need of any exploration license. Moreover, it is supplementary and cheaper to existing geophysical methods, can be used as pre-bid screening or comparative analysis of license blocks, and can optimize the planning of expensive seismic surveys.

10428-26, Session 6

Can porosity affect the hyperspectral signature of sandy landscapes?

Gladimir V. G. Baranoski, Bradley W. Kimmel, Univ. of Waterloo (Canada)

Porosity is a fundamental property of sand deposits found in a wide range landscapes, from beaches to desert dune fields. As a primary determinant of the density and permeability of sediments, it represents a vital input for basin modeling and studies involving coastal erosion. Moreover, the porosity of a sand deposit can used to calculate its wet bulk density. This quantity, in turn, is of interest for a variety of geoaccoustics and geochemical investigations aiming at the understanding of sediment transport and water diffusion properties of sandy landscapes. This connection between porosity and water flow is also one of the focal points of hydrological studies involving the permeability of aquifers. Despite the importance of porosity, however, its quantification remains difficult since techniques for obtaining in situ samples of sand deposits from which porosities can be measured are often undermined by core disturbance problems. In fact, the effective sampling of sand deposits without disturbing their loosely packed grains continues to be an elusive task. In this work, we investigate the effects of porosity on the hyperspectral signatures of sandy landscapes. Our goal is to assess the feasibility of initiatives aimed at the remote quantification of this property. Although our investigation is focused on surficial, noncemented sand deposits, it takes into account a wide range of sand characterization properties, including, but not limited to, grain size, moisture saturation, roundness and sphericity. In order to overcome the difficulties involving in situ studies, we employ an in silico approach. More specifically, we perform predictive computer simulations using a hyperspectral model for particulate materials, known as SPLITS (Spectral Light Transport Model for Sand), which takes into account actual sand characterization data. Through this approach, we can perform controlled experiments on sand samples, i.e., we can assign different values to specific parameters and analyze their effects on the sample's hyperspectral responses while keeping the other parameters constant. We remark that such controlled experiments are difficult to be effectively performed under actual laboratory conditions. To the best of our knowledge, this work represents the first comprehensive investigation relating porosity and the hyperspectral signature of sandy landscapes presented in the scientific literature. Our findings demonstrate that future initiatives for the detection of porosity variations through changes in the hyperspectral reflectance responses of sand deposits would required sensors with a degree of sensitivity several orders of magnitude superior to the existing ones. Previous studies have indicated that the permeability

of sand deposits may be correlated with sand grains' size and sphericity in addition to porosity. Our experiments have also indicated that variations on porosity are more susceptible to detection when the target samples are characterized by sphericity values at the lower and upper bounds of the observed range for this parameter. Furthermore, the interplay between porosity and sphericity can result in distinct reflectance variations at distinct regions of the light spectrum. Our findings are expected to strengthen the knowledge basis to be used in the development of new high-precision technology for the monitoring of environmentally-triggered changes in sandy landscapes.

10428-27, Session 6

Mapping above ground biomass in lowland Amazon forest gradient using canopy texture index derived from WorldView-2 satellite data

Mike Harvey Salazar Villegas, TU Dresden (Germany)

Very High Resolution (VHR) imagery enable reliable measurement of forest canopy grain and crown size distribution, with high potential to map forest standing biomass. The production of such map across landscape scale is crucial as international efforts to protect forest ecosystems, such as Reduced Emissions from Degradation and Deforestation (REDD+) and Payments for Ecosystem Service (PES) conservation mechanisms. However, landscape-scale mapping Above Ground Biomass (AGB) over complex canopy structure is challenging as (1) saturation of remote sensing signals a at high AGB values, (2) instrumental effects due variations in sun– scene–sensor geometry, (3) steep topography, making the use of imagery data complex. This study, attempts to develop an approach by using a Fourier transform textural ordination (FOTO) method from a Worldview-2 multispectral imagery and 15 ground control forest plots sampled across a gradient of forest types for AGB estimation in lowland Amazon.

For our dataset we find that FOTO is effective in differentiate the range of forest types from low-impacted logged to young secondary forest. For low-impacted forest, the relationship between field derived and texture derived AGB is consistent, which exhibited a R2 = 0.84 of the variability of field data (relative RMSE = 10%). For young secondary forest, relationship between observed and predicted AGB, exhibited a R2 = 0.81 of the variability of field data (relative RMSE = 15%). An AGB map (100m spatial resolution) was generated over a heterogeneous landscape of 268 km2 in the Colombian Amazon. These results indicate that estimation of forest AGB, based on VHR satellite data, can be improved by (a) applying forest gradient/range –specific models, and (b) including textural information. Finally, this methodological approach can also be used for integrating limited forest inventory plot AGB data with VHR imagery for low cost PES instruments, to plan appropriate reforestation measures and for carbon offset assessments.

10428-28, Session 6

Discriminating the Mediterranean Pinus spp. using the land surface phenology extracted from the whole MODIS NDVI time series and machine learning algorithms

Victor F. Rodriguez-Galiano, Univ. de Sevilla (Spain); David Aragones, Estación Biológica Doñana, Consejo Superior de Investigaciones Científicas (Spain); Jose A. Caparros-Santiago, Univ. de Sevilla (Spain); Rafael M. Navarro-Cerrillo, Universidad de Córdoba (Spain)

Land surface phenology (LSP) can improve the characterisation of forest areas and their change processes. The aim of this work was: i) to characterise the temporal dynamics in Mediterranean Pinus forests, and ii) to evaluate the potential of LSP for species discrimination.

The different experiments were based on 679 mono-specific plots for the 5 native species on the Iberian Peninsula: P. sylvestris, P. pinea, P. halepensis, P. nigra and P. pinaster, which were obtained from the Third National Forest Inventory of Spain. The entire MODIS NDVI time series (2000–2016) of the MOD13Q1 product was used to characterise phenology at a spatial resolution of 250 m and with a compositing window equal to 16 days. Different terrain variables such as elevation, slope and aspect were computed from the Advanced Spaceborne Thermal Emission and Reflection Radiometer Global Digital Elevation Model (ASTER GDEM V2) as auxiliary information. Additionally, the distance of each plot to the coastline was extracted from the GADM V2.8 world administrative boundaries dataset. The Breaks for Additive Season and Trend (BFAST) algorithm was applied to smooth the NDVI time series, considering a harmonic model and 10 iterations. The following phenological parameters were extracted using the TIMESAT software for each cycle from the smoothed time series: the start, end and median days of the season, and the length of the season in days, as well as the base value, maximum value, amplitude and integrated value. Multitemporal metrics were calculated to synthesise the inter-annual variability of the phenological parameters: the median, 10% percentile, 90% percentile, the difference between the previous percentiles, the standard deviation, the regression slope, the determination coefficient and the number of seasons in each year.

The species were discriminated by the application of Random Forest (RF) classifiers from different subsets of variables: model 1) NDVI-smoothed time series, model 2) multitemporal metrics of the phenological parameters, and model 3) multitemporal metrics and the auxiliary physical variables (altitude, slope, aspect and distance to the coastline). This latter model was also built using a Classification and Regression Tree (CART) algorithm to better explain the variables of the threshold that better discriminate between Pinus spp.

An atypical behaviour was detected for the years 2004 and 2011, and 2000, 2009 and 2015 matching wet and dry cycles, respectively. P. sylvestris had a different phenological behaviour from P. pinea, P. halepensis and P. pinaster. Model 3 was the best, with an overall accuracy of 82%, a kappa coefficient of 0.77 and whose most important variables were: elevation, coast distance, and the end and start days of the growing season. The species that presented the largest errors was P. nigra, (kappa= 0.45), having locations with a similar behaviour to P. sylvestris or P. pinaster, possibly due to repopulation with distinct subspecies. The CART tree model showed that the Pinus spp. might be differentiated considering a threshold value of 24 April as the start date of the growing season, a distance to the coastline of 179 km and a median elevation of 1100 m, among others.

10428-29, Session 6

Vulnerable land ecosystems classification using spatial context and spectral indices

Edurne Ibarrola-Ulzurrun, Univ. de Las Palmas de Gran Canaria (Spain); Consuelo Gonzalo-Martín, Univ. Politécnica de Madrid (Spain); Francisco Javier Marcello-Ruiz, Univ. de Las Palmas de Gran Canaria (Spain)

Natural habitats are exposed to growing pressure due to intensification of land used, tourism development and other activities. Obtaining information on the structure and type of vegetation is necessary for conservation, restoration and management projects. In this context, remote sensing is an important tool for monitoring and managing habitats as it allows the acquisition of data in remote and inaccessible areas, and in different temporal context. This is important since traditional field-based biodiversity assessment methods are sometimes subjective and usually spatially restrained due to constrain in time, finance, or habitat accessibility. Vegetation mapping obtained from classification of remote

sensed imagery also provides valuable information for understanding the natural and anthropogenic environments through quantifying vegetation cover from local to global scales at a given time point or over a continuous periods. Thus, image classification is a crucial stage in remote sensing image analysis. The majority of image classifications techniques are based upon the pixel-based approach, in which pixels are classified individually according to their digital values, but neither spatial concepts nor contextual information are incorporated. An alternative approach is the object-based (OBIA) approach, in which a previous segmentation step merges image pixels to create objects that are then classified as classes, defined by the spectral, spatial, structural and hierarchical properties. Besides, improved results may be gained by incorporating additional spatial information and specific spectral indices into the classification process, which could help separate spectrally confused classes. In this context, the main goal of the work was to implement and assess object-based classification techniques on very high resolution imagery incorporating spectral indices and spatial information in the classification model, in order to improve the resultant thematic map. The study area chosen was the Teide National Park in Canary Islands (Spain). It is a vulnerable heterogeneous ecosystems characterized by its small and mixed vegetation, where the spatial information is critical and should be incorporated in order to generate accurate thematic maps. Worldview-2 orthoready imagery of the ecosystem was used in the study. Firstly, a pansharpening algorithm was applied in the imagery to enhance its spatial resolution. After a detailed study about the different pansharpening techniques that could be suitable for our image and ecosystem type, the Weigthed Wavelet 'à trous' through Fractal Dimension Map algorithm was applied. Afterwards, the image was orthorectified and atmospherically corrected. In the classification model, two common indices were selected Normalized Difference Vegetation Index (NDVI) and Optimized Soil Adjusted Vegetation Index (OSAVI), as well as two specific Worldview-2 sensor indices, Worldview Vegetation Index and Worldview Soil Index. To include the contextual information, Grey Level Co-occurrence Matrices (GLCM) were used taking into account the homogeneity, contrast, dissimilarity, entropy, mean, standard deviation and correlation. The classification was performed applying Support Vector Machine algorithm using a sufficient and representative number of training and testing samples of vegetation species (Spartocytisus supranubius, Pterocephalus lasiospermus, Descurainia bourgaeana and Pinus canariensis) selected by experts of the National Park as well as urban road and bare soil classes. Confusion Matrices have been computed to evaluate the results from each classification model. The highest Overall Accuracy and Kappa Coefficient was obtained combined both Worldview indices with the GLCM-dissimilarity, achieving an accuracy of 90.07% in the classification of the thematic map.

10428-30, Session 6

Analysis of phenological changes of high vegetation in amplitude images of SAR time series

Ramona Ihrig, Karlsruher Institut für Technologie (Germany) and Fraunhofer-Institut für Optronik, Systemtechnik und Bildauswertung (Germany); Silvia Kuny, Antje Thiele, Fraunhofer-Institut für Optronik, Systemtechnik und Bildauswertung (Germany) and Karlsruher Institut für Technologie (Germany); Stefan Hinz, Karlsruher Institut für Technologie (Germany)

In the last 20 years SAR remote sensing has developed strongly and is now an important alternative to multispectral remote sensing due to its independency of weather and illumination. These advantages allow for image stacks to be generated continuously with satellite-based SAR systems, in which changes of various kinds can be detected and analyzed.

This study focuses on an investigation to what extent phenological changes are detectable in X-band SAR amplitude images. More precisely, the seasonal changes of high vegetation in forest areas, in particular deciduous forest areas, are of interest. Since X-band does not penetrate but is reflected by the canopy of trees, the transition of a tree in full foliage to the bare trunk in winter can be assumed to show some impact on the backscattering intensities.

C-band or even longer wavelengths might be the more common choice to observe vegetational properties. However, there are studies that have to deal with the signature of vegetation in X-band imagery and thus have to account for its seasonal inconsistency. Hence, the analysis of phenological changes is also of interest for X-band SAR imagery.

Since the seasonal changes are expected to be quite different depending on geographic latitude and the type of vegetation zone, three representative areas were chosen for this work, located in Germany (Greding), Japan (Towada) and Turkey (Koyulhisar). Each of the chosen areas features forest types, which are characteristic of the respective region. The data set used for the analysis consists of a TerraSAR-X high resolution Spotlight image stack (16 images, 17 images, and 10 images, respectively) for each area spread over roughly a year, with additional optical imagery for reference purposes. Furthermore, data regarding forest borders, height and weather information are available.

Our workflow starts with the coregistration of the image stack, followed by the radiometric calibration. Based on this amplitude image stack statistical texture features of the first (e.g. Mean, Variance, Standard deviation, Kurtosis, Skewness) and second order (e.g. Entropy, Difference Entropy, Energy, Contrast, Correlation) are computed for the different forest areas and observed over the time series. For this, suitable parameter sets are identified and discussed, among others, the patch size, the distance, the orientation and the number of bins for computing the grey level co-occurrence matrix. The subsequent analysis includes the identification of features showing a distinct temporal trend as well as those that prove to be unaffected by seasonal changes. A visual and a numerical evaluation of the results and a subsequent discussion are concluding the paper.

10428-31, Session 7

Quick multitemporal approach to get cloudless improved multispectral imagery for large geographical areas

Nicola Colaninno, Univ. Politècnica de Catalunya (Spain); Alejandro Marambio, Univ. Nacional Autónoma de México (Mexico); Josep Roca Cladera, Univ. Politècnica de Catalunya (Spain)

The increasing availability of satellite information has improved the capability of global land cover monitoring. As a consequence, the demand for remotely sensed data is growing increasingly, due to the possibility of managing information about huge geographic areas, in digital format, at different time periods, and suitable for analysis in GIS platforms. However, primary satellite information is not such immediate as desirable. Often a number of atmospheric occurrences restrict the use of the information for certain specific purposes. Hence, improving the classification results is still an exciting challenge. Actually, beside geometric and atmospheric limitations, which need to be fixed; clouds, cloud shadows, and haze generally contaminate optical remote-sensing images. Indeed, in terms of land cover, such a contamination is intended as missing information and should be replaced.

Nowadays, information reconstruction of images represents an active research topic in the fields of remote sensing. In particular, there are several approaches aimed to detect and mask clouds, and cloud shadows, for returning an uncontaminated image data, although they differ with respect to the general processing strategy. Generally, image reconstruction is classified according to three main approaches, i.e. in-painting-based, multispectral-based, and multitemporal-based methods.

This work refers to the multitemporal-based methods, which

rely on both temporal and spatial coherence to retrieve cloud-free pixels from different time periods for the same image scene. Accordingly, our research explores an automatic methodology for quickly getting daytime cloudless and shadow-free improved image scenes at moderate spatial resolution for large geographical areas. In particular, the methodology relies on two main steps, i.e. a multitemporal effect adjustment of a stack of multitemporal image scenes, in order to avoid significant seasonal variations, and a data reconstruction phase based on automatic selection of the best (uncontaminated) pixels from the stack. The result is a composite multispectral image of Top Of Atmosphere (TOA) reflectance based on middle values of the stack, over a year. Nonetheless, the approach is suitable under certain restrictions. The assumption is that, for specific purposes, land cover changes at a coarse scale are not significant over relatively short time periods.

The structure of the paper relies first on an overall description of motivations and objectives of the research. Moreover, an exhaustive analysis of other related works, and relevant approaches, is provided. Then, because it is largely recognized that satellite imagery along tropical areas are generally strongly affected by clouds, the methodology is tested for the case study of the Dominican Republic at the year 2015. Satellite information employed for the experiment are multispectral imagery from the Landsat 8 mission, which provides information at a spatial resolution of 30 meters per pixel and squared image scenes of about 185 km. In particular, five image scenes are needed to cover the whole Country. Finally, in order to evaluate the improvement achieved by this approach for purposes of land cover monitoring, land cover classification is undertaken either upon original and processed data and compared.

10428-32, Session 7

Simulation of vegetation and relief induced shadows on rivers with remote sensing data

Pierre Karrasch, Sebastian Hunger, TU Dresden (Germany)

Rivers are the lifelines of our environment. For this reason they are always in the focus of environmental studies. With the European Water Framework Directive the European Commission provides a powerful tool to commit the member states to prove the so called good ecological status of all the water bodies in their countries. For the assessment of the ecological status the member states have developed different monitoring programs and approaches. In Germany remote sensing data and methodology are used within the framework of the overview method provided by the German Working Group on water issues of the Federal States and the Federal Government represented by the Federal Environment Ministry (LAWA), for example for the vegetation in the riparian zone, the structure of the river bank or the alignment of a river. Such hydromorphological parameters can have an immediate impact on the chemical and biological status of a river. Thus, the shadowing of a river affects the temperature of the water and also the energy balance of the water body. Therefore changes in temperature also influence the biological and chemical status of rivers or lakes. Two different categories of reasons for the shadowing of waterbodies can be distinguished. Firstly there are the predominant climatic and weather conditions like the air temperature and especially the influence of cloud coverage. The second category comprises influences in the close environment of the waterbody. Especially the vegetation in the riparian zone induces shadows on the water surface. Depending on the surrounding environment of the analyzed waterbody also the relief causes shadows on the waterbody.The main objective of this study is the simulation of the shadowing of a section of the river Freiberger Mulde for a full year. This ensures that effects of different sun positions over the year (azimuth, elevation) are taken into account. For this purpose, a workflow has been developed on the basis of remote sensing data, which comprises two essential stages. For all analyses digital orthophotos (RGBI) with a geometric resolution von 20 cm and a digital surface model with a geometric resolution of 2 m is available. Prior to the actual analysis of shadowing a comprehensive data pre-processing is necessary. At first the water surface has to be extracted using the digital orthophotos. This is done using object-oriented classification methods. However, the riverbank line derived from this information is strongly influenced by overhanging vegetation. To avoid this underestimation of the water surface it is necessary to reconstruct the real river bank line. Karrasch and Hunger (2016) introduced a statistical approach how such mathematical reconstruction can be implemented. On the basis of the available data of the extent of the river section (shapefile), it is now possible to simulate the shadowing of the water body during the course of the year. For this the river section is divided into grid cells. For each of these grid cells simulation of the annual course of the sun is repeated. For every time interval it is verified whether the line of sight between the grid cell and the appropriate sun position (azimuth, elevation), intersect the digital surface model. In this case, the particular grid cell is defined as ‘shadowed’ by an artefact of the surface model (e.g. vegetation, relief) at that time. This algorithm is repeated for a full year and all grid cells in the chosen river section of the study area. The result of this procedure is a raster layer which represents the theoretical annual hours of shadowing of the river section. In future this information can be expanded by means of further affecting factors. This includes the estimation of the phenological status of deciduous trees in the riparian zone, which can have a great influence on the shadowing of the water surface. Furthermore the varying spectral radiance will be considered. On the one hand, this depends on the position of the sun (azimuth, elevation) and on the other hand on the changing distance between the earth and the sun (perihelion, aphelion). Another important aspect is the consideration of cloud coverage and diffuse illumination as weighting factor for the whole modelling of energy flows into rivers caused by sun radiation.

10428-33, Session 7

Hyperspectral signature analysis of three plant species to long-term hydrocarbon and heavy metal exposure

Guillaume Lassalle, ONERA (France); Anthony Credoz, Total S.A. (France); Sophie Fabre, ONERA (France); Rémy Hédacq, Dominique Dubucq, Total S.A. (France); Arnaud Elger, EcoLab (France)

Pipeline leakages and natural oil seepages can be detected on bare soils using hyperspectral remote sensing technics that search for hydrocarbon absorption features at specific wavelengths. However, they remain particularly difficult to identify in regions covered by dense vegetation. Hence, recent studies aim to exploit vegetation as spectral bioindicators by detecting changes in particular wavelengths of the hyperspectral signature, induced by oil exposure. In order to assess the feasibility of the method at larger spatial scale, a study has been carried out in a greenhouse on three species from tropical (Pennisetum alopecuroides and Panicum virgatum) and temperate (Rubus fruticosus) zones. The main purpose was to analyze the variability of vegetation hyperspectral response to long-term oil exposure using common vegetation indices applied at leaf and plant scales. Plants were grown on contaminated soil during 130 days, with concentrations respectively up to 4.5 and 36 g.kg-1 for heavy metals and C10-C40 hydrocarbons. Reflectance data (350-2500 nm) were acquired at several dates (from 1 to 60 days) at both scales under artificial light source with a spectroradiometer ASD FieldSpec Hi-Res. All species showed an increase of reflectance in the visible (VIS, 400-750 nm) and short-wave infrared (SWIR, 1300-2500 nm) under experimental contaminants exposure. However, the responses were contrasted in the near-infrared (NIR, 750-1300 nm), with an increase of reflectance for Panicum and Pennisetum and a decrease for Rubus on contaminated soil. These results were consistent with those of previous experimental studies

conducted on short-term exposure at leaf and plant scales. 47 normalized vegetation indices covering VIS, NIR and SWIR were compared between treatments for all species, and the most sensitive to contamination exposure were retained. The same indices showed significant differences at both leaf and plant scales until 60 days ($p < 0.05$). Indices related to plant pigments (Lichtenthaler Index, Structure Intensive Pigment Index), plant water content (Normalized Difference Water Index, Disease Water Stress Index) and red-edge reflectance (Red-edge Position Index, Normalized Difference Vegetation Index) appeared to be particularly sensitive to soil contamination. In order to validate the selection of indices, hyperspectral measurements were performed outdoor at plant scale at the end of the experiment (130 days). Leaf samples were also collected for pigment analysis to complete this validation stage. Indices selected at day 60 were still sensitive to soil contamination after 130 days, excepted for some indices located in particular wavelengths of the SWIR. In addition, the selected indices from the VIS were also related to pigment concentrations found in leaves to ensure that the corresponding wavelengths were sensitive to the measured pigments. This study demonstrates the interest of hyperspectral data to detect vegetation exposed to soil contamination. The promising results show great potential for oil exploration and environmental diagnosis based on the exploitation of airborne and satellite hyperspectral data.

10428-34, Session 7

Automated flood extent identification using WorldView imagery for the insurance industry

Christina Geller, AIR Worldwide (United States)

The flood extent identification workflow originally began with Digital Globe's protogenV2RAW algorithm to detect the presence of water in the image. This unsupervised process was originally intended to create a water mask producing a binary image where intensity 255 indicates the presence of water while intensity 0 is the absence of water in 8-band optical and VNIR imagery. However, while the protogenV2RAW algorithm was known to display false positives due to the presence of certain types of concrete roofs or shadows, comparison of the results for the August 2016 Louisiana flooding event to the National Geodetic Survey's Nadir aerial imagery for the event showed that the algorithm was unable to identify unclear or "muddy" water and underestimated the extent of the flood. To solve this problem, a spectral library with an expanded understanding of the spectral signature of water, including water filled with silt and debris as a result of a flood, was developed. These unique spectral signatures of these unclear waters were identified using supervised classification on WorldView3 imagery of known flooding events in India, Serbia, Bosnia, the United Kingdom, Brazil, China, and the United States. The global nature of the supervised classification was intended to account for the derivation in soil conditions that might impact the visual appearance of the flood. Floods in the bayous of Louisiana, for example, appeared light brown in color while floods in the neighboring state of Texas appeared green in coloring. The original protogenV2RAW algorithm was then updated to utilize the expanded spectral library in its identification of water and produce an imager where intensity 255 indicates the presence of clear water, intensity 100 indicates the presence of unclear water, and intensity 0 indicates the absence of water within the imagery. (The non-binary nature of the output allows for easy visual inspection by the user, although the later push for full-automation means the intensity 255 and intensity 100 classes are merged together in the final output.) Residual gaps in the output are the result of the presence of the built environment in the study area as the updated algorithm is unable to account for floods passing through buildings. These "holes" are plugged using the nearest neighbor calculation where a 2 meter pixel with "flooded" neighboring pixels, which neighbor defined as a distance of 4 meters, are also assumed to be flooded. Once imagery for a single day from the area of interest are processed into the clear water, unclear water, and no water classification, the results are then merged together and compared to a repository of land cover datasets for around the world. Permanent water bodies and wetlands are then removed in order to create a result identifying flooded areas only.

10428-35, Session 8

Identification and classification of tree species of riparian zones using object-based image analysis

Sebastian Hunger, Pierre Karrasch, TU Dresden (Germany)

Riparian zones which are defined as accompanying areas of flowing and stagnant water bodies exhibit an important factor in a river ecosystem. They are described as the transitional zone between terrestrial and aquatic ecosystems that have a direct impact on aquatic and wildlife habitats and contain a mixture of grasses, shrubs and trees. The diverse characteristics of landscape elements are responsible for different patterns and composition of vegetation as well as the various forms of riparian zones that allow the development of a multitude of habitats and niches. Due to the provision of a variety of environmental, economic and social functions riparian zones and their vegetation are of utmost importance when assessing river ecosystems. They provide a benefit for example by the presence of vegetation as a natural habitat, the linking of different habitats, the protection of river banks and the preservation of water quality due to the reduction of substance intrusion. In this context especially trees fulfill a variety of functions e.g. stabilizing river banks and influencing the microclimate. Restoration represents a common approach for the conservation and protection of riparian zones. In the year 2000 the European Parliament and the Council established the Water Framework Directive at the European level. This directive constitutes a framework for measures in the field of water policy that obliges the Member States to reach and sustain the good ecological status of their water bodies. Every Member State has developed its own monitoring programs. The monitoring of this process constitutes an essential tool for quantitative analyses and evaluation of implemented measures for decision-making and planning of further measures. In addition, the analysis of riparian zones helps to understand the development of vegetation patterns and habitats. Therefor field surveys that are normally carried out to assess the condition and composition of riparian zones are an appropriate method. However they are only suited for small-scale studies.

In this context the application of data and methods belonging to the fields of remote sensing and geoinformatics are a meaningful addition for the assessment across extensive areas. With the increasing availability of high resolution digital imagery it is possible to clearly distinguish individual landscape elements from another. Thus the improved recognizability of details enables not only the separation of vegetation classes but also the identification of individual species. This study aims at the development, application and evaluation of different image processing methods to extract tree populations and parameters to describe individual tree species of a section of the river Freiberger Mulde. High resolution digital aerial imagery and field surveys form the basis for this study. The extraction and identification of trees is conducted by the help of object-based image analysis which is used for a multitude of applications. This method has the advantage that spectrally similar and spatially neighboring picture elements are grouped to form the image objects that are used to identify individual tree species. In addition to the spectral information of the individual image objects it is also possible to consider characteristics such as size, shape and neighborhood. The results indicate that the use of high resolution digital imagery for the identification and classification of tree species can have a substantial additional value.

10428-36, Session 8

SYeNERGY: the satellite data-based platform for energy sector in Poland, the pilot study with PGE S.A. company

Martyna Gatkowska, Wojciech Kiryla, Katarzyna Dabrowska-Zielinska, Institute of Geodesy and Cartography (Poland)

The paper aims at presentation of SYeNERGY project, which is designed to develop the on-line platform applying satellite data in order to support various actors in the Energy Market in Poland.

According to the Amendment of the Law on Renewable Energy Sources from 22.06.2016 r. in Poland, the recipients of the energy biomass – Energy Companies, are obliged to obey to the rules of local biomass (the biomass can be obtained from the distance of maximum 300 km in straight line from the CHP) and biomass' sustainable acquisition (the biomass cannot be collected from the areas under protection of: NATURA 2000, Reservations, National and Regional Parks). The entire responsibility of obtaining the biomass according to the law is put on the recipients of the biomass – Energy Companies. The procedures implemented by them up to now are very time and money consuming.

Since the procedures of verifying the accuracy of information on the delivered biomass are very time and money consuming, the Energy Crops companies are vividly interested in application of supporting tools.

This situation was found by the Institute of Geodesy and Cartography as a motivation for development of the system which would enable to efficiently check if the acquired biomass fulfill the requirements of local biomass and sustainable acquisition.

Moreover, the system was also designed to verify if the information on the energy biomass plantations, delivered by the plantations owners are true. The System enables, on the basis of satellite data based procedures and models, to deliver the following information: the type of energy biomass (multiple years: willow, poplar) and one-year crops (corn, rape, wheat and rye), the area of the plantation, the biomass – yield, the distance from the CHP as well as the distance from the surrounding protection areas.

Moreover, application of archive satellite data and especially the satellite data acquired in winter, enabled to deliver the information if the energy biomass was harvested and what was the harvested area.

In the beginning of 2017, the agreement between the Institute of Geodesy and Cartography and PGE S.A. – one of the biggest energy companies in Poland was signed in order to conduct the pilot application of SYeNERGY platform in their everyday work.

So far two reports containing all information on the biomass plantations were delivered to the PGE employees and their accuracy and content was assessed as sufficient.

The Pilot application is planned to be continued until the end of 2017 and the further cooperation is also planned.

The PGE S.A. company is interested in development of the dedicated satellite data based platform which would enable their employees in whole Poland to perform the verification of the biomass suppliers.

10428-37, Session 8

Modeling and testing of geometric processing model based on double baselines stereo photogrammetric system

Yingbo Li, Sisi Zhao, Bin Hu, Haibo Zhao, Beijing Institute of Space Mechanics and Electricity (China)

Aimed at key problems the system of 1:5000 scale space stereo mapping and the shortage of the surveying capa-bility of urban area, in regard of the performance index and the surveying systems of the existing domestic optical mapping satellites are unable to meet the demand of the large scale stereo mapping, it is urgent to develop the very high accuracy space photogrammetric satellite system which has a 1:5000 scale (or larger).The new surveying systems of double baseline stereo photogrammetric mode with combined of linear array sensor and area array sensor was proposed, which aims at solving the problems of barriers, distortions and radiation differences in complex ground object mapping for the existing space stereo mapping technology. Based on collinearity equation, double baseline stereo photogrammetric method and the model of combined adjustment were presented, systematic error compensation for this model was analyzed, position precision of double baseline stereo photogrammetry based on both simulated images and images acquired under lab conditions was studied. The laboratory tests showed that camera geometric calibration accuracy is better than 1?m, the height positioning accuracy is better than 1.5GSD with GCPs?The results showed that the mode of combined of one linear array sensor and one plane array sensor had higher positioning precision. Explore the new system of 1:5000 scale very high accuracy space stereo mapping can provide available new technologies and strategies for achieving demotic very high accuracy space stereo mapping.

10428-38, Session 8

Modeling chlorophyll-a and turbidity concentrations in river Ganga (India) using Landsat 8 OLI imagery

Satish Prasad, Ridhi Saluja, J. K. Garg, Guru Gobind Singh Indraprastha Univ. (India)

Introduction: Rivers being one of the most complex ecosystems are highly variable both spatially and temporally. Chlorophyll-a (Chl-a) is considered one of the primary indicator for water quality and as a measure of river productivity, while turbidity in rivers is a measure of suspended organic matter. Monitoring of river parameters is challenging, demanding tremendous efforts and resources. However remotely sensed satellite data allows spatial and temporal coverage and monitoring of river water quality variables throughput the year. Numerous algorithms have been developed in the past for deriving environmental parameters such as chlorophyll-a and turbidity from remote sensing imagery. However, most of these algorithms were focused on the lentic systems. There is paucity in such algorithms or methods from which water quality variables can be predicted using remotely sensed satellite imagery.

Objective: The primary objective of our study is to develop algorithms based on Landsat 8 OLI imagery and in-situ observations for prediction of Chl-a and turbidity in river Ganga.

Methodology: In this study, regression models are developed to retrieve Chl-a and turbidity values in Ganga river. Band reflectance from multispectral Landsat-8 OLI images of May and October 2016 representing summer and autumn season were used for model development and validation along with simultaneous ground truth data, and December 2016 image as winter season was used to predict chlorophyll-a and turbidity. Field data from 24 data sampling points distributed along the river stretch were used. Image processing was performed in ENVI 5.3 software. Pre-processing of satellite imagery included conversion of DN values to radiance and then reflectance using ENVI 5.3 FLAASH module. Different combinations of image bands, band ratios, ratios of logarithmically transformed bands and subtraction between bands combinations were tested against chl-a, turbidity and their logarithmically transformed concentrations for model development. The reflectance values derived from satellite imagery were then subjected to regression analysis using field data as the dependent variable SPSS version 16.0 and Microsoft Office XLSTAT. Chlorophyll-a and turbidity maps were generated using ArcGIS 10.3 software.

Results and Conclusion: The band ratio of B3/B2 (R2= 0.69)

and log (B6/B2) (R2= 0.64) proved to be the best applicable algorithms for estimating chlorophyll-a. The best algorithms for turbidity were log (B7/B1) (R2= 0.73) and subtraction combination of bands B2-B6, B4-B5 and B4-B7 (R2= 0.89) for estimating turbidity, based on band combinations tested. The algorithms were used to generate maps showing the chlorophyll-a and turbidity concentration distribution in the study area. The predicted and estimated Chl-a and turbidity were then tested for accuracy assessment using the December 2016 dataset.

10428-39, Session 9

Remote sensing-based identification of NWW strike large-deep fault and Its relation to uranium ore-field in Southeast China

Wei Pan, Zhangfa Yu, Hanbo Li, Qinglin Tian, Beijing Research Institute of Uranium Geology (China)

Southeast China in this paper was allocated between 110°~120° east longitude and 24°~30° north latitude ,which is in joint area of Paleo-Tethys and Pacific tectonic domain. However, few large EW nearly strike fault was discover in the area, this maybe was caused by the strong transformation of NE strike faults in the Late Mesozoic Yansanian and NNE structure in Cenozoic Himalayan to the early formed nearly EW strike Paleotethys faults. In this paper 5°?6° mosaic ETM image download from GLCF was used firstly to interpret the line feature of large-deep fault. The interpretation of large-deep fault was quite different to the small fault, the interpretation criteria should not focuses on the continuous and detail liner feature of the fault, but the vestige of the fault actiction occurred as the boundary of color and texture pattern unit which indicate the lithological association and magmatic intrusion units. Two NWW strike (Tongdao-Longchuan and Yongfu-Fogang) were discovered by contrasting the interpreted line feature and the faults in published geology map. To verify the fault feature of the interpreted line feature, The forming temperature of the surface rock, the regional gravity and magnetism data were registered with the ETM image in ArcGIS platform. The contour map of the forming temperature of surface rock in South China shew clear NWW axial anomalies against the NE axial background anomalies while the NWW strike Tongdao-Longchuan and Yongfu-Fogang passed through the Mesozoic or Cenozoic strata and Yashanian magmatic rocks in Cathaysia landmass, and same axial temperature anomalies along Paleozoic strata in Yangzi landmass. In Bouguer gravity anomaly map, Tongdao-Longchuan and Yongfu-Fogang line feature constitute the boundary of NWW axial low gravity anomalies in Yangzi landmass. The aeromagnetic ?T anomaly contour map shew some NWW axial anomalies along Tongdao-Longchuan line feature and clear NWW axial anomalies along Yongfu-Fogang line feature against the NE axial background anomalies in Cathaysia landmass, but few NWW magnetic anomaly occurred along the two line feature in Yangzi landmass. The above fact suggest that the two line feature are large-deep faults which were formed before Indo-Chinese period and has affect the forming temperature of Mesozoic outcrops and the intrusion of Yanshanian magmatism. Comprehensive study of the spatial relation of large uranium uranium deposits to the faults found that The intersect area of large-deep NWW strike fault formed before before Indo-Chinese and NE strike ,NNE strike fault after Yanshanian control the most of the uranium ore-field in Southeast China.

10428-40, Session 9

Emergency response to landslide using GNSS measurements and UAV

Konstantinos G. Nikolakopoulos, Ioannis Koukouvelas, Univ. of Patras (Greece)

Landslide monitoring can be performed using many different methods: Classical geotechnical measurements like inclinometer, topographical survey measurements with total stations or GNSS sensors and photogrammetric techniques using airphotos or high resolution satellite images. However all these methods are expensive or difficult to be developed immediately after the landslide triggering. In contrast airborne technology and especially the use of Unmanned Aerial Vehicles (UAVs) make response to landslide disaster easier as UAVs can be launched quickly in dangerous terrains and send data about the sliding areas to responders on the ground either as RGB images or as videos. In addition, the emergency response to landslide is critical for the further monitoring. For proper displacement identification all the above mentioned monitoring methods need a high resolution and a very accurate representation of the relief. The ideal solution for the accurate and quick mapping of a landslide is the combined use of UAV's photogrammetry and GNSS measurements. UAVs have started their development as expensive toys but they currently became a very valuable tool in large scale mapping of sliding areas. The purpose of this work is to demonstrate an effective solution for the initial landslide mapping immediately after the occurrence of the phenomenon and the possibility of the periodical assessment of the landslide. Three different landslide cases from the Western Greece are presented in the current study. All three landslides have different characteristics: occurred in different geomorphologic environments, triggered by different causes and had different geologic bedrock. In all three cases we performed detailed GNSS measurements of the landslide area, we generated orthophotos as well as Digital Surface Models (DSMs) at an accuracy of less than ±10 cm. Slide direction and velocity, mass balances as well as protection and mitigation measurements can be derived from the application of the UAVs. Those data in addition are accurate, cost- and time-effective.

10428-41, Session 9

Surface deformation analysis over Vrancea seismogenic area through radar and GPS geospatial data

Maria A. Zoran, Roxana S. Savastru, Dan M. Savastru, National Institute of Research and Development for Optoelectronics (Romania); Florin Serban, Delia Teleaga, TERRASIGNA (Romania); Doru Mateciuc, National Institute for Earth Physics (Romania)

Time series analysis of Global Positioning Systems GPS and InSAR data is an important tool for Earth's surface deformation assessment, which can result from a wide range of geological phenomena like as earthquakes, volcanoes, landslides or ground water level changes. The study of geophysical phenomena which appear prior to and after seismic events involves different scientific fields like geophysics, hydrology, geomagnetism, atmospheric physics, geochemistry, radiopropagation and seismology. Earthquake prediction has two potentially compatible but distinctly different objectives: (a) phenomena that provide information about the future earthquake hazard useful to those who live in earthquake-prone regions and (b) phenomena causally related to the physical processes governing failure on a fault that will improve our understanding of those processes. To understand the exact relationship of a precursor with an impending large earthquake, it is essential to know the geodynamical reason behind the occurrence of that precursor. Validating an earthquake precursor through an acceptable geodynamic modeling and accounting for its occurrence is a challenging task. The aim of this paper was to identify several types of earthquake precursors that might be observed from geospatial data. Precise information concerning surface deformation of the earth in Vrancea region is indispensable to numerical simulation of earthquakes and of other tectonic activity. Surface deformation can be interpreted in relation to an internal mechanical process of the Earth, i.e., stress distribution or fault slips, using the elastic dislocation theory. In spite of providing the best constraints on the rate of strain accumulation on active faults (coseismic, postseismic, and

interseismic deformation; plate motion and crustal deformation at plate boundaries), GPS measurements have a low spatial resolution, and deformation in the vertical direction cannot be determined very accurately. Continuous GPS Romanian network stations and few field campaigns data recorded between 2005-2012 years revealed a displacement of about 5 or 6 millimeters per year in horizontal direction relative motion, and a few millimeters per year in vertical direction. In support of this achievement , time series satellite Sentinel 1 data available for Vrancea zone during October 2014 till October 2016 have been used to generate two types of interferograms (short-term and medium- term) in order to assess possible deformations due to earthquakes and respectively for possible slow deformations. As during last investigated period have not been recorded medium or strong earthquakes, interferograms over investigated test area revealed small displacements on vertical direction (subsidence or uplifts) of 5-10 millimeters per year. Based on GPS continuous network as well as satellite Sentinel 1 results, different possible tectonic scenarios can be developed. The localization of horizontal and vertical motions, fault slip, and surface deformation of the continental blocks provides new information, in support of different geodynamic models. As Vrancea area has a significant regional tectonic activity in Romania and Europe, the joint analysis of geospatial and in-situ geophysical information is revealing new insights in the field of hazard assessment.

10428-43, Session 9

Passive thermal infrared hyperspectral imaging for quantitative imaging of shale gas leaks

Marc-André Gagnon, Pierre Tremblay, Simon Savary, Vincent Farley, Philippe Lagueux, Éric Guyot, Martin Chamberland, Jean Giroux, Telops Inc. (Canada)

There are many types of natural gas fields including shale formations that are common especially in the St-Lawrence Valley (Canada). Since methane (CH4), the major component of shale gas, is odorless, colorless and highly flammable, in addition to being a greenhouse gas, methane emanations and/or leaks are important to consider for both safety and environmental reasons. Telops recently launched on the market the Hyper-Cam Methane, a field-deployable thermal infrared hyperspectral camera specially tuned for detecting methane infrared spectral features under ambient conditions and over large distances. In order to illustrate the benefits of this novel research instrument for natural gas imaging, the instrument was brought on a site where shale gas leaks unexpectedly happened during a geological survey near the Enfant-Jesus hospital in Quebec City, Canada, during December 2014. Quantitative methane imaging was carried out based on methane's unique infrared spectral signature. Optical flow analysis was also carried out on the data to estimate the methane mass flow rate. The results show how this novel technique could be used for advanced research on shale gases.

10428-44, Session 10

Monitoring structural breaks in vegetation dynamics of the nature reserve Königsbrücker Heide

Christine Wessollek, Pierre Karrasch, TU Dresden (Germany)

Nowadays remote sensing is a well-established method and technique of providing data. Especially for regular monitoring of manifold natural and anthropogenic processes satellite imagery, aerial photographs or increasingly images collected by unmanned aerial vehicles (UAV) are playing an important role. This current development shows the availability of systems with very high geometric resolution for the monitoring of vegetation. At the same time, however, the value of temporally high-resolution data is underestimated, particularly in applications focusing on the detection of short-term changes. These can be natural processes like natural disasters as well as changes caused by anthropogenic interventions. These include, for example, economic activities such as forestry, agriculture or mining. On the other hand, there are also processes which are intended to convert previously used areas into natural or near-natural surfaces. Such kind of conversion can take place for example on past mining landscapes or former military training areas. The Königsbrücker Heide is such a former military training site located about 30 km north of the Saxon state capitol Dresden. After the withdrawal of the Soviet forces in 1992 and after nearly 100 years of military use this site was declared as nature reserve in 1996. The management of the whole protection area is implemented in three different management zone. A small buffer zone to the surrounding landscape, a nature development zone and a zone of controlled succession covers an area of about 7.000 ha. This results in different developments of succession on that conversion areas. Analyses by Wessollek and Karrasch (2016) show the development of the Königsbrücker Heide based on MODIS-NDVI time series between 2000 and 2016. As can be seen these data are useful to detect trends in vegetation development. Furthermore different developments are apparent in the nature development zone and the zone of controlled succession even if no general statement regarding the zones can be made. Nevertheless, the analyses also show that short-term changes, so called breaks in the vegetation development cannot be described using linear trend models. The complete understanding of vegetation trends is only given if discontinuities in vegetation development are detected and considered as part of the trend modelling. There are multiple reasons for such breaks. Structural breaks in the NDVI time series can be found simultaneously in the whole study area. Hence it can be assumed that these breaks have a more natural character, caused for example by climatic conditions like temperature or precipitation. Otherwise, especially in the zone of controlled succession structural breaks can be detected which cannot be traced back to natural conditions. The documentation of the tending strategies in the zone of controlled succession allows the validation of these structural breaks. On the other hand, this information also serves to parameterize the algorithms of breakpoint detection. Final analyses of the spatial distribution of breakpoints as well as their frequency depending on the respective protection zone allow a detailed view to vegetation development in the Königsbrücker Heide, which cannot be represented by simple trend models.

10428-45, Session 10

Analyses of GIMMS NDVI Time Series in Kogi State, Nigeria

Jessica Palka, Christine Wessollek, Pierre Karrasch, TU Dresden (Germany)

The value of remote sensing data is particularly evident where an areal monitoring is needed to provide information on the earth's surface development. The use of temporal high resolution time series data allows for detecting short-term changes in different investigation areas. One of these study areas is Kogi State in Nigeria. In the region with an area of approximately 28,000 km? different vegetation types can be found. The northern part is characterized by woody-derived savannah and Guinea savannah while the southern part consists of rainforest. Furthermore gallery forests can be found along the two main rivers in Kogi State. As the major population in this region is living in rural communities with crop farming the existing vegetation is slowly being altered. The expansion of agricultural land causes loss of natural vegetation, especially in the regions close to the rivers which are suitable for crop production.

With regard to these facts, two questions can be dealt with covering different aspects of the development of vegetation in the Kogi state. One task is the determination and evaluation of the general development of the vegetation in the study area (trend estimation). On the other hand, analyses on a short-term behavior of vegetation conditions can provide information

about seasonal effects in vegetation development. These changes can be of natural or anthropogenic origin.

To perform both types of analysis remote sensing data with high temporal resolution are necessary. For this purpose, the GIMMS-NDVI data set, which is provided by the NOAA, provides information on the normalized difference vegetation index (NDVI) in a geometric resolution of approx. 8 km in the study area. Although this resolution must be described as comparatively coarse, the temporal resolution of 15 days allows the already described analyses. For the presented analysis data for the period 1981-2012 (31 years) were used.

The implemented workflow mainly applies methods of time series analysis. These methods are based on the decomposition of the time series by means of an additive model. In this process the time series of each surface element is decomposed into the three components of trend, seasonality and a residual term containing the random portion of the signal. The seasonal component is then used for the analysis of seasonal vegetation development. The results show that in addition to the classical seasonal development, artefacts of different vegetation periods (several NDVI maxima) can be found in the data. The trend component of the time series shows a consistently positive development in the entire study area considering the full investigation period of 31 years. However, the results also show that this development has not been continuous and a simple linear modeling of the NDVI increase is only possible to a limited extent. For this reason, the trend modeling was extended by procedures for detecting structural breaks in the time series. This consideration of breakpoints allows the modeling of the trend behavior in the periods between the breaks. The results of these analyses show an improvement of the quality of the linear modeling of the NDVI development by an average of approx. 30% (RMSE). Furthermore can be seen that not all intervals (periods between the breaks) show positive trends.

In addition to the RMSE, extensive residual analysis were carried out for the qualitative assessment of all performed analyses. This includes the decomposition of the individual time series as well as the modeling of vegetation trends. All results are presented in extensive map representations and thus allow, for example for the breakpoints, the analysis of spatial distributions over time.

In the future, the analyses are planned to be expanded by sensitivity analysis of breakpoint detection as well as investigations on the influence of precipitation on NDVI development, for example by CHIRPS data.

10428-46, Session 10

Distinguishing sliding area by decision analyzing with remote sensing image and lidar data combined

Chia-Hao Chang, Jee-Cheng Wu, National Ilan Univ. (Taiwan)

After the Earthquake 921 in Taiwan, the country has been facing many environmental challenges with the earthquakes, typhoon which brings about abundant rainfall every year resulting in soil liquefaction and collapse of the land, which is seriously affecting the people's lives and property. The landslide attributes to several environmental factors, which could be analyzed to better-helpful for the government and related agent to manage the endangered area. This study has chosen Provincial Highway 14(Taiwan) 34K~38K+500" as a sample area which has devastated by Earthquake 921 and Typhoon Mindulle. The decision analysis is conducted by utilizing Orthophoto to processing band math and Segment Only Feature Extraction and by using Digital Elevation Model(DEM) to compute profile curvature, plane curvature and slope length and slope factor. The comparing has done by following the methods below:

1. The orthophoto have divided by using 'Segment Only Feature Extraction' which is tool in ENVI and combined with profile curvature, plane curvature, slope length and slope factor.

2. The orthophoto have divided by using 'Segment Only Feature Extraction' which is tool in ENVI and combined with profile curvature and plane curvature. The studied has shown that the accuracy could be increased by more than 15% when the slope length and slope factor are considered.

10428-47, Session 10

Research on intelligent extraction method of coastal aquaculture areas on high resolution remote sensing image based on multi-features fusion

Bo Cheng, Yueming Liu, Guizhou Wang, Xiaoxiao Ma, Institute of Remote Sensing and Digital Earth (China)

In this article, an intelligent extraction method of coastal aquaculture area based on multi-features is proposed. Used GaoFen-2 images for experimental data, and chose several Chinese southeastern coastal sea areas as the experimental area, on the basis of analyzed the spectral characteristics of the aquaculture areas, extracted spectrum, texture and other features to constitute the feature set. The feature set is dimension reduced and fusion to generated the new feature of target recognition in coastal aquaculture area, then used the threshold method to extract the aquaculture area on the new feature. Ultimately achieve high precision intelligent extraction and classification of coastal aquaculture area. In addition, the method was used to detect the change of the aquaculture area before and after the disaster. The remote sensing images of different stages before and after typhoon landing were selected and extracted the coastal aquaculture area respectively. By comparing the extracted aquaculture area of the disaster affected area, to statistic the affected area, conduct disaster analysis and study the typhoon disaster damage to the coastal aquaculture area.

10428-48, Session 10

Fusion of remote sensing, DGPS, total station and GPR data for the3-D mapping of Himalayan cryosphere: application and future potential

Pawan Kumar, Milap C. Sharma, Jawaharlal Nehru Univ. (India)

Himalayan Glaciers are a major source of fresh water, and in places are the critical source of water for drinking, irrigation and hydroelectric power generation for South Asia. Modern water resource management requires understanding the volume of source available for a robust planning and development for the future.Glaciers are highly sensitive indicators to any climate change. Contemporary size and volume are critical factors for timely evaluation/assessment for both near-term and long-term changes in both temperature and precipitation and the cryosphere thereupon. Glacier area and surface morphology can be readily mapped from both satellites imagery and aerial photographs. With the help of remotely sensed data and GIS analysis, glacier surface areas have been mapped with mean spatial resolution of 10 meter. The surface mapping with such resolution is neither able to access the exact volume nor determine sensitivity of glacier to the recent climate. Most satellite maps are only two-dimensional mapping of crysophere, but three-dimensional maps of glacier hydrological systems are necessary for volumetric assessment and long-term planning.

Therefore, the integration of survey instrument such as DGPS, Total Station with millimeter accuracy, and simultaneous simulation with Ground Penetrating Radar (GPR) surveys over the mapped conduit systems will help in accessing glacier mass accurately and define subsurface geometry for the 3-D modeling of glaciers for better understanding and estimation of water fresh resource. Further, the 3-D mapping of cryosphere will help us to access accurate the volume of fresh water in the Himalayan cryosphere, along with contemporary dynamics. We show an integrated approach to assess and quantify the

Himalayan cryosphere by integrating such techniques for a better management and understanding of the Himalayan cryosphere to climatic parameters and management of future water requirements. However, it is an established fact that glaciers show varied sensitivity to climate over the time and space, both in growing and receding.Therefore, monitoring this fresh water resource is most essential for an agrarian country like India where demand for irrigation is great in the Great Plains. Present study will represent the seamless integration of field based 3-D Total station mapping of glacier snout of Gangotri Glacier, GPR Profiling of Glacier at selective locations, Volume estimation and annual change in the volume and its integration with the MODIS LST data in a way to access the present glacier sensitivity to climatic variability, as well as help model future scenario more accurately for robust management of this finite water resource.

10428-52, Session 10

SAR and optical data in land degradation processes estimation: a case study from Southeast Bulgaria

Daniela Avetisyan, Roumen Nedkov, Space Research and Technology Institute (Bulgaria); Emiliya Velizarova, Forest Research Institute, Bulgarian Academy of Sciences (Bulgaria); Denitsa Borisova, Space Research and Technology Institute (Bulgaria)

Soil is a dominant factor of the terrestrial geosystems in the dry sub-humid zones, particularly through its effect on biomass production. Due to the climate changes and industrial development, soil resources in these zones are prone to degradation. On the other hand, degradation processes cause changes in land cover. Remote sensing optical data are widely used in the process of determining land cover change whereas SAR data is suitable for determination of soil moisture dynamics. In the present study, Tasseled Cap Transform (TCT) and modified Change Vector Analysis (mCVA) techniques are applied to Landsat data in order to be determined magnitude and direction of land cover changes in the semi-natural areas of Haskovo Region, Southeast Bulgaria. The study of the vector direction presents some distinct changes in the soil characteristics for the whole territory and significant changes in vegetation characteristics and moisture content in part of the semi-mountainous territories of the examined region. It has been found that the magnitude of those changes increases up to 50% in some of the territories under investigation. SAR data has been used to evaluate the relative soil moisture content in various soil differences and to trace its dynamics during growing season. In order to achieve this aim, Relative Soil Moisture Index (RSMI) is used. The index estimates the relative variation of volumetric soil moisture content in a given time period and enables determination of its change in relative values. On the basis of integrated application of aforementioned techniques, a model providing key information about the impact of soil moisture change and dynamics upon processes related to land cover change. The suggested model is appropriate for estimation of ecosystem services and functions delivered by landscapes in dry sub-humid zones.

Conference 10429: Lidar Technologies, Techniques, and Measurements for Atmospheric Remote Sensing

SPIE. REMOTE SENSING

Monday 11–11 September 2017

Part of Proceedings of SPIE Vol. 10429 Lidar Technologies, Techniques, and Measurements for Atmospheric Remote Sensing XIII

10429-1, Session 1

Airborne IPDA lidar development for column measurement of trace gases *(Invited Paper)*

Upendra N. Singh, Mulugeta Petros, Tamer F. Refaat, NASA Langley Research Ctr. (United States); Syed Ismail, Analytical Services and Materials, Inc. (United States)

NASA Langley Research Center (LaRC) has been involved in developing 2-micron lidar technologies for the past two decades. These technologies targets active remote sensing of winds, water vapor (H2O) and CO2. Currently, a novel airborne 2-micron triple-pulse IPDA lidar is under development at NASA LaRC. This instrument is an update for the successful development, demonstration and validation for an airborne 2-micron double-pulse CO2 IPDA lidar. This IPDA lidar targets column measurements of two important trace gases: carbon dioxide (CO2) and water vapor (H2O), simultaneously and independently. This IPDA lidar leverage advanced two-micron triple-pulse high-energy laser transmitter and a state-of-the-art detection system based on a newly developed HgCdTe (MCT) electron-initiated avalanche photodiode array. The IPDA design targets the capabilities of future space-based CO2 sensors set by major world-wide space agencies. Advancements in IPDA lidar development and scaling for space-based measurement will be presented.

10429-2, Session 1

New lidar challenges for gas hazard management in industrial environments

Nicolas Cézard, Anasthase Liméry, Philippe Benoit, Simon Le Méhauté, Didier Fleury, Didier Goular, Christophe Planchat, Matthieu Valla, Béatrice Augere, ONERA (France); Johan Bertrand, ANDRA (France); Agnes Dolfi-Bouteyre, ONERA (France)

The unique capability of Lidars to perform range-resolved gas profiles makes them an appealing choice for many applications, including in the industry. At the crossroads of research and applied physics, Onera develops innovative technologies and lidar systems to address new challenges arising in industrial contexts. This paper focuses on two complimentary lidar developments, one Raman and one DIAL, led at Onera's Optics Department.

On the Raman side, a high spatial-resolution multi-channel Raman Lidar is developed in partnership with the French National Radioactive Waste Management Agency (Andra). This development aims at enabling future monitoring of hydrogen and water vapor profiles inside disposal cells containing radioactive wastes. Andra was commissioned in 2006 to study the design and creation of an industrial site (Cigéo project), for deep geological disposal facility of radioactive wastes. Nuclear wastes may release hydrogen gas under some scenarios. For disposal cell safety and waste management concerns, a remote sensing solution able to monitor hydrogen and humidity profiles along the future disposal cells with high spatial resolution, is desired. We report on the development and first tests of a three-channel Raman Lidar (H2, H2O, N2) designed to address this issue. The emission wavelength is 355 nm, and the instrument takes advantage of SiPM detection technology (silicon photomultiplier, still little used in lidar to date) to provide a robust and fast photon-counting detection chain. To demonstrate the concept, simultaneous hydrogen and water vapor profiles have been recently measured along a 5-meter-long gas cell with 1 meter resolution at a distance of 85 meters.

On the DIAL side, a new instrumental concept is being explored and developed in partnership with Total E&P. The objective is to perform methane plume monitoring and flux assessment in the vicinity of industrials plants or platforms, in case of serious operational accident. In such case, concentrated methane plumes may be released in the atmosphere and may represent a danger for human intervention. For flux assessment, both gas concentration and air speed must be profiled by lidar. Therefore, the concept is to design a bi-function, all-fiber, coherent DIAL/Doppler Lidar. The chosen wavelength is 1645 nm, corresponding to a strong absorption wavelength of methane. The first challenge of this project was to design and build an appropriate fiber laser source. The achieved demonstrator delivers 200 W peak power, polarized, spectrally narrow (<15 MHz), 110 ns pulses of light out of a monomode fiber. It fulfills the requirements for a future implementation in a bi-function Dial/Doppler fiber lidar with km-range expectation. We report on the laser and lidar architecture, and on first lidar tests at 1645 nm.

10429-4, Session 1

Optical parametric oscillator lidar for the gas constituents sensing in the spectral range of 3-4 ?m

Olga V. Kharchenko, Oleg A. Romanovskii, Sergey A. Sadovnikov, Semen V. Yakovlev, V.E. Zuev Institute of Atmospheric Optics (Russian Federation)

The applicability of a KTA crystal-based laser system with optical parametric oscillators (OPO) generation to lidar sounding of the atmosphere in the spectral range 3–4 μm is studied in this work. A technique developed for lidar sounding of trace atmospheric gases (TAG) is based on differential absorption lidar (DIAL) method and differential optical absorption spectroscopy (DOAS). The DIAL-DOAS technique is tested to estimate its efficiency for lidar sounding of atmospheric trace gases. The numerical simulation performed shows that a KTA-based OPO laser is a promising source of radiation for remote DIAL-DOAS sounding of the TAGs under study along surface tropospheric paths. A possibility of using a PD38-03-PR photodiode for the DIAL gas analysis of the atmosphere is shown.

10429-5, Session 2

Arctic aerosol and water vapor profiling of the atmosphere using CAAAL (Canadian Autonomous Arctic Aerosol Lidar): first results *(Invited Paper)*

Kevin B. Strawbridge, Environment and Climate Change Canada (Canada)

The Canadian Autonomous Arctic Aerosol Lidar (CAAAL) developed by Environment and Climate Change Canada (ECCC) was recently deployed to Iqaluit, Nunavut in the Canadian Arctic. The instrument started measuring aerosol profiles at three wavelengths and water vapor profiles from near ground to 10-15 km during the extended night time beginning in November, 2016. The solid state laser based lidar was specifically designed for robust operation in the Arctic environment. The solid state laser emits 115 mJ at 355 nm, 30 mJ at 532 nm and 65 mJ at 1064 nm with a repetition rate of 100 Hz. The lidar is located along with a number of other remote sensors (radars, ceilometer, microwave radiometer) as well as co-located with twice daily balloon soundings. The autonomous operation is possible by employing a vertically-

pointing radar for aircraft detection that turns off laser beam if an aircraft is detected overhead in the nominal hazard zone while also maintaining a climate controlled environment inside the trailer. The health of the system is monitored remotely along with several pan/tilt cameras to ensure consistent results. An automatic wiper system keeps the exit window clean and the data are collected, stored and displayed on a website in near real-time. A detailed description of the instrument will be presented along with the calibration of the water vapor system and early results of both the aerosol and water vapor profiles collected to date. Comparison with other instrumentation will also be shown.

10429-6, Session 2

Strategic positioning of the ERATOSTHENES Research Centre for atmospheric remote sensing research in the Eastern Mediterranean and Middle East region

Rodanthi-Elisavet Mamouri , Cyprus Univ. of Technology (Cyprus); Albert Ansmann, Leibniz Institut für Troposphärenforschung (Germany); Diofantos G. Hadjimitsis, Argyro Nisantzi, Cyprus Univ. of Technology (Cyprus); Johannes Bühl, Patric Seifert, Ronny Engelmann, Ulla Wandinger, Leibniz Institut für Troposphärenforschung (Germany); Charalampos C. Kontoes, National Observatory of Athens (Greece); Gunter Schreier, Deutsches Zentrum für Luft- und Raumfahrt e.V. (Germany); Georgios Komodromos, Ministry of Transport, Communications and Works (Cyprus); Silas C. Michaelides, Kyriacos Themistocleous, Cyprus Univ. of Technology (Cyprus)

The aim of this paper is to present the importance of a permanent state- of-the-art atmospheric remote sensing ground based station in the region of the Eastern Mediterranean and Middle East (EMME). The ERATOSTHENES Research Centre (ERC) with the vision to become a Centre of Excellence for Earth Surveillance and Space-Based Monitoring of the Environment (EXCELSIOR H2020: Teaming project) in close collaboration with the German Leibniz Institute for Tropospheric Research (TROPOS), already operates within Phase 1, a fully established PollyNet-CLOUDNET supersite in Cyprus for a period of 1 year. The first results of the Cy-CARE (Cyprus Cloud Aerosol and Rain Experiment) - a common initiative between the Cyprus University of Technology (CUT), Limassol and TROPOS, Germany- are presented in this paper. The Cy-CARE has been designed by TROPOS and implemented at CUT to fill a gap in the global understanding of aerosol-cloud interaction, answering the question how rain patterns will develop in future and what the effect of climate change on arid regions as EMME might be. The EXCELSIOR is a team effort between CUT (acting as the coordinator), the German Aerospace Centre (DLR), the Institute for Astronomy and Astrophysics Space Applications and Remote Sensing of the National Observatory of Athens (NOA), the TROPOS and the Cyprus' Department of Electronic Communications of the Ministry of Transport, Communications and Works (DEC-MTCW) who will work together to improve the network structures significantly, resulting in Cyprus being regarded as a cornerstone of a European Network of active remote sensing of the atmosphere.

10429-7, Session 2

Retrieval of microphysical properties of liquid water clouds from atmospheric lidar measurements: comparison of the Raman dual field of view and the depolarization techniques

Cristofer Andres Jimenez Jimenez, Albert Ansmann, Leibniz Institut für Troposphärenforschung (Germany); David Donovan, Koninklijk Nederlands Meteorologisch Instituut (Netherlands); Ronny Engelmann, Jörg Schmidt, Ulla Wandinger, Leibniz Institut für Troposphärenforschung (Germany)

Since 2010, the Raman dual-FOV lidar system of TROPOS, Leipzig, permits the retrieval of microphysical properties of liquid-water clouds during nighttime. The methods makes use of the total nitrogen Raman lidar return and the respective nitrogen Raman signal caused by multiple-scattering (forward scattering by droplets) and one Raman backscatter process. Recently a robust optimal estimation procedure to retrieve this microphysical properties from lidar depolarization measurements was developed, in addition. This method makes use of the relationship between cloud multiple scattering effects and light depolarization by cloud droplets. Three telescopes for high accuracy depolarization measurements were implemented in the Multi-wavelength Atmospheric Raman lidar for Temperature, Humidity, and Aerosol profiling (MARTHA, Leipzig), being calibrated by an absolute three signals procedure. For the first time, two different lidar-based methods are now available to study microphysical properties of liquid-water clouds (liquid water content, effective droplet radius, droplet number concentration) with one lidar system. Results of the comparison between the two methods in terms of the retrieved cloud microphysical and optical properties for several liquid-water cloud measurements cases will be presented. Potential and limits will be discussed.

10429-8, Session 2

Lidar and in situ observations of aerosols, radiation fluxes, and meteorological parameters during the 20 March 2015 solar eclipse over southern Italy

Maria-Rita Perrone, Pasquale Burlizzi, Salvatore Romano, Univ. del Salento (Italy)

The effects of the 20 March 2015 partial solar eclipse on irradiance measurements, Planetary Boundary Layer (PBL) height, meteorological variables, and near surface particle properties have been investigated at Lecce (lc, 40.3°N, 18.1°E) in southeastern Italy. Each solar eclipse is always a unique event, since it is characterized by a particular time of the day, season, location, and synoptic conditions, and allows investigating the atmospheric processes driven by a fast decrease of the solar and terrestrial radiation. According to astronomic data, the eclipse started at lc at about 08:30 UTC and ended at 10:47 UTC, reaching the maximum obscuration of the solar disk (43.6%) at about 09:37 UTC. Short wave irradiance measurements revealed that the eclipse direct radiative forcing at the surface was equal to -307 Wm-2 at the maximum obscuration of the solar disk.

A lidar system identified as UNILE (UNIversity of LEcce) lidar and operating since May 2000 within the European Aerosol LIdar NETwork (EARLINET) was used to investigate both the atmospheric turbulence weakening driven by the eclipse cooling effect at different altitudes from the ground and the PBL height time evolution. It has been found that the PBL height that was equal to 660±20 m before the eclipse onset decreased up to 330±60 m at the eclipse full phase. Measurements from a micrometeorological station located at 16

m height over a grass soil have instead been used to investigate the atmospheric turbulence weakening at the ground level by the changes of the buoyancy and momentum fluxes and the turbulent kinetic energy. Nephelometer and aerodynamic particle sizer measurements revealed that the solar eclipse was also responsible for the increase of the near surface particle scattering coefficient, mainly because of the increase of the fine particle concentrations.

10429-9, Session 3

Advancement of coherent Doppler wind lidar at NASA Langley Research Center *(Invited Paper)*

Upendra N. Singh, Michael J. Kavaya, NASA Langley Research Ctr. (United States); George D. Emmitt, Simpson Weather Associates, Inc. (United States)

The first earth science "Decadal Survey" issued by the U.S. National Research Council (NRC) in 2007 identified the need for a space based lidar mission to measure three-dimensional tropospheric winds. This NRC recommendation went on to state that reliable global analyses of three-dimensional tropospheric winds are needed to improve the depiction of atmospheric dynamics, the transport of air pollution, and climate processes. A National Aeronautics and Space Administration (NASA) Weather Focus Area workshop held in April 2015 has also identified Global wind measurement as the next frontier for satellite remote sensing, particularly for weather research and forecasting.

NASA LaRC is developing high-energy 2-micron lasers and coherent-detection wind lidar systems to advance technology that is needed for global wind measurements from space. The wind lidar systems utilized the advanced laser technology available at the time in the development progress. The first 2-micron airborne wind lidar system was developed over 2005 – 2010. The Doppler Aerosol WiNd (DAWN) lidar system featured a 250 mJ, 10 Hz, 190 ns laser, an optical wedge-based conical scanner approximately centered on nadir, and a 15-cm receiver aperture. We are planning to fly DAWN in NASA's Convective Processes Experiment (CPEX) in May-June 2017. In preparation for CPEX, DAWN is being upgraded to improve its photon efficiency and to permit more operator test and alignment options in the field. NASA LaRC is also developing a second generation airborne lidar system that will have a different laser operating point to reduce risk, to greatly decrease the heat to be removed from the laser, and to improve the science product from future use in space. The status of the wind lidar systems, and aircraft science campaign results will be presented.

10429-10, Session 3

Siberian lidar station: the basic complex of remote laser sounding of the atmosphere

Oleg A. Romanovskii, Gennadii G. Matvienko, Yurii S. Balin, Sergey M. Bobrovnikov, Aleksey V. Nevzorov, V.E. Zuev Institute of Atmospheric Optics (Russian Federation)

The Siberian Lidar Station created at V.E. Zuev Institute of Atmospheric Optics and operating in Tomsk (56.5° N, 85.0° E) is a unique atmospheric observatory. It combines up-to-date instruments for remote laser and passive sounding for the study of aerosol and cloud fields, air temperature and humidity, and ozone and gaseous components of the ozone cycles. In addition to controlling a wide range of atmospheric parameters, the observatory allows simultaneous monitoring of the atmosphere throughout the valuable altitude range 0–75 km. In this paper, the instruments and results received at the Station are described.

10429-11, Session 3

Two wavelengths Mie-Raman lidar for full-time measurements of aerosol characterization

Longlong Wang, Samo Stanic, Univ. of Nova Gorica (Slovenia); William E. Eichinger, The Univ. of Iowa (Armenia); Asta Gregoric, Maru?ka Mole, Univ. of Nova Gorica (Slovenia); Klemen Bergant, Univ. of Nova Gorica (Slovenia) and Slovenian Environment Agency (Slovenia)

Multiple wavelength measurements of extinction and backscatter coefficients can provide information on aerosol size distributions and single scatter albedo.

We have developed a two wavelengths Mie-Raman lidar system to produce profiles of the extinction coefficient, backscatter coefficient and lidar ratio based on a 355 nm laser and the backscatter coefficient at 1064 nm at University of Nova Gorica, Slovenia. The lidar system includes four separate channels: vibrational nitrogen Raman signal at 387nm, and two Mie-Rayleigh signals caused by atmospheric molecules and aerosols at 355 nm and 1064 nm separately. The key features of this lidar system are long distance and full-time detection. These are obtained using a 600 mm aperture of cassegrain telescope and 150 mJ Nd:YAG pulsed laser at 355 nm and 50 mJ Nd:YAG pulsed laser at 1064 nm. The lidar is used for long-term observation of the evolution planetary boundary layer and for aerosol characterizations.

10429-12, Session 3

A graph signal filtering-based approach for detection of different edge types on airborne lidar data

Eda Bayram, Elif Vural, A. Aydin Alatan, Middle East Technical Univ. (Turkey)

Airborne Laser Scanning is a well-known remote sensing technology, which provides very dense and highly accurate, yet unorganized point cloud of earth surface. In the last decade, extracting information from data generated by airborne LIDAR systems has attracted many studies in geo-spatial analysis and urban applications. However, processing of LIDAR point cloud is challenging due to its irregular structure and 3D geometry. In this study, we propose a novel framework for detection of points on the boundaries of a LIDAR object or a LIDAR scene. Our approach is enlightened by the edge detection techniques in conventional vision applications and it is based on graph signal filtering which is a rising field of signal processing for irregular structured data types. Due to the convenient use of graph signal processing on unstructured LIDAR point clouds, we accomplish to detect the edge points directly on 3D data using a graph structure which is constructed exclusively to answer the needs of the application. Moreover, considering the elevation data as the graph signal, we leverage aerial characteristic of the airborne LIDAR data. Our proposed method can be employed both for discovering the jump edges on a segmentation problem and for exploring the crease edges on a LIDAR object on a reconstruction/modeling problem by only adjusting the filter characteristics. Therefore, it is much more practical than calculating surface normals or other geometric primitives for each point on the dataset.

10429-13, Session 3

The vertical correction of point cloud strips performed over the coastal zone of changing sea level

Ewa Gasinska-Kolyszko, Kazimierz Furmanczyk, Univ. of Szczecin (Poland)

The main principle of LIDAR is to measure the accurate time of the laser pulses sent from the system to the target surface. In the operation, laser pulses gradually scan the water surface and in combination with aircraft speed they should perform almost simultaneous soundings of each strip. Vectors sent from aircraft to the Sea are linked to the position of the aircraft. Coordinates of the points - X, Y, Z, are calculated at the time of each measurement .

LIDAR crosses the surface of the sea while other impulses pass through the water column and, depending on the depth of the water, reflect from the seabed. Optical receiver on board of the aircraft detects pulse reflections from the seabed and sea surface.

On the tidal water basins lidar strips must be adjusted by the changes in sea level. The operation should be reduced to a few hours during low water level. Typically, a surface of 20 to 30 km2 should be covered in an hour . The Baltic Sea is an inland sea, and the surveyed area is located in its South - western part, where meteorological and hydrological conditions affect the sea level changes in a short period of time.

A lidar measurement of sea surface, that was done within 2 days, in the coastal zone of the Baltic Sea and the sea level measured 6 times a day at 8, 12, 16, 20, 00, 04 by a water gauge located in the port of Dziwnów (Poland) were used for this study.

On the basis of the lidar data, strips were compared with each other . Calculation of time measurement was made for each single line separately. Profiles showing the variability of sea level for each neighboring and overlapping strips were generated. Differences were calculated changes in sea level were identified and on such basis, an adjustment was possible to perform.

Microstation software and terrasolid application were used during the research. The latter allowed automatically and manual classification of the point cloud. A sea surface class was distinguished that way. Point cloud was adjusted to flight lines in terms of time and then compared and corrected.

10429-14, Session 3

Polarization lidar observations of elevated aerosol layer over a tropical rural site in India

Vishnu R., Bhavani Kumar YellaPragada, National Atmospheric Research Lab (India); James Jebaseelan Samuel, VIT University (India)

Polarization lidar observations have been carried out for the elevated aerosol layer transport over Gadanki (13.45 N, 79.17 E) during the month of April 2009. The layer occurrence, height distributions and transport processes have been investigated. Eight clear air cases were considered for the current study. For understanding the origin of these elevated aerosol layers, NOAA-HYSPLIT trajectory analysis were carried out. It is found that the transported layer originated from the central Indian region and have depolarization ratio between 0.05 and 0.1. From the NAAPS model analysis and MODIS fire count images, it is found that the source for the aerosol layer were originated from the wild fire events at the central Indian region.

10429-15, Session PS

Atmospheric lidar co-alignment sensor: flight model electro-optical characterization campaign

Angel Luis Valverde Guijarro, Gonzalo Ramos Zapata, Tomás Belenguer-Dávila, Hugo Laguna Hernandez, INTA Instituto Nacional de Técnica Aeroespacial (Spain)

Due to the difficulty in studying the upper layer of the troposphere by using ground-based instrumentation, the conception of a space-orbit atmospheric LIDAR (ATLID) becomes necessary. ATLID born in the ESA's EarthCare Programme framework as one of its payloads, being the first instrument of this kind that will be in the Space. ATLID will provide vertical profiles of aerosols and thin clouds, separating the relative contribution of aerosol and molecular scattering to know aerosol optical depth. It operates at a wavelength of 355 nm and has a high spectral resolution receiver and depolarization channel with a vertical resolution up to 100m from ground to an altitude of 20 km and, and up to 500m from 20km to 40km. ATLID measurements will be done from a sun-synchronous orbit at 393 km altitude, and an alignment (co-alignment) sensor (CAS) is revealed as crucial due to the way in which LIDAR analyses the troposphere.

As in previous models, INTA has been in charge of part of the ATLID instrument co-alignment sensor (ATLID-CAS) electro-optical characterization campaign. CAS includes a set of optical elements to take part of the useful signal, to direct it onto the memory CCD matrix (MCCD) used for the co-alignment determination, and to focus the selected signal on the MCCD. Several tests have been carried out for a proper electro-optical characterization: CAS line of sight (LoS) determination and stability, point spread function (PSF), absolute response (AbsRes), pixel response non uniformity (PRNU), response linearity (ResLin) and spectral response. In the following lines, a resume of the flight model electro-optical characterization campaign is reported on. In fact, results concerning the protoflight model (CAS PFM) will be summarized. PFM requires flight-level characterization, so most of the previously mentioned tests must be carried out under simulated working conditions, i.e., the vacuum level (around 10-5 mbar) and temperature range (between 50ºC and -30ºC) that are expected during ATLID Space operation.

10429-16, Session PS

Space-based lidar for monitoring the Martian canyons

Alexsandr S. Grishkanich, Leonid Smirnov, ITMO Univ. (Russian Federation); Dmitry N. Redka, Saint Petersburg Electrotechnical Univ. "LETI" (Russian Federation)

With the passage of time and advancement of technology and technology exploration of Mars has become more detailed We present the substance indicators, which are the main constituents of the aqueous suspension found on the surface of Mars. According to studies selected for the study of the spectrum of substances. Choose a method of remote sensing surface. Selected scheme of the lidar.

10429-17, Session PS

Research on the temporal and spatial distribution characteristics of ozone based on differential absorption lidar and WRF-Chem model over the Yangtze River Delta, China

Yan Xiang, Anhui Institute of Optics and Fine Mechanics (China) and Univ. of Science and Technology of China (China); Jianguo Liu, Anhui Institute of Optics and Fine Mechanics (China); Yafang Cheng, Max-Planck-Institut für Chemie (Germany) and Institute for Environmental and Climate Research (China); Tianshu Zhang, Guangqiang Fan, Yunsheng Dong, Zhenyi Chen, Anhui Institute of Optics and Fine Mechanics (China); Lihui Lv, Anhui Institute of Optics and Fine Mechanics (China) and Univ. of Science and Technology of China (China)

Surface ozone, an important secondary air pollutant, has become one of Chinese major atmospheric pollutants. In summer 2016,3 times of ozone heavy pollution appeared in 12 days in the Yangtze River Delta (YRD), one of Chinese most

developed areas, it lasting 2 to 3 days every time, the maximum concentration reaching to 550ppb, a high concentration of ozone pollution layer with vertical and horizontal transmission showing at altitude 1-2km, which has a significant impact of near-grounded ozone pollution. It has been observed simultaneously by two differential absorption lidars(DIAL). Diurnal variation in near-grounded ozone concentration of a single peak and single valley, the average minimum value is 75ppb, appearing at around 02:00 LST, and the average maximum value is 90ppb, appearing at around 12:00 LST. However, the daily ozone concentration of the upper air is not obvious. In order to obtain the temporal and spatial variation characteristics of ozone concentration in the whole YRD region and the influence of meteorological factors on ozone concentration, the WRF-Chem model is used to simulate the pollution process. The results show that the simulation results of ozone concentration are in good agreement with the lidar monitoring values, and the correlation between 300 meters on the ground reaches 0.8. The meteorological elements play an important role in the change of ozone concentration. Strong solar radiation, high temperature and low relative humidity are favorable environmental conditions for ozone pollution, while high wind speed has a diffusion effect on ground ozone, and rainfall has a good effect on ozone removal.

10429-18, Session PS

Data processing technique for the all-fiber wind profiler

Gleb Petrov, International Aeronavigation Systems Concern (Russian Federation); Nikolay A. Baranov, Dorodnicyn Computing Ctr. (Russian Federation)

It's considers the data processing for a wind lidar profilometer based on a continuous laser source. This lidar allows to solve the task of wind profile restoration up to 300 m altitude.

One of the main problem of such lidar is the necessity of local oscillator in optic scheme. The local oscillator (acousto-optic modulator - AOM) makes task of determination low speed wind enough hard. Also, it makes additional noise to the signal processing tract. At the other hand, AOM is needed to solve the problem of wind direction sign determination.

In [1], the lidar architecture based on the quadrature reception of signals is described. This scheme makes it possible to build an optical scheme without a local oscillator. In this case, an element of the phase shift for the reference optical signal is needed in the optical scheme. A fiber optic element is used to form a phase shift of a quarter wavelength.

The backscattered radiation enters the optical hybrid receiver. At the output there are two pairs of optical signals for connection to two balanced photodetectors. Let's introduce the following notations for optical signals: S_b – reference signal without phase shift; S_bs – reference signal with a phase shift of a quarter wavelength; D – backscattered signal.

Photodetectors receive two mixtures of signals: S_b+D, S_bs+D. At the outputs, electrical signals are formed: E_b and E_bs.

The disadvantage of the above described model without a local oscillator is two separate computational modules FFT: F_b=FFT(E_b) and F_bs=FFT(E_bs). Spectra F_b and F_bs are used for calculation of cross-spectra C1 and C2: C1=Im(F_b)?Re(F_bs), C2= Im(F_bs)?Re(F_b). Cross-spectra include information about wind direction sign.

This study shows the joint processing of E_b and E_bs in one FFT module, which reduces the computational complexity and improves the energy efficiency due to joint processing of correlated signals. So, it's necessary to generate a complex signal for FFT: F_c=FFT(E_b+ i?E_bs)

A characteristic feature of the resultant spectrum F_c is the asymmetry with respect to the maximum detected frequency. According to the our results, it can be seen that the amplitudes of the power spectrum are being added and, consequently, the signal-to-noise ratio is increasing when determining the Doppler frequency.

This spectrum makes it possible to determine both the positive and negative Doppler shift. Described technique:

- simplifies the scheme of signal processing;
- facilitates the search for Doppler frequency;
- reduces computing requirements.

10429-19, Session PS

Observations of aerosol characteristics by mobile vehicle lidar in summer 2016 in central plains of China

Lihui Lv, Wenqing Liu, Tianshu Zhang, Zhenyi Chen, Yunsheng Dong, Guangqiang Fan, Yan Xiang, Yang Liu, Fengcheng Wu, Anhui Institute of Optics and Fine Mechanics (China)

Observations of aerosol based on a mobile vehicle lidar were performed in Shangqiu, Central Plains of China in July 2016. Spatial and temporal distributions of aerosol in this area were obtained and sources were determined with the observations using mobile vehicle lidar. Results showed that the particles mainly gathered below 1.5 km near the ground, the depolarization ratio was relatively small, and the area was polluted mainly by fine particles. In spatial distribution, the aerosol extinction coefficient in the north was higher than that in the south. In the temporal distribution, diurnal change of aerosol extinction coefficient had a dropping trend in the daytime and a rising trend at night, which accorded with the daily change of atmospheric boundary layer height. By investigating the variations of aerosol extinction coefficient before and after traffic restrictions policy, it was found that the traffic emission was considered to be the one of the main sources of pollution in the northeast of the area. The traffic emission on national roads in northern and eastern Shangqiu would contribute to haze formation in the center of the city under easterly wind. In addition, the adverse meteorological conditions of small wind speed and high relative humidity were also the cause of haze formulation in summer. Thus, more attention should be paid to reduce local emission on the upwind, especially in poor diffusion conditions.

10429-20, Session PS

Enhanced air pollution associated with wind in northern China

Zhenyi Chen, Hefei Institutes of Physical Science (China); Tianshu Zhang, Yunsheng Dong, Guangqiang Fan, Lihui Lv, Yang Liu, Yan Xiang, Xiaowen Shu, Anhui Institute of Optics and Fine Mechanics (China)

We present Mie lidars observations in three cities in north China and obtained the formation processes of an pollution episode. The evolution of particle extinction coefficients and boundary layer heights in Beijing (BJ), Yongledian (YLD) and Tangshan (TS) along the southern transportation pathway are measured and then the particle transportation flux from/to Beijing during this period can be obtained. From December 17, BJ, YLD and TS experienced this severe pollution nearly at the same time. The average values of particle extinction coefficients for particles in BJ,YLD and TS cities were 0.78 km-1, 0.82 km-1, and 0.89 km-1, respectively , indicating that the short-distance regional transport indeed exists in the southeast direction. The mean value of depolarized ratio in TS was 0.12 ,which suggests that there existed predominant amounts of fine particles in this pollution. The boundary layer height sharply decreased and reached the lowest value of 175m in TS. Then the boundary layers in this three cities were stable at the height of roughly 0.2 km . Furthermore,the typical weather conditions during this episode were stable high pressure system, sustained southwest wind, and shallow inversion layer near the surface. Therefore it was difficult for pollutants to diffuse.The four-day back trajectories from a HYSPLIT model indicate that the air masses

in the lower boundary layer were mostly advected from the densely populated south regions of China.

10429-21, Session PS

Recovery of wind field characteristics by lidar data

Gleb Petrov, JSC "International Aeronavigation Systems Concern" (IANS) (Russian Federation); Nikolay A. Baranov, Dorodnicyn Computing Ctr. (Russian Federation); Ilia Shiriaev, JSC "International Aeronavigation Systems Concern" (IANS) (Russian Federation)

In this paper, the wind field model is based on the hypothesis of uncorrelated linear variable for each horizontal coordinate of the wind speed horizontal component variability. The wind speed vertical component is assumed spatially uniform throughout the volume of measurement at each height. The wind speed gradients for the directions can be set.

Let us set:

u_0, v_0 – wind speed horizontal component spatially averaged over the measurement volume at a fixed height values of the

u_x – gradient alteration of the u – wind speed component along the axis x,

u_y- gradient alteration of the u – wind speed component along the axis y,

v_x- gradient alteration of the v – wind speed component along the axis x,

v_y- gradient alteration of the v – wind speed component along the axis y.

The usage of a gradient wind field model allows to obtain additional wind characteristics that determine horizontal wind shear at each height.

Linear coordinates are functions of the azimuthal measurements direction angle. It provides a linear system of equations for determining the unknown parameters of the wind field, but the system is inconsistent.

Consider the possibility of function bell shaped.

The values of the azimuthal angle range from $-\varpi$ to ϖ radians. The normalization index must provide a single value of the f_x function in 0 radians point and f_y function when the azimuth angle of $\varpi/2$ radians. In addition, the values of bell shaped functions should fall to 0 within the range of the azimuth angle change. When normalization index is close to the 1, the listed conditions are satisfied.

So, the result system to solve has seven parameters.

For the exact restoration of the seven parameters of the numerical simulation model it is not enough to have a connection of the radial projection from the azimuthal angle. Solving the wind field parameters restoration problem by an available set of the wind speed radial projections, the solutions of the optimization problem is linearly independent on (u_0,v_0) and (u_x,u_y,v_x,v_y) parameters. The model, includes an additional optimization parameter - w, which does not have any function of the azimuth angle. Thus, the determination of the wind speed vertical component in the recovery issue, considering the spatial inhomogeneity is possible only with the introduction of additional modulation for the vertical component of the wind speed. This modulation is possible by changing the scan beam angle of elevation.

From the mathematical modeling, and taking into account the impact of noise, it implies that the value of the elevation angle should be 20 and 40 degrees from the vertical direction, and the azimuthal direction should be evenly spaced in a circle scan. The number of fixed positions azimuth angle is 10-15. Such scanning order will ensure the scan data processing, considering the spatial distribution of the wind field, and in addition, will not lead to a decrease in the wind speed and direction results calculation updating frequency on the output of the algorithm.

10429-22, Session PS

The vertical profiles and comparison of ozone observed by differential absorption lidar and captive balloon in Shanghai, 2016

Fan Guangqiang, Tianshu Zhang, Anhui Institute of Optics and Fine Mechanics (China); Dongfang Wang, Shanghai Environmental Monitoring Ctr. (China); Wenqing Liu, Jianguo Liu, Yibin Fu, Yunsheng Dong, Anhui Institute of Optics and Fine Mechanics (China)

The differential absorption lidar is an advanced instrument for monitoring atmospheric ozone profile. A new coaxial differential absorption lidar was developed. The accuracy of measurement system is discussed and analyzed. The lidar system and ultraviolet fluorescence ozone analyzer placed in captive balloon undertook experiment at the same time, at May in Shanghai.The experiment results show that tropospheric ozone profiles derived from lidar and ozonesonde have good consistency, suggesting that result derived from lidar was reliability. A ozone pollution process was discussed combing with meteorological data.

Conference 10430: High-Performance Computing in Geoscience and Remote Sensing

SPIE. REMOTE SENSING

Tuesday 12–12 September 2017

Part of Proceedings of SPIE Vol. 10430 High-Performance Computing in Geoscience and Remote Sensing VII

10430-1, Session 1

On the use of Jetson TX1 board for parallel hyperspectral compressive sensing

José M. P. Nascimento, Gabriel Martin, Instituto de Telecomunicações (Portugal)

Hyperspectral imaging instruments allow data collection in hundreds or even thousands of spectral bands (at different wavelength channels) for the same area on the surface of the Earth. The resulting multidimensional data cube typically comprises several GBs per flight. Due to the extremely large volumes of data collected by imaging spectrometers, hyperspectral data compression, dimensionality reduction and Compressive Sensing (CS) techniques has received considerable interest in recent years. These data are usually acquired by a satellite or an airbone instrument and sent to a ground station on Earth for subsequent processing. Usually the bandwidth connection between the satellite/airborne platform and the ground station is reduced, which limits the amount of data that can be transmitted. As a result, there is a clear need for (either lossless or lossy) hyperspectral data compression techniques that can be applied on-board the imaging instrument.

Typical compression and dimensionality reduction techniques include complex algorithms that are characterized for recovering the signal from a low number of linear measurements thereof. This reduces the amount of data that needs to be measured, transmitted and stored in first place. The CS paradigm is based on performing random projections over the signal of interest and the bulk of the processing to reconstruct the original image is performed on the Earth station, where plenty of computing and storage resources are available compared with the scare resources available onboard.

Due to the fact that hyperspectral images are focused on increasing the spectral resolution rather than the spatial, typically they are more compressible in the spectral domain than the spatial domain. Thus we are able to reconstruct the original hyperspectral image from a low number of random projections in the spectral domain. This is only possible if the spectral vectors live in a low dimensional subspace.

In recent years, graphics processing units (GPUs) have evolved into highly parallel and programmable systems. However one of the main problems for the use of this hardware onboard is the high power and energy consumption that they require. Remote sensing missions are frequently performed onboard airborne devices and satellites, which may impose severe constraints on the power and energy consumption.

In this paper, a parallel implementation for a spectral compressive acquisition method on a Jetson TX1 platform is evaluated, both in terms of computational performance and energy consumption. In this paper we focus on the coder-side of the method because it is the one to be performed onboard, while the decoder side may be performed on Earth station where plenty of hardware may be available. In this implementation, the measurement process is carried out with Gaussian i.i.d. matrices of double precision.

The Jetson TX1 used in the experiments is a low power consumption platform that works with a maximum power of 15W with a voltage input of 5.5V-19.6V DC. It incorporates a Nvidia Maxwell GPU with 256 NVIDIA CUDA cores, a quad-core ARM cortex-A57 MPCore processor, 4GB LPDDR4 memory and 16GB eMMC 5.1 flash storage.

Our study, based on a hyperspectral image of total size of $600 times 512$ pixels (275 MB), reveals that the implementation of the proposed method using the Jetson TX1 board has promising results what concerns with real-time response under onboard energy constraints. In the future, it would be also possible to perform the coding process with single precision, or with Rademacher or Bernoulli matrices which may speedup the measurement process due to the fact that it would be possible to work with integers operations instead of with floating point operations.

10430-2, Session 1

Low-complexity multiple collaborative representations for hyperspectral image classification

Yan Xu, Qian Du, Mississippi State Univ. (United States); Wei Li, Beijing Univ. of Chemical Technology (China); Nicolas Younan, Mississippi State Univ. (United States)

Collaborative representation has been a popular classifier for hyperspectral image classification because it can offer excellent classification accuracy with a closed-form solution. Collaborative representation can be implemented using a dictionary with training samples of all classes, or using class-specific sub-dictionaries. In either case, a testing pixel is assigned to the class whose training samples offer the minimum representation residual. The Collaborative Representation Optimized Classifier (CROC) was developed to combine these two types of collaborative representations to achieve the balance for optimized performance. The class-specific collaborative representation involves inverse operation of matrices constructed from class-specific samples, and the all-class version requires inversion operation of the matrix constructed from all samples. In this paper, we propose a low-complexity CROC to avoid redundant operations in all-class and class-specific collaborative representations. It can further reduce the computational cost of CROC while maintaining its excellent classification performance.

10430-3, Session 1

Real-time implementation of digital stabilization for high-resolution Earth observation imaging

Carole Thiebaut, Sophie Petit, Jean-Marc Delvit, Christophe Latry, Ctr. National d'Études Spatiales (France); Emma Bousquet, Magellium (France); Guillaume Laurent, Ctr. National d'Études Spatiales (France)

In order to increase Signal to Noise Ratio of very high resolution Earth observation satellites images, Time Delay Integration (TDI) sensors are usually used. A TDI device synchronizes the electronic charge transfer with the satellite speed to virtually increase exposure time and thus signal to noise ratio. In this paper, we present an on-board satellite implementation of multiframe registration to improve classical TDI performances. With current TDI, only a limited number of lines can be summed up because of the lack of high frequencies satellite stability which could induce motion blurring on the final image. A solution to no longer constrain the number of lines to be accumulated would be to compute, in real-time, the shift between each line and resample them before summation. For example, a hundred lines TDI could be reached by registering and adding 10 images of sub-TDI of 10 lines each, each sub-TDI having a classical behavior. This real-time processing has to be done on-board at the frequency of each sub-TDI line of the final image. A sensor dedicated to shift measurements would be added in the focal plane: the motion sensor. This sensor would see the same landscape possibly with a lower resolution but at a higher frequency than the principal mission's integration time. Then a fast real-

time algorithm will compute shift between two consecutives images delivered by the motion sensor. In [1], a gradient-based (optical flows) algorithm for shifts estimation between images delivered by the motion sensor has been studied. The proposed algorithm has low complexity in comparison with classical correlation methods which is a significant advantage for being used on-board a satellite at high instrument data rate and in real-time. In [2], a hardware implementation of the same algorithm studied by CNES in another application case is presented. The implemented version of the algorithm uses only two iterations to reach the final shift measurement with image resampling between two iterations and gives good results in terms of shift estimation. The optimization study of the motion sensor and the performances oh the gradient-based algorithm on these images will be presented. Then, computed shifts are used to resample images delivered by sub-TDI devices. Resampled images of each sub-TDI are summed up to obtain the final image. Optimization trade-off study between resampling performances and implementation complexity will also be presented. This paper shows that, in our case, SNR is improved while image sharpness is preserved. An on-ground demonstrator of the presented chain is currently operated in CNES. A dedicated sensor as well as the gradient-based algorithm and the resampling one are under development on representative spatial hardware components.

[1] “A tight multiframe registration problem with application to Earth observation satellite design”, M. Rais, C. Thiebaut, J.M. Delvit, J.M. Morel, in Proc. of IEEE International Conference on Imaging Systems and Techniques, 2014.

[2] “Fast gradient-based algorithm on extended landscapes for wave-front reconstruction of Earth observation satellite”, C. Thiebaut, L. Perraud, J.M. Delvit, C. Latry, in Proc. SPIE 9909, Adaptive Optics Systems V, 99096V, July 27, 2016.

10430-4, Session 1

Deducing scheme for atmosphere information with optical observations of Aurora spectral images

Wanqiu Kong, Jiaji Wu, Tao Wu, Xidian Univ. (China); Gwanggil Jeon, Incheon National Univ. (Korea, Republic of)

When the electron plasma is blown from the solar wind and enters into the earth atmosphere, a large number of neutral particles are excited to cause the significant event called aurora phenomenon. In this process, there are several sources of excitation including electron impact, dissociative recombination, thermal electron excitation. Primary electrons directly cause ionization and dissociation of neutral concentrations and produce a large amount of excited atoms and ions. This process further leads to multiple physics and chemical reactions radiate lights. The emission features radiated from the electron collisions relate to each other with the total flux of the specific electrons.

Aurora imagery is a helpful technique to explore ionospheric reactions. Since the first rocket-placed detector was fired to measure the visible aurora spectrum, this kind of measurements has been performed for almost half a century. Although the emissions observed on the ground accounts for few of the deposited energy in the atmosphere, the rocket and satellite based spectroscopy has too high acquisition cost to be widespread available. Based on the ground observations of aurora spectral images, the emission characteristics reveal the primary electron energy and flux, the basic atmosphere of species concentration and electron temperature, abundant information of the deposited particles. The power of ground-based imagery still lies in the fact that it implicitly gives rich information about the atmosphere condition and the characteristics of the incident primary electron.

The calculations of the primary electron and secondary electron energy distribution are independent based on the excitation theory. Particularly, the oxygen significant spectral lines, green line at 5577 ? and multiplet at 6300/6364 ?, both are originated from the secondary electron impact. As a matter of fact, auroral radiation attenuates along with its transmission through the atmosphere. Hence, the spectral images actually represent the attenuated radiation information. An inverse transform to compensate such reduction is required. In this paper,

In this paper, auroral optical radiation produced by electron impact on oxygen atoms is investigated to explore the relationship between secondary electron energy and spectroscopic emission features. With the consideration that the radiations of atomic oxygen 5577 ? and 6300 ? are representative spectral lines in aurora, we designed a scheme to determine the radiation feature at other spectral bands by using the emission rate ratios of 5577/6300. And the according numerical results are represented with approximated curves varies with the secondary electron energy, which uses atmospheric radiation attenuation to deduce the real-time total flux of bombarding electrons in the atmosphere corresponding to each ground-based image’s hiding radiation condition.

10430-5, Session 1

The implementation of aerial object recognition algorithm based on contour descriptor in FPGA-based on-board vision system

Valery V. Strotov, Pavel V. Babayan, Sergey A. Smirnov, Ryazan State Radio Engineering Univ. (Russian Federation)

The object recognition is one of most complicated tasks that can be solved using image processing. In this work we understand the aerial object recognition as a determination of object type. The set of aerial object types includes various kinds of airplanes, UAVs and helicopters.

The algorithm implementation in real time aerial object recognition systems is the most significant part of this task. It allows solving the wide range of the complex problems including real time air traffic control, emergency search and rescue, aircraft collision avoidance etc.

The common approaches for recognition task solving are the descriptor based approaches and convolution neural networks. The descriptor based approaches include a number of object description techniques based on features (SURF, ORB), Fourier descriptors, Hough moments etc. All these approaches are invariant to object image shift and rotation. However, the most of the listed approaches have some significant problems. The algorithms based on Fourier descriptors and Hough moments are computationally complicated for FPGA based systems. The neural networks require larger FPGA chips. Instead, contour descriptor based algorithm is less computationally complicated. It is invariant to the object shift, rotation and scaling, insensitive to the additive noise and precise enough. Thereby, the algorithm, based on contour description calculation is most suitable for object recognition in real time image processing systems.

The proposed orientation estimation algorithm consists of 2 stages: learning and recognition. Learning stage is devoted to the exploring of studied objects. Using 3D model of the reference objects we can collect the set of training images by capturing 3D model from viewpoints evenly distributed on a sphere. Sphere points distribution is made by the geosphere principle. It minimizes the training image set. Gathered image database is used for calculating the reference object contour descriptors, which will be used in the recognition stage of the algorithm. The object contour can be produced using various border extraction techniques, active contour method etc. The learning stage includes the most computationally complicated operations and processed preliminary.

The recognition stage is focusing on matching process between an observed image descriptor and the reference image descriptors. FFT-based matching approach is used here to obtain real-time performance. The contour descriptor of the object is shifted cyclically to archive the rotation invariance. The result of the matching produces the measure of the

difference between the captured object and the n-th reference object from the database. The object recognition is processed by minimization of this measure. The recognition stage includes the limited number of the operation and can be processed in the real time image processed systems.

The hardware implementation of this algorithm is divided into two parts. The learning is performing on PC. The estimation is performing on-board using the result object descriptor set loaded to on-board computation system memory. The on-board system model was designed on Virtex 7 evaluation kit.

The proposed algorithm was modeled using Matlab. The experimental examinations of the algorithm were performed. We use a number of natural and synthesized videos to determine the algorithm performance. The reference database includes various kinds of airplanes, helicopters and UAVs. The examination result shows that the proposed algorithm reaches the relatively high precision and insensitive to the additive noise.

10430-10, Session 1

Convolutional generative adversarial networks for hyperspectral image analysis

Mercedes Eugenia Paoletti Ávila, Juan Mario Haut, Javier Plaza, Antonio Plaza, Univ. de Extremadura (Spain)

Artificial neural networks (ANNs) have been intensively used the analysis of remotely sensed imagery mainly due to to their success in the fields of pattern recognition [1], [2]. Since the 90s, ANNs have attracted the attention of a large number of researchers, particularly in the area of hyperspectral image classification and analysis [3], [4].

Hyperspectral images are composed by hundreds of contiguous spectral bands [5], creating a huge three-dimensional data cube which comprises an extensive observation area. The processing and classification of these images is very useful in fields such as monitoring and management of the environment, agriculture or security and defense issues.

Convolutional neural networks (CNNs) have been used for the processing of this type of images [6], [7], [8] due to their effectiveness in areas such as image recognition and classification of large datasets composed by two-dimensional images. However, the special computing and storage requirements of hyperspectral images, coupled with the limited availability of labeled training samples, complicate their exploitation in supervised and semi-supervised classification scenarios.

One of the most common problems in this context is overfitting, which results from the complexity of the CNN model which involves a large number of parameters that must be learned, what is also aggravated by the limited availability of labeled training samples. This causes a remarkable loss of precision in such networks, which usually lead to poor predictive performance. To address this issue, several techniques have been developed to reduce the negative impact of overfitting. Strategies include data normalization, dropout methods and synthetic pixel generation.

In this paper, we discuss the use of deep convolutional generative adversarial networks (DCGANs) [9], [10] for the generation of additional (virtual or unlabeled) training samples, and thus alleviate the negative issues introduced by the limited availability of labeled training samples and overfitting. Specifically, we use DCGANs to generate additional (unlabeled) samples, thus improving the predictive performance of the network and reducing the overfitting problem [11].

REFERENCES

[1] Christopher M Bishop. Neural Networks for Pattern Recognition. Clarendon Press, 1995.

[2] P. M. Atkinson and A. R. L. Tatnall. Introduction Neural networks in remote sensing. International Journal of Remote Sensing, 18(4):699–709, 1997.

[3] J. A. Benediktsson, P. H Swain, and O. K. Ersoy. Conjugate gradient neural networks in classification of very high dimensional remote sensing data. International Journal of Remote Sensing, 14(15):2883–2903, 1993.

[4] H. Yang. A back-propagation neural network for mineralogical mapping from AVIRIS data. International Journal of Remote Sensing, 20(1):97–110, 1999.

[5] Chein-I Chang. Hyperspectral Imaging: Techniques for Spectral Detection and Classification. Springer US, 2003.

[6] Liangpei Zhang, Lefei Zhang, and Bo Du. Deep Learning for Remote Sensing Data Advances in Machine Learning for Remote Sensing and Geosciences. IEEE Geoscience and Remote Sensing Magazine, 4(2):22–40, 2016.

[7] Wei Hu, Yangyu Huang, Li Wei, Fan Zhang, and Hengchao Li. Deep convolutional neural networks for hyperspectral image classification. Journal of Sensors, 2015.

[8] Yushi Chen, Hanlu Jiang, Chunyang Li, Xiuping Jia, and Pedram Ghamisi. Deep Feature Extraction and Classification of Hyperspectral Images Based on Convolutional Neural Networks. IEEE Transactions on Geoscience and Remote Sensing, 54(10):6232–6251, 2016.

[9] Alec Radford, Luke Metz, and Soumith Chintala. Unsupervised representation learning with deep convolutional generative adversarial networks. CoRR, abs/1511.06434, 2015.

[10] Ian J Goodfellow, Jean Pouget-Abadie, Mehdi Mirza, Bing Xu, David Warde-Farley, Sherjil Ozair, Aaron Courville, and Yoshua Bengio. Generative Adversarial Nets. In Z. Ghahramani and M. Welling and C. Cortes and N. D. Lawrence and K. Q. Weinberger, editor, Advances in Neural Information Processing Systems, volume 27, pages 2672–2680. Curran Associates, Inc., 2014.

[11] Shiqi Yu, Sen Jia, and Chunyan Xu. Convolutional neural networks for hyperspectral image classification. Neurocomputing, 219:88–98, 1 2017.

10430-9, Session 3

Spectral matching-based mineral mapping in Hyperion images to estimate the grades of iron ore, limestone and magnesite deposits of India

Sanjeevi Shanmugam, Padma Srinivasa Perumal, Anna Univ., Chennai (India)

The aim of using hyperspectral data for mineral exploration is its potential in depicting typical absorption features of the minerals at specific wavelengths along the Visible/Near Infrared (VNIR) and Shortwave Infrared (SWIR) regions. The EO-1 Hyperion with contiguous 242 spectral bands in the range of 400 to 2500 nm confirmed the efficiency of hyperspectral images in mineral mapping. With the advent of such hyperspectral datasets, it has been observed that certain minerals like iron ore (at 865 nm), carbonates (at 2350 nm) and clays (at 2200 nm) can be identified and mapped at large scale. However, accurate grade-wise categorization of such deposits carried out by traditional classification and multispectral images does not yield acceptable results.

Use of appropriate spectral matching approaches, followed by classification using the inputs of spectral matching can give better results. This paper proposes a novel mineral mapping approach based on spectral matching algorithms namely (Jeffries-Matusita (JM) distance, Spectral Angle Mapper (SAM), Spectral Correlation Mapper (SCM), combined JM-SAM and JM-SCM). The spectral matching approaches are applied to the EO-1 Hyperion images of three mining sites in India (magnesite in Chalk Hills of Salem, South India; limestone in Vriddhachalam, South India; iron ore in Noamundi mines, Eastern India). The reference spectra of pure magnesite, limestone and iron ore are extracted from the Hyperion image itself after the application of a detailed radiometric correction. The discriminatory ability of the JM-SAM matching approach is evaluated using the performance measures of relative spectral discriminatory probability (RSDPB) and relative spectral discriminatory

entropy (RSDE). This matching process is extended to the classification framework, wherein the spectra of each target pixel in the image is matched with the image derived reference spectra compiled in a spectral library. Based on the degree of match (or mismatch), a map indicating grade-wise categorization of the ores is obtained. Accuracy assessments compared the matching-based classification results with the minimum distance based classifier. Validation was done by comparing with the ground data obtained from various locations in all the three mining sites. Further, the mineral maps are evaluated by computing SMI (Spectral Matching Index), a parameter that indicates the relationship between false alarms and detection rate yielded by each spectral matching algorithm during mapping. Thus, this study shows that spectral matching based approach is a rapid and reliable tool for grade-wise categorization of minerals and ores using Hyperion images. From the results, it could be inferred that SCM identifies the linear relationship between the target and unknown spectral vectors thereby detecting the linear shape, while JM computes the band-wise spectral information between the two vectors. Besides, this study evaluates the effectiveness of deterministic and stochastic matching approaches in identifying the spectral characteristics of minerals for precise mapping.

10430-12, Session 3

Spaceborne synthetic aperture radar signal processing using FPGAs

Yohei Sugimoto, Satoru Ozawa, Noriyasu Inaba, Japan Aerospace Exploration Agency (Japan)

SAR data consists of a bundle of successive radar echoes (i.e., received signal records) from distributed back-scattering objects on the ground and looks like a sandstorm image on TV. SAR imagery therefore requires image formation through signal processing of the data before browsing images and acquiring information from them. It is hard to distinguish which part of the received signal data includes valuable information before image formation.

For the conventional spaceborne SAR systems such as ALOS-2/PALSAR-2, the received signal records are stored in an onboard data storage. The signal records stay there and wait for transmission until network connection becomes online, or unless real-time transmission is available although only a handful of them may conceal meaningful information.

Conventionally, not only signal data compression techniques (e.g., DS-BAQ) are applied to reduce the transmission data volume but also the operation duty and the operation modes for global observations are limited. For example, the operation duty of PALSAR-2 is about 50% per revolution and the 3m resolution imagery is mostly planned for domestic land observations whereas global areas are observed with the 10m and 100m resolution modes unless otherwise demanded.

With such efforts, the storage usage and the volume of transmittable data through both ground-based and space-based communication networks are balanced. This balance strongly relies on the transmission network availability and easily fails when the network systems are busy or shut down unexpectedly. The observation operations of the present spaceborne SAR systems are rigorously planned by simulating the balance, given multiple user demands under the basic observation scenario. The operation planning has been therefore a pain in the neck for spaceborne SAR remote sensing because the multiple user demands are often conflicting, resulting in compromised operations and the potential of the present spaceborne SAR systems.

This problem should be solved such that we do not have to compromise the operations and the potential of the next-generation spaceborne SAR systems. One of the solutions is to further compress the SAR data through onboard signal processing and information extraction from images. This is also beneficial for event-driven observations and fast delivery of information products.

JAXA is developing evaluation models of FPGA-based signal processing system for onboard SAR image formation. Multiple FPGAs are used to achieve near real-time processing that will be the second most important factor for onboard signal processing of the SAR data after the data reduction.

The evaluation model developed in 2016 can process a 10m resolution single look complex image from ALOS/PALSAR data. The hardware consists of four Xilinx's FPGAs. Hardware architecture that performs the Range-Doppler algorithm is designed and coded in VHDL and implemented on the FPGAs.

The processing speed of the present model resulted in promising. Single image formation of PALSAR will complete in 20 seconds even if the clock speed limited to 100MHz that is equal to the clock speed of Xilinx's space grade FPGA such as Virtex-5QV. The image processed by the model is in no way inferior to the image processed with single precision computing in MATLAB.

10430-13, Session 3

Parallel exploitation of a spatial-spectral classification approach for hyperspectral images on RVC-CAL

Raquel Lazcano López, Daniel Madroñal Quintín, Univ. Politécnica de Madrid (Spain); Himar Fabelo Gómez, Samuel Ortega, Univ. de Las Palmas de Gran Canaria (Spain); Ruben Salvador, Univ. Politécnica de Madrid (Spain); Gustavo M. Callicó, Univ. de Las Palmas de Gran Canaria (Spain); Eduardo Juárez Martínez, César Sanz Álvaro, Univ. Politécnica de Madrid (Spain)

Hyperspectral Imaging (HI) assembles high resolution spectral information from hundreds of narrow bands across the electromagnetic spectrum, thus generating 3D data cubes in which each pixel gathers the spectral information of the reflectance of every spatial pixel. As a result, each image is composed of large volumes of data, which turns its processing into a challenge, as performance requirements have been continuously tightened. For instance, new HI applications demand real-time responses. Hence, parallel processing becomes a necessity to achieve this requirement, so the intrinsic parallelism of the processing algorithms must be exploited.

In this paper, a spatial-spectral classification approach has been implemented using a dataflow language known as RVC-CAL. This language represents a system as a set of functional units, and its main advantage is that it simplifies the parallelization process by mapping the different blocks over different processing units. The spatial-spectral classification approach aims at refining the classification results previously obtained by using a K-Nearest Neighbors (KNN) filtering process, in which both the pixel spectral value and the spatial coordinates are considered. To do so, KNN needs two inputs: a one-band representation of the hyperspectral image and the classification results provided by a pixel-wise classifier. Thus, this algorithm is divided into three different stages: a Principal Component Analysis (PCA) algorithm for computing the one-band representation of the image, a Support Vector Machine (SVM) classifier, and the KNN-based filtering algorithm itself.

The parallelization of these algorithms shows promising results in terms of computational time, as the mapping of them over different cores presents an important speedup. Consequently, experimental results demonstrate that real-time processing of hyperspectral images is achievable.

The paper is structured as follows. Section 1 introduces the motivation and the main objectives of this work. After that, Section II describes the state of the art of the related technologies, i.e., spatial-spectral algorithms and dataflow languages. Once the theoretical bases have been described, Section III addresses the implementation of the three algorithms composing the spatial-spectral classification approach. The obtained results have been tested in terms of accuracy and processing time, and they are analyzed and compared to those obtained in a sequential version in Section IV. These results are first compared individually –i.e., algorithm by algorithm– and as a spatial-spectral classifier as a whole. To finish the system analysis, some conclusions related with

algorithm behavior, time processing and system performance are drawn. Finally, the paper concludes with some future research lines related with the implementation of this algorithm on a high-performance embedded system, such as the Massively Parallel Processor Array (MPPA) multicore platform developed by Kalray.

10430-14, Session 3

Technology for organization of the onboard system for processing and storage of ERS data for ultrasmall spacecraft

Valery V. Strotov, Alexander I. Taganov, Aleksandr N. Kolesenkov, Yuriy V. Konkin, Ryazan State Radio Engineering Univ. (Russian Federation)

There is a trend to develop swarm groups of ultra-small spacecraft (USS) in the area of Earth remote sensing (ERS) that led to a necessity to miniaturize computers and USS software without damage of their functional qualities. Task of processing and analysis of obtained ERS data on USS board is actual taking into consideration significant expenditures of energy for data transfer and low productivity of computers. Thereby, there is an issue of effective and reliable storage of the general information flow obtained from onboard systems of information collection, including ERS data, into a specialized data base (DB).

The paper has considered peculiarities of database management system (DBMS) operation with the multilevel memory structure. Analysis of above mentioned methods of access have shown that the method of the binary aligned tree for access by the primary, unique or external key better corresponds to task terms. For storage of data in DB the format has been developed that describes a DB physical structure which contains required parameters for information loading. Such structure allows reducing a memory size occupied by DB because it is not necessary to store values of keys separately.

Experiments of the developed USS realization have executed in language ?++ with possibility of cross-platform transfer of the executable code. Data changed within operation are stored in the random-access memory and, if necessary, can be copied into the nonvolatile FLASH-memory.

The paper has shown architecture of the relational DBMS oriented into embedment into the onboard USS software. DB for storage of different information, including ERS data, can be developed by means of such DBMS for its following processing. Suggested DBMS architecture has low requirements to power of the computer systems and memory resources on the USS board. Data integrity is ensured under input and change of the structured information.

10430-15, Session 3

Wavelet-based multicomponent denoising on GPU to improve the classification of hyperspectral images

Pablo Quesada-Barriuso, Dora B. Heras, Francisco Argüello, Univ. de Santiago de Compostela (Spain); J. C. Mourino, Fundacion Publica Galega Centro Tecnologico de Supercomputacion de Galicia (Spain)

Supervised classification allows handling a wide range of remote sensing hyperspectral applications. The spatial organization of the pixels over the image has proven to be beneficial for the interpretation of the image content, thus increasing the classification accuracy. Different methods are widely used to this end: segmentation, morphological profiles, attribute profiles, etc. Denoising in the spatial domain of the image has also been shown as a technique that enhances the structures in the image.

In this paper the authors propose in a multi-component noise reduction method in order to increase the classification accuracy. The method com- bines a feature extraction based on a 1D-discrete wavelet transform (DWT) applied in the spectral dimension followed by an Extended Morphological Profile (EMP) and a classifier (SVM or ELM). The multi-component noise reduction is applied to the EMP just before the classification.

The proposed noise reduction is applied to each component of the EMP. The denoising recursively applies a separable 2-D DWT after which the number of wavelet coefficients is reduced by using a threshold. Finally, inverse 2D-DWT filters are applied to reconstruct the noise free original component. The impact of the number of times that the wavelet filter is applied and of the threshold value are studied, as they determine the amount of noise removed.

The accuracy improvements obtained by this classification scheme de- pend on characteristics of the images such as their spatial resolution and on characteristics of the reference data used for the supervised classifica- tion. The computational cost of the classifiers as well as the cost of the whole classification scheme is high but it is much reduced achieving real time behavior for some applications through their computation on Nvidia GPU platforms.

10430-16, Session 3

A FPGA implementation for linearly unmixing a hyperspectral image using OpenCL

Raúl Guerra, Institute of Applied Microelectronics (Spain); Sebastián López, Roberto Sarmiento, Institute of Applied Microelectronics, Univ. de Las Palmas de Gran Canaria (Spain)

Hyperspectral imaging systems provide images in which single pixels have information from across the electromagnetic spectrum of the scene under analysis. These systems divide the spectrum into many contiguos channels, which may be even out of the visible part of the spectra. The main advantage of the hyperspectral imaging technology is that certain objects leave unique ‘fingerprints’ in the electromagnetic spectrum, known as spectral signatures, which allow to distinguish between different materials which may look like the same in a traditional RGB image. Accordingly, the most important hyperspectral imaging applications are realted with distinguishing or identifying materials in a particular scene.

In hyperspectral imaging applications under real-time constraints, the huge amount of information provided by hyperspectral images have to be rapidly processed and analysed. For such purpose, parallel hardware devices, such as Field Programmable Gate Arrays (FPGAs) are typically used. However, developing hardware applications typically requires expertise in the specific targeted device, as well as in the tools and methodologies which can be used to perform the implementation of the desired algorithms in the specific device. In this scenario, the Open Computing Language (OpenCL) emerges as a very interesting solution in which a single high-level synthesis design language can be used to efficiently develop applications in multiple and different hardware devices.

In this work, the Fast Algorithm for Linearly Unmixing Hyperspectral Images (FUN) has been implemented into a Bitware Stratix V Altera FPGA using OpenCL. The obtained resutls demonstrate the suitability of OpenCL as a viable design methodology for quickly creating efficient FPGAs designs for real-time hyperspectral imaging applications.

10430-8, Session PS

Location of High-Speed Train

Liwen Ma, Jiaji Wu, Yan Wang, Chunyuan Li, Xidian Univ. (China)

In the high-speed railway environment, users in high-speed railway network who abnormal access to the network that seriously affected the users perception of the internet. High-speed railway network users abnormal access to private network is mainly due to weak coverage of the 4G mobile network in the high-speed railway network. Currently, the best solutions rely on manual detect the state of radio remote unit of base station. This process is time-consuming and needs a lot of technical staff. In this work, we propose to use Long short-term memory model to significantly lower the work-force burden of the localization system design, while still achieving satisfactory results. Base station collect users information that including high-speed railway network users information and ordinary network users information, So we first make a model for high-speed railway network users to analyze whether the current user is a high-speed railway network user, and then detect the user's real-time location using the Long short-term memory network. In the process of modeling high-speed railway network users, analyzing the data of high-speed railway users which is collected by base stations is paramount, the base station belongs to one high-speed railway line and its location distribution is continuous, by analyzing of the data, we can obtain the base station's location and its corresponding Radio Remote Unit position, then drawing the Radio Remote Unit distribution on the map. We count the user information one by one that access to the network, and find out high-speed railway network user by the status of his/her location and its corresponding time for high-speed railway network user will pass through several base stations in a short time. LSTM is classical deformation of recurrent neural networks(RNN). LSTM is characterized by the addition of layers of the valve gate nodes outside the RNN structure. There are three types of valve gates: forget gate, input gate and the output gate. These valve gates can be opened or closed for judging whether the output of at the layer of the memory state of the model network has reached the threshold value and added to the current layer computing. LSTM is clearly designed to avoid long-term dependency issues, and remembering the information for a long time is almost their inherent behavior, so it is very suitable for high-speed railway network users' location detection. When using the LSTM model to identify the user location, for preventing over-fitting, the data set is randomly divided into training set and verification set according to the ratio of 4:1, the activation function of LSTM module is set as hyperbolic tangent function, and activation function of the fully connected artificial neural network that receive LSTM output is linear function, and using the mean square error as the error calculation method, and using the RMSprop algorithm to update the weight parameter. The multiple user sequences were input to the independent LSTM module and then combine the output results that later were input to the common layer. The results demonstrate that the method we proposed can locate the high-speed railway network user's position.

10430-11, Session PS

GPU implementation of discrete particle swarm optimization algorithm for endmember extraction from hyperspectral image

Chaoyin Yu, Zheng-Wu Yuan, Chongqing Univ. of Posts and Telecommunications (China); Yuanfeng Wu, Institute of Remote Sensing and Digital Earth (China)

Hyperspectral image unmixing is an important part of hyperspectral data analysis. The mixed pixel decomposition consists of two steps, endmember (the unique signatures of pure ground components) extraction and abundance (the proportion of each endmember in each pixel) inversion.

Many algorithms have been proposed so far, including the pure pixel index (PPI), N-FINDR and so on. Particle Swarm Optimization (PSO) was proposed for finding the global optimal solutions of optimization problems in 1995. Recently, the PSO, which was improved into a discrete particle swarm optimization (DPSO) algorithm, has been applied to accurately extract endmembers with high optimal performance. The feasible solution space of endmember extraction combinational optimization model was improved while using PSO to make the positions of particles can be defined. The velocity and velocity updating functions are specified. And by defining the particles adaptive function according to the object function of combinational optimization model, a Discrete-PSO (DPSO) method for endmember extraction was implemented.

The reasonability and effectiveness of the algorithm was verified by simulate data and real data experiments, as shown in Fig. 1, compared to the traditional methods, like VCA and N-FINDR, the RMSE value of the endmember extraction obtained by the D-PSO method is the lowest. In addition, the RMSE value is much lower; the difference from the original image is smaller. In other word, D-PSO could acquire higher extraction precision. Therefore, the D-PSO algorithm can effectively extract the endmember combination.

The D-PSO algorithm needs a large number of iterative loops which takes a lot of time. Considering the high computational amount, the DPSO endmember extraction algorithm is time-consuming for hyperspectral image analysis. As can be seen from Fig. 2, the time complexity of the D-PSO algorithm is affected by the number of particles and the number of endmembers that to be extracted. Given for the random probability of 0.2, the number of endmember should to be extracted as well as the number of the particles to be defined are the important factors in the total time affected. Besides above, according to Figure 3, another factor that affects the total time is a random probability. The larger random probability means the range of the irregular motion of the particles is also wider, which result in converging slowly and time consuming. Developing fast processing techniques for DPSO has received considerable attention, especially in analysis scenarios with real-time constraints.

The DPSO endmember extraction algorithm was first implemented with MATLAB, then accelerated by using NVIDIA Tesla K20GPU with 2496 CUDA cores. In the experiment, several key calculation nodes of the algorithm was designed in parallel (see figure 4): the update of the best fitness, the update of the optimal positions (both each particles' best position and global best position), and the update of the particles' speed and positions. Meanwhile, different combination schemes of particles were tested in the experiments. The global memory, shared memory, L1 cache, L2 cache and L3 cache were carefully designed in the proposed parallel implementation for further improving the performance of the algorithm. And real hyperspectral data collected by the Airborne Visible-Infrared Imaging Spectrometer (AVIRIS), which was built by the National Aeronautics and Space Administration (NASA)'s Jet Propulsion Laboratory, used in the experiments. Results show that the computational performance of DPSO based on GPU has significantly improved in the analysis of hyperspectral images.

10430-17, Session PS

Performance tuning Fu-Liou-Gu radiative transfer scheme on Intel Xeon Phi

Jarno Mielikainen, Bormin Huang, Univ. of Wisconsin-Madison (United States)

Next-generation mesoscale numerical weather prediction system, the Weather Research and Forecasting (WRF) model, is a designed for dual use for forecasting and research. WRF offers multiple physics options that can be combined in any way. One of the physics options is radiance computation. The major source for energy for the earth's climate is solar radiation. Thus, it is imperative to accurately model horizontal and vertical distribution of the heating. Goddard solar radiative transfer model includes the absorption duo to water vapor,ozone, ozygen, carbon dioxide, clouds and aerosols. The model computes the interactions among the absorption and scattering by clouds, aerosols, molecules and surface. Finally, fluxes are integrated over the entire longwave spectrum. Code modernization is essential for a good performance on the multicore processors and many-core coprocessors. In this paper, we present our results of optimizing the Fu–Liou–Gu radiative transfer scheme on the Intel Xeon Phi coprocessor.

10430-18, Session PS

Optimizing the rapid radiative transfer model (RRTM) radiation scheme for Intel Many Integrated Core (MIC) architecture

Jarno Mielikainen, Bormin Huang, Univ. of Wisconsin-Madison (United States)

Atmospheric radiative transfer models calculate radiative transfer of electromagnetic radiation through a planetary atmosphere. Both shortwave radiance and longwave radiance parameterizations in an atmospheric model calculate radiation fluxes and heating rates in the earth-atmospheric system. One radiative transfer model is the rapid radiative transfer model (RRTM), which calculates of longwave atmospheric radiative fluxes and heating rates. The molecular species treated in the model are water vapor, carbon dioxide, ozone, methane, nitrous oxide, and the common halocarbons. The Intel Xeon Phi coprocessor is the first product based on Intel MIC architecture, and it consists of up to 61 cores connected by a high performance on-die bidirectional interconnect. The coprocessor supports all important Intel development tools. Thus, the development environment is familiar one to a vast number of CPU developers. Since the coprocessor has more processor cores and wider vector units than a regular CPU, code modernization is imperative for a good code execution speed. Therefore, we have optimized the existing RRTM source code for modern CPUs and Xeon Phi coprocessors. The existing code was ported to Xeon Phi with a simple recompile. Furthermore, the same optimized code can be compiled for both targets. In this paper, we discuss our code optimizations, which achieved 1.9x speedup compared to the original code on both Intel Xeon CPU and Xeon Phi 7120P coprocessor.

10430-20, Session PS

Development of GNES (Geometry Normalized Electromagnetic System) instrument for metal fefect detection

Zakaria Zakaria, Syiah Kuala Univ. (Indonesia); Mohamad Zubir Mat Jafri, Univ. Sains Malaysia (Malaysia); Muhammad Syukri Surbakti, Saumi Syahreza, Syiah Kuala Univ. (Indonesia); Kok Chooi Tan, Univ. Sains Malaysia (Malaysia)

It has been already made, calibrated and tested a geometry normalized electromagnetic system (GNES) for metal defect examination. The GNES has an automatic data acquisition system which supporting the efficiency and accuracy of the measurement. The data will be displayed on the computer monitor as a graphic display then saved atomatically in the Microsoft Excel format. The transmitter will transmit the frequency pair (FP) signals i.e. 112.5 Hz and 337.5 Hz; 112.5 Hz and 1012.5 Hz; 112.5 Hz and 3037.5 Hz; 337.5 Hz and 1012.5 Hz; 337.5 Hz and 3037.5 Hz. Simultaneous transmissions of two electromagnetic waves without distortions by transmitter will induce an eddy current in the metal. This current in turn will produce secondary electromagnetic fields which are measured by the receiver together with the primary fields. Measurement of percent change of vertical component of the fields will give the percent response caused by the metal or the defect. The response examinations were performed by the models with various type of defect for the master curves. The materials of samples as a plate were using Aluminium, Brass, and Copper. The more of the defects is the more reduction of the eddy current response. The defect contrasts were tend to decrease when the more depth of the defect position. The magnitude and phase of the eddy currents will affect the loading on the coil thus its impedance. The defect must interrupt the surface eddy current flow to be detected. Defect lying parallel to the current path will not cause any significant interruption and may not be detected. The main factors which affect the eddy current response are metal conductivity, permebility, frequency and geometry.

10430-21, Session PS

High-performance technology for indexing of high volumes of Earth remote sensing data

Valery V. Strotov, Alexander I. Taganov, Aleksandr N. Kolesenkov, Boris V. Kostrov, Ryazan State Radio Engineering Univ. (Russian Federation)

Development of high volumes of heterogeneous spatial-temporal data, detection of significant information and knowledge, application of geoinformation methods for analysis and processing of geographical information on spatial-temporal objects, actions and processes allow increasing efficiency of application of Earth remote sensing (ERS) data. There is an issue of availability of obtained data for finite users taking into account an access rate to information within usage of ERS instruments. So, task of development of effective algorithms for search, indexing and cataloging of aerospace images is topical taking into consideration fast increasing volumes and heterogeneity of ERS results.

Cataloging of aerospace images is considered as creation of an archive for images and metadata attached to them with additional characteristics. Application of the geoinformation platform mutually with operative aerospace information allows significantly reducing time of access, processing and preparation of data that will increase quality of the provided information under solution of tasks of applied nature.

Combined storage of aerospace images, digital terrain maps and relational databases generates a geo-relational structure based on geometrical cartographic models. Three-stage algorithm has been suggested for combination of aerospace images being heterogeneous in time on the basis of automatic fitting of reference fragments, removal of information redundancy and sub-pixel improvement. Modernized algorithm of the fuzzy clustering compares a RGB-value of each pixel with a value of the group center: the higher the value of belonging is, the higher possibility that the pixel belongs to this group is.

Suggested algorithms are oriented to realization in systems for data processing on the basis of neural networks being able to training and self-training. Principles of such systems are realized in high-performance central processing units for digital signal processing of original architecture. Complex usage of visual and instrumental approaches allows significantly expanding an application area of ERS data.

10430-22, Session PS

Scattering of a multilayered sphere by Laguerre-Gaussian vortex beam

Tan Qu, Jiaji Wu, Zhensen Wu, Qingchao Shang, Zheng Jun Li, Xidian Univ. (China)

Particle scattering theory is the theoretical basis for the research on the scattering and absorption properties of atmospheric clouds, rain, fog, haze and other particles, which has an important significance in remote sensing. Usually, atmospheric clouds, rain, fog and haze are all nuclear particles. Thus, it is necessary to study on the scattering problem of multilayered inhomogeneous particles.

As a higher order solution to the wave equation in cylindrical coordinate system, Laguerre-Gaussian vortex beam is one of the typical vortex beams in theoretical and experimental research. With the helical phase front carrying orbital angular momentum, it can be used to rotate the particles in interaction. Its annular intensity distribution conquers the shortcoming of Gaussian beam in trapping the particles with lower and higher refractive index than that of the surrounding medium simultaneously. Therefore, the interaction between Laguerre-Gaussian vortex beam and particles is the typical problem of beam scattering.

In this paper, analytical solution to the scattering of a

multilayered sphere by Laguerre-Gaussian vortex beam is investigated. Based on the expansion of Hermite Gaussian beam in terms of spherical vector wave functions (SVWFs) utilizing complex source point method and the relation between Hermite Gaussian beam and Laguerre-Gaussian vortex beam, the expansion of Laguerre-Gaussian vortex beam in terms of SVWFs is derived. The convergences of the expansion coefficients of Laguerre-Gaussian vortex beam are analyzed. Internal fields in each region are expanded in terms of SVWFs. To calculate the scattering coefficients of the field in outer space, an iterative form is constructed according to reflection and refraction on each interface of multilayered sphere, and the continuous boundary conditions. The iterative relations are expressed in forms of ratios and logarithmic derivatives of Riccati-Bessel functions, which can be calculated by their recurrence relations conveniently. The results of multilayered sphere degenerated into single layered sphere illuminated by Laguerre-Gaussian vortex beam are compared with the reference to verify the accuracy of the theory and codes. The effects of the topological charge of LG vortex beam, particle position, radius and layer distribution on the angular distribution of scattering field are numerically discussed in detail. The results show that the handness of the topological charge will influence the scattered field distribution obviously especially when the particle has a shift off the beam propagation axis. The scattered field distribution can be used for the inversion of the particle configuration, position and structure characteristics which is useful for the atmospheric composition detection and particle sizing. In addition, the scattering properties will provide guidance for the beam trap, tractor and rotation as well as other optical noncontactable manipulation which is quite meaningful for the biomedical diagnosis and treatment.

With the increase of the layer and the size of the particle, the computation increases largely. In our near future work, high-performance computing is used for efficient computation without loss of accuracy to calculate the complex particle system.

10430-23, Session PS

Remote sensing for aerosol particles in marine atmosphere using scattering of optical vortex

Mingjian Cheng, Lixin Guo, Qingqing Huang, Jiangting Li, Xu Yan, Songhua Liu, Xidian Univ. (China)

Research on the scattering of aerosol particles has been a hot topic, since it could be great potentially applied in atmospheric radiation, climatic variation, environmental monitoring and other fields. Although aerosol particles are different in shape in the real atmosphere, it can be simplified approximately to a spherical particle and Mie scattering theory can be employed to study the scattering properties of aerosol particles. In this paper, we have employed the complex point method and the generalized Lorenz-Mie theory to study the scattering properties of aerosol particles by LG beam in marine atmosphere. Based on the scattering effect of LG beam, the remote sensing for aerosol particles in marine atmosphere was investigated. The influence of LG modes p (l), the beam waist width w0 and relative humidity Hr were considered. Result indicated that as the number of mode p (l) of LG beam increased, the RCS of aerosol particles alternating appeared maximum and minimum in the forward and backward scattering because of its special ring-shaped distribution. When the beam waist width w0 was added from 0.3?m to 2?m, there appeared obvious extremes gradually in xoz plane. As beam waist was smaller than the particle radius in size, there existed a minimum in the forward direction in yoz plane. According to the mathematical model between aerosol size, refractive index and relative humidity, the comparison of the scattering properties of aerosol particles in different relative humidity between plane wave, Gaussian beam and LG beam were made, and it showed that the effects of Hr on plane wave were almost the same as those for the GB. LG beam had better ability for detecting the changes of relative humidity than plane and GB. The results can provide the theoretic basis for marine atmospheric exploration.

Conference 10431: Remote Sensing Technologies and Applications in Urban Environments

SPIE. REMOTE SENSING

Monday - Tuesday 11–12 September 2017

Part of Proceedings of SPIE Vol. 10431 Remote Sensing Technologies and Applications in Urban Environments II

10431-1, Session 1

Anthropogenic heat flux estimation from space: results of the final phase of the URBANFLUXES Project *(Invited Paper)*

Nektarios Chrysoulakis, Foundation for Research and Technology-Hellas (Greece)

No Abstract Available

10431-2, Session 1

The impact of urban morphology and land cover on the sensible heat flux retrieved by simultaneous satellite and in-situ observations

Lech Gawuc, Lech ?obocki, Joanna Struzewska, Warsaw Univ. of Technology (Poland)

Land surface temperature (LST) is a key parameter in various applications for urban environments research. It is commonly applied in the studies focused on, e.g.: quantification of surface urban heat island intensity (Azevedo et al., 2016), spatial analyses of urban thermal comfort and heat risk (Dousset et al., 2011), relationship with urban land cover (Weng et al., 2008; Zhou et al., 2014). Remotely-sensed radiative surface temperature is not equivalent to kinetic nor aerodynamic surface temperature (Becker and Li, 1995; Norman and Becker, 1995). Thermal satellite observations of urban areas are also prone to angular anisotropy which is directly connected with the urban structure and relative sun-satellite position (Hu et al., 2016).

Sensible heat flux (Qh) is the main component of surface energy balance in urban areas. Retrieval of Qh, requires observations of, among others, a temperature gradient. The lower level of temperature measurement is commonly replaced by remotely-sensed radiative surface temperature (Chrysoulakis, 2003; Voogt and Grimmond, 2000; Xu et al., 2008). However, such replacement requires accounting for the differences between aerodynamic and radiative surface temperature (Chehbouni et al., 1996; Sun and Mahrt, 1995). Moreover, it is important to avoid micro-scale processes, which play a major role in the roughness sublayer. This is due to the fact that Monin-Obukhov similarity theory is valid only in dynamic sublayer.

We will present results of the analyses of the impact of urban morphology and land cover on the seasonal changes of sensible heat flux (Qh). Qh will be retrieved by two approaches. First will be based on satellite observations of radiative surface temperature and second will be based on in-situ observations of kinetic road temperature. Both approaches will utilize wind velocity, and air temperature observed in-situ. We will utilize time series of MODIS LST observations for the period of 2005-2014 as well as simultaneous in-situ observations collected by road weather network (9 stations). Ground stations are located across the city of Warsaw, outside the city centre in low-rise urban structure.

We will account for differences in urban morphology and land cover in the proximity of ground stations. We will utilize DEM and Urban Atlas LULC database and freely available visible aerial and satellite imagery. All the analyses will be conducted for single pixels, which will be closest to the locations of the ground stations (nearest neighbour approach). Appropriate figures showing the seasonal variability of Qh will be presented.

Azevedo, J.A., Chapman, L., Muller, C.L., 2016. doi:10.3390/rs8020153

Becker, F., Li, Z.-L., 1995. doi:10.1080/02757259509532286

Chehbouni, A., Lo Seen, D., Njoku, E.G., Monteny, B.M., 1996. doi:10.1016/S0034-4257(96)00037-5

Chrysoulakis, N., 2003. doi:10.1029/2003JD003396

Dousset, B., Gourmelon, F., Laaidi, K., Zeghnoun, A., et al. doi:10.1002/joc.2222

Hu, L., Monaghan, A., Voogt, J.A., Barlage, M., 2016. doi:10.1016/j.rse.2016.03.043

Norman, J.M., Becker, F., 1995. doi:10.1016/0168-1923(95)02259-Z

Sun, J., Mahrt, L., 1995. doi:10.1175/1520-0469(1995)052<1096:DOSFFT>2.0.CO;2

Voogt, J.A., Grimmond, C.S.B., 2000. doi:10.1175/1520-0450-39.10.1679

Weng, Q., Liu, H., Liang, B., Lu, D., 2008. doi:10.1109/JSTARS.2008.917869

Xu, W., Wooster, M.J., Grimmond, C.S.B., 2008. doi:10.1016/j.rse.2008.04.009

10431-3, Session 1

Urban design and urban heat island

Blanca Arellano, Josep Roca, Univ. Politècnica de Catalunya (Spain)

The Land Surface Temperature (LST) plays a key role in the generation of the Urban Heat Island (UHI), representing a determining factor of the radiation of the surface and the exchange of energy and control the distribution of heat between the surface and the atmosphere. The composition of the land covers is one of the main factors that influence the LST. The literature had emphasized that the different types of land cover materials, their albedo and roughness, degree of impervious as well as the quality and quantity of vegetation, can have a significant impact on the generation of the UHI.

The overall objective of the paper is to investigate whether urban design, on a scale of detail, can mitigate the Urban Heat Island. Specifically, the question is if the morphology of the public space, especially of the green areas and open spaces, affects surface (LST) and air (LSAT) temperatures, in addition to the traditional elements (type of land covers, impervious, vegetation, ...) affect the UHI. The case studies are two urban expansion areas of the municipality of Sant Cugat del Vallés (in the metropolitan area of Barcelona), Parc Central and Coll Favà, with similar characteristics, but with a clearly differentiated public space design: while in Parc Central buildings are structured around the open space, in Coll Favà, the vast majority of open spaces are located peripherally, surrounding the built-up areas. The hypothesis is that the morphology of public space is a significant element in the generation of the UHI. And therefore, an adequate design of open spaces can help to increase the resilience of cities to Climate Change (CC).

The research methodology consisted in: a) studying the urban and climatic parameters of Parc Central and Coll Favà (building index, percentage of public land, degree of waterproofing, quality of vegetation, urban canopy, ...); b) to analyze the spatial distribution of the LST using remote sensing technologies (Landsat 8), at a resolution of 30x30 meters / pixel; c) obtaining LST and LSAT through field work, during day and night time; and d) construction of a model of the surface and air temperatures as a function of the different types of land cover, for each of the areas of analysis.

The study confirms the research hypothesis: from the perspective of the LST, Parc Central is cooler than Coll Favà, both during daylight hours (about 10 degrees) and at nighttime (1.5 degrees). Likewise, the LSAT confirms the better thermal behavior of Parc Central. The urban design, the morphology of public space, is very significant in the regulation of temperature and in the control of the UHI.

This work is part of the research project (Urban CLIM-PLAN) aimed at studying the UHI of the Barcelona Metropolitan Area. The Metropolitan Master Plan of Barcelona is currently being developed. Said plan should direct the urban development of 36 municipalities in the metropolitan area, bringing together about 3.5 million inhabitants. For the first time, the aim is to include climate assessment in urban planning in Barcelona in order to mitigate the effects of the UHI.

10431-4, Session 1

Social vulnerability to heat in Greater Atlanta, USA: spatial pattern of heat, NDVI, socioeconomics and household composition

Sunhui Sim, Univ. of North Alabama (United States)

Social Vulnerability to Heat in Greater Atlanta, USA: Spatial Pattern of Heat, NDVI, socioeconomics and household composition.

Extreme heat is one major weather hazard accounting for nearly 8000 heat-related deaths since 1979 in the US. Spatial Interaction between the geographic locations of social vulnerability to heat is important to understand urban heat environment. Some studies showed that there is the relationship between heat-related death and social variables including socioeconomic status and neighborhood characteristics. The purposed of the article is evaluating global and local indicators of spatial autocorrelation of social vulnerability to heat in Greater Atlanta in 2015.

The research focus is on the variation of heat vulnerability in Greater Atlanta. The study site consists of 46 counties and 1009 census tracts. The social vulnerability to heat is an index of socioeconomic status, household composition, land surface temperature and normalized differential vegetation index (NDVI). Land surface temperature and NDVI were derived from the red, NIR and thermal infrared (TIR) bands of Landsat OLI/TIRS images collected on September 14, 2015. These values were summarized by US census track. Social, economic and household variables were downloaded from Agency for Toxic Substances and Disease Registry – the social vulnerability index (SVI) in 2014. The socioeconomic variables include poverty, unemployment rate, income and education levels. Household composition includes percentage of people older than 65 and people younger than 16, civilian with a disability and single-parent households.

The study derived a composite heat vulnerability index from those four measures (Temperature, NDVI, socioeconomic status and household condition). Each measure was normalized for each tract varied from 0 to 1, with higher magnitudes indicating more vulnerable. Sequential order process was used to determine spatial autocorrelation in R software (R Core Team 2012). First, a neighborhood criterion was chosen based on the geographic arrangement of the census tract. Next, a weight needed to be assigned to the areas that are linked as neighbors. Finally, a statistical test to examine spatial autocorrelation in R results in the functions “moran.test” (test of spatial autocorrelation) and “moran.plot” (a plot of the spatial data against its spatially lagged values, showing any existing linear relationships).

The results showed a significant degree of global spatial autocorrelation ($p < 0.001$) at a 99 percent confidence interval. Moran’s I statistics in Heat vulnerability was 0.58. The study found that heat vulnerability is highly clustered spatially, resulting in “hot spots” and “cool spots”. The results show significant health disparities. The hotspots of social vulnerability to heat occurred in neighborhoods with lower socioeconomic status as measured by low education, low income and more poverty, greater proportion of elderly people and young children. The findings of this study are important for identifying clusters of heat vulnerability and the relationships with social factors. These significant results provide a basis for heat intervention services.

10431-5, Session 3

Mapping urban porosity and roughness characteristics as a mean of defining urban ventilation corridors

Marzena Wicht, Warsaw Univ. of Technology (Poland); Andreas Wicht, GfK (Germany); Katarzyna Osi?ska-Skotak, Warsaw Univ. of Technology (Poland)

Cities can be characterised with the roughest aerodynamic boundaries [1], what results in enhanced turbulent motion and increased drag effect. This leads to reduced wind speeds and directly increases negative effects of living within urban areas. Urban Heat Islands, decreased air quality or densely build-up residential/industrial areas occur in many cities both in temperate and tropical regions and can be included in these negative effects. This case study investigates Warsaw, the capital of Poland, representing a dense, urban environment, located in the temperate zone. It suffers from immensely exceeded air pollution levels as well as Urban Heat Island, and the local government is seeking ways to resolve these issues [2]. Among many mitigation techniques, air restoration and exchange system was suggested as appropriate measure [3], as it addresses many of the mentioned issues. The essential elements of such system are ventilation corridors. This paper describes mapping these corridors utilising the morphometric methods of urban roughness aided by remote sensing data. The focus lies especially on the terrain topology and texture of single elements, including high vegetation canopy layer. The methods include calculation of zero plane displacement height (zd) and roughness length (z0) and their distribution for the eight (inter-)cardinal wind directions [4] based on a hybrid lot-grid approach. The roughness mapping is based on LiDAR data and secondary products like a normalised DTM, which includes all potential obstacles. Cadastral databases including building footprints are available for most developed countries, therefore, the proposed method can be utilised in many areas across the world. This study considers the normalised DTM and different porosity of obstacles, deriving a new outlook at the morphometric methods as a way to improve their accuracy. The mapped areas of low roughness characteristics might be appointed as ventilation corridors and play a crucial role in air restoration and exchange system. They may also be included in further planning process by the local government as the preservation areas.

1. Oke, T. R. (1978). Boundary layer climates, 372. Methuen, New York.

2. Halicki, P. (2017). Smog w Warszawie. “Tak ?le nie by?o od wielu lat”. Warszawa Onet.pl.

3. Rizwan, A. M., Dennis, L. Y., & Chunho, L. I. U. (2008). A review on the generation, determination and mitigation of Urban Heat Island. Journal of Environmental Sciences, 20(1), 120-128.

4. Gál, T., & Unger, J. (2009). Detection of ventilation paths using high-resolution roughness parameter mapping in a large urban area. Building and Environment, 44(1), 198-206.

10431-8, Session 3

Seasonal and temporal dynamics of urban heat island: Jaipur City

Surbhi Gaur, Jawaharlal Nehru Univ. (India)

Presently India is experiencing rapid urbanization, which is skewed and bias towards the mega urban centers. Urban population of India grew to 377 million during 2001-2011, with a growth rate of 2.76% annual. The total urban population share increased from 27.7% to 31.1% during the same period, with adding 3.3 percentage points to previous decade. To accommodate the rapid rapidly growing population in urban we required more physical spaces and dwelling. Both the vertical and horizontal expansion of cities in an unplanned way leads to degradation of green spaces. Distance from the natural environment, enormous heat generation, high absorption and

obstruction of heat exchange by high rise building leads to the development of urban heat islands (UHI). The urban heat island effect is a positive temperature anomaly that occurs over urban areas relative to surrounding non-urban areas. Urban heat island effect, and its mostly negative consequences of modified temperature, wind, precipitation, and air quality patterns, is the primary instigator of local climate change. The increasing impact of urban heat islands on local climates may eventually translate to more widespread climate change, possibly global, if left unchecked. An elevated temperature is making dual impact by increasing peak energy demand, air conditioning costs, air pollution levels, and heat-related illness and mortality, which has been exacerbate especially during the summer seasons. More precisely, it becomes a priority to understand the strong interactions between urban micro-meteorology and urban land cover area in order to better map the spatial (day and night) and seasonal characteristics of UHI.Characterization and modeling of UHIs must consider the inherent spatial non-stationary within land surface variables. Permanent meteorological station data, based on air temperatures are not able to map the spatial component and micro variability of temperature in accordance to the land use and land cover. In way to achieve spatial pattern of urban heat island, LST data can provide a continuous and simultaneous view of urban surface climate and gradient also. In present study land surface temperature (LST) and emissivity data from satellite thermal infrared (TIR) imagery have been used for the spatio-temporal mapping of urban heat island of Jaipur City.

10431-10, Session 3

Identifying the sources of radon gas in the city of Mumbai and minimizing its impact on the health of the people using remote sensing and GIS solutions

Leon Cruz Ratinam, Don Bosco Institute of Technology (India)

A city like Mumbai which is congested and polluted has very high chances that people are continuously being exposed to high concentrations of radon gas thereby harming their health to a great extent. This research attempts to identify sources of radon concentrations and also create GIS solutions to minimise the harm done to the people.

There has been no major research in studying the presence and effects of radon gas in a city like Mumbai. There is also a lack of awareness both among the public and the medical fraternity. For example there are very less chances that a doctor in Mumbai will tell a patient that his/her respiratory ailment is directly related to the radon gas concentration in his/her home.

Identifying the sources of Radon is the first challenge this research is directed towards. Precision testing instruments and methods need to be established to identify the major pockets of high concentration radon in the city of Mumbai. A GIS solution using remote sensing techniques is being used to record, analyse and identify the high concentration pockets of radon gas. Also the presence of radon in water, its movement and effects too needs to be explored.

This research also links the impact of the exposure of radon to the various health problems faced by the people living in those radon zones of study. This includes collaboration with the hospitals in identifying patients who could be probable victims of radon gas concentrations. This research hopes to be of great help in the proper diagnosis of the causes of certain ailments caused by exposure to radon gas and also provide solutions to minimize its effects.

10431-12, Session 3

Concentrations retrieving by BP-ANN algorithm for multi-component air VOCs

Yudi Zhao, Ruyi Wei, Xi'an Institute of Optics and Precision Mechanics, CAS (China); Xuebin Liu, Xi'an Institute of Optics and Precision Mechanics, CAS (China); Yishan Wang, Tao Yu, Xi'an Institute of Optics and Precision Mechanics, CAS (China)

RS-FTIR (Remote sensing-Fourier Transform infrared spectroscopy) is one of the most important technologies in atmospheric pollutant monitoring. It is very appropriate for on-line dynamic remote sensing monitoring of air pollutants, especially for the toxic VOCs (volatile organic chemicals). However, their absorption spectra are often seriously overlapped in the atmospheric infrared window bands, i.e. MWIR(3 - 5?m) and LWIR(8 - 12?m). Major traditional algorithms retriving and de-mixing the spectra to distinguish multi-component air VOCs include CLS (Classical Least Squares), PLS (Partial Least Squares) and KFM (Kalman Filtering Methods). ANN (Artificial Neural Network) is an algorithm based on the theory of the biological neural network, which simplifies the partial differential equation with complex construction. For its preferable performance in nonlinear mapping and fitting, in this paper we utilize BP-ANN (Back Propagation-Artificial Neural Network) to quantitatively analyze the concentrations of eight typical industrial VOCs, including Benzene, Ethenyl-Ben, 1,3-Butadiene, 1,2-Dimethylbenzene, 1,3-Dimethylbenzene, 1,4-Dimethylbenzene, Ethenyl-Benzene and Ethylene.

We extracted the original infrared spectra of these VOCs as FTIR input spectra from the NIST (National Institute of Standards and Technology) website, most of which virtually overlapped, and established a mixed multi-component simulation environment. Based on Beer-Lambert Law, concentrations can be retrieved from the absorbance of spectra. Parameters including learning rate, momentum term, the number of hidden nodes and iterations were obtained when the BP network was trained with 100 groups of input data. By improving these parameters, the network can be optimized to produce necessarily higher precision for the retrieved concentrations. Results of tests show that not only each component of the eight VOCs can be distinguished, but also high precisions of their concentrations can be reached. The MRE (Mean Relative Error) of them is lower than 0.094, the mean of the SEP (Standard Error of Prediction) is below 0.0014% and the MPE (Mean Predictive Error) can reach to -8.25. This BP-ANN method proves to be an effective and promising algorithm on dealing with multi-component analysis of VOCs.

10431-13, Session 3

Seasonal variability of aerosols and their characteristics in urban and rural locations of Delhi-NCR

Purnima Bhardwaj, Alok K. Pandey, Krishan Kumar, Vinod K. Jain, Jawaharlal Nehru Univ. (India)

Present study shows the seasonal variation of Aerosol Optical Depth (AOD) and aerosols characteristics over an urban and rural environment in New Delhi and National Capital Region (NCR) in the summer and winter seasons of the year 2015. NASA's Terra satellite MODIS sensor AOD data have been used for spatial distributions of aerosols over the New Delhi and surrounding rural area. The PM2.5 aerosols sampling was carried out over this region at an urban and rural locations using a Mini-Volume sampler and further analyzed on Scanning Electron Microscope (SEM) and Energy Dispersive X-Ray Spectroscopy (EDX). A relatively higher PM2.5 concentration is observed at the urban sampling site in the summer as well as winter season. Spatial AOD maps show a higher AOD in the Delhi compared to relatively lower AOD in NCR in both summer and winter season. In summer season, Delhi-NCR is affected by the frequent dust storm events and wind-blown dust which increases the amount of coarser particles in the atmosphere which plays a greater role in the scattering and absorption of solar radiation. In summer season, coarser mode aerosols are the major factor affecting the AOD in the rural area whereas in urban area it is a combination of both the higher concentration of anthropogenic aerosols and coarser

particles. However, in winter season, AOD is affected mainly by the fine mode aerosols which are anthropogenic in nature. SEM and EDX analyses results are a powerful tool to understand the elemental composition and morphology of the aerosols which helps in understanding the origin of the aerosols and their optical properties as they depend greatly upon the chemical composition of the particles. SEM analysis results showed flaky, aggregates, spherical and irregular shaped particles dominated in both the urban and rural areas. In winters, in rural area, spherical particles were found to be in abundance which could be due to wood burning for various purposes such as cooking or keeping warm whereas in urban area particles were found to be more spherically chain-like structures and in condensed form. EDX analysis showed the abundance of Oxygen (O) followed by Silicon (Si) followed by other elements such as C, Cu, Zn, Ga and Fe in both the urban and rural areas, however, not much significant difference could be seen in their concentrations at both the sampling sites. Presence of these elements in rural area indicates the presence of long range transport.

10431-38, Session 3

Urban heat island and its relationship with land-use/land-cover classification over Delhi-NCR during

Shivesh Berwal, Krishan Kumar, Jawaharlal Nehru Univ. (India)

This study attempts to examine the role of land-use/land-cover (LULC) classification in the variable behaviour of day-time Urban Heat Island over Delhi. LISS-III data of Resourcesat-I and MODIS (Moderate Resolution Imaging Spectroradiometer) Aqua 8-day Land Surface Temperature Product have been used to investigate the spatial variations in land cover and land surface temperature for the month of March, 2015. The LISS-III image shows the predominance of built-up area over Delhi, which is surrounded by agricultural land covered by crop vegetation at this time of the year. The Enhanced Vegetation Index (EVI) Map of Delhi for March 2015 retrieved from MODIS dataset reveals that EVI over Delhi varies from 0.06 to 0.29 whereas EVI over the surrounding regions reaches up to 0.66, which confirms the prevalence of crop vegetation in the surrounding regions. The day and night-time land surface temperature maps reveal that temperatures over Delhi are significantly higher (8°C -10°C) than those over the surrounding regions. A strong negative correlation is found between day-time and night-time land surface temperature with EVI over study area. Urban heat island intensity (UHII) is found to be positive in both day-time and night-time. An attempt has also been made to study role of thermal inertia in the diurnal variation of land surface temperature and a negative correlation is found between them.

10431-15, Session 4

Use of multitemporal lidar data to extract changes due to the 2016 Kumamoto earthquake

Fumio Yamazaki, Wen Liu, Chiba Univ. (Japan); Luis Moya, Tohoku Univ. (Japan)

An automatic procedure to extract collapsed buildings from a pair of Lidar data taken before and after the 2016 Kumamoto, Japan, earthquake on was performed. Lidar surveys were carried out for the affected areas along the causative faults by Asia Air Survey Co., Ltd. [1]. The density of the collected Lidar data was 1.5 - 2 points/m2 for the first flight on April 15, 2016 and 3 - 4 points/m2 for the second flight on April 23, 2016. This LiDAR pair dataset is one of the few cases in which pre- and post-event digital surface models (DSMs) were obtained from the same airplane, instrument, and pilot.

The spatial correlation coefficient of the two Lidar data was calculated using a 101 x 101 pixels window (50 m x 50 m), and the horizontal shift of the April-23 DSM with the maximum correlation coefficient was considered as the crustal movement by the April-16 main-shock. The horizontal component of the calculated coseismic displacement was applied to the post-event DSM to cancel it, and then the vertical displacement between the two DSMs was calculated [2]. The both horizontal and vertical coseismic displacements were removed to extract collapsed build in the study area.

Then building-footprints were employed to assess the changes of the DSMs within them. Three parameters were selected to evaluate whether a building is collapsed or not: the average of the differences between the pre-event and post-event DSMs within a building footprint, the standard deviation of that differences, and the correlation coefficient between the DSMs. The extracted parameter values were then compared with the result of the field damage investigation conducted by an academic group.

From the comparison, the difference value was found to be the most suitable parameter to extract collapsed buildings. From a total of 26,071 evaluated buildings in Mashiki town, the method extracted 1,300 collapsed buildings. It was also observed that in order to improve the quality of the parameters, it is recommended to discard the elevation points located close to the boundaries of the footprint polygons because the matching between the DSMs and footprints was not so accurate. These preliminary results are helpful to extract collapsed buildings at an early stage of the occurrence of a damaging even.

References:

[1] Asia Air Survey Co., Ltd. the 2016 Kumamoto Earthquake. An approach of crustal deformation analysis based on comparison of two periods of Lidar measurement.

[2] L. Moya, F. Yamazaki, W. Liu, T. Chiba, Calculation of coseismic displacement from Lidar data in the 2016 Kumamoto, Japan, earthquake, Natural Hazards and Earth System Sciences, 17, 143-156, 2017.

10431-16, Session 4

Multitemporal synthetic aperture radar for bridges monitoring

Serena Tessitore, Diego Di Martire, Domenico Calcaterra, Univ. degli Studi di Napoli Federico II (Italy); Donato Infante, Federico II University of Naples (Italy); Massimo Ramondini, Gianpiero Russo, Univ. degli Studi di Napoli Federico II (Italy)

The present work is devoted to analyze the potentiality of satellite-based techniques for structural monitoring of bridges. Specifically, the well-known case study of the cable stayed bridge across the river Garigliano and Ausente stream is presented. The available “in situ” data have been compared and integrated with satellite-based measurements (ERS, ENVISAT satellites) for the common monitoring period (1993-2004); thus, the temporal observation window has been extended until 2010 (ENVISAT satellite). InSAR represents one of the more innovative tool for deformation monitoring and its application on manmade structure and infrastructure can make easier the detection of potential problems with a consequent improvement of risks management.

10431-17, Session 4

The Interaction between building load and ground subsidence based on multisource remote sensing data

Qin Yang, Yinghai Ke, Capital Normal Univ. (China)

Beijing is the capital of China with a population of about 21,729million people, inhabiting an area of about 1,641 million square kilometers. Beijing has suffered land subsidence since 1935 and gradually formed five large land subsidence area.

With rapidly development of urban area, the constructions of multi-storey and high-rise buildings could accelerate land subsidence, and the uneven land subsidence could also affect building stability. This study focuses on the relationship between land subsidence and building load from regional scale and single building scale using Permanent Scatterer for SAR Interferometry (PS-InSAR), Geographic information system (GIS) and optical remote sensing techniques based on multi-source remote sensing data, and carries out the following aspects:

Firstly, PS-InSAR technique was used to obtain time-series surface displacement information of Beijing urban area based on more than 50 scenes of TerraSAR-X images during the periods of 2010-2016. The deformation results are evaluated and validated using the existing leveling surveys and GPS survey measurements. Five regions representing different compressible layer thickness, geological structure and groundwater level were selected. For each region, stereo pair of high spatial resolution panchromatic images acquired from Pleiades satellite are used to derive Digital Surface Model (DSM). In order to verify the accuracy of DSM, we choose 15 measured points in the 1:2000 topographic map to compare difference between values combine with visual interpretation and check point method. Meanwhile, building contours are extracted in each of the five typical regions through Object Oriented Classification (OOC) method based on the combination of multi-spectral images and DSM. Then, GIS analysis methods has been utilized to calculate the building floor area ratio of the typical area based on DSM and building contours. Finally, we received the spatial distribution map of building load in five typical area.

Secondly, in order to explore spatial difference of the urban ground subsidence under the influence of building load, we execute a correlation analysis with respect to ground subsidence and building load from regional scale. Moreover, at single building scale, we compared the PS point subsidence velocity of single building in all directions to study the uneven displacements on the building. Furthermore, we establish a risk assessment system around the stability and security of the residential area to diagnose the health of urban buildings.

Results shows that subsidence velocity in Beijing is ranging from -143.6mm/year (sinking) to 23.2 mm/year (uplift), and subsidence velocity in urban districts is obviously exceed in suburbs. Statistical analysis showed positive correlation between the density of building load and subsidence rate. Through correlation analysis we will further prove that the greater the building floor area ratio was, the more severe the land subsidence will be. Additionally, we discovered that some building suffer obvious uneven settlement. The results indicate that ground subsidence has been posed a great threat to the stability and security of the urban building after evaluating. Thus we may verify that the uneven land subsidence do harm to the building stability.

10431-18, Session 5

Defining urban and rural areas: a new approach

Josep Roca, Blanca Arellano, Univ. Politècnica de Catalunya (Spain)

The separation between the countryside and the city, from rural and urban areas, has been one of the central themes of the literature on urban and territorial studies. The seminal work of Kingsley Davis in the 1950s introduced a wide and fruitful debate which, however, has not yet concluded in a rigorous definition that allows for comparative studies at the national and subnational levels of a scientific nature. In particular, the United Nations (UN) definition of urban and rural population is overly linked to political and administrative factors that make it difficult to use data adequately to understand the human settlement structure of different countries.

The present paper seeks to define a more rigorous methodology for the identification of rural and urban areas. For this purpose it uses the night lights supplied by the SNPP satellite, and more specifically by the VIIRS sensor for the determination of the urbanization gradient, and by means of the same construct a more realistic indicator than the statistics provided by the UN. The arrival of electrification to nearly every corner of the planet is certainly the first and most meaningful indicator of artificialization of land. In this sense, this paper proposes a new methodology designed to identify highly impacted (urbanized) landscapes worldwide based on the analysis of satellite imagery of night-time lights. The application of this methodology on a global scale identifies the land highly impacted by light, the urbanization process, and allows an index to be drawn up of Land Impacted by Light per capita (LILpc) as an indicator of the level of urbanization.

The methodology used in this paper can be summarized in the following steps: a) a logistic regression between US Urban Areas (UA), as a dependent variable, and night-time light intensity, as an explanatory variable, allows us to establish a nightlight intensity level for the determination of Areas Highly Impacted by Light (AHIL); b) the delimitation of the centers and peripheries is made by setting a threshold of night-time light intensity that allows the inclusion of most of the centers and sub-centers; c) once identified urbanized areas, or AHIL, it is necessary to delimit the rural areas, or Areas Little Impacted by Light (ALIL), which are characterized by low intensity night light; d) finally, rurban landscapes are those with nightlight intensities between ALIL and AHIL.

The developed methodology allows comparing the degree of urbanization of the different countries and regions, surpassing the dual approach that has traditionally been used. This paper enables us to identify the different typologies of urbanized areas (villages, cities and metropolitan areas), as well as “rural”, “rurban”, “periurban” and “central” landscapes. The study identifies 186,134 illuminated contours (urbanized areas). 404 of these contours have more than 1,000,000 inhabitants and can be considered real “metropolitan areas”; on the other hand there are 161,821 contours with less than 5,000 inhabitants, which we identified as “villages”. Finally, the paper shows that 40.26% live in rural areas, 15.53% in rurban spaces, 26.04% in suburban areas and only 18.16% in central areas.

10431-19, Session 5

Predicting urban expansion in Moscow based on night lights

Demetris N. Stathakis, Univ. of Thessaly (Greece); Karen Seto, Yale Univ. (United States); Igor Savin, RUDN Univ. (Russian Federation)

Forecasting has always been central to urban planning in order to accommodate future needs and mitigate future side effects of urbanization. Having an estimate of how cities will evolve in the future has recently gained more importance due to the rapid pace of urbanization globally and also due to the significant impact of urbanization to the environment. Forecasting methods in urban planning can be either of broad scale, focusing on broad administrative devisions, or fine grained, focused on sub-city level e.g. at the pixel level. In this paper we deploy a fine grained method.

The study area is Moscow, the capital of the Russian Federation. It is one of the largest cities worldwide and the largest in the European continent, with approximately 12 million inhabitants. A significant increase in population (+35%) and a rapid increase in terms of Gross Domestic Produce (GDP) has taken place.

The data used is the intercalibrated DSMP/OLS time series. The correlation coefficient of the SoL, calculated on the intercalibrated images for the existing data (1992-2013), with the total population and the GDP is 0.62 and 0.84 respectively.

The method used to forecast is exponential smoothing. In specific, for each pixel in the intercalibrated raster time series an exponential model is fitted. The smoothing constants alpha (weight of recent data) and beta (trend) range in (0,1), depending on each individual pixel’s time series. The gamma parameter (seasonality) is set to zero. Forecasted values over 63 are truncated to 63. The estimates produced include a mean value along with the upper and lower bounds of a 95% confidence interval.

The results include forecasted rasters, calculated globally for each year in [2014, 2025]. Focusing on Moscow, the impact of the strong expanding trend noticed in the previous two decades is clearly visualized by projecting it to the year 2025. Peri-urban areas as well as areas along the road network show the largest magnitude of change. In the case of Moscow region it is mostly positive change because the area has been growing rapidly. The model also provides reasonable results even on declining areas, with negative urbanization trends. This is because it is purely data-driven, free of any assumptions on the expected trend in the area.

In conclusion, the method provides a means of projecting the trend captured by past intercalibrated night lights in the future. The prediction is spatially and temporally fine grained and can provide an insight on where urbanization pressures are expected to emerge. The forecast comes with confidence intervals that can be exploited to better interpret future values, as error is inherent in any forecasting attempt.

10431-20, Session 5

Contribution of a local segmentation parameters optimization approach for mapping urban areas

Tais Grippa, Stefanos Georganos, Sabine G. Vanhuysse, Moritz Lennert, Eléonore Wolff, Univ. Libre de Bruxelles (Belgium)

Mapping urban area from earth observation data has known major breakthrough with the increasing spatial resolution of spaceborne and the revolution of methods from pixel-based to Object-based image analysis (OBIA).

When producing LULC maps in OBIA, the segmentation step still remains a crucial point, as it could have an influence on the quality of the produced maps, at least to a certain extent [1]. Therefore, there is a need to evaluate if the quality of segmented images is sufficient. The main objective of the segmentation step is to obtain uniform objects which are significantly different from their neighbours. Very often, evaluation of segmentation results is undertaken by visual interpretation of the segmented image. It the results are not satisfying, segmentation parameters are gradually adjusted in a trial-and-error manual process. Beyond the fact that it represents a time-consuming task, this approach has the major inconvenient of being subjective, as it relies on the judgement of the interpreter. Objectives evaluation methods allow to face these issues as they either rely on comparing the segmented image to a reference segmentation, using 'discrepancy measure' (supervised evaluation methods) or compute 'goodness metrics' using the intrinsic information of the segmented maps to evaluate how well the objects correspond to some desired characteristics (unsupervised evaluation methods). The latter, as they do not rely on a-priori knowledge contrarily to the former, can be used for automated selection of segmentation parameters [2]. They usually consist in finding segmentation parameters which maximize both intra-object homogeneity and inter-object heterogeneity. Unfortunately, even when using segmentation parameters optimization techniques, finding 'the perfect' segmentation is nearly impossible. Usually the finally selected segmentation result is more a satisfying solution containing persisting oversegmented and/or undersegmented objects.

Mapping urban area using OBIA is challenging since those consist in a highly complex arrangement of heterogeneous land-cover classes. In this context, achieving satisfying segmentation results using a single segmentation parameter combination might be impossible, even when using unsupervised optimization methods. However, it is often possible to divide the whole city into smaller and quite homogeneous urban neighbourhoods by visual photo-interpretation based on criteria like building size or density. Those neighbourhoods could then be processed individually by applying segmentation parameter optimization of each of them. Previous study [3] applying this approach on agricultural plot showed interesting results.

This paper assess the contribution of a local segmentation parameter optimization approach for the classification of large urban areas. First, the whole scene is segmented using a single globally-optimized segmentation parameter. Second, the city is divided by into 290 homogeneous neighbourhoods in terms of building size and density. Each neighbourhood is then segmented using a locally-optimized segmentation parameter. Finally, a LULC classification is performed using the random forest classifier. Contribution of a local optimization is assessed both in terms of segmentation results and thematic accuracy.

REFERENCES:

1. Räsänen, A.; Rusanen, A.; Kuitunen, M.; Lensu, A. What makes segmentation good? A case study in boreal forest habitat mapping. Int. J. Remote Sens. 2013, 34, 8603–8627.

2. Zhang, H.; Fritts, J. E.; Goldman, S. A. Image segmentation evaluation: A survey of unsupervised methods. Comput. Vis. Image Underst. 2008, 110, 260–280.

3. Cánovas-García, F.; Alonso-Sarría, F. A local approach to optimize the scale parameter in multiresolution segmentation for multispectral imagery. Geocarto Int. 2015, 30, 937–961.

10431-21, Session 5

Urban land cover and land use classification based on high-spatial resolution satellite image using deep learning

Pengbin Zhang, Yinghai Ke, Capital Normal Univ. (China)

Urban land cover and land use mapping is one of the major applications of satellite image classification. Machine learning algorithms such as random forest, support vector machine, have played a key role in previous research. However, they can't extract adequately discriminative features as the uncertainty caused by high resolution images. Compared to these shallow architectures, deep learning can obtain higher level features, which is particularly effective to classification. After Hinton proposed the method to train deep neural network effectively in 2006, deep learning has developed several models include deep belief networks(DBN), stacked denoising auto-encoder(SDAE), convolutional neural networks(CNN) and recurrent neural networks(RNN).

In our work, SDAE and CNN were selected as the bases of our image classification framework. SDAE and CNN are both powerful deep learning algorithms and have been widely investigated. As for the research region, worldview-2/3 data covering several typical parts of Beijing were selected. We also collected sufficient ground truth samples for model training and testing through field investigation and artificial interpretation. According to the ground truth, we divided the samples into six classes represent six land cover types.

Next step, in order to improve the accuracy, image preprocessing include radiometric calibration, atmospheric correction, geometric correction and image sharpen are all applied in advance. Considered the uncertainty and to increase the dimension of raw feature, we extracted the 3*3 neighborhood pixels of sample points as the input vector. And the whole image pixels are ready for prediction in the same form as sample points.

And then two network structures need to be confirmed. Because there is no standard architecture of CNN and SDAE and the proper layer-depth is usually decided by the specific application and dataset. In order to establish suitable networks, we need to try several times and confirm the best depth. We have preliminary realized the two networks with tensorflow library, which is an open-source software library for machine Intelligence supplied by google. The procedure can be divided into two parts 1) Training stage: the vector of training samples are assigned to networks separately and through a greedy layer-wise training strategy. 2) Fine-turning stage: after the feed-forward propagation was accomplished, the output results were compared with the labels of samples and the error would be back-forward to adjust the weights and bias in order to improve the capacity of networks. Finally, the trained models

will be used to predict the whole region into six classes, after we obtain the final model structures.

AS a comparison, we also adopted Radial Basis Function Kernel as the kernel function of SVM and set the parameter C and g through grid search using the libSVM package. We will compare the classification results of CNN-based model ,SDAE-based model and SVM and expect the proposed two deep learning algorithms will perform better than SVM. In the future, we will try to design models combine unsupervised and supervised advantages to train the model with less label-points.

10431-22, Session 6

Optimizing classification performance in an object-based very-high-resolution land use-land cover urban application

Stefanos Georganos, Tais Grippa, Sabine G. Vanhuysse, Moritz Lennert, Eléonore Wolff, Univ. Libre de Bruxelles (Belgium)

In Remote Sensing (RS) classification applications and especially in object-based image analysis (OBIA), massive amount of redundant data are often used as input. The effects of high dimensionality can have consequences ranging from increased processing time and unnecessary computational effort, to negative effects in algorithm performance (Pal and Foody 2010), while making variable assesment a challenging task. Thus, finding appropriate methods in order to reduce the number of features and select the most significant variables might be particularly beneficial. As there is no standardized way to select features for a classification, the choice of method is usually based on intuition and individual assessment (Tokarczyk et al. 2015). The most common FS techniques are i) embedded methods from Classification and Regression Trees (CART) classifiers (e.g. Random Forest, Boosting Trees), ii) wrappers, which combine embedded methods with model performance such as Recursive Feature Elimination (RFE) and iii) filter approaches, which are used as a preprocessing step and usually utilize simple statistical measures such as Pearson's Correlation Coefficient to remove collinear features as a pre-processing step. A few studies have explored FS but they are usually constrained to a single classifier (Pal and Foody 2010; Kuo et al. 2014). In this study, we applied various algorithms from the whole range of the aforementioned FS spectrum, in the context of an object-based Land Use/ Land Cover (LULC) classification of Ouagadougou, Burkina Faso. The state-of-the-art classifiers involved in the study are Gradient Boosting Machine (GBM), Adaboost, Random Forest, Support Vector Machine (SVM), Extreme Gradient Boosting (Xgboost) and Rotation Forest (RotFor). The aim is to compare different FS methods in terms of computational time, classification performance and the amount of features required for achieving optimal results, to conclude if the amount of complexity and time which is required for complex FS methods, justifies their use over simple or even no FS in the selected classifiers.

References

Kuo, Bor Chen, Hsin Hua Ho, Cheng Hsuan Li, Chih Cheng Hung, and Jin Shiuh Taur. 2014. "A Kernel-Based Feature Selection Method for SVM with RBF Kernel for Hyperspectral Image Classification." IEEE Journal of Selected Topics in Applied Earth Observations and Remote Sensing 7 (1): 317–26. doi:10.1109/JSTARS.2013.2262926.

Pal, Mahesh, and Giles M. Foody. 2010. "Feature Selection for Classification of Hyperspectral Data by SVM." IEEE Transactions on Geoscience and Remote Sensing 48 (5): 2297–2307. doi:10.1109/TGRS.2009.2039484.

Tokarczyk, Piotr, Jan Dirk Wegner, Stefan Walk, and Konrad Schindler. 2015. "Features, Color Spaces, and Boosting: New Insights on Semantic Classification of Remote Sensing Images." IEEE Transactions on Geoscience and Remote Sensing 53 (1): 280–95. doi:10.1109/TGRS.2014.2321423.

10431-23, Session 6

Building change detection via a combination of CNNs using only RGB aerial imageries

Keisuke Nemoto, Ryuhei Hamaguchi, Masakazu Sato, Aito Fujita, Tomoyuki Imaizumi, Shuhei Hikosaka, PASCO Corp. (Japan)

The extraction of building change information, for example construction of a new building, from the remote sensing imageries is a valuable source for various applications such as urban management and marketing purpose. Currently, much of the information extraction is performed by human experts, making the process slow and costly. The main goal of this work was to develop a methodology for automatically capturing the changes of buildings from remote sensing imageries.

Recent studies have proposed several methodologies for achieving the goal by requiring 3-D information such as building height in order to improve performance of the building change detection. The 3-D information often used includes Light Detection and Ranging (LiDAR) point cloud data, Digital Elevation Models (DEMs) and Digital Surface Models (DSMs).

Differently from the past literature, we do not rely on the 3-D information but focus on using only RGB aerial imageries because it is not always possible to prepare the 3-D information due to higher data acquisition and processing cost from an application point of view. For creating pipelines for the building change detection with no height information but with only RGB imageries, one must address the practical challenge, i.e., a necessity to extract discriminative features for distinguishing buildings from other irrelevant objects, only based on the colour information. This is generally quite difficult because the visual appearance of buildings can be highly variable due to several factors such as atmospheric conditions, different viewpoints of sensors, shadows, occlusions and so on. To this end, we employ deep Convolutional Neural Networks (CNNs) to extract effective features from RGB aerial imageries.

In our present methodology we treated the building change detection aspects as two issues, the building detection and the subsequent change detection. A brief description of the proposed pipeline to do these is as follows: (1) In the building detection phase, we use CNN models to perform a pixel-wise segmentation over an input, RGB imagery. This generates a probability map (where each pixel indicates the probability of the pixel belonging to building) as a coarse estimation for building regions. As a post-processing, the coarse building regions are refined by separating wrongly coalesced buildings and eliminating falsely detected regions. This process is required to obtain the instance-level results. (2) In the change detection phase, we build another CNN models to classify each detected building into one of the change categories (e.g., new construction, no change and so on). For improving the accuracy of the change detection, the probability map along with the RGB imageries were jointly fed into this classification model.

The proposed pipeline was tested on two types of high resolution imageries (aerial and satellite) which contain several types of building changes such as reconstruction, demolition and new construction. On both imageries, our methodology showed remarkably good results which are competitive to those that depend on 3-D information. We also presented the performances in each phase of the entire pipeline. We concluded that by virtue of CNNs it was possible to detect building changes accurately even without 3-D information.

10431-24, Session 6

Using remote sensing and GIS in addressing the future decisions regarding underused urban spaces; Hajj sites in Mecca as case study

Ayman Imam, Univ. Politècnica de Catalunya (Spain) and

King Abdulaziz Univ. (Saudi Arabia); Josep Roca, Univ. Politècnica de Catalunya (Spain)

The term Underused Urban Spaces (UUS) refers to spaces within urban areas that have become unused, or that are being used to a lesser degree than they could or should be. The Islamic pilgrimage sites known as Hajj sites (HS) are considered form of the UUS concept as they are used lesser degree than they should be. However, the emergence of such spaces has therefore encouraged researchers, urban planner, social and local authorities to discuses about the appropriate decision regarding their future towards conversion or alternatively using those spaces in order to achieve positive social, economic and environmental benefits, according to Pagano & Bowman (2000), UUS can be a powerful tool for governments and investors to use during the urban growth (UG) of their cities. Since, remote sensing and GIS technologies are used recently to study and analyze the UG of cities; the main objective of this paper is to demonstrate the efficiency of those technologies in addressing the future decisions regarding the underused status of Hajj sites in relation to UG of the city of Mecca. Tow classified land cover maps of Mecca for two years (1998 and 2013), in addition to entropy index and multiple regression analyses were utilized in order to quantify the relationship between HS and Mecca UG. The results showed that the urban growth of Mecca has increased by approximately 56%, and almost 32% of that increased were around HS in on hand, and on the other hand the entropy and the regression analysis showed that there is 51% probability that the future growth to be also around HS. These findings will better addressing the future decisions regarding the underused status of HS, simultaneously revel that the use of RS and GIS was highly effective to be adopted within similar cases of UUS.

10431-25, Session 6

2D Intensity images from sparse lidar data in urban environment

Imran Ashraf, Soojung Hur, Yongwan Park, Yeungnam Univ. (Korea, Republic of)

Light Detection And Ranging (LIDAR) has become part and parcel of ongoing research in remote sensing. Although LIDAR efficiently captures data during day and night alike, yet data accuracy is affected involving altered weather conditions. LIDAR data fusion with sensors like color camera, hyperspectral camera and RADAR proves to be a viable solution not only to improve quality of data but to produce high definition color data; as LIDAR cannot capture color information and is low resolution. LIDAR 3D point cloud is transformed in 2D intensity images for the said purpose. In spite that LIDAR produces a large number of points per frame (between 1 to 1.3 million for 360° scan), while generating images for limited Field of View (FoV) data sparsity results in poor quality images. Moreover, 3D to 2D data transformation also involves data loss which further deteriorates the quality of images. This research focuses on generating intensity images from LIDAR data by utilizing interpolation techniques including Bi-linear, Nearest Neighbor and Bi-cubic interpolation. The main focus is to test the suitability of interpolation methods for 2D image generation, evaluate the performance of interpolation methods and analyze the quality of the generated 2D image. Furthermore, since the generated images contain noise and blur; Symmetric Median, Weiner, Hybrid Median filter and morphological operations are used to improve the quality of images. Generated images can further be used for data fusion purpose. Results show that Bi-linear interpolation and Symmetric Median filter outperforms other selected methods.

10431-26, Session 6

Implication of relationship between natural impacts and land use/land cover (LULC) changes of urban area in Mongolia

Byambakhuu Gantumur, Falin Wu, Yan Zhao, BeiHang Univ. (China); Battsengel Vandansambuu, Enkhjargal Dalaibaatar, National Univ. of Mongolia (Mongolia); Fareda Itiritiphan, Dauryenbyek Shaimurat, Beihang Univ. (China)

Urban growth can profoundly alter the urban landscape structure, ecosystem processes, and local climates. Timely and accurate information on the status and trends of urban ecosystems is critical to develop strategies for sustainable development and to improve urban residential environment and living quality. Ulaanbaatar city was urbanized very rapidly caused by herders and farmers, many of them migrating from rural areas, have played a big role in this urban expansion (sprawl). Today, 1.3 million residents for about 40% of total population of Mongolia are living in the Ulaanbaatar region. The human activities of these 1.3 million residents influence stronger to green environments. The aim of this study is to detect the change of land use/land cover (LULC) caused by human activities and estimate the trend of this area future by remote sensing and statistical methods. The implications of analysis are provided by change detection methods of LULC, remote sensing spectral indices including normalized difference vegetation index (NDVI), normalized difference water index (NDWI) and normalized difference built-up index (NDBI). In addition, it can relate to urban heat island (UHI) provided by using Land surface temperature (LST) with local climate issues. Statistical methods for image processing are used to define relations between those spectral indices and change detection images and regression analysis for time series trend in future. Remote sensing data are used by Landsat (TM/ETM+/OLI) satellite images over a period of five years from 1990 to 2016. The advantage of this study is that the methods are to detect the change with statistical analysis on LULC image processing. The experimental results show that forests, pastoral land, protected green area and water buffer zones are decreased and ger area (Mongolian housing districts) in green belt, urban expansion area and agricultural lands are increased in this urban area.

10431-27, Session 7

Towards a rational use of loading and unloading areas in urban environments

Daniel Barba, Sergio Garcia-Villanueva, Hector Del-Campo-Pardo, Univ. de Valladolid (Spain); Juan A. March, RDNest (Spain); Diego R. Llanos, Univ. de Valladolid (Spain) and RDNest (Spain)

Despite the efforts of the authorities, that promote the use of other transportation systems, the traffic still increases in European cities, leading not only to traffic jams but also to pollution episodes. Delivery vehicles are part of both problems, because of their intensive use, the advent of e-commerce, the limited number and sizes of loading and unloading areas in many ancient European cities, and the difficulties associated to keeping track of the correct use of these spaces.

In this work we propose an holistic solution to the management of delivery vehicles in urban environments. Our solution is based on the use of LEB (Low-Energy Bluetooth) devices provided by the local authority to delivery vehicles. With the help of low-cost, low-power antennas with Bluetooth and 4G capabilities installed next to each loading and unloading area, the authorities are able to know in real time (a) the use of these areas by delivering vehicles, (b) the paths of the vehicles while they travel across the city, (c) the time spent in each area by each one of them, and (d) with the help of a mobile/tablet App,

the local police can check in seconds the permissions of each vehicle using these public spaces. Moreover, the use of a GIS-based platform allows the Traffic Department to track online each particular vehicle, based on the loading/unloading spaces being used, and to infer the most representative paths they follow, an information that may guide the decision about where these spaces are really necessary and whether each particular vehicle follows their associated usage rules.

One of the main advantages of this solution is that the technology involved is relatively inexpensive: LEB emissors cost are falling, and many DIY platforms such as Raspberry Pi 3 comes with Bluetooth and WiFi connectivity. In this paper we will examine in detail the design space of each solution, with the main advantages and drawbacks for each alternative. Moreover, we will explore the possibility of using these antennas to also measure pollution, thanks to the use of ozone, particulate matter, carbon monoxide, suflur dioxide, and nitrous oxide solid-state sensors. Other sensors to measure light and noise pollution are also simple to add, making these antennas the all-in-one solution for smart cities sensing.

10431-28, Session 7

Valorisation of urban elements through 3D models generated from image matching point clouds and augmented reality visualization based in mobile platforms

Luís F. E. S. C. Marques, Univ. Politècnica de Catalunya (Portugal); Josep Roca, Univ. Politècnica de Catalunya (Spain); José A. Tenedório, Univ. Nova de Lisboa (Portugal)

The use of multiple sets of images with high level of overlapping to extract 3D point clouds has increased progressively in recent years. There are two main fundamental factors in the origin of this progress. In first, the image matching algorithms has been optimised and the software available that supports the progress of these techniques has been constantly developed. In second, because of the emergent paradigm of smart cities which has been promoting the virtualization of urban spaces and their elements. The creation of 3D models for urban elements is extremely relevant for urbanists to constitute digital archives of urban elements and being especially useful for enrich maps and databases or reconstruct and analyse objects/areas through time, building and recreating scenarios and implementing intuitive methods of interaction. These characteristics assist, for example, higher public participation creating a completely collaborative solution system, envisioning processes, simulations and results.

This paper is organized in two main topics. The first deals with technical data modelling obtained by terrestrial photographs: planning criteria for obtaining photographs, approving or rejecting photos based on their quality, editing photos, creating masks, aligning photos, generating tie points, extracting point clouds, generating meshes, building textures and exporting results. The application of these procedures results in 3D models for the visualization of urban elements of the city of Barcelona. The use of Augmented Reality through mobile platforms allows understanding the city origins and the relation with the actual city morphology, (en)visioning solutions, processes and simulations, making possible for the agents in several domains, to fundament their decisions (and understand them) achieving a faster and wider consensus.

10431-29, Session 7

On-field mounting position estimation of a lidar sensor

Owes Khan, René Bergelt, Wolfram Hardt, Technische Univ. Chemnitz (Germany)

In order to retrieve a highly accurate view of their environment, autonomous cars are often equipped with LiDAR sensors. These sensors deliver a three dimensional point cloud in their own co-ordinate frame, where the origin is the sensor itself. However, the common co-ordinate system required by HAD (Highly Autonomous Driving) software systems has its origin at the center of the vehicle's rear axle. Thus, a transformation of the acquired point clouds to car co-ordinates is necessary, and thereby the determination of the exact mounting position of the LiDAR system in car coordinates is required. Unfortunately, directly measuring this position is a time-consuming and error-prone task. Therefore, different approaches have been suggested for its estimation which mostly require an exhaustive test-setup and are again time-consuming to prepare.

When preparing a high number of LiDAR mounted test vehicles for data aquisition, most approaches fall short due to time or money constraints. In this paper we propose an approach for mounting position estimation which features an easy execution and setup, thus making it feasible for on-field calibration.

10431-30, Session 7

Application of Hymap image in the environmental survey in Shenzhen, China

Wei Pan, Beijing Research Institute of Uranium Geology (China); Xiaomao Yang, Peking Univ. (China); Xuejiao Chen, Beijing Research Institute of Uranium Geology (China); Ping Feng, National Key Lab. of Remote Sensing Information and Image Analysis Technology (China)

Illegal excavation of the land surface and discharge of unqualified water are the main reason to cause environmental pollution in the urban development, and high efficient methods to localization the source area are requested for the supervision and monitoring by the administration. In this paper, airborne Hyperspectral HyMap image with Synchronous in-situ spectral data were used in mapping the distribution of granite, excavated construction site, eroded land-soil, polluted water and vegetation in Shenzhen of South China. HyMap image was measured in March 2003 with 3.5 m spatial resolution and 15 nm spectral resolution from 0.44 ?m-2.5 ?m. The Airborne raw data was calibrated and corrected with Modtran5 model and synchronous solar illuminance and atmospheric visibility to the reflectance image on the ground. The spectra of rocks, soils, water and vegetation and artificial material were obtained by ASD Field pro spectrometer in reflectance with a white reference board. In order to identify the target objects in hyperspectral image , we extracted the spectral feature of the object with their ground spectra. Both the fresh granite and sandy soil shew clearly absorption at 2200 nm ±, but the weathered granite and sandy soil will have another absorption at the wavelength from 880 nm~940 nm. The water polluted by living Sewage which is high in ammonia nitrogen and phosphorous and BOD5 get the strongest reflectance at 550 ~570 nm, while water polluted by industry sewage which is high in CODcr and heavy metal ions get the peak reflectance at 350~400 nm. Most vegetation have the same absorption wavelength but with different reflectance. In order to localize the granite and the erode soil with the corrected HyMap image with the in-situ spectral endmember, we need to resample the ground spectra of the target object to the wavelength range and spectral resolution of Hymap sensor. We tried several algorithm to identify the object in the Hymap image and find the best is spectral angle mapping (SAM) in the absorption wavelength. With this algorithm, we discriminate the unpaved granite among cement paved mine pits, the newly excavated sandy soil in the construction site and the eroded soil in the bank of reservoir with the accuracy over 95%. We fails to discriminate the artificial forest from the natural forest and grass land in the airborne image with the in-situ spectral endmember, but succeeded with the image spectral endmember extracted from the image. We did not discriminate the different water pollution in the image, but find some texture analysis method to map the possible underwater terrain and the sea farming field in the coast area.

10431-9, Session PS

Estimation and modelling of land surface temperature from Landsat images using GIS and remote sensing: a case study of Khulna City Corporation (KCC)

Tahmid Hossain, Rashed U. Zaman, Khulna Univ. of Engineering & Technology (Bangladesh)

Surface temperature increasing has become an important issue for the upcoming days and a factor in global studies. In developing countries like Bangladesh, population has been increasing rapidly with rapid change of urban environment as well as land surface temperature has been increasing with this rapid growth of urbanization. In this paper, we tried to find out the impact of land use/ land cover change on the land surface temperature of Khulna City Corporation (KCC) area. Measuring land surface temperature is one of the way to find out the urban growth of this region as it will become a vibrant area because of the construction of Padma Multipurpose Bridge connecting Khulna region to other parts of the country. Land surface temperature (LST) were estimated from the thermal bands of the Landsat 5 TM and Landsat 7 ETM+ using remote sensing and geographic information system (GIS) techniques. We used the Landsat image of 1990, 1995, 2000, 2005, 2010 and 2015 to estimate the land surface temperature of 2030. To estimate the temperature we used a regression analysis which 'r' value was 0.85. Spatial variability of surface radiant temperature caused by thermal behavior of different land cover was retrieved from satellite data by using NDVI and used to estimate LST. The land surface temperature map revealed that the land surface temperature has increased with the growth of urban areas in Khulna area and the temperature will increase about 5 degree in 2030 from the last calculated temperature of 2015.

10431-11, Session PS

Contributions of dust aerosol from riverbeds of Taiwan

Fujung Tsai, National Taiwan Ocean Univ. (Taiwan)

High concentrations of dust aerosols are often generated from the riverbeds of Taiwan. During strong winds, the PM10 (particular matter greater than 10 um) concentrations of more than 400 ug m-3 are often observed by the riverbed monitoring stations, especially in central and southern Taiwan. This study analyzes the PM10 concentrations and the meteorological data of the eight major riverbed stations in Taiwan from Sept 2010 to August 2011. The eight major rivers from north to south are Daan, Dajia, Dadu, Zhuoshuei, Gaoping, Lanyang, Beinan, and Tsengwen Rivers. To calculate the contributions of the dust particles, local riverbed dust emissions are added into a regional dust model, and two cases are selected for analyzing their contributions.

The results show that the annual averaged values for the observed PM10 range from 21 to 73 ug m-3 for the eight riverbed stations. The maximum annual averaged value is obtained from the Tsengwen riverbed station in southern Taiwan, where monthly averaged PM10 concentrations reach more than 100 ug m-3 during the months of northeasterly monsoon. The hourly PM10 concentrations of the station also exceeds the air quality standard of 125ug m-3 during 10% of the hours within a year. On the other hand, in central Taiwan where four major rivers are located, the exceedance of hourly PM10 concentrations ranges from 2% to 7% of the hours within a year, depending on the stations.

In simulating the riverbed dust concentration, the locations of the eight major river basins are compiled into 0.01 degree by 0.01 degree grid point data, and their dust emission intensities are calculated. For calculating the emission intensity, the Asian dust emission formula from Tsai et al. (2004) is applied to Taiwan's riverbeds, except that the threshold wind speed and humidity for dust generation is analyzed from each local riverbed stations. In addition, the dust emission intensity is adjusted according to the local observations. Two dust events, including Oct 26-27 and Nov 11-12, 2010, are selected for model simulation. Both observations from riverbed monitoring stations and the aerosol optical depths from satellite are used for comparison. The simulated results show that with the riverbed emissions included, the PM10 enhancement reaches a maximum of about 200 ug m-3 in central Taiwan, where the major rivers of Daan, Dajia, Dadu, Zhuoshuei are located. Vertically, the PM10 concentrations are enhanced by more than 10 ug m-3 within 1-2 km above surface in central Taiwan, and by 100 ug m-3 within 1 km above surface in southern Taiwan. The contribution of riverbed emission in Taiwan depend on the wind intensity. In the first dust event when northeasterlies are weak, dust emissions from the major riverbeds of Taiwan accounts for less than 10% of the atmospheric PM10 concentrations of the island, while in the second dust event when northeasterlies are strong, the dust contributions reach more than 30%.

10431-31, Session PS

State estimation with incomplete nonlinear constraint

Yuan Huang, Xueying Wang, Wei An, National Univ. of Defense Technology (China)

Kalman filters are commonly used to estimate the state of a dynamic system based on its state process and measurement models. In practice, a large amount of prior knowledge can be used to enhance the filter performance. For example, when a vehicle is traveling on a known road, be it straight or curved, the state of vehicle is constrained. Recently, a rigorous analytic method was proposed to incorporate the linear constraint into state estimation. However, the work about nonlinear constraint is rare. Actually, nonlinear constraint is more common, the road is almost curved. Unfortunately, it is hard to find the close-form solution for state estimation with nonlinear constraint. Project method and numerical optimization method are combined to obtain result in many papers. It is usually assumed that the nonlinear constraint is known prior. However, this prior knowledge may be not available in practice scene. In this paper, we present a method that deal with the state estimation with unknown nonlinear constraint.

In this paper, we consider a second-order sate constraint function. An ellipse can be viewed as a second-order approximation to an arbitrary nonlinearity. A fitting algorithm of ellipse is proposed firstly. In many geometric fitting algorithms, the error distance is usually defined with the orthogonal distance from the given points to the geometric feature to be fitted. It is suppose that the mean of the error distance is zero. However, it is not apply to the scene mentioned in this paper. In this paper, a 2D radar is assumed to report measurements in polar coordinates, including range and azimuth, the measurement noise assumed to be zero-mean white Gaussian noise with known variances. Then, the statistic properties of the target position in X-Y plane is complicate because of the nonlinear relationship with original radar measurements. Furthermore, the mean of error distance defined above is nonzero, the unscented transform (UT) is adopted to obtain the statistic properties of error distance defined above and a new error distance is redefined. The fitting problem is transformed to the nonlinear estimation problem. Various numerical methods can be used to address the nonlinear estimation problem. In this paper, it is based on a computational algorithm that iteratively finds the ellipse parameters. The Golub method is used to obtain the inverse of the Jacobian matrix. Further, an approximate method is used to obtain the step size for reducing the iterations. The estimated ellipse function is used to approximate the nonlinear constraint. Then, the typical nonlinear constraint methods proposed in recent works can be used to constrain the target state.

A ground vehicle is assumed to travel along a circular road segment in the simulation part. The proposed Kalman filter is evaluated with a comprehensive comparison against recently work, unconstrained nonlinear filtering methods as well as the Posterior Cramer-Rao Lower Bound(PCRLB). The proposed method achieve a better performance than unconstrained

nonlinear filter. However, it is sensitive to the measurement noise. Monte-Carlo simulation results are presented to illustrate the effectiveness of the proposed method.

10431-32, Session PS

City landscape changes effects on land surface temperature in Bucharest metropolitan area

Dan M. Savastru, Maria A. Zoran, Roxana S. Savastru, National Institute of Research and Development for Optoelectronics (Romania); Adrian I. Dida, Transylvania Univ. of Brasov (Romania)

Knowledge of the current changes and dynamics of different urban land cover types in relation to climate changes and anthropogenic activities is critical for mitigation strategies to address the thermal environment challenges for ecosystem. Due to several anthropogenic sources and climate changes, cities are vulnerable to climate extremes like heat waves. The overwarming of urban areas due to the urban heat island effect in synergy with heat waves adds to the general effect of global temperature increase. Associated meteorological variables like humidity, wind speed or radiation significantly affects human health and urban ecosystems. From an energetic perspective, a side effect coming along with the excessive warming is an increase of cooling demand in summer and a projected decrease of heating load in winter. This aspect can result on the one hand in increased demand of energy and higher emissions in summer, but on the other hand, a positive feedback on wintertime energy consumption and an increase of air pollution. This study investigated the influences of city land cover changes and extreme climate events on land surface temperature in relationship with several biophysical variables in Bucharest metropolitan area of Romania through satellite and in-situ monitoring data. Remote sensing data from IKONOS, Landsat TM/ETM+ and time series MODIS Terra/Aqua and NOAA AVHRR sensors have been used to assess urban land cover– temperature interactions over 2000 - 2016 period. Time series Thermal InfraRed (TIR) satellite remote sensing data in synergy with meteorological data (air temperature- AT, precipitations, wind, solar radiation, etc.) have been applied mainly for analyzing land surface temperature (LST) patterns and its relationship with surface landscape characteristics, assessing urban heat island (UHI), and relating urban land cover temperatures (LSTs) with surface energy fluxes to characterize landscape properties, patterns, functions and processes. Vegetation abundances and percent impervious surfaces were derived by means of linear spectral mixture model, and a method for effectively enhancing impervious surface has been developed to accurately examine the urban growth. The land surface temperature, a key parameter for urban thermal characteristics analysis, was also analyzed in relation with the Normalized Difference Vegetation Index (NDVI) at city level. Based on these parameters, the urban size dynamics, urban heat island effect (UHI) and the relationships of LST to other biophysical and meteorological parameters (surface albedo, precipitations, wind intensity and direction, air temperature) have been analyzed. Results show that in the metropolitan area ratio of impervious surface in Bucharest increased significantly during investigated period, the intensity of urban heat island and heat wave events being most significant. The correlation analyses revealed that, at the pixel-scale, LST and AT possessed a strong positive correlation with percent impervious surfaces and negative correlation with vegetation abundances at metropolitan scale respectively. The NDVI was significantly correlated with precipitation. The spatial average air temperatures in urban test areas rise with the expansion of the urban size. This analysis provided an integrated research scheme and the findings can be very useful for urban ecosystem modeling, mitigation strategies and future planning.

10431-33, Session PS

Urban green land cover changes and their relation to climatic variables in an anthropogenically impacted area

Maria A. Zoran, National Institute of Research and Development for Optoelectronics (Romania); Adrian I. Dida, Transylvania Univ. of Brasov (Romania)

Urban vegetation land cover change is a direct measure of quantitative increase or decrease in sources of urban pollution and the dimension of extreme climate events and changes that determine environment quality. The shape and form of urban vegetation reflectance spectra depends on many factors such as vegetation structure, leaf biochemical composition, soil background, and the view and illumination geometry.

With the rapid change of Bucharest metropolitan area in Romania, during the past decades, urban green was fragmented and dispersed causing impairment and dysfunction of these important urban elements. Climate variability and change can exert profound stresses on urban green environment, which are sensitive to heat waves, droughts, and changes in the frequency of precipitations. As future climate trends have been predicted to increase the magnitude and negative impacts of urban heat waves in metropolitan areas, there is an urgent need to be developed adequate strategies for societal vulnerability reducing. Urban green areas are experiencing rapid land cover change caused by human-induced land degradation and extreme climatic events. Vegetation index time series provide a useful way to monitor urban vegetation phenological variations. This study quantitatively describes Normalized Difference Vegetation Index NDVI) /Enhanced Vegetation Index (EVI) and Leaf Area Index (LAI) temporal changes for Bucharest metropolitan region land cover in Romania from the perspective of vegetation phenology and its relation with climate changes and extreme climate events. The time series from 2000 to 2016 of the NOAA AVHRR and MODIS Terra/Aqua satellite data were analyzed to extract anomalies. Urban/periurban vegetation phenology analyses were developed for diverse urban green land-covers test sites providing a useful way to analyze and understand the phenology associated to those land-covers. Time series of climatic variables were also analyzed through anomaly detection techniques and the Fourier Transform. Correlations between NDVI/EVI time series and climatic variables were computed. Temperature, rainfall and radiation were significantly correlated with almost all land-cover classes for the harmonic analysis amplitude term.However, vegetation phenology was not correlated with climatic variables for the harmonic analysis phase term suggesting a delay between climatic variations and vegetation response. Training and validation were based on a reference dataset collected from IKONOS high resolution remote sensing data. The mean detection accuracy for period 2000- 2016 was assessed to be of 87%, with a reasonable balance between change commission errors (19.3%), change omission errors (24.7%), and Kappa coefficient of 0.73. This paper demonstrates the potential of moderate - and high resolution, multispectral imagery to map and monitor the evolution of the physical urban green land cover under climate and anthropogenic pressure.

10431-34, Session PS

Metal-coated optical fibers for high temperature sensing applications

Janusz D. Fidelus, Karol Wysokinski, Tomasz Stanczyk, Agnieszka Kolakowska, Piotr Nasilowski, Stanislaw Lipinski, Tadeusz Tenderenda, Tomasz Nasilowski, InPhoTech (Poland)

Recently, tremendous attention is focused on fiber optic sensors (FOS). Due to their remarkable properties fiber optics have revolutionized a multitude of various sensing applications, including sensing in harsh environments [1].

Although, the technology for manufacturing FOS is already highly developed, there are still a few aspects that are severely problematic, such as performance of optical fibers in high temperatures. The problem of increasing fibers' temperature reliability becomes very important when FOS have to operate at elevated temperatures (above 400°C). Although, silica is a material which is commonly recognized as a high temperature resistant material, silica optical fibers degrade quickly when exposed to temperatures above 300 - 400 ?C because of formation of microcracks due to hydrolysis taking place on the surface of the fiber [2]. These microcracks can initiate a critical gap creation leading to severe deterioration of mechanical parameters of the fibres or even their destruction. This obstacle can be overcome by deposition of metals on the fiber's surface, which will protect it from external environment.

In this work we discuss the impact of a high-temperature and different gasses on the mechanical parameters of developed metal coated fibers and compare their reliability with commercially available copper coated fibers. The technology of deposition different metals (such as copper, nickel and gold) as well as their combination were elaborated by InPhoTech.

Characterization of elaborated materials and selected study such as thermal shock, cyclic tests together with tensile and bending tests will be presented.

The obtained results may find application in both the scattered sensors of temperature and strains based on the Brillouin/ Raman scattering, point sensors based on Bragg gratings and point gas sensors operating in the steel industry, mines and chemical industry.

[1] B. Culshaw et al. "Fiber-Optic Sensing: A Historical Perspective," J. Light. Technol., vol. 26, no.9, May (2008).

[2] Rayss, J.; Widomski, J.; Podko?cielny, W.M. Optoelectron. Rev., 3–4, 107–109, (1995).

10431-35, Session PS

Monitoring and localization hydrocarbon and sulfur oxides emissions by SRS-lidar

Alexsandr S. Grishkanich, ITMO Univ. (Russian Federation); Dmitry N. Redka, Saint Petersburg Electrotechnical Univ. "LETI" (Russian Federation)

We developed lidar for UAV drone with hyperspectral resolution ? / ?? ≥ 1000. Hyperspectral resolution is realized by a polychromator based on stigmatic holograms gratings with an auto-alignment system. Field tests were conducted. At a distance of 150 m, the lidar detects sulfur oxides and hydrocarbons with 1 ppm sensitivity.

10431-36, Session PS

Speed scanning system based on solid-state microchip laser for architectural planning

Alexsandr S. Grishkanich, ITMO Univ. (Russian Federation); Dmitriy N. Redka, Saint Petersburg Electrotechnical Univ. "LETI" (Russian Federation); Konstantin Tsvetkov, JSC Shipbuilding & Ship Repair Technology Ctr. (Russian Federation)

According to the current great interest concerning Large-Scale Metrology applications in many different fields of manufacturing industry, technologies and techniques for dimensional measurement have recently shown a substantial improvement. Ease-of-use, logistic and economic issues, as well as metrological performance, are assuming a more and more important role among system requirements. The project is planned to conduct experimental studies aimed at identifying the impact of the application of the basic laws of solid-state microchip as radiators on the linear-angular characteristics of existing measurement systems. The project is planned to conduct experimental studies aimed at identifying the impact of the application of the basic laws of microlasers as radiators on the linear-angular characteristics of existing measurement systems for architectural planning. The system consists of a distributed network-based layout, whose modularity allows to fit differently sized and shaped working volumes by adequately increasing the number of sensing units. Differently from existing spatially distributed metrological instruments, the remote sensor devices are intended to provide embedded data elaboration capabilities, in order to share the overall computational load.

10431-37, Session PS

Spatio-temporal variability of urban heat islands in local climate zones of Delhi-NCR

Bakul Budhiraja, Shiv Nadar Univ. (India); Prasad Pathak, Nalanda Univ. (India); Girish Agrawal, Shiv Nadar Univ. (India)

Land use change is at the nexus of human territory expansion and urbanization which causes significant variation in climatological interactions between the land surface and earth's atmosphere. Human intrusion disturbs the natural heat energy balance of the area, although a new equilibrium of energy flux is attained but with greater diurnal range and adversely affecting the geo/physical variables. Urban or regional climate is determined by these geo/physical variables namely soil moisture, vegetation cover, land surface temperature, surface net radiation, albedo, downward and upward long wave flux. Modification in the trend of these variables causes a phenomenon known as urban heat Island i.e. a dome of heat is formed around the city which has 7-10 ?C high temperature than the nearby rural area at night.

The study focuses on Surface UHI conventionally studied using thermal band of the remotely sensed satellite images. All matter with a temperature greater than absolute zero emits thermal radiation which is determined through Land Surface Temperature (LST) to understand SUHI. Monthly Land Surface Temperature is determined for the year 2005 and 2015 using Landsat archive for Delhi National Capital Region (NCR). This region was chosen because it is the biggest urban agglomeration in India, many satellite cities are coming in periphery and it has temperate climate with no sea nearby to balance rising urban heat. The mono-window algorithm has been applied using NDVI for emissivity correction as even for Landsat 8 split window techniques is not advisable for LST retrieval according to USGS. Quantification of UHI is predictably done using UHI intensity that is the difference between representative Urban and rural temperature. Recently the definition of urban and rural has been questioned because of various kinds of configurations of urban spaces across the globe. Delhi NCR urban configurations vary spatially - thus one UHI intensity does not give a deep understanding of the micro-climate.

Advancement was made recently to standardize UHI intensity by dividing city into Local climate Zones (LCZ) which goes beyond the division of urban and rural, comes with 16 broad categories with scientific parameter limits to be applied to cities. LCZ map of Delhi NCR has been created with modifications to apply to this specific city. Zonal analysis is performed to check the frequency distribution of LST in each LCZ for normal distribution fitting. One way ANOVA F-test in R is used to delineate the LCZ which have significant differences in there means across the year. The monthly LST variation produces heat islands as well as inverted cool islands in the months of harvest of wheat and rice. UHI intensity comparison across LCZ for SUHI yielded the changing dynamics of UHI on a temporal and micro-spatial scale.

Conference 10432: Target and Background Signatures

Monday - Tuesday 11–12 September 2017

Part of Proceedings of SPIE Vol. 10432 Target and Background Signatures III

10432-1, Session 1

Spectral characterisation of natural backgrounds

Max E. Winkelmann, Fraunhofer-Institut für Optronik, Systemtechnik und Bildauswertung (Germany)

As the distribution and use of hyperspectral sensors is constantly increasing, the exploitation of spectral features is a threat for camouflaged objects. To improve camouflage materials at first the spectral behaviour of backgrounds has to be known to adjust and optimize the spectral reflectance of camouflage materials.

In an international effort, the NATO CSO working group SCI-295 “Development of Methods for Measurements and Evaluation of Natural Background EO Signatures” is developing a method how this characterization of backgrounds has to be done. It is obvious that the spectral characterization of a background will be quite an effort. To compare and exchange data internationally the measurements will have to be done in a similar way.

To test and further improve this method an international field trial has been performed in Storkow, Germany.

We will report about the field trial and the lessons learned derived from the trial. Furthermore an outlook will be provided about the findings and results of the measurement campaign.

10432-2, Session 1

Angular dependance of spectral reflection for different materials

Pascal Kiefer, Max E. Winkelmann, Fraunhofer-Institut für Optronik, Systemtechnik und Bildauswertung (Germany)

Reflectance spectra of different vegetative background areas are measured and their features analyzed. It is shown that the measurement angle has an important impact on the absolute reflection values. Furthermore the influence of humidity is discussed.

By analyzing bark samples one could verify that the amount of chlorophyll in the scenery has a direct impact on the reflectance values, resulting in strong chlorophyll absorption at around 0.7μm. Two different bark measurements with a time interval of two years showed the same qualitatively behavior, so the results are reproducible.

Different grass sceneries with flowers also were discussed. The analyzed spectra also showed absorption due to the presence of chlorophyll. The qualitative behavior of all flower sceneries is the same, while deviations in the absolute value of the reflectance lead to the conclusion that the measurement angle has a significant impact on the absolute reflectance. A comparison with measurement values of another grass scenery from the ASTER database strengthens the produced arguments by showing the same qualitative behavior.

The analysis of the impact of the measurement angle on the reflectance values was continued by analyzing spectroscopic data of tarmac and cobblestone. While showing the same qualitative behavior, the measurement values differed greatly for different measurement angles. Just by varying the measurement angle the reflectance values changed up to 20%. Therefore, one should always take into account the sun angle and the measurement angle. A comparison with reflectance data of the ASTER database justified the measurement results.

Analyzed measurements of dry grass were similar to the flower and grass scenery. By comparing the measured data with the data of the ASTER database, one could notice a deviation at 0.7μm. The measurement data of the ASTER database does not show any presence of an absorption peak, while the measured data did. This lead to the conclusion that the analyzed grass of the ASTER data had to be a lot drier than the analyzed one. The analyzed grass scenery had a small portion of green grass, which leads to light absorption due to chlorophyll.

By comparing the measurement data of the different sceneries, one could verify that the humidity of the sample has a direct impact on the magnitude of the water absorption. Dry grass only shows a weak absorption due to the presence of water while the grass and flower scenery with living plants show a strong absorption. Even bark shows signs of water absorption. Of course, the absorption there is a lot smaller due to the thick bark layer between the tree trunk and the measurement sensor. Tarmac and cobblestone do not show any signs of water absorption.

10432-3, Session 1

Optical polarization: background and camouflage

Christina Åkerlind, Tomas Hallberg, Johan Eriksson, Hans M. Kariis, David Bergström, FOI-Swedish Defence Research Agency (Sweden)

The infrared polarimetric sensor technology development has matured in terms of availability and performance in recent years. The technology aims at revealing difficult, concealed and camouflaged targets.

A signature is nothing on its own, but always something that results as a contrast between a target and a background. To enable a reinforced signature reduction against this approaching technology threat, there is a need to polarimetrically study the background and possibilities of improved concealment and disguise from an optical polarimetric sensor technology. A brief review is made of the available literature on background and environmental optical (mainly IR) polarization properties.

Polarimetric imaging sensors in the electro-optical region, already military and commercially available in both the visual and infrared, show enhanced capabilities for advanced target detection and recognition. The capabilities arise due to the ability to discriminate between man-made and natural background surfaces using the polarization information of light. A brief overview will be given on polarimetric sensor functionality.

In the development of materials for signature management in the visible and infrared wavelength regions, different criteria need to be met to fulfil the requirements for a good camouflage against modern sensors. In conventional camouflage design, the aimed design of the surface properties of an object is to spectrally match or adapt it to a background and thereby minimizing the contrast given by a specific threat sensor. Dimensioning properties relevant in an optical camouflage polarimetric perspective (such as degree of polarization and the azimuth angle) will be discussed.

A discussion is included on potential military uses for polarimetric technologies for sensing as well as of how polarimetric countermeasures can be realized.

Optical polarization properties will be discussed from different aspects, and an attempt to illustrate relevance from different perspectives; from physical properties to military utility.

Together with a sensor analysis this paper will contribute to understanding of the sensor-signature duel at a future battlefield comprising polarization sensitive optical sensors.

10432-4, Session 1

Selected issues connected with determination of requirements of spectral properties of camouflage patterns

Franti?ek Racek, Univ. of Defence (Czech Republic); Adam Jobánek, Military Research Institute, s. p. (Czech Republic); Teodor Balá?, Jaroslav Krejcí, Univ. of Defence (Czech Republic)

Despite of the design details of individual CC&D concepts, camouflage pattern creation usually begins with relevant backgrounds scientific mapping and ends with set of requirements for camouflage material production. Once the material or product is manufactured, it is necessary to control if desired parameters are achieved and in case of camouflage properties, it should be done quite properly since it is directly connected to soldiers' safety. Validation process of initial spectral requirements fulfilment carrying out with the camouflage materials (e.g. prints) in lab conditions plays crucial role on a way to the better camouflage. One of the important issues within this procedure is how to DEFINE spectral properties of final camouflage materials.

Traditionally spectral reflectance of the material is measured and compared with permitted spectral reflectance boundaries. The boundaries are limited by upper and lower curve of spectral reflectance. The boundaries for unique color has to fulfil the operational requirements as a versatility of utilization through the all year seasons, day and weather condition on one hand and chromatic and spectral matching with background as well as the manufacturability on the other hand. The interval between the boundaries suffers with ambivalent feature. Camouflage pattern producer would be happy to see it much wider, but blending effect into its particular background could be better with narrower tolerance limits. From the point of view of long time user of camouflage pattern battledress, there seems to be another ambivalent feature. Width of the tolerance zone reflecting natural dispersion of spectral reflectance values allows the significant distortions of shape of the spectral curve inside the given boundaries.

It will be presented in the paper the overview of the selected method of determination of requirements on properties of chromatic and spectral features of the camouflage patterns across the European, NATO or armed forces of advanced countries. Furthermore, it will be illustrated the potential variability of shape of spectral curves still fit into the boundaries of exemplar standard tolerance zone. It will be also presented the example of measurement of spectral features of camouflage battledresses affected by different time and way of usage. It will illustrate a variability span of spectral features with regard to requested initial spectral boundaries for newly acquisitioned materials. Such ageing aspects are currently usually out of the subject of defense standards for military acquisition of camouflage materials.

Presented experimental data indicate, that the factual battledress color patch can vary inside the tolerance boundaries the way that can change the overall chromatic and spectral properties of the camouflage. Authors denote how tracking of two significant features (the chlorophyll peak and red edge) could be used for advanced determination of the spectral properties of the camouflage pattern. The explicit shape of spectral curves leads to employment of techniques of spectral curves similarity comparison together with the traditional defining the limits of spectral boundaries. It will also be included the introduction of possible technique for spectral similarity determination.

Research of impact of extended spectral requirements on patterns camouflage effectiveness improvement is considered follow-on activity.

10432-6, Session 1

Methods for evaluation of camouflage effectiveness: a comparison of assessment methods based on human observers and CAMAELEON simulations

Daniela H. Heinrich, Gorm K. Selj, Norwegian Defence Research Establishment (Norway)

Military operations in different environments all over the world require adapted camouflage patterns. Developing optimized camouflage patterns relies on valid methods. In this paper we focus on evaluation methods for military textiles which are an important part of protection measures for soldiers. To find the best performing pattern for given environments we applied observer trials. The observer trials used human observers for camouflage evaluations. Qualified military observers did search for targets placed in natural settings presented on a high resolution PC screen and the detection times were recorded. Effectiveness of camouflage patterns could be ranked according to the recorded times of detection. We found this method to be reliable and to give valid results. CAMAELEON is another camouflage evaluation method which bases the evaluation on simulations. CAMAELEON is a licensed tool that uses pictures of camouflaged targets in chosen surroundings and ranks the camouflaged targets by their similarity with local backgrounds. The similarity is estimated through the parameters local contrast, orientation of structures in the pattern and spatial frequency, by mimicking the response/signal processing in the visual cortex of the human eye. Appling those two methods to the same images with camouflaged targets we found that CAMAELEON simulations results didn't match observer trials results for targets with disruptive patterns. This induced us to do a follow up study to learn more about the advantages and pitfalls of CAMAELEON. During recent observer trials we studied new camouflage patterns and the effect of additional equipment, namely combat vests. In this paper we will present the results from a study comparing evaluation results of observer trials and CAMAELEON.

10432-7, Session 1

Hyperspectral discrimination of camouflaged target

Vojtech Bárta, Franti?ek Racek, Univ. of Defence (Czech Republic)

The acquisition system takes place as an initial part of Fire Control System (FCS) of general weapon system. The elements of acquisition system discriminate the target on the background and it distinguish all the required information for the FCS correct operation. A plenty of different systems and physical principles can be used to fulfil the tasks of acquisition system. Besides the conventional target location techniques, all the appropriate modern techniques are brought into the service. Generally, to maximize the effect of acquiring system the number of optical, electro-optical, acoustic, and radio frequency sensors are combined as well as usage of the advanced data processing.

The modern electro-optical observation device capable of acquisition of complex target data is imaging spectrometer, in other words the hyperspectral camera. Hyperspectral imaging is utilised for both its wide spectral range possibility and above all, its high spectral resolution. Due to its significant spectral properties, the HS Imaging is destined for discrimination of camouflaged targets.

In the introduced study, the hyperspectral imaging has been utilized for discrimination of camouflaged targets on the background. A lots of identification methods are known. Among them, we used a supervised method of classification which has made use of spectral similarity measurements as for example spectral angle mapper (SAM), spectral cross correlation (SCC) or spectral information divergence (SID). It was tested the proposed methodology to discriminate the

camouflaged targets from the background upon the arranged scenery. Considering the arranged scenery allowed us, not only verify the performance results, but also to determine its efficiency. The presented methodology can in future find its utilization in advanced acquiring systems of upcoming FCS.

10432-8, Session 2

Hyperspectral target detection analysis of a cluttered scene from a virtual airborne sensor platform using MuSES *(Invited Paper)*

Corey D. Packard, Timothy S. Viola, Mark D. Klein, ThermoAnalytics, Inc. (United States)

The ability to predict spectral electro-optical (EO) signatures for various targets against realistic, cluttered backgrounds is paramount for rigorous signature evaluation. Knowledge of background and target (with plume) signatures is essential for a variety of defense-related and scientific applications including contrast analysis, camouflage development, automatic target recognition (ATR) algorithm development and scene material classification. The capability to simulate any desired mission scenario with forecast or historical weather is a tremendous asset for defense agencies, serving as a complement to (or substitute for) target and background signature measurement campaigns. In this paper, a systematic process for the physical temperature and visible-through-infrared radiance prediction of several diverse targets in a cluttered natural environment scene is presented. The ability of a virtual airborne sensor platform to detect and differentiate targets from a cluttered background, from a variety of sensor perspectives and across numerous wavelengths in differing atmospheric conditions, is considered. The process described utilizes the thermal and radiance simulation software MuSES and provides a repeatable, accurate approach for analyzing wavelength-dependent target and background signatures in multiple band-integrated wavebands (multispectral) or hyperspectrally. This virtual radiance prediction procedure has been extensively validated and provides a flexible process for signature evaluation and algorithm development.

Accurate thermal-band infrared signature prediction of targets (such as ground vehicles with engine and exhaust heating) depends primarily on the realistic prediction of physical temperatures. These temperatures must be calculated by a transient solver that combines environmental effects and all modes of heat transfer to incorporate wind convection, solar insolation, thermal radiation and vertical/lateral conduction. Historical or forecast meteorological conditions from a specified date and global location can be used to predict target and background signatures under desired weather conditions, while locally-measured weather data can be used to obtain validation-fidelity simulation outputs. Geometric descriptions of the targets and faceted background elements (via 3D surface meshes) are characterized by database-specified material thermal properties and layer thicknesses. Optical surface properties of objects in the scene are described spectrally with wavelength-dependent emissivity and (diffuse and specular) reflectivity components and Sanford-Robertson BRDF parameters. Non-homogenous surface descriptions such as camouflage patterns can be employed via texture maps. Various terrain descriptions can be employed as backgrounds, and faceted topography (e.g., digital elevation maps) can be included, as can explicit representations of tree canopies, vegetation, buildings and other clutter.

Once thermal solutions have been obtained, (multi or hyper) spectral signature predictions can be generated. The resulting rendered images include thermal emissions, diffuse/specular reflections, spectral plume radiance and MODTRAN-based atmospheric effects to portray scenes from an optical sensor's perspective. In addition, scene radiances in non-thermal wavebands driven primarily by reflections of natural light (solar or lunar) can be predicted. In this work, the hyperspectral prediction of various targets in a cluttered surveillance scene is demonstrated with MuSES, and the impact of atmospheric degradation on target discernment and background characterization is illustrated. The process described in this paper provides a rigorous scientific approach for analyzing hyperspectral or band-integrated target and background signatures.

10432-9, Session 2

Hyperheat, a thermal signature model for super- and hypersonic missiles

Sven A. van Binsbergen, TNO (Netherlands); Bas van Zelderen, TNO (Netherlands) and Technische Univ. Delft (Netherlands); François Bouquet, TNO (Netherlands); Ronald G. Veraar, TNO Defence, Security and Safety (Netherlands); Ric H. M. A. Schleijpen, TNO (Netherlands)

In performance prediction of IR sensor systems for missile detection, sensor specifications and target signature are essential variables. So far, for velocities up to Mach 2-2.5, a simple model based on the aerodynamic heating of an ideal gas was used. This typically results in an overestimate of the target temperatures with correspondingly large signatures and detection ranges. Especially for even higher velocities, this approach is no longer accurate. More accurate alternatives include CFD calculations, although these typically require significant computing power.

Within TNO, the Matlab code Hyperheat was developed to calculate the time-resolved skin temperature of axisymmetric high speed missiles during flight, taking into account the behaviour of non-ideal gas and proper heat transfer to the missile surface. Allowing for variations in parameters such as missile shape, altitude, atmospheric profile, angle of attack, flight duration and super- and hypersonic velocities up to Mach 30 enables more accurate calculations of the actual target temperature. The generated skin temperature maps are calculated within minutes, even for >100 km trajectories, and can be easily converted in thermal signatures for further processing.

This paper discusses the approach taken in Hyperheat. Then, the thermal signature of a set of typical missile threats is calculated using both the simple aerodynamic heating model and the Hyperheat code. The respective signatures are compared, as well as the difference in the corresponding externally calculated detection ranges when using both methods.

10432-10, Session 2

Infrared measurements of launch vehicle exhaust plumes

Caroline Schweitzer, Norbert Wendelstein, Karin U. Stein, Fraunhofer-Institut für Optronik, Systemtechnik und Bildauswertung (Germany)

In the fields of early warning, one is depending on reliable analytical models for the prediction of the infrared threat signature: By having this as a basis, the warning sensors can be specified as suitable as possible to give timely threat approach alerts.

In this paper, we will present preliminary results of measurement trials that have been carried out during 2015 and 2017, where the exhaust plume of two different launch vehicles has been measured under various atmospheric conditions. The gathered data will be used to validate analytical models for the prediction of the plume signature.

10432-11, Session 2

Analysis of passive signatures UAV targets recorded by multispectral systems in visible and infrared ranges

Mariusz Kastek, Krzysztof Firmanty, Jaroslaw Barela, Tomasz Sosnowski, Military Univ. of Technology (Poland); Stanislaw Milewski, Jacek Zalewski, Michal Zablotny, Polish Naval Academy (Poland)

Detection of UAV (especially small drones) objects is a very demanding problem of public safety. So far, the problem of detecting small drones was considered only in the case of airports but it is becoming more and more important for public places like metro stations, and government buildings. Multispectral imaging - detection systems operating in wide spectral ranges from visible up to infrared will increase the ability to detect threats.

The measurement laboratory stand consists of multiple multispectral cameras: visible and thermal camera. The systems give possibility to record the signatures of drones. The registration was made in NWIR, SWIR and LWIR spectral bands simultaneously. The infrared cameras have possibilities install optical filters for multispectral measurement. Additionally the measurement of signatures in test fields give more information according the changes of weather conditions. The signatures recorded by cameras were analysis and some of the results as well as the measurement methodology are presented in the article.

The paper present results of field measurement signatures of a few types of UAV drones and shows results analysis of statistical parameters of that signatures, according the changes of parameters during the time and weather conditions. Presented method gives some results for the method of automatically detection of the drones which can be implemented in multispectral detection system.

10432-12, Session 2

Novel conductive polymer composite for radar signature management

Marek Strandberg, Katrin Idla, Tallinn Univ. of Technology (Estonia)

The present study is a continuation of our previous studies investigating the radar absorption properties of electrically conductive polymer, polypyrrole coated materials.

We show that lightweight panels made of non-conductive polymer and conductive polymer can reduce significantly radar cross-section (RSC). Conductive polymer composites have the reduction of reflectance as follows:

<Figure Unavailable>

These panels are lightly modified Salisbury Screen type absorbers where reducing the cross-sectional area is based on the electrical properties of the material. The key variables in our studies were the geometry of the panels and the different patterns of electrically active polymer. Both, laboratory and field tests have shown that the composite works well in frequency ranges X and Ku. The good sides of the developed panels are their lightness (600-1000 g/m2), customizability of the RSC reduction properties in a particular specific frequency range and durability of the material.

Field test results confirmed that the RSC of unmanned aerial vehicle (UAV), covered with the lightweight panels, can be reduced in X band. Radar absorbing composite can be embedded into the airplane fuselage during manufacturing process.

10432-13, Session 2

Simulation of an oil film at the sea surface and its radiometric properties in the SWIR

Frédéric Schwenger, Fraunhofer-Institut für Optronik, Systemtechnik und Bildauswertung (Germany); Alexander M. J. van Eijk, TNO Defence, Security and Safety (Netherlands) and Fraunhofer-Institut für Optronik, Systemtechnik und Bildauswertung (Germany)

The knowledge of the optical contrast of an oil layer on the sea under various surface roughness conditions is of great interest for oil slick monitoring techniques. This paper presents a 3D simulation of a dynamic sea surface contaminated by a floating oil film. The simulation considers the damping influence of oil on the ocean waves and its physical properties. It calculates the radiance contrast of the sea surface polluted by the oil film in relation to a clean sea surface for the SWIR spectral band.

Our computer simulation combines the 3D simulation of a maritime scene (open clear sea/clear sky) with an oil film at the sea surface. The basic geometry of a clean sea surface is modeled by a composition of smooth wind driven gravity waves. Oil on the sea surface attenuates the capillary and short gravity waves modulating the wave power density spectrum of these waves. The radiance of the maritime scene is calculated in the SWIR spectral band with the emitted sea surface radiance and the specularly reflected sky radiance as components. Wave hiding and shadowing, especially occurring at low viewing angles, are considered. The specular reflection of the sky radiance at the clean sea surface is modeled by an analytical statistical bidirectional reflectance distribution function (BRDF) of the sea surface. For oil at the sea surface, a specific BRDF is used influenced by the reduced surface roughness, i.e., the modulated wave density spectrum. The radiance contrast of an oil film in relation to the clean sea surface is calculated for different viewing angles, wind speeds, and oil types characterized by their specific physical properties.

10432-14, Session 3

Examination of soldier target recognition with direct view optics

Frederick Long, U.S. Army Armament Research, Development and Engineering Ctr. (United States); Gabriella Larkin, U.S. Army Research Lab. (United States); Danielle M. Bisordi, Shauna Dorsey, Damien Marianucci, Lashawnta Goss, Michael M. Bastawros, U.S. Army Armament Research, Development and Engineering Ctr. (United States); Paul Misiuda, Glenn A. Rodgers, U.S. Army Aberdeen Test Ctr. (United States); John P. Mazz, U.S. Army Materiel Systems Analysis Activity (United States)

Target recognition and identification is a problem of great military and scientific importance. However, the observation and identification of a target with a direct view optic (DVO) is a complex process involving both the optical performance characteristics of the DVO and the image processing capabilities of the human eye and brain. The initial goal of this work was to examine the threshold of target recognition with DVOs of varying magnification and to correlate DVO magnification level with a probability of recognition. In the experiment, ten U.S. Army soldiers were tasked with identifying letters on targets at 800 and 1300 meters away. Letters were selected to assess visual performance because they are a standard method for measuring visual acuity. The letters were Rockwell font letters written in black with a dark Army green background. The exact colors used were characterized using laboratory color measurements and by monitoring the illumination conditions during the experiment. The letters were approximately 90 cm high since this is the size of a well-known rifle. Four DVOs with angular magnifications of

1.5x, 4x, 6x, and 9x were used. For a set of measurements, the target range was fixed and a soldier used different magnification DVOs. The staircase method was used during the experiments to concentrate the test trials near the threshold level of performance. More specifically, to increase in DVO magnification (i.e., move up the staircase), the soldier needed to provide one incorrect letter identification; to decrease in DVO magnification (i.e., move down the staircase), the soldier needed to provide four consecutive correct identifications. This adaptive sampling approach enabled calculation of actual probabilities for correct identification.

Previous scientific literature suggests that human target recognition can be viewed as a linear response problem in angular frequency space using the established values for the contrast sensitivity function for a healthy human eye and the experimentally measured modulation transfer function of the optic. This physics based approach allows target recognition to be described in terms of measurable parameters, such as luminance and target contrast. At the highest magnification of 9x, the soldiers could identify the letters with almost no errors (i.e., 97% probability of correct recognition). At lower magnification, errors in letter identification were more frequent. Moreover, it was found that the identification errors for the letters were not random, but occurred most frequently with a few pairs of letters, such as O and Q. This observation is consistent with the literature for letter recognition and can be attributed to the high angular frequency components that differentiate the O and Q. In the small subject sample of ten soldiers, there was considerable variation in the observer recognition capability at 4x and a range of 800 meters. This can be directly attributed to the variation in the observer visual acuity. Ultimately, even though quantification of human variability in target recognition is limited, an understanding of the role of human variability in target recognition is of considerable scientific and practical importance.

10432-15, Session 3

Dependency of human target detection performance on clutter and quality of supporting image analysis algorithms in a video surveillance task

Samuel W. Huber, Forventis-GmbH (Switzerland); Patrick Dunau, Fraunhofer-Institut für Optronik, Systemtechnik und Bildauswertung (Germany); Peter Wellig, Armasuisse (Switzerland); Karin U. Stein, Fraunhofer-Institut für Optronik, Systemtechnik und Bildauswertung (Germany)

In target detection, the success rates depend strongly on human observer performances. Two prior studies tested the contributions of target detection algorithms and prior training sessions. The studies used simulated, highly cluttered video sequences. The aim of this Swiss-German cooperation study is to evaluate the dependency of human observer performance on the quality of supporting image analysis algorithms. The evaluation is done by measuring the workload using the reaction times for a concurrent task.

To test the human observer performances video simulation trials are conducted. The organization of these trials can be split into a training and a test phase. During the training phase, the human observers watch typical video sequences and still images of the desired target objects. They then are being trained to detect avatars wearing backpacks within a cluttered public area. The second phase of the trial contains the video sequence tests. The participants have to watch 15 different video sequences. Each video sequence shows a heavily cluttered public area. In each video sequence, the viewing angle and also the number of subjects walking in the area are altered. The number of presented avatars in the area is fixed to 100, 150 and 200 subjects. The number of targets appearing is kept constant at a prevalence rate of 10%. Furthermore, the number of marked targets by the target detection system has been varied from 0, 5, 10, 20 up to 40 marked subjects while keeping the positive predictive value of the detection algorithm at 20%. Hence, in the 100 avatars condition, 10 targets will appear. For this case, the numbers of targets included in the marks are given in brackets after the number of marks: 0 (0), 5 (1), 10 (2), 20 (4), 40 (8). Equivalently, these numbers are given for 15 targets (150 avatars condition) and 20 targets (200 avatars condition), respectively; 15 targets: 0 (0), 5 (2), 10 (3), 20 (6), 40 (12); 20 targets:

0 (0), 5 (2), 10 (4), 20 (8), 40 (16). The task for the observers is to detect all targets in the shortest possible time. Additionally, a secondary task to measure the workload condition is applied where the participants have to react upon the appearance of a visual stimulus by pressing an assigned key on a keyboard. From the trials, the detection rates and detection times for the target subjects are recorded. Furthermore, the reaction times to acknowledge the secondary stimulus are recorded.

The trial tests for the hypothesis that an increase of avatars decreases detection rates and increases detection times while increasing workload at the same time. Additionally, it is expected that the increase of marks lowers detection performances, hence decreasing detection rates, increasing detection times and increasing workload. The evaluation is done using inferential and descriptive statistics.

Consequently, the results of this study reveal guidelines for the training and support of observers in observational tasks.

References

[1] S. Huber and P. Wellig, “Human factors of target detection tasks within heavily cluttered video scenes,” in SPIE Security + Defence: SPIE, 2015, 96530R.

[2] P. Dunau, S. W. Huber, K. U. Stein, and P. Wellig, “Asynchronous threat awareness by observer trials using crowd simulation,” in Proc. SPIE 9997, Target and Background Signatures II: SPIE, 2016, 99970K.

10432-16, Session 3

Mirage: a visible signature evaluation tool

Joanne B. Culpepper, Defence Science and Technology Group (Australia); Alaster J. Meehan, YTEK Pty Ltd (Australia); Q. T. Shao, Thermovoltaic Technologies Pty Ltd (Australia); Noel J. Richards, YTEK Pty Ltd. (Australia)

Understanding and evaluating visible signatures has long been a focus of military research. Early work began by evaluating camouflage and disruptive pattern effectiveness through straightforward human observer evaluation, where observers viewed scenes in the field or in photographs, and used various ranking or rating criteria to judge the best options. This approach still underpins evaluation of camouflage and platform signature today. However, it is impractical to run human observer experiments to cover the gamut of proposed applications for Army platforms: to conduct field experiments in every operating environment, or even to collect photographs of the platforms in each environment. Additionally, human observation experiments are expensive in dollar, time and human resource costs. DST Group therefore aims to provide a capability to evaluate visible signatures by computer modelling, and has developed a tool called Mirage.

This paper presents the Mirage visible signature evaluation tool, designed to provide a visible signature evaluation capability for land vehicles. Mirage will evaluate the effect of scene content on the detectability of targets, providing a capability to assess the signature in context of the environment. Mirage is based on a parametric evaluation of input images, assessing the value of a range of image metrics and combining them using a machine learning method to produce target detectability estimates.

Mirage has been developed using experimental data from photo-simulation experiments, where human observers search for vehicle targets in a variety of digital images. The images used for model development are synthetic (computer generated) images, showing vehicles in many different scenes and exhibiting a wide variation in scene content. This wide variety is vital to understanding the critical parameters that

affect detectability in the land environment, including the effect of terrain types (e.g. desert or rainforest), weather conditions (e.g. clear or overcast) and time of day. This knowledge and understanding assists in developing Mirage's capability to assess vehicle visible signature across a wide variety of operational environments and conditions.

Synthetic images with variations in scene content have been used to develop Mirage. The synthetic images have been analysed using image metrics, which measure how the target in the image differs from the background and how scene content affects detectability. Machine learning has been used to develop an initial model to predict detection probability, using the results from the metrics analysis and the detection results from human observer experimentation. The machine learning technique is also used to determine the relative importance of the image metrics for predicting detectability. Analysis of the relative importance of the image metrics is used to refine Mirage's ability to accurately predict detection probability of a target in an image.

10432-17, Session 3

Comparing synthetic imagery with real imagery for visible signature analysis: human observer results

Joanne B. Culpepper, Defence Science and Technology Group (Australia); Noel J. Richards, YTEK Pty Ltd. (Australia); Christopher S. Madden, Neal Winter, Defence Science and Technology Group (Australia)

Synthetic imagery could potentially enhance visible signature analysis by providing a wider range of target images in differing environmental conditions than would be feasible to collect in field trials. Achieving this requires a method for generating synthetic imagery that is both verified to be realistic and produces the same visible signature analysis results as real images. Is target detectability as measured by image metrics the same for real images and synthetic images of the same scene? Is target detectability as measured by human observer trials the same for real images and synthetic images of the same scene?

This paper focuses upon the second verification step using human observer trials to compare the similarity of target detection results between real digital (photographs) images and synthetic images generated of the same scene. Two sets of synthetic images were created, one using an image generation tool, E-on Vue, and the other using a gaming engine, Unity 3D. These tools both employ a 3D model of the target platform and recreate a set of 22 scenes observed in the real images using a height map, aerial imagery and models of the vegetation. Care was taken to ensure the realism of the scene and that they closely matched the original imagery in terms of scene colouring, topography, target positioning and arrangement and density of vegetation and other scene content, though the image fidelity differed between E-on Vue and Unity 3D.

The synthetic scenes and real images were used in a photosimulation experiment in March 2017. Twenty four Australian Army Observers participated in the photosimulation trial. In the photosimulation trial, the observers were tasked to search each scene and to identify the target location. A time limit of 50 s was placed on the visual search task, after which the next image was presented.

In this paper we present analysis of the target detection results will determine if there is any significant difference between the real images and the synthetic images generated in E-on Vue and Unity 3D. If the results indicate that there is an equivalency achievable between real and synthetic images, this would open up the next steps of generating synthetic videos and conducting visible signature analysis of moving platforms and investigating the replication of multiple environmental conditions to better evaluate their impact on a target's signature. Additionally, it provides an important validation step for visible signature evaluation tools developed from synthetic images, such as DST's Mirage visible signature evaluation tool for land vehicles.

10432-18, Session 3

Target acquisition modeling over the exact optical path: extending the EOSTAR TDA with the TOD sensor performance model

Johan-Martijn ten Hove, TNO Defence, Security and Safety (Netherlands); Martien Oppeneer, VORtech BV (Netherlands); Piet Bijl, Judith Dijk, Miranda van Iersel, TNO Defence, Security and Safety (Netherlands)

The Electro-Optical Signal Transmission and Ranging (EOSTAR) model is an image-based Tactical Decision Aid (TDA) for thermal imaging systems (MWIR/LWIR) developed for a sea and littoral environment with an extensive atmosphere model. The Triangle Orientation Discrimination (TOD) model calculates the sensor and signal processing effects on a set of input triangle test pattern images, judges their orientation using a Human Visual System (HVS) model and derives the system image quality from the correctness of the responses. Combination of the TOD model and EOSTAR, basically provides the possibility to model Target Acquisition (TA) performance over the exact path from scene to observer: ship representative TOD test patterns are placed at the position of the real target; the combined effects of the environment (atmosphere, background, etc.), sensor and signal processing on the image are calculated using EOSTAR; and the results are judged using the HVS model. The thresholds are converted into Detection-Classification-Identification (DCI) ranges of the real target.

10432-19, Session 4

Automatic target recognition and detection in infrared imagery under cluttered background

Erhan Gundogdu, Aselsan Research Ctr. (Turkey) and Middle East Technical Univ. (Turkey); Aykut Koc, Aselsan Research Ctr. (Turkey); A. Aydin Alatan, Middle East Technical Univ. (Turkey) and Ctr. for Image Analysis (Turkey)

Visual object classification has long been studied in visible spectrum by utilizing conventional cameras. Since the labelled images has recently increased in number, the great amount of parameters are optimized in the context of deep Convolutional Neural Networks (CNN). Moreover, a human-level performance is achieved in terms of recognition accuracy by the trained models. As the infrared (IR) sensor technology has been improved during the last two decades, labelled images extracted from IR sensors have been started to be used for object detection and recognition tasks. However, datasets for IR sequences are still not adequate to train state-of-the-art CNN models when compared to the available datasets of visible spectrum. To this end, we address the problem of infrared object recognition and detection by collecting 15K images from the real-field with longwave and midwave IR sensors. In order to recognize objects, a tree-structured object recognition model is proposed. At each node of the constructed tree, a separate CNN classifier is trained by the subset of the available dataset, which is determined by the decision functions of the parent node of the corresponding node. The decision functions are designed such that the whole data is hierarchically balanced within the nodes of the tree. Once the training is completed, the test samples are propagated over the tree, and the probability of the test sample being at the tree nodes are computed. These probabilities are employed in the process of combining the classifier decisions of the nodes visited by the test samples. The node classifiers are trained on the constructed dataset with four IR target types: marine vessels, tanks, airplanes and helicopter. Moreover, the trained ensemble of classifier is utilized in a detect-by-classification method, where the classification is performed in a set of candidate object boxes

and the maximum confidence score in a particular location is accepted as the score of the detected object. The experiments conducted on the real-field experiments demonstrate that the proposed classifier on the selected object proposals presents satisfactory results for detecting subtle IR targets, such as tanks and maritime vessels, in the cluttered background.

10432-20, Session 4

Video change detection for fixed wing UAVs

Jan Bartelsen, Thomas Müller, Jochen Ring, Fraunhofer-Institut für Optronik, Systemtechnik und Bildauswertung (Germany); Bastian Erdnüß, Karlsruhe Institute of Technology (Germany); Klaus Mück, Stefan Brüstle, Bastian Lutz, Fraunhofer-Institut für Optronik, Systemtechnik und Bildauswertung (Germany); Theresa Herbst, Ruprecht-Karls-Univ. Heidelberg (Germany) and Fraunhofer-Institut für Optronik, Systemtechnik und Bildauswertung (Germany)

In this paper we proceed the work of Bartelsen et al.[1] We present a draft of a process chain for an image based change detection which is designed for videos acquired by fixed wing unmanned aerial vehicles (UAVs). From our point of view, automatic video change detection for aerial images can be useful to recognize functional activities which are typically caused by the deployment of improvised explosive devices (IEDs) e.g. excavations, skid marks, footprints, left-behind tooling equipment, and marker stones. Furthermore, in case of natural disasters like flooding, imminent danger can be recognized quickly. Due to the necessary range, we concentrate on fixed wing UAVs. Automatic change detection can be reduced to a comparatively simple photogrammetric problem when the perspective change between the “before” and “after” image sets is kept as small as possible. Therefore, the aerial image acquisition demands a mission planning with a clear purpose including flight path and sensor configuration. While the latter can be enabled simply by a fix and meaningful adjustment of the camera, ensuring a small perspective change for “before” and “after” videos acquired by fixed wing UAVs is a challenging problem. Concerning this matter, we performed tests with an advanced commercial off the shelf (COTS) system which comprises a differential GPS and autopilot system and estimated the repeat accuracy of its trajectory. Although several similar approaches have been presented,[2] [3] as far as we are able to judge, it has not been estimated yet where the limits for this important issue are. Furthermore, we designed a process chain to enable the practical utilization of video change detection. It consists of a front end of a database to handle large amounts of video data, an image processing and change detection implementation, and the visualization of the results. We applied our process chain on the real video data acquired by the advanced COTS fixed wing UAV and synthetic data acquired by simulation. For the image processing and change detection, we used the approach of Müller.[4] It enables a near real time video change detection for aerial videos although it was developed for unmanned ground vehicles (UGVs). Concluding, we discuss the demands on sensor systems in the matter of change detection.

References

[1] Bartelsen, J., Saur, G., Teutsch, C. “Evaluation of Experimental UAV Video Change Detection”, Proc. SPIE 9997, Target and Background Signatures II, (2016).

[2] Donzelli, T. P., Jackson, L., Yeshnik, M., Petty, T.E. “Airborne Change Detection System for the Detection of Route Mines. Proc. SPIE 5089, Detection and Remediation Technologies for Mines and Minelike Targets VIII, (2003).

[3] Ugliano, M., Bianchi, L., Bottino, A., Allasia, W. “Automatically Detecting Changes and Anomalies in Unmanned Aerial Vehicle Images”, In: International Forum on Research and Technologies for Society and Industry 2015 (RTSI 2015), Torino, 16-18 September 2015. pp. 484-489

[4] Müller, T. “Change Detection on UGV Patrols with Respect to a Reference Tour Using VIS Imagery”, Proc. SPIE 9460, Airborne Intelligence, Surveillance, Reconnaissance (ISR) Systems and Applications XII, 94600I (2015).

10432-21, Session 4

Automatic visibility retrieval from thermal camera images

Céline Dizerens, Univ. Bern (Switzerland); Beat Ott, Peter Wellig, Armasuisse (Switzerland); Stefan Wunderle, Univ. Bern (Switzerland)

Detection, Recognition and Identification (DRI) ranges are important parameters to determine operating conditions but also the quality of thermal infrared sensors. As these range parameters are often based on numerical simulations or laboratory measurements, they may differ from the actual visibility that can be derived from thermal camera images. Moreover, visibility measurements reflect different physical properties of the atmosphere (scattering and absorption) and thus are highly variable in space and time.

This study presents an automatic visibility retrieval of a FLIR A320 Stationary Thermal Imager installed on a measurement tower on the mountain Lägeren located in the Swiss Jura Mountains. Our visibility retrieval makes use of edges that are automatically detected from thermal camera images. Predefined target regions, such as mountain silhouettes or buildings with high thermal differences to the surroundings, are used to derive the minimum distance that is detectable in the image. The retrieval examines natural edges within 12 selected target regions located at different distances to the camera. We use Canny edge detection using adapted thresholds, which is a robust algorithm that removes noise and detects edges at the same time. Additionally, our procedure includes automatic image alignment to correct small shifts of the camera caused by wind and the thermal expansion of the measurement tower. These approaches enable a stable, automatic processing of the thermal images. We carried out a detailed analysis of visibilities derived from more than 24000 thermal images of the years 2015 and 2016 by comparing them to (1) measurements of a forward-scatter visibility meter (Vaisala FD12 working in the NIR spectra), (2) visibilities derived from a panoramic camera image (VIS-range), and (3) modeled visibilities using the Thermal Range Model TRM4. Atmospheric conditions, mainly water vapor from European Center for Medium Weather Forecast (ECMWF), were considered to calculate the extinction coefficients using MODTRAN. The FD12 and the panoramic camera were both installed on the same measurement tower as the FLIR camera to allow a direct comparison of visibility measurements in the visible, thermal infrared, and near-infrared spectra of the different instruments. Similar to the automatic visibility retrieval of the FLIR camera, edges are detected in predefined target regions of the panoramic camera image. Wherever possible, the same target regions as for the FLIR visibility retrieval are selected, complemented with additional targets that have similar distances to the camera. Moreover, DRI ranges using TRM4 were modeled using different target sizes to make them comparable to the camera-based visibility retrieval and FD12 measurements. Because the spatial resolution of the FLIR camera prevents to apply the Johnson criteria (target size: 2.3m x 2.3m), which is part of STANAG 4347, the target size is increased in TRM4 to model DRI ranges. The automatic visibility retrieval based on FLIR A320 images is often in good agreement with the retrieval from the systems working in different spectral ranges, but some significant differences were detected as well, depending on weather conditions and thermal differences of the monitored landscape.

10432-22, Session 4

A comparative study on methods of improving SCR for ship detection in SAR image

Haitao Lang, Hongji Shi, Yunhong Tao, Beijing Univ. of Chemical Technology (China); Li Ma, China Three Gorges Corp. (China)

Knowledge about ship positions plays a critical role in a wide range of maritime applications, such as traffic safety, fisheries control, search and rescue, border surveillance, etc. Thanks to its many advantages, including wide coverage, all-time and almost all-weather operational capabilities, space-borne synthetic aperture radar (SAR) offers a great potential in monitoring ships at sea.

Ship detectors based on constant false alarm rate (CFAR) framework have been extensively studied and implemented in several operational maritime surveillance systems [1]. In general, CFAR ship detector operates by identifying pixels with higher brightness compared to clutters in the surrounding areas. Therefore, to improve the performance of ship detector in SAR images, an effective strategy is improving local signal-to-clutter ratio (SCR) before conducting detection.

Various methods for improving SCR of digital images have been developed in literature. In this paper, we present a comprehensive comparison to several representative methods, including: for single polarization SAR images, (1) spatial neighborhood enhancement, (2) wavelet transform based enhancement, and for full polarization SAR images, (3) scattering mechanism analysis based method.

Specifically, we implement two local contrast enhancement methods, i.e., a traditional Max-mean/max-median method proposed by [2], a more recent locally adaptive regression kernel (LARK) based method proposed by [3]. LARK can obtain the local structure of images by analyzing the radiometric differences based on estimated gradients to reveal the distinguishable characteristics between ships and surrounding clutter. To conduct a wavelet based image enhancement, we propose a multi-scale multi-channel wavelets selective fusion based method. Three selective channels of three different scales are fused to enhance the SCR. For pol-SAR data, we improve a four-component model-based polarization decomposition method [4] and combine several scattering mechanisms to generate a novel metric for ship detection.

The real full polarization Radarsat-2 images are used to evaluate the methods in the experiments. The methods are evaluated from two perspectives: (a) the ability of enhancing the SCR and (b) the performance of ship detection. To conduct ship detection, the CA-CFAR algorithm is used in the SCR enhanced images. Pre-experimental results prove that (1) all these methods can significantly improve the SCR of the original SAR images leading to a performance improvement of ship detector. (2) when combining a polarized metric to spatial neighborhood operations or wavelet based method, the SCR can be improved further.

Reference

[1] M. Stasolla, J. J. Mallorqu´ı, G. Margarit, C. Santamaria, and N. Walker, “A comparative study of operational vessel detectors for maritime surveillance using satellite-borne synthetic aperture radar,” IEEE Journal of Selected Topics in Applied Earth Observations and Remote Sensing, vol. 9, no. 6, pp. 2687–2701, 2016.

[2] S. Deshpande, M. Er, and R. Venkateswarlu, “Max-mean and max-median filters for detection of small-targets,” in Proc. SPIE, Oct. 1999, vol. 3809, pp. 74–83.

[3] Takeda H, Farsiu S, Milanfar P. Kernel Regression for Image Processing and Reconstruction. IEEE Transactions on Image Processing, 2007, 16(2):349-366.

[4] Chen, S.W.; Wang, X.S.; Xiao, S.P.; Sato, M. General polarimetric model-based decomposition for coherency matrix. IEEE Transactions on Geoscience and Remote Sensing. 2014, 52, 1843–1855.

10432-23, Session 4

SAR image dataset of military ground targets with multiple poses for ATR

Carole Belloni, Alessio Balleri, Nabil Aouf, Cranfield Univ. (United Kingdom); Thomas J. Merlet, Thales Optronique S.A.S. (France); Jean-Marc Le Caillec, Télécom Bretagne (France)

Automatic Target Recognition (ATR) is the task of automatically detecting and classifying targets and is an active area of research that includes both civilian and defense applications. Recognition using Synthetic Aperture Radar (SAR) images is interesting because SAR images can be acquired at night and under any weather conditions, whereas optical sensors operating in the visible band do not have this capability.

A large portion of the existing SAR ATR algorithms have been evaluated using the widely used MSTAR dataset [1]. The problem with the MSTAR dataset is that some of the proposed ATR methods have shown good classification performance even when targets are hidden [2], suggesting the presence of a bias in the dataset. Evaluations of SAR ATR techniques with an alternative database is currently difficult due to the lack of publicly available data in the SAR domain.

In this paper, we present a high resolution SAR dataset consisting of images of a set of ground military targets taken at various aspect angles. The measurements were carried out in a controlled environment and can be used for a fair evaluation and comparison of SAR ATR algorithms. In order to acquire each image in the new dataset, we applied the Inverse Synthetic Aperture Radar (ISAR) technique to a target rotating on a turn-table. The target range profiles were collected with a Vector Network Analyser (VNA) transmitting a stepped frequency waveform every 0.2° degrees of the whole rotation. Artefacts in the image are improved by waiting for the target to stabilize after the rotation before emitting a new pulse.

The targets consist of four variants of two 1.7m-long, 0.9m-wide model sized T-64 and T-72 tanks. The gun, the turret position and the depression angle are changed to form 26 different sequences of data. The emitted signal spanned the frequency range from 13GHz to 18GHz to achieve a bandwidth of 5 GHz. The bandwidth was sampled with 4001 frequency points. The ratio between the size of the target and the wavelength was 88 which is 3.6 times lower than that of the MSTAR. The range resolution of the data is 3cm on a 1.7m tank, which is equivalent to a 17cm resolution on a real-sized tank, and that is comparable to the resolution that can be currently obtained using SAR airborne systems. From the radar data, single polarized images are obtained using the matched filter algorithm. With a 20° integration angle, 936 images are produced, each depicting a view of one of the total four target variants. These images are separated in a suggested training and testing set to have a standard evaluation of SAR ATR algorithms.

[1] “Sensor data management system website, MSTAR database”, https://www.sdms.afrl.af.mil/index.php?collection=mstar, last accessed: 2016-07-12.

[2] R. Schumacher and K. Rosenbach, “ATR of battlefield targets by SAR classification results using the public MSTAR dataset compared with a dataset by QinetiQ UK,” in RTO SET Symp. Target Identification and Recognition Using RF Systems. Citeseer, 2004.

10432-24, Session 4

Automatic X-ray image segmentation and clustering for threat detection

Odysseas Kechagias-Stamatis, Nabil Aouf, David Nam, Carole Belloni, Cranfield Univ. (United Kingdom)

The proposed object segmentation and clustering pipeline is a blend of image processing and computer vision concepts applied on a dual-view imaging scheme (Figure 1).

A. Triple-layered X-ray segmentation:

The first phase of our solution consists of a triple-layered segmentation scheme that is based on the effective atomic number of each object contained in the baggage, parcel etc. under inspection. This number defines the object's density and Aim of this segmentation scheme is to break down the contents the density related subcomponents. Density based categories are low, medium and high, which in the X-ray image are represented with different coloring i.e. orange, green and blue/black. Hence, the density based segmentation is transformed into a color based one depending on the dominant color response of each pixel. If the dominant response in any color is less than 33% of the maximum possible, then this pixel is classified as of high density. From the three subcomponent images, only the high-density one is further propagated through the proposed architecture. For enhanced performance, closed contour objects are filled with their material (soft/ medium) (Figure 2).

B. Mild object clustering:

Objects in the high-density image are disconnected using the morphological operations of image opening and closing using a small structuring element to preserve the object's shape. This methodology affords disjoining objects that are not overlapping or heavily connected. The latter cases require a hard object clustering scheme that is presented in section (C).

Artefacts smaller than 400 pixels are discarded as noise (Figure 3) while the remaining are clustered based on their pixel-pair connectivity. Pixel-pairs that meet the 8-connectivity criteria are assigned under the same cluster, otherwise to a different cluster (Figure 4).

C. Hard object clustering:

To compensate overlapping or highly connected objects within the same cluster, we force disjoining objects within the same cluster by exploiting sophisticated computer vision concepts in combination with a complementary view of the same baggage etc. where objects are observed from a different angle. This hard object clustering scheme is applied sequentially to each cluster obtained from section (b).

Initially, we apply a local feature based description technique on each mild cluster Ci and on the second X-ray image Im. Although a few methods exist, we chose SURF as it balances performance and processing time.

Cluster and image features are matched using a Nearest Neighbor Distance Ratio criterion and matches are refined based on RANSAC (Figure 5 (a)). These matched keypoints leverage a rigid transformation between cluster Ci and image Im that is applied on the latter, providing the Transformed Im i.e. TIm (Figure 5 (c)). A rigid transformation requires at least three matches and thus if these are not present, we consider that the cluster cannot be sub-clustered.

TIm is then fused with the cluster image Ci (Figure 5 (d)) and their intersection area is extracted and is then fused with cluster Ci. Based on the second image fusion, the intersecting area is considered as sub-cluster-A of cluster Ci while the remaining, sub-cluster-B (Figure 5 (e)).

10432-26, Session PS

Research on weak chirp signal detection based on cubic spline interpolation

Yu Duan, Zhaodong Niu, National Univ. of Defense Technology (China); Peiliang Jing, Huayin Ordnance Test Ctr. (China)

Chirp signals are extensively used in many applications of signal processing, such as in radar and wireless communications. Therefore, how to extract the effective information of the chirp signals from noise, clutters and complex backgrounds, is pivotal problem for reconnaissance receivers. In practical applications, the signal-to-noise ratio (SNR) of the received chirp signals tends to be quite low, for instance, below -10dB. As a consequence, the chirp signals are often weak and difficult to be detected. In the circumstances, many traditional analysis methods are not available to detect chirp signals effectively, thus it is meaningful to propose a new detection scheme with an acceptable computation and good detection performance in low SNR.

In this paper, we first expatiate the research background and introduce merits and demerits of several existing methods. Afterwards, we study on the properties of chirp signals, and according to the continuous time-frequency characteristic of this kind of signal, we propose a new algorithm in response to the problem of weak chirp signal detection. There are two theoretical components in the proposed scheme. The first one is a detector which, exploiting a time-frequency analysis approach to obtain the time-frequency feature of a signal with noise. After that, a numerical analysis method is employed to extract chirp signals from samples. Specifically, to start with, input signals are short-time Fourier transformed into coherent integration of frequency-shift sample sequences with complex envelopes, to achieve a time-frequency curve. And then, the time-frequency curve is numerically analyzed with cubic spline interpolation, in order to eliminate the noise to the utmost extent as well as to extract the straight lines that represent chirp signals. By doing so, the chirp signals are detected from noise effectively. In low SNR conditions, the process of detection in frequency domain after STFT, as a matter of fact decreases the power of noise and increases the SNR objectively. Moreover, the interpolation reconstruction mitigates the effect of noise ulteriorly, to a certain degree. It can be seen as a process of denoising, and the process makes it easy to estimate the parameters of the chirp signal.

The results of this work may be of utility to the application where chirp signals need to be detected in environments of low SNR. We test our approach using simulated data. In the experiments, we employ simulated chirp signals with strong noise to test the proposed method and several detection methods in open literature. We compare the processing results of these methods and analyze the experimental results. The simulation results show that the proposed method remains effective when the SNR is about -18dB. Finally we come to the conclusion that the proposed method presents better performance in comparison with the other methods.

10432-27, Session PS

Small target detection using objectness and saliency

Naiwen Zhang, Yang Xiao, Huazhong Univ. of Science and Technology (China); Zhiwen Fang, Hunan Univ. of Humanities, Science and Technology (China); Jian Yang, Huazhong Univ. of Science and Technology (China); Li Wang, Tao Li, Beijing Institute of Control Engineering (China)

Object detection without category information arises as a critical standalone preprocessing step in many applications, such as object recognition and object tracking. Recently, many object proposal algorithms have been proposed to discovery objects in complex scenes. However, for small objects, these methods often loss the effectiveness. The main reason may be that the structure information of small objects is ambiguous.

Generally, the existing of object detection methods can be categorized into three groups: (i) superpixel-based methods, (ii) edge-based methods, and (iii) CNN-based methods. The first group mainly focuses on constructing the connectivity graph of superpixels, defining the energy function of superpixels, or designing the grouping mechanism of superpixelss. Nevertheless, they suffer from low computational efficiency because of segmentation algorithms, especially for segmenting the small objects from their surround. The methods in group (ii) extract the structure information from the edges. For instance, BING adopted normed gradient features to describe the proto-objects and utilized SVM to detect the objects at 300 fps. EdgeBoxes is proposed to estimate the objectness using contour information. In general, edge-based algorithms are faster than segmentation-based algorithm. However, it is hard to obtain high quality proposals on small objects because the edge information of small objects

is inadequate. CNN-based methods (iii) often achieve high performance in object detection. But these methods rely on special hardware GPU, which cannot be widely used in limited resource systems, such as small UAV and mobile phone.

In order to achieve good performance on detecting smaller than 30*15 pixels targets, we propose a real-time method combining objectness and saliency to detect small targets. Firstly, we use BING[1] to propose less than 200 bounding boxes, whose maximal size is 32*16. Secondly, K-means algorithm is applied to cluster these bounding boxes into K classes according to their locations. These classes are ranked in descending order by the number of boxes, and we extract the top k classes whose centroid is set as the seed points. According to the seeds, k potential object regions are proposed to calculate local saliency maps using MBS[2]. Finally, we fuse these saliency maps and use EdgeBoxes[3] to accurately detect the small targets.

The proposed method is compared with several methods, such as BING and EdgeBoxes. Over 200 images, where the range of target size is from 10*7 to 30*15, are used to test our method. The experimental results show that our method outperforms other comparison methods in recall rate and meet the real-time requirement.

[1] M.-M. Cheng, Z. Zhang, W.-Y. Lin, and P. H. S. Torr, "BING: Binarized normed gradients for objectness estimation at 300fps," in CVPR, 2014.

[2] J. Zhang, S. Sclaroff, Z. Lin, X. Shen, B. Price, R. Mech, " Minimum Barrier Salient Object Detection at 80 FPS," in ICCV, 2015

[3] C. L. Zitnick and P. Dollár, "Edge boxes: Locating object proposals from edges," in ECCV, 2014.

10432-28, Session PS

An object detection and tracking system for unmanned surface vehicles

Jian Yang, Yang Xiao, Huazhong Univ. of Science and Technology (China); Zhiwen Fang, Hunan Univ. of Humanities, Science and Technology (China); Naiwen Zhang, Huazhong Univ. of Science and Technology (China); Li Wang, Tao Li, Beijing Institute of Control Engineering (China)

Object detection and tracking are critical parts of unmanned surface vehicles (USV) to achieve automatic obstacle avoidance. Automatic navigation of USV is based on high quality localization of obstacle, which can be obtained by object detection and tracking. Off-the-shelf object detection methods have achieved impressive accuracy in public datasets, though, they still meet bottlenecks in practice, such as high time consumption and low detection quality. In terms of object tracking, a key shortcoming is its infeasibility of locating new targets.

Recently, CNN-based object detection methods, such as Fast R-CNN and Faster R-CNN, have achieved promising accuracy. However, the high time consumption makes them hard to be directly used in USV. The state-of-the-art Faster R-CNN method operates at only 7 frames per second. In addition, low detection quality is another demerit. The existing methods focus on how to improve the detection precision. The predicted regions often cover parts of objects rather than the whole one, because 0.5-citerion of Intersection over Union (IoU) is employed to measure the detection precision. The 0.5-criterion, to be specific, means that the object is judged as being successfully detected when the IoU between the predicted region and the ground-truth region is more than 50%. Unfortunately, inaccurate object localizations are therefore resulted. This makes it rather difficult for USV to compute the optimal navigation route. As for the object tracking part, existing approaches such as the renowned KCF , perform favorably regarding efficiency, accuracy and robustness. While they cannot be employed for USV alone owing to that new objects cannot be found during tracking.

Towards this end, we propose a novel system for USV, which is able to locate the object more accurately while being fast and stable simultaneously. The key insight of our method is a hierarchical leverage of object detection and tracking techniques, aggregating their advantages to allow for in practice performance. Firstly, we employ Faster R-CNN to acquire several initial raw bounding boxes. Secondly, the image is segmented to a few superpixels using EGBS. For each initial box, the superpixels inside will be grouped into a whole according to a combination strategy, and a new box is thereafter generated as the circumscribed bounding box of the final superpixel. Thirdly, we utilize KCF to track these objects. After several frames, Faster-RCNN is again used to re-detect objects inside tracked boxes to prevent tracking failure as well as remove empty boxes. Finally, we utilize Faster R-CNN to detect objects in the next image, and refine object boxes by repeating the second module of our system. To figure out whether new objects are detected, we propose a new similarity measure to compare these objects with those tracking objects. Tracking objects and new objects are retained, which will be tracked in the next several frames.

Our system delivers several advantages towards the application of USV, including high detection accuracy, high localization accuracy, being fast and robust. We test our method on video sequences recorded in real marine environments. The experimental results demonstrate that our system is fast, robust and accurate, which can be applied to USV in practice.

10432-29, Session PS

Airport object extraction based on visual attention mechanism and parallel line detection

Wen Lv, Libao Zhang, Beijing Normal Univ. (China)

With the rapid development of remote sensing technology, specific target detection in high resolution remote sensing images has become an important and challenging task. Thanks to the selective visual attention mechanism in human visual systems (HVS), human beings can rapidly distinguish and extract the most salient region from a complicated image without effort. However, computational saliency analysis and target recognition is still facing great difficulties.

The airport is one of the most crucial traffic facilities in military and civil fields. Automatic airport extraction in remote sensing images has many applications such as regional planning and military reconnaissance. It is observed that previous works on the airport extraction can be generally concluded as the following two categories: One is based on edge or line segments extraction. The other is based on texture analysis and image segmentation. For the first category, the line segments of the airport runways are detected by Hough transform, Radon transform, and Line Segment Detector (LSD). These methods simply focus on the outline of the airport runways and the quality of extraction results is usually degraded by the disturbing line segments such as highway, residential area, long rivers or farmland. For the second category, the adaboost algorithm is employed as a feature selector to provide the discriminative textural properties for the airport runways. The texture features can also be classified by support vector machine (SVM). However, the texture-based method can be time-consuming when the imagery data increases.

Visual attention mechanism and saliency analysis are widely used to extract the salient objects and regions of interest that distinguishes itself from other parts of the image quickly. By this mechanism, we can extract the airport target in a relatively smaller remote sensing image region and remarkably save computational cost. In this paper, we propose a reliable airport extraction model combining visual attention mechanism and parallel line detection algorithm. First, a novel saliency analysis model for remote sensing images with airport region is proposed to evaluate both global contrast and spatial unity. The proposed model can precisely extract the most salient region and preferably suppress the background interference. Second, the prior geometric knowledge is analyzed and airport runways contained two parallel lines with similar length are detection efficiently. Finally, we use the improved Otsu method

to segment and extract the airport regions from the salient map of remote sensing images.

In the experiments, we select eighty high resolution remote sensing images acquired from Google Earth. Compared with other seven models, our proposed model achieves the best visual effects and uniformly emphasizes the foreground objects with little background interference. Furthermore, we also use the receiver operator characteristic (ROC) curves, the area under the ROC curve (AUC), Precision, Recall and F-measure to compare our proposed model with the other seven models. The experimental results demonstrate that our proposed model outperforms existing saliency analysis models and shows good performance in the extraction of the airports.

10432-225, Session PS

Flare dispensing program optimization against third generation infrared seekers via genetic algorithm

Ragip Yurttas, Kaan Ergöz, Emrah Oduncu, TÜB?TAK B?LGEM ?LTAREN (Turkey)

MANPADS (Man-portable-air Defense System) missile having infrared detectors, aiming to destroy air platforms, determine the position of targets based on the infrared energy radiating from air platforms. It is possible to detect infrared signals radiating from an air platform by a missile seeker. This will enable the missile to estimate target position. On the other hand, there are many advanced techniques developed to prevent missiles to damage targets. It is a real need for the missiles to overcome these ECM (Electronic-Counter-Measures) techniques such as flare dispensing programs. In order to satisfy this basic need of missiles, certain techniques called ECCM (Electronic-Counter-Counter-Measures) techniques have been developed.

In this paper, to neutralize the MANPADS missile, flare dispensing programs which is optimized by Genetic Algorithm are generated. To generate optimum program, the simulation software on MATLAB are developed. This simulation has infrared background model to calculate background radiation, path radiance and spectral transmittance in the spectral range of modelled missile seeker's infrared detector. Modelled missile which has third generation cooled infrared seeker has gimbal, 3D PPN guidance and thrust model. This missile has also ECCM technique. This technique allows missile not to deceive by common type flares. The reason of that, common type flares have too high radiation than air platform. However spectral flare's radiation is similar with air platform radiation. To break lock of missile on target, two type flares which are common and spectral are modelled. Modelled flares have infrared signature with respect to time and kinematic motion model. As target model, simulation has F-16 jet platform which has 3D infrared signature model with different temperature zones and 6-DOF dynamic motion models.

Third generation infrared seekers can distinguish angular positions of more than one targets radiated on its FOV. Then, it can choose one of them with regard to their radiation levels. So as to break lock of missile, flares are dispensed. The most crucial parameters of dispensing flare programs are initiating of flare dispensing program, time sequences between dispensed flares, dispensed flare number and dispensed flare types. To initiate flare dispensing program, two different approaches are developed. These approaches are user defined time and distance between missile and target. Dispensed flare numbers are pre-determined. For each run, 2 common type flares from left and right side of platform at time synchronized, 2 spectral type flares from left and right side of platform at time synchronized are dispensed. To determine the time sequence between dispensed flares, optimization algorithm is used. This algorithm is Genetic Algorithm which is used for searching optimum solution with minimizing cost function recursively. In this simulation, cost function is defined as minimum miss-distance between missile and target. For each run, Genetic Algorithm tries to minimize this miss-distance with optimizing dispensing time of flares. At the end of algorithm, miss-distance cost function is less than threshold level which is set to 10 meters and simulation is terminated. As a result, effective flare dispensing programs are generated with Genetic Algorithm.

Conference 10433: Electro-Optical and Infrared Systems: Technology and Applications

Wednesday - Thursday 13–14 September 2017

Part of Proceedings of SPIE Vol. 10433 Electro-Optical and Infrared Systems: Technology and Applications XIV

10433-31, Session PS

Optoelectronics applications in multimedia shooting training systems: SPARTAN

Tomasz Glogowski, Pawel Hlosta, Slawomir Stepniak, Waldemar Swiderski, Military Institute of Armament Technology (Poland)

Multimedia shooting training systems are increasingly being used in the training of security staff and uniformed services. An advanced practicing–training system SNIEZNIK/SPARTAN for simulation of small arms shooting has been designed and manufactured by Autocomp Management Ltd. and Military Institute of Armament Technology for the Polish Ministry of National Defence.

SNIEZNIK/SPARTAN is a stationary device designed to teach, monitor and evaluate the targeting of small arms and to prepare soldiers for:

firing the live ammunition at open ranges for combat targets and silhouettes

detection, classification and engagement of real targets upon different terrains, weather conditions and periods during the day

team work as a squad during the mission by using different types of arms

suitable reactions in untypical scenarios.

Placed in any room the training set consists of:

the projection system that generates realistic 3D imaging of the battlefield (such as combat shooting range) in high-resolution

system that tracks weapons aiming points

sound system which delivers realistic mapping of acoustic surroundings

operator station with which the training is conducted and controlled

central processing unit based on PC computers equipped with specialist software realizing individual system functions

units of smart weapons equipped with radio communication modules, injection laser diodes and pneumatic reloading system.

The system make possible training by firing in dynamic scenarios, using combat weapons and live ammunition against visible targets moving on a screen. The use of infrared camera for detecting the position of impact of a projectile.

10433-32, Session PS

Detection of defects in multi-layered aramide composites by ultrasonic IR thermography

Monika Pracht, Waldemar Swiderski, Military Institute of Armament Technology (Poland)

In military applications, laminates reinforced with aramid, carbon, and glass fibers are used for the construction of protection products against light ballistics. Material layers can be very different by their physical properties. Therefore, such materials represent a difficult inspection task for many traditional techniques of non-destructive testing (NDT). Defects which can appear in this type of many-layered composite materials usually are inaccuracies in gluing composite layers and stratifications or delaminations occurring under hits of fragments and bullets. IR thermographic NDT is considered as a candidate technique to detect such defects. One of the active IR thermography methods used in non-destructive testing is vibrothermography. The term vibrothermography was created in the 1990s to determine the thermal test procedures designed to assess the hidden heterogeneity of structural materials based on surface temperature fields at cyclical mechanical loads. A similar procedure can be done with sound and ultrasonic stimulation of the material, because the cause of an increase in temperature is internal friction between the wall defect and the stimulation mechanical waves. If the cyclic loading does not exceed the flexibility of the material and the rate of change is not large, the heat loss due to thermal conductivity is small, and the test object returns to its original shape and temperature. The most commonly used method is ultrasonic stimulation, and the testing technique is ultrasonic infrared thermography. Ultrasonic IR thermography is based on two basic phenomena. First, the elastic properties of defects differ from the surroundings, and acoustic damping and heating are always larger in the damaged regions than in the undamaged or homogeneous areas. Second, the heat transfer in the sample is dependent on its thermal properties. In this paper, both modelling and experimental results which illustrate the advantages and limitations of ultrasonic IR thermography in inspecting multi-layered aramide composite materials will be presented.

10433-33, Session PS

Analysis of the development of missile-borne IR imaging detecting technologies

Jinxiang Fan, Feng Wang, Shanghai Institute of Mechanical and Electrical Engineering (China)

Today's infrared imaging guiding missiles are facing many challenges. With the development of targets' stealth, new-style IR countermeasures and penetrating technologies as well as the complexity of the operating environments, infrared imaging guiding missiles must meet the demands of efficient target detection, capability of anti-interference and anti-jamming and the operational adaptability in complex, dynamic operating environments. Missile-borne infrared imaging detecting systems are constrained by practical considerations like cost, size, weight and power(SWaP), and lifecycle requirements. Future-generation infrared imaging guiding missiles need to be resilient to changing operating environments and capable of doing more with fewer resources. Advanced IR imaging detecting and information exploring technologies are the key technologies that affect the future direction of IR imaging guidance missiles. Infrared imaging detecting and information exploring technologies research will support the development of more robust and efficient missile-borne infrared imaging detecting systems. Novelty IR imaging technologies, such as infrared adaptive spectral imaging, are the key to effectively detect , recognize and track target under the complicated operating and countermeasures environments. Innovative information exploring techniques for the information of target, background and countermeasures provided by the detection system is the base for missile to recognize target and counter interference, jamming and countermeasure. Modular hardware and software development is the enabler for implementing multi-purpose, multi-function solutions. Uncooled IRFPA detectors and high-operating temperature IRFPA detectors as well as commercial-off-shelf(COTS) technology will support the implementing of low-cost infrared imaging guiding missiles. In this paper, the current status and features of IR imaging detecting technologies for anti-air, anti-missile and air-surface missiles are summarized. The key technologies and the development trends of missiles' IR imaging detecting technologies are analyzed.

10433-34, Session PS

Research of validity of the vibration measurement on absolute gravimeter based on interferometric technology

Zhenyu Xiong, Xudong Yu, Xingwu Long, National Univ. of Defense Technology (China)

An improved interferometric system aiming at measuring micro displacement is put forward on the basis of phase generated carrier(PGC) demodulation of space optics. This system can improve the accuracy of Absolute Gravimeter(AG) by measuring the amplitude and direction of ground vibration. While the carrier frequency is between 1K and 2K, ground vibration with low frequency (10Hz to 100Hz) and micro vibration amplitude (30nm to 300nm) can be obtained, which satisfies the requirements of AG. And the details are shown below.

1. Setting up the whole interferometer system in an horizontal plane, then the phase of the interference signal is modulated by the piezoelectric ceramic (PZT) and the signal is detected with self-designed photoelectric detector. The frequency of initial referenced vibration signals are given by 20Hz, 40Hz, 60Hz, 80Hz. After phase compensation of the demodulation, the demodulated vibration signal is compared with the amplitude and frequency of the PZT which is calibrated before to validate this algorithm.

2. Changing the measuring prism from horizontal direction into vertical direction and adopting an extra vibration signal generator. Vibration isolation platform Minus K and vibration detector 991B are used to make comparison with results from the interferometer system synchronously in order to validate this system. Comparing with the vibration detector, it can be seen that the accuracy of the interferometer can match with that of the detector in 10-8m and the range of signal frequency it can detect is less than 100HZ, which quite meet requirements of the micro vibration measurement. And this result can also help broaden the application of interferometer and provide new guideline for vibration isolation.

10433-35, Session PS

Comparison of parameters of modern cooled and uncooled thermal cameras

Jaroslaw Barela, Mariusz Kastek, Krzysztof Firmanty, Michal Krupinski, Wojskowa Akademia Techniczna im. Jaroslawa Dabrowskiego (Poland)

During the design of a security system employing thermal cameras one always faces a problem of choosing the camera types best suited for the task. In many cases such a choice is far from optimal one, and there are several reasons for that. System designers often favor tried and tested solution they are used to. They do not follow the latest developments in the field of infrared technology and sometimes their choices are based on prejudice and not on facts.

The paper presents the results of measurements of basic parameters of MWIR and LWIR thermal cameras, carried out in a specialized testing laboratory. The measured parameters are decisive in terms of image quality generated by thermal cameras. All measurements were conducted according to current procedures and standards. However the camera settings were not optimized for a specific test conditions or parameter measurements. Instead the real settings used in normal camera operations were applied to obtain realistic camera performance figures. For example there were significant differences between measured values of noise parameters and catalogue data provided by manufacturers, due to the application of edge detection filters to increase detection and recognition ranges. The purpose of this paper is to provide help in choosing the optimal thermal camera for particular application, answering the question whether to opt for cheaper microbolometer device or apply slightly better (in terms of specifications) yet more expensive cooled unit. Measurements and analysis were performed by qualified personnel with several dozen years of experience in both designing and testing of thermal camera systems with both cooled and uncooled focal plane arrays. Cameras of similar array sizes and optics were compared, and for each tested group the best performing devices were selected.

10433-36, Session PS

Range-gated system for far observing

Denis Shabrov, Ilya Puchkouski, Vadim A. Gorobets, Boris Kuntsevich, B.I. Stepanov Institute of Physics (Belarus)

The range-gated system for far observing have been developed and tested.

This system can use for detecting and tracking objects at night time at long distances. Also it can work in conditions of limited transparency of the atmosphere (the presence of atmospheric phenomena such as rain, snow, drizzle and fog). With the help of the system it is possible to distinguish details of objects with a size of 0.5 m at the maximum distance up to 7 km.

The system is based on the cut-off of the background optical signal from the near zone by the method of active range-gated imaging.

The system provides the ability to observe when exposed to powerful light interference. The wide aperture lens optics (diameter 300 mm) and pulsed laser emitters of the IR spectral range as the illumination of the observation zone have been used. Fifteen laser diodes (wavelength 840 nanometers, the peak power – 200 W, the pulse duration – 100 nanoseconds, repetition rate – 5200 Hz) were used for illumination. Laser diodes were competed by the special developed lens objectives. The 3-rd generation imaging tube with the electronic gate block is used as a photo-detector. The image from the imaging tube screen is moved to a sensitive camera on the basis of the CCD matrixes and further on the LCD-monitor screen.

The conducted tests of the system showed its working capacity and efficiency. The carried out researches have revealed essential advantages of the range-gated in comparison with traditional systems without synchronized laser illumination. They enable to apply on qualitative higher level not only to already known applications for the night vision aims, but also opens for them new prospects in earlier unknown areas. For example, our experiments show a lot of possibilities for such systems in the field of the 3D vision.

10433-37, Session PS

A method for distance determination using range-gated imaging suitable for the arbitrary pulse shape

Vitaliy P. Kabashnikov, Boris Kuntsevich, B.I. Stepanov Institute of Physics (Belarus)

There are three methods for distance determination using range-gated viewing systems. In the time slicing method, distance is computed by weighted averages of 2D gated images that are obtained by variation of delay time between laser and gate pulses. In range-intensity correlation method two overlapped images with specific range-intensity profile (RIP) are used. Range information is deduced from range-intensity correlation of plateau and rising/falling ramp (in the case of trapezoid RIP) or rising and falling ramp (in the case of triangular RIP). More sophisticated variant of range-intensity correlation method includes coding approach with the specific algorithm of the gate opening. In the gain modulation method distant information can be obtained by a 2D gain-modulated gate image and 2D gain-constant gate image. Range-intensity correlation method needs laser pulses with rectangular or Gauss time dependences. Time slicing and gain modulation methods are free of the laser pulse shape.

A method we propose for distance determination with the help of range-gated viewing systems is also suitable for the arbitrary shape of the illumination pulse. The method is based on fixating of the delay time at which maximum of the pulse energy reflected from an object takes place. This method is close to the time slicing method because we need a sequence of 2D images with different delay times to find the maximum. The delay time corresponding to the maximum, depends on the pulse and gate durations and, generally speaking, on the shape of the pulse. For the pulse with the power time dependence in the form of a trapezoid an analytical relationship is obtained between the delay time corresponding to the energy maximum, pulse length, gate duration and the distance to the target. If the pulse length is less than or equal to the gate duration, the delay time corresponding to the maximum does not depend on the pulse shape. This circumstance simplifies greatly the determination of the distance. At the equal durations of the pulse and gate, there is a strict local maximum, which turns into a plateau when the pulse is shorter than the gate duration. A delay time corresponding to the strict local maximum or the far boundary of the plateau (where improper maximum is) is directly related to the distance to the object by means of the factor which equals half of the light velocity. These results are illustrated by a numerical study of the dependence of the detected energy of the reflected pulse on the delay time for the real pulse shape. To verify the proposed method we used the AISV1 range-gated viewing system [1]. The observed object was a vertical wall located at distances 32.1 and 61.7m. Maximum of the signal was determined by visual observation of the object on the monitor screen. The distance defined by the proposed method coincided with the direct measurement with the accuracy 1m, which is comparable with the delay time step multiplied by half of the light velocity. The obtained results can be useful in the development of 3-D vision systems.

10433-38, Session PS

Tools virtualization for command and control systems

Marek Piszczek, Marcin Maciejewski, Wojskowa Akademia Techniczna im. Jaroslawa Dabrowskiego (Poland); Mateusz Pomianek, Military Univ. of Technology (Poland); Mieczys?aw Szustakowski, Wojskowa Akademia Techniczna im. Jaroslawa Dabrowskiego (Poland)

Information management is an inseparable part of the command cprocess. The specificity of actions may often require use of large quantities of advanced data providing equipment. When you look at solutions of stationary and mobile command centers, you will see a multitude of devices. Person taking the decision interacting with them in various ways (change parameters, observe indications). Each of these physical devices requires power supply and most have access to the information network. Some of them are equipped with user interface.(73) (83)

Tools virtualization process can introduce a number of significant modifications in the design of solutions for management and command. The general idea involves replacing physical devices user interface with their digital representation. Many of currently used device provides functionality of the so-called virtual instrument. So, in the simplest case, the interaction is done with the mouse and keyboard and visualization is presented on the monitor screen. Use of such systems does not require physical contact with specific device. It has been replaced by a standard computer input and output interface. This approach allows to look at the design of devices differently and, where it is possible, to replace advanced and expensive physical human machine interface (HMI).

A more advanced level of the systems “digitalization” is to use the augmented and virtual reality (VR) environment.

With territorially distributed devices (With the stationary/ mobile command center), we handle them with the use of augmented reality (AR) technology. With such arrangement there is no need to equip each device with input-output interface. Customized HMI is displayed to the operator when he approaches to each device. Identification of device is done by image recognition of characteristic graphic markers (photo codes). Visualization is achieved by (optical) see-through head mounted display (HMD). Control can be done for example by means of a handhold touch panel, which together witch the HMD is an operator equipment called wearable computer.

Equally interesting solution is the use of immersive virtual environment. The command center can for example be reconstructed or designed from scratch in digital form. In this case, the physical location of the operator not must consist of any special equipment beyond the VR system and access to information network. Operator (with the use of HMD) by immersing in virtual environment is transferred to his work place. Of course this is not only the digital representation of rooms and equipment. Operator can interact with devices in such a way as it would perform in real world (for example with the virtual hand). Information from device (for example indication form digital display, image on the monitor) are visualized in a manner striking resemblance actual operation of equipment. Data are also presented in real time (including network delays).

In the classic information systems, each device has its own on the data rate and the system is the sum of requirements of its components. However, it is known that at the moment we focus on the single device. Because of their procedures (an analysis of central vision, tracking eye movement) AR and VR systems offers another interesting and useful feature of reducing requirements for system data throughput.

Experiments carried out using Moverio BT-200 and SteamVR systems and the results of experimental application testing clearly indicate the ability to create a fully functional information system with the use of augmented and virtual reality technology.

10433-39, Session PS

Method of attack on schemes of optical encryption with spatially incoherent illumination

Pavel A. Cheremkhin, Nikolay N. Evtikhiev, Vitaly V. Krasnov, Vladislav G. Rodin, Anna V. Shifrina, National Research Nuclear Univ. MEPhI (Russian Federation)

Applications of optical methods for encryption purposes have been attracting interest of researchers for decades. The first and the most popular is double random phase encoding (DRPE) technique. There are many optical encryption techniques based on DRPE. Main advantage of DRPE based techniques is high security due to transformation of spectrum of image to be encrypted into white spectrum via use of first phase random mask which ensures that encrypted image also has white spectrum. Downsides are necessity of using holographic registration scheme in order to register not only light intensity distribution but also its phase distribution, and speckle noise occurring due to coherent illumination. Elimination of these disadvantages is possible via usage of incoherent illumination instead of coherent one. In this case, phase registration is not required, which means that there is no need for holographic setup, and there is also no speckle noise. This technique does not have drawbacks inherent to coherent methods, however, as only light intensity distribution is considered, mean value of image to be encrypted is always above zero which leads to intensive zero spatial frequency peak in image spectrum. Consequently, in case of spatially incoherent illumination, image spectrum, as well as an encryption key spectrum, cannot be white. This can be used to crack encryption system. If encryption key is very sparse, encrypted image might contain parts or even whole unhidden original image. In case of denser keys, original image boundaries still might be partially visible. This will not provide correct decryption key, but will allow to significantly narrow the search for one. Therefore, in this paper new attack method on schemes of optical encryption with spatially incoherent illumination is presented. Method is based on detection of

original image boundaries in the encrypted image. Because encryption is accomplished via optical convolution of original image with encryption key, encryption key can be found if original image is known. In proposed method, in place of original image (which is unknown to the attacker) we use random matrices. Because encryption key consists of number of white points on black background, its normalized average energy (NAE), i.e. ratio of mean matrix value to its maximum value, is much lesser than 0.5. In case of incorrect decryption attempt, reconstructed image will have NAE close to 0.5. In this way "correctness" of reconstructed key is evaluated. First, correct original image size is found by varying size of random matrices. Then, other parameters, such as filtration threshold and Tikhonov regularization parameter, are adjusted in order to provide minimum reconstructed key NAE value. Reconstructed in this way keys are extremely noisy even in case of simplest keys, but after binarization they provide areas of encryption key points possible locations. In case of simplest keys proposed method allows to acquire correct key. In case of complex keys it allows to narrow the search for one. Results of numerical experiments on breaking the system of optical encryption with spatially incoherent illumination are presented.

10433-40, Session PS

Fiber-optic perimeter security system based on WDM technology

Alexandre V. Polyakov, Belarusian State Univ. (Belarus)

There is a great variety of perimeter security systems: capacitive, vibration, radio wave, radio beam, IR and others. The perimeter protection system always is the first technical boundary of object protection; reliability and efficiency of this boundary is very important for early detection of the trespasser. highly demanded fiber-optic systems feature intellectuality, advance information capacity, reliability and extended functionality. Use of fiber-optical alarm sensors in perimeter protection systems or protection of approaches to objects or prohibited zones is perspective. To advantages of fiber-optical systems it is possible to relate their immunity to influence of electromagnetic and radio-frequency noises, and also lightning discharges that reduces probability of a false alarm. Sensor cables do not radiate electromagnetic energy and they are difficult for finding out with the help of search equipment. Attractive feature of systems is absence on perimeter of the active electronic equipment; it allows to cut expenses on installation and service of security system and also to use these sensors on explosive objects or under water.

Intelligent underground fiber optic perimeter security system is presented. Their structure, operation, software and hardware with neural networks elements are described. System allows not only to establish the fact of violation of the perimeter, but also to locate violations. This is achieved through the use of WDM-technology division spectral information channels. As used quasi-distributed optoelectronic recirculation system as a discrete sensor. The principle of operation is based on registration of the recirculation period change in the closed optoelectronic circuit at different wavelengths under microstrain exposed optical fiber. As a result microstrain fiber having additional power loss in a fiber optical propagating pulse, which causes a time delay as a result of switching moments of the threshold device. Emerging delay using time-amplitude converter are transformed to a set of amplitude, the value of which corresponds to time intervals. These amplitude at the output of the multi-channel amplitude analyzer form the histogram distribution. By this displacement of the histogram can determine the change of time intervals in the nanosecond and sub-nanosecond scale. The system detects walking, running or crawling intruder, as well as undermining attempts to register under the perimeter line. To separate the signals generated by intruder noise and interference, the signal analyzer is used, based on the principle of a neural network. Application of neural network ensures high reliability at a low level detection of false positives. When applied to the problems of recognition signal invasion from sensors in security systems, neural network or neurocomputer - a computer system, an algorithm for solving problems which is presented as a network of threshold elements with dynamically tunable coefficients and algorithms settings that are independent of the dimension of the threshold elements of the network and their input space. These alarm systems can be used to protect the perimeters of facilities such as airports, nuclear reactors, power plants, warehouses, and other extended territory.

10433-41, Session PS

The second bias compensation of ring laser gyro in inertial navigation system

Chunfeng Gao, Qi Wang, Guo Wei, Zhihui Ying, Zhimin Ouyang, Xingwu Long, National Univ. of Defense Technology (China)

For the ring laser gyro inertial navigation system (INS), the intrinsic temperature characteristics of the gyro restrict the accuracy of the system. There are a lot of papers on the temperature compensation and bias calibration of ring laser gyro INS. However, it is found in practical application that the gyro bias will still vary with different temperatures after the full temperature field compensation and systematic calibration. This is because the two beams in the gyro will be locked in different modes at different starting temperatures, which will result in the variation of gyro bias. Thus, it is necessary to compensate the second bias compensation of the gyros in full temperature range to achieve the goal of improving the accuracy of ring laser gyro INS. In this paper, the bias of gyros ware measured under the different startup temperature, and emulation analysis and analogue loading verification are conducted.

10433-42, Session PS

Enhancement of tracking performance in electro-optical system based on servo control algorithm

WooJin Choi, SungSu Kim, DaeYoon Jung, Agency for Defense Development (Korea, Republic of); HyoungKyu Seo, Hanwha System Co. (Korea, Republic of)

Modern electro-optical surveilance and reconnaissance systems require tracking capability to get an exact images of target or to accurately direct the line of sight to targets which is moving or still. This leads to the tracking system composed of image based tracking algorithm and servo control algorithm.

The image tracking algorithm calculates pixel error between center of image and target in the image within the prescribed image region. The servo control algorithm convert pixel error from image tracking algorithm into the angular velocity error and move the line of sight of system by the angular velocity.

Image tracking algorithm starts to find target within a prescribed searching area. After finding target, image tracking algorithm set new searching area using target position of previous image. Image tracking algorithm search target within new searching area. This process is repeated continuously until finishing tracking. Movement of line of sight should be limited to the range of searching area. Fast movement of line of sight results in missing targets in the consecutive image tracking algorithm. Delay in transmitting image between camera and image tracker causes instability in tracking system. This instability makes overshooting in response of tracking system. In particular, the large angle error leads to overshooting which should be alleviated.

Therefore, the performance of tracking system can be enhanced by considering both of problems.

This research proposes method to adaptively tune the velocity limiting parameters and acceleration limiting parameters. Tracking system is composed of tracking control loop and rate control loop for line of sight stabilization. Rate control loop is based on PI-Lead controller using gyro as feedback sensor. And rate control loop tune both limiting parameters.

Velocity limit makes the image tracking algorithm not to miss target. Trackable area within image and size of target determine the velocity limit. Acceleration limit make it possible target to move to the center of image without overshooting. The first lockon needs acceleration limit to prevent overshooting. The acceleration limit comes from the size of target in image and angle error.

Tracking simulation using both velocity limit and acceleration limit shows that the proposed tracking system can track all targets within image. Several experiments using electro-optical system demonstrate the effectiveness of the proposed tracking system.

10433-43, Session PS

Attempt to find optimal selections of EO systems for good results of imaging in real environment surveillance process

Octavia Violeta C. Borcan, Danut Ursu, Constantin Marin, Alexandru Toma, Anca Beldiceanu, S.C. Institutul de Optoelectronica S.A. (IOEL) (Romania)

In this paper the authors try to determine a procedure for the best choice in selecting one or other type of sensors as a function of the object under observation, background and environmental conditions.

In surveillance activities related to different missions and scenarios occurred in day and/or night time, the proper choice and use of video surveillance sensors is of huge importance.

Depending on the spectral signatures of background area and those of the objects of interest and environmental conditions, each video technology has its own limits. Used in a multispectral system the visual information received is complementary.

These spectral signatures can be due to either differences in reflectivity, differences in temperatures or differences in emissivity and the appearance in image is different.

Starting from specific scenarios of surveillance, as for example the surveillance of the sky to detect drones, or surveillance of the sea to detect boats in maritime environment, or surveillance of the ground area to detect some manmade objects, this paper approaches the problem of the image appearance in VIS, NIR, SWIR and LWIR spectral ranges, using different passive technologies of surveillance with CCD/CMOS, InGaAs, microbolometers detectors. These images are comparatively presented in relation to some theoretical quantifications made either through mathematical models or through software simulations in order to calculate the detection and recognition distances for specific targets in some specific conditions. Starting from a few targets and backgrounds with known spectral reflectivity or emissivity, usual contrast of reflectivities or emissivities are calculated, in pairs of target material and background area, in spectral ranges between 0.4 – 0.7, 0.7 – 0.9, 0.9 - 1.7 ?m, respectively 8 – 12 ?m. These calculated contrast differences are then used in the so called „camera formula", a theoretical relation revealed in the specific literature and where all the important parameters which have influences on an electro-optical (EO) system are considered: the lens, the detector, the target, its illumination and the atmosphere.

Based on this model, the authors show the influence of the reflectance contrast on the signal strength reaching the surface of the video detector, in similar environment conditions and using the same optical system. Then, different environmental influences are introduced and analyzed, one by one. Finally, the authors of this paper seek certain characteristics of the electro-optical system itself that can influence most the strength and quality of the optical signal, with respect to influences on detection and recognition distances of the target. The influence of the optical system is analyzed starting with the F# number and optical coating variation and also with the influence of the detector responsivity. The possibility of using an active technology instead of a passive one, by introducing a pulsed laser illuminator, is also analyzed, underlying its advantages. The use of some spectral or polarizing filters is also considered, in order to highlight various target features in some special environmental circumstances that might arise during real-world operations. Relevant images are presented to exemplify these techniques along with a few laboratory setups through which these were acquired.

10433-44, Session PS

Velocity correction of a laser Doppler velocimeter based on the Janus configuration

Qi Wang, National Univ of Defense Technology (China); Chunfeng Gao, Guo Wei, Zhimin Ouyang, Xingwu Long, National Univ. of Defense Technology (China)

A reference-beam laser Doppler velocimeter (LDV) can measure the velocity of a vehicle for an inertial navigation system, but the LDV is sensitive to the inclination angle of the laser beam. When the vehicle jolts, the measurement error will increase. In order to reduce the measurement error produced by the jolt of the vehicle, a LDV based on the Janus configuration has been proposed by other researchers. The system mounted at the bottom of the vehicle consists of two single reference-beam subsystems, where the laser probe of a subsystem looks forward and the other looks backward with the same inclination angle. The velocity measurement of the vehicle can be compensated by the pitch angle calculated by the two detected Doppler frequencies and the inclination angle. But the compensation formula has not the highest accuracy in some cases. The paper proposes a new compensation formula which is complemented with the old formula, and then derives the application conditions of the two formulas. Simulations show that the error of the Janus configuration LDV using the new formula is 0.6% and the error using the old formula is 2% when the vertical velocity to horizontal velocity ratio (VHR) reaches 0.2 and pitch angle is . Experiments verify that the velocity measurement accuracy of the Janus configuration LDV is enhanced, so the LDV with velocity correction is more suitable for vehicle self-contained inertial navigation systems.

10433-45, Session PS

Adaptive fault-tolerant method for SINS/LDV integrated system in land vehicle navigation

Guo Wei, Chunfeng Gao, Qi Wang, Zhenyu Xiong, Zhimin Ouyang, Xingwu Long, National Univ. of Defense Technology (China)

As a new velocity sensor, laser Doppler velocimeter (LDV) is gradually applied in vehicle navigation field. It has many advantages such as high accuracy, rapid dynamic response and large measuring range. Similar to odometer, LDV cannot be used alone for navigation without orientation information, while SINS/LDV integration can achieve. Reliability and accuracy are severely influenced when signals of LDV are out of Accuracy in conditions of high vibration strength, large heading maneuvering, surface gathered water and etc. Therefore, it is very important to study how to improve reliability of signals from LDV in the SINS/LDV integrated system. This paper analyses typical physical constraints in land used condition, then probable fault types of LDV are sorted out and fault signals can be denied in time by reasonable failure criteria. Meanwhile, new information matrix is introduced into closed-loop Kalman filtering gain matrix to achieve fault-tolerant filter. The research reveals that the adaptive fault-tolerant method proposed by this paper can effectively improve reliability and accuracy of the SINS/LDV integrated system.

10433-46, Session PS

Accurate estimation of camera shot noise in the real-time

Pavel A. Cheremkhin, Nikolay N. Evtikhiev, Vitaly V. Krasnov, Vladislav G. Rodin, Rostislav S. Starikov, National Research Nuclear Univ. MEPhI (Russian Federation)

Nowadays digital cameras are essential parts of various technological processes and daily tasks. They are widely used in optics and photonics, astronomy, chemistry, biology and other various fields of science and technology such as control systems and video-surveillance monitoring.

One of the main information limitations of photo- and videocameras are noises of photosensor pixels. Camera's photosensor noise can be divided into random and pattern components. Temporal noise includes random noise component while spatial noise includes pattern noise component. Spatial part usually several times lower in magnitude than temporal. At first approximation spatial noises might be neglected. Temporal noise includes signal-dependent shot noise and signal-nondependent dark temporal noise.

For measurement of camera noise characteristics, the most widely used methods are standards (for example, EMVA Standard 1288). It allows precise shot and dark temporal noise measurement but difficult in implementation and time-consuming. Earlier we proposed method for measurement of temporal noise of photo- and videocameras. It is based on the automatic segmentation of non-uniform targets (ASNT). Only two frames are sufficient for noise measurement with the modified method. In result, proposed ASNT modification should allow fast and accurate measurement of temporal noise.

In this paper, we registered frames and estimated shot and dark temporal noises of cameras consistently. The modified ASNT method was used. Temporal noise was estimated in the real-time using the MATLAB program environment. Estimation was performed for cameras: consumer photocamera Canon EOS 400D (CMOS, 10.1 MP, 12 bit ADC), scientific camera MegaPlus II ES11000 (CCD, 10.7 MP, 12 bit ADC), industrial camera PixeLink PL-B781F (CMOS, 6.6 MP, 10 bit ADC) and video-surveillance camera Watec LCL-902C (CCD, 0.47 MP, external 8 bit ADC). Experimental dependencies of temporal noise on signal value are in good agreement with fitted curves based on a Poisson distribution excluding areas near saturation.

Compared to the EMVA Standard 1288 we can obtain shot noise significantly faster. Time of registering and processing of frames used for temporal noise estimation was measured. Using standard computer, frames were registered and processed during a fraction of second to several seconds only.

Also we accelerated the process by reducing of data points of the dependency of temporal noise on signal value. Application of this method allows to significantly increase of processing rates. Frames processing times were decreased up to several tens of times.

The accuracy of the obtained shot noise and dark temporal noise values were estimated.

10433-47, Session PS

Modified two-point calibration algorithm for infrared focal plane arrays

Tomasz Orzanowski, Wojskowa Akademia Techniczna im. Jaroslawa Dabrowskiego (Poland)

This paper presents a modified two-point calibration algorithm with useful method of pixel offset correction coefficients update for infrared focal plane arrays (IRFPAs). The new approach to IRFPA response nonuniformity correction (NUC) consists in the use of pixel response change determined at the actual operating conditions in relation to the reference ones by means of shutter to compensate a pixel temporal drift. This approach permits to estimate a pixel offset efficiently and remove any optics shading effect in the corrected output image as well. Moreover, the proposed NUC algorithm is easy to implement by hardware too. To show efficiency of the modified two-point calibration algorithm some test results for microbolometer IRFPA are presented.

10433-48, Session PS

The analysis of functional regions in the long-wavelength-infrared interband cascade photodetector

Krzysztof Czuba, Iwona Sankowska, Agata Jasik, Ewa Papis-Polakowska, Janusz B. Kaniewski, Institute of Electron Technology (Poland)

Long-Wavelength Infrared (LWIR) photodetectors have numerous scientific, civilian and military applications, including trace substance detection, medical diagnostics, missile guidance and defence systems, environmental and industrial process monitoring. Presently, Mercury-Cadmium-Telluride-based (MCT) devices are commonly used in this spectral range due to their good performance and mature production technology. Recently, Interband Cascade Infrared Photodetectors (ICIP) based on antimonide superlattices are emerging as a strong candidate to outperform them, especially at high operating temperatures. In spite of their rapid development there are still some issues to overcome to fully utilize their potential.

In this paper, the analysis of the properties of functional regions in LWIR ICIP under various perturbations are presented. The absorption region based on the InAs/GaSb type-II broken-gap superlattice is considered. Furthermore, type-II staggered InAs/AlSb multiple-quantum-well-based (MQW) hole barrier-intraband relaxation region and type-I AlSb/GaSb superlattice-based electron barrier-injection tunnelling region are investigated. Second-nearest neighbour sp3s* tight binding model is used for electronic structure calculations. It allows for proper reproduction of X-valley E(k) dispersion and transverse effective mass, which is especially important in indirect-gap materials and heterostructures. Furthermore, it provides the possibility to use ternary alloys as layers.

The influence of simple change in well and barrier widths in InAs/AlSb MQW region on its basic properties is investigated. Moreover, the effects of the structural perturbations caused by variation in the composition of MQW and superlattices constituent layers are demonstrated. The electronic structure calculations are complemented by simulations of x-ray diffraction curves, to further validate obtained results. The analysis of the shape and Full Width at Half Maximum values of the simulated superlattice diffraction peaks is used to predict the material quality. In addition, the change of the strain due to the variation of the composition in MQW and superlattices is investigated. A tolerance limit of each perturbation is determined that still allows for proper operation of the LWIR ICIP devices. The design rules that would simplify their practical realization are proposed.

10433-1, Session 1

Pulsed holographic system for imaging through spatially extended scattering media *(Invited Paper)*

Andrey V. Kanaev, K. Peter Judd, Paul Lebow, Abbie Tippie Watnik, U.S. Naval Research Lab. (United States); Kyle Novak, Tekla Research Inc. (United States); James R. Lindle, U.S. Naval Research Lab. (United States)

Imaging through scattering media is a highly sought capability for military, industrial, and medical applications. Unfortunately, nearly all recent progress was achieved in microscopic light propagation and/or light propagation through thin or weak scatterers, which is mostly pertinent to medical research

field. Sensing at long ranges through extended scattering media, for example turbid water or dense fog, still represents significant challenge and the best results are demonstrated using conventional approaches of time- or range-gating. The imaging range of such systems is constrained by their ability to distinguish a few ballistic photons that reach the detector from the background, scattered, and ambient photons, as well as from detector noise. Holography can potentially enhance time-gating by taking advantage of extra signal filtering based on coherence properties of the ballistic photons and by employing coherent addition of multiple frames. In holographic imaging scheme ballistic photons of the imaging pulse are reflected from a target and interfered with the reference pulse at the detector creating a hologram. Related approaches were demonstrated previously in one-way imaging through thin biological samples and other microscopic scale scatterers. In this work, we investigate performance of holographic imaging systems under conditions of extreme scattering (less than one signal photon per pixel signal), demonstrate advantages of coherent addition of images recovered from holograms, and discuss image quality dependence on the ratio of the signal and reference beam power.

10433-2, Session 1

Shortwave infrared laser range-gated viewing based on accumulation mode

Yves Eugene Lutz, Emmanuel Bacher, Stephane Schertzer, Institut Franco-Allemand de Recherches de Saint-Louis (France)

Laser gated viewing in the short wave infrared (SWIR) spectral region is widely developed and presents very high efficiency for several night vision applications. The most advantage of those systems in comparison to more classical near infrared (NIR) systems is that the nominal ocular hazard distance (NOHD) can be dramatically reduced thanks to the wavelength emission located in the eye safe spectral region. Most SWIR gated viewing systems are based on solid state laser illuminators which work in flash mode whereas the NIR systems are principally based on accumulation mode operation. Flash mode requires high energy and short laser pulses which can only be provided by solid state lasers. In this case two main limitations occur, one concerning the image quality which is affected by interference effects like speckle noise which is related to the coherence of the laser source. Another limitation concerns the detection range which is limited by the laser pulse energy available with solid state laser in this spectral region. The maturity of high power laser diode stacks with emission in the SWIR spectral region and moreover the availability of new image detectors able to work with high repetition gates open new perspectives for laser range gated viewing working in accumulation mode. In this work such a system is presented, described and used for experimental recordings. In a first step a powerful illuminator based on QCW InGaAsP high power laser diode stack is designed and developed, special care has been done to the development of the current driver able to generate sub-microsecond steep edges current pulses with corresponding duty cycle. Beam shaping and collimation allow homogeneous rectangular illumination patterns matched to the detector geometry. In a second step, two experiments are conducted to validate the proper operation of the emitter and transmitter. The system is placed in a tunnel equipped with bar charts placed at different distances. By varying of the delay between laser firing and gate opening all charts could be spatially isolated. The addition of multiple laser echo's with a linear increasing in image brightness even with longer acquisition time also confirm low dark current and low jitter making the system definitively able for proper accumulation mode operation.

Images of the same scene and the same conditions are recorded with two different SWIR active imaging systems working in flash and accumulation mode respectively. The analysis of the images confirms the same global intensity whereas the speckle contrast dramatically decreases in accumulation mode. The potential of the range detection increasing in the accumulation mode is also described and experimentally confirmed. Accumulation mode opens new opportunities for compact, efficient and cost controlled SWIR active imaging.

10433-3, Session 1

Optical fundamentals of an adaptive substance-on-surface chemical recognizer

Richard W. Fauconier, Precisyx, LLC (United States); Mandoye Ndoye, Tuskegee Univ. (United States); Webert Montlouis, Johns Hopkins Univ. (United States)

In recent years, widely-tunable laser sources have been used in handheld, monostatic configurations to identify the chemical compositions of thin liquid and gel films on various surfaces by their infrared reflectance spectra. However, several challenges continue to plague this type of substance-on-surface recognition with ambiguous determinations. Among the problems: (1) unknown optical properties of the supporting surface beneath the chemical layer, (2) unknown thickness and refractive index of the chemical film and (3) unknown angles of incidence and detection.

A bistatic optical sensing concept is proposed here in which a multi-wavelength laser source and a detector are physically displaced from each other. It is shown that, with the aid of the concept apparatus proposed, the unknown variables can be measured in real time. An adaptive signal-processing algorithm then allows the unambiguous identifications of the unknown chemicals by their infrared spectra despite their variable presentations.

The proposed bistatic sensor system consists of an optical transmitter and an optical receiver. The whole system is mounted on a stable platform. Both the optical transmitter subsystem and the optical receiver subsystem contain auxiliary sensors to determine their relative spatial positions and orientations. For each subsystem, these auxiliary sensors include an orientation sensor, and rotational sensors for absolute angular position. A profilometer-and-machine-vision subsystem is also included. It determines how much of the support surface is covered by the unknown substance-to-be-identified, whether the illuminating laser beam is falling fully or partially on the unknown substance or on the supporting surface, and the local shape of the target's supporting surface, and its approximate dimensions. It also allows the apparatus to automatically realign transmitter and receiver so that the target is unambiguously illuminated by the interrogating laser beam.

The optical transmitter and receiver subsystems are described in sufficient detail to justify the proffered analysis of concentric visible and infrared beams on their way through the system. To determine dimensions of the unknown substance layer, a circularly polarized and phase-modulated green laser and a similar red laser are employed. A similarly polarized and modulated 1550 nm infrared laser also provides ancillary data. Sufficient feasibility details are also presented on achieving the 1-10 GHz modulation and circular polarization with off-the-shelf components. To determine the infrared absorbance spectrum of the unknown substance, three unmodulated quantum cascade lasers are employed across the range of 860-1500 nm.

A set of vector and scalar equations is developed to characterize the changes to a coherent laser beam of Gaussian cross-section, phase-modulated and elliptically polarized, as it propagates from its source, through a transparent thin film layer, undergoing multiple reflections before emerging as multiple beams, to be gathered by an appropriate detector having an optical aperture of known size. Absorptive and non-absorptive propagation are both considered, as well as propagation for a flat and a convex supporting surface. The results of finite-difference time domain simulations are reported.

They show how the conceptual sensor system's data can be used to make unambiguous in-the-field spectral determinations of a sample's identity, regardless of thickness, or shape of supporting surface.

10433-4, Session 1

Atmospheric effects on laser eye safety and damage to instrumentation

Arkadi Zilberman, Natan S. Kopeika, Ben-Gurion Univ. of the Negev (Israel)

Electro-optical sensors as well as unprotected human eyes are extremely sensitive to laser radiation and can be permanently damaged from direct or reflected beams.

The purpose of this study was to determine the effects of the atmospheric channel on laser eye/detector safety and how such effects can be minimized for personnel or electro-optical system, located at target range, being illuminated by a single pulse or train of pulses from a laser transmitter. Since military and civilian forces use many electro-optical surveillance instruments, the laser radiation may overload or damage the light-sensitive sensor and thus, temporarily or permanently, disable the targeted device.

A fundamental problem in analysis of laser-based systems is the determination of the total optical power density or irradiance that is present at the receiver aperture or laser-guided weapon seeker and, consequently, the total optical power incident on the photosensitive element of the receiver (i.e., photo-detector, CCD, etc.) or eye of observer.

Laser detector/eye hazard depends on the interaction between the laser beam and the media in which it traverses. The environment conditions, including terrain features, particulate and water content, and atmospheric turbulence may alter the laser's effect on the detector/eye. It is possible to estimate the performance of an electro-optical system, e.g., aircraft/ground-based laser target designators, as long as the atmospheric propagation of the laser beam can be adequately modeled. More recent experiments and modeling of atmospheric optics phenomena (e.g., inner scale effect, aperture averaging, atmospheric attenuation in NIR-SWIR, and Cn2 modeling) justify an update of previous eye/detector safety modeling.

In the present work, the influence of the atmospheric channel on laser safety for personnel and instrumentation is shown on the basis of theoretical and experimental data of laser irradiance statistics for different atmospheric conditions. A method for evaluating the probability of damage and hazard distances associated with the use of laser systems in a turbulent atmosphere operating in the visible and NIR-SWIR portions of the electromagnetic spectrum is presented.

The probabilistic approach for ocular hazard distance estimation is revised to address turbulence and particulate scattering effects on ocular exposure levels for a given set of input parameters. The analysis yields a computation of probability of damage and hazard distance for a chosen level of threshold energy density. The multiple experimental data shows that the log-normal distribution can be adopted as a convenient basis for a probability analysis of laser hazards.

This work can result in further development of a general hazard evaluation procedure based on atmospheric effects and laser operating conditions and scenarios. The present work can also result in development of a guide to estimate the probability of eye/detector damage and hazard distance, and it can be used as a performance prediction model for directed energy engagement of ground-based or air-based systems.

10433-5, Session 1

Design and performance of a SWaP short-range fully fibered monostatic laser rangefinder

Gwenn Pallier, SensUp (France); Augustin Portalis, SensUp (France) and Keopsys (France); Guillaume Canat, Keopsys SA (France); Frederic J. L. Chiquet, Patrick Auffray, Sy Dat Le, SensUp (France); Marc Le Flohic, Keopsys SA (France)

The development of a multisensor optronic device requires Size, Weight and Power (SWaP), cost-effective and modular rangefinders while keeping a good range performance. We report on a fully fibered monostatic laser rangerfinder based on a one lens collimator used as the aperture of both the emission and reception channels. This has been possible thanks to the use of a multimode fiber coupler multiplexer (MUX).

This design makes the system compacter and achieves a less than 200g full system weight. In addition to its low volume, the fully fibered architecture allows designing a building block rangefinder with the collimator sub-system on one side and the laser and electronics cards module on the other side. Both are linked up by only an optical fiber. This kit format enables the rangefinder to better fit in any available space in higher level systems such as gimballs and multi-function imagers. Besides, no alignment is needed, and no parallax error is possible: the alignment between channels is guaranteed by design over the whole range.

The emission/reception channels of the first prototype has a 28mm diameter 80mm focal length lens, and a 1.55µm 22µJ pulsed laser firing in a burst mode. The rangefinder is set in a class 1 configuration, and measures at 3Hz. The achieved TEX is 23dB, and targets up to 4.3km have been easily measured in that configuration.

Many improvements are possible leading to a perspective of reaching a 28dB system in that same configuration.

10433-7, Session 1

High-resolution 3D laser imaging based on tunable fiber array link

Sisi Zhao, Ningjuan Ruan, Song Yang, Beijing Institute of Space Mechanics and Electricity (China)

Airborne photoelectric reconnaissance system with the bore-sight down to the ground is an important battlefield situational awareness system, which can be used for reconnaissance and surveillance of complex ground scene. Airborne 3D imaging Lidar is recognized as the most potential candidates for target detection under the complex background and is progressing in the directions of high resolution, far distance detection, high sensitivity, low power consumption, high reliability, low cost, eye safety and multi-function. However, the traditional 3D laser imaging system has the disadvantage of low imaging resolution because of the small number of pixels, or in other words, the small scale of the existing detector. Besides, due to the two dimensional mechanism scanning, traditional 3D LIDAR usually has a large volume and hence cannot be equipped on the small platform. This paper proposes a high-resolution 3D laser imaging technology based tunable fiber array link, which can solve the problem of the small scale of the existing detector and is likely to be a potential candidate for the receiving system of the fiber phased array LIDAR. The laser echo is received and travels through a tunable fiber array link with modulated variables (for example: phase, array arrangement, and fiber inherent parameters), and then transmits to the focal plane detector. The optical signal received by the detector is converted into electrical signal which is obtained by the computer. The computer accomplishes the signal calculation and image restoration based on the modulated information, and then reconstructs the target image. The mathematical model of tunable optical fiber array link for signal receiving and transmitting is established. Based on the model, the complete imaging link of the 3D LIDAR is simulated, including signal emission, free space transmission, fiber array link receiving, image restoration and reconstruction. The influencing impact factors on high density three dimensional point cloud reconstruction are analyzed. The results show that the resolution of the 3D laser imaging based tunable fiber array link, with the wavelength of 1550nm, can be improved by three times at least. Moreover, a design of the compact fiber-based receiving system is also put forward for the future airborne reconnaissance application.

10433-8, Session 2

Dynamic turbulence mitigation with large moving objects *(Invited Paper)*

Robert P. J. Nieuwenhuizen, Adam W. M. van Eekeren, Judith Dijk, Klamer Schutte, TNO (Netherlands)

Long range imaging with visible or infrared observation systems is typically hampered by atmospheric turbulence. The fluctuations in the refractive index of the air produce random shifts and blurs in the recorded imagery that vary across the field of view and over time. The resulting unsharp and unstable videos severely complicate their utility for visual detection, recognition and identification at large distances. Software based turbulence mitigation methods aim to restore such recorded image sequences based on the image data only. This should produce sharp and stable imagery of the observed scene, thus enabling visual identification at larger distances.

Although successful restoration has been achieved on static scenes in the past, there remains a significant challenge in handling moving objects. An important issue here is how to distinguish between the true motion of the moving objects and the apparent motion in the background. Under moderate turbulence conditions the apparent shifts will have similar magnitudes and length scales. Inaccurate segmentation of these moving objects may lead to several problems. On the one hand, moving objects classified as background may result in motion blur on these objects. Also larger moving objects may affect the estimation of background motion due to camera tip and tilt for example. On the other hand, turbulence mitigation methods typically represent moving objects using their pixel values in the input frames. Therefore regions in the background that are classified as moving objects will not be corrected for the effects of turbulence.

Here we investigate how turbulence mitigation can be accomplished in the presence of large moving objects, i.e. moving objects that have linear dimensions on the order of tens of pixels or more. We consider two different scenarios, both under moderate turbulence conditions with turbulence induced shifts magnitudes of several pixels. In the first scenario we have recorded imagery in a land scene with moving persons and vehicles. In the second scenario we have recorded imagery of heaving ships at sea. For both these scenarios we consider the use of optical flow estimation methods to estimate both the turbulence induced shifts in the images as well as the motion of large moving objects. These motion estimates are then used to register the contents from earlier frames in a video to a dynamic but stabilized reference. This reference allows for some motion of the background itself, to account for example for shifts or rotations of the camera, but leaves moving objects in approximately their current position. Moreover, the motion estimates are used with our TNO turbulence mitigation software, which cancels turbulence induced shifts at small scales by time averaging of the registered input frames followed by an image sharpening step. We investigate how different regularization methods for the optical flow affect the accuracy of the segmentation between moving object motion and the background motion. Moreover we qualitatively asses the quality improvement of the resulting imagery in sequences of output images, and show a substantial gain in their apparent sharpness and stability on both the background and moving objects.

10433-9, Session 2

Evaluation of deep neural networks for single image super-resolution in a maritime context

Robert P. J. Nieuwenhuizen, Maarten C. Kruithof, Klamer Schutte, TNO (Netherlands)

High resolution imagery is of crucial importance for the performance on visual recognition tasks. Super-resolution (SR) reconstruction algorithms aim to enhance the image resolution beyond the capability of the image sensor being used. Traditional SR algorithms approach this inverse problem using physical models for the image formation combined with a regularization function to prevent instabilities in the solution. Recently deep neural networks have been put forward as an alternative approach to the SR reconstruction problem. They learn a mapping from low resolution images to their high resolution counterparts from pairs of training images, which allows them to capture more specific information about the space of possible solutions than traditional regularization functions. These networks have achieved state-of-the-art performance on single image SR for sets of generic test images.

Here we investigate whether the same performance can be realized when these neural networks for single image SR are applied specifically in the maritime domain. In particular we investigate their ability to reconstruct undersampled images of ships at sea, and demonstrate that the performance is similar to what is achieved on generic test images. In addition we quantify the gain in performance that is achieved when the networks are trained specifically on images of ships, which allows the networks to capture more prior knowledge about the space of possible solutions. Finally we show that the performance deteriorates when the resolution of test images is limited by image blur, for example due to diffraction, rather than undersampling. This highlights the importance of using representative training data that account for the part of the image formation process that limits the resolution in the sensor data.

10433-11, Session 3

InAs/GaSb type-II superlattices versus HgCdTe ternary alloys: future prospect *(Invited Paper)*

Antoni Rogalski, Wojskowa Akademia Techniczna im. Jaroslawa Dabrowskiego (Poland)

Recently, there has been considerable progress towards III-V antimonide-based low dimensional solids development and device design innovations. From a physics point of view, the type-II InAs/GaSb superlattice is an extremely attractive proposition. Their development results from two primary motivations: the perceived challenges of reproducibly fabricating high-operability HgCdTe FPAs at reasonable cost and theoretical predictions of lower Auger recombination for type-II superlattice (T2SL) detectors compared to HgCdTe. Lower Auger recombination should be translated into a fundamental advantage for T2SL over HgCdTe in terms of lower dark current and/or higher operating temperature, provided other parameters such as Shockley-Read-Hall lifetime are equal.

In fact, investigations of antimonide-based materials began at about the same time as HgCdTe in the 1950's, and the apparent rapid success of their technology, especially low-dimensional solids, depends on the previous five decades of III-V materials and device research. However, the sophisticated physics associated with the antimonide-based bandgap engineering concept started at the beginning of 1990's gave a new impact and interest in development of infrared detector structures within academic and national laboratories. In addition, implementation of barrier in photoconductor structure, in so called barrier detector, prevents current flow in the majority carrier band of detector's absorber but allows unimpeded flow in the minority carrier band. As a result, this concept resurrects the performance of antimonide-based focal plane arrays and give a new perspective in their applications. Apart from barrier structures, a new emerging strategy includes multi-stage/ cascade infrared devices.

InAs/GaSb T2SL photodetectors offer similar performance to HgCdTe at an equivalent cutoff wavelength, but with a sizeable penalty in operating temperature, due to the inherent difference in Shockley-Read lifetimes. It is predicted that since the future IR systems will be based on the room temperature operation of depletion-current limited arrays with pixel densities that are fully consistent with background- and diffraction-limited performance due to the system optics,

the material system with long Shockley-Read lifetime will be required. Since T2SLs are very resisted in attempts to improve its SR lifetime, currently the only material that meets this requirement is HgCdTe. In this contest, the performance of both material systems are compared.

10433-12, Session 3

HgCdTe and Sb-based infrared detection modules for gas sensing manufactured at VIGO System S.A.

Adam Piotrowski, Zbigniew Orman, Jozef Piotrowski, Artur Keblowski, Lukasz Kubiszyn, VIGO System S.A. (Poland)

This article reports the parameters and characteristics of recently introduced mid Infrared (3-12um) detection modules for gas sensing applications. In Mid infrared range one can detect almost every simple or complex compound existing on earth. Currently a driving factors for development of gas sensors are related to air/water quality, explosive material detection and medical applications, especially breath analyzers. Gas sensors require source (thermal, diode or laser), sampling compartment and detection module. At VIGO System we are concentrated on designing and manufacturing high operating temperature detectors, fast, sensitive, affordable and reliable required for development of such platforms. We are using active, absorber elements based on complex HgCdTe or InAsSb heterostructures monolithically integrated with optical immersion lens. Additional collective optics, signal amplification, temperature control and heat dissipation will be also discussed in this article. Those functions are critical for ultimate performance of gas sensors.

10433-13, Session 3

Present status of metrology of electro-optical surveillance systems

Krzysztof Chrzanowski, INFRAMET (Poland)

Electro-optical imaging and laser systems (thermal imagers, night vision devices, visible/NIR cameras, SWIR imagers, laser range finders, laser designators, laser pointers, fused images, multi-sensors systems, fused systems, UV cameras, optical sights) are one of most important technologies for modern armed forces. A short review of present status of metrology of electro optical imaging and laser systems for surveillance applications has been presented in this paper. It has been shown that is quite common that test systems from different manufacturers generate significantly different measurement results, different test teams using the same test system obtain sometimes different measurement results, measured data obtained during customer acceptance tests differ from manufacturer data sheets, and parameters of the same names are sometimes understood in different ways. There are also some parameters of EO systems that are extremely difficult to be accurately measured and measurement uncertainty at level of 10-20% is considered as a success. This situation can be unexpected for many readers because nowadays in many areas of metrolology (example : measurement of electrical quantities) measurement uncertainties are below 0.1%. After this initial introduction complex reasons that have created this poor situation of EO metrology are presented like big size and dynamic growth of EO technology, subjective measurement of some parameters, poor standardization, metrology infrastructure of EO metrology still at beginner stage.

The first limiting factor is a size of EO technology. It should be remembered that EO metrology covers test methods and test equipment of more than a dozen of different types of EO systems. There are more than a hundred of parameters used to characterize different types of electro optical imaging and laser systems. Some parameters used to characterize different types of EO systems have the names but actually are defined and measured in different ways. Therefore it is extremely difficult to master testing all groups of EO systems and is difficult even to master testing a single EO group. Further on, different types of EO systems have been developed by different communities that sometimes use specific terminology for internal communication. The result is that specialists in design of thermal imagers understand quite well designers of VIS/NIR or SWIR cameras but often have problems to understand night vision technology due to its hermetic terminology and big design differences.

Second, EO technology is quickly expanding and improving. This dynamic growth is a difficulty for an adept in EO metrology who must have at least basic understanding of design of EO systems to do proper tests. Next, technology improvements can create big obstacles for metrologists. Totally different test system is needed to measure resolution of old image intensifier tubes at level of 32 lp/mm (level 30 years ago) and resolution of modern image intensifier tubes at level about 64 lp/mm. Next, imaging EO systems have become increasingly intelligent and capable to do advance image processing automatically or semi automatically. Image quality and indirectly test results depends on a set of parameters of tested system that can be regulated by system test operator.

Third, some of parameters of EO imaging systems (MRTD for thermal imagers, MRC for VIS/NIR cameras) are subjective parameters. Human operator is expected to make decision about measurement results. If tests are done by several operators and results are averaged then this subjectivity does not automatically means low measurement accuracy. However, high measurement accuracy of subjective parameters of EO systems could be be achieved only if such tests are done world wide by well trained test operators who use the same test criterion. Unfortunately different test teams often use slightly different test criterion when measuring subjective parameters of imaging EO systems.

Fourth, poor standardization is probably the most important factor that generates negative impact on present situation in EO metrology. Majority of manufactures of EO system have implemented so called ISO 9000 quality systems and buyers of EO systems sometimes expect high quality of purchased products because the products are supposed to fulfill “requirements of ISO 9000 standards”. However, ISO 9000 family standards are basically quality management systems standards designed to help organizations ensure that they meet the needs of customers and other stakeholders while meeting statutory and regulatory requirements related to a product. The problem is that there is almost no international or even national standards that would present regulatory requirements on EO systems. The author is not aware about any standards that would present regulatory requirements on EO systems except a series of MIL standards that present requirements on night vision devices and image intensifier tubes. However these standards are old (issued in 1970-1990s) and the requirements are low and easy to fulfill. Therefore practically information that manufacturer of EO system has implemented ISO 9000 quality systems give warranty that management of the company and may be production is done in standardized way but gives no warranty on high performance parameters of manufactured EO systems.

Lack of statutory requirements on EO systems in form of modern standards is still of minor importance because such standard requirements can be easily replaced by requirements presented in tenders issued by big buyers on EO market (example Ommnibus program in US). The real big problem is lack of modern and internationally accepted standards that could regulate definitions, measurement methods and equipment to measure parameters of EO systems. Present situation is rather gloomy: a series of old MIL standards (field of night vision technology) that need to be updated, two old NATO standards on testing and evaluation thermal imagers, two old and formally canceled NATO standards on testing and evaluation image intensifier systems, relatively new ISO standard on testing night vision devices having little chance to be accepted by international community, several standards on test of VIS/NIR cameras issued by different organizations that differ in recommendations, no any standard on testing SWIR cameras, UV cameras, laser range finders, multi sensor system and fused systems. The logical consequence of lack of standards on test methods is that different manufacturers

of EO systems use often slightly different test methods and get slightly different measurement result. It is also a common situation for tender evaluation committee to find situation that different tenderers calculate detection, recognition and identification ranges of thermal imagers, VIS-NIR cameras or night vision devices in different ways.

Fifth, poor metrology infrastructure of EO metrology is another important factor that has negative impact on accuracy of equipment for testing EO imaging and laser systems. The reason is rather simple. EO metrology is young comparing to metrology of physical quantities listed in SI system. The system of metrology of physical quantities has been developed during at period of hundred of years when we can talk about beginning of EO metrology about fifty years ago and real growth during last thirty years. Therefore is a natural that all technologically advanced countries have national metrological institutes capable to calibrate meters of physical quantities listed in SI system (examples national metrological organizations like NIST in USA, PTB in Germany, NIM in China, KRISS in Korea) but very few have a center capable to calibrate stations for testing EO systems (example Night Vision and Electronic Sensors Directorate (NVESD) in USA). This situation is a big problem for manufacturers of EO test stations who are forced typically to use indirect calibration methods to calibrate manufactured test equipment.

There have been presented earlier a rather gloomy picture of EO metrology and reasons that generates such rather poor status of this metrology. However, EO technology is expanding and improving quickly. Importance EO technology is growing for both military and civilian customers. Therefore it can be expected that next decades will bring significant positive changes in metrology of electro-optical imaging and laser systems.

10433-14, Session 3

Interband cascade type-II infrared InAs/GaSb - current status and future trends

Klaudia Hackiewicz, Piotr Martyniuk, Wojskowa Akademia Techniczna im. Jaroslawa Dabrowskiego (Poland)

Type-II InAs/GaSb interband supperlattice quantum cascade infrared detectors (QCD) proved to be promising candidate for short response time devices operating in room and higher temperatures. The spectral responsivity of mid- wave (MWIR) T2SLs InAs/GaSb based QCD has been observed even up to 380 K.

Short time constant is directly related to the unique carrier transport properties of the interband QCD structures, where at 380 K ~ 4 ns time constant was observed. What is more, thermal generation recombination rates of interband QCDs are orders of magnitude reduced in comparison with corresponding intersubband quantum cascade infrared detectors giving flexibility in higher operating temperature (HOT) applications. The most important feature is that the multiple-stage architecture is useful for improving the sensitivity of HOT detectors, where the quantum efficiency is limited by short diffusion length. Assuming that absorption depth for IR radiation is longer than the diffusion length only a limited fraction of the photogenerated carriers contribute to the quantum efficiency. That could be circumvented by fabrication of multi-stage devices where each equal stage consist of active, relaxation and barrier layer. Significant improvement in detectivity will be visible for the active layer meeting the requirement of ?L ≤ 0.2, where ? is the absorption coefficient and L is the diffusion length. QCD T2SLs InAs/GaSb detector operating at 380 K exhibits Johnson noise limited detectivity at the level of ~ 1E8 Jones without implementation of immersion lens.

In this paper the current status of novel HOT interband cascade infrared detectors is presented. Analysis of the detector's performance versus bias voltage and operating temperatures and future trends in development of the quantum cascade detectors are shown.

10433-15, Session 3

Electrical and optical performance of mid-wavelength infrared InAsSb heterostructure detectors

Emilia Gomulka, Malgorzata Kopytko, Wojskowa Akademia Techniczna im. Jaroslawa Dabrowskiego (Poland); Krystian Michalczewski, Institute of Applied Physics, Military Univ. of Technology (Poland); Lukasz Kubiszyn, Artur Keblowski, Waldemar Gawron, VIGO System S.A. (Poland); Piotr Martyniuk, Wojskowa Akademia Techniczna im. Jaroslawa Dabrowskiego (Poland); Jozef Piotrowski, VIGO System S.A. (Poland); Jaroslaw Rutkowski, Wojskowa Akademia Techniczna im. Jaroslawa Dabrowskiego (Poland)

The materials belonging to the nearly lattice-matched family of semiconductors known as the "6.1Å family" are important for the preparation of the heterostructure infrared (IR) detectors, in particular barrier detectors. All kind of heterostructure devices involve at least two or three semiconductors of the family and their ternary alloys. Ternary alloys at different compositions provide the device engineer with a larger flexibility in the tuning of the band gabs and band offsets between the components. Band-gap engineering is the principle of operation of barrier detectors. The barrier detector concept assumes large offset in one band and almost zero offset approximation throughout the heterostructure in the other, allowing flow of only minority carriers in a photoconductor.

InAs1–xSbx ternary alloy has the lowest band gap among all III-V semiconductors, with a values as small as 0.1 eV at room temperature, can be considered as an alternative to HgCdTe for the mid- wavelength infrared (MWIR), as well as the long-wavelength infrared (LWIR) applications. The development of this ternary alloy has a long history. The properties of InAsSb were first investigated by Woolley et al. in the 1960s. Recently, the rapid progress of InAsSb crystal growth techniques and detector fabrication procedure has been observed due to development of barrier IR detector design. InAsSb is interest principally for heterostructures, especially combining with InAs and Al-based ternary alloys for band-gap engineered barriers.

In this work we investigate the high-operating temperature performance of MWIR InAsSb-AlAsSb heterostructure detectors with cut-off wavelengths near 5 ?m at 230 K. The devices have been fabricated with different type of the absorbing layer: nominally undoped absorber, and both n- and p-type doped. The results show that the device performance strongly depends on absorber layer doping. Generally, p-type absorber provides higher values of current responsivity than n-type absorber, but at the same time also higher values of dark current. The device with nominally undoped absorbing layer shows moderate values of both current responsivity and dark current. Resulting detector detectivities D* varies from 2?109 to 5?109 cmHz1/2/W at 230 K, which is easily achievable with a two stage TE cooler.

10433-16, Session 3

Calculation of optimal absorber thickness in interband cascade type-II infrared InAs/GaSb superlattice photodetectors

Klaudia Hackiewicz, Jaroslaw Rutkowski, Piotr Martyniuk, Tetjana Manyk, Wojskowa Akademia Techniczna im. Jaroslawa Dabrowskiego (Poland)

The paper presents the performance of the interband cascade type-II infrared InAs/GaSb superlattice photodetectors. Such photodetectors are made up of multiple stages, which are connected in series using an interband tunneling heterostructure. Each stage can be divided into three regions:

absorber region, relaxation region and interband tunneling region. Cascade configurations allows to achieve fast response detectors. Making the assumption of bulk-like absorbers, we show how the standard semiconductor transport and recombination equations can be extended to the case of multiple-stage devices. We report the dependence of the Johnson-noise limited detectivity on the absorber thickness for a different number of stages. This allows optimization of the detector architecture, necessary to achieve high value of the detectivity. For this purpose, we make comparison of collection efficiency in single- and multiple-stage absorbers for detectors using a intrinsic absorber material with ?L product. Moreover, we compare our theoretical values of detectivity with experimentally measured data.

10433-17, Session 3

Optical fiber strain sensor for application in intelligent intruder detection systems

Tomasz Sta?czyk, InPhoTech (Poland); Tadeusz Tenderenda, Lukasz Szostkiewicz, InPhoTech (Poland) and Warsaw Univ. of Technology (Poland); Beata Bienkowska, Polish Ctr. of Photonics and Fiber Optics (Poland); Daniel Kunicki, InPhoTech (Poland); Michal Murawski, Polish Ctr. of Photonics and Fiber Optics (Poland); Pawel Mergo, Univ. of Maria Curie-Sklodowska (Poland); Tomasz Nasi?owski, InPhoTech (Poland)

Nowadays technology allows to create highly effective Intruder Detection Systems (IDS), that are able to detect the presence of an intruder within a defined area. However, such systems are subject to different types of non-intruder related inputs (e.g. pet movement, light reflection, wind-caused plant movement), all of which must be distinguished from an intruder related input, if the system is to prove practical in use. The amount of false alarm generated by the IDS is one of the main factors that defines the reliability and quality of the system. There are different detection techniques that are being used in IDSs (e.g. Passive Infrared Detection, MicroWave detection, ultrasonic) and all of them have their advantages and disadvantages. This is why the best results in avoiding false alarms, can be achieved by combining different detection techniques in one system. Such integrated systems, are able to collect and analyze data not only from motion sensors, but also from different devices and sensors distributed in the investigated area.

One group of devices that can be applied in the Intruder Detection System, are devices based on Fiber Optic Sensors (FOS). Components, and elements based on FOS, benefits from numerous advantages of optical fibers like: small size, light weight, high sensitivity, robustness and distributed sensing possibility. Especially low weight and small size of optical fibers, allows them to be integrated with other materials in a way that makes them unnoticeable.

In this work we present an optical fiber sensor based on dedicated Microstructured Optical Fibers (MOF) characterized by increased strain sensitivity. By designing the MOF with large air holes in close proximity to a fiber core, we increased the effective refractive index sensitivity to longitudinal strain. The presented sensor can be easily integrated in the floor system in order to detect any movement in the investigated area. What is more, such sensor, placed under the floor is invisible to the potential intruder and allows to gather much more information than standard motion detectors. By using several FOS connected in one system, and distributed under the floor, we are able to determine not only the mass of the detected object but also its distribution on the floor and its movement in time. Such information allows to distinguish the intruder related signals from non-intruder related signals, and determine weight, and number of the intruders.

The presented fiber optic sensor, based on the specialty optical fibers, due to its numerous advantages, can find application in Intelligent Intruder Detection Systems. Integrated with other detectors, it allows not only to avoid the false alarms, but also to precisely define size and number of intruders.

10433-18, Session 3

All-fiber intensity bend sensor based on photonic crystal fiber with asymmetric air-hole structure

Dawid Budnicki, Lukasz Szostkiewicz, InPhoTech (Poland); Michal O. Szymanski, Polish Ctr. for Photonics and Fibre Optics (Poland); Lukasz Ostrowski, InPhoTech (Poland); Zbigniew Holdynski, InPhoTech (Poland); Stanislaw Lipinski, InPhoTech (Poland); Michal Murawski, Polish Ctr. of Photonics and Fiber Optics (Poland); Grzegorz Wójcik, Maria Curie-Sklodowska Univ. (Poland); Mariusz Makara, InPhoTech (Poland); Krzysztof Poturaj, Pawel Mergo, Univ. of Maria Curie-Sklodowska (Poland); Marek Napierala, Tomasz Nasi?owski, InPhoTech (Poland)

Monitoring the geometry of an moving element is a crucial task for example in robotics. The robots equipped with fiber bend sensor integrated in their arms can be a promising solution for medicine, physiotherapy and also for application in computer games. Optical fibers are very interesting for sensors application due to their small size and weight, ability to perform remote measurements up to several kilometers from sensing point, high safety - no sparks nor EM interference and high fatigue strength (over 20 years).

Fiber sensors measure at least one of the parameters of light (e.g. intensity, phase or polarization state), that are changed by external factors. The bend sensors proposed in the literature are based on interferometric method or long-period gratings. The main disadvantage of such sensors is their high sensitivity to different external factors (temperature, stress and pressure). We report an all-fiber intensity bend sensor, which is based on microstructured multicore optical fiber. It allows to perform a measurement of the bending radius as well as the bending orientation. The reported solution has a special air-hole structure which makes the sensor only bend-sensitive.

Our solution is an intensity based sensor, which measures power transmitted along the fiber, influenced by the bend. The sensor is based on a multicore fiber with the special air-hole structure that allows detection of bending orientation in range of 360°. Each core in the multicore fiber is sensitive to bend in specified direction.. The principle behind sensor operation is to differentiate the confinement loss of fundamental mode propagating in each core. Thanks to received power differences one can distinguish not only bend direction but also its amplitude. Multicore fiber is designed to utilize most common light sources that operate at 1.55 μm thus ensuring high stability of operation. The proposed solution is able to detect the fiber end point with 0.84 dB/cm accuracy for 15 cm fiber length with up to few degree accuracy of bend direction. Such sensitivity allows to perform end point detection with millimeter precision.

10433-19, Session 4

The European Computer Model for Optronic System Performance Prediction (ECOMOS)

(Invited Paper)

Stefan Kessler, Fraunhofer-Institut für Optronik, Systemtechnik und Bildauswertung (Germany); Piet Bijl, TNO Earth, Life & Social Sciences (Netherlands); Luc Labarre, ONERA (France); Endre Repasi, Fraunhofer-Institut für Optronik, Systemtechnik und Bildauswertung (Germany); Wolfgang Wittenstein, Consultant (Germany); Helge Bürsing, Fraunhofer-Institut für Optronik, Systemtechnik und Bildauswertung (Germany)

ECOMOS is a multinational effort within the framework of an

EDA Project Arrangement. Its aim is to provide a generally accepted and harmonized European computer model for computing nominal Target Acquisition (TA) ranges of optronic imagers operating in the Visible or thermal Infrared (IR). The project involves close co-operation of defense and security industry and public research institutes from five nations: France, Germany, Italy, The Netherlands and Sweden. ECOMOS will use and combine existing European tools, to build up a strong competitive position.

In Europe, there are two well-accepted approaches for providing TA performance data: the German TRM (Thermal Range Model) model and the Netherlands TOD (Triangle Orientation Discrimination) method. ECOMOS will include both approaches. The TRM model predicts TA performance analytically, whereas the TOD prediction model utilizes the TOD test method, imaging simulation and a Human Visual System model in order to assess device performance. For the characterization of atmosphere and environment, ECOMOS uses the French model and software MATISSE (Modélisation Avancée de la Terre pour l'Imagerie et la Simulation des Scènes et de leur Environnement).

In this presentation, the central idea of ECOMOS is exposed. The overall structure of the software and its underlying models are shown and elucidated. The status of the project development is given and the work share between participating nations is addressed.

10433-20, Session 4

Corner-point criterion for assessing nonlinear image processing imagers

Stéphane Landeau, Laurent Pigois, Jean-Paul Foing, Gilles Deshors, Greggory G. Swiathy, Delegation Generale Pour L'Armament (France)

Range performance modeling of optronics imagers attempts to characterize the ability to resolve details in the image. Today, digital image processing is systematically used in conjunction with the optoelectronic system to correct its defects or to exploit tiny detection signals to increase performance. In order to characterize these processing having adaptive and non-linear properties, it becomes necessary to stimulate the imagers with test patterns whose properties are similar to the actual scene image ones, in terms of dynamic range, contours, texture and singular points. This paper presents an approach based on a Corner-Point (CP) resolution criterion, derived from the Probability of Correct Resolution (PCR) of binary fractal patterns. The fundamental principle lies in the respectful perception of the CP direction of one pixel minority value among the majority value ??of a 2?2 pixels block. The evaluation procedure considers the not degraded actual original image as its multi-resolution CP transformation, taking the role of Ground Truth (GT). After a spatial registration between the degraded image and the original one, the degradation is statistically measured by comparing the GT with the degraded image CP transformation, in terms of localized PCR at the region of interest dynamic range. The paper defines this CP criterion and presents the evaluation procedure applied to non-linear processing cases. Then, this criterion is compared with the standard Johnson criterion, in the case of a linear blur and noise degradation. In a next paper part, the evaluation of an imaging system integrating an image display and a visual perception is considered, by proposing an analysis scheme combining two methods: a CP measurement for the highly non-linear part (imaging) and conventional methods for the more linear part (displaying). Finally, an application to color imaging is proposed, for which the choice of the working color space is made in accordance with the type of image enhancement processing used.

10433-21, Session 5

The utility of polarimetry within passive military imaging systems *(Invited Paper)*

Duncan L. Hickman, Moira I. Smith, Tektonex Ltd. (United Kingdom); Kyung Su Kim, Hyun-Jin Choi, Agency for Defense Development (Korea, Republic of)

An ongoing challenge for many military imaging systems is the detection and classification of targets in a cluttered environment. In many instances, the use of contrast and relative motion alone do not offer a sufficient level of discrimination to give operational confidence in an automated system and it is therefore necessary to exploit additional discriminatory scene information. Polarisation offers one such source of information and this paper reports on an extensive series of polarimetric trials undertaken across the visible, NIR, SWIR, MWIR, and LWIR spectral bands. This is a unique trials data set and some examples will be given to illustrate the variation in polarisation content across the different bands. The benefits and limitations of polarimetry are described for both visual display and autonomous imaging systems using sample imagery and pertinent metrics. Visual display methods will include standard techniques as well as alternative image manipulation schemes. In general, polarimetric signature levels are low and this can introduce both noise and system bias in derived parameters such as AOP and DOLP. These limitations are considered and the impact on the sensor processing is discussed with particular emphasis on optimising the various system threshold settings. In terms of polarisation across the different spectral bands, one potential limitation is the reduction of the degree of polarisation in the MWIR due to the presence of both reflected and thermally-emitted radiation. This is discussed in the context of the observed polarimetric signatures during trials. Image fusion methods have been previously applied to polarimetric sensors and these will be considered in the context of operational benefits and implementational challenges. To further illustrate the utility of image fusion, a comparison will be made between MWIR polarimetric imagery and that derived from the fusion of visual and LWIR polarimetric imagery.

10433-22, Session 5

Common aperture multispectral spotter camera: Spectro XR

Vladimir Petrushevsky, Dov Freiman, Idan Diamant, Shira Giladi, Maor Leibovich, Elbit Systems Electro-Optics El-Op Ltd. (Israel)

The paper outline:

Introduction: overview of the current state and development trends in the electro-optical surveillance payload technology, particularly regarding high-resolution, narrow field-of-view cameras.

General description of the Spectro payload recently developed by ELOP

Main technical characteristics of the multispectral (VNIR/SWIR/MWIR) spotter camera

Parametric study illustrating the effect of aperture diameter and F-number on effective range of EO and SWIR imaging at different Sun angles. Advantages of the Spectro spotter design point.

Optical design overview. The optics includes a front reflective (Cassegrain) telescope, spectral beamsplitter, and three refractive rear channels (VNIR, SWIR and MWIR). The telescope mirrors are made of aluminum alloy and diamond turned to optical quality suitable for visible-band imaging. The telescope is aligned in a special interferometric setup. There is a single field-of-view in the MWIR band, and dual field-of-view (narrow / super-narrow) in both VNIR and SWIR bands. Both VNIR and SWIR have a filter wheel with three spectral filters.

Mechanical design overview. In particular, the telescope design was especially challenging because of wide range

of temperature, high levels of operational vibration at some of platforms of application, and dense packaging inside the payload where multiple heat sources are located in close vicinity of the telescope. Finite element analysis was extensively used in the design. The telescope was thoroughly tested and maintains its optical performance under the difficult conditions.

Overview of the three spectral channels (main features, focal plane array versions)

Color calibration and correction in visible band. Special calibration method and correction algorithm were developed. Combined with relatively large aperture and low F-number of the optics, this results in significant extension of useful range of color imaging.

Examples of images taken by the camera in the three spectral bands

Summary

10433-23, Session 5

Extension to NIR and visible ranges of high-resolution relative spectral response measurement using Fourier Transform Infrared Spectrometer (FTIR) of CMOS FPAs

Catherine Barrat, Thierry Lepot, Michaël Ramamonjisoa, Sébastien Fradcourt, HGH Systèmes Infrarouges (France)

The accurate knowledge of detectors specifications becomes of higher importance whatever the application. Among these specifications is the relative spectral response. Spectral response measurement of CMOS Focal Plane Arrays is now possible either thanks to a grating-based monochromator or through an FTIR spectrometer. In both cases, the relative response is computed by comparing the response of the detector under test with the response of a reference detector which is supposed to be constant whatever the wavelength. The difference of the results between the 2 methods is of course the spectral resolution: limited to 1% of the wavelength using the dispersive method, the spectral resolution is easily better than 1cm-1 using the FTIR. However, the implementation of the FTIR method remains rather complex due for instance to the temporal difference between the response of the detector under test and the response of the reference detector.

Through the FTIR method, the spectrum is calculated as the Fourier Transform of the signal of the detector, i.e. the interferogram of the input optical source through the interferometer and received by the detector. A Fast Fourier Transform algorithm (FFT) is then applied which requires a sampling frequency. Sampling points are selected at most at every zero-path difference of the interferogram of an internal He-Ne laser. The maximum sampling frequency is consequently the laser frequency and, theoretically, measurements of sources with higher frequencies or wavenumbers than the laser He-Ne, i.e. in the visible spectral range, become impossible. Indeed, considering that the FFT result also includes the symmetric curve about the sampling frequency, the measurements below the He-Ne laser wavenumber, i.e. in the NIR range, may be affected by the overlapping of the main spectrum curve with its symmetric.

An apparently easy solution would be to increase the sampling frequency by using a lower wavelength laser but this solution just moves the problem to a lower range and happens to be expensive. Our paper presents the method to pass over the sampling limitation thus extending measurements over the visible and NIR for CMOS detectors. This method uses the re-combination of the main curve and its symmetrical replica. The paper also explains the drawbacks of this method: the existence of a blind range and the limitations toward UV range. Of course, the principle of the high resolution spectral response measurement through FTIR is also reminded. This method is now implemented into BIRD210, the universal testing bench of FPAs.

10433-24, Session 5

Hazardous gas detection for FTIR-based hyperspectral imaging system using DNN and CNN

Yong Chan Kim, Hyeong-Geun Yu, Jai-Hoon Lee, Dong-Jo Park, KAIST (Korea, Republic of); Hyun-Woo Nam, Agency for Defense Development (Korea, Republic of)

Recently, a hyperspectral imaging system (HIS) with a Fourier Transform InfraRed (FTIR) spectrometer has been extensively used due to its strengths of detecting gaseous fumes. Even though numerous algorithms for detecting gaseous fumes have already been studied, it is still difficult to detect target gases perfectly, because of interference signals of the FTIR spectrometer and unclear characteristic of low concentration gases. In this paper, we propose detection algorithms for classifying hazardous gases using a deep neural network (DNN) and a convolutional neural network (CNN), which recently show state-of-the-art performance in extensive fields. In both the DNN and the CNN algorithms, spectral signal preprocessing is carried out by selecting 118 spectral inputs which visibly represent characteristic of each gaseous fume, and removing offsets of each spectrum. Also, we implement a denoising process due to the interference signals of the FTIR spectrometer, and eliminate baselines with the K-matrix of broad Gaussian and least-square fitting (LSF). Then, in the DNN algorithm, preprocessed spectral signals (118 input data) are used as feature maps of the DNN with 4 layers, and it is trained by the a stochastic gradient descent (SGD) algorithm (50 batch size), and dropout regularization (0.7 ratio). In the CNN algorithm, preprocessed spectral signals (118 input data) are trained with 1x3 convolution layers and 1x2 down sampling layers. As a result, the proposed algorithms improve a 5% accuracy rate (from 94% to 99%) compared with the existing SVM algorithm for detecting and classifying hazardous gases and show robustness against an unremoved noise from FTIR spectrometer.

10433-25, Session 6

Device physics of III-V SLS detectors: current status and challenges *(Invited Paper)*

Sumith Bandara, US Army NVESD (United States)

This talk highlights recent progress and challenges in bandgap engineering of antimony (Sb)-family III-V binary materials followed by discussion of current device and material research being conducted to address these technical hurdles. It describes the formation of superlattices with different alloy combinations and material system properties such as variable bandgap, electron and hole mobility, and minority carrier lifetime a critical factor for detector performance. It discusses widely varying results of experimentally measured minority carrier lifetimes, which range from 30 nanoseconds to 9 microseconds depending on the bandgap and the inclusion of gallium compounds in the superlattice material, and explains present understanding of the minority carrier lifetime and its dependence on the material parameters. It balances advantages and disadvantages of SLS in both device performance and FPA fabrication, and details technical challenges such as lower hole mobility in n-type SLS materials, surface pinning of p-type material and their effect on performance of infrared detectors are detailed. Finally, the presentation concludes with recent results from (Vital Infrared Sensor Acceleration) VISTA Program on imaging FPAs.

10433-26, Session 6

Modelling and measurement of bandgap behaviour in MWIR InAs/InAs(0.815) Sb(0.185) strained-layer superlattices

Veronica Letka, James Keen, Adam P. Craig, Andrew R. J. Marshall, Lancaster Univ. (United Kingdom)

Infrared photodetectors based on strained-layer superlattices (SLS) have recently been subject to attention due to their inherent bandgap tunability. The two alloys most commonly used in type II SLS detectors, InAs and GaSb, are believed to suffer from decreased minority carrier lifetimes due to the presence of defect centres in GaSb [1]. In the gallium-free alternative the GaSb layer is replaced with an InAs(1-x) Sb(x), layer, where the valence band offset can be tuned by the antimony fraction, and by optimising the energy miniband sizes.

Undoped medium-wavelength InAs/InAs(0.82)Sb(0.18) SLS transmission samples were grown by molecular beam epitaxy on semi-insulating GaAs with the use of the strain-relieving interfacial misfit array technique. Their superlattice periods were varied in the range of 4.2 to 13.7 nm in order to study the effect of their size on the bandgap and the resulting photoluminescence and absorption spectra. An nBn device was also grown on native n-GaSb, and was processed into a series of large area devices using photolithography and standard wet etching.

The band structure of each sample was calculated using Krijn's interpolation scheme of van de Walle's 'model-solid' derivation of band offsets [2]. The minibands were obtained with Shen's k.p model of carrier dispersion relations in a semi-infinite superlattice [3]. 4 K photoluminescence measurements demonstrate the predicted increase of peak wavelength with increasing superlattice period: a 4.2 nm period corresponds to a PL peak at 4.3 μm, a 9.2 nm period to 4.9 μm, and 13.7 nm to a 5.1 μm peak. There is, however, no major effect on magnitude of the room-temperature absorption coefficients, which retain values of ~ 1000 /cm up to the cut-off wavelength predicted by the model. Since spectral response measurements of the nBn device demonstrate a Varshni-like behaviour in response to temperature, it is hoped that the model can be adapted to reliably predict the bandgap behaviour at all temperatures in the 4 – 300 K range, and for long wavelength (9 – 12 μm) photodetectors.

References

[1] S P Svensson et al, J. Cryst. Growth 334, 103 (2011)

[2] M P C M Krijn, Semicond. Sci. Technol. 6, 27 (1991)

[3] M Shen et al, Mat. Sci. Eng: B 103, 122 (2003)

10433-27, Session 6

Evaluation of a HDR image sensor with logarithmic response for mobile video-based applications

Marco Tektonidis, Mateusz Pietrzak, David Monnin, Institut Franco-Allemand de Recherches de Saint-Louis (France)

The performance of mobile video-based applications in the field of security and defence (e.g., change detection, automatic navigation) that use conventional low dynamic range (LDR) sensors highly depends on the illumination conditions. Typical issues with image data acquired by LDR image sensors are overexposure, dark shadows, and intensity and color inconsistencies under varying illumination conditions. These issues influence the visual inspection of the video data, as well as the employed image analysis techniques (e.g. feature extraction) required for image stabilization or matching of corresponding images in multi-sequence image data. In contrast to LDR sensors, high dynamic range (HDR) image sensors are able to capture scenes with high dynamic range, and are thus less dependent on illumination conditions and variations. HDR sensors with logarithmic response allow for a single-shot image acquisition and are suitable for mobile applications (e.g., vehicles, UAVs, UGVs).

We have developed a complete image processing framework for a logarithmic HDR image sensor, including the preprocessing of the captured image data as well as tone mapping. The preprocessing methods comprise non-uniformity correction, cross-talk compensation and demosaicing. The implemented two-point non-uniformity correction method uses a dark frame and a flat-field frame to reduce the typically high levels of inherent fixed-pattern noise. Subsequently, the cross-talk correction compensates blocking artifacts, and demosaicing interpolates the missing RGB values on the acquired Bayer color filter array. The employed combined cross-talk correction and demosaicing approach allowed for a more accurate interpolation, improving the quality of the computed HDR RGB images. To display the HDR images on conventional LDR monitors, we have developed global as well as local tone mapping approaches. The global tone mapping approaches use a spatially invariant mapping function based on the global image statistics, for all pixels of an image. Instead of using global statistics, the local tone mapping approaches use local image information to map the HDR image values to a lower dynamic range. For local tone mapping we employed stacked integral images (SII) to reduce computation times and to allow computation in real-time.

We investigated the performance of the logarithmic HDR image sensor as well as the performance of the implemented image processing methods. We evaluated the preprocessing methods with reference to image quality, and we compared global and local tone mapping. For the evaluation we have used static images as well as dynamic image sequences. For the acquisition of the dynamic image data we mounted the HDR image sensor on a vehicle. We have assessed the performance of the HDR sensor and the tone mapping approaches based on the contrast in scenes with high dynamic range, and based on the consistency of intensities and colors in dynamic image sequences acquired under varying illumination conditions. In addition, we have simultaneously acquired image data using a conventional LDR image sensor, and compared the results with the HDR image data.

10433-28, Session 6

High-speed infrared imaging for material characterization in experimental mechanics experiments

Marc-André Gagnon, Frédérick Marcotte, Philippe Lagueux, Vincent Farley, Éric Guyot, Telops Inc. (Canada); Vince Morton, Telops Inc. (United States)

Heat transfers are involved in many phenomena such as friction, tensile stress, shear stress and material rupture. Among the challenges encountered during the characterization of such thermal patterns is the need for both high spatial and temporal resolution. Infrared imaging provides information about surface temperature that can be attributed to the stress response of the material and breaking of chemical bounds. In order to illustrate this concept, tensile and shear tests were carried out on steel, aluminum and carbon fiber composite materials and monitored using high-speed (Telops FAST-M2K) and high-definition (Telops HD-IR) infrared imaging. Results from split-Hopkinson experiments carried out on a polymer material at high strain-rate are also presented. The results illustrate how high-speed and high-definition infrared imaging in the midwave infrared (MWIR, 3 – 5 μm) spectral range can provide detailed information about the thermal properties of materials undergoing mechanical testing.

10433-29, Session 6

Passive ranging effectiveness and related metrics in realistic flight scenarios

Francesco Castaldo, Leonardo S.p.A (Italy); Roberto Conte, Leonardo (Italy); Luca Fortunato, Leonardo (Italy)

Passive ranging is the process of estimating the distance between an observer (own-ship) and one or more moving objects (targets) by using passive sensors only, without electromagnetic or acoustic emissions. In the specific case of airborne Infra-Red Search and Track (IRST) systems, they are increasingly used in the advanced sensor suites of modern fighter aircrafts. IRST systems automatically search, detect and track targets with generally better higher angular resolution than Radars. Being passive systems, they are particularly eligible for silent operations, where any signal emission can unveil the presence in the operative scenario; this is a major tactical advantage with respect to Radars.

On the other hand, one of the major drawbacks of the IRST systems is the lack of direct range measurement. Still, as well-known from literature, range is univocally linked to angle only data, when specific dynamics occur. In all the other cases, range estimation is still considered an open research topic.

In this paper, we analyze several available passive ranging algorithms, as pure geometrical solution, EKF and Range-Parametrized EKF, from a user perspective. A stable system, robust to noise and exempt from flickering range values, which provides reliable estimations and trustworthy confidence indications, is considered indispensable for assuring the operability of the system in real situations.

Algorithms based on filters (as Kalman Filters) require a certain amount of time to converge over a meaningful value. Casting out the range before reaching a stable state usually yields to unreliable estimates and greatly degrades the usability of the system in warfare scenarios.

In situations where no reliable range estimation is available, a possible option is not to provide any range at all. However, by blindly following this criterion we may reduce the operative usability of the system. For this reason, we discuss the existing trade-off between estimation error and length of the estimation.

Another key element is to provide, together with range estimation, a reliable confidence score, indicating the “quality” of the provided target distance. This score should be high during optimal functioning conditions and low when we expect a poor estimation. In general, this information is considered important because it can be used, together with a series of other statistical quantities provided by the IRST to the aircraft, to trigger the sensor fusion processes at aircraft level.

In this paper we select and discuss a set of informative cases which have been derived from our experience in analyzing real sorties data. Such cases are generated by a simulator of flight scenarios, where both own-ship and target ship are allowed to steer and maneuver in realistic fashion.

We also propose a set of new metrics that, in our opinion, captures the system performance in terms of usability and effectiveness. In literature the performance of ranging algorithms is usually done by means of distance-based metrics (as RMSE); on the basis of the points raised above, we enrich the algorithm evaluation process by also considering additional features as estimation declaration length and the frequency of estimated confidence score representing the truth.

10433-30, Session 6

MTF measurement of IR optics in different temperature ranges

Hannes Duncker, TRIOPTICS GmbH (Germany)

Infrared (IR) optical systems are at the core of many military, civilian and manufacturing applications and perform mission critical functions. To reliably fulfill the demanding requirements imposed on today’s high performance IR optics, highly accurate, reproducible and fast lens testing is of crucial importance. Testing the optical performance within different temperature ranges becomes key in many military applications.

The MTF (Modulation Transfer Function) test bench presented in this contribution is a turn-key device to precisely characterize a wide range of optical parameters of mid- and long-wave IR optics with effective focal lengths between 10mm and 300mm and clear apertures up to 100mm.

Due to highly complex IR-Applications in the fields of aerospace, military and automotive industries, MTF Measurement under realistic environmental conditions become more and more relevant. Therefore an integrated thermal chamber application allows measuring several sample sizes in a temperature range from -40 °C to +120°C. To reach reliable measurement results under these difficult conditions, a specially developed temperature stable design including an insulating vacuum are used.

The main function of this instrument is the measurement of the MTF both on- and off-axis at up to +/-70° field angle, as well as measurement of e.g. effective focal length, distortion, field curvature and chromatic aberration, etc.

The vertical configuration of the system guarantees convenient and highly reproducible sample mounting onto an air-bearing based sample holder in combination with a small overall footprint. By integrating a high-resolution IR camera with area sensor (FPA) in the detection unit, we avoid time consuming and high maintenance detection schemes such as the scanning slit method with liquid nitrogen cooled detectors. Thus reducing the time needed for a measurement from minutes to single-digit seconds and dramatically increases throughput.

To achieve the highest MTF measurement accuracy, we use a custom relay lens with large NA exclusively designed for the application. The specified absolute accuracy of +/- 3% MTF is validated using internationally traceable reference optics.

Together with a complete and intuitive software solution, this makes the instrument a turn-key device for today’s state-of-the-art optical testing.

10434-1, Session 1

Overview of sources for ISR applications *(Invited Paper)*

Eric D. Park, Christopher M. DePriest, Kevin M Ezzo, Kevin F. Wall, Q-Peak, Inc. (United States)

Intelligence, Surveillance, and Reconnaissance applications for defense and security continue to broaden to encompass broad swaths of the EM spectrum. We will confine the discussion to the optical wavelengths ranging from the UV to the Long Wave IR. This remains so broad as to encompass virtually all lasers so a review of system requirements and performance parameters will help to establish the most meaningful spectral windows and laser technologies. A projection to leading edge and future requirements will help sort down to the most promising approaches for continuing development.

10434-2, Session 1

New microwave modulation LIDAR scheme for naval mines detection

Nour Alem, Fabrice Pellen, Bernard Le Jeune, Univ. de Bretagne Occidentale (France)

Lidar is currently employed for civilian activities, such as bathymetric measurement, maritime security, pollution measurement or detection of items lost in seawater, and for military activities, such as shallow underwater target detection [1]. The goal of this research is to study a LIDAR system mounted on a ship and looking for underwater targets in front of the ship like mines and obstacles with immersion depths between 0 and 10 m. Detection distances covered ranges from 500 to 1000 m in order to allow appropriate evasive action from the ship if an obstacle is detected.

In a conventional lidar system, the optical source frequently used is a pulsed Nd:YAG laser, frequency-doubled at 532 nm : a wavelength enables one to work in the transparency window of seawater [2]. Nevertheless, the volume backscattering in the water column can be considered as a low-frequency component deterministic noise because it superimposes onto the target echo [3]. This phenomenon can be intuitively understood by analogy with night-driving: when a driver turns on his high-beams in dense fog conditions, he cannot see farther because he is blinded by the backscattered light. Indeed, the use of a higher optical power, sending more photons to the medium, does not produce an enhancement of the detection range under predominant backscattering conditions. Therefore, hybrid LIDAR radar was proposed [4] to improve system detection performances by applying a radar intensity modulation on emitted signal. (Nanosecond) pulsed modulated light is required in order to precisely locate the target.

Many specifications are prerequisite to facilitate the processing of the radiofrequency envelope, to which is added the specifications required to reach the target and thus to be able to detect. Modulation frequency is the key parameter to dissociate the target reflection from the medium backscattered signal by choosing a modulation frequency upper than several megahertz. Another crucial requirement consists in generating a powerful modulated pulse considering the scattering and the absorption undergone by the optical pulse while propagating through the water column. A polarimetric emitted signal is also used to discriminate the target return. In this paper, we will present a novel hybrid LIDAR radar emitter that we have developed. This new design allows emitting a powerful signal at 532 nm lasting only few nanoseconds. We will expose the advantages and the problems encountered while conception and implementation and how we managed to overcome them. The results will be compared with theoretical predictions.

References:

[1] G. C. Guenther, Airborne laser hydrography: System design and performance factors NOAA Professional Paper Series (National Ocean Service 1, Rockville, 1985).

[2] J. Lotrian, J. Cariou, and Y. Guern, “Attenuation measurement in liquids by analysis of space-time structure of backscattered laser light pulses,” Appl. Opt.29, 1593–1594(1990).

[3] F. Pellen, X. Intes, P. Olivard, Y. Guern, J. Cariou, and J. Lotrian, “Determination of sea-water frequency response by backscattering transfer function measurement,” J. Phys. D 715 33, 349–354 (2000).

[4] L. J. Mullen, P. R. Herczfeld, R. Fischl, and V. M. Contarino, “ Evaluation of hybrid lidar-radar for ocean exploration,” in 26th European Microwave Conference (1996), pp. 1015–1018

10434-3, Session 1

UTOFIA: an underwater time-of-flight image acquisition system

Adrian Driewer, Fraunhofer-Institut für Mikroelektronische Schaltungen und Systeme (Germany); Igor Abrosimov, Jonathan Alexander, odos imaging ltd. (United Kingdom); Marc Benger, Fraunhofer-Institut für Mikroelektronische Schaltungen und Systeme (Germany); Marion E. O’Farrell, Karl H. Haugholt, SINTEF Digital (Norway); Chris Softley, odos imaging ltd. (United Kingdom); Jens T. Thielemann, Jostein Thorstensen, SINTEF Digital (Norway); Chris Yates, odos imaging ltd. (United Kingdom)

This contribution describes the development of a newly designed Time-of-Flight (ToF) image sensor for underwater application. The sensor is part of the project UTOFIA (underwater time-of-flight image acquisition) funded by the EU within the Horizon 2020 framework. This project aims to develop a camera based on range gating that extends the visible range compared to conventional cameras by a factor of 3 and delivers real-time range information by means of a 3D video stream at the same time. The system determines the distance by sending a very short laser pulse and measuring the time the pulse needs to travel to an obstacle and back to the sensor. The light intensity is attenuated by passing through the water. In addition, particles in the water reflect the light partially back onto the sensor. This makes underwater range measurements exceptionally challenging.

In order to suppress the influence of the backscattered light the integration of signal is activated only after that unwanted signal has passed the system. By systematically delaying the emission of the laser pulse relative to the integration the system can identify the distance to an object. Within a first prototype of the UTOFIA system built with off-the-shelf components the concept and interaction between the system elements could be verified. Even this prove-of-concept system shows an expansion of the visible range of a factor of 2.5 compared to a consumer underwater camera and delivers decent distance precision.

In order to enhance the capabilities for underwater range imaging the applied sensor needs to fulfill certain requirements such as fast charge transfer and high responsivity. Within the first prototype a test image sensor with various pixel designs has been examined in order to find the optimal pixel structure for under water range gating in poor water conditions. These tests have been performed in air in a lab measurement setup as well as underwater in measurements in a pool with different turbidities of the water. By analyzing the distance measurement performance for different test targets a pixel structure with the best tradeoff between the sensor parameters could be found.

Based on the results of these investigations an image sensor with a lateral resolution of 320x240 (QVGA) pixels has been designed at IMS. Each pixel consists of two identical sub-pixels which enables operation modes with enhanced signal-to-noise ratio or higher frame rate respectively. The functionality and

basic characteristic has been tested with respect to the EMVA Standard 1288 with constant LED illumination and a pulsed diode laser in air. With the camera integrated in the second prototype the performance of underwater range gating has been evaluated.

10434-4, Session 1

Experimental evaluation of penetration capabilities of a Geiger-mode APD array laser radar system

Per Jonsson, Julia Hedborg, Markus Henriksson, Lars J. Sjöqvist, Michael Tulldahl, FOI-Swedish Defence Research Agency (Sweden)

Laser radar 3D imaging has the potential to improve target recognition in many scenarios. One case that is challenging for most optical sensors is to recognize targets hidden in vegetation or behind camouflage. The range resolution of time-of-flight 3D sensors allow segmentation of obscuration and target if the surfaces are separated far enough that they can be resolved as two distances. Systems based on time-correlated single-photon counting (TCSPC) have the potential to resolve surfaces closer to each other than laser radar systems based on proportional mode detection technologies and is therefore especially interesting. Photon counting detection is commonly performed with Geiger-mode Avalanche Photodiodes (GmAPD) that have the disadvantage that they can only detect one photon per laser pulse per pixel. A strong return from an obscuring object may saturate the detector and thus limit the possibility to detect the hidden target even if photons from the target reach the detector. The operational range where good foliage penetration is observed is therefore relatively narrow for GmAPD based systems. In this paper we investigate the penetration capability through semitransparent surfaces for a laser radar with a 128?32 pixel GmAPD array and a 1542 nm wavelength laser operating at a pulse repetition frequency of 90 kHz. In the evaluation we placed a screen behind different curtains with varying transmissions and measured the detected signals from the surfaces for different laser intensities. The maximum return from the second surface occurs when the probability to get a detection from the first surface is around 0.5-0.7 per pulse. At higher laser excitation power the signal from the second surface decreases. To optimize the foliage penetration capability it is thus necessary to adaptively control the laser power to keep the returned signal within this region.

10434-5, Session 1

Laser SRS tracker for reverse prototyping tasks

Alexsandr S. Grishkanich, ITMO Univ. (Russian Federation); Dmitriy N. Redka, Saint Petersburg Electrotechnical Univ. “LETI” (Russian Federation); Konstantin Tsvetkov, JSC Shipbuilding & Shiprepair Technology Ctr. (Russian Federation)

According to the current great interest concerning Large-Scale Metrology applications in many different fields of manufacturing industry, technologies and techniques for dimensional measurement have recently shown a substantial improvement. Ease-of-use, logistic and economic issues, as well as metrological performance, are assuming a more and more important role among system requirements. The project is planned to conduct experimental studies aimed at identifying the impact of the application of the basic laws of chip and microlasers as radiators on the linear-angular characteristics of existing measurement systems. The project is planned to conduct experimental studies aimed at identifying the impact of the application of the basic laws of microlasers as radiators on the linear-angular characteristics of existing measurement systems. The system consists of a distributed network-based layout, whose modularity allows to fit differently sized and shaped working volumes by adequately increasing the number of sensing units. Differently from existing spatially distributed metrological instruments, the remote sensor devices are intended to provide embedded data elaboration capabilities, in order to share the overall computational load

10434-6, Session 2

Characterization and performance of a LWIR polarimetric imager *(Invited Paper)*

Johan Eriksson, David Bergström, FOI-Swedish Defence Research Agency (Sweden); Ingmar Renhorn, Renhorn IR Consultant AB (Sweden)

The polarimetric dimension has been shown to provide means for potentially enhancing the capacity of electro-optical sensors in areas such as anomaly detection, identification and material characterization. Any potential benefit weigh against the added complexity of the sensor and the occurrence and robustness of polarimetric signatures. While progress in the design of novel systems for snapshot polarimetry may result in compact and lightweight polarimetric sensors, the aim of this work is to address the nature of polarimetric signatures and put that in relation to the noise properties of polarimetric sensors. Initial progress on the design, characterization and performance of a polarimetric imager, primarily designed for static scenes in the long wave thermal infrared, is presented. The system utilize the division-of-time principle and is built around an uncooled micro-bolometer camera and a rotating polarizing filter. Methods for radiometric and polarimetric calibrations are presented and residual polarimetric noise properties are explored. It is shown that the ability to characterize, model and compensate for instrument effects play a crucial role for the separation of radiometric and polarimetric effects. The robustness of polarimetric signatures are illustrated by examples of diurnal variations in outdoor scenery. Limitations and growth potential of the current system are discussed.

10434-7, Session 2

Single vs. dual color fire detection systems: operational tradeoffs

Meir Danino, Yosef Danan, Moshe Sinvani, Bar-Ilan Univ. (Israel)

In attempt to supply a reasonable fire plume detection, multinational cooperation with significant capital is invested in the development of two major Infra-Red (IR) based fire detection alternatives, single-color IR (SCIR) and dual-color IR (DCIR). False alarm rate was expected to be high not only as a result of real heat sources but mainly due to the IR natural clutter especially solar reflections clutter. SCIR uses state-of-the-art technology and sophisticated algorithms to filter out threats from clutter. On the other hand, DCIR are aiming at using additional spectral band measurements (acting as a guard), to allow the implementation of a simpler and more robust approach for performing the same task.

In this paper we present the basics of SCIR & DCIR architecture and the main differences between them. In addition, we will present the results from a thorough study conducted for the purpose of learning about the added value of the additional data available from the second spectral band. Here we consider the two CO2 bands of 4-5 micron and of 2.5-3 micron band as well as off peak band (guard). The findings of this study refer also to Missile warning systems (MWS) efficacy, in terms of operational value. We also present a new approach for tunable filter to such sensor.

10434-8, Session 2

A method of recognition of maritime objects based on FLIR (forward looking infra-red) sensor images using dynamic time warping

Tadeusz Pietkiewicz, Wojskowa Akademia Techniczna im. Jaroslawa Dabrowskiego (Poland)

Passive infra-red sensors FLIR (forward looking infra-red) used for the recognition of maritime objects are deployed on maritime surveillance aircraft or ships. They are used primarily for short- to medium-ranged recognition and identification of surface ships (civilian or military). A FLIR sensor yields achromatic digital images in which every pixel is characterized by one number – a pixel luminance.

A FLIR sensor can be practically implemented to recognize and identify maritime objects when a classifier (performing object identification) has a database of images of maritime objects. The classifier can then decide which object in the database is the closest to the observed object due to the values of specific objects attributes and the value of distance criterion. In this paper FLIR images of maritime objects from the Baltic Sea have been used.

In the first part of the paper a model of the process of image recognition of maritime objects based on FLIR images is presented.

In the next chapters selected algorithms used in the classification process are presented.

The paper presents a segmentation algorithm based on the Otsu method, which main advantage is a possibility of full automation of the segmentation process, but the quality of the maritime object silhouette is not the highest.

In the paper as a second segmentation algorithm (for comparison) is used a segmentation algorithm VPS (Visual Perception - based Segmentation). Its operation is based on the imitation of the adaptability of the human vision system.

The result of these algorithms are maritime object silhouettes represented by binary images. The product function of the brightness of silhouette binary image pixels and the original grayscale image results in a silhouette image containing information on temperature distribution.

As distinctive features of silhouettes two histograms of each image: a histogram of vertical projection of pixel brightness on the horizontal axis and a histogram of horizontal projection of pixels brightness on the vertical axis has been adopted. These histograms are subsequently used for determining the distance between the recognized FLIR image and images contained in the pattern database. The basis of this process is an algorithm of time series comparing DTW (Dynamic Time Warping). This algorithm determines the global distance of two time series.

The problem of assessing the similarity of objects silhouettes has been brought to the problem of assessing the distance between pairs of histograms: a pair of vertical histograms, a pair of horizontal histograms and a pair of histograms obtained by the concatenation of vertical and horizontal histograms.

In the next part of the paper the classification algorithm is presented. It chooses the best (most similar) images contained in the database of pattern FLIR images. This classifier is a one-dimensional distance classifier with Euclidean distance function over the distance space created by the DTW algorithm.

In the last part of the paper the results of the developed method to recognize maritime objects based on FLIR images are presented. The results relate to two methods of segmentation and three different types of histograms as distinctive features of silhouettes. In conclusions proposals for the development of the method and directions for further research have been formulated.

10434-9, Session 2

Fine-grained visual marine vessel classification for coastal surveillance and defense applications

Berkan Solmaz, ASELSAN A.S. (Turkey); Erhan Gundogdu, ASELSAN A.S. (Turkey) and Middle East Technical Univ. (Turkey); Kaan Karaman, ASELSAN RESEARCH CENTER (Turkey); Veysel Yucesoy, ASELSAN A.S. (Turkey) and Bilkent Univ. (Turkey); Aykut Koç, ASELSAN A.S. (Turkey)

The need for capabilities of fully automatic categorization and recognition of visual content has substantially improved due to presence of large number of images captured by surveillance cameras. Computer vision researchers have been working on development of effective methods for learning compact representations of visual data. During the recent years, compared to the hand-crafted visual representations, deep learning based architectures have received great attention due to their success in visual categorization of generic user uploaded images. Moreover, fine grained image categorization, a closely related research problem to generic image categorization aiming classification of fine subcategories within coarse object categories, was studied for developing diverse applications such as classifying images of vehicles, birds, dogs, food and plants. Higher visual similarity between species of coarse groups makes fine-grained categorization a more challenging problem compared to generic image categorization.

In this paper, we propose the use of several deep learning based architectures for categorizing and recognizing marine vessels for defense and security applications. First, we gather a large number of marine vessel images via online sources, then we group them into three coarse categories such as defense vessels, civil and commercial vessels. Next, we subgroup all defense vessels into fine categories such as landing ships, mine warfare, destroyers and aircraft carriers. For use in experiments we split collected images into two non-overlapping groups; training and testing. For describing each image and distinguishing thousands of images belonging to coarse and fine categories, we extract state-of-the-art hand-crafted and deep visual representations and train a multi-class support vector machine. As more effective representations, we also fine tune convolutional neural network based deep architectures for marine vessel images. Then, we perform extensive experiments mainly on two beneficial scenarios, classification and recognition of marine vessels, and provide a detailed performance comparison of hand crafted representations and deep architectures for both scenarios. First experiment involves coarse categorization of marine vessel images. Second experiment aims learning fine categories belonging to coarse categories. Third experiment, embroils recognition of specific defense vessels, since availability of multiple images for each marine vessel makes discrimination achievable. As an additional experiment, we attempt joint learning of coarse and fine labels for deep representations when no prior information is present prior to analysis of marine vessel images. Obtaining high performance on classification of both coarse and fine categories and encouraging results for recognition of marine vessels using deep architectures, we believe the capabilities presented in this work may be essential components of future coastal and on board surveillance and security systems.

10434-10, Session 2

Real-time moving objects detection and tracking from airborne infrared camera

Andrea Zingoni, Marco Diani, Giovanni Corsini, Univ. di Pisa (Italy)

Detecting and tracking moving objects from an airborne infrared (IR) camera offers interesting possibilities in video surveillance, remote sensing and computer vision applications, like monitoring large areas simultaneously, quickly changing

the point of view on the scene and pursuing the objects of interest. To fully exploit such a potential, versatile solutions are needed, but, in the literature, the majority of them works only under specific conditions about the considered scenario, the characteristics of the moving objects or the aircraft flight modes.

Therefore, we proposed a novel approach to the problem and developed a detection and tracking algorithm that overcomes these limitations. The algorithm works independently from the monitored scenario and is suitable to detect small objects and robust to changes in the point of view of the camera and to possible abrupt movements of the aircraft, allowing this either to monitor the scene from afar or to approach and pursue a specific object. In addition, it performs in real-time even using cheap processors, thanks to a light computational load.

The algorithm consists of three main stages, namely detection, registration and tracking, performed iteratively at each acquired frame. In the first stage, an initial coarse detection map is computed by using a particular local statistic robust to noise and clutter and fast to calculate at the same time. The detection map is then refined through morphological operations to reduce false alarms, label the candidate moving objects and provide their position.

In the second stage, exploiting the information about attitude and velocity of the aircraft provided by a low-cost inertial navigation system (INS) on board, the candidates position is registered on a frame chosen as reference. This contains the position of each candidate at each acquired frame, so as to recreate the favorable situation of steady camera. To correctly register the candidates position, an estimation of their distance from the aircraft is performed with a fast structure-from-motion algorithm based on INS data.

In the third stage, the candidates are tracked using a Kalman filter, on the basis of their previous positions within the reference frame. The steady ones are rejected and excluded from the detection in the subsequent iterations, whereas the moving ones are declared as detected. The detection map is finally registered on the next acquired frame to retrieve information on the moving objects appearance and position referred to the current camera viewing geometry, which will be used to compute the statistic in the detection stage of the new iteration.

The algorithm has been tested on a large dataset of simulated IR video sequences, recreating various scenarios and various points of view and flight trajectories, in order to evaluate quantitatively its performance in different conditions. Promising results have been obtained, either in terms of detection and false alarm rate or in terms of accuracy in position and velocity estimation. In addition, the algorithm has been capable to perform in real-time. Then, to assess its behavior also in real cases, it has been used to pursue cars or people with a drone, completing the task successfully and confirming its effectiveness.

10434-11, Session 3

Active multispectral reflection fingerprinting of persistent chemical agents *(Invited Paper)*

Hans Dieter Tholl, Diehl BGT Defence GmbH & Co. KG (Germany); Marcel Rattunde, Fraunhofer-Institut für Angewandte Festkörperphysik (Germany); François Gutty, Thales Research & Technology (France); Mariusz Kastek, Wojskowa Akademia Techniczna im. Jaroslawa Dabrowskiego (Poland); François Brygo, Bertin Technologies (France); Frank Wilsenack, Wehrwissenschaftliches Institut für Schutztechnologien (Germany)

Reliable and sensitive standoff detection of C agents has considerable operational implications. Available instruments are based on passive spectroscopic techniques. Currently, there is a need to specifically detect liquid or powder contamination with very low vapour pressure and non-persistent chemical warfare agents or toxic industrial chemicals at stand-off and remote distances.

The project AMURFOCAL is conducted under the Joint Investment Programme (JIP) on CBRN protection funded through the European Defence Agency (EDA). The project has the research topic of C agent detection and identification at stand-off distance with amplified quantum cascade laser technology in the long wave infrared spectral range, where the C agents have typically strong absorptions bands.

The project is seeded by two recent developments in infrared lasers in the spectral range between 8-12μm: tunable external cavity quantum cascade lasers and tunable parametrical optical amplification to boost the output power to 100 W peak power at the wavelength of the emission of the EC-QCL. The receiver is based on a broadband infrared detector with a few detector elements. The output is transmitted to a target in a distance of 10 - 20 m. A 3D data cube is registered by wavelength tuning the laser emission while recording a synchronized signal received from the target. A chemometrics software tool analyzes the backscattered laser light. A particular CWA is identified and localized through the extraction of its characteristic spectral fingerprint out of the 3D data cube.

The talk reviews the detection of chemical warfare agents, describes the AMURFOCAL instrument, its functional units, and its principles of operation.

10434-12, Session 3

Simultaneous remote measurement of CO2 concentration, humidity and temperature with a matrix of optical fiber sensors

Karol Wysokinski, Marta Filipowicz, Tomasz Stanczyk, Stanislaw Lipinski, InPhoTech (Poland); Marek Napierala, InPhoTech (Poland) and IPT Safety (Poland); Michal Murawski, Polish Ctr. of Photonics and Fiber Optics (Poland); Tomasz Nasilowski, InPhoTech (Poland)

A matrix of optical fiber sensors eligible for remote measurements is reported in this paper. The aim of work was to monitor the air quality with a device, which does not need any electricity on site of the measurement. The matrix consists of several sensors detecting carbon dioxide concentration, relative humidity and temperature. Sensors utilize active optical materials, which change their colour when exposed to varied conditions. All the sensors are powered with standard light emitting diodes. Light is transmitted by an optical fiber from the light source and then it reaches the active material layer which changes its colour, when the conditions change. This results in a change of attenuation of light passing through the active layer. Modified light is then transmitted by another optical fiber to a detector, where a simple photoresistor is used. It is powered by a stabilized DC power supply and the current is measured. Each light source used for the measurements requires a reference optical fiber, which is not used for sensing, but it transmits the light to the detector, so any differences of the basic power output level can be recorded. Polymer optical fibers are used for light transmission, which makes the light coupling into the fiber simple, and reduces the cost of a device. Since no expensive elements are needed to manufacture such a matrix of sensors, its price may be competitive to the price of the devices already available on the market, while the matrix also exhibits other valuable properties. Such a sensor may be used for monitoring the air quality in manifold places including explosion endangered areas. It is possible, since the sensors are all-optical and thus they are inherently non-sparking and intrinsically safe. For instance they may be used for the monitoring of underground mines, oil refineries, natural gas production sites or places, where fossil fuels are being stored. An increase of carbon dioxide concentration may be an indicator of fire or explosion. There is also an another emerging application of CO2 measurement, which is a supervision of key points of buildings, since carbon dioxide is produced by human breath and therefore the rise of the carbon dioxide concentration may indicate an unauthorised intrusion.

10434-13, Session 3

New optical scheme of the intensity control for a remote gas analyzer

Denis Shabrov, Vadim A. Gorobets, Ilya Puchkouski, Boris Kuntsevich, B.I. Stepanov Institute of Physics (Belarus)

Usually in the optical scheme of the reference channel of a remote gas analyzer on the base of a TEA CO2 laser the part of the laser radiation reflects from a IR material plate (for example ZnSe) and goes to a photodetector. In this case it is necessary to provide the full interception of a laser beam especially for lasers with non-uniform distribution of radiation energy on the spot. However the big lack of such simple optical circuit of the reference channel of a gas analyzer is too big amplitude of a basic signal. The simple attenuation of the signal by the plates with a limited transmission does not solve the problem, since IR materials normally used for these purposes are semitransparent in the middle IR region of matter either having a small attenuation factor (which leads to unacceptable dimensions) or a strong dependence on the wavelength of the radiation.

The new scheme of the reference channel of a remote gas analyzer has been offered and realized. The use of additional reflective elements with the low reflection factor allows to receive full interception of laser radiation and to provide a linear operating mode of a photodetector even for the strongest laser lines. Analysis of the spectra of possible plates for use has shown that it is most convenient to use as a weakly reflecting plate of LiF and ZnSe. The spectral dependence of their reflection factors in the range 9.2-10.8 micrometers is practically linear.

At the measurement of a concentration of air pollutions on a differential method the weak dependence of reflection factors for used reflecting plates from wavelength can be easy to take into account by adding corresponding factors in the formula for calculations of air pollution concentrations..

The application of the new optical scheme of the reference channel for the gas analyzer has allowed carrying out correct measurements of air pollutants with the high accuracy.

10434-14, Session 3

Passive fiber optic temperature sensor for safety applications

Agnieszka Kolakowska, InPhoTech (Poland) and Warsaw Univ. of Technology (Poland); Karol Wysokinski, Janusz D. Fidelus, Stanislaw Lipinski, InPhoTech (Poland); Malgorzata Kuklinska, Polish Ctr. of Photonics and Fiber Optics (Poland); Anna Pytel, InPhoTech (Poland) and Warsaw Univ. of Technology (Poland); Pawel Mergo, Univ. of Maria Curie-Sklodowska (Poland); Tadeusz Tenderenda, InPhoTech (Poland); Miroslaw A. Karpierz, Warsaw Univ. of Technology (Poland); Tomasz Nasilowski, InPhoTech (Poland)

Energy blackouts are one of the most critical problems in nowadays safety management. An energy blackout can occur as a result of an electrical fault at a power station or a transmission line, which can be caused by temperature increase at transformers or other electrical devices where electromagnetic (EM) fields are high enough to disturb the temperature measurement. To prevent such incidents Fiber Optic Sensors (FOS) can be applied. Devices based on optical fiber technology are insensitive to external EM fields and are intrinsically safe (as no electrical power is needed at the sensing point), so the temperature measurement can be performed in areas where standard electronic devices cannot be easily applied. What is more, due to very low silica fiber attenuation the measurement point can be located kilometers away from a light source and detector, what makes the sensors independent on a local power source. Furthermore due to small size FOS can be also used for temperature sensing in mechanical mechanisms where the amount of free space is very low. They can be also integrated with the structure of different materials for military applications (e.g. in tanks and airplanes).

In this work we propose an intrinsically safe temperature sensor based on fiber optic technology. The presented sensor is entirely passive and benefits from all of the above mentioned advantages, which allows it to be applied in most demanding environments. The construction of the presented sensor is based on a dedicated microstructured optical fiber what allows to adjust both the range and sensitivity of the sensor to a specific application.

We present the results of temperature measurements with a series of sensors designed for operation in the temperature range between 30˚C to 100˚C. The experimental investigation proved that the sensors have linear temperature to power characteristic, and the measurement resolution is 0.1 ˚C. The developed sensors, due to its numerous advantages (namely intrinsic safety, EM field insensitivity, limited strain cross sensitivity and possibility of remote sensing), may be used in safety applications, such as preventing energy blackouts or continuous mechanical elements temperature monitoring.

10434-15, Session 3

Dual-core optical fiber based strain sensor for remote sensing in hard-to-reach areas

Anna Makowska, Lukasz Szostkiewicz, InPhoTech (Poland) and Warsaw Univ. of Technology (Poland); Agnieszka Kolakowska, Dawid Budnicki, InPhoTech (Poland); Beata Bienkowska, Lukasz Ostrowski, Michal Murawski, Polish Ctr. of Photonics and Fiber Optics (Poland); Marek Napierala, InPhoTech (Poland) and Warsaw Univ. of Technology (Poland); Pawel Mergo, Univ. of Maria Curie-Sklodowska (Poland); Tomasz Nasilowski, InPhoTech (Poland)

In many different applications, detection of strain is necessary. For example, strain measurements gives us information about mass movements, working load of machines, intrusion appearance etc. Using optical fibers is advantageous especially when one is focused on assuring the maximum level of security. In various application electrical devices are not welcome, wherever there are explosive substances, e.g. in mine-like objects. By using optical fibers, one can realize non-spark measurements. Taking advantage of the fact, that optical fibers can play both the role of sensing elements and they can realize signal delivery, we can effectively realize remote sensing in hard-to-reach areas.

We present research on optical fiber sensors including simulation and model validation. As a base for the strain remote sensor we use dual-core fibers. Although multi-core fibers are recognized mostly as a base for the next generation telecommunication systems, at the same time, they can be advantageously used in sensor technology. Multi-core fibers possess a characteristic parameter called crosstalk, which is a measure of the amount of signal which can pass to the adjacent core. High level of crosstalk is found to be highly undesirable for telecommunication applications. However, for construction of new types of fiber optic sensor, this phenomenon can be advantageously used.

The proposed fiber structure is distinguished by the presence of the air-holes. The fiber itself exhibits very low crosstalk – the interference of the supermodes in the structure is non-efficient. In order to create a strain-sensitive area, we take advantage of the fiber post-processing, namely fiber tapering. In the tapered section, the air-holes are collapsed, so locally we increase the crosstalk parameter. Strain measurement is realized thanks to the fact that depending on the strain applied, the power distribution between the cores of dual-core fibers changes. Principle of operation allows realization of measurements both in wavelength and power domain. The second option is cost-effective as far as there is no need for interrogators.

We elaborated the numerical model in order to simulate the effect of applying strain to the sample. Experimental results are in very good compatibility with stimulated values. Both numerical and experimental results confirmed that performance of the sensor can be adjusted by changing taper parameters, particularly its length and ratio. Strain sensitivity can reach the values above 15nm/m? (experimental value), what is a value an order of magnitude bigger than in commercially available strain sensors based on Fiber Bragg Gratings. In the research framework, we examined also temperature sensitivity, proving that it has negligible level.

10434-16, Session 4

Low cost SWIR imager for remote sensing on small UAVs *(Invited Paper)*

Ethan J. D. Klem, Dorota S. Temple, RTI International (United States); Christopher W. Gregory, Allan H. Hilton, Micross Components, Inc. (United States); Nathan Reim, Joseph Eyerman, RTI International (United States)

The rapid growth of security and commercial applications of small autonomous moving platforms like unmanned aerial vehicles (UAVs) has further increased interest in low-cost infrared sensors. While such low-cost sensors exist for the long-wave infrared (LWIR) portion of the spectrum, commercial focal plane arrays (FPAs) for the short-wave infrared (SWIR) range (wavelengths between 900 nm to 1700 nm) are much more expensive, and therefore not practical for implementation on small UAVs (sUAVs). And yet, there is considerable interest in adding SWIR imagers to the sUAV sensor suite, particularly for surveillance in haze or smoke, and for agricultural applications. SWIR imaging can provide information on water and nutrient content in plants and soil, facilitating monitoring of the health of crops and crop yield forecasts. In this paper, we will describe the fabrication and performance of SWIR FPAs developed at RTI International that are based on heterojunctions incorporating colloidal quantum dots (CQDs) of lead sulfide (PbS) and carbon fullerenes (C60). P-type PbS CQD films are deposited by spin coating of the CQD solution directly on readout integrated circuit (ROIC) wafers, and are chemically and thermally treated to tailor electro-optical properties of the CQD film. N-type C60 films are deposited by thermal evaporation. The wafer-level deposition techniques executed at low temperature and the monolithic integration of the photodiode arrays with the ROICs are key to the low cost of the CQD FPA. In addition, the monolithic integration facilitates decreasing the pixel size and increasing the array format, leading to the reduction of the size, weight and power (SWAP) of the camera. We will conclude the presentation with the report on the integration of the CQD SWIR camera on a hexacopter UAV and the imaging performed during the test flights.

10434-18, Session 4

Research methods of video stabilization and object detection on the video

Anton Chukhlamov, Kseniia V. Ezhova, ITMO Univ. (Russian Federation)

When developing software for auto detection and tracking objects on video in real time, it is necessary to additionally provide for the possibility of stabilizing the original video.

If there is a beating of the image that occurs when the optical system moves in the transverse direction, program image stabilization, viewing images without shaking, and, in case of blurring of the image, it is much easier to optimize for objects on it.

Within this work there were used several numbers of actual algorithms, that can solve the computer vision problems (with using openCV library and C++).

Introduction. Results of development of the software for the video stabilization and object detection on the video. The processes of stabilization of a flow of images are described and detecting of objects on the image, in this case, it is the person, are also described. There are different parallelizing computing methods, are described.

Problem definition. An initial task – to analyse the existing algorithms of stabilizatioan and detecting. The developed Software has to:

- stabilize the video with a minimum time delay;

- detect in a flow of images of the person (a face, eyes, a mouth, a nose, hair);

- watch the movements of the person;

- work quickly and correctly (real time)

The following goals were reached:

1. The existing algorithms for face recognition were analyzed and a person tracking system was created using openCV algorithms.

2. The existing algorithms of video stabilization were analyzed.

3. Using QT (cross-platform).

4. To parallelize the calculations, the GPU is used.

5. At the moment, the possibility of creating a hardware-software system (a special camera that accepts the same calculations and software) is being considered.

10434-33, Session 4

The photonic technology revolution Influence on the defence area

Jacek Galas, Dariusz Litwin, Narcyz Blocki, Marek Daszkiewicz, Institute of Applied Optics (Poland)

The revolution in photonic technology is comparable to the revolution in electronics provided by transistors, integrated circuits, microprocessors and computers. Development of technology of photonic integrated circuits and photonics components will lead to deep changes in military technique and then to build military systems with new features not possible to achieve with classical electronic techniques. The most important changes will concern the radar and radiolocation techniques as well as radiocommunication and telecommunication systems together with quantum cryptography devices. This paper will describe the progress in photonic technology and how it influences the above military applications.

10434-20, Session 5

Imaging and laser profiling for airborne target classification

Ove Steinvall, FOI-Swedish Defence Research Agency (Sweden)

Optical imaging for long range target classification has its practical limitations due to the demand on high transverse sensor resolution connected to small pixel sizes, long focal lengths and large aperture optics. It is therefore motivated to look for 1D laser range profiling for target classification.

Laser range profiling is attractive because the maximum range can be substantial, especially for a small laser beam width. A range profiler can also be used in a scanning mode to detect targets within a certain sector. The same laser can also be used for active imaging when the target comes closer and is angular resolved. Although the profiling may by itself be sufficient for target classification the discrimination capabilities among a group of anticipated targets candidates may be uncertain due to uncertainty in the target aspect angles, atmospheric effects and sensor noise. It is therefore motivated to look at a sensor fusion approach in which the profiling data is combined with imaging data even when these data have a rather low resolution.

Example of both simulated and experimental data will be investigated and analyzed for target classification purposes.

10434-21, Session 5

Person detection and tracking with a 360° lidar system

Marcus Hammer, Marcus Hebel, Michael Arens, Fraunhofer-Institut für Optronik, Systemtechnik und Bildauswertung (Germany)

Today it is easily possible to generate dense point clouds of the sensor environment using 360° LiDAR (Light Detection and Ranging) sensors which are available since a number of years. The interpretation of these data is much more challenging. For the automated data evaluation the detection and classification of objects is a fundamental task. Especially in urban scenarios moving objects like persons are of special interest. Examples can be found in automatic collision avoidance for mobile sensor platforms or surveillance tasks.

In literature there are several approaches for automated person detection in point clouds. While most techniques show acceptable results in object detection, the computation time is often crucial. The runtime can be problematic, especially due to the amount of data in the panoramic 360° point clouds. On the other hand, for most applications a real time object detection and classification is needed.

The paper presents a proposal for a fast, real-time capable algorithm for person detection, classification and tracking in panoramic point clouds.

To achieve sufficient fast object detection we use the dense and organized structure of the point clouds. The typical 360° point cloud consists of up to 250000 individual “pixels” (range values) in up to 64 rows, representing a time interval of 0.1 s. For each pixel the immediate horizontal vicinity is checked to find range differences. If there is no substantial range difference, the two pixels are attributed to the same structure. On the other hand, if there is a range difference, the two pixels are assumed to belong to two different structures. In this way, a 2D line clustering is done.

For all line clusters with a suitable width the vertical neighborhood is checked for other clusters with similar horizontal coordinates to form 3D clusters. When a 3D cluster roughly meets the dimensions of a human body in height and width it is classified as a person hint. With this approach a person classification rate of over 99 % can be achieved, but the precision is poor.

To improve the precision these person hint objects are further classified using Bayesian probabilities of several object features like the cluster width or the amount of points in the cluster. In this way the precision can be raised to an adequate but not optimal amount, unfortunately the classification rate gets slightly worse.

This drawback can be reduced by a global tracking of all person hint objects. If the object stays on a stable position, it is most likely not a person and the person probability is not altered. In contrast the person probability of moving objects with a trajectory correlating to human movement can be increased.

With this fast geometric approach it is possible to detect and track persons in panoramic views in real time (that is up to 10 frames per second) with a high detection rate and an acceptable false positive rate. The motion vector of the detected pedestrians, which is a result of the tracking, can be used for pedestrian route estimation.

10434-22, Session 5

Super-resolution depth information from a shortwave infrared laser-gated viewing system by using correlated double sampling

Benjamin Göhler, Peter Lutzmann, Fraunhofer-Institut für Optronik, Systemtechnik und Bildauswertung (Germany)

A laser gated-viewing (GV) system provides range-gated images without any range resolution within a pre-defined range gate. The only depth information that is obtained is that all objects visible in the GV image are located within the range gate. Of course, the range gate can be moved in depth from frame to frame yielding a tomographic sequence of the scene which can be used for 3D reconstruction. However, each GV image of this sliding gates sequence requires a separate laser pulse and thus additional capturing time which may be not available for a real-time system or in a dynamic scenario with moving objects.

There is also another, more sophisticated approach for deriving 3D information from only two GV images with slightly different positions of the range gate. This approach makes use of the shape of the gate profile which is not a perfect box function but consists of rising and falling slopes with a plateau region in between. By comparing the pixel gray values of an object located within a slope region in the first GV image with the pixel gray values of this object within the plateau region in the second GV image, the corresponding ranges can be calculated with a higher depth resolution (super-resolution) than the minimal gate shift step size.

Following this idea, we have applied this approach to the reset and signal images of a new short-wave infrared (SWIR) GV camera whose read-out integrated circuit (ROIC) supports correlated double sampling (CDS) actually intended for the reduction of kTC noise (reset noise). The reset and signal images, and thus the derived depth information, are extracted from only one single laser pulse.

The SWIR GV camera consists of a 640 x 512 avalanche photodiode (APD) array based on mercury cadmium telluride (MCT) with a pixel pitch of 15 ?m. A Q-switched, flash lamp pumped solid-state (FPSS) laser with 1.57 ?m wavelength (OPO), 52 mJ pulse energy after beam shaping, 7 ns pulse length and 20 Hz pulse repetition frequency is used for flash illumination.

In this paper, the approach for calculating super-resolution depth information from only one GV image by using CDS is introduced. The range accuracy of this method is determined from real measurements and compared to results of the sliding gates technique. Finally, 3D reconstructions of different objects are presented.

10434-23, Session 5

Robust eye-safe pulsed fiber laser source for 3D ladar applications

Lars G. Holmen, Norwegian Defence Research Establishment (Norway) and Univ. I Oslo (Norway); Gunnar Rustad, Magnus W. Haakestad, Norwegian Defence Research Establishment (Norway)

Ladar (laser detection and ranging) systems are finding important applications within 3D imaging for use with autonomous vehicles, topographic mapping, and remote sensing. To a large extent, the performance of the laser source determines the capabilities of a given ladar system, and the advances in laser technology opens up possibilities for new designs and applications. In particular, fiber laser technology has driven the power scaling needed for developing sources for high-performance scanning ladar systems with several kilometer detection ranges. Such ladar systems require several tens of μJ laser pulse energy at several tens of kHz pulse rate

with nanosecond pulse duration and good beam quality.

Pulsed laser sources with a wavelength of 1.55 μm are attractive for remote sensing applications as 1.55 μm is considered to be an "eye-safe" wavelength. This wavelength is readily available from erbium-doped fiber lasers, which are attractive due to compatibility with the mature technology of fiber optic telecommunication. For practical applications, fiber laser sources can be realized in mechanically robust "all-fiber" designs, where all components are fused or spliced together.

Commonly, pulsed fiber laser sources are implemented as master oscillator power amplifiers (MOPAs) due to the power scalability and possible flexibility in seeding conditions. Direct control over the pulse repetition frequency and pulse duration is readily achieved using for example gain switched diode lasers as seed sources. Furthermore, seed diode current-modulation can be used to control the exact pulse shape, which can correct for pulse distortion caused by gain saturation in the final amplification stage of a MOPA.

The power available from commercial seed diodes has generally been limited to a few tens of mW. Thus, multistage amplification is needed to achieve nanosecond pulses of ~100 μJ energy, and typical setups that have demonstrated this performance have been implemented with at least three stages of amplification. In turn, this means that several stages of isolation and filtering of amplified spontaneous emission (ASE) between stages are required – both spectrally with band pass filters, and temporally through time-gating with e.g. acousto-optic modulators. Multistage designs thus increase the cost and complexity of the systems, and should from practical points of view be limited when possible.

We present an all-fiber MOPA at 1.55 μm wavelength, producing 140 μJ pulses at 50 kHz repetition rate with a full-width half-maximum duration of 5 ns, and a M^2 beam quality factor of 1.2. By using a high-power (100 mW) distributed feedback (DFB) laser diode as the seed source, we were able to reduce the system complexity down to two amplification stages. Furthermore, we achieve high operational flexibility by using a directly current-driven seed source, and the MOPA has been successfully operated at pulse repetition frequencies between 25 kHz and 100 kHz.

Our two-stage fiber MOPA delivers high performance while maintaining a low complexity. Combined with a robust all-fiber design, our design is well suited as a field source for remote sensing applications such as 3D imaging.

10434-24, Session 5

Velocity and range measurement optical frequency stepped chirp modulated coherent lidar for space application

Xiaolin Sui, North China Research Institute of Electro-optics (China); Xiaojun Shi, CETC, Science and Technology Dept. (China); Shouhuan Zhou, North China Research Institute of Electro-optics (China)

Coherent doppler lidar has been widely used in the 1960s, which can be used to measured range, speed of moving targets, wind speed and vibrations. The performance of the coherent radar has advantages compared to the direct detection radar. It has strong anti-jamming capability, high detection sensitivity and access to large amount of information, which are important direction of future development of lidar.

The structure of coherent doppler lidar is complex and bulky, which limited its application before the year of 2000. With the development of laser technology, in particular, the tunable diode laser technology, which leads to coherent laser radar can be realized compact in size. Master oscillator power-amplifier (MOPA) structure of the coherent light source has frequency modulation function in distributed feedback semiconductor (DBF) lasers and erbium doped fiber amplifier (EDFA), which is a new type emission source of coherent radar. The emergence of the source caused coherent laser radar technology innovation, which made it possible to achieve frequency modulation continuous wave coherent doppler lidar.

We introduced Structural theory and key technologies of frequency modulated continuous wave coherent doppler lidar in detail and experimental results are presented in this paper.

In order to test the performance of the FM continuous wave CDL, we use a rotating flywheel to build the experimental platform. Then we use a tunable laser that can control the frequency difference of laser, aiming at the edge of the flywheel that has some known speed. The reflected signal light and a local oscillator light are coupled into an optical fiber and received by the detector. Finally, the signal is sampled and processed by some algorithms to compute the line speed of the flywheel. Flywheel with high-precision servo motor driving and shaft angle encoder calibrating, the relative accuracy of 0.1%.The signal waveform is shown and the experimental results are shown By comparison of different speed settings of the flywheel and the actual measurement value, the signal processing system is able to get the correct measurement results.

10434-25, Session 6

Multimodal UAV detection: study of various intrusion scenarios

Sebastien Hengy, Martin Laurenzis, Stéphane Schertzer, Institut Franco-Allemand de Recherches de Saint-Louis (France); Alexander Hommes, Franck Kloeppel, Alex Shoykhetbrod, Thomas Geibig, Winfried Johannes, Fraunhofer-Institut für Hochfrequenzphysik und Radartechnik (Germany); Oussama Rassy, Frank Christnacher, Institut Franco-Allemand de Recherches de Saint-Louis (France)

Small unmanned aerial vehicles (UAVs) are becoming increasingly popular and affordable the last years for professional applications as well as for the private consumer market, with varied capacities and performances. Recent events showed that illicit or hostile uses are possible and constitute an emergent, quickly evolutionary threat. Recent developments in UAV technologies tend to bring autonomous, highly agile and capable unmanned aerial vehicles to the market. These UAVs can be used for spying operations (data collection for mission planning or infringing the sphere of privacy) as well as for transporting illicit or hazardous material (smuggling, flying improvised explosive devices).

The scenario of interest concerns the protection of sensitive zones (military or industrials) and individuals against the potential threat constituted by small drones. In the recent past, field trials were carried out to investigate the detection and tracking of multiple UAV flying at low altitude. Here, we present results which were achieved using a heterogeneous sensor network consisting of acoustic antennas, small FMCW RADAR systems and optical sensors. While acoustics and RADAR was applied to monitor a wide azimuthal area (360°) and to simultaneously track multiple UAV, optical sensors were used for sequentially identification.

Ground truth data has been measured thanks to an RTK-GPS added to the flying UAVs. The localization results have been compared to the ground truth data to estimate the efficiency of each detection system. The 7 microphones acoustic arrays are constituted with two interlocked tetrahedrons of 2.5 and 10 centimeters in width. For single source localization, the mean azimuth and elevation estimation error has been measured equal to 1.5 and -2.5 degrees respectively. The associated standard deviation is 4.4 and 3.5 degrees. The FMCW radar allows tracking of multiple UAVs by estimating their range, azimuth and motion speed. Both technologies can be linked to the electro-optical system for final identification of the detected object. The developed electro-optical prototype is a passive and active imaging system delivering images close to the natural perception of human operators. Fusion of RADAR and acoustic data is studied for threat position estimation to orientate the optical system.

10434-26, Session 6

Open architecture of smart sensor suites

Wilmuth Müller, Achim Kuwertz, Fraunhofer-Institut für Optronik, Systemtechnik und Bildauswertung (Germany); Christina Grönwall, Henrik Petersson, FOI-Swedish Defence Research Agency (Sweden); Rob J. Dekker, TNO (Netherlands); Frank Reinert, Fraunhofer-Institut für Optronik (Germany)

Experiences from recent conflicts show the strong need for smart sensor suites comprising different multi-spectral imaging sensors as core elements as well as additional non-imaging sensors. The smart sensor suites should be part of a smart sensor network – a network of sensors, databases, evaluation stations and user terminals. Its goal is to optimize the use of various information sources for military operations like situation assessment, intelligence, reconnaissance, target recognition and tracking. Such a smart sensor network will enable commanders to achieve higher levels of situational awareness.

Within the study at hand, it is analyzed how the efficiency of sensor suites can be increased by using an Open System Architecture. The open system architecture, based on a system-of-systems approach, enables combining different sensors in multiple physical configurations, like distributed sensors, co-located sensors combined in a single package, sensors mounted on a tower, sensors integrated in a mobile platform, and use of trigger sensors. The mode of operation is adaptable to a series of scenarios with respect to relevant objects of interest, activities to be observed, available transmission bandwidth, etc. The designed open architecture based on system requirements defined within the study at hand will be presented.

The sensor suites, linked to a sensor planning system and a C4ISR centre, may thus be part of a surveillance network. A smart sensor suite may be used in combination with future RPAS (Remotely Piloted Aircraft Systems) to support a more flexible dynamic configuration of the payloads.

Starting from a set of system requirements and relevant scenarios, an open system architecture of a smart sensor suite has been designed. The system architecture has been designed in accordance with the NATO Architecture Framework, version 3.1.

A series of views from the NATO All View (NAV), NATO Capability Views (NCV), NATO Operational View (NOV), NATO System View (NSV) and NATO Technical View (NTV) have been developed. The developed views together with the element library, containing descriptions of the architectural elements which have been used in the views' description will be presented.

10434-27, Session PS

Fiber optic perimeter system for security in smart city

Jakub Cubik, Stanislav Kepak, Marcel Fajkus, Jan Nedoma, Ondrej Zboril, Vladimír Va?inek, Jan Jargus, Martin Novak, V?B-Technical Univ. of Ostrava (Czech Republic)

Protection of persons and assets is the key challenge of Smart City safeguards technologies. Conventional security technologies are often outdated and easy to breach. Therefore, new technologies that could complement existing systems or replace them are developed. The use of optical fibers and their subsequent application in sensing is a trend of recent years. This article discusses the use of fiber-optic sensors in perimeter protection. The sensor consists of optical fibers and couplers only and being constructed without wires and metal parts bring many advantages. These include an absence of interference with electromagnetic waves, system presence can be difficult to detect as well as affect its operation. Testing installation of perimeter system was carried out under reinforced concrete structure. Subjects walked over the bridge at different speeds and over the different routes. The task for the system was an absolute detection of all subjects. The proposed system should find application mainly in areas with the presence of volatile substances, strong electromagnetic fields, or in explosive areas.

10434-29, Session PS

Automatic oil tank recognition in optical UAV imagery based on detection of elliptic roof

Zhaodong Niu, National Univ. of Defense Technology (China); Da Tang, Beijing Institute of Tracking and Telecommunication Technology (China); Yu Duan, Jiameng Pan, Weihua Wang, National Univ. of Defense Technology (China)

Oil tank is one kind of foundational industrial facility for storage of oil and petrochemical products. Automatic recognition of the oil depot in the remote sensing image is of important practical significance in many fields such as oil leakage prevention, disaster monitoring and environmental conservation. As so far, there have been some efforts paid on automatic oil tank detection from near-nadir optical satellite image, in which rooftop of the oil tank is similar to a circle region. Therefore, circle detection methods are widely used to extract the oil depot from the satellite image efficiently. However, it costs too much money and preparation time to obtain remote sensing images of oil depot by means of satellite. Nowadays, the Unmanned Aerial Vehicle (UAV) provides a valid alternative solution to the satellite for monitoring the oil depot, owing to its advantages of flexibility, rapid response and minimal cost. Distinct from the near-nadir satellite image, the circular roof of oil tank appears as ellipse in the oblique UAV image. What is more, recognition of oil tank in the forward-looking optical image suffers from some problems, including interference by complex ground scenes and occlusion between buildings.

In order to cope with aforementioned difficulties, a novel oil tank extraction method based on detection of the elliptic rooftop is proposed. To start with, the straight line segments of ground objects are detected in the image. Secondly, based on these detected straight lines, the candidate rooftops are extracted to form hypotheses of oil tanks. Finally, facade contours of oil tanks are extracted and used to verify hypotheses in the chosen Region of Interest (ROI).

Step one: Straight line segments extraction.

Firstly, edge points of ground objects are extracted in the optical UAV image by the Canny detector, and then these edge points are connected to form curve segments using the Kovesi algorithm. Finally, the iterative endpoint fit-and-split procedure is used to partition sequences of edge pixels that belong to the same curve into subsequences which are sufficiently straight.

Step two: Oil tank hypotheses formation using elliptic roofs.

In view of the fact that the circular rooftop of the oil tank appears as ellipse in the oblique UAV image, it is advisable to detect the elliptical contour in the edge image to generate hypotheses of oil tanks. Firstly, based on the geometric principles including connectivity, continuity and convexity, the detected line segments are linked to form arc segments, which are selected as ellipse candidates. Unlike previous ellipse detection methods, we do not use strict criterion and complicated strategy during the line grouping process, so as to reduce the computational requirement. As a result, the extracted arc may contain some outlier pixels which do not belong to the ellipse. Then, an ellipse is fitted to each arc segment by an iterative least square method. To eliminate the negative effect of the outliers, we randomly select a number of edge pixels from arc segment to estimate ellipse parameters, and count the number of edge pixels that support the estimated ellipse. Repeating aforementioned process enough times, if the normalized maximal number of supporter pixels is greater than predefined threshold, the corresponding fitted ellipse is taken as oil tank hypothesis.

Step three: Oil tank verification based on facade contours.

Since oil tank hypotheses may include some false alarms such as buildings, facade of oil tank should be used to verify the existence of real oil tank. Verification of oil tank is accomplished primarily by detection of facade contours including elliptic bottom boundaries and straight side boundaries under the rooftop.

Synthetic and real UAV images containing complex ground scenes are used to validate the performance of the proposed algorithm. Compared with state-of-the-art methods, the proposed algorithm can recognize oil tanks more accurately from UAV images including a variety of objects, such as roads and buildings. The proposed algorithm achieves probability of correct recognition greater than 95% with false alarms rate less than 0.01 per image.

10434-30, Session PS

Infrared small target detection in a wide field imaging system

Jinyan Gao, Zai-ping Lin, Wei An, National Univ. of Defense Technology (China)

Small target detection in wide-area surveillance is a challenging task. Current imaging staring sensors in practical systems are characterized by large pixel counts and wide field of view (WFOV). Therefore, it is not suitable to detect targets simply via a single algorithm in different background types. In this paper, we solve the problem by background type classification and take different background suppression methods to meet the high efficiency and accuracy detection requirements.

The wide field imaging system has the following advantages. First, the WFOV stairing IR data can contains the cooperative IR targets and targets of opportunity under a wide range of weather and seasonal conditions. Second, the WFOV sensors eliminate the requirement for mechanical balancing devices and have relatively stable platforms. This ensures that there is a lower jitter in multi-frame images. Third, the ability of WFOV sensors to download information is limited per unit time, so we take the local window approach to Improve the local area's SNR, and finally inprove the detection probability.

Our method contains three parts. First, different image pro-processing is compared, such as mean filter, median filter, high pass filter, top-hat filter and directional median filter, but the directional median filter is finally used. Second, considering most of the research on regional complexity is based on the information entropy of the image, it is applied to the binary background after adaptive thresholding, thus far, we get the intensive candidate regions in an image. Third, we performed high frame rate imaging (100 frames/second) on the intensive regions. Finally, after analysis, the targets presence sub-pixel motion characteristics in high frame rate image sequences, we proposed to employ the temporal variance filter to detect the target.

Monte Carlo implementation of the proposed detection method in the framework of wide field imaging system is provided. Experiment demonstration involves the quantitative analysis of different pro-processing methods by the SNR gain and the background suppression factor (BSF), and the directional median filter shows obvious advantages than the methods. In addition, the information entropy is verified by extracting the salience regions of the image. The final simulation results show that the proposed detection framework can successfully detect targets in typical surveillance scenarios.

10434-31, Session PS

Opto-digital complex for remote mine detection and minefields mapping

Arsenii Golovin, A. V. Demin, Dmitrii Abramov, Ekaterina Seledkina, ITMO Univ. (Russian Federation)

As a result of 2016, the number of dead and maimed people as a result of explosions of landmines and explosive devices has reached its maximum in the past 10 years, according to the International Movement for the Prohibition of Anti-Personnel Mines (ICBL).

Since this problem is especially actual, and effective solution has not been found yet, the task was set for a group of ITMO University scientists to develop a remote sensing search system capable of detecting and identifying hidden ground and subsurface objects with high detection rate and low level false alarms.

Many modern methods for the detection of mines and minefields are based on the use of primary (external contour and mine shape, contrast with respect to the surrounding background, uniformity of the image within the mine contour, etc.) and secondary features (wilted vegetation, loosened soil, traces left by the mine-laying machine, etc.)

Hyperspectral infrared imaging allows detecting both primary and secondary features and has higher informativity before broadband IR sounding, since it allows dividing the spectral range of the infrared device into a group of hundreds of different wavelengths with a high spectral resolution, the intensity of each depends on the emissivity and the true temperature of the soil surface.

The article proposes to use stereoscopic hyperspectral IR remote sensing in order to increase the reliability of detecting and reducing the frequency of false alarms. Stereoscopic surveying allows to exclude skipping of objects masked in vegetation and laid at an angle, and to separate the disturbed surface (friable signs) from ordinary soil and embankments. The results of processing hyperspectral data from two channels are combined into a thematic thermal stereomodel of the terrain, on which the anomalies found by the algorithm are highlighted.

The concept of an optical-electronic complex for remote sensing of minefields, structural and optical schemes, applied calculations and design solutions are presented in the first part of article. The second part of the article describes the basic algorithms for processing hyperspectral data, the method of combining them into a thermal stereomodel of the terrain, with the possibility of classifying objects. The concept of an ultimate geoinformation system is also provided that allows to combine a digital terrain model in the visible range with a thermal stereomodel for further solving the problems of detection and identification of hidden ground and subsurface objects, reconnaissance and planning of humanitarian demining missions.

10434-32, Session PS

Analysis of the inversion of winter wheat leaf area index based on the data of the double bases of satellite to land and MODIS

Hong-Wei Zhang, Key Lab. of Agrometeorological Safeguard and Applied Technique (China)

Winter wheat leaf area index Monitoring based on remote sensing was an important method to quickly acquire the growth status and spatial distribution in a large scale. In order to establish an accurate and convenient method for monitoring leaf area index, the methods of Co-inversion of "the Double Bases of Satellite to Land" & MODIS was utilized in the inverse of Winter wheat leaf area index in March of 2015 and 2016 respectively in Hebi city, Henan Province, China. The results showed that the two methods of LAI inversion could reflect the spatial distribution characteristics of winter wheat, and the MODIS stability was better, but the inversion value was lower than the observation in site. The method of "the Double Bases of Satellite to Land" had a better fitting effect than MODIS, and could be promoted in business.

1. Study Area & Data

The study area is located in Hebi city, Henan Province(35°26?—36°02?N?113°59?—114°45?E), which belong to warm temperate monsoon climate. The Date of observation was chose in Mid. March of 2016. There were 15 sites were selected.

2. Methods & Data Processing

2.1 LAI Calculating method based on in situ observation

(1)

There? ? is Leaf length and Max width respectively, n is the No. per wheat plant, k=0.83 is LAI corrected factor?m is the total plant number in 1 m2?S=10000 cm2?

2.2 The inversion of LAI based on MODIS

Radiative transfer model was used in this study, and described as:

(2)

There, S is canopy reflectance or transmittance, ? is wavelength, ?S, ?S is solar zenith angle and azimuth angle respectively, ?v, ?v is observed zenith angle and azimuth angle respectively, C is the physical structure parameters of vegetation canopy (such as vegetation-LAI, leaf inclination angle & distribution etc.)

2.3 The inverse of LAI based on “the Double Bases of Satellite to Land”

The Co-inversion of leaf area index is the 2th inversion in which set up the correlation between Land LAI observation & Satellite LAI inversion.

(3)

There, p is the canopy gap ratio which is the ratio of background pixels to all pixels, ? is zenith angle of instrument.

And the experience formula was set as follow.

(4)

3. Results Analysis

Tab. 1 the Analysis on the inversion of LAI of Winter Wheat based on MODIS & “the Double Bases of Satellite to Land”

Methods Model Mean square deviation F value

MODIS

0.47 349

the Double Bases of Satellite to Land

0.05 1377

4. Conclusions and Discussions

(1) Two methods of LAI inversion could reflect the spatial distribution characteristics of winter wheat, and the MODIS stability was better, but the inversion value was lower than the observation in site.

(2) The method of “the Double Bases of Satellite to Land” had a better fitting effect than MODIS, and could be promoted in business.

At the same time, due to the limitation of observation data, the study was just carry on in jointing stage of winter wheat, and it is necessary to establish inverse models in the whole stage.

Conference 10435: Technologies for Optical Countermeasures

Tuesday - Wednesday 12–13 September 2017

Part of Proceedings of SPIE Vol. 10435 Technologies for Optical Countermeasures XIV

10435-1, Session 1

The scientists' war: essential research areas for technological superiority in future conflicts *(Invited Paper)*

Philip Perconti, U.S. Army Research Lab. (United States)

During World War II thousands of scientists and engineers were working diligently on military applications in government laboratories, and the American people was increasingly aware and proud of their contribution. The press often referred to World War II as "the physicists' war". Military historians designated this period as the First Offset, where the scientific discoveries produced from government projects such as the Manhattan Project and the radar system (referred to as the powerful electronic eye at Bell Labs) ended the war. During the Cold War, the Second Offset emphasized surveillance, and reconnaissance platforms, precision-guided weapons, and stealth technology. The open question is, where will the US achieve its next technological superiority in future conflicts?

The intent of the presentation is to answer this question while considering nonlinear, multi-domain future conflicts with increased operational tempo, velocity of human interaction and events, vulnerabilities in cyberspace and space domains, and operations in highly populated regions. ARL scientists and engineers identified Essential Research Areas (ERAs) that are critical to ensuring the US Army technological superiority. The presentation descripts the ERAs formulation analysis, scientific gaps, and technical objectives, where we recognize that future warfare will be fought in three domains: (i) the physical, activities defined in space and time; (ii) the virtual, activities defined by thought and perception; and (iii) the human, the activities defined by the interaction of people and societies. The ERAs represent the highest scientific research priorities on which ARL focuses its resources. The ERAs are designed to enable the Army to dominate the theater of operations, project national power robustly, and execute combined arms maneuver in air, land, maritime, space, and cyberspace domains.

10435-2, Session 1

Innovation within defence *(Invited Paper)*

Paul A. Winstanley, UK Defence Solutions Ctr. (United Kingdom)

The UK Defence Solutions Centre (UKDSC) was formed and an independent partnership between the UK Government and the UK Defence Industry. The UKDSC operates pre-competitively and works on a 0 to 15-year horizon with the objectives of achieving better alignment between UK Government and International requirements, improving collaboration in the value chain and stimulating innovation and investment from a broad range of sources. Against this framework specific case studies of optical countermeasure activities will be described.

10435-4, Session 2

Testing missile warning and countermeasure systems (MWCS): instrumentation for development, production and maintenance of MWCS *(Invited Paper)*

Dario Cabib, CI Systems (Israel) Ltd. (Israel); ILya Koshkin, AltaSens, Inc. (United States)

CI has adopted a unique, all-encompassing approach to testing missile warning and countermeasure systems (MWCS). This is an integrated approach from two points of view: i) It specifically answers the testing needs of all stages in the life of an MWCS, from development to maintenance in the field, and ii) it is capable of carrying out all needed tests of most electro-optical subsystems of the MWCS.

For this purpose CI has developed unique equipment and methodology, examples of which are: i) a small, cost effective, easy-to-use, thermal envelope allowing environmental tests of MWCS sensor performance on a bench instead of the need to use cumbersome testing in a chamber: this solution is implemented on the detector manufacturing level as well as the complete sensor, ii) a complex missile simulator for a civilian aircraft MWCS, including both scenario feedback loop for acquisition and tracking by multi IR sensors and a radiometer for jamming code emission testing, and iii) a thermal signature simulator/theodolite combined system that easily allows mutual alignment, coverage zones along with field of view calibration of MWCS sensors mounted on the aircraft for threat detection and acquisition, and iv) a laboratory level multi channel threat simulation and counter measure receptor for integration and evaluation of the complete MWCS pod performance.

The general approach, specific solutions, methodology and other examples of unique instrumentation for this MWCS testing application will be presented in this paper.

10435-5, Session 2

Flare dispensing program optimization against third generation infrared seekers via genetic algorithm

Ragip Yurttas, Kaan Ergöz, Emrah Oduncu, TÜB?TAK B?LGEM ?LTAREN (Turkey)

MANPADS (Man-portable-air Defense System) missile having infrared detectors, aiming to destroy air platforms, determine the position of targets based on the infrared energy radiating from air platforms. It is possible to detect infrared signals radiating from an air platform by a missile seeker. This will enable the missile to estimate target position. On the other hand, there are many advanced techniques developed to prevent missiles to damage targets. It is a real need for the missiles to overcome these ECM (Electronic-Counter-Measures) techniques such as flare dispensing programs. In order to satisfy this basic need of missiles, certain techniques called ECCM (Electronic-Counter-Counter-Measures) techniques have been developed.

In this paper, to neutralize the MANPADS missile, flare dispensing programs which is optimized by Genetic Algorithm are generated. To generate optimum program, the simulation software on MATLAB are developed. This simulation has infrared background model to calculate background radiation, path radiance and spectral transmittance in the spectral range of modelled missile seeker's infrared detector. Modelled missile which has third generation cooled infrared seeker has gimbal, 3D PPN guidance and thrust model. This missile has also ECCM technique. This technique allows missile not to deceive by common type flares. The reason of that, common type flares have too high radiation than air platform. However spectral flare's radiation is similar with air platform radiation. To break lock of missile on target, two type flares which are common and spectral are modelled. Modelled flares have infrared signature with respect to time and kinematic motion model. As target model, simulation has F-16 jet platform which has 3D infrared signature model with different temperature zones and 6-DOF dynamic motion models.

Third generation infrared seekers can distinguish angular positions of more than one targets radiated on its FOV. Then, it can choose one of them with regard to their radiation levels. So as to break lock of missile, flares are dispensed. The most crucial parameters of dispensing flare programs are initiating of flare dispensing program, time sequences between dispensed

flares, dispensed flare number and dispensed flare types. To initiate flare dispensing program, two different approaches are developed. These approaches are user defined time and distance between missile and target. Dispensed flare numbers are pre-determined. For each run, 2 common type flares, 2 spectral type flares are dispensed. To determine the time sequence between dispensed flares, optimization algorithm is used. This algorithm is Genetic Algorithm which is used for searching optimum solution with minimizing cost function recursively. In this simulation, cost function is defined as minimum miss-distance between missile and target. For each run, Genetic Algorithm tries to maximize this miss-distance with optimizing dispensing time of flares. At the end of algorithm, miss-distance cost function is more than threshold level and simulation is terminated. As a result, effective flare dispensing programs are generated with Genetic Algorithm.

10435-6, Session 2

Higher operation temperature quadrant photon detectors of 2-11 μm wavelength radiation with large photosensitive areas

Jaroslaw Pawluczyk, Andrzej Sosna, Dariusz Wojnowski, A. Kozniewski, Mariusz Romanis, Waldemar Gawron, Jozef Piotrowski, VIGO System S.A. (Poland)

We report on the status of quadrant photon detectors optimized for 2-11 μm wavelength spectral range, with photosensitive area of a (single) quadrant of 1 to 4 mm in transverse size. They are based on HgCdTe multilayer (100) and (111)B oriented heterostructures grown by metal organic vapor phase epitaxy on CdTe-buffered semi-insulating (100) GaAs substrates. The devices are fabricated as photoconductors (PC) or multiple photodiodes (PVM). The former are characterized by the uniformity of few per cent of responsivity along the wafer surface. The latter consist of multiple photovoltaic cells connected in series and distributed along the wafer surface, comprising a periodical stripe structure with a period of 20 μm. Within each period, there is an insensitive gap/trench of <9 μm in width between stripe mesas, which dramatically worsens the uniformity of the responsivity at the spot size close to the period. Because bias is necessary for operation of the photoconductors, they produce 1/f noise with few kHz knee frequency. The photodiodes are typically operated at 0 V bias, so there is no 1/f noise and operation from DC is enabled. Upper corner frequency is several dozen of MHz for both the types with Peltier cooling. Both have similar normalized detectivity D*>1.4E8 cm·Hz1/2/W at 230 K, allowing for position control of the laser beam with accuracy of around 1 μm at 100 KHz, 10.6 μm wavelength of pulsed radiation spot of ~0.3 mm dia at the close to maximal input radiation power density in a range of detector linear operation. Several measures countering fringing effects and crosstalk have been implemented. The transverse size of the active area of the quadrant, especially that of PVM, could be easily increased even beyond 4 mm with greater size of the cold finger of the thermoelectric cooler (TEC). The assembled detectors are sealed and coupled with preamplifiers ensuring, besides amplifier's low noise, also low amplifier's input resistance and stable detector bias voltage in order to prevent degradation of responsivity, linear operation range and time response. TEC controller stabilizes detector temperature with ±0.01 K accuracy in a wide range of ambient temperature. The detector with the integrated proprietary electronics makes a compact detection module of low power consumption.

The devices facilitate precise and fast positioning of radiation/laser spot, required for such applications as infrared laser range finders, closed-loop directed infrared countermeasures, advanced photolithography systems. The detectors are attractive due to their useful performance at higher operating temperature, achieved by Peltier coolers, which work effectively even at higher, e.g. 70 C, ambient temperature. The advantages owed to the thermoelectrical cooling are: long lifetime, no moving parts, reduced weight and price. Operation in the 8-11 ?m, long-wavelength range makes the system less vulnerable to change in atmospheric conditions. Possibility to work at various wavelengths in a system utilizing several wavelengths of laser radiation can also be advantageous.

10435-7, Session 3

Continuous wave optical power scaling with lateral dimensions for high-power quantum cascade lasers *(Invited Paper)*

Arkadiy A. Lyakh, Univ. of Central Florida (United States)

Significant increase in continuous wave optical power from a single quantum cascade laser emitter beyond its current record of five watts will likely require power scaling with active region lateral dimensions. Active region overheating presents a major technical problem for such broad area devices. Laser thermal resistance can be reduced and laser self-heating can be suppressed by significantly reducing active region thickness, i.e. by reducing number of active region stages and by reducing thickness of each stage in the cascade. The main challenge for quantum cascade lasers with a "thin" active region is to ensure that optical power emitted per unit area of the active region stays high despite the reduction in active region thickness, a condition critical for the power scaling. Various aspects of bandgap engineering, waveguide design, and thermal design pertinent to the broad area configuration will be discussed in this presentation. Also, high duty cycle and continuous wave data collected for first broad area quantum cascade lasers developed by the group will be presented and analyzed.

10435-8, Session 3

Advanced thermal management of high-power QCL arrays for infrared countermeasures *(Invited Paper)*

Philip Barletta, Micross Advanced Interconnect Technology (United States); Laurent Diehl, Pendar Technologies (United States); Mark T. North, Aavid Thermacore, Inc. (United States); Bao Yang, Sevket Yuruker, Univ. of Maryland, College Park (United States); Nicholas G. Baldasaro, Dorota S. Temple, RTI International (United States)

Next-generation infrared countermeasure (IRCM) systems call for compact and lightweight high-power laser sources. Specifically, optical output power of tens of Watts in the mid-wave infrared (MWIR) is desired. Monolithically fabricated arrays of quantum cascade lasers (QCLs) have the potential to meet these requirements. Single MWIR QCL emitters operating in continuous wave at room temperature have demonstrated multi-Watt power levels with wall-plug efficiency of approximately 15%. However, tens of Watts of output power from an array of QCLs translates into the necessity of removing hundreds of Watts per cm2, a formidable thermal management challenge.

A potential thermal solution for such high-power QCL arrays is active cooling based on high-performance thin-film thermoelectric coolers (TFTECs), in conjunction with pumped porous-media heat exchangers. The use of active cooling via TFTECs makes it possible to not only pump the heat away, but also to lower the QCL junction temperature, thus improving the wall-plug efficiency of the array. TFTECs have shown the ability to pump >250W/cm2 at ?T=0K, which is 25 times greater than that typically seen in commercially available bulk thermoelectric devices.

The thin-film materials used in the present work were a p-type Bi2Te3/Sb2Te3 nanostructure, and an n-type d-doped Bi2Te3-xSex alloy. Both materials were grown heteroepitaxially on GaAs substrates using metalorganic chemical vapor deposition. These materials were then fabricated into TFTECs using standard bonding, etching, photolithography, metallization, and electroplating techniques. Minimization of parasitic electrical and thermal resistances was the primary concern when

developing and optimizing the fabrication procedure.

The completed TFTECs were tested for both maximum temperature difference (?Tmax) between the hot and cold sides (i.e, heat source side and heat sink side, respectively) and heat pumping, Q, at several ?T values.

The present work also explored the integration of the TFTECs into a full thermal management package in conjunction with a porous metal heat exchanger (PMHX) for heat rejection. A detailed design for a fully-integrated QCL/TFTEC/PMHX package was developed.

This work was supported in part by the DARPA MATRIX project (Contract No. W31P4Q-16-C-0019).

10435-9, Session 3

Recent results on performance optimization of mid-infrared quantum cascade lasers for infrared countermeasure applications

Richard Maulini, Ilia Sergachev, Dana Nevou, Stéphane Blaser, Tobias Gresch, Alfredo Bismuto, Antoine Muller, Alpes Lasers SA (Switzerland)

We will present our latest results on high power quantum cascade lasers (QCLs). QCLs optimized for high peak or average power were realized to provide extensive coverage of the mid-wave and long-wave infrared regions for directional infrared countermeasures and remote sensing applications.

We report QCLs with watt-level average output power QCLs at wavelengths of 3.95, 4.55, 4.65, 4.90, and 9.70 μm. In the second atmospheric window, at a wavelength of 9.70 μm, thermoelectrically-cooled devices emit a continuous-wave output power in excess of 2.0 W and 1.2 W at temperatures of -20ºC and +20ºC, respectively, and conductively-cooled devices emit an average power of 1.05 W at room temperature without the need for a thermoelectric cooler.

We also report gain-guided broad area QCLs emitting at the wavelength of 4.55 ?m. The devices were processed in a buried heterostructure configuration with a narrow current injector section and the mode size is determined by lateral current spreading in the active region. With this novel device configuration, we demonstrate 23.5 W peak power at a temperature of 20ºC and duty cycle of 1%, with a far field consisting of a single symmetric lobe centered on the optical axis. These experimental results are supported well by 2D numerical simulations of electric currents and optical fields in a device cross-section.

10435-10, Session 3

Comparison of performance of high-power mid-IR QCL modules in actively and passively cooled mode

Franz Münzhuber, Hubert Denzel, Hans Dieter Tholl, Diehl BGT Defence GmbH & Co. KG (Germany)

We report on the effects of active and passive cooling on the performance of high power mid-IR QCL modules (? ≈ 3.9 μm).

In active cooling mode, a thermo-electrical cooler attached with its hot side to a heat sink of constant temperature, a local thermometer in close proximity to the QCL chip (epi-down mounted) as well as a control unit have been used for temperature control of the QCL submount. In contrast, the passive cooling was performed by attaching the QCL module solely to the heat sink.

Electro-optical light-current- (L-I-) curves are measured in a quasi-cw mode, from which efficiencies can be deduced. Waiving of the active cooling elements results in a drop of the maximum intensity of less than 5 %, compared to the case wherein the temperature of the submount is stabilized to the temperature of the heat sink.

The application of a theoretical model of electro-optical performance to the data shows good agreement and captures the relevant observations.

We further determine the heat resistance of the module and demonstrate that the system performance is not limited by the packaging of the module, but rather by the heat dissipation on the QCL chip itself.

10435-11, Session 4

Compact 2100 nm laser diode module for next-generation DIRCM *(Invited Paper)*

Edgaras Dvinelis, Mindaugas Greibus, Augustinas Trink?nas, Greta Naujokaite, Augustinas Vizbaras, Brolis Semiconductors UAB (Lithuania); Dominykas Vizbaras, Brolis Photonics Solutions Ltd. (United Kingdom); Kristijonas Vizbaras, Brolis Semiconductors UAB (Lithuania)

Compact high-power 2100 nm laser diode module for next-generation directed infrared countermeasure (DIRCM) systems is presented. Next-generation DIRCM systems require compact, light-weight and robust laser modules which could provide intense IR light emission capable of disrupting the tracking sensor of heat-seeking missile. Currently used solid-state laser solutions for mid-IR band are bulky and heavy making them difficult to implement in smaller form-factor DIRCM systems. Recent development of GaSb laser diode technology greatly improved optical output powers and efficiencies of laser diodes working in 1900 - 2450 nm band while also maintaining very attractive SWAP (size, weight and power) characteristics. Today single GaSb laser diode emitters are capable of providing Watt level emission of optical output power with high efficiency values. Multiple emitters may be stacked spatially in order to achieve higher optical output power levels.

2100 nm laser diode module presented in this work performance is based on high-efficiency broad emitting area GaSb laser diode technology. Epitaxial laser diode structures were grown by an in-house multi-wafer Veeco Gen200Edge MBE system. After the growth wafers were processed into double-trench ridge waveguide devices with an emitting area of 120 x 2 ?m. Finally AR/HR optical coatings were applied and chips were mounted on custom heatsink mounts. Each laser diode emitter is able to provide 1 W of CW output optical power with working point efficiency up to 20% at temperature of 20 °C. Due to the nature of wide emitter aperture beam astigmatism is introduced - fast and slow axes of output laser diode beam have different locations of virtual emission origin points inside the chip. For this reason rotationally symmetric lenses cannot be used for beam collimation, instead custom designed fast-axis collimator (FAC) and slow-axis collimator (SAC) lenses were used. These lenses were actively aligned and attached by UV epoxy curing using custom designed “NanoGlue” machine from “nanosystec”. Beam divergence in fast-axis is limited by diffraction and can be collimated down to 2-3 mrad full angle (1/e2). Beam parameter product (BPP) in slow-axis is limited by 120 ?m wide aperture and full angle divergence of ~15° (1/e2, also depends on driving current), this allows to achieve ~8 mrad full angle (1/e2) beam divergence after SAC lens. Total 2 emitters stacked vertically were used in the 2100 nm laser diode module. Final optical output power of the module goes up to 2 W with working point efficiency up to 20% at temperature of 20 °C. For DIRCM applications raw optical power values usually are not sufficient so another important parameter to consider is output beam radiant intensity, which can go up to 100 kW/str depending on the level of collimated beam divergence. Laser diode emitters and collimating optical system are placed inside small sealed aluminum package. Total dimensions of the module are below 40 x 30 x 20 mm (L x W x H) with a weight of <50 grams. Finally output beam is bore-sighted to mechanical axes of the module housing allowing for easy integration into next-generation DIRCM systems.

10435-12, Session 4

Radiation-hardened optical amplifier based on multicore fiber for telecommunication satellites

Marta Filipowicz, Marek Napierala, InPhoTech (Poland); Michal Murawski, Polish Ctr. of Photonics and Fiber Optics (Poland); Lukasz Ostrowski, Lukasz Szostkiewicz, InPhoTech (Poland); Pawel Mergo, Univ. of Maria Curie-Sklodowska (Poland); Marios Kechagias, Jihan Farzana, Leontios Stampoulidis, Efstratios Kehayas, Gooch & Housego (United Kingdom); J. Crabb, Gooch & Housego (Torquay) Ltd. (United Kingdom); Tomasz Nasilowski, InPhoTech (Poland)

We present research results concerning a space-dedicated optical amplifier for application in telecom satellites. The unit is a part of a photonic payload, which aims to provide higher capacity for satellite transmission, meaning a throughput up to 1 Tb/s. Achieving such a result with electronics architecture comes at expense of a highly complicated design and an increase in mass and volume, what cannot be accepted by satellite operators. Thus, there is a need to create enabling technologies that would allow sustained entry of photonics into space equipment. These technological advancements will (i) enable faster and more efficient inter satellites links as well as satellite to ground links, (ii) fuel new satellite based services that require high-speed satellite communication (iii) allow for greater area coverage with only a single satellite.

The optical amplifier is based on a 7-core microstructure Er-doped fiber. The use of space division multiplexing technique (SDM) in such a volume-hungry application is highly advantageous in terms of volume as well as fiber count reduction. The seven fiber's cores are distributed in a hexagonal arrangement and embedded in a common glass cladding. Each core is surrounded by the ring of air holes. There are also additional air holes that allow for unambiguous structure orientation. Such architecture allows for independent signal propagation in every elementary cell and ensures negligible core-to-core crosstalk value (less than -37 dB according to experimental results). As for the fiber' external dimension it is not greater than the one of a standard telecommunication single mode fiber (125 um).

Regarding the gain properties the amplifier is characterized by flat gain in C band equal to 23.4 dB for a pump power of 250 mW and input signal power of -6 dBm. At the same time the noise figure (NF) is lower than 5.1 dB. Also, what is crucial the fiber is hardened against disruptive influence of ionizing radiation. This eliminates the need to incorporate thick shielding and allows to make the overall element's weight smaller. According to experimental results the radiation induced gain drop (RIGD) is less than 0.6 dB for a dose of 20 krad.

10435-13, Session 4

Pathways to higher mid-IR laser sources *(Invited Paper)*

Eric D. Park, Kevin F. Wall, Kevin M Ezzo, Wenyan Tian, Q-Peak, Inc. (United States)

No Abstract Available

10435-14, Session 5

Atmospheric and laser propagation *(Invited Paper)*

Alexander M. J. van Eijk, TNO Defence, Security and Safety (Netherlands) and Fraunhofer-Institut für Optronik, Systemtechnik und Bildauswertung (Germany)

The presentation will be an overview of atmospheric effects on the propagation of electro-optical radiation, including specific effects related to laser radiation and the maritime environment.

10435-15, Session 5

Experimental validation of a phase screen propagation model for nanosecond laser pulses travelling through turbulent atmospheres

Christopher D. Burgess, Christopher Westgate, Defence Science and Technology Lab. (United Kingdom)

Applications involving the outdoor use of pulsed lasers systems can be effected by atmospheric turbulence and scintillation. In particular, deterministic prediction of the risk of injury or damage due to a laser pulse can be difficult due to uncertainty over the focal plane fluence of a pulse that has traversed through a turbulent medium.

In this study, focussed beam profiles of nanosecond laser pulses are recorded for visible laser pulses that have traversed 500m and 1400m paths through turbulent atmospheres. Beam profiles are also taken under laboratory conditions. These pulses are characterised in terms of their peak focal plane fluence, total collected energy and Strehl ratio. Measured pulses are then compared statistically to pulse profiles generated by a phase screen propagation model based on the Von Karman phase screen distribution. The model takes into account the refractive index structure constant (Cn2), the wavelength, the path geometry and macroscopic beam steering due to scintillation.

Analysis shows good correlation between the measured and simulated data, inferring that the Von Karman phase screen model can be used to predict focal plane fluence distributions for outdoor applications.

10435-16, Session 5

Power in the bucket and angle of arrival modelling in the presence of an airborne platform-induced turbulence

Marie-Thérèse Velluet, ONERA (France)

In the framework of a European collaborative research project called ALWS (Airborne platform effects on lasers and Warning Sensors), the effects of platform-related turbulence on MAWS (missile approach warning systems) and DIRCM (directed infrared countermeasures) performance are investigated.

Field trials have been conducted to study the turbulence effects around a hovering helicopter and behind a turboprop aircraft on the ground, with engines running. In particular, intensity patterns of laser beam degraded by this strong turbulence were recorded by high speed cameras. The time dependence of the power in the bucket (PIB) and the amplitude of the angle of arrival (AOA) have been characterized during the trial. Temporal spectrums of these two parameters present an asymptotic behaviour typical of optical beams propagating through developed turbulence (Kolmogorov). Based on the formalism developed in the case of propagation through atmospheric turbulence, we have first estimated the turbulence strength and the wind velocity inside the plume for different flight conditions during the helicopter field trial as well the turboprop aircraft one. By applying analytical temporal spectrum of the PIB and the AOA, it is possible to perform numerically times series of these two quantities in the same conditions as the experimental ones. These simulated time series have been compared with the recorded data to assess the validity domain of the simplified proposed model. Then, this model will be integrated in a simulator to estimate the impact of the turbulence induced by the platform and to evaluate the system performance degradation. In this model dedicated to plume and downwash effects, aero-optical effects are not taken into account.

10435-17, Session 6

Enhancing the applications of chalcogenide glass for passive and active multispectral applications *(Invited Paper)*

Daniel W. Hewak, Andrea Ravagli, Christopher Craig, Armen Aghajani, Brian E. Hayden, Univ. of Southampton (United Kingdom); Ajoy K. Kar, Mark D. MacKenzie, Heriot-Watt Univ. (United Kingdom)

In the last decades, the commercial availability of chalcogenide glasses has strongly enhanced the development of infrared optics and technology. However, their production in large batches, the optimization of optical, thermal and mechanical properties and their use as active light sources, in particular lasers, are still not fully addressed.

The production of Ga-La-S glass received much attention as a candidate for the production of stable chalcogenides. The high melting point of the precursors allowed a significant improvement of the melting process. In addition, the addition of elements such as Se, Te, In, rare earths and transition metals were proved to enhance the glass forming ability of the glass and its applications. Ga-La-based glasses are characterised by high thermal and mechanical stability and high resistance to acids and solvents and the ability to be readily doped with active light emitting ions.

In this talk we discuss four areas of current research; the upgrading of the production of Ga-La-based glasses from laboratory to commercial level, glass optimization through high throughput modifications, compositional modification for multispectral applications and doped glasses with mid-infrared emission.

10435-18, Session 6

Chalcogenide negative curvature fibers *(Invited Paper)*

Curtis R. Menyuk, Univ. of Maryland, Baltimore County (United States); Chengli Wei, Baylor Univ. (United States); R. Joseph Weiblen, Univ. of Maryland, Baltimore County (United States); Jonathan Hu, Baylor Univ. (United States); Rafael R. Gattass, L. Brandon Shaw, Jasbinder S. Sanghera, U.S. Naval Research Lab. (United States)

Negative curvature fibers have demonstrated remarkably low loss over a broad bandwidth in silica optical fibers with reported losses of 2–5 ?m of less than 1 dB/m [1]. Losses of 11 dB/m have been reported in a chalcogenide fiber that was used to deliver light from a CO2 laser (9.8 ?m) [2]. Negative curvature fibers are particularly attractive for applications that require hollow-core chalcogenide fibers because they are less sensitive to fabrication imperfections than are photonic crystal fibers [3]. We have demonstrated losses as low as 2.1 dB/m at 10 ?m in a chalcogenide negative curvature fiber that as fabricated through extrusion [4]. In this presentation, we describe theoretical and experimental work that we have carried out to design and fabricate chalcogenide negative curvature fibers.

1. A. N. Kolyadin et al., Opt. Exp. 21, 9514–9519 (2013).

2. A. F. Kosolapov et al., Opt. Exp. 19, 25723–25728 (2011).

3. R. J. Weiblen et al., Opt. Lett. 41, 2624–2627 (2016).

4. R. R. Gattass et al., Opt. Exp. 24, 25697–25703 (2016).

10435-19, Session 6

Chalcogenide glass and fiber technology for countermeasure and other applications *(Invited Paper)*

Ishwar D. Aggarwal, The Univ. of North Carolina at Charlotte (United States); W. J. Kim, Viet K. Nguyen, L. Brandon Shaw, Lynda E. Busse, U.S. Naval Research Lab. (United States); Catalin Florea, US Naval Research Lab. (United States); Daniel Gibson, Rafael R. Gattass, Shyam S. Bayya, U.S. Naval Research Lab. (United States); Frederic Kung, U.S. Navy (United States); Geoffrey D. Chin, U.S. Naval Research Lab. (United States); Fritz Miklos, Sotera Defense Solutions, Inc. (United States); Jasbinder S. Sanghera, U.S. Naval Research Lab. (United States)

Glasses based on the elements S, Se, and Te are called chalcogenide glasses. These glasses are transparent in the infrared (IR), possess low phonon energies, are chemically durable, and can be drawn into fiber. Recent research progress at the Naval Research Laboratory (NRL) to develop chalcogenide glass fibers for applications in the mid- and long-wave IR wavelength regions from 2 to 12 μm will be reviewed. Our recent effort in the development of low loss chalcogenide fibers, by describing the synthesis and purification methods, fiber drawing techniques, and highlighting the best results, will be summarized. Various applications of these high quality chalcogenide fibers, including IR countermeasures, multimode beam combiners, mid-infrared supercontinuum sources, fiber Bragg gratings, fiber bundles for IR imaging, anti-reflecting surface structures, and modal filters, will be described. Novel infrared (IR) lenses that enable a reduction in the size and weight of IR imaging optics through the use of layered glass structures with broad IR transmission will also be presented.

10435-3, Session 7

Physics based performance model of a UV missile seeker *(Invited Paper)*

Itor James, Cranfield University (United Kingdom)

Modelling of missile seekers operating in the UV has been undertaken owing to their perceived future proliferation risk and subsequent threat to aircraft operations. There is little to no current understanding as to whether or not this modelling is correct. A generic, physics based model has therefore been developed, which is able to produce similar data to the higher fidelity seeker models and which is subject to the same variables. This generic model is unclassified and open source in its approach. The assumptions and data included in this model will be presented along with initial results showing the ability to detect an object is dependent on range, object size and reflectivity to various degrees. Discussion and critique is invited.

10435-20, Session 7

Anti-aliasing algorithm development *(Invited Paper)*

Frances Bodrucki, The Univ. of North Carolina at Charlotte (United States)

In this paper, we discuss the testing of sensor-imbedded algorithms for mitigation of aliasing artifacts under pulsed illumination. Previous sensors tested, one with a fixed frame rate and one with an adjustable frame rate, showed different degrees of operability when subjected to a QCL laser pulsed at the frame rate of the fixed-rate sensor. We implemented algorithms to allow the adjustable sensor to detect the presence of aliasing artifacts, and in response, to adjust the

frame rate of the sensor. The result was that the sensor output showed a varying laser intensity (beat note) as opposed to a fixed signal level.

We present results of a new sensor which implements a tracking functionality, and investigate the degree to which this sensor can be controlled to produce similar operability advantages when illuminated with pulsed QCL radiation.

A MIRAGE infrared scene projector will be used to explore the efficacy of the new algorithms implemented, with possibility of additional polarization-based discriminants.

10435-21, Session 7

Airborne platform effects on lasers and warning sensors *(Invited Paper)*

Markus Henriksson, FOI-Swedish Defence Research Agency (Sweden); Christian Eisele, Dirk P. Seiffer, Fraunhofer-Institut für Optronik, Systemtechnik und Bildauswertung (Germany); Lars J. Sjöqvist, FOI-Swedish Defence Research Agency (Sweden); Fabio Togna, Aeronautica Militare Italiana (Italy); Marie-Thérèse Velluet, ONERA (France)

Airborne platform effects on lasers and warning sensors (ALWS) has been a European collaborative research project to investigate the effects of platform related turbulence on optical countermeasure systems, especially missile approach warning systems (MAWS) and directed infrared countermeasures (DIRCM). Field trials have been carried out to study the turbulence effects around a hovering helicopter and behind a turboprop aircraft with engines running on the ground. In addition different methods for modelling the effects have been investigated.

In the helicopter trials significant beam wander, scintillations and beam broadening were experienced by narrow divergence probe beams when passing through the down- wash of the hot engine exhaust gases. The measured effects considerably exceed the effects of atmospheric turbulence. Extraction of turbulence parameters for modelling of DIRCM relevant scenarios show that in most cases the reduction of jamming power and distortion of jamming waveform can be expected to be small. The reduction of effects of turbulence is mainly related to the larger beam divergence and shorter Rayleigh length of DIRCM lasers compared to the experimental probe beams. Measurements using the turboprop platform confirm that tolerable effects on laser beam properties are found when the laser beam passes through the exhaust 15 m behind the outlet where the exhaust gases are starting to cool down.

Modelling efforts have shown that time resolved computational fluid dynamics (CFD) calculations can be used to study properties of beam propagation in engine exhaust related turbulence. Because of computational cost and the problem of validating the CFD results the use for system performance simulations is however difficult.

The hot exhaust gases emitted from aircraft engines create extreme optical turbulence in a local region. The effects on countermeasure system performance depend both on the system parameters and on the threat characteristics. With present day DIRCM systems the effects of even severe turbulence are often tolerable.

10435-22, Session 7

Brillouin scattering effect in the multicore optical fiber applied to fiber optic shape sensing

Anna Pytel, Agnieszka Kolakowska, Michalina Józwik, Lukasz Szostkiewicz, InPhoTech (Poland) and Warsaw Univ. of Technology (Poland); Zhisheng Yang, Ecole Polytechnique Fédérale de Lausanne (Switzerland); Barbara Wajnchold, Michal Murawski, Polish Ctr. of Photonics and Fiber Optics (Poland); Marek Napierala, InPhoTech (Poland); Luc Thévenaz, Ecole Polytechnique Fédérale de Lausanne (Switzerland); Pawel Mergo, Univ. of Maria Curie-Sklodowska (Poland); Tomasz Nasilowski, InPhoTech (Poland)

Shape sensing is a subject, which has drawn much interest in the past few years [1, 2]. Determining the shape of materials and devices finds applications in various industries, mainly in medical engineering, robotics and civil engineering. Such sensors can be used to monitor the shape of medical instruments, for example in robotic-assisted minimally invasive surgery technologies, but also in controlling the exact position of the flexible arm of robots. There is certainly a plethora of various optical fiber sensors architectures, but generally speaking, shape sensing is possible if exact bend radius, its location and orientation can be measured along the whole optical fiber. This is why authors propose to take advantage of distributed sensing using Brillouin scattering in multicore optical fibers [3].

The measurement of the exact bending radius is deduced from the strain induced in lateral cores, which impacts on the Brillouin frequency shift (BFS). Additionally, comparing the differential strain between cores constellating the fiber enable to distinguish the bending orientation. The bending location is identified by performing a distributed measurement using an optical time-domain method, for example in the Brillouin Optical Time Domain Analysis (BOTDA).

Presented sensor is based on the 7-core microstructured fiber designed for telecommunication application [4, 5]. The fiber has low loss and now cross-talk between the cores. The design of the shape sensor is carefully analyzed and the theoretical background is presented. Authors report the first experimental results for the mentioned sensor. The multicore fiber was measured using a BOTDA set-up and the response clearly showed differential responses of the Brillouin frequency shift for all cores. Moreover the response from the outer cores was strongly dependent on the bend's orientation. These results confirmed that developing a shape sensor based on the proposed design is fully realistic.

[1] R. G. Duncan et al., "High-accuracy fiber-optic shape sensing. Proc. SPIE 6530, Sensor Systems and Networks: Phenomena, Technology, and Applications for NDE and Health Monitoring" 2007, 65301S (2007)

[2] J. P. Moore et al., "Shape sensing using multi-core fiber optic cable and parametric curve solutions", Opt. Express, 20 (3), 2967 (2012)

[3] Z. Zhao et al., "Distributed shape sensing using Brillouin scattering in multi-core fibers", Optics Express, 24, 25211 (2016)

[4] A. Ziolowicz et al., "Hole-assisted multicore optical fiber for next generation telecom transmission systems", Appl. Phys. Lett., 105, 81106 (2014)

[5] M. Napierala et al., "Multicore optical fibres for next generation telecommunication transmission systems and components", Photonics Lett. Pol., 7, 3, (2015)

10435-23, Session 7

Polarization analysis of retroreflection from COTS sensors

Frances Bodrucki, The Univ. of North Carolina at Charlotte (United States)

Previous work involved detection of retroreflected signals, focusing on polarization as a discriminator. We continue to explore the formalisms of the Stokes vector and Mueller matrix for characterization of retroreflection for common sensors such as cell phones and commercial cameras, as well as various optical materials. The experimental setup up for the Stokes vector data is a four-channel analyzer designed to simultaneously detect and record all four Stokes parameters. The Mueller matrix data is collected via a commercial (Scatterworks, Inc.) Complete Angle Scatter Instrument (CASI) scatterometer.

10435-24, Session 7

Artificial saturable absorbers based on nonlinear phenomena in optical fibers

Jan Szczepanek, Univ. of Warsaw (Poland); Tomasz M. Karda?, Institute of Physical Chemistry, Polish Academy of Sciences (Poland); Witold Stepie?, Warsaw Univ. of Technology (Poland); Czeslaw Radzewicz, Univ. of Warsaw (Poland); Yuriy Stepanenko, Institute of Physical Chemistry, Polish Academy of Sciences (Poland)

All-fiber ultrafast laser oscillators can be mode-locked with various Saturable Absorbers (SA). Techniques which use nonlinear optical phenomena to mimic saturable absorption such as: Nonlinear Optical Loop Mirror (NOLM), Nonlinear Amplifying Loop Mirror (NALM) or Nonlinear Polarization Evolution (NPE) can be implemented in all-fiber cavities. Those artificial SA are based on the phenomena which occur inside optical fibers thus no additional technology or material is needed. In this work we present the results of modelling and the performance of NOLM and a novel NPE method both using Polarization Maintaining (PM) fibers and PM fiber components only. Both methods were successfully used for starting mode-locking in all-PM-fiber laser cavities [1-2].

Both NOLM and NPE rely on nonlinear phase shift between pulses with different intensities in the fiber. In the case of NOLM the pulse is split at a non-symmetrical fiber coupler and the two copies propagate in a closed fiber loop in the opposite directions, gain different nonlinear phase and interfere at the coupler. With proper parameters only the part of the pulse with high intensity is transmitted – NOLM works as an artificial saturable absorber. NPE is based on the temporal filtration of the pulse polarization state affected by a self-action due to the instantaneous Kerr nonlinearity. In our approach based on PM fibers the pulse is split with an angle splice between birefringent fibers, which results in two copies of the pulse with non-equal intensity and orthogonal polarizations. The nonlinear polarization change resulting from nonlinear phase difference between propagating pulses is governed, in this case, by self- and cross-phase modulation and thus temporal overlap of the pulses is of essence. The two pulses with linear perpendicular polarizations travel at different group velocities. The resulting Group Velocity Mismatch has to be compensated and this is achieved by using pieces of fiber with alternating orientation. The two copies of the pulse interfere at the output fiber-coupled polarizer and one is filtered out of the cavity. With a proper angle splice between last fiber piece and the polarizer, the device works as an artificial SA with zero transmission in the low intensity limit.

We present an experimental study and numerical simulations of NOLM's performance for different coupling ratios and loop lengths and the performance of PM NPE for a variety of splice angles and fiber lengths. We have measured saturable absorption characteristic of the artificial saturable absorbers described above. The pulses used in the experiment were positively chirped to simulate conditions in all-normal-dispersion fiber cavities. These are of interest because of the high pulse energy and increased environmental stability achievable in such setups. The measured saturable absorption characteristics indicate which parameters are responsible for oscillator performance, e.g. self-starting. The comparison of the modelling results and the experimental parameters of oscillators using such SA allow us to get better understanding how the studied SA affect pulse dynamics in the cavity.

1. Szczepanek et al., Opt. Lett. 40, 3500 (2015).

2. Szczepanek et al., Opt. Lett. 42, 575 (2017).

10436-10, Session PS

Experimental investigation of the photodarkening induced core laser leakage in a 3kW co-pumping fiber amplifier

Lingchao Kong, Miao Li, Jinyong Leng, Xiaolin Wang, Pu Zhou, Xiaojun Xu, Jinbao Chen, Zongfu Jiang, National Univ. of Defense Technology (China)

The photodarkening effect is one of the bottle necks for the long term operation of the high power fiber laser and amplifier. This effect will induce additional loss to the signal laser and increase the heat load in the active fiber. Thus the threshold of the thermally induced nonlinear effect will be reduced by the photodarkening.

In our previous work, we demonstrated the thermally induced core laser leakage phenomenon in the large mode area single trench fiber, in which the core laser started to leakage into to the inner cladding after input pump power reached certain threshold. The thermal effects was the key reason that additional heat load lead to the higher order mode loss degradation and power coupling from the fundamental mode to the higher order mode.

In this work, we demonstrated photodarkening induced core laser leakage phenomenon in the long term operation of a 3kW co-pumping fiber amplifier. The fiber amplifier was seed by a 1080nm fiber oscillator of 100W signal power and pumped with 915nm laser diode modules of 4290W total pump power. A high power cladding stripper was made on the output fiber to strip out the cladding light. The maximum output power was 3.05kW and the slope efficiency was 68%. Then a 12 hours full power operation was performed and the output power evolution was monitored. The result showed that the output power decreased from 3 kW to 2.65kW. However the output power does not decreased monotonically but with a perturbation period about 4.5min. We also monitored the scattering light power of the output beam and the temperature of the cladding power striper to make sure this perturbation was not caused by the water cooling of the power meter. The power of the scattering light also showed the same evolution trend with the perturbation period about 4.5min. The temperature variation of the cladding power stripper was opposite that it increased as the output power decreased and decreased as the output power increased. The highest temperature was also increased from 74? to above 100? before and after the long term operation. This indicated that the output power decrease was caused by the core laser leakage into the inner cladding and the co-pumping scheme may not be suitable to achieve high power fiber laser with long term output stability. The power perturbation was also an evidence of the thermally induced mode instability. Future work was needed to explain the difference between this work and our previous work that no characteristic frequency was observed when the output power decreased.

10436-11, Session PS

Optimization for the fiber laser source through its temporal and spectral characteristics

Wei Liu, Pengfei Ma, Pu Zhou, Zongfu Jiang, National Univ. of Defense Technology (China)

Ytterbium-doped fiber amplifier (YDFA) based on master oscillator power amplifier (MOPA) architecture is an effective solution for power scaling in the high-power laser system. Due to the influence of nonlinear effects and the related spectral broadening effect, it is challenging to realize high-power and narrow-band output simultaneously. In this report, we show that the spectral properties and the stimulated Raman scattering (SRS) threshold of the MOPA structure could be optimized through the spectral-temporal characteristics shaping of the fiber oscillator. We propose the spectral models for the fiber oscillator and the MOPA structure together with the SRS effect. Both the spectral formation in the fiber oscillator and the spectral evolution during amplification are divided into two main processes: the amplification of the optical field in active fiber and the energy transfer between different spectral components due to the nonlinear propagation. Accordingly, we use an amplitude equation to describe the nonlinear propagation by the nonlinear Schrödinger equation (NLSE) with the electric field description of the initial spontaneous emission noise and the steady-state rate equations to calculate the wavelength-dependent gain in the active fiber. And the set of bidirectional spectral-spatial equations describing the optical field in the active fiber are given by the combined simulation of the NLSE and steady-state rate equations. For a fiber oscillator, its structure and parameters, such as the structure of the cavity, the length of the cavity or the pump power, will have a significant effect on the spectral and temporal characteristics. Thus, it is possible to design the spectral and temporal characteristics of the fiber oscillator through changing its structure and parameters. In addition, the spectral-temporal characteristics of the fiber oscillator could be further optimized through the wavelength filters in fiber optics. In the MOPA structure, the output root-mean-square (RMS) spectral width almost increases linearly along with the power scaling process, while the growth rate of the spectral width and the SRS threshold are all closely related to the spectral-temporal characteristics of the fiber oscillator. The preliminary analysis of the simulation results shows that the noise floor, the temporal fluctuations and the spectral properties of the fiber oscillator will significantly impact the spectral broadening properties and the SRS threshold of the MOPA structure. The developed model represents a powerful tool for the design of a fiber oscillator through its structural parameters. This work could provide a good reference for optimal performance high-power fiber laser system.

10436-20, Session PS

Simulation study of the lethality effect of high-power laser: a different shape light spot

Xin Peng, Guomin Zhao, Houman Jiang, Minsun Chen, National Univ. of Defense Technology (China)

Numerical simulation method is used in this paper to analyze the high-power laser lethality effect on the target with different light spot shapes. Three kinds of light spot shapes (circle, square, triangle) are used in the simulation, while a piece of aluminum sheet is used as the target under the exposure of the high-power laser. Results show that the lethality effects are different with different light spot shapes after 10 seconds exposure, while the power density and the area of the light spot are kept as constant in these three cases. In the temperature field analysis, the maximum temperature in the case of circle light spot is the highest within the three cases, while the case of triangle light spot is the lowest. In the equivalent stress analysis, the equivalent stress is maximum in the case of triangle light spot while are equal in the other cases. It also shows that area of the maximum equivalent stress in the case of square light spot is larger than in the other cases. We can conclude that the target under high-power laser irradiation is easier to be breakdown with a triangle light spot, while a square light spot can be used to generate larger area destruction.

10436-21, Session PS

Study of reflectivity to different probe lasers by 45# steel heated in air

Houman Jiang, Xinmeng Li, Minsun Chen, National Univ. of Defense Technology (China)

The reflectivity vs time curves are measured and analyzed for 45# steel samples heated in air under the same heating procedure while irradiated by probe lasers with different wavelength. The curves are obtained with a setup in which an integrating sphere is used to collect the reflected energy from the probe laser by the sample, and a lock-in amplifier together with a chopper is adopted to suppress the influence of the thermal radiation from the heated sample, and another integrating sphere is used to monitor the power fluctuation for the probe laser. CW Lasers with wavelength of 0.532?m, 0.975?m and 3.8?m are respectively used as the probe laser, and it is found that the corresponding reflectivity vs time curve shows cyclical variation of different cycle length for the three probe lasers in an overall trend of decrease during the heating process. The overall trend of reflectivity decrease is attributed to the oxidation in the sample surface as the sample is heated in air, and the cyclical variation is thought to be the result of the multi-beam interference as the thickness of the oxidation layer increases. A numerical model is built to describe the growth of the oxidation layer and to reveal the mechanism behind the cyclical variation in the reflectivity vs time curve.

10436-22, Session PS

Small laser cutting head of kilowatt fiber laser for rescue service

Qiong Zhou, Wenguang Liu, BaozHu Yan, Xiaojun Xu, Jinbao Chen, National Univ. of Defense Technology (China)

Because of the high efficiency, laser cutting device is typically used for industrial manufacturing applications. But the currently used laser cutting head is large, costly, complex operation and the space locality, so it cannot be used in some special occasions, such as traffic accident rescue, fire rescue and earthquake relief. Considering the special requirements for rescue service, this paper designed a kind of small fiber laser cutting head and its optical properties are studied.

The size of small laser cutting head is designed as 180 mm?15 mm ?15 mm (length * width?height), and the main parts include focusing optical component and mechanical component. Focusing optical component integrates the functions of laser tube and the focusing lens in ordinary laser cutting lead, and is used in focusing laser output beam. Mechanical component integrates the functions of nozzle and mechanical structure of the laser head, and is used in protection of focusing optical component and formation of supersonic assisted gas. Small optical component is directly spliced to kW level fiber laser through the optical fiber. Beam quality of output laser is 0.9 mm? mrad (diameter?full Angle), the focal length is 100 mm, the focal spot diameter is about 30 um, and the maximum cutting depth can be up to 25 mm, which can ensure implementation of high efficient laser cutting.

In laser cutting process focusing optical component will absorb laser and will lead to axial thermal deformation, in this paper we analyze the distribution of axial thermal deformation of focusing optics components by using Comsol Multiphysics simulation software. The results showed that the maximum axial thermal deformation of focusing optical component is 2 um (the output power of fiber laser is 500W), the focal length changes to 99.7 mm, and the thermal deformation will not affect the cutting effect. Considering the fiber optic axis deflection caused by the fiber splicing process, assuming that the off-axis deflection of incident laser is 8 mrad the laser beam propagation in focusing optical component is studied by Zemax optical design program. The results show that the PV value of wavefront aberration is 1.99? (not including the piston ,tilt and defocusing aberration items) and the wavefront aberrations mainly include 0o astigmatic, coma and primary spherical aberration. The intensity of the focal spot distributes asymmetrically. The focal spot diameter increased to 42 um, the beam quality of output laser is 1.26 mm?mrad (diameter ?full Angle). However, the intensity of is more than 2.5MW/cm2 ,which means that the target can be effectively cut by the small laser cutting head.

10436-23, Session PS

Experimental study on the energy coupling characteristic of 45# steel to near-infrared laser

Minsun Chen, Xinmeng Li, Guomin Zhao, Houman Jiang, National Univ. of Defense Technology (China)

Based on a dynamic measurement apparatus for energy coupling coefficient / radiation coefficient of opaque objects, the energy coupling characteristic of 45# steel to near infrared laser was studied experimentally. The influence of the oxidation film structure on the energy coupling coefficient was studied by controlling the heating rate and the maximum temperature of the sample. The thickness of the oxidation film was measured by a scanning electron microscope. The energy coupling coefficient will change greatly from the room temperature to 480?. It will increase slowly at the initial rising temperature stage and then increase rapidly to the maximum value. After reaching the maximum, the energy coupling coefficient will take place periodic fluctuation, and reach a stable value finally. Preliminary analysis shows that the change of the conductivity with temperature results in the slow increase of the energy coupling coefficient. The rapid increase of the energy coupling coefficient is due to the absorptive Fe3O4 film, which is produced by the surface oxidation reaction of the sample. The periodical fluctuation of the energy coupling coefficient is due to the interference effect of the oxidation films.

10436-24, Session PS

Gas-assisted metal cutting by a fiber laser for rescue service

Wenguang Liu, Baozhu Yan, Qiong Zhou, Cheng Luo, National Univ. of Defense Technology (China)

Fiber laser cutting machine with small volume and light weight can be a promising tool in the rescue services. In this paper, a kW level fiber laser with special designed cutting head was used to cutting titanium and aluminum alloy. The cutting head is designed with a focal length of 100mm, and focal depth 20mm. And gas assisted cutting parameters are optimized for different samples by the cutting experiments. For a 6mm titanium alloy plate, the cutting parameter is optimal with 500W laser power, 0.8g/s oxygen flow assisted, and the cutting velocity is 3mm/s. For a titanium alloy tube with outer diameter of 30mm and inner diameter of 18mm, the cutting parameter is optimal with 500W laser power, 0.8g/s oxygen flow assisted, and the cutting velocity is 1mm/s. For a 3mm aluminum plate, the cutting parameter is optimal with 800W laser power, 1g/s air flow assisted, and the cutting velocity is 1mm/s. The cutting parameters optimized by experiment are consultative for the use of kW level compact fiber cutting machine in the rescue services.

10436-26, Session PS

High-peak power, athermal Nd:YAG transmitter

Mateusz Ka?ków, Jan K. Jabczynski, Waldemar Zendzian, Lukasz Gorajek, Zbigniew Puzewicz, Wojskowa Akademia Techniczna im. Jaroslawa Dabrowskiego (Poland)

The modern battlefield operations, such as target designation or ranging, require laser sources to be very bright, robust and versatile. The well-known, Q-switched Nd:YAG laser systems meet these conditions. From an end-user point of view, the laser device should be simple in use, insensitive in certain temperature range and immune to moderate mechanical shocks. The most demanding aspect of a laser system is its thermal management. Laser diodes (LD), used as pumping units, are the best choice to decrease the heat load inside the gain medium and to provide high pumping rates. On the other hand, narrow absorption spectra of Nd-doped laser media imposes temperature stabilization of LD emission spectrum. The thermo-electric Peltier module seems to be the best approach, but it requires TEC driver and additional heatsink, what makes the whole system unreliable in combat environment.

In this paper we present diode-side-pumped, Q-switched Nd:YAG laser with partial athermalization, achieved by application of two 2D laser diode stack (2D-LDS) with separated central emission wavelengths. The 1% at. Nd:YAG plane-parallel rod used in experiments had diameter of 5 mm and was 50 mm long. The average absorption coefficient was maintained at level of 4 cm-1 in 20-36oC temperature range. The two uncollimated, conduction-cooled, quasi-continuous-wave vertical 2D-LDS provided up to 4 kW of pump peak power in duration of 0.2 ms with repetition rate up to 25 Hz (0.625% duty factor). Pumping beam was focused into the gain media only through its cylindrical surface, which acted as a cylindrical lens. The laser resonator consisted of a flat rear mirror (HR@1064 nm), thin-film polarizer, RTP Pockels cell, aperture and a flat output coupler (T = 60%). In free-running operation output energy of 88 mJ was obtained. In case of Q-switching operation, pulse energy of 59 mJ with duration of 10 ns was achieved. This corresponds to 5.9 MW of pulse peak power. In the LD temperature range of 20-36oC, output pulse energy varies between 84-100% of maximum value. The full-angle divergence was measured to be 4.5 mrad and 6.3 mrad in x-direction and y-direction, respectively. The limiting factor in pulse energy scaling was the presence of amplified spontaneous emission (ASE), which occurred at pump energy level above 0.5 J.

10436-1, Session 1

Analysis of optical scheme for medium-range directed energy laser weapon system *(Invited Paper)*

Jan K. Jabczynski, Mateusz Kaskow, Lukasz Gorajek, Krzysztof Kopczy?ski, Wojskowa Akademia Techniczna im. Jaroslawa Dabrowskiego (Poland)

From the point of view of optical engineering, the general task of directed energy laser weapon system is to deliver the laser beam of given beam waist size on the medium or long distances of a few km. For the purposes of this work we have assumed that beam quality M2 parameter should be < 2 at 1 um wavelength and laser power is few tens of kWatts. In preliminary range analysis the relations between range of operation and aperture were investigated, taking into account the diffraction and technical limitations as beam quality, accuracy of point tracking, technical quality of optical train, losses inside optical elements, atmosphere influence etc. As a result for the medium ranges of 2 - 3 km being our scope of interest we restricted the analysis to apertures not wider than 150 mm and the optical system without adaptive optics. The typical laser beam forming optical train for such purposes consists of about 10 elements including mirrors and a few refractive elements, each experiences the thermo-optic distortions as a result of residual absorption on surfaces and in the volume. Thus the laser beam profile in near field should take into account the minimization of aperture losses and thermo-optical effects as well as the effective width of laser beam in far field. Let us notice that optimal from the thermo-optic problems 'top-hat' profile results in far field in poor 'sombrero' like profile which has wider diameter than equivalent Gaussian profile. On the other hand for Gaussian profile of given 1/e2 diameter in the near field the clear aperture should be much wider (~ 2 times) to neglect aperture losses. Thus, it is evident tradeoff between the above requirements in near and far fields. We have analyzed theoretically such problem for the group of a few most interesting from that point of view profiles including for reference two limiting cases of Gaussian beam and near 'top hat' profile. For each beam profile we have designed the two element beam shaper optics applying semi-analytical approach and ZEMAX software for final optimization. Further applying COMSOL software we have determined the thermo-optic aberrations induced for such profile in the volume and on surfaces of optical element. We have found that the most promising is the SuperGaussian profile of index = 2 for which the surfaces of beam shaper elements can be manufactured in the acceptable cost-effective way and far field diameter has low value. In last part of work the tolerance analysis was performed to determine the technical limitations and problems with manufacturing and mounting of optics.

10436-2, Session 1

High-beam quality, all-solid-state 5J, 200Hz nanosecond Nd:YAG laser system *(Invited Paper)*

Xiongxin Tang, Academy of Opto-Electronics, CAS (China)

The laser system is constructed in a master oscillator power amplifier (MOPA) configuration, with four components: a single-frequency seed laser, pre-amplifier unit, beam control unit, and post-amplifier unit. The pre-amplifier consists of a three-stage side-pumped rod amplifier. The stimulated Brillouin scattering phase-conjugate mirror (SBS-PCM) technique is implemented in the control unit to correct the wavefront distortion dynamically. The post-amplifier unit is composed of a three-stage large slab amplifier. The single-frequency seed laser produces an output power of 8.58 ?J with a pulse duration of 33.9 ns (FWHM) at 200 Hz repetition rate. The root-mean-square (RMS) fluctuation in pulse energy is smaller than 1% and the beam quality is better than 1.12 times DL. The seed pulses then pass through the pre-amplifier and then the control unit at which the beam shaping is applied. The pulse energy is amplified to 300 mJ. The pulse duration is 30.5 ns and the beam quality is better than 1.4 times DL. After passing through the post-amplifier, the pulse energy reaches 5 J with the beam quality 3.2 times DL. Adaptive optics system is applied for wavefront correction, and the beam quality is improved to 1.7 times DL. A pulse energy of 5 J at 1064 nm is first-ever achieved with a pulse duration of 6.6 ns at a repetition rate of 200 Hz, and the output energy stability is 4.9% peak-to-valley.

10436-3, Session 1

Mult-terawatt OPCPA system designed with acurate non-collinear pulse propagation model

Tomasz M. Karda?, Yuriy Stepanenko, Institute of Physical Chemistry, Polish Academy of Sciences (Poland); Czes?aw Radzewicz, Univ. of Warsaw (Poland)

Recently some of us have shown that the use of a correct ab initio approach to nonlinear pulse propagation simulations during nonlinear optical device designing can result in threefold efficiency increase with respect to the efficiency of existing solutions [1]. In that work we have focused on small beam size, and thus, high divergence regime where the effects of diffraction, spatial and temporal walk-off are difficult to separate and thus require numerical approach. Our collinear model of pulse propagation enabled modelling and optimization of a cascade third harmonic generation in a single element tripler. Herewith, we present the results of expanding our model to treatment of non-collinear optical configurations and the model application to our OPCPA design [2,3]. To the best of our knowledge this is a first propagation

model that enables non-collinear configurations while in minimal assumptions regime: unidirectionality and paraxial approximation.

By definition the non-collinear propagation is required when interaction of two or more beams is considered. In this case the use of not necessarily slowly varying envelope for each interacting beam is justified from both physical and computational reasons. In case of 3D non-collinear propagation the above conclusion leads to the concept of reference wavevector. Our model is based on unidirectional pulse propagation equation (UPPE [4]) in a rotated frame of reference. Rotation by a different angle has to be, however, performed separately for each of the interacting beams. Apparently even for quite high mutual beam angles it is enough to solve scalar, rather than vectorial, version of UPPE and sustain accuracy. Finally the initial conditions (rotated optical pulses) can be prepared through arbitrary 3D rotation through Fourier Transform shear operations. The idea, realization and advantages of the above mentioned, novel concepts: reference wavevector, rotated UPPE and arbitrary Fourier rotation will be discussed in the presentation.

The real life examples of model results for the usage will be presented: an LBO based chirped pulse non-collinear optical parametric amplifier working in “exotic” (off major plane) phase matching conditions and the redesigned multiterawatt BiBO based OPCPA system [2].

1. T. M. Karda?, M. Nejbauer, P. Wnuk, B. Resan, C. Radzewicz, and P. Wasylczyk, “Full 3D modelling of pulse propagation enables efficient nonlinear frequency conversion with low energy laser pulses in a single-element tripler,” Scientific Reports 7, 42889 (2017).

2. P Wnuk, Y Stepanenko, C Radzewicz “Multi-terawatt chirped pulse optical parametric amplifier with a time-shear power amplification stage”, Optics Express 17(17), 15264 (2009)

3. Y. Stepanenko, “On the efficiency of a multiterawatt optical parametric amplifier: numerical model and optimization,” JOSA B 28, 2337–2346 (2011).

4 M. Kolesik and J. V. Moloney, “Nonlinear optical pulse propagation simulation: From Maxwell’s to unidirectional equations,” Phys. Rev. E 70, (2004).

10436-5, Session 1

Tunable-line-width all-solid-state double-spectral-line sodium beacon laser

Yanhua Lu, Huaijin Ren, Lei Zhang, Xiafei Xu, Min Wan, Institute of Applied Electronics (China); Guobin Fan, China Academy of Engineering Physics (China)

We demonstrated a tunable-line-width 101 W average-power all-solid-state 589nm double-spectral-line sodium beacon laser. We took the technical route of the 1064nm and 1319nm Nd:YAG lasers extra cavity sum frequency generation. The laser contained two spectral lines: 589.1591 nm and 589.1571 nm. The former line was matched to the sodium D2a absorption line with the average power of 81W, while the other line matched to the D2b absorption line with the average power of 20W. The two lasers were generated by two individual lasers with the similar principle. It was quite different with the traditional method which used phase-modulating onto the D2a line laser. Although the volume and the cost increased in our method, its difficulty and complexity reduced. Furthermore, it avoided the energy loss of the unexpected generated frequency (central wavelength of about 589.1601nm, which had no use for the sodium beacon return light) by phase modulating. The beam quality of the two spectral line lasers was both less than 1.3. The two lasers were polarized-combined to transmit coaxially.

The initial line width of the laser was about 0.3GHz, which was in the comb-like discrete structure of about three longitudinal modes. Because the nature line width of the sodium atoms was about 10 MHz with the Doppler line width of about 1.2GHz, it was necessary to broaden the line width of the sodium beacon laser to avoid the low threshold effect of the narrow line width sodium beacon laser, to excite more sodium atoms and then increase the return light’s intensity. We used a white noise generator to modulate the 1064nm single frequency seed laser in frequency domain. The white noise could be treated as the sum of discrete frequencies by Fourier expansion. Each individual frequency would modulate the single frequency laser and generate the +1 and -1 side frequencies. Finally the whole line width was broadened by summing all of the side frequencies. Beside of the line width broadening by this method, the obtained spectral was continuous in the frequency domain, whereas it was discrete by directly output of the multi longitudinal mode laser. The line width tenability was accomplished by tuning the driver power of the white noise generator. The line width became wider with the increasing of the driver power. The line width of the 1064nm single frequency seed laser was less than 100kHz, and its broadening tuning range was 0 to 0.7GHz. Therefore, the finally line width tuning range of the 589nm laser was 0.3GHz to 1.0GHz.

10436-29, Session 1

The High Energy Laser Joint Technology Office: a historical perspective *(Invited Paper)*

Albert A. Ogloza, Naval Surface Warfare Ctr. Port Hueneme Div. (United States)

At the turn of the century the US was a world leader in the development of large chemical laser systems. Most of the DoD funding was directed to the major aerospace contractors, while limited funds were available for basic and applied research within the Service and Agency laboratories, academic institutions and small businesses. Advancements in the telecommunication industry led to increased, world-wide, interest solid state lasers. The US found itself lagging behind the International S&T community in this area of HEL technology development. The High Energy Laser Joint Technology Office (HEL JTO) was established in 2000 for the purpose of developing and executing a comprehensive investment strategy for HEL science and technology. HEL JTO investments focused laboratory curiosities into state of the art building blocks (components, sub-systems and systems). The success of “Flagship” laser programs, the Joint High Power Solid State Laser (JHPSSL) and the Robust Electric Laser Initiative (RELI), stimulated DoD interest in integrating HELs onto militarily useful platforms. The significance of the numerous HEL JTO accomplishments over the past 17 years will be discussed. So, with a new name, the Directed Energy Joint Transition Office (DE JTO), a meager budget, and increased interest within the DoD community to integrate HELs on military platforms, what’s next for the HEL JTO (DE JTO)?

10436-6, Session 2

Recent advances in average power scaling of fibers *(Invited Paper)*

Till Walbaum, Franz Beier, Nicoletta Haarlammert, Marco Plötner, Victor Bock, Gonzalo Palma-Vega, Christian Hupel, Fraunhofer-Institut für Angewandte Optik und Feinmechanik (Germany); Stefan Kuhn, Friedrich-Schiller-Univ. Jena (Germany); Johannes Nold, Matthias Heinzig, Fraunhofer-Institut für Angewandte Optik und Feinmechanik (Germany); Jens Limpert, Friedrich-Schiller-Univ. Jena (Germany); Thomas Schreiber, Ramona Eberhardt, Andreas Tünnermann, Fraunhofer-Institut für Angewandte Optik und Feinmechanik (Germany)

As they are inherently resilient to environmental perturbations and provide an excellent interface for integration into complex beam direction systems, fiber lasers with high output power are highly interesting for long distance sensing and directed energy applications. In particular, the good beam quality available from single-mode fiber systems allows for an increase in efficiency,

since high intensity can be obtained at long range. However, also applications requiring tight focusing on short distance benefit from the properties.

In this presentation, we will give an overview of our recent advances in fiber laser power scaling, the required components and their characterization and application.

To begin with, we will give an overview of the current challenges faced by developers of kilowatt class fiber lasers. New results concerning the power scaling of single fiber systems in the one micron range will be presented. By optimization of fiber design and fabrication, we were able to extract more than 4.4 kW from a step index fiber while maintaining high beam quality. We will also present how to adapt a fiber amplifier system for different output wavelengths, in particular for the amplification at 1018 nm. Output powers in excess of 660 W were achieved at this wavelength, which is of interest for tandem pumping as well as for further frequency conversion.

High power fiber laser systems require specific components to be run reliably, and in-depth knowledge about the characteristics of all their constituents. We will present measurements precisely characterizing the properties of cladding light strippers as well as double clad fibers, considering numerical aperture of the guided light and cladding light content, respectively.

As an application, we will present recent achievements on the wavelength conversion of high power fiber laser systems, making use of the Raman shift in single crystal diamonds. This allows spectrally shifting the emitted light to regions inaccessible for normal gain media, which may be of interest for material processing, medical applications or when eye-safety is an issue.

Another aspect that is currently highly sought after is the generation of ultrashort pulses at high average power. Recent results have shown the advantages of femtosecond pulse bursts in material processing as compared to other alternatives. We will show how to generate sub-picosecond pulses at high repetition frequencies and an average power in the kW region without having to rely on mode-locked oscillators. This is done by generating spectral side bands of a dual-wavelength continuous wave laser via self phase modulation and then compressing the spectrum. The resulting pulse train has a repetition frequency equal to the initial frequency distance between the two laser wavelengths and was generated at 930 fs pulse duration and more than 700 W average power.

10436-7, Session 2

Thermal Distortion of 960l/mm Broadband Polarization-independent Reflective Diffraction Gratings as Beam Combiner

Jiao Xu, Peng Chen, Yibin Zhang, Yonglu Wang, Junming Chen, Yanzhi Wang, Shanghai Institute of Optics and Fine Mechanics (China); Yun Cui, Changchun Institute of Optics, Fine Mechanics and Physics (China); Yunxia Jin, Jianda Shao, Shanghai Institute of Optics and Fine Mechanics (China)

Spectral beam combined technique has promising potential in improving output power and brightness. However, the technique could not play the role without beam combiner. In report of Lockheed Martin Corporation, 30KW combined power, the highest, was obtained by polarization-dependent reflective diffraction gratings as beam combiner and in report of SIOM, 10.88KW combined power was obtained by polarization-independent reflective diffraction gratings as beam combiner. Though 10.88KW is not the highest combined output power, polarization-independent reflective diffraction beam combiner has many priorities in simplifying and lightweight the high power fiber laser system compared with polarization-dependent optics. In our report, we will give some design results of broadband polarization-independent all-dielectric reflective diffraction gratings as beam combiner and provide some fabrication results including diffraction efficiency and laser induced damage mechanism.

In process of the grating fabrication, there are many impacting factors, such as the line density, the bandwidth, the tolerance of the process and so on, in which the line density is a parameter which can improve the design results and adjust the whole optical system structure. In this paper, we optimized 3 kinds of different line densities polarization independent gratings with different relief structures and focused on diffractive efficiency and reliable process evaluation of the gratings with 960 line/mm samples from reflective coatings to gratings. Furthermore, we investigated the morphology of laser-induced damage patterns irradiated on the continue wave laser power.

10436-8, Session 2

Toward Watt-level, compact and rugged mid-IR fiber laser sources

Louis-Rafaël Robichaud, Simon S. Duval, Jean-Christophe Gauthier, Vincent Fortin, Pascal Paradis, Louis-Philippe Pleau, Michel Olivier, Michel Piché, Réal Vallée, Martin Bernier, Ctr. d'Optique, Photonique et Laser (Canada)

The keen interest for mid-IR (3-20 μm) laser sources over the last decade was driven by several applications in the field of standoff remote sensing, infrared countermeasures and medical/industrial laser processing. Among the available laser sources in the mid-IR, fiber based sources are one of the most promising technologies because they offer power scalability, beam quality and reliability in a compact and robust system design. Currently, the most mature systems are based on fluoride glass fibers mainly because of their low losses and high gain around 2.8 μm. In fact, all-fiber laser cavities generating up to 30 Watts CW average power were previously reported at 2.94 μm using erbium doped fluoride fibers These active fibers can also be used as efficient nonlinear converters for the generation of either mid-IR tunable femtosecond pulses or supercontinuum.

In this report, we show that the amplification of picosecond pulses can lead to a 0.5 W average power supercontinuum generation (SCG) extending up to 4.2 μm. Then, by cascading an indium fluoride or an arsenide selenide step-index fiber to the setup, the supercontinuum is broadened up to 5.4 μm and 8 μm, respectively. The amplification of femtosecond pulses, on the other hand, produces a 3.5 W ultrafast tunable output up to 3.6 μm through Raman soliton self-frequency shift (SSFS).

To achieve these results, one needs (1) an appropriate seed laser either for SCG (OPG, T0 = 400 ps, Wavelength = 2.75 μm, Rep. rate = 20 kHz, E = 1.5 μJ, P0 = 3.5 kW) or for SSFS (mode-locked fiber oscillator [6], T0 = 440 fs, Wavelength = 2.8 μm, Rep. rate = 57.9 MHz, E = 4.7 nJ, P0 = 9.5 kW), (2) an erbium-doped fluoride fiber amplifier (Øcore= 15 μm, NAcore = 0.125, Er3+ doping level = 7 mol%) pumped in co-propagation with a high-power 980 nm diode laser (average power ~52 W) via a dichroic mirror and a ZnSe coupling lens and (3) several meters of passive fiber (ZrF4, InF3, As2Se3) in order to maximize the Raman redshift. The output spectrum and average power are measured by a grating-based monochromator and a thermopile, respectively.

During our talk, we will review our versatile in-amplifier approach based on a simple erbium doped fluoride fiber amplifier, which is revealed to be an excellent non-linear red-shifter and a high power scalable system A detailed experimental and theoretical optimization of this approach as well as its current limitations will be discussed in the context of defense and security. This fiber-based source could have a great impact in countermeasure and standoff remote sensing applications.

10436-9, Session 2

All-glass microstructured fiber cladding light stripper for kW-class laser systems

Mateusz Wysmolek, Christoph Ottenhues, Tony Pulzer, Michael Steinke, Laser Zentrum Hannover e.V. (Germany); Uwe Morgner, Leibniz Univ. Hannover (Germany); Jörg Neumann, Dietmar Kracht, Laser Zentrum Hannover e.V. (Germany)

In a typical fiber laser system there are five major contributors to generation of cladding light: unabsorbed pump light, splice loss, bending loss, isotropic amplified spontaneous emission in active fibers, and coupling loss. There are many variations of cladding mode strippers (CMS) which rely on different physical phenomena, but generally they can be divided into two groups: by altering the refractive index around the fiber or by changing fiber's geometry to suppress waveguiding. Refractive index alteration is mostly done with different polymers with higher refractive index than the cladding material. Thereby, the cladding light expands into the polymer where it is dumped. Careful choice appropriate polymers can provide very good results, but the biggest disadvantage is that polymers are susceptible to high temperatures and degrade, putting a limit to the highest applicable pump power which can be extracted to around 100 W. Furthermore, such components can be only utilized at wavelengths below 1.2 μm. Fiber geometry alteration for cladding light stripping is achieved mostly with etching. Fibers are tapered and the fiber surface is roughened by hydrofluoric (HF) acid. The process is time consuming and control is very low. Since the device is not polymer-based the power handling can be enhanced greatly up to 500 W but the efficiency is not as high (approx. 20 dB) as with the polymer-based method. Here we propose a (CMS) based on direct micro structuring of the fiber barrel surface with a continuous wave CO2 laser. The approach delivers a device that is suitable for all pump wavelengths and can be adopted for any kind of fiber. With equally spaced grooves simulations and experiments have shown strong near exponential power gradient along the CMS, which could ultimately cause device failure due to strongly elevated component temperatures in the very first part of the CMS. To overcome this problem we have investigated theoretically and experimentally two CMS structures: the first with equidistant spacing (160 μm) of grooves and the second was such that the groove spacing gradually changed from 750 μm to 160 μm to flatten out the intensity profile of stripped light. Both CMS structure types were stress-tested under 335 W coupled power. The two were able to withstand the launched power of 335 W. However, the package temperature with equally spaced groves case reached 60 °C and failed catastrophically after few minutes of operation. Although same strip efficiency (equidistant 22.9 dB, graded 23.2 dB), CMS with graded structure performed much better in terms of reliability. The maximum temperature was reduced to 52 °C and device's reliability could be tested in a 500 hours long stress test. To the best of our knowledge this is the first demonstration of all-glass micro-structured fiber cladding mode stripper with optimized micro-structure pattern capable of handling 350 W with >22 dB cladding light attenuation.

10436-25, Session 2

Numerical study of the measurement capability of quadriwave lateral shearing interferometry for multimode fiber laser

Kun Xie, Wenguang Liu, Qiong Zhou, Hongmiao Zhao, Xiaojun Xu, National Univ. of Defense Technology (China) and Hunan Provincial Key Lab. of High Energy Laser Technology (China) and Hunan Provincial Collaborative Innovation Ctr. of High Power Fiber Laser (China)

Quadriwave lateral shearing interferometry (QWLSI) could acquire the phase and intensity distribution of laser beam with remarkable resolution in only one measurement. It's a potential method to measure the phase step of multimode laser. However, the discontinuity point of intensity will reduce the quality of interferogram and lead to wrong wavefront retrieve result. In this paper, analysis and simulations have been conducted on the measuring ability of the QWLSI for the higher-order modes (HOM) in large mode area (LMA) fiber. A set of interferogram image of ideal linearly polarized (LP) mode are calculated and analyzed by a commercial retrieve software. The results show that the proper ratio of the shearing distance to the gap size between HOM petals is the critical parameter to retrieve wavefront correctly. To study the influence of coherence on wavefront retrieving, we calculated the interferogram of multimode laser with different modal phase fluctuation. The results indicate that the partially coherent beam will introduce significant ambiguity into the retrieved wavefront. Finally, the feasibility of wavefront correction of multimode laser with LSI and spatial light modulator is demonstrated with simulations.

10436-27, Session 2

Eye safer silica fiber lasers *(Invited Paper)*

Colin C. Baker, U.S. Naval Research Lab. (United States)

No Abstract Available

10436-28, Session 2

Beam shaping by using small-aperture SLM and DM in a high power laser

Sensen Li, Zhiwei Lu, Pengyuan Du, Harbin Institute of Technology (China); Yulei Wang, Harbin Engineering Univ. (China); Lei Ding, China Academy of Engineering Physics (China); Xiusheng Yan, Science and Technology on Electro-optical Information Security Control Lab. (China)

High-power laser plays an important role in many fields, such as directed energy weapon, optoelectronic contermeasures, inertial confinement fusion, industrial processing and scientific research. The uniform nearfield and wavefront are the important part of the beam quality for high power lasers, which is conducive to maintaining the high spatial beam quality in propagation. We demonstrate experimentally that the spatial intensity and wavefront distribution at the output is well compensated in the complex high-power solid-state laser system by using the small-aperture spatial light modulator (SLM) and deformable mirror (DM) in the front stage. The experimental setup is a hundred-Joule-level Nd:glass laser system operating at three wavelengths at 1053 nm (1?), 527 nm (2?) and 351 nm (3?) with 3 ns pulse duration with the final output beam aperture of 60 mm. While the clear arperture of the electrically addressable SLM is less than 20 mm and the effective diameter of the 52-actuators DM is about 15 mm. In the beam shaping system, the key point is that the two front-stage beam shaping devices needs to precompensate the gain nonuniform and wavefront distortion of the laser system. The details of the iterative algorithm for improving the beam quality are presented. Experimental results show that output nearfield and wavefont are both nearly flat-topped with the nearfield modulation of 1.26:1 and wavefront peak-to-valley value of 0.29 ? at 1053nm after beam shaping.

10436-12, Session 3

New results for temperature rise in gain medium of operating DPAL causing its degradation *(Invited Paper)*

Boris V. Zhdanov, Matthew D. Rotondaro, Michael

K. Shaffer, Randall J. Knize, U.S. Air Force Academy (United States)

Diode Pumped Alkali Laser (DPAL) is one of the main candidates for development of a high power directed energy system producing laser beam from a single aperture with high spatial quality. Currently, several groups in the US and abroad demonstrated DPAL systems with kW level output power and efficiency higher than 50% [1,2]. At the same time, the DPAL power scaling experiments revealed some limiting effects, which require detailed study to understand the nature of these effects and ways to mitigate them. Examples of such effects are output power degradation in time, alkali cell windows and gain medium contamination and damage that causes lasing efficiency decrease or even lasing termination [3]. These problems can be connected to thermal effects, ionization, chemical interactions between the gain medium components and alkali cells materials. Study of all these and, possibly, other limiting effects and ways to mitigate them is very important for high power DPAL development.

In this talk we present our new results of experiments on measurements of temperature rise in the gain medium of operating DPAL leading to the output power degradation even before visible damage in the gain cell occurs. This degradation can be both recoverable and non-recoverable, depending on operation conditions and the system design. This paper is a continuation of the experiments published in [4]. For precise contactless in situ temperature measurements, we used interferometric technique slightly modified compared to one described in [5].

1. A.V. Bogachev, S.G. Garanin, A.M. Dudov, V.A. Yeroshenko, S.M. Kulikov, G.T. Mikaelian, V.A. Panarin, V.O. Pautov, A.V. Rus, S.A. Sukharev, “Diode-pumped caesium vapour laser with closed-cycle laser-active medium circulation”, Quantum Electronics 42 (2), 95-98 (2012)

2. G.A. Pitz, D.M. Stalnaker , E.M. Guild, B.Q. Oliker, P.J. Moran, S.W. Townsend, and D.A. Hostutler “Advancements in flowing diode pumped alkali lasers”, Proc. SPIE 9729, 972902-1 – 972902-8 (2016)

3. B.V. Zhdanov, M.D. Rotondaro, M.K. Shaffer, and R.J. Knize, “Power Degradation Due to Thermal effects in Potassium Diode Pumped Alkali Laser ”, Opt. Comm. 341, 97-100 (2015).

4. Boris V. Zhdanov, Matthew D. Rotondaro, Michael K. Shaffer and Randall J. Knize, “Measurements of the gain medium temperature in an operating Cs DPAL”, Optics Express, 24(17), 19286-19292 (2016)

5. M. K. Shaffer, T. C. Lilly, B.V. Zhdanov, R. J. Knize, “In situ non-perturbative temperature measurement in a 133Cs alkali laser”, M. K. Shaffer, T. C. Lilly, B.V. Zhdanov, R. J. Knize, Optics Letters 40(1) 119-122 (2015)

10436-13, Session 3

Experimental studies and modeling of static Cs DPALs: dependence of the power and beam shape on different parameters *(Invited Paper)*

Salman Rosenwaks, Ilya Auslender, Eyal Yacoby, Boris D. Barmashenko, Ben-Gurion Univ. of the Negev (Israel)

The pump-to-laser beam overlap and the cell length of static diode-pumped Cs lasers are crucial parameters for optimization of these lasers. In previous publications we modeled the influence of the pump-to-laser beam overlap on the performance of optically pumped cesium vapor laser (T. Cohen, E. Lebiush, I.Auslender, B.D. Barmashenko and S. Rosenwaks, Opt. Exp. 24, 14374 (2016)), and the laser power, cell temperature and beam quality dependence on the cell length of static Cs DPALs, (K. Waichman, B.D. Barmashenko and S. Rosenwaks, J. Opt. Soc. Am. 34, 279 (2017)). In the present paper we report on experiments in progress aiming at comparing the models to the experimental results.

10436-14, Session 3

Scaling up and controlling beam quality of flowing-gas diode pumped potassium laser with different pumping geometries: 3D CFD modeling

Eyal Yacoby, Karol Waichman, Oren Sadot, Boris D. Barmashenko, Salman Rosenwaks, Ben-Gurion Univ. of the Negev (Israel)

Comprehensive analysis of the performance and beam quality of subsonic flowing gas K diode-pumped alkali lasers (DPALs) with different pumping geometries using 3D computational fluid dynamics model is reported. The model is applied to a K DPAL with transverse pumping and parameters similar to those of the 1.5 kW K DPAL [Pitz et al, Proc. SPIE 9729, 972902 (2016)] and calculated results are in satisfactory agreement with the measurements. To study the possibility of scaling up the K DPAL the model was applied to 100- kW class device with transverse and end pumping geometry. Dependence of the output power on flow velocity and pumping geometry is studied. It is found that for the flow velocity Vi > 4 m/s the power Plase >100 kW is nearly independent of Vi, whereas for lower Vi the power decreases due to gas heating.

Comparison between end and transverse pumping by beams with the same rectangular cross section and uniform intensity shows that the output power is almost not affected by the pump geometry. However, in the case of end pumping the output laser beam has a uniform spatial intensity distribution in the beam cross section, whereas for transverse pumped DPALs with high temperature Ti at the laser section inlet the intensity is strongly non-uniform and has a bimodal shape in the pumping direction. To achieve more uniform laser intensity spatial profile it is necessary to decrease Ti. It is seen that decrease of Ti from 460 K to 449 K corresponding to K density of nk = 5 - 8.4 ? 10^13 cm^-3, respectively, results in a decrease of the beam width at the far field by more than three times.

The model is applied to evaluation of the beam quality of the flowing-gas K DPAL which strongly depends on the refractive index distribution in the gain medium. The beam divergence and the width of the intensity distribution in the far field for the end pumping appear to be much narrower than for the transverse pumping. Wave front corrections of the transversely pumped device using cylindrical lens results in substantial reduction of the laser beam divergence and improvement of its quality which becomes comparable with that of the end pumped laser.

Comparison between the far field intensity profile after the phase correction shows that for the end pumping geometry the intensity and phase distributions at the output coupler are uniform so that for the transverse pumping the beam width is by ~30% larger than that in the end pumping case. However, as Ti decreases to 453 K it is almost the same for both pumping geometries.

10436-15, Session 3

Modeling of multi-transversal mode lasing in static alkali vapor lasers

Ilya Auslender, Boris D. Barmashenko, Salman Rosenwaks, Ben-Gurion Univ. of the Negev (Israel)

In most alkali vapor lasers, pumped by Ti:Sapphire or low power diode lasers with well collimated output beams, only the fundamental transverse mode of the stable resonator oscillates. The reason is that the beams of such pump sources are focused to small spots with the radii close to those of the fundamental laser modes. However, in the case of pumping by high power diode laser arrays it is difficult to focus the pump beam to small spot and usually its radius in the laser cell is several times larger than that of the fundamental laser mode. In this case several high order transverse modes of the resonator participate in the lasing. In the present paper we use a simple optical model to describe multi-transverse mode operation of alkali lasers. The

model is based on calculations of the pump and laser beam intensities in the gain medium, where the laser beam intensity is a linear combination of the azimuthally-symmetric Laguerre-Gaussian modes. The model was applied to optically pumped cesium vapor laser studied experimentally and theoretically in [1]. It was found in our calculations that for low pump power and small pump beam radii applied in [1], only fundamental lasing mode oscillates, just as shown experimentally in [1]. However, for higher pump powers and larger pump beam diameters several transverse modes participate in oscillation. The number and intensities of the oscillating modes as a function of the pump beam power and radius are found. The number of lasing modes increases with the increase of the pump beam radius when the latter becomes larger than the fundamental laser mode radius. It was shown that for a given pump power, there is an optimal pump beam radius corresponding to the maximum laser power and determined by the modal composition of the laser beam. In order to check the validity of the model, it was applied to pulsed static Cs DPAL [2] with the pump beam radius much larger than that of the fundamental laser mode and constant gas temperature. The model predicts linear dependence of the laser power on the pump power, the values of the former being in agreement with the experimental results.

1. T. Cohen, E. Lebiush, I. Auslender, B. D. Barmashenko and S. Rosenwaks, “Influence of the pump-to-laser beam overlap on the performance of optically pumped cesium vapor laser,” Opt. Express 24, 14374 (2016).

2. B. V. Zhdanov, J. Sell, and R. J. Knize, “Multiple laser diode array pumped Cs laser with 48W output power,” Electron. Lett. 44, 582-583 (2008).

10436-16, Session 3

Three-Dimensional simulation of beam propagation and heat transfer in static gas Cs DPALs using wave optics and fluid dynamics models

Karol Waichman, Boris D. Barmashenko, Salman Rosenwaks, Ben-Gurion Univ. of the Negev (Israel)

An analysis of beam propagation, kinetic and fluid dynamic processes in diode pumped alkali laser (DPAL) using wave optics model and gasdynamic code is reported. The analysis is based on a three-dimensional, time-dependent computational fluid dynamics (3D CFD) model. The Navier-Stokes equations for momentum, heat and mass transfer are solved by a commercial ANSYS FLUENT solver based on the finite volume discretization technique. The CFD code which solves the gas conservation equations includes effects of natural convection and temperature diffusion of the species in the DPAL mixture. The DPAL kinetic processes in the Cs/He/C2H6 gas mixture considered involve the three low energy levels, (1) n2S1/2, (2) n2P3/2 and (3) n2P1/2 (where n=6 for Cs). The Cs states are considered as separate species in the species conservation equations, each containing sources arising from the Cs kinetics. The kinetic processes include absorption due to the D2 transition followed by relaxation 3 to 2 fine structure levels and stimulated emission due to the 2?1 D1 transition. Collisional quenching of levels 2 and 3 and spontaneous emission from theses levels are also considered. The gas flow conservation equations are coupled to the fast-Fourier-transform algorithm for the transverse mode propagation to obtain a solution of the scalar paraxial propagation equation for pump and laser beams propagation. The wave propagation equation is solved by the split-step beam propagation method where the gain and refractive index in the DPAL medium affect the wave amplitude and phase. Using the CFD and beam propagation models, the gas flow pattern and spatial distributions of the pump and laser intensities in the resonator were calculated for end-pumped Cs DPAL. The laser power, DPAL medium temperature and the far-field laser beam quality were calculated as a function of pump power. The results of the theoretical model for laser power were compared to experimental results of Cs DPAL.

10436-4, Session 4

High-efficiency mid-infrared optical parametric amplifier with approximate uniform rectangular pump distribution

Xingbin Wei, Yuefeng Peng, Xingwang Luo, Tangjian Zhou, Jue Peng, Zan Nie, Jianrong Gao, Institute of Applied Electronics (China)

We present a high-efficiency mid-infrared optical parametric amplifier (OPA) pumped by a Nd:YAG slab laser with approximate uniform rectangular distribution. Output power of 40.3 W at 3.82 ?m was achieved for 293.4 W of pump. To the best of our knowledge, this is the highest power at 3.82 ?m from a mid-IR OPA.

To improve the conversion efficiency of OPA, we used an approximate uniform pump beam, which helped most of the pump area maintain the optimal intensity. This reduced the back conversion effect in which the signal and idler lasers began to sum back to the pump laser and decreased the conversion efficiency of OPA. The uniform pump distribution without any peak intensity also reduced the damage chances of the nonlinear crystal of PPMgOLN and increased its pump power capability in power-scaling operations. To make sufficient usage of the narrow and small interface of PPMgOLN (3T?5W?50L mm^3), we chose a rectangular pump shape whose size (~2.1?3.5 mm^2) was adjusted to match the maximum effective interface of PPMgOLN (~75% of its clear aperture). A Nd:YAG slab laser was an ideal pump source for PPMgOLN OPA because of its high power (>300 W) and good beam quality (M^2<3) with uniform rectangular distribution.

The idler laser of 3.82 ?m from an optical parametric oscillator (OPO) was power-scaled in the following OPA system. The seed-OPO was singly resonated at its idler wave in P-P cavity. We used two 1.064 ?m lasers to pump the OPO and OPA separately. The pulse-width adjustment and pulse synchronization of the 1 ?m pump laser and 3.82 ?m seed laser were realized by changing the parameters of the two acoustic-optical Q-switches in the two pump lasers. The pulse widths (FWHM) of the pump and idler seed lasers at their maximum powers were 58 ns and 61 ns, respectively.

The two PPMgOLN crystals for OPO and OPA had the same grating period of 29.2 ?m, and were placed in two ovens whose operation temperatures were adjusted separately according to the phase-matching conditions at different pump powers. The operation temperature of PPMgOLN in OPA was 116.5 °C, which was 3.5 °C lower than the temperature of the crystal in OPO due to the higher thermal effect for higher pump power. This was verified by observing the thermal distribution and gradient along the two crystals.

With the input pump power of 293.4 W, the amplified 3.82 ?m laser power was 40.3 W deducting the injected seed laser power of 2.9 W from OPO. The corresponding conversion efficiency from the pump to the idler was 13.7% for the PPMgOLN OPA. The slab laser had potential of offering higher output power. However, the pump power was limited to below the damage threshold of PPMgOLN and infrared coatings of its surfaces. Considering the conversion efficiency curve without decreasing with the increase of the pump power, higher output power of the amplified idler laser could be expected with higher pump power.

10436-17, Session 4

Standoff spectroscopic interrogation of samples irradiated by high energy lasers

Jean-François Daigle, Defence Research and Development Canada, Valcartier (Canada); Dominik Pudo, Francis Théberge, Defence Research and Development Canada (Canada)

We report on a novel method that shows the potential to provide real-time, standoff forensic analysis of samples being

irradiated by a high energy laser (HEL). The interaction of the HEL beam with matter produces specific optical signatures that can be detected from the location of the HEL weapon system. A spectroscopic analysis of these signals can then provide useful information to the operator including the impact the laser has on the sample as well as providing data about the its structure and composition.

When a HEL is fired on a solid sample, a portion of the incident laser energy is absorbed by the material resulting in a temperature elevation. Depending on its composition, the irradiated material can then be vaporized, burn or melt. All of those processes are usually accompanied by the emission of light with a spectral signature, specific to the material and to the process taking place. These signals can be detected remotely using passive spectroscopic sensors positioned at the location of the HEL. The hardware has a small footprint, is independent of the HEL system, and is based on commercial off-the shelf components.

In order to demonstrate the potential of the method for standoff analysis/identification of solid materials, it was tested with different metallic surfaces interrogated over propagation paths of several hundreds of meters. The different samples tested were AISI 1020 grade carbon steel, aluminum 6061-T6, SAE 202 stainless steel and alpha-type copper brass.

Each measured spectrum exhibited distinct features corresponding to the predicted fluorescence lines of the metal, thus enabling the identification of the exposed material. Depending on the exposed metallic sample, emission lines corresponding to iron oxide (FeO), chromium oxide (CrO), manganese oxide (MnO), copper oxide (CuO) and aluminum oxide (AlO) were observed since the laser beam is sufficiently intense to induce rapid oxidation on the target surface. These features are unique and offer the possibility to discriminate the different samples.

The results obtained show a clear potential for standoff target identification and discrimination during a HEL exposition of metallic samples. In addition, it allows monitoring of the engagement process itself, potentially permitting to identify the extent to which the laser penetrates a target. This, in turn, would contribute to increased control over HEL lethality and precision, circumventing the limitations of conventional video monitoring systems.

10436-19, Session 4

Investigations of high power laser beam interaction with composite materials by means of digital image correlation and thermovision methods

Malgorzata Kujawi?ska, Marcin Malesa, Kamila Kustron, Warsaw Univ. of Technology (Poland); Roman Ostrowski, Wojskowa Akademia Techniczna im. Jaroslawa Dabrowskiego (Poland)

The effects of interaction between a variety of solid state materials and high power laser beam have been extensively demonstrated in many scientific and industrial domains, including laser material processing, 3D manufacturing and laser cleaning of artworks. Most of the works are focused on interaction with more or less homogeneous materials such as metals, ceramics, glass, stones and the processes which can be optimized for the chosen functionality (drilling, cutting, cleaning) and processing conditions. Now days in defense applications it is necessary to address also structures, which are as light as possible and at the same time sufficiently strong i.e. which are constructed of composite materials. Many such structures are basically composed of : (1) sandwich structures of GraphiteEpoxy plies and (2) Nomex honeycomb or Rohacell foam core. Additionally they are often covered with different paints or radar absorbing materials, which might dramatically change the interaction conditions. Therefore in this paper we present systematic investigation of a variety composite material structures exposed to a high power beam. The laboratory experiments are performed by two full-field optical measurement methods namely: thermovision and 3D Digital image Correlation methods. Both systems utilize high speed cameras which enable to monitor in time the maps of temperature T(x,y;t), in-plane displacements u(x,y;t), v(x,y;t) and out-of-plane displacement w(x,y;t). The experiments are performed at selection of materials with typical coatings and for different conditions of interaction. The full-field character of results allows to estimate not only local effect of interaction but also predict the model of destruction of a structure.

Conference 10437: Advanced Free-Space Optical Communication Techniques and Applications

SPIE. SECURITY+ DEFENCE

Monday - Tuesday 11–11 September 2018

Part of Proceedings of SPIE Vol. 10437 Advanced Free-Space Optical Communication Techniques and Applications III

10437-1, Session 1

Free Space Optical Interconnect (FSOI) modules for short range data transfer applied to board to board high rate communication

Myriam Kaba, Maxime Mallet, Laurence Pujol, Christian Claudepierre, Radiall SA (France); Johannès Veyron, RADIALL IDA (France); Romain Giroud, Daniel Mouseaux, Radiall SA (France); Mathias M. Pez, Radiall AEP, Inc. (United States); Francois Quentel, Vincent Foucal, Radiall SA (France)

On the way of the tremendous increasing of interconnection needs whether its improving board density or linking handset devices to networks, free space technology (FSOI: Free Space Optical Interconnect) provides an interesting alternative to wired devices.

Using optical high speed signal transmission through air FSOI provide extra ways to interconnect devices when space is too tight for optical fiber interconnection. As a contactless technology, FSOI allow data transfer between mobile devices and docking systems or between isolated media through window.

We developed a FSOI module dedicated to short range data transfer and compliant with milaero environments, called F-light. Target application is a board to board high rate communication providing more flexibility in the chassis functionality. Adding F-light on board enable extra communication channels without changing back or front panel architecture of the equipment.

Opto mechanical modelizations have been done to design robust configuration and provide good mechanical misalignment tolerances between emitter and receiver components. The FSO link exhibits an optical transmission at a 850nm-wavelength over a communication distance of 15mm. The emitter and receiver are based on a 850nm-VCSEL and a 100μm-photodetector, respectively; and both integrate short focal length ball lenses. We have chosen to position the photodetector before the receiver focal point. This designing choice was made to recover data over an enlarged optical plan, in order to guarantee adequate geometrical tolerances. Our design's performances have been optimized over temperature through an accurate adjustment of VCSEL's driving currents. Indeed, a current mapping, via I2C control, has been performed in order to extract values compliant over the full temperature range from -40°C until +90°C. Design validations tests have also included additional measurements under stress environment. These verifications have first involved tentative HALT (highly accelerated life test) measurement at temperature as low as -70°C and as high as +160°C. Secondly, tentative endurance testing has been performed over a long period around tens of hours at both -30°C and +90°C.

F-light has demonstrated longitudinal tolerance of +1.5/-1 mm (optical axis), lateral tolerance of +/-1 mm and angular tolerances of +/-1.5° over large range of temperature from -40°C up to 90°C for 5 Gbps balanced data link. Prototypes have been fabricated and reliable performances have been demonstrated through environmental constraints: thermal cycles and shocks, vibrations as defined in the standard MIL-STD-883 and damp heat cycle as defined in the standard MIL-STD-810G.

Increasing the data rate beyond 10 Gbps will have impact on lasers and photodiodes selection and may lead to a cramped alignment tolerances. We propose a set of solutions to enlarge both optical and mechanical performances of higher speed F-Light device.

10437-2, Session 1

Review of optical wireless communications for data centers *(Invited Paper)*

Shlomi Arnon, Ben-Gurion Univ. of the Negev (Israel)

A data center is a physical or virtual group of numerous servers, for the searching, storage, management and dissemination of information, which consume huge amount of energy. DC includes servers, communication and storage equipment and a support system including an air conditioning system and electricity regulator units. Datacenter operators face with the challenges of meeting exponentially increasing demands for network bandwidth without unreasonable increases in operation and infrastructure cost. In order to meet the requirements of moderate increase in operation and infrastructure cost technology revolution is required. One way to overcome the shortcomings of traditional static (wired) data center architectures is using the augmented network based on optical wireless communication (OWC) or free space optics (FSO). The OWC link could be deployed on top of the existing cable/fiber network layer, such that live migration could be done easily and dynamically. In that case the network topology is flexible and adapts quickly to changes in traffic, heat distribution, power consumption and characteristics of the applications. In addition, OWC could provide an easy way to maintains and scale up data centers. As a result total cost of ownership could be reduced and the return on investment could be increased. In this talk we will review the main OWC technologies, algorithms concepts and configurations which improve the performance of next generation data centers.

10437-3, Session 1

Energy reduction using multi channels optical wireless communication based OFDM

Laialy Darwesh, Shlomi Arnon, Ben-Gurion Univ. of the Negev (Israel)

In recent years, an increasing number of data center networks (DCNs) have been built to provide various cloud applications. Major challenges in the design of next generation DC networks are high flexibility and scalability, high data rates, minimum latency and high cyber security. Use of optical wireless communication (OWC) to augment the DC network could help to confront some of these challenges.

In this paper we compare different methods of optical orthogonal frequency division multiplexing (O-OFDM), asymmetrically clipped optical OFDM (ACO-OFDM), DC-biased optical OFDM (DCO-OFDM), and layered ACO-OFDM, used for intensity-modulation and direct-detection in optical wireless communication for DCNs. In DCO-OFDM a DC bias is added to the signal to make it positive. In ACO-OFDM the transmitted signal is formed by clipping the original bipolar OFDM signal at zero and transmitting only the positive parts which are founded in the odd subcarriers. In layered ACO-OFDM the subcarriers are divided into different layers and modulated by different kinds of ACO-OFDM which are combined for simultaneous transmission.

We compare these three methods in a DCN scenario and evaluate their performance.

10437-4, Session 1

OWC with vortex beams in data center networks

Judy Kupferman, Shlomi Arnon, Ben-Gurion Univ. of the Negev (Israel)

Data centers are a key building block in the rapidly growing area of internet technology. A typical data center has tens of thousands of servers, and communication between them must be flexible and robust. Light beams that have orbital angular momentum (OAM) can provide a useful and flexible method for optical wireless communication in data centers. OAM beams can be generated in a very large number of modes, independent of polarization. This can provide a large alphabet for communication. Detection of OAM beams and sorting of modes is generally done using a spatial light modulator, or a dedicated sorting device. However it is possible to design a simple OAM detector that takes advantage of the spatial pattern of the beam to distinguish between modes. We propose such a type of system for OAM detection in optical wireless communication for data center networks, and evaluate performance.

10437-5, Session 2

International standards for optical wireless communications: state-of-the-art and future directions *(Invited Paper)*

Marian Marciniak, National Institute of Telecommunications (Poland)

International standards of Optical Wireless Communications will be reviewed and discussed in the talk. As the number of active OWC installations is growing fast, the standards for compatibility of co-existing neighbouring systems are being developed. The talk will address the Laser Safety (IEC standards), ITU-T Study Group 15 standards (G.640 Co-location longitudinally compatible interfaces for free space optical systems), ITU-Radiocommunication Sector standards (P.1817-1 Propagation data required for the design of terrestrial free-space optical links), and the IEEE Work in Progress - standardization activity on Visible Light Communications. The author's long-term cooperation with Prof. Erich Leitgeb, Graz University of Technology (AT), recently in the framework of COST Action MP1401 Advanced fibre laser and coherent source as tools for society, manufacturing and lifescience is kindly acknowledged. Long-term interactions with IEC, ITU, IEEE, and COST Actions are acknowledged.

10437-6, Session 2

Acquisition and tracking for underwater optical communications

Andrew J Williams, Leslie Laycock, Michael S. Griffith, Andrew G. McCarthy, Duncan P. Rowe, BAE Systems (United Kingdom)

A wide array of underwater platforms are used in both the civil and military domain for various applications. This includes autonomous systems such as mobile Unmanned Underwater Vehicles (UUVs) and static deployed sensor networks. There is a growing requirement to transfer large volumes (many Gigabytes) of data between these platforms. Seawater transmission at Radio Frequencies (RF) is poor which limits their use to very short range or low bandwidth links. Although acoustic links offer data transmission over long ranges, the bandwidth is typically low and the link is not particularly covert. As seawater is transmissive in the visible band, underwater optical communications is an active area of interest since it offers the potential for power efficient, covert and high bandwidth (Gbps) datalinks at short to medium ranges.

Short range underwater optical communications systems have been successfully demonstrated using sources with low directionality such as LEDs. The deployment of such systems, combined with the effects of scattering from water-borne particulates, results in little requirement being placed on the relative alignment of each node. However, efficient systems operating at higher data rates and/or longer ranges dictate the use of more directional beams, which must be sufficiently aligned to achieve the required link margin. This introduces a challenge for mobile platforms, since the precise initial node locations may not be accurately known (e.g. due to lack of GPS and drift of the Inertial Navigation System), and the relative position of each node may change during the course of a link. The acquisition and tracking of each node is therefore critical in order to establish and maintain an optical datalink.

This paper describes work undertaken to investigate these challenges, and to demonstrate acquisition and tracking in a 3D underwater environment. A range of optical sources, beam steering technologies, and tracking sensors have been investigated and assessed for suitability. Various acquisition strategies were also investigated. Since the uncertainty zone and maximum range of the system can vary significantly with mission and local conditions, the acquisition strategy must be robust whilst still aiming to minimise the acquisition time. A novel scanning strategy exploiting variable beam divergence was therefore developed to meet this requirement.

A prototype optical acquisition and tracking system was developed and demonstrated at the A.B. Wood Laboratory Underwater Test Tank at the University of Southampton. The system utilised custom quadrant detectors based on Silicon PhotoMultiplier (SiPM) arrays for fine tracking, and a Wide Field of View (WFoV) sCMOS camera for link acquisition. The tracking beams exploited fluidic lenses to provide variable beam divergence for implementing the acquisition strategy, and AC modulation/filtering for background light rejection. The system successfully demonstrated robust optical acquisition and tracking between two nodes with only nanowatt received optical power levels. The acquisition time was shown to be dependent on the initial node conditions and the transmitted optical power. The SiPM quadrant detectors also demonstrated tracking over a large dynamic range (several orders of magnitude) in the laboratory.

This work was supported by the UK Defence Science and Technology Laboratory (Dstl).

10437-7, Session 2

Detection modules for FSO receivers operating in the wavelength range of 8-12 um

Waldemar Gawron, Przemys?aw Kalinowski, Maciej Fimiarz, VIGO System S.A. (Poland); Janusz Miko?ajczyk, Jacek Wojtas, Wojskowa Akademia Techniczna im. Jaroslawa Dabrowskiego (Poland)

In this paper we present the construction and test results of new detection modules for Free Space Optical Data Link (FSO) operated in the 8-12 ?m wavelength range. FSO communication in this spectrum is less sensitive to atmosphere conditions. The main requirements for detectors applied in FSO receivers correspond to both operational and functional parameters. These devices should be characterized by high sensitivity and operation speed. It is necessary to achieve low value of error rate using low-power laser beam and small-aperture optics. Therefore, detection performance close to fundamental limits are required.

Additionally, for the present optical links, sub-nanosecond response time of photoreceivers is also required. This can be achieved using of HgCdTe photodiodes in the form of modified N+pP+ heterostructures with immersion lens, reverse biasing and cooling by means of the thermoelectric coolers. TEC controller stabilizes detector temperature with high precision in wide ambient temperature range taking into account compact dimension and low-power consumption. Immersion lens enables optimization of the detector physical dimensions,

decreasing detector capacity and its time constant. Further improving of the photoreceiver sensitivity can be achieved by both matching the photodiode to the preamp and minimizing the noises. Basing on both signal and noise characteristics, it is possible to choose the operating point of the detector and preamp for the highest signal to noise ratio while maintaining high signal gain.

The paper shall review of designing and investigation process of photoreceivers for FSO application. Some results of the performed simulations and experiments are also discussed. Finally, further refinements will be conducted taking into account parameters of FSO photoreceiver.

This research was supported by The Polish National Centre for Research and Development grant DOB-BIO8/01/01/2016.

10437-8, Session 2

Analysis of mid-IR InP-based QCLs designed for application in optical transmitter of ffree-space optics

Kamil Pierscinski, Institute of Electron Technology (Poland); Janusz Miko?ajczyk, Dariusz Szabra, Wojskowa Akademia Techniczna im. Jaroslawa Dabrowskiego (Poland); Dorota Pier?ci?ska, Piotr Gutowski, Institute of Electron Technology (Poland); Zbigniew Bielecki, Wojskowa Akademia Techniczna im. Jaroslawa Dabrowskiego (Poland); Maciej Bugajski, Institute of Electron Technology (Poland)

In this paper, theoretical and experimental analysis of AlInAs/InGaAs/InP Quantum Cascade Lasers are presented towards application in FSO systems. QCLs possess inherent advantage that makes them ideal candidates for optical communication systems. Due to operation in infrared spectral range and high speed of modulation, they are very attractive sources for optical transmitter construction

In the frame of this work, series of QCLs (designed and fabricated at the ITE), for application in FSO system, were examined. These lasers were grown by molecular beam epitaxy (MBE) method combined with MOVPE technique to improve waveguiding in the devices. Some devices were also fabricated as buried heterostuctures, characterized by improved thermal performance. They are characterized by different geometries and constructions towards best performance in optical link systems operated in the wavelength range of 8-12 microns. The preliminary test of QCLs included standard electrical measurements of pulsed light-current-voltage characteristics. The obtained results made it possible to determine operation point for modulation work. These modulation performances were tested using some laboratory laser drivers. Basing on these measurements, both power and time parameters of QCLs pulses were investigated. These results defined critical values for FSO system.

The second part of the analysis concerned the spatial parameters of QCLs radiation. Due to low quality of the beam, which is a feature specific to all kinds of edge-emitting semiconductor lasers, knowledge of spatial characteristics of emission is very important for FSO optics construction. The problem becomes more challenging if broad area devices are considered as a sources of radiation, as their far field pattern is typical for higher order optical mode propagating in the laser cavity. Typically, 35 micrometer wide device emits a TEM10 mode. This results in highly non-uniform radiation distribution. In order to characterize spatial properties of beams, far field patterns of emission were registered. Finally, the obtained results made it possible to discusses some aspects of FSO transmitter construction, wherein the investigated QCLs can be used.

This research was supported by The Polish National Centre for Research and Development grant DOB-BIO8/01/01/2016.

10437-9, Session 2

Aspects of scintillation modelling in LEO-ground free-space optical communications

Florian Moll, Christian Fuchs, Deutsches Zentrum für Luft- und Raumfahrt e.V. (Germany)

Free-space optical communications can be used to transmit data from low Earth orbit satellites to ground with very high data rate. In most cases the data content arises from earth observation missions but other use cases are also possible.

In the last section of the downlink, the electro-magnetic wave propagates through the turbulent atmosphere which is characterized by random index of refraction fluctuations. The propagating wave experiences phase distortions that lead to intensity scintillation in the aperture plane and power scintillation in the focus plane of the receiving telescope. For an assessment of the degradation of communication performance, an appropriate channel model to quantify the severity of scintillation is needed.

Approaches to analytically model wave propagation through atmospheric turbulence are well known, like the Rytov method, the parabolic equation method, the extended Huygens-Fresnel principle and the extended Rytov method. These methods are then usually used to calculate the statistics of scintillation phenomena. Parameterization of these models by selecting the correct turbulence profile is however difficult. The turbulence profiles are often either too inaccurate or too complex for a feasible deployment.

An approach that directly models the scintillation effect without claiming to be a generic description of optical turbulence is therefore more feasible, i.e. the direct model would be more tailored to the specific application, in the actual case LEO-ground free-space optical communications. Information on the strength of scintillation as well as spatial and temporal correlation is needed in this case.

Measurements together with the existing theoretical framework shall be used to develop a new scintillation model that focuses on low earth orbit to ground free-space optical communications link design. By using measurements, many inaccuracies arising from lack of knowledge of the correct turbulence profile and limitations of the analytical method are taken out.

The current paper addresses the aspects one has to obey on the way to a feasible scintillation model. We focus on systems with intensity modulation and direct detection. Suitable profiles of index of refraction structure parameter are discussed to compare measurements with model calculations. Validity of the plane wave assumption in the downlink is discussed based on model evaluations of plane wave and Gaussian beam wave propagation. Inaccuracies when using the plane earth model instead of the spherical earth model are investigated by analysing the Rytov index. Impact of beam wander and non-ideal tracking are also discussed. The measurements of scintillation index and fading statistics are compared to calculations with results from the extended Rytov theory. The used satellite sources are the Optical Inter-orbit Communications Engineering Test Satellite (OICETS), the International Space Station (ISS) and the Small Optical TrAnsponder (SOTA). The first source has a transmission wavelength of 847 nm, the second and third 1550 nm. Measurement station is the Optical Ground Station Oberpfaffenhofen near Munich which its 40 cm Cassegrain receiver telescope. Deployed measurement devices are a focal plane photo diode and a pupil plane camera.

10437-16, Session 2

Underwater Wireless Acousto-Optic Waveguide (UWAOW)

Giovanni Giuliano, BAE Systems (United Kingdom) and University of Glasgow (United Kingdom); Lionel William John Kent, Leslie Laycock, BAE Systems (United Kingdom)

A novel technique is described for laser based underwater communication systems. Electromagnetic waves that fall in the blue-green region of the visible spectrum have received the most interest since they correspond to the minimum of optical attenuation within the medium. Nevertheless, the optical transmission losses of seawater range from 0.1 dB/m in clear ocean waters to several dB/m in a harbour. These values impose several limitations on the maximum communication distance for the system. This is because optical power decreases exponentially with the distance from the laser source, and it is dominated by the total extinction coefficient which is the sum of both absorption and scattering by the seawater. These, in turn, are Inherent Optical Properties (IOPs) and thus they are dependent only upon the medium. For this reason, it is not possible to overcome the exponential attenuation of seawater. The Underwater Wireless Acousto-Optic Waveguide (UWAOW) described aims to minimise the adverse effect of scattering within the communication channel. Scattering losses is one of the current technical challenges associated with any underwater free-space communication due to the inherent properties of the medium. The main expected benefit arising from the implementation of the proposed novel technique is minimised photon time of flight dispersion, as discussed above, that would result in an augmented collected optical power at the photoreceiver. This, in turn, would increase the electrical signal-to-noise ratio that is directly related to the data throughput and the maximum achievable range under varying conditions. A novel technique based on a simple but powerful concept is here described. We targeted our research on two different embodiments in order to efficiently establish and maintain a free-space wave-guiding along the optical communication channel. In this work we present a comparison of their advantages and disadvantages, and we provide numerical examples for their implementation. Ongoing work will further develop this model.

The present study was spawned by the lack of research into achieving underwater total internal reflection (TIR) via the acousto-optic effect. The uniqueness of this technique exists in the fact that it is based on a high sound pressure level which induces a localised change in refractive index of seawater sufficient to achieve total internal reflection within the communication channel. Different transducer systems for generating the pressure wave have been investigated and take the form of wave which may be either a standing wave, or novel beamforming technique. The former is based on an array of transducers and with an acoustic mirror at the receiver in order to establish the standing wave. The alternative approach relies on the high intrinsic directionality of a novel beamforming where an annular transducer array is examined as an acoustic source. In this paper, the main characteristics of the acoustic optic waveguide will be presented. This will include both sound and light propagation in the ocean, TIR, novel beam propagation, the refractive index of water as function of the externally applied acoustic pressure, and the SONAR technology. The modelled results, the limitations imposed by the challenging medium, and the system requirements required to obtain an UWAOW will be also be addressed.

10437-10, Session 3

TBA2 *(Invited Paper)*

Arnesh Vijay, Nokia Mobile Networks (Poland)

No Abstract Available

10437-11, Session 3

A new encoding scheme for visible light communications with applications to mobile connections

David Benton, Aston Univ. (United Kingdom)

A new, novel and unconventional encoding scheme called concurrent coding, has recently been demonstrated and shown to offer interesting features and benefits in comparison to conventional techniques, such as robustness against burst errors and improved efficiency of transmitted power. Free space optical communications can suffer particularly from issues of alignment which requires stable, fixed links to be established and beam wander which can interrupt communications. Concurrent coding has the potential to help ease these difficulties and enable mobile, flexible optical communications to be implemented through the use of a source encoding technique. This concept has been applied for the first time to optical communications where standard LEDs have been used to transmit information encoded with concurrent coding. The technique successfully transmits and decodes data despite unpredictable interruptions to the transmission causing significant drop-outs to the detected signal. The technique also shows how it is possible to send a single block of data in isolation with no pre-synchronisation required between transmitter and receiver, and no specific synchronisation sequence appended to the transmission. Such systems are robust against interference – intentional or otherwise – as well as intermittent beam blockage. Applications to mobile optical communications systems will be discussed.

10437-12, Session 3

Delayed frame repetition with forward error correction for variable data rate free space optical communications system

Amita Shrestha, Dirk Giggenbach, Deutsches Zentrum für Luft- und Raumfahrt e.V. (Germany); Norbert Hanik, Technische Univ. München (Germany)

Variable data rate is an attractive technique for free space optical (FSO) communication to cope against dynamic channel conditions. Different schemes for adopting the data rate to channel conditions have been investigated theoretically and experimentally according to literature. However, mainly considering satellite terminals, a simple technique that does not require hardware modifications and many resources and that can be easily configured, is of major importance. With this motivation, a simple technique called Delayed Frame Repetition (DFR) with standard forward error correction (FEC) is proposed in this paper. Main idea is that the system is running at a maximum data rate in good channel condition, and when scintillation strength increases, the system can lower its effective data rate, maintaining the link and channel symbol rate. This can be achieved by retransmitting the encoded frames number of times, each after certain delay that is longer than the fade time. Forward error correction protects the data from distributed bit errors, whereas retransmission of frames protects it against longer fades. This paper will present results using different types of FEC in combination with DFR, and an optimum for FSO channel is selected. For simulation, various artificially generated vectors representing different channel conditions are used. Different channel conditions are characterized by the parameter Scintillation Index (SI) that quantifies the fluctuation of the received signal, which is cause by atmospheric effects and residual pointing error of the transmit beam. In addition, some existing power vectors measured during real experiments are also used for verification.

Performance of the system also depends on correlation behavior of the channel. For long autocorrelation times, longer delays are necessary for DFR in order to make sure that the repeated frames are not experiencing same channel conditions.

Therefore, some evaluations are done to determine optimum/minimum delay required to retransmit frames for particular channel, and compare it with the delay and amount of memory required by systems with standard FEC and long bitwise interleaving. Results for using different types of receiver types - namely ideal shot-noise limited (SNL), thermal-limited (TL) and realistic Avalanche Photodiodes (APD) - are also presented. Performance of the system is evaluated in terms of number of photons required per data bit to achieve certain bit error rate. Reducing the data rate for challenging channel conditions already brings gain to the system in terms of link margin. However, our goal is to optimize a technique to vary the data rate that can either stay constant or if possible even improve the receiver sensitivity in terms of required photons per data bit.

10437-14, Session 3

Intensity properties of Bessel vortex beam in atmospheric turbulence

Wuming Wu, Dong Zhi, Yu Ning, Cheng Luo, Wenguang Liu, Zongfu Jiang, National Univ. of Defense Technology (China)

The Bessel beam is an important member of the family of non-diffracting beams, which can overcome the losses of quantum entanglement between photon pairs in communication system. And the vortex beam can be also utilized as an information carrier in communication system, because the topological charge can carry an unlimited number of bits. Many methods have been proposed to generate Bessel vortex beams. Among of these methods, coherent combining technology is a most promising way to generate this beam with high power scaling capacity. The vortex phase of combined Bessel can be formed approximately by applying discontinuous piston phase on an array of fiber lasers. And another advantage of the method is a possibility of fast (with a frequency of more than 109Hz) phase shift of subapertures providing a charge in the orbital angular momentum.

In free-space optical communication systems based on Bessel vortex beams, the effects caused by turbulent atmosphere should not be ignored, even for weak turbulence. Based on the extended Huygens–Fresnel diffraction integral, the average intensity properties in the far field of a ideal Bessel-Gaussian beam with optical vortices propagating in turbulent atmosphere have been investigated. And the intensity properties of a ideal Bessel vortex beams propagation in atmospheric turbulence have also been numerically studied, including the intensity distribution and fluctuations. However, to the best of our knowledge, the intensity properties vary as the turbulence strength and topological charges change of a combined Bessel vortex beam are not reported, which is formed by an array of fiber lasers.

In this paper, we use numerical wave optics simulation to investigate the intensity-hole radius, energy efficiency and aperture averaged scintillation of two types of beams. One type is the combined Bessel vortex beam, another type is the ideal Bessel-Gaussian vortex beam. The simulation software is see-light, which developed by National University of Defense Technology and Institute of software Chinese academy of Sciences. And the principle of the software is based on the angular spectrum theory and fast Fourier transform. Numerical examples reveal that the spreading of a combined Bessel vortex beam is more serious than that of a ideal Bessel-Gaussian vortex beam with the same topological charges. That is because the initial intensity and phase distributions of a combined Bessel beam are discontinuous, but that of a Bessel-Gaussian beam are smooth. The intensity-hole radius and aperture averaged scintillation of a combined Bessel vortex beam are much bigger, and the energy efficiency is much smaller. In addition, the intensity-hole radii and aperture averaged scintillation of the two types of Bessel vortex beam all increase, but the energy efficiency all decrease with the increasing of the topological charges. All of these results of the Bessel vortex beams can be useful for the future practical optical links.

10437-17, Session 3

15 Gb/s OFDM-based VLC using direct modulation of 450 GaN laser diode

Shaun Viola, Univ. of Glasgow (United Kingdom); Mohamed Sufyan Islim, The Univ. of Edinburgh (United Kingdom); Scott Watson, Univ. of Glasgow (United Kingdom); Stefan Videv, Harald Haas, The Univ. of Edinburgh (United Kingdom); Anthony E. Kelly, Univ. of Glasgow (United Kingdom)

A record data rate for visible light communications (VLC) using a transistor outline (TO) packaged Gallium Nitride (GaN) laser diode is reported. Using a system 3 dB bandwidth of 1.4 GHz data transmission at 15 Gb/s is reported. This is achieved due to the use of orthogonal frequency division multiplexing (OFDM) in combination with a high system signal to noise ratio (SNR) and adaptive bit loading extending the effective bandwidth to 2.5 GHz. To the best of authors knowledge this is the highest reported data rate for single channel VLC.

10437-15, Session PS

The development of HgCdTe detectors for free space optics

Piotr Martyniuk, Wojskowa Akademia Techniczna im. Jaroslawa Dabrowskiego (Poland); Waldemar Gawron, VIGO System S.A. (Poland); Janusz Miko?ajczyk, Zbigniew Bielecki, Wojskowa Akademia Techniczna im. Jaroslawa Dabrowskiego (Poland)

Free Space Optics (FSO) is wireless technology providing data transmission physical links for contemporary telecommunication. It consists of a laser transmitter to send of optical radiation through the atmosphere and a photoreceiver to process the received signal. The one of the most important part of photoreceiver is detector. The performance of FSO system strongly depends on the wavelength range of operation. Usually in the case of fog, rain or scintillations, operation at longer range of wavelength has a significant advantage over shorter wavelengths for FSO systems. Therefore HgCdTe long-wave (8?12 micrometer – LWIR) infrared detectors reaching ultra-fast response (time < 1 ns) and nearly background limited infrared photodetection (BLIP) condition are very attractive for these applications.

Both nearly BLIP detectivity and ultra-fast response time is obtained by implementation of the hyper-hemispherical GaAs immersion lens into structure to increase optical to electrical area ratio giving flexibility in terms of response time optimization. The optimization approach depends on voltage condition. The generation - recombination (GR) mechanism within active layer was found to be important for forward and weak reverse conditions while photogenerated carrier transport is significant for higher reverse bias. Except of applied voltage, the drift time strongly depends on thickness of the absorption region. Reducing the thickness of the active region, the short drift times could be reached, but that solution significantly reduces quantum efficiency and decreases detectivity. Taking that into consideration, a special multilayer heterostructure designs are developed. The p-type absorber in multilayer heterostructures was found to be favorable due to both high ambipolar mobility and low thermal GR driven by the Auger mechanism.

Theoretical simulations indicate that LWIR HgCdTe structure could reach response time below < 100 ps while biased and ≤ 1 ns while unbiased (at T = 300K). Immersed detectivity exceeds 109 cmHz1/2/W.

Finally, taking into account FSO link equation, comparison of the FSO system performances operating at the wavelength range of 8-12 um using different constructions of detectors and their preamps is presented.

This research was supported by The Polish National Centre for Research and Development grant DOB-BIO8/01/01/2016.

Conference 10438: Emerging Imaging and Sensing Technologies

Wednesday - Thursday 13–14 September 2017

Part of Proceedings of SPIE Vol. 10438 Emerging Imaging and Sensing Technologies for Security and Defence II

10438-1, Session 1

Single photon depth imaging *(Invited Paper)*

Gerald S. Buller, Aongus McCarthy, Ximing Ren, Aurora Maccarone, Rachael Tobin, Abderrahim Halimi, Yoann Altmann, Yvan R. Petillot, Stephen McLaughlin, Andrew M. Wallace, Heriot-Watt Univ. (United Kingdom); Agata M. Pawlikowska, Robert A. Lamb, Leonardo MW Ltd. (United Kingdom)

Time-of-flight single-photon detection is a candidate technology for a variety of depth imaging applications, including long-range free-space imaging and underwater sensing. This presentation will describe recent experiments and image processing analysis which highlight the key aspects of the approach, including sensitivity, accuracy and resolution, long range and eye-safe capabilities. These applications include long-distance depth imaging (ie > 1km) where both superconducting and semiconductor-based single-photon detectors have been used to operate within the atmospheric windows around the 1550nm wavelength. We will also examine the possibilities of extending the operational wavelength to greater than 1550nm. In underwater applications, the operational wavelength is typically between 450nm to 700nm, within the high-efficiency band of high-performance, near-room temperature silicon-based single photon avalanche diodes. In underwater imaging, depth and intensity measurements were made at up to nine attenuation lengths between transceiver and target. Another area of emerging interest is the use of multiple wavelength single-photon LIDAR which may prove suitable for investigation of distributed targets. For example, an appropriate selection of wavelengths can reveal indications of the structural and physiological parameters of vegetation to provide a valuable insight into the carbon dioxide cycle for environmental research. Single photon lidar has also been used to both reconstruct and classify color detail of targets, even at low signal levels equivalent to less than 1 photon per pixel, on average.

10438-2, Session 1

Highly birefringent dual-mode nonlinear fibers for customised supercontinuum generation

Zbyszek Holdynski, Marek Napierala, Michalina Jó?wik, InPhoTech (Poland); Pawel Mergo, Univ. of Maria Curie-Sklodowska (Poland); Tomasz Nasilowski, InPhoTech (Poland)

Nonlinear effect control by microstructured fiber geometry and mode dispersion is extensively explored in various types of applications (sensing, fluorescence microscopy, spectroscopy, etc.). Strong dependence between zero dispersion wavelength and domination mechanism of proper nonlinear effects can be used for efficient spectral bandwidth control. The few mode operation in nonlinear fibers enables to obtain even more flexibility in nonlinear effects control and their dominance in generated spectra. In the paper we present possibility of supercontinuum generation in dual mode highly birefringent microstructured fibers. Unique birefringent fiber geometry enables precise dispersion control in both fundamental and second order modes. Our results are aimed at creating new functionality in generated supercontinua, i.e. polarization based spectrum tunability and flatness control. We show the role of fiber geometry influence on dual mode propagation condition changes. We show also the role of polarization coupling condition in fundamental and second order modes in a process of nonlinear effect generation. Furthermore, we analyse experimentally the stability of nonlinear effects generation in our fibers, related to polarization coupling and dispersion changes. Our results should be suitable for supercontinuum optimization for analysis spectral reflectivity of a variety of both retro-reflecting and diffuse targets in booth defense (in air) and health care (in tissue) applications.

The domination of nonlinear effects can be changed in fundamental and second order mode according to fiber geometry to generate spectrally flat broadband source. We show three fibers with slightly different core diameters. Difference between fibers geometry is used to obtain appropriate mode domination condition during pump laser source coupling. Our spectra can be generated in three excitation regimes, i.e. when only fundamental mode is excited at fiber input, when second order mode or both modes are excited. Controlled mode excitation can be used for more precise nonlinear domination control, and consequently allows controlling flatness and bandwidth (from ultraviolet and visible to near infrared spectral region) of generated spectra.

10438-3, Session 1

Self-assembled micro-apertures for low-cost, field-deployable microscopes

Bhuvaneshwari Karunakaran, Debjani Paul, Soumyo Mukherji, Indian Institute of Technology Bombay (India)

This paper describes a method to fabricate and self-assemble micro-apertures on miniature elastomer lenses using a fast, low-cost approach. Here, we show that by using capillary encapsulation technique, elastomer lenses and micro-apertures can be precisely aligned with least effort. A visual feedback system is combined to the capillary encapsulation technique to control the micro-aperture size. The resultant micro-aperture sizes range between 200μm to 650μm.

Portable low-cost microscopes, such as, smartphone based, have potential applications in defence, healthcare, forensics, environmental monitoring, etc. A miniature lens can readily transform a smartphone into a field-deployable microscope. These lenses are highly low-cost and disposable. However, use of such miniature lenses requires micro-apertures to effectively produce an image. The process of mounting miniature lenses and micro-apertures precisely is crucial in governing the lens performance, and is challenging in terms of alignment. Cybulski et al. reported a novel self-assembly technique of mounting a miniature glass ball-lens and micro-aperture using capillary encapsulation [1]. In comparison to glass ball lens, elastomer lenses made of polydimethylsiloxane (PDMS) are easy to fabricate, low-cost and have better performance [2].

In this work, we present the capillary encapsulation technique to fabricate micro-apertures for miniature PDMS lenses. The lens is fabricated using a previously reported technique [3]. It is nearly hemispherical, 1 mm in diameter with ~1mm base thickness.

The micro-aperture fabrication process involves two steps: (1) capillary formation by flattening the lens, and (2) partial encapsulation of the lens by an opaque polymer solution. In step (1), the lens is sandwiched between two glass slides (G1 and G2). G2 is coated with a ~1mm thick PDMS layer and cured. The lens is placed on G1 non-permanently. The curved side of the lens faces the PDMS coated surface of G2. The distance between G1 and G2 is decreased to cause the lens to flatten, and a capillary to form. An opaque and low viscous polymer solution (Smooth-on Smooth-Cast ONYX® Fast) is passed into the capillary and cured (curing time: 15 minutes). The polymer solution encapsulates the lens except the flattened portion. After the polymer solution cures, G2 is removed. The lens attains its original shape due to the elastic nature of PDMS. Thus, a micro-aperture is self-assembled onto the lens.

The size of the micro-aperture is governed by the flattened area of the lens. The aperture size is tuned by varying the distance between G1 and G2. In the setup, G2 is placed on a micrometer stage. An imaging system used in [3] is used to get a visual display of the flattened area of the lens. Using the visual feedback system, aperture sizes ranging between 200μm to 650μm were fabricated reproducibly.

This low-cost technique allows self-assembly of micro-apertures on miniature elastomer lenses, with control on the aperture size ensuring reproducibility. Future research work will focus on integrating these lens modules to develop a low cost, portable cell counter.

[1] Cybulski et al., PLoS one, 2014.

[2] Lee et al., Biomedical Optics Express, 2014.

[3] Karunakaran et al., MicroTAS 2016.

10438-4, Session 1

Infrared detector based on interband transition of semiconductor quantum well

Ling Sun, Jie Liu, Haiqiang Jia, Institute of Physics (China); Wenxin Wang, Lu Wang, Institute of Physics, Chinese Academy of Sciences (China); Hong Chen, Institute of Physics (China)

Inter band transition in bulk material and inter subband transition in quantum well material are two main working mechanism of infrared detector. Inter band transition of quantum well was not considered as a good option to build infrared detectors. However, recent experimental findings that confined optical generated carriers within a PN junction can be extracted with a very high efficiency, and such phenomenon leads to a great improvement of the absorption process.Up to 88% localized carrier extraction efficiency from spacial localized state was measured. And a obivous increase in absorption coefficient was also found. Those findings provide the possibility to fabricate novel high performance detectors which was verified through a short wavelength prototype device.

10438-5, Session 2

Challenges for the future of imaging: what's next and where can we draw inspiration from? *(Invited Paper)*

Marc P. Christensen, Prasanna Rangarajan, Southern Methodist Univ (United States)

Recent advances in computation, optical projection, and non-traditional imaging sensor designs are making it possible to overcome classical optical challenges which have stood for centuries: breaking resolution "limits" in real world scenarios and capturing indirect images of obscured objects.

10438-6, Session 2

The simplicity, complexity, and benefits of multi-aperture imaging in the thermal infrared *(Invited Paper)*

Andrew R. Harvey, Guillem Carles Santacana, Laura V. Cowan, Miguel A. Preciado, Univ. of Glasgow (United Kingdom); Jason F. Ralph, Univ. of Liverpool (United Kingdom); James Babington, Andrew P. Wood, Excelitas Qioptiq (United Kingdom)

We will describe multiple practical solutions that we have developed to exploit the unique capabilities of multi-aperture imaging in the medium-wave and long-wave infrared. The conventional approach of imaging with a single optical aperture, established for more than a century, requires a single optical lens system able to provide sufficient performance across an extended field of view and wavelength range. The diffraction limit, or the so-called Shannon limit, can be achieved for only; relatively low angular resolution, or restricted field of view, or restricted wavelength range, or by use of highly complex lens designs. This yields a major penalty in cost, size and weight. Imaging with arrays of similar or diverse imaging systems, individually optimised for a small field of view or wavelength range, means that each lens can be considerably simpler.

This paper will describe how the use of multiple-camera imaging systems provides an alternative imaging modality, but with a different challenge: to computationally integrate diverse images while demonstrating an overall system benefit. As a compelling example, we have employed an array of thirteen individually spectrally filtered cameras to yield a snapshot multi-spectral imaging system covering the near, medium and longwave infrared bands for a range of applications. Possible applications include video-rate multi-gas imaging; for pollution monitoring and hydrocarbon leakage for example; to the classification of plastics. The use of individual spectrally filtered cameras means that chromatic aberration is not significant and optical throughput is very high. The exploitation of cameras that have been mass produced for the consumer market means that overall system costs are more than an order of magnitude lower than that for conventional multi-spectral systems. We have developed techniques to co-register images and calibrate the inevitable parallax within the camera array and, furthermore, we demonstrate how this parallax may be exploited to image through obscurants, such as foliage for example, or to employ tomographic techniques to improve the accuracy of gas-concentration measurement in the thermal infrared.

We report the use of superresolution with arrays of nominally identical cameras (without spectral filtering) to yield high-resolution imaging with reduced track length. The use of thinner lenses, enables high-resolution imaging to be achieved with low-cost silicon, despite its relatively high absorption which prevents its use in traditional high-resolution imaging.

While conventional foveal-imaging systems are restricted to complex designs yielding foveal ratios of up to 2:1, we have rigorously designed multiple-aperture imaging systems with computational recovery for 3:1 ratios (greater ratios are possible) using arrays of simple but dissimilar lenses and a single detector. While spatial separation of the images on a single detector array provides a simple solution, we show through modelling, how multiple images with dissimilar fields of view can be superimposed on a single detector array and the how computational recovery can be used to separate out the images and yield a single foveal, wide-field-of-view image from a reduced-cost system.

10438-7, Session 2

An analytical model for weak hyperspectral signal performance prediction of anomaly detection

Pierre Lahaie, Defence Research and Development Canada, Valcartier (Canada)

Introduction

Advances in physical detector technology for the detection of very low to medium intensity light signal will become possible in the near future. The application of these detectors for hyperspectral detection in active and passive configuration is of great interest and the prediction of the detection performance is required for planning the introduction and use of these technologies. In a previous paper [1], simulation analysis has been produced in the case of the additive hyperspectral signal model to evaluate the performance of detectors in the case of photon counting and intensified physical detectors. These detectors influence the noise model,

which is Poisson only for a photon counting detector and a convolution of the distribution of intensified counts with a Poisson distribution is used for an intensified detector. In the paper an analytic Receiver Operating Characteristics (ROC) curve computation method is developed for the case of an integrated signal and the matched filter anomaly detection algorithms [2-7].

Analysis

The signal is assumed to respect the additive linear model:

r=x+as (1)

Where: r is a measurement, x is the realization of a background, s is the signature of a contaminating material and a is the intensity of the signal. Bold characters denote spectral vector quantities. It is assumed in the development that the signal from the background is strict sense stationary. Many operators can be used to perform anomaly detection. An obvious detector uses the signal integration (2) D_is and another one arises from the matched filter development of a classifying detector D_mf(3):

D_is=∑?r_n (2)

D_mf=((r-?x?).s_d)/(s_d.s_d) (3)

In these detectors, the index d denotes a particular signature used in the detection which is not necessarily the signature of the material that generated the signal and ?x? is the mean of the background. These two detectors are analyzed with respect to the noise generated by the physical detector. The expression of the noise distributions are respectively for the Poisson shot noise and the intensified signal:

p(n)=(e^(-?) ?^n)/n! (4)

And:

f_x (x)=∑_n??(e^(-?) ?^n)/n! f_x^((n)) (x) ? (5)

Where: f_x^((n)) (x) is the distribution of counts when n photons strike the physical detector. Such a distribution can be found in [8]. A computation result is given in figure 1. Theoretical and simulated ROC curves are computed and compared in the same conditions for intensified and photon counting physical detectors.

Conclusion

Figure 1 shows an excellent agreement between simulated and analytic data. The analytic results are important because they enable the use of performance results for very small probability of errors that are very difficult to produce in simulation and almost impossible to produce experimentally. The method is also developed for the matched filter detection algorithm and ROC curves have been obtained. The results show an increase in performance of the matched filter when the signature is closer to the spectral shape. When compared to the integrated signal algorithm, the matched filter gives better results when the signature is close to the spectral shape and the integrated signal algorithm is better when the spectral shape of the signal is far from the signature.

[1] Lahaie, P., Simard J.R., Buteau S.,"Evaluation of adaptive algorithms for detection and classification of fluorescent aerosols in the atmosphere", Proc. SPIE, Optics and Photonics for Counterterrorism, Crime Fighting and Defence IX, October 2013

[2] Robey F.C., Kelly E.J., Nitzberg R., "A CFAR Adaptive matched filter detector", IEEE Transactions on aerospace and electronic systems, Vol. 28, no 1, January 1992, PP. 208-216

[3] Scharf L., McWhorter L.T., "Adaptive matched subspace detectors and adaptive coherence estimators", Prof Asilomar Conf. on signals, systems and computer, November 1996.

[4] E.J. Kelly, "An adaptive detection algorithm", IEEE Transactions on aerospace and electronic system, vol. AES 22, no1, March 1986,PP. 115-127

[5] Theiler J., Foy B.R, "EC-GLRT: Detecting weak plumes in non-Gaussian hyperspectral clutter using an elliptically contoured generalized likelihood ratio test", Proceedings of IGARSS 2008, Boston,

[6] Scharf L., Friedlander B., "Matched subspace detectors", IEEE Transactions on signal processing, vol. 42, no 8, August 1994, PP 2146-2157.

[7] Kraut S., Scharf L., McWhorter L.T., "Adaptive subspace detectors". IEEE Transactions on signal processing Vol. 49, No 1, January 2001, PP. 1-16

[8] Sandel B.R., Broadfoot A.L. "Statistical performance of the intensified charged coupled device", Applied Optics, Vol. 25, No. 22, November 1986

10438-8, Session 2

Digital holographic correction of distortions inside the Michelson interferometer using the phase-only LCOS modulator

Dmitriy V. Venediktov, Saint Petersburg State Univ. (Russian Federation); Nikolay V. Petrov, ITMO Univ. (Russian Federation); Sergey A. Pul'kin, Saint Petersburg State Univ. (Russian Federation); Alexander A. Sevryugin, Saint Petersburg Electrotechnical Univ. "LETI" (Russian Federation); Vladislav Shoev, Saint Petersburg State Univ. (Russian Federation); Ibragim M. Tursunov, Vladimir Y. Venediktov, Saint Petersburg Electrotechnical Univ. "LETI" (Russian Federation)

The paper reports the results of experimental demonstration of correction of distortions, imposed by the defects of optical elements inside the Michelson (Twyman-Green) interferometer for the high-accuracy measurement of nanosize steps on the surface of one of its mirrors. The correction is provided by the use of the overlapped digital holograms, one bearing the information about the intra-interferometer distortions and about the measured object, and another – only about the same distortions. Consequent diffraction of the beam on both holograms provides elimination of the distortions' effect and thus "cleaning" of the information beam.

10438-9, Session 3

Image enhancement framework for low-resolution thermal images in visible and LWIR camera systems

Thapanapong Rukkanchanunt, Masayuki Tanaka, Masatoshi Okutomi, Tokyo Institute of Technology (Japan)

Infrared (IR) thermography camera became an essential tool for monitoring applications such as pedestrian detection and equipment monitoring. Most commonly used IR cameras are Long Wavelength Infrared (LWIR) cameras due to their suitable wavelength for environmental temperature. Even though the cost of LWIR cameras had been on a decline, the affordable ones only provided low-resolution images. Enhancement techniques that could be applied to visible images often failed to perform correctly on low-resolution LWIR images. Many attempts on the thermal image enhancement had been on high-resolution images. Stereo calibration between visible cameras and LWIR cameras had recently been improved in term of accuracy and ease of use. Recent visible cameras and LWIR cameras are bundled into one device, giving the capability of simultaneously taking visible and LWIR images. However, few works take advantage of these camera systems. In this work, image enhancement framework for visible and LWIR camera systems is proposed. The proposed framework consists of two inter-connected modules: visible image enhancement module and LWIR image enhancement module. The enhancement technique that will be experimented is image stitching which serves two purposes: view expansion and super-resolution. The visible image enhancement module uses SIFT algorithm for feature extraction and matching while homography is estimated via RANSAC. The stitching order is determined by minimum spanning tree of the relation graph. Seam carving and fast Poisson blending are employed to reduce the artifacts caused by misalignment. The intermediate

results such as homography and seam carving's labels are passed to LWIR image enhancement module. The LWIR image enhancement module aligns LWIR images to visible images using stereo calibration's results and utilizes already computed homography from visible images to avoid feature extraction and matching on LWIR images. Seam carving's labels from visible images help eliminating ghost effects while the cost value associated with seam carving determines the strength of pixel value in the overlapping regions during the guided upsampling process. The framework is able to handle the difference in image resolution between visible images and LWIR images by performing sparse pixel-to-pixel version of image alignment and image projection, followed by guided upsampling. Experiments show that the proposed framework is able to correctly produce stitched images even when visible and LWIR images are loosely aligned. Our stitched images are sharper and have higher resolution compared to the results from existing methods. This framework can be used in many applications such as thermal image super-resolution and thermal image view expansion.

10438-10, Session 3

A self-assembly optimization method for BAW filter layout design

Yang Gao, China Academy of Engineering Physics (China); Da-Peng Zhang, Le Jia, Southwest Univ. of Science and Technology (China); Shu-Wen Wen, Southwest Univ. of Science and Technology (China) and Institute of High Energy Physics (China)

Nowadays, primarily acoustic wave devices are used for filtering in front ends of modern mobile transceivers. No competitive technology providing the same performance at the same size and cost exists at the moment. At higher frequencies mainly BAW filters are used [1]. BAW filter can provide lower insertion loss, better selectivity, higher power handling, higher operation frequency, and better ESD protection [2]. With these advantages, BAW filter technology has been gaining more market share in wireless communication, radar and GPS applications. A BAW filter is consisted of several series/parallel connected BAW resonators (BAWR), sometimes a few inductors or capacitors, and their interconnects [3]. Layout is the very last BAW filter design procedure. How to get a device footprint as small as possible to improve chips per wafer, while maintaining designed filter specifications (e.g. performance degradation induced by EMI coupling between any two closely adjacent BAWRs [4]), is urgently needed for cos-effective mass production considerations. Although there are so many commercial-off-the-shelf BAW filters, few publications on this topic can be found [5]. This paper presents a self-assembly like BAW filter layout design method to bridge the obvious technology gap.

Firstly, 11 layout design constraints are summarized and explained. They are: 1) each BAWR should has an apodized shape (i.e. irregular convex square or pentagon without two parallel sides) to suppress spurious modes (Fig.2) [6]; 2) FBAR shape should be as close as possible to the square or pentagon to avoid small acute angle or big obtuse angle [6]; 3) pentagon is more suitable for BAWRs with a relative large active area and square for a relative small one, which helps saving the overall resonators area; 4) electrically-connected BAWRs should be layout-neighboring [7]; 5) any two layout-neighboring BAWRs should have a pair of most aligned but no parallel sides; 6) layout-neighboring BAWR pair has a minimum gap Gneighboring (e.g., Gneighboring = 20 ?m) according to EM calculations (Fig.3); 7) the first series BAWR and the last series BAWR in a BAW filter circuit schematics should keep a minimum gap Gfirst-last no less than Gneighboring, this is naturally satisfied in most situations; 8) BAWRs adjacent to the surrounding G-S-G pads should be placed with a side as parallel as possible; 9) and keep a minimum gap GFBAR-Pad no less than Gneighboring; 10) interconnects of BAWRs and BAWR-Pad should be as wide as possible to ensure high quality electronical signal; 11) the overall filter layout is rectangular or even square.

Secondly, we present the detailed optimization process and which is illustrated with a 5-order BAW ladder filter case, as shown in Fig.1. There are two kinds of layout inputs: 1) filter circuit schematics, which defined series/parallel resonators and their connections; 2) specific areas of each resonator, which is determined by the filter performance design process. Layout optimization has 6 steps. 1) Preset the shape of each BAWR (square/pentagon) according to its active area value. Note that in a BAW ladder filter, a series resonator always has a smaller active area than its neighboring parallel one, thus results in initial square series resonators and pentagon parallel ones. 2) Add an auxiliary circumcircle for each BAWR, tightly align all the series resonator circumcircles along a central line in order, and mate the corresponding electronically neighboring parallel resonator circumcircles one by one at a position above/below the center line. This makes an initial 3-row and N-column 2D arrangement, and the column number N is determined by the filter order. It is worth mentioning that, the circumcircle can be slightly scaled, e.g. enlarged for more robust EMC consideration, FBARs' buried/backside air cavity preservation etc., or reduced for more effective layout. 3) Fix the very first series resonator circumcircle position and incrementally "compress" the initially self-assembled 3-row structure along the row width direction, which transfer the central line into a slight center-fluctuated zigzag line (i.e. smaller row width) and accompanied by less row height expansion at the positive stage. This "compress" try procedure end at a turning point where the layout area (row width ? row height) cease to decrease, i.e. those row height for row width bargain is no more cost effective. 4) Apodize the square series resonators and fine-tune each resonator's shape and rotation according to above-mentioned related design rules. 5) Wiring BAWRs and pads together. If the filter circuit do has some monolithic integrated inductors/capacitors, such an element can also be treated as a circumcircle in step 2). 6) A combined acoustic-electromagnetic BAW filter simulation method is used to verify the layout result. If the specific values in the design constraints are reasonably set, the layout design iteration is usually not necessary.

In the 5-order BAW ladder filter layout demo case, a fill ratio over 44% is obtained. The method is patent filing and an auto-layout program is developing.

10438-11, Session 3

BAW sensor read-out circuit based on Pierce oscillator architecture

Yang Gao, China Academy of Engineering Physics (China); Xi-Yang Yin, Bin Han, Yu-Hang Wang, Southwest Univ. of Science and Technology (China)

Bulk Acoustic Wave Resonators (BAWRs) have been well developed both as filters [1] and as high sensitivity sensors in recent years [2]. In contrast to traditional megahertz quartz resonators, BAWRs offer significant increases in resonant frequency, typically operating in gigahertz regimes. This translates into a potential sensitivity increase of more than three orders of magnitude over traditional QCM systems [3]. Additionally, shear-mode resonators are effective in both air and water, a necessity for real-time biomolecular detection [4]. ZnO BAWRs are also shown potentials for high sensitivity UV light and gamma ray detection. With 365 nm UV light of intensity 1.7 mW/cm2, a BAWR with n-ZnO/Au Schottky diode has 250 kHz frequency downshift [5]. The maximum gamma sensitivity of 2300 kHz/krad was also demonstrated [6]. However, macroscale cabling and microwave instrumentation for gigahertz drive and readout add considerable expense and complexity to the measurement platform and spatially prevent array integration. Given the micrometer-scale size of BAW sensor-head, read-out circuitry can monolithic integrated with this GHz transducer is urgently needed to produce small, robust, and inexpensive sensor systems [4].

A BAW sensor read-out circuit design based on Pierce oscillator architecture [7] is presented in this paper. The circuit schematic shown in Fig.1 is a differential structure with two identical BAW oscillator channels for reference and

measurement respectively, but the reference one is isolated from the physical quantity to be measured. The two BAW oscillators are configured as the Pierce oscillator architecture for simple electronics and high frequency stability, enabling a compact, power-saving, high sensitivity sensor system. A BAW oscillator design for an illustrated 2 GHz BAW mass sensor is shown in Fig.2. After mixing, measurand induced frequency shift of the sensing BAWR is picked up. Followed by signal filtering, amplification and shaping processing (corresponding to the so-called "signal converting module"), the analogue sensing signal is converted into digital one. Fig.3 is signal converting module design case. Fig.3a) is the EM field-circuit co-simulation model of a mixer, Fig.3b) shows good match between the simulated mixer output signal spectrum (left) with the measured one (right). Fig.3c) presents the simulation model (left) and measured output (right) of a amplifying and shaping circuit. Fig.3d) is the photo of a signal converting module. Finally, the frequency detecting can be done in a FPGA. There are many frequency detection methods, and the pulse synchronization detection method is used to ensure high precision. Principle and FPGA fulfillment of the method is shown in Fig.4.

Taking 2 GHz BAW mass sensor as a case study, deign procedure are given in details. Simulation and experimental results reveal a 0-99 MHz frequency shift measurement range. Main factors affecting phase noise of the BAW oscillator are also discussed, for further read-out circuit optimizations.

10438-12, Session 3

Simulation of continuously logical base cells (CL BC) with advanced functions for analog-to-digital converters and image processors.

Vladimir G. Krasilenko, Vinnitsa Social Economy Institute (Ukraine); Alexander Lazarev, Vinnitsa National Technical Univ. (Ukraine); Diana V. Nikitovich, Vinnitsa Social Economy Institute (Ukraine)

The paper considers results of design and modeling of continuously logical base cells (CL BC) based on current mirrors (CM) with functions of preliminary analogue and subsequent analogue-digital processing for creating sensor multi-channel analog-to-digital converters (SMC ADCs) and image processors (IP). For such with vector or matrix parallel inputs-outputs IP and SMC ADCs it is needed active basic photosensitive cells with an extended electronic circuit, which are considered in paper. Such basic cells and ADCs based on them have a number of advantages: high speed and reliability, simplicity, small power consumption, high integration level for linear and matrix structures. We show design of the CL BC and ADC of photocurrents and their various possible implementations and its simulations. We consider CL BC for methods of selection and rank preprocessing and linear array of ADCs with conversion to binary codes and Gray codes. In contrast to our previous works here we will dwell more on analogue preprocessing schemes for signals of neighboring cells. Let us show how the introduction of simple nodes based on current mirrors extends the range of functions performed by the image processor. Each channel of the structure consists of several discharge-analog cells (DC) on 20-40 CMOS. The amount of DC does not exceed the number of digits of the formed code, and for an iteration type, only one cell of DC, complemented by the device of selection and holding (SHD), is required. One channel of ADC with iteration is based on one DC-3(G) and SHD, and it has only 40 CMOS transistors. In such ADCs easily parallel code can be realized and also serial-parallel output code. The circuits and simulation results of their design with OrCAD are shown. The supply voltage of the DC is 2.4÷3.3V, the range of an input photocurrent is 0.1÷10?A, the transformation time is 30 ns at 5-8 bit binary or Gray codes. The general power consumption of the ADC with iteration is only 50÷100?W, if the maximum input current is 1?A. Such simple structure of linear array of ADCs with low power consumption and supply voltage 3÷5V, and at the same time with good dynamic characteristics (frequency of digitization even for 1.5?m CMOS-technologies is 40 MHz, and can be increased up to 10 times) and accuracy characteristics are show. The SMC ADCs based on CL BC and CM opens new prospects for realization of linear and matrix IP and photo-electronic structures with matrix operands, which are necessary for neural networks, digital optoelectronic processors, neural-fuzzy controllers.

10438-13, Session 3

Optical parallel DNA sequence alignment based on metamaterials

Hossein Babashah, Zahra Kavehvash, Somayyeh Koohi, Amin Khavasi, Sharif Univ. of Technology (Iran, Islamic Republic of)

In this paper, a new optical structure is proposed for DNA sequence alignment based on metamaterials. The location and length of deletions and insertions are determined via an optical processor. The optical processor includes an optical correlator and an integrator. The optical correlator is implemented based on metasurfaces which help in making the whole structure small enough to be implemented in an integrated photonic system. The location of the deletions or insertions are detected via optical correlator while the deletion length is specified through the difference length of the ramp function produced from integrating the multiplication of the reference and query genome. The metasurface implementation helps in miniaturizing the structure to process the long length DNA sequences in parallel making DNA sequence alignment procedure considerably faster.

10438-14, Session 4

Atmospheric sensing with single photon counting *(Invited Paper)*

Agata Pawlikowska, Leonardo MW Ltd (United Kingdom); Brian Flemming, Leonardo MW Ltd. (United Kingdom); Abderrahim Halimi, Gerald S. Buller, Heriot-Watt Univ. (United Kingdom); Robert A. Lamb, Leonardo MW Ltd. (United Kingdom)

Understanding the effect of turbulence on both the signal-to-noise and image quality in 3D imaging lidar for long-range targeting is critical to the assessment of system and operational performance. In this work we experimentally determine Cn2 and angle-of-arrival (AOA) fluctuations using a single photon counting lidar. These parameters characterise the strength of optical turbulence. However, as single photon counting lidar gains greater prominence, the high speed data acquisition afforded by this technique suggests that it can be used to make near real-time measurements of the state of the atmosphere. We present results from a 3D lidar which is reconfigurable to operate with InGaAs/InP single photon detectors: the first is a single element single photon avalanche diode (SPAD) and the second is a 32 x 32 Geiger mode array. The operational wavelength for both detectors is 1550 nm. We assess the effect of background noise and signal strength on the measured scintillation index and AOA. Our results show reasonable agreement with those from a commercial scintillometer. We conclude that 3D photon counting lidar can be used to simultaneously acquire images and deduce the level of turbulence. This allows automated post processing of images to correct for turbulence and improve the special resolution in long-range active and passive imaging sensors.

10438-16, Session 4

Assessment of tunnelling magnetoresistors for magnetic imaging tomography

Abigail Langley, Maxim B. Joseph, Robert Ward, Joseph C. Watson, AWE plc (United Kingdom)

Imaging of potential threat objects within shielded containers can be difficult, such as x-ray through dense metals e.g. Pb. Magnetic imaging tomography (MIT) offers a method by which imaging is performed on the basis of electrical conductivity and magnetic permeability rather than density. MIT has been used widely in the non-destructive evaluation (NDE) field to detect flaws and defects in solid objects, usually using inductance coils to generate and detect the magnetic field. Here, we use a tunnelling magnetic resistor (TMR) to detect a field generated by a drive coil and use this data to image objects of interest within shielded enclosures.

10438-17, Session 4

Detection of underground structures using UAV and field spectroscopy for defence and security in Cyprus

George Melillos, Kyriacos Themistocleous, Maria Prodromou, Diofantos G. Hadjimitsis, Cyprus Univ. of Technology (Cyprus)

The purpose of this paper is to present the results obtained from unmanned aerial vehicle (UAV) and field spectroscopy campaigns for detecting underground structures. Underground structures can affect their surrounding landscapes in different ways, such as soil moisture content, soil composition and vegetation vigor. The latest is often observed on the ground as a crop mark; a phenomenon which can be used as a proxy to denote the presence of underground non-visible structures. A number of vegetation indices such as the Normalized Difference Vegetation Index (NDVI), Simple Ratio (SR), Difference Vegetation Index (DVI) and Soil Adjusted Vegetation Index (SAVI) were utilized for the development of a vegetation index-based procedure aiming at the detection of underground military structures by using existing vegetation indices or other in-band algorithms. The measurements were taken at the following test areas such as: (a) vegetation area covered with the vegetation (barley), in the presence of an underground military structure (b) vegetation area covered with the vegetation (barley), in the absence of an underground military structure (c) vegetation area covered with the existing natural soil, in the presence of an underground military structure (d) vegetation area covered with the existing natural soil, in the absence of an underground military structure. Leaf Area Index (LAI) and Crop Height (CH) measurements were also taken simultaneously to spectroradiometric measurements and following the same phenological cycle of each crop for the corresponding cultivating periods.

10438-18, Session 4

Magnetic induction tomography imaging of objects for security applications

Robert Ward, Abigail Langley, Joseph C. Watson, Maxim B. Joseph, Maxim B. Joseph, AWE plc (United Kingdom)

A coil array system has been developed at AWE that performs image capture based on Magnetic Induction Tomography and eddy-current principles. Using a function generator to drive a primary Helmholtz coil and a 20x21 array of secondary receiver pick-up coils, measurements of signal strength and relative phase can be made using a lock-in amplifier. Switching over each receiver pick-up coil a pixelated 2D conductivity map of an object has been obtained in just 10 seconds. This technique provides as a solution to interrogating complex conductive targets in a non-destructive manner and provide as a complementary threat evaluation technique to the more conventional X-Ray/radiography solutions.

10438-19, Session 5

Active optical atomic clock for gravitational anomalies detection

Marcin Bober, Michal Zawada, Nicolaus Copernicus Univ. (Poland)

Optical atomic clocks are the most precise measurements ever build by the mankind. Accuracy at the level of 10^-18 [1,2] and instability in mid 10^-17 after 1 s of averaging [3] was already presented. With all perturbation under control one can use a clock not only for precise time measurements but also for other physical quantity measurements, e.g. for looking for fundamental constants variations [4] or dark matter in form of topological defects [5]. Atomic clocks are also directly sensitive to the gravitational potential, i.e. they can be used as a gravitational waves detectors [6] and in relativistic geodesy [7,8].

All modern optical atomic clocks are passive, with an oscillator in the form of ultra-stable laser and a frequency discriminator in the form of cold atomic sample. We would like to propose instead an active optical atomic clock [9] as a gravitational detector. Such an active frequency standard would take advantage form both better instability and higher time resolution over already existing optical clocks. Its construction will provide a high degree of mobility, since its performance would not be limited by an instability of a fragile optical cavity.

We will present potential advantages of using active optical clocks as gravitational potential detectors along with gravimeters measuring acceleration. A combination of both devices can remotely detects not only small gravitational anomalies or objects, but also precisely locate them. Moreover, shape and mass distribution can also be derived.

[1] T. Nicholson et al., Nat. Commun. 6, 6896 (2015),

[2] I. Ushijima et al., Nat. Photon. 9, 185 (2015),

[3] M. Schioppo et al., Nat. Photon. 11, 48 (2017),

[4] T. Rosenband et al., Science 319, 1808 (2008),

[5] P. Wcis?o et al., Nat. Astronomy 1, 0009 (2016),

[6] S. Kolkowitz et al., Phys. Rev. D, 94, 124043 (2016),

[7] A. Bjerhammar, NOAA Technical Rep. NOS 118 NGS 36 (1986), Available at: http://www.ngs.noaa.gov/PUBS_LIB/RelativisticGeodesy_TR_NOS118_NGS36.pdf,

[8] R. Bondarescu et al., Geophys. J. Int. 191, 78 (2012),

[9] G. A. Kazakov et al., arXiv:1503.03998v1 [physics.atom-ph].

10438-20, Session 5

Single-particle imaging for biosensor applications

Mustafa Yorulmaz, Berkan Solmaz, Elif Ç. Seymour, Aykut Koç, ASELSAN A.S. (Turkey); M. Selim Ünlü, Boston Univ. (United States)

Imaging of nanoparticles at the single particle level is an important subject of recent research especially for the applications in bio-imaging and photovoltaics. Developing techniques in order to image nanoparticles for early detection of diseases, such as viral infections and cancer, as well as the use of nanoparticles for the treatment of certain types of cancers has gained considerable attention.

We put our research efforts to develop an in-vitro point-of-care biosensor that can be used for diagnostic purposes. For this purpose, an imaging technique that is sensitive, easy-to-

implement, low-cost, and easy-to-miniaturize is essential. Such a technique will be useful to develop biosensors which will transform into portable medical imaging and detection devices, allowing for disease diagnostics in remote locations and subsequent planning for clinical therapy.

Optical interferometric techniques have proven utility in sensitive imaging of individual nanoparticles in wide-field. In our research, We implement various optical schemes to improve the sensitivity of this biosensor, targeting to detect smaller biomolecules that would normally go undetected. For this purpose, we implement a specific surface made of Silicon and Silica of certain heights. Moreover, we employ polarization techniques, which help reducing the background.

We put efforts in creating practical, robust, and cost-effective solutions for non-laboratory environments. Optical Interference Microscopy has been successfully applied in detecting synthetic nanoparticles and viruses. In spite of the strong imaging capability of the technique, it does not require advanced optics parts. Moreover, it can be developed using halogen light sources instead of expensive lasers. It requires the use of a silicon-silicon dioxide substrate as a common-path interferometer.

The interferometric detection of scattering signal generated by the nanoparticle upon its excitation with the light source is different than in the case of detecting the direct scattered light, such as the scattering signal in the dark field scattering microscopy. The signal measured using the solely scattering-based detection scales with r^6. The direct scattering signal therefore drops notably for particles with small sizes. For example, it becomes challenging to image gold nanoparticles with sizes below 40 nm using direct scattering signal. Whereas, the interferometric signal scales with r^3. Therefore, it becomes possible to measure nanoparticles with small sizes. For example, we can measure gold nanoparticles of diameters of ~20 nm and polyester dielectric nanoparticles of diameters of 60 nm using interference signal.

Our goal is to enhance the sensitivity of this technique through integration of polarization optics, and achieve accurate sizing as well as shape and orientation determination of nanoparticles in conjunction with the physical theory based forward model and various reconstruction models. This enhancement will allow us to extend the use of this technique for detecting a wide variety of diseases including cancer using minute amounts of sample.

10438-21, Session 6

Investigation of the properties of the confocal ring resonators as sensitive elements of microoptical gyroscopes

Ekaterina R. Govorenko, Yurii V. Filatov, Egor V. Shalymov, Vladimir Y. Venediktov, Saint Petersburg Electrotechnical Univ. “LETI” (Russian Federation)

Often resonators with an equidistant spectrum are required in optics. One of ways of their receiving is the degeneracy of the frequencies of the resonator modes. For example, it is observed in the well-known classical confocal (linear) resonator. At the same time exist similar to him on properties of the configuration of the ring resonators – the ring confocal resonators. In the first approximation they can be received using in the resonator at least one concave toroidal reflective surface with the values of the radiuses of curvature in the two main meridional sections providing performance of the confocal condition and degeneration of the spectrum. For example, such resonators can be used as sensitive elements of miniature optical gyroscopes. To date properties of the confocal ring resonators have not been practically studied. This work is devoted to investigation of the properties of the confocal ring resonators.

Conference 10439: Millimetre Wave and Terahertz Sensors and Technology

Monday 11–11 September 2017
Part of Proceedings of SPIE Vol. 10439 Millimetre Wave and Terahertz Sensors and Technology X

10439-1, Session 1

Gas spectroscopy system with transmitters and receivers in SiGe BiCMOS for 225-273 GHz

Klaus Schmalz, IHP GmbH (Germany); Nick Rothbart, Deutsches Zentrum für Luft- und Raumfahrt e.V. (Germany) and Humboldt-Univ. zu Berlin (Germany); Johannes Borngräber, IHP GmbH (Germany); Selahattin Berk Yilmaz, Silicon Radar (Germany); Dietmar Kissinger, IHP GmbH (Germany) and Technische Univ. Berlin (Germany); Heinz-Wilhelm Hübers, Deutsches Zentrum für Luft- und Raumfahrt e.V. (Germany) and Humboldt-Univ. zu Berlin (Germany)

The implementation of mm-wave transmitters (TXs) and receivers (RXs) in SiGe BiCMOS or CMOS offers a path towards a compact and low cost system for gas spectroscopy of breath and toxic gases, including the detection of nitrogen oxides. This paper updates results of our work on gas spectroscopy based on TXs and RXs in IHP's 0.13 ?m SiGe BiCMOS technology. We demonstrated spectroscopic results at 238 - 252 GHz for methanol at pressures of 50 and 13 Pa. The 2f (second harmonic content) of the absorption spectrum was obtained by detecting the IF power of the RX using a diode power sensor connected to a lock-in amplifier. In this work, the improved performance of our system is shown by the absorption spectra of gaseous methanol at 241 - 242 GHz at 1.5 Pa, corresponding to a line width of about 1 MHz. The signal-noise ratio (SNR) for the absorption line of methanol at 241.7 GHz is used as measure. The system includes two fractional-n phase-locked loops (PLLs), which allow frequency ramps for the TX and RX, and a superimposed frequency shift keying (FSK) modulation for the TX. Another option includes reference frequency ramps for the PLLs in integer-n mode, which are realized by a direct digital synthesizer (DDS), including superimposed FSK modulation for the TX. In contrast to our results at 13 Pa, the DDS inclusion does not increase the SNR at 1.5 Pa. An SNR of 450 is observed within 25 s acquisition at 1.5 Pa. By inserting attenuators between the TX and the RX, the SNR decreases proportionally to the received power for our experimental conditions. We have extended our single band TX/RX system without the DDS option to a multiband system to cover the frequency range 225 - 273 GHz. It is built by combining corresponding pairs of TXs and RXs up to three frequency bands in this range. By modifying the local oscillator of the RX and TX previously used for 238 - 252 GHz, the following bands are realized: a) 225-258 GHz, b) 245-263 GHz, and c) 253-273 GHz. The multiband operation allows parallel spectra acquisition for these bands. The subharmonic RXs for the bands a) and b) use a low noise amplifier (LNA) with a gain of 18 dB at 245 GHz, and the RX for the band c) includes an LNA with a gain of 11 dB at 265 GHz. For the TXs and RXs appropriate frequency ramps are generated by their corresponding external fractional n PLL devices. The carrier boards with the TXs or RX-chips, and the PLLs are mounted to the input and output windows of the absorption cell, respectively. The 1.9 m folded gas absorption cell and the vacuum pumps are placed on a portable breadboard with dimensions of 75 cm x 45 cm.

10439-2, Session 1

Investigation of radiant millimeter wave/ terahertz radiation from low-infrared signature targets

Berat Aytaç, TÜB?TAK B?LGEM ?LTAREN (Turkey) and Middle East Technical Univ. (Turkey); Ümit Alku?, Middle East Technical Univ. (Turkey); Mustafa Sivasligil, TÜB?TAK B?LGEM ?LTAREN (Turkey); Asaf Behzat Sahin, Yildirim Beyazit Univ. (Turkey); Hakan Altan, Middle East Technical Univ. (Turkey)

Millimeter (mm) and sub-mm wave radiation is increasingly becoming a region of interest as better methods are developed to detect in this wavelength range. The development of sensitive focal plane array (FPA) architectures as well as single pixel scanners has opened up a new field of passive detection and imaging [1]. Spectral signatures of objects, a long standing area of interest in the Short Wave Infrared (SWIR), Mid-Wave (MWIR) and Long Wave-IR (LWIR) bands can now be assessed in the mm-wave/terahertz (THz) region. The advantage being that this form of radiation is not as adversely affected by poor atmospheric conditions compared to other bands. In this study, a preliminary experiment in a laboratory environment is performed to assess the radiance from targets with low infrared signatures in the millimeter wave/terahertz (THz) band (90-700GHz). The goal of this approach is to be able to model the experimental results to better understand the mm-wave/THz signature of targets with low observability in the IR bands.

In order to develop a model to understand the effect of targets at stand-off distances in various atmospheric conditions, first experiments were done to characterize the sensitivity of a commercially available FPA camera (Terasense TERA-256). In laboratory conditions (ambient temperature around 28°C), a differential blackbody source (aperture size of 4"x4" and absolute temperature range adjustable between -40°C to 175°C) whose absolute temperature is changed between 10°C to 100°C with 10°C increments is used to simulate a target signature with low temperature. The blackbody source and the camera are aligned with at a stand-off distance of 15cm such that the blackbody radiation covers full focal plane array of the camera of size 16x16, no other optical elements were used. The 8-bit camera has a reported noise equivalent power (NEP) of 1 nW/ [2].

For each temperature between 10°C to 100°C, the corresponding average readout value/pixel is computed. Starting from approximately 60°C, the average readout values increase and no significant change is observed for the temperatures between 10°C and 50°C. The main reason might be the minimum detectable power reported for the camera. Starting from 90°C, the average readout value/pixel decreases, the reason of which may be the increase in the camera housing temperature (the operating temperature of the camera is reported to be 15°C-30°C). Using the Planck radiation law and the responsivity of the camera, the incident power captured by the camera for each temperature is computed. These preliminary results show that mm-wave/THz radiation from a blackbody at temperatures between 50°C to 90°C can be detected using room temperature FPA cameras with nominal sensitivity. The advantage of such methods will allow for one to understand the impact of adverse environments on mm-wave/THz signatures of targets such as rain, dust and/or fog. The development and extension of atmospheric models to this region of the electromagnetic spectrum will be especially useful for defense applications such as surveillance, target detection and tracking, where low visibility of targets in certain bands is difficult.

References

[1]. T. Maya, G. Ziegera, S. Andersa, V. Zakosarenkoa, M. Starkloff, H.G. Meyera, G. Thorwirthb and E. Kreysac, "Passive stand-off Terahertz imaging with 1 Hertz frame rate," Proc. of SPIE ,vol. 6949, 2008.

[2]. Imaging of beams from TDS and FDS spectroscopy systems (n.d.), retrieved March 1, 2017 from http://terasense.com/applications/tds-fds-systems/.

10439-15, Session 1

Signatures of human skin in the millimetre wave band (80-100) GHz

Amani Yousef Owda, Nacer Ddine Rezgui, Neil A. Salmon, Manchester Metropolitan Univ. (United Kingdom)

With the performance of millimetre wave security screening imagers improving (reduced speckle, greater sensitivity, and better spatial resolution) attention is turning to identification of anomalies which appear on the human body. Key to this identification is the understanding of how the emissive and reflective properties vary over the human body and between different categories of people, defined by age and gender for example. As the interaction of millimetre waves with the human body is only a fraction of a millimetre into the skin, precise measurement of the emission and reflection of this radiation will allow comparisons with the norm for that region of the body and person category. On an automated basis at security screening portals this will increase detection probabilities and reduce false alarm rates, ensuring high through-puts at entrances to future airport departure lounges and transport networks.

A technique to measure the human skin emissivity in vivo over the frequency band 80 GHz to 100 GHz is described. The emissivities of the skin of a sample of 60 healthy participants (36 males and 24 females) measured using a 90 GHz calibrated radiometer was found to range from 0.17?0.002 to 0.68?0.002. The radiometric measurements were made at four locations on the arm, namely: palm of hand, back of hand, dorsal surface of the forearm, and volar side of the forearm, where the water content and the skin thickness are known to be different. These measurements show significant variation in emissivity from person to person and, more importantly, significant variation at different locations on the arms of individuals. Males were found to have an emissivity 0.03 higher than those of females. The emissivity of the back of the hand, where the skin is thinner and the blood vessels are closer to the skin surface, was found to be lower by 0.0681 than the emissivity of the palm of the hand, where the skin is thicker. The measurements also show that the emissivity of the volar side location where the blood vessels are closer to the skin surface is lower by 0.0677 than the emissivity of the dorsal surface location. The measured differences agree with those differences estimated by a half space electromagnetic model of the interaction and can be interpreted in terms of the differing water contents and skin thickness of those regions of the body.

10439-5, Session 2

Experiments in passive millimetre wave imaging of extended sources in the near-field regime of a security screening portal using aperture synthesis

Neil A. Salmon, MMW Sensors Ltd. (United Kingdom)

Aperture synthesis for passive millimetre wave imaging provides a means to screen people for concealed threats in the extreme near-field of a portal, a regime where the imager to subject distance is of the order of both the required depth-of-field and the field-of-view. Due to optical aberrations, focal plane array imagers are in effective in this regime. Operation of active sensors in this regime may also prove challenging due to illumination problems and multi-path when imaging canyon regions of the body. An aperture synthesis passive millimetre wave imaging system suffers none of these problems, it can image with microscope (~half-wavelength) resolution, through the clothing, down to the skin, for all regions of the human body.

Some recent measurements are presented that demonstrate the three-dimensional imaging capability of extended sources using a 22 GHz aperture synthesis system. An analysis of fix pattern artefacts in the images is made. A comparison is made between imagery generated via a direct inverse Fourier transform of the visibility function and the faster gridded inverse fast Fourier transform method. The direct inverse Fourier transform enables aliasing in the imagery to be more clearly identified. It also enables better understanding of how the fixed pattern artefacts arise in the imagery. Some initial results are also presented of how the Gerchberg technique, an image enhancement algorithm used in radio astronomy, is adapted for three-dimensional imaging in security screening.

10439-6, Session 2

Full polarimetric millimetre wave radar for stand-off security screening

Edward J. Blackhurst, The Univ. of Manchester (United Kingdom); Neil A. Salmon, MMW Sensors Ltd. (United Kingdom); Dean R. O'Reilly, Manchester Metropolitan Univ. (United Kingdom)

The challenge for millimetre wave stand-off security screening of personnel for concealed threats lies in how to optimise the information gathering capability in a regime where the diffraction limited sensor spot size, at ranges out to tens of metres, is considerably greater than the target. Minimising this spot size may favour operating at higher radiation frequencies, but operation at too high a frequency may introduce unacceptable levels of clutter due to the scattering by clothing. Measurements to date using active stand-off security screening systems have revealed considerable levels of cross-polar scattering in the intensity of electric field returns from targets over the whole of the millimetre wave band. Therefore characterising the full-polarimetric complex electric field amplitude return over a wide bandwidth will provide considerably more information about the target. This may enable stand-off threat recognition, possibly identification, with sufficiently good receiver operating characteristics for operational scenarios. The opportunity for this relatively new area of research for security screening is that the algorithms for full-polarimetric target analysis have been develop by the remote sensing community and are extensively published in the open literature.

Measurement and analysis of the full-polarimetric Sinclair (back) scatter matrices over a frequency band of 18 GHz to 26 GHz for a number of stand-off targets will be presented. A vector network analyser, an orthomode transducer and a conical ridged horn antenna enable a monostatic measurement configuration. The system will be calibrated using the known polarimetric responses from canonical scatterers, such as odd number bounce reflectors (planes, spheres and trihedrals) and even number bounce reflectors (eg. dihedrals). Calibration takes the form of the subtraction of backgrounds (to minimise spurious signals) and deconvolution (to remove system dispersion effects). Measurements will be conducted in an anechoic region and where possible in the far field, to simplify analysis. Results will be analysed for repeatability and consistency, and compared with the known canonical scatterer signatures. Non-repeatability in the Sinclair matrices may be interpreted as depolarisation, which can be further quantified and analysed by constructing the full-polarimetric coherency (alternatively the covariance or Kennaugh) matrices.

10439-7, Session 3

Detection of terahertz radiation using submicron field effect transistors and their use for inspection applications

Juan Antonio Delgado Notario, Univ. de Salamanca (Spain); Elham Javadi, Univ. of Tehran (Iran, Islamic Republic of); Yahya M. Meziani, Jesus Enrique Velázquez-Perez, Univ. de Salamanca (Spain); Kristel Fobelets, Imperial College London (United Kingdom); Enrique Diez, Univ. de Salamanca (Spain)

We investigated room temperature detection of terahertz radiations by using different types of transistors (Strained Silicon Modulation field effect transistor, GaAs FET, and GaN HEMT). Experimental results show a good level of response to terahertz radiation at 300 GHz and 150 GHz. Competitive performance parameters were obtained (NEP and responsivity) in comparison with other detectors. Enhancement of the photoresponse signal by imposing a dc drain-to-source current (Ids) was observed experimentally. A 2D numerical study was performed using Synopsys TCAD to understand the response found in THz measurements. Simulation results show a non-resonant response in agreement with measurements showing a significant impact of the Ids applied on the THz response. The bias current induces a large asymmetry degree in the boundary conditions of the plasma waves and, accordingly, a significant enhancement of the detector responsivity is observed. Inspection of hidden objects by using those devices within a terahertz imaging setup was demonstrated at both 150 and 300 GHz.

10439-8, Session 3

Applications of lateral Schottky barrier diodes based on 2DEG at terahertz devices

Grzegorz Cywinski, Institute of High Pressure Physics (Poland); Wojciech Knap, Institute of High Pressure Physics (Poland) and Lab. Charles Coulomb, Univ. Montpellier (France); Piotr Kruszewski, Institute of High Pressure Physics (Poland); Ivan Yahniuk, Pawel Prystawko, Institute of High Pressure Physics (Poland); Dmytro B. But, Univ. Montpellier (France); Krzesimir Szkudlarek, Grzegorz Muziol, Czeslaw Skierbiszewski, Institute of High Pressure Physics (Poland); Tomasz Waliwande, Farran Technology Ltd. (Ireland); Sergey Rumyantsev, Ioffe Institute (Russian Federation)

Due to physical properties of nitrides and especially GaN/AlGaN two-dimensional electron gas (2DEG) one can foresee wide range potential application of nitrides. Recent developments in nitride technology and their device processing lead to increasing of interest for nitride based high frequency (HF) devices. Improvements in GaN substrate technology and epitaxy already resulted in a few important achievements in High Electron Mobility Transistors (HEMT), which are currently compete with commercially available devices based on arsenides. An another important device based on 2DEG is lateral Schottky diode, which due to special geometry design is forming one-dimensional (1D) Schottky contact. This 1D Schottky contact together with commonly used for HF devices regrown ohmic contact are significantly reducing RC product and this results in possible ultrahigh values of cutoff frequencies of such devices.

We have grown 2DEG GaN/AlGaN high quality structures in metalorganic vapour phase epitaxy (MOVPE) and molecular beam epitaxy (MBE) on different types of commercially available substrates, including free standing ones, which are important in sense of low density of extended defects. Typical room temperature electron mobilities and electron sheet densities were within the range (1925-1760) cm2/(V?s) and (4-10)?1012 cm-2, respectively. Our devices were fabricated using our standard HEMT processing based on a laser writing-based photolithography method, where insulation of devices is performed using 150 nm shallow mesa etching. The 1D contact was formed to 2DEG on the mesa side and the contact area was estimated on ~12?10-9cm2/mm. This extremely small area results in exceptional small value of capacitances of 1D Schottky junction, which for all our devices fabricted in 2 ?m technology, were estimated below 50 fF. The DC characterization shows small values of reverse currents, which do not exceed 1 ?A/mm for reverse voltage of-5 V and reasonable breakdown voltage in the range of -90 V. Our studies showed that this kind of Schottky diodes has close to unity ideality factor and low level of the 1/f noise. Test devices were DC characterized and investigated towards terahertz detection in probe station on wafer and later on for spectral and polarization dependences for bonded chips (selected diode devices). For these experiments needles of our probe station and bonds play roles of antennas for terahertz radiation coupling. Results of photoresponse in range 110-170 GHz of GaN/AlGaN lateral Schottky diodes are showing feasibility of usage similar devices towards HF multiplication and mixing to outperform existing arsenide devices in sense of maximal power, robustness against electrical discharge, elevated temperatures etc. This paves the way towards new high power terahertz Schottky multipliers.

This work was supported partially by the National Science Centre, Poland allocated on the basis of the Decision Nos. DEC-013/10/M/ST3/00705 and DEC-2016/22/E/ST7/00526 and National Centre for Research and Development, Poland Grant PBS3/A3/23/2015.

10439-14, Session 3

Efficient and tunable THz emitters from Dirac-like fermions in HgCdTe alloys

Dmytro B. But, Christophe Consejo, Univ. Montpellier (France); Sergey Krishtopenko, Univ. of Montpellier (France); Nina V. Dyakonova, Univ. of Montpellier (France); Vladimir I. Gavrilenko, Institute of Applied Physics of the Russian Academy of Sciences (Russian Federation); Sergey A. Dvoretsky, A.V. Rzhanov Institute of Semiconductor Physics (Russian Federation); Frédéric Teppe, Univ. Montpellier (France); Wojciech Knap, Univ. of Montpellier (France)

Terahertz (THz)/Far infrared (FIR) magnetically tunable emission were subject of intense studies for decades [1, 2]. Impressive results have been obtained using GaAs and InSb semiconductors leading to the design of cyclotron resonance (CR) emitters based THz/FIR spectrometers [3]. Recent emergence of extremely high crystalline quality MBE grown HgCdTe alloys with extremely narrow band gap and even Dirac-like linear energy spectra rises questions about band structure related modification of electron heating and hope for THz cyclotron emission of high efficiency and tunability [4]. Indeed, decrease of the band gap and the cyclotron mass may lead to magnetic field tunability, greater by an order of magnitude than the one in GaAs or InSb semiconductors and non-equidistant Landau Levels (LLs) may help in decreasing of the parasitic self-absorption phenomena.

In this work we present experimental results on magnetically tunable THz emission from several HgCdTe bulk layers with extremely narrow energy band gaps (below 50meV). In Fig.1 we show a typical emission spectra for Hg0.81Cd0.19Te sample. One can clearly see CR emission lines moving to higher energies with increasing magnetic field. In Fig.1b a comparison between experimental and calculated transition energies is shown. Points are experimental results and two lines (for each alloy composition) correspond to calculated two lowest conduction band CR transitions –not resolved in the experiments. Transition energies were calculated using 8 band Kane Hamiltonian [5]. Nonlinear character of transition energies versus magnetic field increases with lowering Cd alloy composition showing transition from linear to square root behavior characteristic for Dirac-like band structure. A good agreement between theoretical curves and experimental results demonstrates that emission from our sample can indeed be attributed to the CR excitations in the conduction band. We have also performed preliminary experiments with lower energy bandgaps (going to zero) expecting higher tunability and efficiency of THz emission. Surprisingly we have observed decrease or complete absence of THz emission. Our results paves the way towards new Terahertz spectrometers based on solid state magnetically tunable resonant detectors and emitters.

References

[1] W. Müller, F. Kohl, E. Gornik, Infrared Physics, vol. 18, p. 691 (1978).

[2] W. Zawadzki, C. Chaubet, D. Dur, W. Knap, A. Raymond, Solid-State Electronics, vol. 37, p. 1213 (1994).

[3] W. Knap et al., Rev. Sci. Instrum., vol. 63, p. 3293 (1992).

[4] F. Teppe et al., Nat. Commun., 7, p. 12576 (2016).

[5] M. Zholudev et al., Phys. Rev. B vol. 86, p. 205420 (2012).

10439-9, Session 4

Super-resolution image reconstruction applied to an active millimeter wave imaging system based on compressive sensing

Ümit Alku?, Middle East Technical Univ. (Turkey); Esra Sengün Ermeydan, Asaf Behzat Sahin, Ilyas Cankaya, Yildirim Beyazit Univ. (Turkey); Hakan Altan, Middle East Technical Univ. (Turkey)

The development of passive and active millimeter wave (mm-wave) imaging systems is progressing rapidly fueled by the need for many applications in the area of security and defense. Imaging schemes that may either utilize array detectors or single detectors in scan architectures suffer from poor resolution due to the longer wavelengths used and the limits of the optical system in terms of lens and mirror dimensions. In order to overcome this limit, super-resolution techniques can be employed to enhance the resolution of the imaging system. Here, a form of this technique based on oversampling is applied to reconstruct the image of a target which is acquired using compressive sensing based on scanning the image plane using randomly patterned masks with fixed pixel sizes. The mm-wave stand-off imaging system uses a 99 GHz center frequency source and heterodyne sub-harmonic receiver placed in a bi-static configuration to image a target in reflection mode. The image of the target is projected onto a mechanically scanned spatial light modulator (SLM), which is a patterned two-dimensional mask that is translated along one axis. The SLM made by patterning copper on a plastic substrate is comprised of square 10x10 randomized patterns where each pixel has a dimension of 5x5mm. A total of 42 distinct patterns along one dimension is scanned and the image of the target is reconstructed using compressive sensing (CS) based algorithms. The target, a circular metallic object is placed at a distance of 20 cm from the imaging lens as shown in Fig. 1a. Typically the SLM is scanned one pixel at a time to shift the pattern during the reconstruction (See Fig 1b). To enhance the resolution of the image, the patterns are shifted by smaller steps, thereby each pixel is oversampled. Accordingly, the resulting new pattern and detected intensity are fed into the CS algorithm to reconstruct the image of the target. As a result, for a half pixel shift of 2.5mm, instead of 10x10 patterns, the measurement masks are newly created mathematically as 20x20 patterns where each 5x5mm pixel is divided into 4 to obtain smaller pixels each of size 2.5x2.5mm. As it is seen from the 400 pixel image obtained after the 45th measurement (Fig.1.c), the circular object of 12mm diameter brings more edge information than the 100 pixel image (Fig.1.b) obtained by 5mm motion, that is, it rounds the image and approximates the shape of the original object. The enhancement is due to a noise reduction as well as oversampling of the target. The speed of the current system is limited by the mechanical scanning; however with an optimized design of the imaging system, precise images of targets can be acquired more rapidly in a stand-off configuration.

10439-10, Session 4

About efficiency of correlation function using with Fourier transform for the passive THz image quality

Vyacheslav A. Trofimov, Vladislav Trofimov, Ivan Shestakov, Roman Blednov, Valentine Kovalev, M.V. Lomonosov Moscow State Univ. (Russian Federation)

We investigate new approach for THz image quality enhancing using correlation function (convolution function) between Fourier transform of the image under consideration and Fourier transform of a standard image. Main difficulty of this approach concludes in choosing of the standard image in that way to see in its Fourier spectrum the spectrum harmonics of well-known forbidden objects.

We compare the results of computer processing based on developing approach with the results which were obtained early using various other approaches.

10439-11, Session 4

Review terahertz image enhancement techniques

Piotr Garbat, Bartosz Ko?ciug, Warsaw Univ. of Technology (Poland)

In recent years we have seen significant progress in the terahertz emission and detection technologies. This development allowed the broad application of the terahertz imaging technology. THz imaging systems are usually less sensitive, and the acquired images are of insufficient quality. The improvement of imaging quality is significant an imaging system. The search for efficient terahertz image enhancement methods is still a great challenge. The goal of this paper is to define the experimental methodology to compare image enhancement algorithms.

This article focuses on analyzing image enhancement methods for two types imaging systems: time-domain terahertz imaging (THz-TDS) and single-band imaging system. Time-domain terahertz (THz) modalities can provide spectral information, and image from this type system can be considered as a hyperspectral image. Also, a signal acquired by time-domain THz systems are complex. Most hyperspectral image denoising algorithms are efficient with real-valued signals, but filtration aphorisms for complex-valued images are still under investigation Here, we present a complex terahertz image denoising method. We investigate methods based on multidimensional image decomposition. These include among other things: discrete wavelet transform, empirical mode decomposition, short fast Fourier transform. The second group of methods based on nonlinear image filters adapted to hyperspectral image representation.

The second aim of this paper is, to propose an algorithm that preserves structure in a terahertz image. Presented algorithm of image processing based on coincident analysis of image structure and quality parameter optimization.

For imaging systems using single spectral band information we compare and classify classical image enhancement algorithms. The review includes bilateral filter and guided bilateral filter (BF, GBF), nonlocal means filter (NLM), group of BM3D filers, total variation filters (TV).

Experimental results demonstrate the results of image enhancement algorithms analysis. The image enhancement performances of all considered methods are compared for experimental image data.

10439-12, Session PS

Computer modelling study on diffractive structures for broadband THz range beam shaping

Karolina Liebert Wegrzynska, Martyna Rachon, Agnieszka Siemion, Jaroslaw Suszek, Warsaw Univ. of Technology (Poland); Maciej Sypek, Warsaw Univ. of Technology (Poland)

The THz and sub-THz radiation can be used in many different domains like, defense, security, medicine, telecommunication, industrial non-destructive testing and many others. To fully exploit the potential of the THz range it is necessary to provide effective both sources and detectors. Also a high performance optics systems seems to be necessary to design and manufacture useful devices.

Different solutions in the case of the optical path in such devices were applied. Generally refractive and reflective optics is considered. It was noticed a technological breakthrough in the field of the flat optics systems manufactured by 3D print technology (sub-wave optics, diffractive optics, metamaterials) during last years. Significant results in the field of THz beam shaping were obtained by the use of the diffractive optics. The diffractive structures have many advantages such as light weight and small thickness (therefore lower absorption) and compactness. In addition, in the case of applying them for THz radiation range, they are relatively cheap to produce by mechanical milling or 3D printing. However, the main disadvantage of the diffractive structures is their huge chromatic aberration.

Diffractive optics is very efficient in the case of the narrowband (quasi-monochromatic) illumination. For example the existing postal scanner works using only well-defined wavelength. On the other hand – due to the narrowband illumination - it cannot proceed real-time spectral analysis of the envelopes. Designing of the broadband diffractive optical systems could significantly increase range of application for existing THz and sub-THz devices. In this paper we evaluate the chromatic properties of selected diffractive elements useful in THz and sub-THz range: higher order kinoform (HOK) and structures with extended depth of focus (EDOF).

Typically – during designing process of the diffractive element – we assume well-defined wavelength called designed wave length (DWL). The first type of diffractive optical element being analyzed for broadband illumination is HOK. In opposite to the traditional kinoform (maximal phase retardation 2 pi for DWL) HOK exhibits maximal phase retardation of 2 n pi for DWL where n is an integer number greater than 1. Diffractive optics in the form of the HOK can suppress chromatic aberration for wavelengths shorter than DWL. Typically HOK is thicker than the first order kinoform but it is still thinner than the corresponding refractive structure.

As it was mentioned the second method of reducing chromatic aberration is application of the structures with extended depth of focus (EDOF). An axicon (AX) or Light Sword Optical Element (LSOE) are examples of such structures. Increased depth of focus can spread focal spot along the optical axis. Due to this the different wavelengths can overlap and therefore suppress chromatic aberration.

In this paper we present theoretical considerations and numerical modeling devoted to the HOK and EDOF diffractive optics components. Furthermore comparison of the designed HOK and corresponding EDOF elements is presented and discussed.

10439-13, Session PS

An equivalent method of mixed dielectric constant in passive microwave/millimeter-wave radiometric measurement

Jinlong Su, Yan Tian, Fei Hu, Liangqi Gui, Yayun Cheng, Xiaohui Peng, Huazhong Univ. of Science and Technology (China)

Passive microwave radiometric measurement has been extensively used in remote sensing and target detection where dielectric constant plays an important role. It can provide significant information for scene understanding such as soil moisture and ocean salinity retrieval, material classification and so on. Generally, the dielectric constant is retrieved from brightness temperature (TB) in passive microwave radiometric measurement. However, since TB is a real number, multiple solutions of the complex dielectric constant based on TB will be obtained.

Therefore, we propose the mixed dielectric constant (MDC) to stand for the constant dielectric constant and the corresponding calculation method in passive microwave radiation related application. Based on the forward model simulations, we define a parameter named Ratio of Angle-Polarization Difference (RAPD), which is a ratio of the vertical polarized TB difference and the horizontal polarized TB difference between the two observation angles. RAPD is utilized as an intermediate quantity to solve material MDC which is a real number that can be used to calculate TB by the forward model.

In order to apply the MDC to practical applications, some scientific questions should be investigated. On the one hand, dielectric constant is the key parameter influencing MDC, which characterizes the intrinsic property of materials (the materials we investigated are non-magnetic with the permeability of 1.0). However, there is not a consistent one-to-one correspondence between MDC and dielectric constant. For definite the relationship between MDC and dielectric constant, we set up a congruent relationship with dielectric constant?real part ranges from 1 to 80 and imaginary part ranges from 0 to 80?for uniform non transmitting materials. When materials have the same MDC, it means that these materials have the same RAPD. On the other hand, MDC is calculated for various objects (including aluminum plate, grass, concrete, soil, ocean and so on) at 94GHz and 10GHz. We use the MDCs of various objects to calculate the TBs in multiple angles and in vertical and horizontal polarizations, then compare the calculated results with the theoretical TBs. Results indicate that using RAPD to retrieve MDC is feasible. Thus, material type can be discriminated by using MDC. Finally, the stability of the measurement error is analyzed with results suggesting that MDC has a good stability for the output voltages of passive microwave/millimeter radiometer.

One of the most notable merits of our method is that the MDC retrieved from RAPD is free of system additive error and multiplicative error. Thus, the calibration is not necessary for a linear radiometer system. The MDC solved by using our method could lead to possible new applications, such as metal target detection in security inspection and surveillance. In future work, we will conduct relevant microwave/millimeter radiometric measurement to verify our method.

Conference 10440: Optical Materials and Biomaterials in Security and Defence Systems Technology

SPIE. SECURITY+ DEFENCE

Monday - Tuesday 11–12 September 2017

Part of Proceedings of SPIE Vol. 10440 Optical Materials and Biomaterials in Security and Defence Systems Technology XIV

10440-1, Session 1

Core/shell semiconductor quantum dots for lighting and display: exciton interactions and dynamics *(Keynote Presentation)*

Renato Bozio, Marcello Righetto, Alessandro Minotto, Ilaria Fortunati, Raffaella Signorini, Univ. degli Studi di Padova (Italy)

The widespread application of quantum dots greatly profits from their broad absorption band. However, the variable nature of excitations within these bands is expected to result in undesired excitation energy dependence of steady state emission properties. We demonstrate the different role played by hot and cold carrier trapping in determining fluorescence quantum yields. Our analysis relates the energetic parameters with the available knowledge on the dynamics of charge trapping. It turns out that de-trapping processes play a pivotal role in determining steady state emission properties. We studied excitation dependent photoluminescence quantum yields (PLQY) in different CdSe/CdxZn1-xS (x = 0, 0.5, 1) quantum dots to identify best performing heterostructures, in terms of shell thickness and composition. Our rationalization of the observed behavior is focused on the modulation of trapping and de-trapping rates. The combination of experimental results and PLQY kinetics modeling reveals the need to consider hot-carrier trapping, supporting recent dynamics observations. This work provides a deeper insight into trapping process in quantum dots, relating its energetics and dynamics.

Understanding and controlling fast recombination in quantum dots (QDs) is prerequisite for most of QDs-based devices operation. Through identification of factors lengthening recombination, current research aims to achieve rationally tailored synthesis, pursuing better-performing nanostructures. Here we investigate the effects of core/shell interface on recombination in CdSe/CdxZn1-xS QDs. The complementary use of global and inversion analysis allows disentangling complex transient absorption signal. Smoothing of interface potential, together with effective surface passivation, appear to be crucial factors in slowing down both Auger-based and exciton trapping recombination. Either thick CdS shell or alloyed CdZnS shell efficiently suppress these process. Therefore, they stem as possible candidates for realization of QDs lasers and LEDs. Through kinetic modelling, we managed to related these processes to parameters quantifying emission efficiency, such as QY. Recombination rates, extracted from transient absorption data, provide direct evidences for trap mediated Auger recombination, completing the picture of exciton dynamics in CdSe/CdxZn1-xS.

[1] A. Minotto, F. Todescato, et al., J. Phys. Chem. C 118, 24117 (2014).

[2] R. Signorini et al., Nanoscale 3, 4109 (2011); F. Todescato et al., Adv. Funct. Mater. 22, 337 (2012).

10440-2, Session 1

Photon management in polymer nanofibers: emission, scattering and amplification of light *(Keynote Presentation)*

Andrea Camposeo, Maria Moffa, Istituto Nanoscienze (Italy); Vito Fasano, Martina Montinaro, Vincenzo Resta, Univ. del Salento (Italy); Luana Persano, Istituto Nanoscienze (Italy); Dario Pisignano, Univ. del Salento (Italy)

Polymer nanofibers are innovative nanostructured materials with anisotropic shape and intriguing multiscale optical properties, which make them exploitable as both active and passive miniaturized photonic components [1]. Individual polymer filaments, being composed by dielectric materials with refractive index in the range 1.5-1.8, can confine and transport light between distant locations, on typical spatial scales of the order of 100 microns, suitable for on-chip applications. In addition, nanofibers can be arranged in 2-dimensional (2D) and 3-dimensional (3D) macroscopic, disordered or partially-ordered architectures, which feature interesting light diffusion properties, arising from the microscopic inhomogeneity of the multi-filament networks [2]. Nanofibers can be also functionalized for emitting light by embedding molecular and inorganic (such as quantum dots, nanorods, 2D materials) emitters, which might feature enhanced photon emission rates, polarized emission, optical gain and improved coupling to waveguide modes [3,4]. The understanding of the interplay between the optical properties of individual filaments and of multi-particle networks is fundamental for the realization of nanostructured, complex photonic structures, with tailored scattering, absorption end emission properties. These disordered photonic media are currently being exploited in many technological fields, including photovoltaics, laser devices, and optical imaging [5]. However, light scattering and emission by nanofibers and photon channeling into polymer subwavelength waveguides depend on many variables, being often limited by the uniformity of the fiber morphology, the mutual arrangement of the nanofibers into complex structures, and the positioning of the molecular and inorganic nanoscale light-sources within individual fibers. Here we report on the fabrication of active and passive polymer nanofibers and nanofibrous macroscopic networks by electrospinning. These nanostructured media display enhanced emission and optical gain, improved surface properties, and controlled light diffusion properties. Polarization fluorescence spectroscopy of light emitted by molecular and polymeric conjugated compounds embedded in single electrospun polymer fibers, and optical spectroscopy analysis of multifilament networks evidence that efficient, nanostructured photon sources with targeted polarization, light-scattering, and optical gain can be realized, paving the way for nanofiber-based random lasers. The research leading to these results has received funding from the European Research Council under the European Union's Seventh Framework Programme (FP/2007-2013)/ERC Grant Agreement n. 306357 (ERC Starting Grant "NANO-JETS", www.nanojets.eu).

[1] Persano, L., Camposeo, A., and Pisignano, D., "Active polymer nanofibers for photonics, electronics, energy generation and micromechanics," Prog. Polym. Sci. 43, 48-95 (2015).

[2] Pisignano, D., Persano, L., Camposeo, A., "Perspectives: Nanofibers and nanowires for disordered photonics," APL Mater. 5, 035301 (2017).

[3] Gaio, M., Moffa, M., Castro-Lopez, M., Pisignano, D., Camposeo, A. and Sapienza, R., "Modal coupling of single photon emitters within nanofibre waveguides," ACS Nano 10, 6125-6130 (2016).

[4] Camposeo, A., Pensack, R. D., Moffa, M., Fasano, V., Altamura, D., Giannini, C., Pisignano, D., Scholes, G. D., J. Am. Chem. Soc. 138, 15497–15505 (2016).

[5] Wiersma, D. S., "Disordered photonics," Nat. Photon. 7, 188-196 (2013).

10440-3, Session 1

Analysis of deformation of aluminum plates under the influence of nano- and microsecond laser pulses

Karol Jach, Roman Ostrowski, Robert ?wierczy?ski, Antoni Rycyk, Krzysztof Czy?, Marek Strzelec, Antoni Sarzy?ski, Wojskowa Akademia Techniczna im. Jaroslawa Dabrowskiego (Poland)

The paper presents numerical modeling of interaction of strong laser radiation with conventional aluminum sheets, similar to those used in military technology. The theoretical model uses equations of continuum mechanics (equations of hydrodynamics and the equations of mechanics of solid bodies in a cylindrical coordinates r, z), enriched with equations describing the typical high temperature effects, such as absorption of laser radiation within the Al shield, electronic and radiative thermal conductivity, and energy loss on phase transitions (melting, evaporation, ionization). Semiempirical equations of state were used to describe the properties of material in the conditions of large deformation and the Johnson-Cook's model. The equations were solved using the method of free points developed by one of the authors.

Despite the difficulties associated with the numerical solution of the equations, the uncertainty in determination of factors describing material properties, as well as an approximate description of some phenomena (eg. transport of radiation), solutions of this type are extremely valuable because they allow, even from the qualitative point of view to: interprete the experimental results, assess the influence of various parameters (eg. laser pulse) on the qualitative and quantitative characteristics of some phenomena, setting directions for experimental work to achieve the intended results.

Two kinds od laser pulses were considered: microsecond pulse with duration of 200 ??s and a low peak power of 10 kW/cm2 (CW laser), and nanosecond pulse with duration of 10 ns and high peak power of 5 GW/cm2 (pulsed laser). The aim of this study was to determine the shapes and temperatures of Al plates under the influence of these pulses for the comparison of the numerical results with future experiments and to verify the possibility to determine the distribution of the energy density of the laser beam on the basis of the plate deformation. In case of relatively low peak laser power (long pulse) observed were only slightly attenuated vibrations without plastic deformation of Al plate. The plate was rigidly fixed at its edges. The visualisation of transverse cross-section of samples in case of short nanosecond pulses have shown temperature distributions in distorted Al plate with exemplary maximum value of around 600 K after 1200 ns from the beginning of laser pulse. In this case, numerical procedure included rejection of vapour cloud after 20 ns from the plate, because this cloud was not further interacting, but caused clearly numerical (not physical) plate deformation.

Short, nanosecond laser pulses with high peak power of Q0=6?109 [W/cm2] start evaporation of target surface and significant distortion of the remaining area. The distortion remains fixed in the target, which is strongly deformed plastically. It seems to be difficult to corelate the final target shape with laser beam spatial power distribution.

Acknowledgements. The work was performed as part of project No DOB-1-6/1/PS/2014, funded by the National Centre for Research and Development in Poland, entitled "Laser Systems of Directed Energy Weapons, Laser Systems of Non-Lethal Weapons".

10440-4, Session 2

Surface relief gratings: experiments, physical scenarios and photoinduced (anomalous) dynamics of functionalized polymer chains *(Keynote Presentation)*

Antoni C. Mitu?, Wojciech Radosz, Michal A. Szczesniak, Tomasz Wysoczanski, Grzegorz Pawlik, Wroclaw Univ. of Science and Technology (Poland)

Surface Relief Gratings were demonstrated experimentally more than 20 years ago [1,2]. Despite many years of research efforts the underlying mechanism remains unclear [3]. We discuss briefly the evolution of the physical concepts in this period and, in particular, the importance of the hypothetical photofluidization scenario and its counterpart, the orientational approach: a sound analysis of experimental data in this context was recently presented by Saphiannikova et al. [4]. Very recent results obtained within the latter approach [5] validate the generic Monte Carlo model for the photoinduced build up of the density grating and surface relief grating (SRG) in a model polymer matrix functionalized with azo-dyes [6]. Mass transport from illuminated to dark places was demonstrated and ascribed to a hypothetical complex dynamics of polymer chains in bond-fluctuation model. In this paper we characterize the motion of single functionalized chains as well as an ensemble of such chains, dependent on two factors: intensity of light illumination and its gradient. Various regimes of diffusion are found: subdiffusion, normal diffusion and superdiffusion. The conditions which promote those motions are discussed. The origin of the effect of "fine structure" of SRG close to the maximum of its density [6] is discussed and a simple mechanism of mass transport which might be responsible for it is put forward. The results provide a deeper insight into the mechanisms responsible for inscription of SRG as well as for single functionalized nanoparticle studies [7].

[1] P. Rochon, E. Batalla, A. Natansohn, Appl. Phys. Lett., 66 (1995) 136.

[2] D.Y. Kim, S.K. Tripathy, L. Li, J. Kumar, Appl. Phys. Lett., 66 (1995) 1166.

[3] S. Lee, H.S. Kang, J.-K. Park, Adv. Mater., 24 (2012) 2069.

[4] M. Saphiannikova, V. Toshchevikov, Journal of the Society for Information Display, 23 (2015) 146.

[5] V. Toshchevikov, J. Ilnytskyi, M. Saphiannikova, to appear in J. Phys. Chem. Lett. (2017).

[6] G. Pawlik, A. Sobolewska, A. Miniewicz, A.C. Mitus, EPL 105 (2014) 26002.

[7] J-P. Abid, M. Frigoli, R. Pansu, J. Szeftel, J.Zyss, C. Larpent, S. Brasselet, Langmuir 27 (2011) 7967.

10440-5, Session 2

Induced circular dichroism and laser action of hemicyanine dyes coupled to DNA and DNA-complex *(Keynote Presentation)*

Yutaka Kawabe, Yuki Suzuki, Takuya Tanaka, Kento Okoshi, Chitose Institute of Science and Technology (Japan)

Strong fluorescence enhancement was induced for many organic dye systems by the coupling to DNA or DNA-surfactant complex, prompting the development of thin film laser devices. Since fluorescence characteristics of the dyes were very sensitive to the interaction mode, it is worthwhile to elaborate their optical properties when interacting with DNA and its complexes. In this study, absorption and circular dichroic (CD) spectra were examined for solutions and films composed of hemicyanines and DNA, and the details of laser emission were studied with the complex films prepared with multiple methods.

Absorption spectra for the dyes changed remarkably by the interaction with pure DNA, while DNA-complex caused blue shift in fluorescence. In typical cases, red shift of 50nm was observed, indicating strong interaction in the ground state of the dyes. Reflecting the interaction, clear Cotton effect in CD spectra in dye absorption band was observed, and the spectral shape indicated that their direct interaction was caused presumably caused by groove binding to pure DNA. Meanwhile, weak CD signal from the dyes mixed with DNA-

complex suggested indirect interaction between them. Shift of fluorescence peak was negligible for the dyes interacting with DNA, while relatively large blue shift was observed when interacting with DNA-complex. In both cases, fluorescence was enhanced and the highest emission was obtained from the dyes interacting with DNA-complex. These facts suggested that interaction with dye and surfactant should be substantially important for efficient light emission.

Stimulated emission properties depended on the film formation method, maybe because interaction between the dye and DNA, and also that between dye and surfactant should have strong influence. In this study, two fabrication means were employed. Other than conventional method in which the mixed solution of DNA-complex and the dyes was casted, in recently developed 'immersion method', pre-fabricated DNA-complex films were stained in dye solution. The difference of spectral bands of the dyes in two types of films was about 20 ~ 30nm, and immersion method gave longer wavelength partially due to dye aggregation. Strong ASE (amplified spontaneous emission) and laser emission under optical pumping with population grating were given by the films of three types of the dyes and prepared by the two methods. The superior performance was obtained for the samples made by the immersion method. Laser threshold values were about 0.1mJ/cm2, which was close to the lowest record. Initial output emission was two orders of magnitude greater than that from conventionally prepared films. Low threshold and long durability of the immersion made devices were obtained in three types of hemicyanine dyes, making them promising for future application.

10440-6, Session 2

LIBS spectra of multicomponent Al, Fe, Cu alloys and composite materials used for selected elements of armament and munition

Roman Ostrowski, Wojciech Skrzeczanowski, Antoni Rycyk, Krzysztof Czy?, Antoni Sarzy?ski, Marek Strzelec, Karol Jach, Robert ?wierczy?ski, Wojskowa Akademia Techniczna im. Jaroslawa Dabrowskiego (Poland)

Spectral investigations in the UV-VIS range of Al, Cu, and Fe alloys and composite materials were performed using LIBS technique. The investigated objects were typical rifle bullets, mortars, rocket launchers and samples of different type steel, Cu and Al alloys, as well as composite materials of special chemical composition. Two Nd:YAG lasers were applied: a short 4 ns 60 mJ Brio Quantel/BigSky laser and a long pulse 200/400 (up to 1000) μs (~ 2/4 up to10 J) laser constructed at the Institute of Optoelectronics MUT. Both lasers used 1064 nm wavelength. In each case laser beam was directed through a 100 mm focal lens to focus the laser energy into a fine spot which allowed to register a LIBS spectrum with the ?/?? ≈ 20000 resolution. The spectra were recorded in air under atmospheric pressure.

All spectra were recorded in the 200 – 800 nm interval which allowed to qualitatively find chemical compositions and their similarity using statistical data processing (Factorial Analysis).

This spectrochemical analysis was possible for metal alloys objects for both lasers, and in case of composites only if samples were irradiated by short laser pulse since for long pulse all composite materials spectra were very similar to each other – they imitated a grey/black body spectra. For metal alloys a major difference was observed for irradiation of samples with short and long laser pulse – for short laser pulse only atomic spectra were observed while for long microsecond laser pulses molecular transitions were registered. Analogous molecular transitions were seen in composite samples spectra but for both lasers.

However, the types of registered transitions were different. For Al samples many transitions of AlO molecule were observed. These were oscillation-rotational spectra which could be surely a result of interaction of Al plasma and the atmosphere due to long interaction time between laser radiation and a sample surface. For Cu and Fe alloys – molecular spectra were not observed, mainly due to relatively narrow spectral range of the spectrometer – the transitions are outside the VIS range. For composites – the molecular transitions in molecules of CN, CH, C2 and N2 (in the latter the transition could be of atmospheric origin), mainly present in sample matrix. For long pulses UV transitions are not observed – this indicates lower plasma temperatures.

Electron temperatures of plasma created on different materials were found on the base of Boltzmann plots. Temperatures are clearly higher for plasmas generated with a short laser pulse which results from much higher laser power density on the sample surface for short pulse but not from fluence which is 20-40 times larger for long pulse. The presented results show that plasma radiation characteristics mainly depend on power density not on energy density, "long pulse" plasma is colder, and long living plasma generates more effective interaction between ambient medium and irradiated material which should be taken into consideration for laser plasma – matter processing.

Acknowledgements. The work was performed as part of project No DOB-1-6/1/PS/2014, funded by the National Centre for Research and Development in Poland, entitled "Laser Systems of Directed Energy Weapons, Laser Systems of Non-Lethal Weapons".

10440-7, Session 3

Emission properties of DNA/metal complex-based electrochemiluminescent cell *(Invited Paper)*

Norihisa Kobayashi, Chiba Univ. (Japan)

DNA has been collecting a lot of interests as novel optical and electronical materials because DNA is an environmentally-friendly material with a unique ordered one-dimensional structure with the sequence of these four bases. We are conducting some projects concerning DNA to open up field of "DNA photonics and DNA electronics

10440-8, Session 3

Protein-based visual receptive fields for image processing *(Invited Paper)*

Yoshiko Okada-Shudo, The Univ. of Electro-Communications (Japan)

We propose two types of optical filters, difference of Gaussians (DOG) and Gabor filters, with the use of the light sensitive receptor protein bacteriorhodopsin (bR). Our DOG and Gabor filters mimic on-center ganglion cell and simple cell receptive fields, respectively. The potential ability of bR to exhibit both excitation and inhibition is applied to construct artificial receptive fields. We exploit bR characteristics to fabricate bR receptive fields consisting of two oppositely coated bR films by using dip-coat and inkjet printing method.

We demonstrate that our DOG ntrol in industrial manufacturing. The goal of this research is the development of artificial DOG and Gabor optical filters for improving the filter has the function of a Laplacian filt particular

spatial-frequency and orientation. Future plans include combining bR based Gabor filter and high-speed image processing for detecting defects in electronic cir

cuits and quality co analog image processing performance. Notably, the low cost and simplicity of fabricating single element bR filters, and no requirement for external connections are two of the major advantages over conventional silicon semiconductor technology.

10440-9, Session 3

Quantum dot geometry effect on first and third order optical susceptibility

Mohammad Hossein Alam, Hossein Babashah, Zahra Kavehvash, Somayyeh Koohi, Amin Khavasi, Ali Gholamrezaei, Sharif Univ. of Technology (Iran, Islamic Republic of)

Solving Schrödinger equation for quantum dots and wetting layer reveals that the corresponding eigenvalues and eigenfunctions are considerably dependent on quantum dots size, wetting layer height, and quantum dot geometry. Moreover, first and third order susceptibilities (?(1) , ?(3)) depend on eignevalues and eignefunctions overlap. In this paper, we solve Schrödinger equation for three different geometry of quantum dots including rectangular, elliptic, and conical. The results obtained from eignefunctions overlap indicate that ?(1) and ?(2) strongly depend on the quantum dots geometry.

10440-10, Session 4

Alternative energy for advanced security and defence: organic photovoltaics, current commercial and scientific status *(Keynote Presentation)*

Vaidotas Ka?ukauskas, Vilnius Univ. (Lithuania)

The situation and tendencies of organic (nano-) photovoltaics will be reviewed, starting from the underlying physics up to the current achievements and perspectives of commercialization. The noticeable advances in the efficiency and price of the organic PV cells took place in a few recent years. Now these parameters are already suitable to start the commercial production. However, the first commercialization attempts failed several years ago. The poor marketing and business strategy were claimed to be the reason. Nowadays several institutes and companies are competing in the field, exploring possibilities of different physical approaches and device engineering solutions. The new generation prototype devices were announced recently. Nevertheless, it is clear that the commercial success will depend not only on the suggested solutions and price, but also on their popularity among end-users, and the commercial management, which is not directly associated with the physical issues and economic indicators.

Microscopic charge transport properties are of primary importance in organic material and device engineering, as they determine macroscopic material parameters, thus conditioning device efficiency. Due to the hoping nature carrier mobility is one of the main factors limiting charge transport in disordered organic materials. Thus, understanding of the fundamental transport properties is an absolute must for the purposeful device engineering.

We will demonstrate that in materials and structures that are promising for organic and hybrid photovoltaics (MDMO-PPV, P3HT, P3HT with CdSe nanocrystals, DCV6T-ZnPC, also in inorganic ?-Si with Au nanoparticles and others) carrier transport phenomena are influenced in a complex way by the light-, electric field- and thermally- stimulated mobility and trapping effects, depending on the excitation conditions. Carrier mobility measurements were performed by the CELIV (Charge Extraction by Linearly Increasing Voltage) method, carrier traps were analyzed by the Thermally Stimulated Current spectroscopy, and Current-Voltage characterization was used to investigate carrier injection and contact properties.

We will show that such complex experimental analysis by complementary methods enables discrimination and evaluation of numerical parameters of the mobility and trapping phenomena at different excitation conditions. Moreover, to correctly address transport and trapping issues, distribution of the density of transport states has to be taken into account.

10440-11, Session 4

Optical and photochemical properties of diarylethylenes

Oksana Krupka, Vitalii Smokal, Taras Shevchenko National Univ. of Kyiv (Ukraine); Beata J. Derkowska-Zielinska, Nicolaus Copernicus Univ. (Poland); Alexey Kolendo, Taras Shevchenko National Univ. of Kyiv (Ukraine)

Organic photochromic molecules have been widely investigated as promising materials for different optoelectronics application such as switching elements for microelectronics, high-density data storage, nonlinear optics, etc. Diarylethylenes and polymers based on them are known for their excellent photochemical and photophysical properties. The interesting aspect concerning styrylquinoline polymers is the possibility of switching between two independently addressable states trans form and the metastable cis form upon exposure of the light or thermal stimulation. And as result, this leads to reversible structural and electronic changes geometry of molecules, dipole moments, ϖ-conjugation, HOMO-LUMO gap in the other side on the molecular level that affect macroscopic properties. The isomerization process of styrylquinoline containing compounds plays significant role in the unique optical properties of polymers based on them.

The styrylquinaline containing derivatives were synthesized and their structures determined by UV- and HNMR- spectroscopies. The polymerization was carried out in DMF with AIBN as initiator. The products of polymerization were characterized by HNMR, GPC, DSC.

10440-12, Session PS

Analysis of the use of fiber-optic technology for the monitoring heart rate of the pregnant and fetus

Jan Nedoma, Marcel Fajkus, Radek Martinek, Jan Jargus, Ondrej Zbo?il, Vladimír Va?inek, V?B-Technical Univ. of Ostrava (Czech Republic)

This article describes an analysis of the use of fiber-optic technology in biomedical applications, specifically for the monitoring heart rate of the pregnant (mHR) and fetal (fHR). Authors focused on the use of Fiber Bragg Grating (FBG) and Fiber-Optic Interferometers (FOI). Thanks to the utilization of conventional method so-called cardiotocography (CTG), the mortality of newborn babies during delivery has decreased. Generally, among disadvantages of this method, there is a high sensitivity to noises caused by the movement of a mother, and it is connected with the frequent transfer of ultrasonic converters. This method is not suitable for a long-term continuous monitoring due to a possible influence of ultrasonic radiation on the fetus. Use of fiber-optic technology offers many advantages, for example, use measuring probes based FBG or FOI does not represent any additional radiation burden for the pregnant woman or fetus, fiber-optic measurement probes are resistant to technical artifacts such as electromagnetic interferences (EMI), thus they can be used in situations where it is impossible to use classic methods, e.g. examination by magnetic resonance (MR) or in case of delivery in water. The article describes the first experimental knowledge of based on real measurements.

10440-13, Session PS

Fiber-optic sensor based on Mach-Zehnder interferometer for securing entrance areas of buildings

Jan Nedoma, Marcel Fajkus, Radek Martinek, Pavel Mec, Martin Novák, Luká? Bednárek, Vladimír Va?inek, V?B-

Technical Univ. of Ostrava (Czech Republic)

Authors of this article focused on the utilization of fiber optic sensors based on interferometric measurements for securing entrance areas of buildings such as windows and doors. We described the implementation of the fiber-optic interferometer (type Mach-Zehnder) into the window frame or door, sensor sensitivity, analysis of the background noise and methods of signal evaluation. The advantage of presented solution is the use of standard telecommunication fiber standard G.652.D, high sensitivity, immunity of sensor to electromagnetic interference (EMI) and passivity of the sensor regarding power supply. Authors implemented the Graphical User Interface (GUI) which offers the possibility of remote monitoring presented sensing solution.

10440-14, Session PS

Analysis of chromaticity temperature of novel bulb composed of PDMS and phosphor

Martin Novák, Marcel Fajkus, Jan Jargus, Lukas Bednarek, Jakub Cubik, Daniel Cvejn, Vladimír Va?inek, V?B-Technical Univ. of Ostrava (Czech Republic)

The authors of this article focused on the issue of measurement of the chromaticity temperature of proposed bulbs made from polydimethylsiloxane, depending on the temperature of proposed bulbs. The advantage of this solution is the immunity to electromagnetic interference (EMI) and the ability to use, for example in dangerous environments (such as mines, factories, etc.). For the realization of incandescent bulbs was used transparent two-component elastomer Sylgard 184. A mixture of polydimethylsiloxane (PDMS) and a curing agent in a defined ratio (10:1) and admixture with garnet phosphor YAG: Ce was cured in the temperature box at temperature 90 °C ± 3 °C in the shape of the bulbs. All experiments were realized with eight different weight ratios of phosphor and Sylgard 184. Optical power (5 W) from a laser with a wavelength of 455 nm was fed to the proposed bulbs using the cylindrical waveguide of polydimethylsiloxane with a diameter of 5 mm. Chromaticity temperature was measured by two temperature sensors for 12hours. The outcome of this study is the evaluation of the chromaticity temperature of output light depending on temperature variations of proposed bulbs due to the conversion of optical power into heat.

10440-15, Session PS

Fiber-optic sensor for monitoring a density of road traffic

Jan Nedoma, Marcel Fajkus, Radek Martinek, Pavel Mec, Martin Novák, Jan Jargus, Vladimír Va?inek, V?B-Technical Univ. of Ostrava (Czech Republic)

Authors of this article have focused on the use of fiber-optic technology in the car traffic. The article describes the use of fiber-optic interferometer for the purpose of the dynamic calculation of traffic density and subsumption the vehicle into the traffic lane. The objective is to increase safety and traffic flow. Presented solution is characterized by the non-destructive character to the road - sensor no need built into the roadway. The sensor works with standard telecommunications fibers of the G.652.D standard. Other hallmarks are immunity to electromagnetic interference (EMI) and passivity of concerning the power supply. The massive expansion of optical cables within telecommunication needs along roads offers the possibility of connecting to the existing telecommunications fiber-optic network without a converter. Information can be transmitted at distances of several km up to tens km by this fiber-optic network. Set of experimental measurements in real traffic flow verified the functionality of presented solution.

10440-16, Session PS

Analysis of the influence location of the fiber-optic sensor on the measurement and determination the heart rate of the human body

Jan Nedoma, Marcel Fajkus, Radek Martinek, Jakub ?ubík, Stanislav Kepak, Jan Vanus, Ondrej Zbo?il, Vladimír Va?inek, V?B-Technical Univ. of Ostrava (Czech Republic)

Authors of this article focused on the analysis of the influence location of the fiber-optic sensor on the measurement and determination the heart rate (HR) of the human body. The sensor uses a Fiber Bragg Grating (FBG) and is encapsulated in the polymer polydimethylsiloxane (PDMS). The combination of fiber-optic technology and its encapsulation in a polymer PDMS allows the use of the sensor e.g. in magnetic resonance environments (MRI). Among currently solved doctors requirements belongs field focusing on the study of hyperventilation and panic attacks of patients during MRI examination due to their very frequent occurrence. Proposed FBG sensor can help doctors to predict (based on heart rate) hyperventilation and panic attacks of patients during MRI examinations. For the most accurate determination of the heart rate, it is necessary to know the influence location of the sensor on the human body. The sensor functionality and analysis of the sensor placement on the heart rate has been verified by a series of real experimental measurements of test subjects in the laboratory environment.

10440-17, Session PS

Characterization and visual illustration of the consequences motion of human body for the determination of heart rate

Jan Nedoma, Marcel Fajkus, Radek Martinek, Stanislav Kepak, Jakub ?ubík, Vladimír Va?inek, V?B-Technical Univ. of Ostrava (Czech Republic)

The team of authors focused on analyzing of using fiber-optic sensor based on Fiber Bragg Grating (FBG) for the monitoring of heart rate (HR) of long-term ill patients with a minimum of physical movement load. During all experiments, test subjects were asked to simulate their natural behavior in the most accurate way (for instance, the focus was on the use of fine motor skills - not only movements of hands and arms, legs, and feet, coughing, changes in body positions, but also walking). All these external aspects are taken into account in the bellow-described results of the probe efficiency and show that it is very necessary to know the impact of these artifacts for the determine the heart rate of the human body. Final results were discussed with the senior doctor of the long-term care department.

10440-18, Session PS

Analysis of non-invasive FBG sensor for monitoring patient vital signs during MRI

Jan Nedoma, Marcel Fajkus, Radek Martinek, Vladimír Va?inek, V?B-Technical Univ. of Ostrava (Czech Republic)

This article focuses on the analysis and verification of a non-invasive fiber Bragg grating (FBG) sensor used for the monitoring of a patient`s heart rate (HR) and respiratory rate (RR) in a magnetic resonance environment (MRI). Measuring heart and respiratory rate were carried out on a group of five volunteers with their written consent during MRI examinations. The type of the scanner used in the experiment was GE Signa HDxt 1.5T. The benefit of this article lies in the

design of a sensor in the form of a sensor pad. The sensor is placed beneath a patient`s body lying supine. The purpose is to increase and improve the patient`s safety as well as to help doctors to predict panic and hyperventilation attacks of patients during MRI examinations. Provided Bland-Altman statistical analysis demonstrates the heart and respiratory rate detection with a satisfactory accuracy for all five volunteers.

10440-19, Session PS

The methodology of preparing the end faces of cylindrical waveguide of polydimethylsiloxane

Martin Novák, Jan Nedoma, Jan Jargus, Luká? Bednárek, Daniel Cvejn, Vladimír Va?inek, V?B-Technical Univ. of Ostrava (Czech Republic)

Polydimethylsiloxane (PDMS) can be used for its optical properties and its composition offers the possibility of use in the diverse environments. Therefore authors of this article focused on more detailed working with this material. The article describes the methodology of preparing the end faces of the cylindrical waveguide of polymer polydimethylsiloxane (PDMS) to minimize losses during joining. The first method of preparing the end faces of the cylindrical waveguide of polydimethylsiloxane is based on the polishing surface of the sandpaper of different sizes of grains (3 species). The second method using so-called heat smoothing and the third method using aligning end faces by a new layer of polydimethylsiloxane. The outcome of the study is to evaluate the quality of the end faces of the cylindrical waveguide of polymer polydimethylsiloxane based on evaluating the attenuation. For this experiment, it was created a total of 140 samples. The attenuation was determined from both sides of the created samples for three different wavelengths of the visible spectrum.

10440-20, Session PS

Analysis of the bending radius of the cylindrical waveguide of polydimethylsiloxane for the purpose of lighting

Martin Novák, Jan Jargus, Marcel Fajkus, Luká? Bednárek, Vladimír Va?inek, V?B-Technical Univ. of Ostrava (Czech Republic)

Polydimethylsiloxane (PDMS) can be used for its optical properties and its composition offers the possibility of use in the diverse environments. Therefore authors of this article focused on more detailed working with this material. The authors describe the use of PDMS polymer for the light transmission over short distances (up to tens of centimeters). PDMS offers good prerequisites (mechanical properties) for the creating cylindrical lighting waveguide e.g. for the purpose of the automotive industry. The objective is to determine the maximum bending radius of the cylindrical waveguide of polydimethylsiloxane for different wavelengths of the visible spectrum and thus extend the knowledge for subsequent use in lighting. The created cylindrical waveguide consist of a core and a cladding. Cladding was formed by a PDMS having a lower refractive index in order to respect the condition of total reflection.

10440-21, Session PS

Analyzing of using PDMS polymer as the sensors of the pressure or weight

Jan Jargus, Jan Nedoma, Martin Novák, Marcel Fajkus, Pavel Mec, Daniel Cvejn, David Bujdos, Vladimir Vasinek, V?B-Technical Univ. of Ostrava (Czech Republic)

Polydimethylsiloxane (PDMS) can be used for its optical properties, and its composition offers the possibility of use in the diverse environments (industry, medicine applications, security devices and etc.). Therefore authors of this article focused on more detailed working with this material. This material could be use for the sensory applications such as the sensor of pressure or weight, which may find use also in the field of security and defense. The article describes the process of making the prototype of the sensor and its verification based on laboratory results. Measurement methodology is based on the determination of the change of optical power at the output of the sensor prototype depending on the change in pressure or weight. We estimate the maximum load of the sensor on the basis of the laboratory results in the units of tons. Using a calibration measurement can determine the amount of pressure and weight with an accuracy of ± 2 %.

10440-22, Session PS

Noninvasive encapsulated fiber-optic probes for interferometric measurement

Ondrej Zbo?il, Jakub ?ubík, Stanislav Kepak, Jan Nedoma, Marcel Fajkus, Petr Závodn?, Vladimír Va?inek, V?B-Technical Univ. of Ostrava (Czech Republic)

This article focuses on the sensitivity of encapsulated interferometric probes. These probes are used mainly for BioMed and security applications. Fiber-optic sensors are interesting for these applications, as they are resistant to electromagnetic interference (EMI) and that also do not affect the surrounding medical and security equipment. Using a loop of the optical fiber with is not a suitable for these measurements. The optical fiber should be fixed to one position, and should not significantly bend. For these reasons, the optical fiber is encapsulated. Furthermore, it is necessary that the encapsulated measuring probes were flexible, inert, water resistant and not toxic. Fiber-optic sensors shouldn't be magnetically active, so they can be used for example, in magnetic resonance environments (MR). Probes meeting these requirements can be widely used in health care and security applications. Encapsulation of interferometric measuring arm brings changes in susceptibility of measurements in comparison with the optical fiber without encapsulation. To evaluate the properties of the encapsulated probes, series of probes made from different materials for encapsulation was generated, using two types of optical fibers with various degrees of protection. Comparison of the sensitivity of different encapsulated probes was performed using a series of measurements at various frequencies. The measurement results are statistically compared in the article and commented. Given the desired properties polydimethylsiloxane (PDMS) polymer has been proven the most interesting encapsulating material for further research.

10440-23, Session PS

Analysis of creating an innovative microlens made of polydimethylsiloxane polymer on the end of the optical fibers

Ondrej Zbo?il, Jan Nedoma, Marcel Fajkus, Martin Novák, Jan Jargus, Tomá? Stratil, Vladimír Va?inek, V?B-Technical Univ. of Ostrava (Czech Republic)

The article describes a method for fabrication of polymer optical micro-lenses using polydimethylsiloxane (PDMS) at the end of optical fibers. PDMS is an optically clear substance having a refractive index very similar to the optical fibers. Therefore it is an interesting material for optical purposes. PDMS is characterized by resistance to electromagnetic interference (EMI), enabling the use in electromagnetically noisy environments. These lenses could be used for example for the security applications. For the manufacture of the micro-

lenses is used Sylgard silicone elastomer 184. When applied to the end of conventional optical fiber is cured by treatment at 100 °C ± 5 °C. Authors performed a series of experimental measurements. The optical characteristics of the treated fibers compared with conventional fibers without micro-lenses. The fibers provided with optical lenses made of PDMS may be used for security applications, in the visible light communication (VLC) or as a microprobe.

10440-24, Session PS

Device for the alternative option of temperature measurement based on the polydimethylsiloxane polymer

Jan Jargus, Jan Nedoma, Marcel Fajkus, Martin Novák, Jakub Cubik, Daniel Cvejn, Vladimir Vasinek, V?B-Technical Univ. of Ostrava (Czech Republic)

Polydimethylsiloxane (PDMS) has good optical properties, and its composition offers the possibility of use in many applications (industry, security device, medicine applications and etc.). We focused on the alternative option of temperature measurement in this article. Our approach is based on measuring changes of chromaticity correlated temperature corresponding to changes in temperature. Described device uses an optical fiber with a defined layer of PDMS and luminophore and we assume that it can find use also in the field of security. The article describes the process of making the prototype of the device and its verification based on laboratory results. The measured temperature depends mainly on the type of optical fiber and the measured temperature range is determined by the thermal resistance of used optical fiber. Using a calibration measurement can determine the value of temperature with an accuracy of ± 2,5 %.

10440-25, Session PS

Hybrid optical security system using photonic crystals and MEMS devices

Jerzy Ciosek, Wojskowa Akademia Techniczna im. Jaroslawa Dabrowskiego (Poland)

An important issue in security systems is the selection of appropriate detectors or sensors, whose sensitivity parameters will guarantee the functional reliability and elimination of false alarms.

Modern technological level enables us to make optimized sensor systems for selective action tailored to specific types of common risk factors.

In optical security systems, one of the safety parameters considered is the spectral range in which the excitation signal is associated with a risk factor. Advanced safety systems should be designed taking into consideration the possibility of the occurrence of complex and often at the same time a number of factors, which can be selectively recognizable.

Analyzed chemical hazards are chemical warfare agents and toxic industrial compounds present in the form of gases and aerosols.

The proposed solution is a hybrid optical system consisting of a multi-spectral structure of photonic crystals associated with MEMS (Micro Electro-Mechanical System) resonator. Very good properties for use in detectors have crystallographic structure of carbon: micro-diamond and graphene doped with nitrogen.

The advantage of this system is a multi-spectral sensitivity at the same time narrow-band selectivity for the identification of a risk factor. It is possible to design a system optimized for fixed types expected though of very complex signals.

10440-26, Session PS

Fiber-optic sensor system for entrance areas monitoring

Marcel Fajkus, Jan Nedoma, Stanislav Kepak, Jakub ?ubík, Jan Jargus, Ond?ej Zbo?il, Radek Martinek, Vladimír Va?inek, V?B-Technical Univ. of Ostrava (Czech Republic)

Authors of this article present the fiber-optic system based on fiber Bragg gratings (FBGs) which are used to secure the entrance areas such as buildings, halls, warehouses, etc. The system uses the specially encapsulated sensory array of fiber Bragg gratings which are implemented into the floor or on the floor and allows for monitoring the area of 1x1 m up to 100x100 m. Depending on the number of FBG sensors. The sensory array is characterized by immunity to electromagnetic interference (EMI), passivity regarding electrical power supply, the possibility of remote evaluation (up to units of km) and high sensitivity. Proposed sensor system has detection capability greater than 99 % and furthermore, provides information about the weight load to an accuracy of ± 5 kg. The concept has been tested in a real environment within the test polygon for several weeks. As the reference devices, we used the CCTV (Closed Circuit Television).

10440-27, Session PS

Bragg grating sensors for the monitoring load of production press machines

Marcel Fajkus, Jan Nedoma, Pavel Mec, Jakub ?ubík, Stanislav Kepak, Jan Jargus, Martin Novák, Radek Martinek, Vladimír Va?inek, V?B-Technical Univ. of Ostrava (Czech Republic)

This article discusses the topic of the monitoring of the operating condition of the pressing machines. In the process of pressing there are a large acting of the forces of the press machine on the machined material. It is accompanied by an expression of deformation of parts of the pressing machines. Knowledge about the resulting loading is important for the final product quality and durability of these machines. In the case of multi-columned presses is important even load distribution among the individual columns. For this reason, it is necessary to monitor the load of the hydraulic pistons. Conventional approaches of load monitoring utilize piezoelectric sensors and strain gauges, which are sensitive to electromagnetic interference, require electrical power, subject to corrosion and action of moisture. A suitable alternative is the fiber Bragg gratings (FBGs) sensors, that those failures have. Their use for load monitoring production presses have been verified by the real measurement on a four-post hydraulic press ALPHA 4 from the company FORM + TEST Seidner. For measurements were used the FBG sensors and classic foil strain gauges (reference). Real measurement was performed during a load of press in the range from 0 to 2000 kN with a step of 500 kN.

10440-28, Session PS

Monitoring of the structural loads of tunnels using a distributed optical system BOTDR

Marcel Fajkus, Jan Nedoma, Pavel Mec, Martin Novák, Tomas Kajnar, Radek Martinek, Jakub Jaros, David Hruby, Vladimír Va?inek, V?B-Technical Univ. of Ostrava (Czech Republic)

Authors of this article focused on the analysis of the use of distributed fiber-optic technology for security monitoring of structural loads of road and motorway tunnels. Authors focused on measurements of deformation utilizing Brillouin

Time Domain Reflectometry (BOTDR). The principle is based on the measurement of the stimulated Brillouin scattering. The article describes the load of tunnel based on the real measurements made during the construction of the motorway tunnel in the Slovakia Republic in a time horizon of several months. Experiments were carried out with standard optical telecommunication cable with water-absorbing aramid yarns and jacketing of diameter 4.2 mm. The outcome of this article is an introductory analysis the use of fiber-optic technology for security monitoring of structural loads for road and motorway tunnels.

10440-29, Session PS

Monitoring system of hydraulic lifting device based on the fiber-optic sensors

Marcel Fajkus, Jan Nedoma, Martin Novák, Radek Martinek, Jan Vanus, Pavel Mec, Vladimír Va?inek, V?B-Technical Univ. of Ostrava (Czech Republic)

This article deals with the description of the weighing dynamic system for the weighing the municipal waste based on the fiber-optic grating sensors. For minimize the financial costs of the proposed weighing system, the power evaluation of measured signal has been chosen. The solution is based on an evaluation of the signal obtained using the fiber Bragg grating (FBG) sensors with overlapping reflective spectra. For encapsulation of the sensors was used polydimethylsiloxane (PDMS) polymer. To obtain a weight of the waste is uses the action of deformation of the lifting device on the pair of the Bragg grating sensors mounted on the lifting device of the dumpster car. According to the proposed algorithm is determined weight with an accuracy of +/- 1.5% in the range of 0 to 100 kg for standard containers designed for the municipal waste collection. Verification of the proposed system was realized on the various types of the standard containers intended for the collection of municipal waste and on the various types of garbage trucks in real traffic. The original contribution of the paper is to verify the new low-cost fiber-optic system for weighing municipal waste with the aim of streamline garbage collection.

10440-30, Session PS

Processing of fetal heart rate through non-invasive adaptive system based on recursive least squares algorithm

Marcel Fajkus, Jan Nedoma, Radek Martinek, Vladimír Va?inek, V?B-Technical Univ. of Ostrava (Czech Republic)

In this article, we describe an innovative non-invasive method of Fetal Phonocardiography (fPCG) using fiber-optic sensors and adaptive algorithm for the measurement of fetal heart rate (fHR). Conventional PCG is based on a non-invasive scanning of acoustic signals by means of a microphone placed on the thorax. As for fPCG, the microphone is placed on the maternal abdomen. Our solution is based on patent pending non-invasive scanning of acoustic signals by means of a fiber-optic interferometer. Fiber-optic sensors are resistant to technical artifacts such as electromagnetic interferences (EMI), thus they can be used in situations where it is impossible to use conventional EFM methods, e.g. during Magnetic Resonance Imaging (MRI) examination or in case of delivery in water. The adaptive evaluation system is based on Recursive least squares (RLS) algorithm. Based on real measurements provided on five volunteers with their written consent, we created a simplified dynamic signal model of a distribution of heartbeat sounds (HS) through the human body. Our created model allows us to verification of the proposed adaptive system RLS algorithm. The functionality of the proposed non-invasive adaptive system was verified by objective parameters such as Sensitivity (S+), Signal to Noise Ratio (SNR), and Positive Predictive Value (PPV).

10440-31, Session PS

Thermal and light-induced properties of a series of azobenzene poly(ester imide)s

Anna Kozanecka-Szmigiel, Warsaw Univ. of Technology (Poland); Jolanta Konieczkowska, Ewa Schab-Balcerzak, Ctr. of Polymer and Carbon Materials (Poland); Jerzy Antonowicz, Warsaw Univ. of Technology (Poland); Dariusz Szmigiel, Institute of Electron Technology (Poland)

Azobenzene polymers belong to very important light-responsive materials exhibiting photoinduced orientation and photoinduced mass transport arising from efficient and reversible trans-cis-trans photoisomerization cycles. Polyimides are considered as attractive hosts for functionalized or supramolecular materials due to their high glass transition and decomposition temperatures, good mechanical properties and chemical resistance. In addition, azo polyimides are known for an enhanced temporal stability of the generated azo chromophore alignment and a high thermal stability of the inscribed gratings. In this study we present a series of amorphous side-chain azo poly(ester imide)s possessing the chromophores directly attached to the backbone via one of their phenyl rings. The polymers differ in a chromophore content in a repeating unit and in a type of the neighbouring chain groups (either the ester or/and the imide groups). A proper design of a chemical architecture allowed for getting a closer insight into certain structure-property relations. We present the details of the preparation route of azo poly(ester imide)s from their poly(amic acid)s precursors as well as investigate thermal and light-induced properties of the materials. The photoinduced birefringence measurements at 445-nm excitation wavelength showed a large amount of chromophore alignment in the poly(ester imide) containing two azo moieties per a repeating unit. The experiments on holographic grating recording with 442-nm writing beams revealed the most efficient mass transport in the material possesing the azo chromophores located between the imide groups, while no mass transport was found for the material containing the chromophores placed exclusively between the ester groups. For all the polymers a relatively slow photoinduced birefringence relaxation in the dark was observed.

Conference 10441: Counterterrorism, Crime Fighting, Forensics and Surveillance

SPIE. SECURITY+ DEFENCE

Monday - Tuesday 11–12 September 2017

Part of Proceedings of SPIE Vol. 10441 Optics and Photonics for Counterterrorism, Crime Fighting, and Defence XIII

10441-1, Session 1

Design optimization of Cassegrain telescope for remote explosive trace detection

Kaushalkumar Bhavsar, The Robert Gordon Univ. (United Kingdom); Kemal Efe Eseller, Atilim Ümiv. (Turkey); Radhakrishna Prabhu, The Robert Gordon Univ. (United Kingdom)

The past three years have seen a global increase in explosive-based terror attacks. The widespread use of improvised explosives and anti-personnel landmines have caused thousands of civilian casualties across the world. Even after years of ending wars, unexploded landmines and other kind of explosives continue to injure and destroy lives and livelihood. Current scenario of globalized civilization threat from terror drives the need to improve the performance and capabilities of stand-off explosive trace detection devices to be able to anticipate the threat from a safe distance to prevent explosions and save human lives.

In recent years, laser-induced breakdown spectroscopy (LIBS) is an emerging approach for material or elemental investigations. All the principle elements on the surface are detectable in a single measurement using LIBS and hence, a stand-off LIBS based method has been used to remotely detect explosive traces from several to tens of metres distance. The most important component of LIBS based stand-off explosive trace detection system is the telescope which enables remote identification of chemical constituents of the explosives. The precision in collection and focusing of the spectral contents (LIBS signals) from the plasma generated by laser irradiation on to the spectrometer enhances the sensitivity of the device. The main objective of this work is to design a robust Cassegrain telescope to detect explosives remotely. The design incorporates various optical aberrations from components. The paper also reports investigations on different designs of Cassegrain telescopes and their suitability for stand-off LIBS system. Then, the analysis of the optimized design with manufacturing tolerances of different optical parts will be investigated to achieve the optimum practical design.

10441-2, Session 1

MMW/THz imaging using upconversion to visible based on glow discharge detector array and CCD camera

Avihai Aharon Akram, Ariel Univ. (Israel) and Ben-Gurion Univ. of the Negev (Israel); Daniel Rozban, Amir Abramovich, Ariel Univ. (Israel); Yitzhak Yitzhaky, Natan S. Kopeika, Ben-Gurion Univ. of the Negev (Israel)

An inexpensive up conversion MMW/THz imaging method is suggested here. The method is based on glow discharge detector (GDD) and silicon photodiode or simple CCD/CMOS camera. The GDD was previously found to be an excellent room-temperature MMW radiation detector by measuring its electrical current. The GDD is very inexpensive, costing about 50 cents, and it is advantageous due to its wide dynamic range, electronic ruggedness, broad spectral range, room temperature operation, simplicity of use, and immunity to high power radiation. An upconversion method is demonstrated here. Upconversion is based on measuring the visual light emitting from the GDD rather than its electrical current. A preliminary experimental result proves that the up-conversion method is preferable. These results showed better response time of 480 ns compared to the electronic detection that was performed in our previous work. Those response time results are limited due to the bandwidth of the optical detector which affects the performance of the detection. Further improvement of the response time and sensitivity can be achieved using a faster optical detector and amplifier. The power measurements and noise equivalent power (NEP) calculation were carried out using a power meter and spectrum analyzer. The power and NEP results of this method show better performance compared to the electronic detection, which is noisier because of the glow discharge plasma. The suggested experimental set up is composed of a GDD imaging array, MMW source based on multipliers, and a basic CCD/CMOS camera. The visual light emitting from the GDD array is directed to the CCD/CMOS camera and the change in the GDD light is measured using image processing algorithms. The combination of charge coupled device (CCD) camera and GDD focal plane arrays can yield a faster, more sensitive, and very inexpensive MMW and THz camera, eliminating the complexity of the electronic circuits and the internal electronic plasma noise of the GDD. Furthermore, three dimensional imaging systems based on scanning prohibited real time operation of the imaging system. In order to enable real time operation a GDD array is required, which is easily economically feasible. This array enables us to acquire information of distance and magnitude from all the GDD pixels in the array simultaneously. The 3D image can be obtained using methods like frequency modulation continuous wave (FMCW) direct chirp modulation, and measuring the time of flight (TOF).

10441-3, Session 1

Peak correlation classifier: a novel means of identifying toxic substances in neutral mixtures

Robert M. French, Univ. de Bourgogne (France); Mathieu Thevenin, Vesna Simic, Karim Boudergui, Commissariat à l'Énergie Atomique (France); Nadine Fourrier, Lab. Central de la Préfecture de Police (France); Thanh-Toan Truong, Lab. Central de la Préfecture de Police (France) and LEAD, Univ. de Bourgogne (France); Bruno Vanlerberghe, LEAD (France); Sandrine Pereira Rodrigues, Lab. Central de la Préfecture de Police (France)

Emergency services are equipped with mobile laboratories in order to react as rapidly as possible in the event a terrorist attack, an industrial disaster, etc. Samples are collected at the site and analyzed immediately. Available analytical tools include various types of spectroscopy equipment (FTIR, Raman, x-ray fluorescence, etc.). However, these analyses produce data that must subsequently be interpreted by an expert, often a time-consuming process constituting a bottleneck for a rapid, subsequent action. In short, there is a pressing need to be able to identify, rapidly and accurately, prohibited, toxic or explosive substances contained in mixtures of other substances. We present a novel algorithm that relies on infrared spectrograms of sampled material, typically taken from a crime scene. The algorithm determines whether or not a given substance is found in the mixture being tested and provides a measure of confidence of its determination.

The proposed algorithm is based on the calculation of a set of correlations between the infrared spectrograms of the Reference-Substance Spectrogram (RSS) and the Unknown-Substance Spectrogram (USS). A simple peak-detection algorithm finds the distinct peaks of RSS. A narrow interval is defined about each peak. If there are N peaks in RSS, then there will be a total of N intervals around these peaks. The derivative of RSS (or, potentially, some other function characterizing the shape of a curve) is calculated at each point in each peak-interval in RSS. At each point in each interval in

USS corresponding to the peak-intervals in RSS, the derivatives of USS are calculated. For each of these intervals, the correlation between the two sets of derivatives is computed. The higher this correlation, the greater RSS and USS resemble each other over that interval. We average these correlations over the N peak intervals. The higher the average correlation, the more likely the Unknown Substance will contain the Reference-Substance.

We present a study of 20 substances containing various levels of 2,4-Dinitrotoluene (2,4-DNT), an impurity present in the explosive TNT at up to 5% by weight. This nitroaromatic was mixed with various percentages of substances with a structure similar to 2,4-DNT (toluene, musc ketone, 4-nitrophenol, flour, saccharose, acetone, sodium bicarbonate, acetylsalicylic acid and hydroquinone). The amount of 2,4-DNT in these test mixtures ranged from none to very low (2%, 5%), up to 71% DNT.

We created narrow intervals about 13 peaks in the 2,4-DNT spectrogram and over these intervals determined the correlations between the derivatives of the 2,4-DNT spectrogram and the corresponding derivatives for each of the 20 test substances. This set of 13 correlations constituted a representation of the Unknown Substance with respect to the Reference Substance.

We then trained a Support Vector Machine (SVM) to classify each of the Unknown Substances as either containing 2,4-DNT or not. The SVM correctly classified all Unknown Substances. In addition, the distance from the separating hyperplane provided a measure of the algorithm's confidence in the accuracy of its classification.

10441-4, Session 2

Banknote authentication using chaotic elements technology

Radhakrishna Prabhu, The Robert Gordon Univ. (United Kingdom); Sajan Ambadiyil, Ctr. For Development of Imaging Technology (India); Krishnendu P.S., Jawaharlal College of Engineering and Technology (India); Vellara Pillai Mahadevan, Univ. of Kerala (India)

The counterfeit banknote is a growing threat to the society since the advancements in the field of computers, scanners and photocopiers, as they have made the duplication process for banknote much simpler. The fake note detection systems developed so far have many drawbacks such as high cost, poor accuracy, unavailability, lack of user-friendliness and lower effectiveness. One possible solution to this problem could be the use of a system uniquely linked to the banknote itself. In this paper, we present a unique identification and authentication process for the banknote using chaotic elements embedded in it. A chaotic element means that the physical elements are formed from a totally random process independent from human intervention. Chaotic elements are physically unclonable in nature. Because of the randomness, it is practically impossible to duplicate the chaotic element, even if the exact manufacturing process is replicated. In a banknote, dual colored optical fibres having fluorescent properties are used as non-diffractive optically variable security devices for preventing counterfeiting and forgery. These Optical fibres are tiny pellets of synthetic material having fluorescent properties which are mixed into the paper pulp in an uncontrolled manner during the paper manufacturing process. Such elements are invisible in white light but emit visible light on excitation with ultraviolet or other actinic radiation. Physical systems with some randomness, which are produced by an uncontrolled process, are good candidates for chaotic elements on the security document. The chaotic elements used in this paper are the random distribution patterns of such security fibres set into the paper pulp. Just like the human biometric traits that have a random pattern and are unique for each, the security fibre pattern is also unique for each banknote. From the ultra-violet (UV) image of the banknote, features of the chaotic element can be extracted. These features are converted into a numerical value and then encrypted. The result is used to create the unique ID in the form of a QR code, and this is printed on the banknote during the production of the banknote. The authenticity of the banknote can be verified by any person who receives the note to decide whether the banknote is authentic or not. Performance analysis of the system is also studied in this paper.

10441-5, Session 2

Active vortex sampling system for remote contactless survey of surfaces by laser-based field asymmetrical ion mobility spectrometer

Gennadii Kotkovskii, Artem E. Akmalov, Alexander A. Chistyakov, Alexey V. Sychev, National Research Nuclear Univ. MEPhI (Russian Federation)

The modern technologies of explosives detection must identify explosive substances with high selectivity and low analysis time, providing the detection limit of about 10-15 g/cm3 for reliable detecting. Ion mobility (IM) and field asymmetric ion mobility (FAIM)–spectrometry satisfy these requirements. To work with traces of explosives IM and FAIM-spectrometers often have a heating module. Another approach uses laser radiation for contactless inspection of objects (including remote objects) by initiating laser desorption [1] jointly with IM and FAIM spectrometry.

The most commonly used schemes of vapor sample collection in IM and FAIM spectrometers are vortex airflows directed to a surface. Inside the vortex there is a volume of reduced pressure having an analytical flow directed to the intake sampling hole of a detector. The vortex flow is typically created by pumping air through a fixed impeller, consisting of a base and blades. Sampling distance for these devices is estimated usually as a diameter of a sampling orifice of a detector that is not more than 10 cm. For laser FAIM spectrometers the opportunity to desorb traces of explosives at large distances contradicts with small sampling distances of fixed-based impeller of sampling systems.

The purpose of this paper is to elaborate a sampling device for a FAIM spectrometer on the basis of a rotating impeller to increase the effective distance of sampling as compared to the existing systems based on fixed impeller.

Numerical simulation of vortex and analytical sampling flows was made for sampling device based on both fixed and high speed rotating impeller. The construction of sampling device based on the rotating impeller located at the same axis as the ion source of a spectrometer was proposed. The device includes a pulley, a belt and a motor.

The dependences of trinitrotoluene (TNT) vapors signal on the rotational speed and the optimization of values of the vortex and analytical sampling flows were obtained.

The proposed construction is capable of creating disturbance of air at a distance of 26 cm and sending it to a spectrometer as results of simulation shows. The experimentally proved sampling distance occurred to be even larger – 30 cm for TNT and cyclotrimethylenetrinitramine (RDX) deposited on various most common surfaces (metal, plastic, paper).

The experimental verification was conducted also in laser desorption mode of FAIM laser spectrometer (?=266nm, 10 Hz, 107 W / cm2). For the use both the laser desorption mode and rotating impeller the amplitude of the signal detected at the distance of 40 cm from spectrometer reaches 25% of the signal for the sample desorbed directly at the spectrometer.

The changes in the scheme of gas internal flows of a FAIM spectrometer necessary for alignment of analytical and vortex flows at increased sampling distances are proposed and discussed.

[1] Akmalov, A. E., Bogdanov, A. S., Kotkovskii, G. E., "A laser desorption ion mobility increment spectrometer for detection of ultralow concentrations of nitrocompounds," Instruments and experimental techniques 56, 309-316 (2013).

10441-6, Session 2

Raman lidar for remote controle explosives in the subway

Alexsandr S. Grishkanich, ITMO Univ. (Russian Federation); Dmitriy N. Redka, Saint Petersburg Electrotechnical Univ. "LETI" (Russian Federation)

Lidar has been designed for remote control of explosives in subway structures. The modular configuration allows detecting more than 4000 Raman shifts of various chemical, toxic or dangerous substances, explosives, derivatives, drugs and drugs. Ultraspectral selection of shifts is implemented. The modular lidar system allows the detection of polynitroaromatic compounds such as trinitrotoluene, trinitrobenzene, esters or nitroamines such as RDX, sentex and nitroglycerin, as well as a large number of various inorganic nitrates and chlorates. The system was developed for the remote search of 2,4,6-trinitrophenylmethylnitramine (tetryl) in a dense subway flow.

10441-7, Session 2

New approach for detection and identification of substances using THz TDS

Vyacheslav A. Trofimov, Dmitry Y. Zagursky, Irina G. Zakharova, M.V. Lomonosov Moscow State Univ. (Russian Federation)

We propose and discuss new effective approach for the detection and identification of substances using a THz TDS. For the detection and identification of substance we propose to use a substance emission at high frequencies corresponding to high energy levels excitation due to cascade mechanism of their excitation under the THz pulse action. The second approach is based on a possibility of observing the absorption frequencies of substance under the frequencies up-conversion.

To explain a physical mechanism of considered possibilities we make a computer simulation using 1D Maxwell's equations and density matrix formalism.

10441-8, Session 3

Automatic assessing properties of dynamic cameras for camera selection and rapid deployment of video-content-analysis tasks in large-scale ad-hoc networks

Richard J. M. den Hollander, Henri Bouma, Jeroen H. C. van Rest, Johan-Martijn ten Hove, Frank B. ter Haar, Gertjan J. Burghouts, TNO (Netherlands)

Video analytics is essential for managing large quantities of raw data that are produced by video surveillance systems (VSS) for the prevention, repression and investigation of crime and terrorism. Analytics is highly sensitive to changes in the scene, and for changes in the optical chain so a VSS with analytics needs careful configuration and prompt maintenance to avoid false alarms. However, there is a trend from static VSS consisting of fixed CCTV cameras towards more dynamic VSS deployments over public/private multi-organization networks, consisting of a wider variety of visual sensors, including pan-tilt-zoom (PTZ) cameras, body-worn cameras and cameras on moving platforms. This trend will lead to more dynamic scenes and more frequent changes in the optical chain, creating structural problems for analytics. If these problems are not adequately addressed, analytics will not be able to continue to meet end users' developing needs. In this paper, we present a three-part solution for managing the performance of complex analytics deployments. The first part is a register containing meta data describing relevant properties of the optical chain, such as intrinsic and extrinsic calibration, and parameters of the scene such as lighting conditions or measures for scene complexity (e.g. number of people). A second part frequently assesses these parameters in the deployed VSS, stores changes in the register, and signals relevant changes in the setup to the VSS administrator. A third part uses the information in the register to dynamically configure analytics tasks based on VSS operator input. In order to support the feasibility of this solution, we give an overview of related state-of-the-art technologies for autocalibration (self-calibration), scene recognition and lighting estimation in relation to person detection. The presented solution allows for rapid and robust deployment of Video Content Analysis (VCA) tasks in large scale ad-hoc networks.

10441-9, Session 3

Face recognition in the thermal infrared domain

Marcin Kowalski, Artur Grudzien, Norbert Palka D.D.S., Mieczyslaw Szustakowski, Wojskowa Akademia Techniczna im. Jaroslawa Dabrowskiego (Poland)

Biometrics refers to unique human characteristics. Each unique characteristic may be used to label and describe individuals and for automatic recognition of a person based on physiological or behavioral characteristics. One of the most natural for humans and the most popular biometric trait is a face. The most common research methods on face recognition are based on visible light. State-of-the-art face recognition systems operating in the visible spectrum achieve very high level of recognition accuracy under controlled environmental conditions. Thermal infrared imagery seems to be a promising alternative or complement to visible range imaging due to its relatively high resistance to illumination changes. A thermal infrared image of the human face presents its unique heat-signature and can be used for recognition. The characteristics of thermal images maintain advantages over visible light images, and can be used to improve algorithms of human face recognition in several aspects. Mid-wavelength or far-wavelength infrared also referred to as thermal infrared seems to be promising alternative. We present the study on 1:1 recognition in thermal domain. The paper presents challenges of face recognition systems in visible and infrared domain. We present step by step recognition process based on extraction of texture oriented facial features.

10441-10, Session 3

Three-dimensional measurement system for crime scene documentation

Marcin M. Adamczyk, Jakub Micho?ski, Elwira N. Ho?owko, Krzysztof Lech, Grzegorz M?czkowski, Pawe? Bolewicki, Warsaw Univ. of Technology (Poland); Kamil Januszkiewicz, Central Forensic Lab. of the Police (Poland); Robert Sitnik, Warsaw Univ. of Technology (Poland)

Three-dimensional measurements (such as photogrammetry, time-of-flight, structure-from-motion or structured-light techniques) are becoming a standard in the crime scene documentation process. The usage of 3D measurement techniques provide an opportunity to prepare more insightful investigation and helps to show every trace in the context of the entire crime scene.

In this paper we would like to present a hierarchical, three-dimensional measurement system that is designed for crime scenes documentation process. Our system reflects the actual standards in crime scene documentation process – it is designed to perform measurement in three stages. First stage of documentation, the most general, is prepared with a scanner

with rather low resolution but also big measuring volume – it is used for the whole scene documentation. Second stage is more detailed: medium resolution and average size of measuring volume for areas that required a more detailed approach. Third stage, most detailed: highest resolution with a small measuring volume for the smallest objects. Every stage of documentation is realized by a different 3D scanner: the first stage is realized by a commercial 3D time-of-flight scanner, the second and third stage are realized by structured-light 3D scanners that were constructed in our laboratory. Each scanner provides its own spatial resolution of 2.0, 0.3, and 0.05 mm, respectively.

The workflow during documentation process assumes using the first scanner for the whole scene documentation (it reflects the manual drawings of the scene that represent the plan of the crime scene). Then, areas that require more detailed scans can be scanned with higher resolution (these can be areas that are indicated by Technicians as significant for the documentation process – it reflects more detailed photos from crime scene). The last stage of documentation assumes the usage of the most precise scanner with the higher resolution: for some particularly important traces, blood spatters or any other important objects. The big advantage of our system is that the 3D model of a scene is built in the real-time on the crime scene.

The documentation process is supervised by a specialised PC application, that is a software platform for measurements management (connecting with scanners and carrying out measurements, automatic or semi-automatic data registration in the real time) and data visualisation (3D visualisation of documented scenes). It also provides a series of useful tools for crime-scenes technicians: virtual measuring tape, searching for sources of blood spatter, virtual walk on the crime scene and many others.

In this paper we present our measuring system and the developed software. We present the principles of operation of our developed structured-light scanners that are used as second and third stages of documentation. We also provide an outcome from research on metrological validation of scanners that was performed according to VDI/VDE standard. We also present an outcome from measurement sessions that were conducted on real crime scenes with cooperation with Technicians from Central Forensic Laboratory of Police.

10441-11, Session 4

Robust visual object tracking with interleaved segmentation

Peter Abel, Hilke Kieritz, Stefan Becker, Michael Arens, Fraunhofer-Institut für Optronik, Systemtechnik und Bildauswertung (Germany)

Visual object tracking is defined as the process of estimating the location and the dimensions of one or more objects over time by using a camera. We particularly focus on single-object short-term tracking in this work. Despite significant progress in this field, there are still challenges posed due to factors such as partial occlusion, deformation, motion blur, illumination variation, scale variations and et cetera. Especially, the tracking of deformable, non-rigid, or size-changing objects poses a challenging task to the trackers.

We present a new approach for tracking non-rigid, deformable objects in a video sequence by merging a tracker based on on-line boosting and a fast foreground background segmentation. Many well-established trackers employ axes-aligned bounding boxes with a fixed aspect-ratio as tracking states. However, this restriction may lead to tracker drifting, especially when non-rigid and articulated motions are involved in an object, since axes-aligned bounding boxes may contain a lot of background in these situations. In order to overcome such limitations, we start with an initial tracker that uses axes-aligned bounding boxes with fixed aspect-ratio as tracking states and extend this tracker by enabling the use of rotated rectangles as tracking states.

We dissolve the fixed aspect-ratio assumption by constructing a confidence map from the on-line boosting-based tracker. This confidence map is constructed by cumulatively adding several axes-aligned rectangular samples inside a map. The samples are additionally weighted by the corresponding sample confidence values which are gathered by applying the appearance model of the initial tracker. The emerging area in this confidence map is not strictly axes-aligned anymore and robustly describes the coarse location and dimension of the object. The precise object boundaries, however, cannot be obtained from this confidence map, since sample sizes and the feature sizes restrict the precision. In order to add precise object boundaries, we embed a foreground background segmentation algorithm which provides a precise, pixel-wise segmentation map of object area. The confidence map and the segmentation map are unified into one map. Inside the unified map, the object location as well as the dimension of the object are estimated via a continuous adaptive mean shift algorithm. As a result, our approach provides a rotated rectangle as tracking states, which enables a more precise description of non-rigid, deformable objects than axes-aligned bounding boxes.

Furthermore, we evaluate our tracker on the visual object tracking (VOT) benchmark dataset 2016 that contains labels for different visual attributes at every frame of a sequences. The attribute labels enable a profound evaluation for specific situations such as size changes of the object in following frames. The evaluation shows an enhancement in performance for objects that change the size in following frames as well as deforming objects. Moreover, our tracker performs better than the initial tracker during camera motion and motion changes of the object. Our evaluation also revealed that our tracker struggles under heavy illumination changes which can be led back on the foreground background segmentation module. This issue, however, is out of the scope of this work.

10441-12, Session 4

Tracking, aiming and hitting the UAV with ordinary assault rifle

Franti?ek Racek, Teodor Balá?, Jaroslav Krej?í, Martin Macko, Stanislav Procházka, Univ. of Defence (Czech Republic)

The usage of small-unmanned aerial vehicles (UAVs) is significantly increasing nowadays. They are being used as a carrier of military spy and reconnaissance devices (taking photos, live video streaming and so on), or as a carrier of potentially dangerous cargo (intended for destruction and killing). Both ways of utilizing the UAV cause the necessity to disable it. From the military point of view, to disable the UAV means to bring it down by a weapon of an ordinary soldier that is the assault rifle. This task can be challenging for the soldier because he needs to visually detect and identify the target, track the target visually and aim on the target. The final success of the soldier's mission depends not only on the said visual tasks, but also on the properties of the gun and ammunition.

Visual tracking of small unmanned aerial vehicles through the opto-mechanical, optical or electro-optical sight of assault rifle is a demanding task connected with many difficulties. First of all, the fundamental sight of the assault rifle is a collimator sight (red dot sight, reflex sight, holo-sight) or an open sight in the case of older rifle types. In both types, the magnification is equal to one. Alternatively, the soldier can use a telescope sight for more precise aiming. Typically, the magnification of the telescope sight of the assault rifle is of factor 3. Thus, the range of the reconnaissance task (detection, recognition or identification) can be determined based on the Johnson criterion. The magnification, properties and qualities of the applied sight determined not only the reach but also the aiming error. The aiming error caused by the weapon operator (soldier) is highly individual and is influenced by the training; let us say subjective influences. Nonetheless, the aiming error is also significantly dependent on the type, parameters and qualities of the used sight; let us say objective influences. Both, the subjective and objective influences are presented in the paper and are evaluated in experimental measurement and theoretical analysis. To disable (destroy) the UAV-type of

target the soldier must hit the target. There are several ways to calculate the hit probability. It is difficult to determine the UAV hit probability because of the target's irregular shape and its ability to maneuver quickly in 3D space. The computational method leads to Monte Carlo computational algorithms.

The paper deals with the usage of assault rifles for shooting aerial targets that have exceptional ability of spatial maneuvering.

10441-13, Session 4

3D noise-resistant segmentation and tracking of unknown and occluded objects using integral imaging

Doron Aloni, Yitzhak Yitzhaky, Ben-Gurion Univ. of the Negev (Israel)

Three dimensional (3D) object segmentation and tracking can be useful in various computer vision applications, such as security and defense. Recently, several methods have dealt with 3D tracking using an integral-imaging system. This kind of imaging system creates 3D computational imaging using a multi channels array that acquires the 3D scene from multiple perspective angles. The use of such data for object tracking can have two main advantages. The first is extra information on occluded objects resulting from the multiple image perspectives, and the second is the ability to detect a static object when it is isolated from its surrounding. The 3D computational reconstruction yields confocal images of different depths, where the focused regions in these images belong to objects at the depths of the computed images, while blurred regions don't. We present a method for 3D multiple-object tracking using computational integral imaging, based on 3D object segmentation. With regard to previous works in such a scenario, the proposed method performs the 3D tracking of objects without prior information about the objects in the scene, and it is efficient under severe noise conditions. The object isolation procedure was published previously (D. Aloni, Y. Yitzhaky, "Automatic 3D object localization and isolation using computational integral imaging", Applied Optics, 54, 6717-6724, (2015)). In this method blur characteristics are used in order to detect the 3D depth localization of the unknown objects. The main assumption is that the focused region consists of the highest frequencies along the reconstructed depth plane and therefore we can separate those regions from the entire image. Chronologically, the algorithm of the 3D tracking makes the following phases:

• Estimation of depth planes where objects exist - using absolute gradient magnitude (AGMR) between neighbored reconstructed planes.

• Object segmentation inside the detected depth plane – in this phase object segmentation is performed in every detected depth plane from phase 1. This segmentation is achieved using the Haar wavelet transform in the first scale with adaptive thresholding method (D. Aloni, Y. Yitzhaky, "Detection of Object Existence from a Single Reconstructed Plane Obtained by Integral Imaging", IEEE Photonics Technology Letters,26, 726-728, (2014)). The result from this operation is an edge image of the objects. This procedure is followed by a process of removing false edges The last operation in this segmentation process finds close contours of the detected objects using active contour method (D. Aloni, Y. Yitzhaky, " Effects of elemental-images' quantity on 3D segmentation using computational integral-imaging ", Applied Optics, 56, (2017)). After this stage we obtain segmented objects including their colors and textures.

• Feature extraction of the segmented objects – in this phase object features are extracted in order to have enough information for the tracking process. We used three intensity-based features and one shape feature.

• Feature-based tracking of the objects in the 3D space along the time axis.

This paper includes experimental results and also an optical design process which indicates the required geometrical parameters that affect the integral imaging system's depth of field and depth resolution.

10441-14, Session 4

Intelligent video monitoring system with the functionality of online recognition of people's behaviour and interactions between people

Konrad Wojciechowski, Marek Kulbacki, Polish Japanese Institute of Information Technology (Poland)

The intelligent video monitoring system entitled SAVA has been implemented as a prototype at the 9th Technology Readiness Level. The source of data are video cameras located in the public space that provide HD video streaming. The system enables identification and classification of such behaviours as: walking, running, sitting down, jumping, lying, getting up, bending, squatting, waving, and kicking. It also can identify interactions between persons, such as: greeting, passing, hugging, pushing, and fighting. The system has module-based architecture. The acquisition module retrieves an image in the MJPEG format from the Axis camera. The compression module, besides conducting trivial operations such as difference and dilatation/erosion, makes use of detection algorithms of background and movable areas. The path detection module searches for paths along which selected key points move. SURF/SIFT descriptors are used for determining the paths, and the Hungarian algorithm is applied for the pairing of the points. The detected paths that satisfy such requirements as the minimum number of frames and the trajectory length are transferred to the subsequent module. The path analysis module reconstructs trajectories of objects in order to determine a minimum bounding box for the object. The result of the module's operation is a contour of the analysed object in time, a unique identifier, and a reference to the source file. On the basis of the paths, the descriptor module determines descriptors of the movement performed by the detected object, constituting the grounds for the behaviour classification. The module of recognising actions classifies the object behaviour on the basis of the determined descriptors and of the base of recordings with annotations. The effect of the module's operation is a recognised action. The system achieves a classification correctness level of 80% when there are more than ten classes.

10441-15, Session 5

Transferring X-ray based automated threat detection between scanners with different energies and resolution

Matthew Caldwell, M. Ransley, Thomas W. Rogers, Lewis D. Griffin, Univ. College London (United Kingdom)

Previously, we investigated the use of Convolutional Neural Networks (CNNs) to detect so-called Small Metallic Threats (SMTs) hidden amongst legitimate goods inside a cargo container. We trained CNNs from scratch using a Threat Image Projection (TIP) framework [1] that generates realistic variation to robustify performance. We showed that by exploiting dual-energy and log-image transforms, tools often used by human operators in commercial cargo screening software, we could achieve 95% detection of containers that contained a single SMT, while raising 0.36% false positives on benign containers [2]. Moreover, the full cargo image was processed in 3s - much faster than a human operator for such complicated images.

One of the main problems in developing high performance Deep Learning algorithms for Automated Threat Detection (ATD) in security imagery, is the difficulty to obtain suitably large training datasets. In our previous work, we circumvented this problem using TIP and data augmentation.

Typically, when one trains an algorithm to perform an ATD task for a given threat on a given modality, one trains the system

on data that is (i) captured by that modality, and (ii) contains examples of the threats to be detected and examples of images with threats absent. So the data corresponds to the same task and same modality (type 1). However, in general there are three other types of data can be used for training ATD: same task and different modality (type 2); different task and same modality (type 3); and different task and different modality (type 4).

Researchers have already investigated performance using type 4 data by transfer learning CNN models from generic object recognition tasks on natural imagery to airport baggage imagery [3]. This gave promising results, even though the system had never previously `seen' X-ray images or threats before.

This paper reports investigations on (i) whether a system trained on type 2 data can improve performance when type 1 data is scant, and (ii) the best way of using types 1-4 in a training protocol using a network or multi-network system architecture. We show that by transfer learning a system trained on ATD for cargo (type 2), one can significantly boost detection performance in baggage and parcels over transfer learning from type 4 data [2].

This is an important result for the Security and Deep Learning communities, since it tests the generalisation ability of a CNN trained without real threat data and applied to a different higher resolution, lower energy imaging modality. And it does so in a real-life security-critical application.

[1] TW Rogers et al. (2016). Threat Image Projection (TIP) into X-ray images of cargo containers for training humans and machines. In: IEEE International Carnahan Conference on Security Technology.

[2] TW Rogers et al. (2017). A deep learning framework for the automated inspection of complex dual-energy x-ray cargo imagery. In: SPIE Defense+Security (to appear).

[3] S Akçay et al. (2016). Transfer learning using convolutional neural networks for object classification within x-ray baggage security imagery. In: IEEE International Conference on Image Processing.

10441-16, Session 5

On the application of semantic technologies to the domain of forensic investigations in financial crimes

Tobias Scheidat, Otto-von-Guericke Univ. Magdeburg (Germany) and Technische Hochschule Brandenburg (Germany); Ronny Merkel, Otto-von-Guericke-Univ. Magdeburg (Germany); Volker Krummel, Andreas Gerlach, Diebold Nixdorf, Inc. (Germany); Michala Weisensee, Jana Zeihe, SBSK GmbH & Co. KG (Germany); Jana Dittmann, Otto-von-Guericke-Univ. Magdeburg (Germany)

In daily police practice, forensic investigation of criminal cases in finance is mainly based on manual work and the experience of individual forensic expert, using only basic storage and data processing technologies. However, an individual criminal case does not only consist of the actual offence, but also of a variety of different aspects involved. Such aspects include, amongst others, the affiliation of an attacker to a criminal organisation, the usage of certain modi operandi, the search and instructing of accomplices, the acquisition of required expert knowledge as well as practical preparation steps (observing the victim, coding malware, stealing a getaway car, etc.). In order to solve a financial criminal case, an investigator has to take these aspects into consideration and to find interrelations between the different case entities (e.g. actors, used tools and weapons, exploited weaknesses, attacked targets, applied modi operandi, etc.) as well as interrelations to other cases (including those investigated by other authorities or other federal states). The required information about these different entities is often stored in distributed databases and mostly requires to be manually requested and processed by forensic investigators.

In this paper, the application of semantic technologies to the domain of forensic investigations is proposed at the example of financial crimes. Such combination allows for the modelling of specific case entities and their interrelations within and between cases. As a result, an explorative search of connections between case entities in the scope of an investigation as well as an automated derivation of conclusions from an established fact base is enabled. The proposed model is presented in the form of a crime field ontology (using the Ontology Web Language OWL), based on different types of knowledge obtained from three individual sources:

1. Online search: Enquiry of official and unofficial websites to gather information about real criminal cases (i.e. police press reports, newspapers), possibilities and/or instructions for concrete attacks, knowledge on buying or building hardware or software tools.

2. Forensic investigators: Interviews of forensic experts about special information regarding individual cases, general procedures of forensic investigations as well as typical modi operandi of crimes.

3. Captive interviews of detained criminals: Interviews of convicted criminals to achieve special and general knowledge on involved actors, criminal procedures, criminal organisations, preparation and execution of offences as well as obtained knowledge, contacts and specific money flows before during and after the crime.

The modelled crime field ontology is illustrated at two examples using the well known crime types of robbery by ATM blasting and data theft by NFC (near field communication) crowd skimming. Of these criminal modi operandi, anonymized fictional versions of real cases are modelled in OWL as well as visualized and exploratively searched using a proposed, Java-based investigators GUI. Modelled case entities include modi operandi, events, actors, resources, exploited weaknesses as well as flows of money, data and know how. The potential exploration of interrelations between the different case entities of such examples is illustrated in the scope of an exemplary fictitious investigation, highlighting the potential of the approach.

10441-17, Session 5

Automatic analysis of online image data for law enforcement agencies by concept detection and instance search

Maaike H. T. de Boer, Henri Bouma, Maarten C. Kruithof, Frank B. ter Haar, Noëlle M. Fischer, Laurens K. Hagendoorn, Bart Joosten, Stephan A. Raaijmakers, TNO (Netherlands)

The information available on-line and off-line, from open as well as from private sources, is growing at an exponential rate placing an increasing demand on the limited resources of Law Enforcement Agencies (LEAs). The absence of appropriate tools and techniques to collect, process, and analyze the volumes of complex and heterogeneous data has created a severe information overload. If a solution is not found, the impact on law enforcement will be dramatic, e.g. because important evidence is missed or the investigation time is too long. Furthermore, there is an uneven level of capabilities to deal with the large volumes of complex and heterogeneous data that come from multiple open and private sources at national level across the EU, which hinders cooperation and information sharing. As such there is a pertinent need to develop tools, systems and processes which expedite online investigations. In this paper, we describe analysis tools to identify and localize generic concepts, instances of objects and logos in images. We also describe how the incremental learning based on only few examples and the large-scale indexing is addressed in the concept detection and instance search. The search technology allows querying of the database by visual examples and by keywords. Our tools are packaged in a Docker container to guarantee easy deployment on a system and our tools exploit possibilities provided by open source toolboxes, to contribute to the technical autonomy of LEAs.

10441-18, Session 5

Optimizing a neural network for detection of moving vehicles in video

Noëlle M. Fischer, Maarten C. Kruithof, Henri Bouma, TNO (Netherlands)

In the field of security and defense, it is extremely important to reliably detect moving objects, such as cars, ships, drones and missiles. Detection and analysis of moving objects in cameras near borders could be helpful to reduce illicit trading, drug trafficking, irregular border crossing, trafficking in human beings and smuggling. Many recent benchmarks have shown that convolutional neural networks are performing well in the detection of objects in images. Most deep-learning research effort focuses on classification or detection on single images. However, the detection of dynamic changes (e.g., moving objects, actions and events) in streaming video is extremely relevant for surveillance and forensic applications. In this paper, we combine an end-to-end feedforward neural network for static detection with a recurrent Long Short-Term Memory (LSTM) network for multi-frame analysis. We present a practical guide with special attention to the selection of the optimizer and batch size. The end-to-end network is able to localize and recognize the vehicles in video from traffic cameras. We show an efficient way to collect relevant in-domain data for training with minimal manual labor. Our results show that the combination with LSTM improves performance for the detection of moving vehicles.

10441-19, Session 5

Deep learning-based fine-grained car make/model classification for visual surveillance

Erhan Gundogdu, ASELSAN A.S. (Turkey) and Middle East Technical Univ. (Turkey); Enes Sinan Parildi, ASELSAN A.S. (Turkey) and Bilkent Univ. (Turkey); Berkan Solmaz, Veysel Yucesoy, Aykut Koç, ASELSAN A.S. (Turkey)

Deep learning based methods have recently dominated the object recognition area. Moreover, fine-grained object recognition is also a potential computer vision problem to be addressed by utilizing the deep Convolutional Neural Networks (CNNs). Nevertheless, the main disadvantage of classification methods relying on deep CNN models is the need for considerably large amount of data. In addition, there exist relatively less amount of annotated data for a real world application, such as the recognition of car models in a traffic surveillance system. To this end, we mainly concentrate on the classification of fine-grained car make and/or models for visual scenarios by the help of two different domains. First, a large-scale dataset including approximately 900K images is constructed from a website which includes fine-grained car models. According to their labels, a state-of-the-art CNN model is trained on the constructed dataset. The second domain that is dealt with is the set of images collected from a camera integrated to a traffic surveillance system. These images, which are over 180K, are gathered by a special license plate detection method on top of a motion detection algorithm. Once the license plate is localized by the system, an appropriately selected size of the image is cropped from the region of interest provided by the detected license plate location. These sets of images and their provided labels for more than 30 classes are employed to fine-tune the CNN model which is already trained on the large scale dataset described above. In order to fine-tune the network, the last two fully-connected layers are randomly initialized. The major reason for this kind of process is that the lower layers of the network learn common car model patterns to both of the domains. On the other hand, the layers towards the top layers learn representations, which are specific to the individual domains. In the transfer learning and domain-adaptation literature, these kinds of approaches are studied in the publicly available datasets. Yet, a real-field implementation integrated to a real world traffic system is required. Hence, in this work, the domain adaptation has been successfully addressed by utilizing both the limited annotated data of the traffic field and a large-scale dataset with available annotations. Our experimental results both in the validation dataset and the real-field results show that the proposed methodology is superior over the conventional deep CNN models. Moreover, a large-scale dataset is exploited to obtain much better recognition results for the relatively limited dataset collected from the field. This leads to a performance uplift of the recognition of this limited dataset.

10441-20, Session 6

Control system of the inspection robots group applying auctions and multi-criteria analysis for task allocation

Wawrzyniec Panfil, Wojciech Moczulski, Silesian Univ. of Technology (Poland)

IMPORTANT: Paper submitted for “Robots for counterterrorism and security / session organized by PIAP”

The goal of the research was to elaborate a control system of a mobile robots group intended for carrying out inspection missions. The main research problem was to define such a control system in order to facilitate a cooperation of the robots resulting in realization of the committed inspection tasks.

Taking into account the current state-of-the-art in the area of the multi-robot control systems it was stated that a significant influence on the effective operation of these systems has an appropriate allocation of tasks among members of the multi-robot group. There were identified two fundamental problems - resolving them will allow to realize the tasks (missions) by the robots more effectively. Many of the well-known control systems use auctions for tasks allocation, where a subject of an auction is a task to be allocated. It seems that in the case of missions characterized by much larger number of tasks than number of robots it will be better if robots (instead of tasks) are subjects of auctions. The second identified problem concerns the one-sided robot-to-task fitness evaluation. It was stated that simultaneous assessment of the robot-to-task fitness and task attractiveness for robot will affect positively for the overall effectiveness of the multi-robot system performance.

To prove the correctness of the mentioned hypotheses there was proposed the methodology of building the control systems of multi-robot groups and basing on that there was elaborated the formal description of the system. This system allows to assign tasks to robots using various methods for evaluation of fitness between robots and tasks, and using some tasks allocation methods. There was proposed the method for multi-criteria analysis, which is composed of two assessments, i.e. robot’s concurrency position for task among other robots and task’s attractiveness for robot among other tasks. Furthermore, there were proposed methods for tasks allocation applying the mentioned multi-criteria analysis method. There was also elaborated a behavior-based controller for robots’ motion control.

The verification of both the elaborated system and the proposed tasks’ allocation methods was carried out with the help of simulated experiments. The object under test was a group of inspection mobile robots being a virtual counterpart of the real mobile-robot group owned by the Department of Fundamentals of Machinery Design, Silesian University of Technology. The analysis of the achieved verification results proved the correctness of the formulated theses.

10441-21, Session 6

Autonomous mobile platform with simultaneous localisation and mapping system for patrolling purposes

?ukasz Mitka, Tomasz Buratowski, AGH Univ. of Science and Technology (Poland)

The work describes an autonomous mobile platform for supervision and surveillance purposes. The system can be adapted for mounting on different types of vehicles. The platform is based on a SLAM navigation system which performs a localization task. Sensor fusion including laser scanners, IMU, odometry and GPS lets the system determine its position in a certain and precise way. The platform is able to create a 3D model of a supervised area and export it as a point cloud. Model generation process is combining laser scanner data, IMU, GPS and odometry with use of the Rao-Blackwellized particle filter. Main concept of this filter in SLAM application is to estimate the joint posterior p(x_(1:t),m|z_(1:t),u_(1:t-1)) about the map m and the trajectory x_(1:t)=x_1,...,x_t of the robot. The estimation is computed using the following equation:

p(x_(1:t),m|z_(1:t),u_(1:t-1))=p(m|?x_(1:t),z?_(1:t))?p(x_(1:t) |z_(1:t),u_(1:t-1))

where z_(1:t)=z_1,...,z_t are the laser scans and u_(1:t-1)=u_1,... ,u_(t-1) is the odometry input obtained by the robot. The estimate of p(x_(1:t) |z_(1:t),u_(1:t-1)) can be obtained with use of the particle filter, where each particle represents a potential trajectory of the robot. Moreover individual map is associated with each particle. The particle filtering process can be performed in the following steps: 1. Sampling: A generation of particles {x_t^((i)) } is obtained from generation {x_(t-1)^((i)) } by sampling from the proposal distribution ϖ, which could be probabilistic odometry motion model.

2. Importance weighting: each particle gets assigned individual importance weight w_t^((i))

w_t^((i))=p(x_(1:t)^((i)) |z_(1:t),u_(1:t-1))/ϖ(x_(1:t)^((i)) |z_(1:t),u_(1:t-1))

3. Re sampling: The particles are drawn with the replacement proportional to their importance weight.

4. Map estimation: For each particle, the corresponding map estimate p(m^((i)) |?x_(1:t)^((i)),z?_(1:t)) is computed based on the trajectory x_(1:t)^((i)) of that sample and the history of scans z_(1:t)

The system can operate both inside and outside as the navigation algorithm is resistant to typical localization errors caused by wheel slippage or temporal GPS signal loss. The system is equipped with a path-planning module which allows operating in two modes. The first mode is for periodical observation of points in a selected area. The second mode is turned on in case of an alarm. When it is called, the platform moves with the fastest route to the place of the alert. The path planning is always performed online with use of the most current scans, therefore the platform is able to adjust its trajectory to the environment changes or obstacles that are in the motion. The control algorithms are developed under the Robot Operating System (ROS) since it comes with drivers for many devices used in robotics. Such a solution allows for extending the system with any type of sensor in order to incorporate its data into a created area model. Proposed appliance can be ported to other existing robotic platforms or used to develop a new platform dedicated to a specific kind of surveillance.

10441-22, Session 6

Unmanned ground systems: state of the art and technology gaps

Józef Wrona, Wojskowa Akademia Techniczna im. Jaroslawa Dabrowskiego (Poland) and Industrial Research Institute for Automation and Measurements (Poland); Jakub Glowka, Mateusz Macia?, Industrial Research Institute for Automation and Measurements (Poland); Tomasz Muszynski, Wojskowa Akademia Techniczna im. Jaroslawa Dabrowskiego (Poland)

The paper presents state of the art and technology gaps of Unmanned Ground Systems (UGS). If it is true that fully autonomous unmanned systems are already a reality, the trend to develop cooperative systems of unmanned systems (system of systems) demands again the availability of reliable technologies.

There will be described an extensive state of the art review to cover the currently available UGS products oriented to the military domain, the research areas that are relevant for the development of new UGS solutions, and, especially, the emerging technologies in the autonomous domain. Technological and non-technological aspects that may hamper the development of UGS solutions that fully achieve the operational requirements will be discussed.

In the state of the art domain there will be discussed the relevant research areas and robot autonomy. However, in the domain of technology gaps identification there will be described gaps identification process, applied methodology and then gaps and measures.

This work was performed in the EDA project UGS-LIS.

10441-23, Session 6

Autonomous mobile robotic system for supporting counterterrorist and surveillance operations

Wojciech Moczulski, Silesian Univ. of Technology (Poland) and SkyTech Research Sp. z o.o. (Poland); Kazimierz Bulandra, KABE Sp. z o.o. (Poland); Marek Adamczyk, SkyTech Research Sp. z o.o. (Poland)

“Robots for counterterrorism and security / session organized by PIAP”

Contemporary research on mobile robots concerns applications to counterterrorist and surveillance operations. The goal of the research is to develop systems that are capable of supporting the police and special forces by carrying out such operations.

The paper deals with a dedicated robotic system that can be implemented for surveillance of large objects such as airports, factories, military bases, and many others. The goal of operation of the system is to trace unauthorised persons who try to enter to the guarded area, document the intrusion and report it to the surveillance centre, and then warn the intruder by sound messages and eventually subdue him/her by stunning through acoustic effect of great power.

The system consists of several parts. An armoured four-wheeled robot assures required mobility of the system. The robot is equipped with a set of sensors including 3D mapping system, IR and video cameras, and microphones. The robot can communicate with the central control station (CCS) by means of a wideband wireless encrypted communication system. A control system of the robot can operate autonomously, and under remote control. In the autonomous mode the robot follows the path that has been planned by the CCS. Once an intruder has been detected, the robot can adopt its plan to allow tracking him/her. Furthermore, special procedures of treatment of the intruder are applied including warning about the breach of the border of the protected area, and incapacitation of an appropriately selected very loud sound until a patrol of guards arrives. In case of getting stuck the robot can contact the operator who can remotely solve the problem the robot is faced with.

The partners expect implementation of an industrial version of the system in late 2018. Integration of the system with a Friend-or-Foe component will be carried out as well.

10441-24, Session 6

Modular robotic system for forensic investigation support

Grzegorz Kowalski, Industrial Research Institute for Automation and Measurements (Poland); Jakub Glowka, Mateusz Macia?, Industrial Research Institute for Automation and Measurements (Poland); Slawomir Puchalski, Industrial Research Institute for Automation and Measurements (Poland)

Forensic investigation on the crime scene is an activity that requires not only knowledge about the ways of searching for evidence, collecting and processing them. In some cases the area of operation might not be properly secured and poses threat to human health or life. Some devices or materials may be left intentionally or not to injure potential investigators.

Besides conventional explosives, threats can be in form of CBRN materials, which have not only immediate effect on the exposed personnel, but can contaminate further people, when being transferred for example on clothes or unsecured equipment.

In this case a risk evaluation should be performed, that can lead to conclusions that it is too dangerous for investigators to work. In that kind of situation remote devices, which are able to examine the crime scene and secure samples, can be used.

In the course of R&D activities we developed a system, which is based on small UGV capable of carrying out inspection of suspicious places and securing evidence, when needed. The system consists of remotely controlled mobile robot, its control console and a set of various inspection and support tools, that enable detection of CBRN threats as well as revelation, documentation and securing of the evidence.

This paper will present main features of the system, like mission adjustment possibilities and communication aspects, and also examples of the forensic accessories.

Conference 10442: Quantum Technologies and Quantum Information Science

Wednesday - Thursday 13–14 September 2017

Part of Proceedings of SPIE Vol. 10442 Quantum Information Science and Technology III

10442-1, Session 1

Device-indpendent randomness amplification against non-signaling adversaries with weakened security assumptions *(Invited Paper)*

Hanna Wojewódka, Univ. of Silesia (Poland); Fernando G. S. L. Brandao, California Institute of Technology (United States); Andrzej Grudka, Adam Mickiewicz Univ. (Poland); Karol Horodecki, Michal Horodecki, Univ. Gdansk (Poland); Pawel Horodecki, Gdansk Univ. of Technology (Poland); Ravishankar Ramanathan, Univ. Libre de Bruxelles (Belgium); Maciej Stankiewicz, Univ. Gdansk (Poland)

The work concerns the problem of finding a protocol for randomness amplification secure against non-signaling adversary with polynomial number of devices, which allows for correlations between

the device and the source of weak randomness. We focus on the epsilon-Santha-Vazirani sources, and provide two results in this direction.

First we revisit the seminal protocol of R. Colbeck and R. Renner (CR protocol) of randomness amplification using Santha-Vazirani (SV) sources, and prove its security relaxing partially assumptions of independence between the devices and the source at a price of narrowed range of epsilon. The relaxation allows that the SV source can indicate as a final device from which randomness is taken choosen with uniform probability from the insecure devices. The proof of relaxation bases on the assumption which is a generalization of Santha-Vazirani condition - the SV condition for boxes: there does not exist a device such that given its inputs and outputs one can get to know the value of SV source by more than epsilon.

Second, we prove security of the CR protocol allowing arbitrary correlations between SV source and device, up to the mentioned SV-box condition, and the assumption that the devices are not correlated with each other. We prove that

if the final device chosen in the protocol was not secure, an independent tester could guess the value of SV source bits more than the SV-box condition allows. The strategy of a tester is to choose a random device out of the ones which do not satisfy condition of the Chain Bell inequality. The idea of the proof of the second result indicates that the CR protocol may be secure under attack which arbitrarily correlates SV with devices of arbitrary type, and is promising in studying this problem.

10442-3, Session 1

On problems in security of quantum key distribution raised by Yuen

Takehisa Iwakoshi, Tamagawa Univ. (Japan)

This study will explain problems in current security proofs in Quantum Key Distribution (QKD) listed by H. P. Yuen [1], especially focusing on the new security criterion named Bit-Error-Rate (BER) Guarantee, which measures BER for the eavesdropper in the guessed key by the eavesdropper compared to the legitimate users' key. Currently, the security of QKD is evaluated by the trace distance between an actually distributed quantum state and the ideal quantum state where the eavesdropper's quantum system is separated from the legitimate users' quantum systems. In 2010, Yuen showed that the success probability for the eavesdropper in guessing the correct key would be given by the trace distance [2], which was shown again by C. Portmann and R. Renner in 2014 [3]. Furthermore, Yuen listed more problems in the current security proofs of QKD, especially emphasized the importance of BER Guarantee. Here the author tries some explanations shortly how such problems were addressed. Firstly, it has been widely perceived that the trace distance is the maximum failure probability in distributing an ideal key [4-6], however, the success probability for the eavesdropper in guessing the correct key can be greater than the trace distance itself. Secondly, Yuen numerically explained that the distributed key is far from the ideal key even with the recent smallest value of the trace distance [7]. Thirdly, he explained the derivation of the secure key rate is not evaluated validly. Fourthly, he criticized the usefulness of Privacy Amplification, that it may rather gain the success probability for the eavesdropper in guessing the correct key. In addition, he proposed a new security measure named BER Guarantee. Therefore, this study also focusses on the BER Guarantee in case of Entangling-Probe Attack [8-10] on BB84 protocol.

References

[1] H. P. Yuen, "Security of Quantum Key Distribution," IEEE Access 4, p724-749, (2016).

[2] H. P. Yuen, "Fundamental Quantitative Security In Quantum Key Generation," Physical Review A 82.6 062304 (2010), or arXiv:1008.0623v3, quant-ph, (2010)

[3] C. Portmann and R. Renner, "Cryptographic security of quantum key distribution," arXiv:1409.3525v1, quant-ph (2014)

[4] R. König, et al., Physical Review Letters 98.14 140502 (2007).

[5] V. Scarani, et al., Reviews of modern physics 81.3 1301 (2009).

[6] F. Benatti, et al., "Quantum Information, Computation and Cryptography: An Introductory Survey of Theory, Technology and Experiments," Springer Science & Business Media, after Eq.(42), (2010).

[7] H. Takesue, et al., "Experimental quantum key distribution without monitoring signal disturbance," Nature Photonics (2015).

[8] C. A. Fuchs, and A. Peres, Phys. Rev. A 53, 2038 (1996).

[9] B. A. Slutsky, R. Rao, P. C. Sun, and Y. Fainman, Phys. Rev. A 57, 2383 (1998).

[10] H. E. Brandt, Phys. Rev. A 71, 042312 (2005).

10442-4, Session 2

Significant-loophole-free test of bell's theorem with entangled photons *(Invited Paper)*

Marissa Giustina, Institut für Quantenoptik und Quanteninformation (Austria) and Univ. Wien (Austria); Marijn A. M. Versteegh, Austrian Academy of Sciences (Austria) and Univ. Wien (Austria); Sören Wengerowsky, Institut für Quantenoptik und Quanteninformation (Austria) and Univ. Wien (Austria); Johannes Handsteiner, Armin Hochrainer, Institut für Quantenoptik und Quanteninformation (Austria) and Univ. Wien (Austria); Kevin Phelan, Institut für Quantenoptik und Quanteninformation (Austria); Fabian O. Steinlechner, Institut für Quantenoptik und Quanteninformation (Austria); Johannes Kofler, Max-Planck-Institut für Quantenoptik (Germany); Jan-Ake Larsson, Linköping Univ. (Sweden); Carlos Abellán, Waldimar Amaya, ICFO - Institut de Ciències Fotòniques (Spain); Valerio Pruneri, Morgan W. Mitchell, ICFO - Institut de Ciències Fotòniques (Spain) and Institució Catalana de Recerca i Estudis Avançats (Spain); Jörn Beyer, Physikalisch-Technische Bundesanstalt (Germany); Thomas Gerrits,

Adriana E. Lita, Lynden K. Shalm, Sae-Woo Nam, National Institute of Standards and Technology (United States); Thomas Scheidl, Institut für Quantenoptik und Quanteninformation (Austria) and Univ. Wien (Austria); Bernhard Wittmann, Anton Zeilinger, Institut für Quantenoptik und Quanteninformation (Austria) and Univ. Wien (Austria)

Local realism is the worldview in which physical properties of objects exist independently of measurement and where physical influences cannot travel faster than the speed of light. Bell's theorem states that this concept is incompatible with the predictions of quantum mechanics, as is expressed in Bell's inequalities. Previous experiments convincingly produced measurement outcomes that violated Bell's inequality and therefore supported the quantum predictions. Yet, every experiment requires assumptions that provide loopholes for a local realist explanation.

The most well-known assumptions and corresponding loopholes are the following:

The detection loophole relates to the fair-sampling assumption, stating that the detected sub-ensemble of the created entangled photon pairs is representative for the entire ensemble. Otherwise, it would be conceivable that the detected sub-ensemble violates the Bell inequality, while the entire ensemble doesn't. This loophole is closed by using a source of entangled photons with a very high heralding efficiency and a highly efficient detection system.

The locality/signaling loophole arises from the assumption that the two parties cannot communicate with each other: the setting choice of one party can not influence the measurement outcome of the other party. To make sure, that this loophole is not exploited, it is necessary to space-like separate the measurement setting choice on one side and the measurement on the other side.

The Freedom-of-Choice assumption is, that that the setting choices are "free and independent" of each other and of the hypothetical hidden variables which could be used to complement quantum mechanics in order to be a local-realist theory. To address this loophole, one has to make an auxiliary assumption to confine the regions in space-time, where hidden influences could be produced. In this case we chose the emission event of the entangled photons. In order to make sure, that this loophole is not exploited, the setting choices have to be space-like separated from the emission event of the photon pair.

Another assumption is the no-memory assumption: Local apparata could remember the outcome of previous trials and therefore alter the statistics. This loophole was closed by avoiding the assumption of independent and identical (i. i. d.) trials and Gaussian statistics.

Here, we report a Bell test that closes the most significant of these loopholes simultaneously. Pairs of polarization-entangled photons are produced by spontaneous parametric downconversion in a ppKTP crystal in a Sagnac-type configuration. The photon pairs are split and coupled into single mode fibers to the detection modules, 28 meters away from the source. At the detection modules, a decision is made by a random number generator based on spontaneous emission, in which basis the photon is measured just before it arrives. The detection is performed using superconducting transition-edge sensors.

Using a well-optimized source of entangled photons, rapid setting generation, and highly efficient superconducting detectors, we observe a violation of a Bell inequality with high statistical significance. The purely statistical probability of our results to occur under local realism does not exceed

3.74?10^-31, corresponding to an 11.5 standard deviation effect.

10442-5, Session 2

On photonic spectral entanglement improving quantum communication

Karolina Sedziak, Mikolaj Lasota, Piotr Leszek Kolenderski, Nicolaus Copernicus Univ. (Poland)

Single-photon sources are crucial components for the implementation of quantum communication (QC) protocols. However, photons emitted by some of the most popular types of realistic sources are spectrally broadband. Due to this drawback, the signal emitted from such sources is typically affected by the effect of temporal broadening during its propagation through telecommunication fibers exhibiting chromatic dispersion. Such problem can be observed e.g. when using sources based on the process of spontaneous parametric down-conversion (SPDC). In the case of long-distance QC the phenomenon of temporal broadening can significantly limit the efficiency of temporal filtering. It is a popular method for decreasing the number of registered errors, basing on the reduction of the duration time of the detection windows.

10442-6, Session 2

Reducing detection noise of a photon pair in a dispersive medium by controlling its spectral entanglement

Mikolaj Lasota, Karolina Sedziak, Piotr Leszek Kolenderski, Nicolaus Copernicus Univ. (Poland)

Single-photon sources are crucial components for the implementation of quantum communication protocols. However, photons emitted by some of the most popular types of realistic sources are spectrally broadband. Due to this drawback, the signal emitted from such sources is typically affected by the effect of temporal broadening during its propagation through telecommunication fibers which exhibit chromatic dispersion. Such problem can be observed e.g. when using sources based on the process of spontaneous parametric down-conversion (SPDC). In the case of long-distance quantum communication temporal broadening can significantly limit the efficiency of temporal filtering. It is a popular method, which relies on the reduction of the duration time of the detection window, used for decreasing the number of registered errors.

In this work we analyzed the impact of the type of spectral correlation within a pair of photons produced by the SPDC source on the temporal width of those photons during their propagation in dispersive media. We found out that in some situations this width can be decreased by changing the typical negative spectral correlation into positive one or by reducing its strength. This idea can be used to increase the efficiency of the temporal filtering method. Therefore, it can be applied in various implementations of quantum communication protocols.

As an example of the application we subsequently analyzed the security of a quantum key distribution (QKD) scheme based on single photons. The investigation was performed for the configuration with the source of photons located in the middle between the legitimate participants of a QKD protocol (called typically Alice and Bob). We demonstrated that when the information about the emission time of the photons produced by the SPDC source is not distributed to Alice and Bob, the maximal security distance can be considerably extended by using positively correlated photons, while in the opposite case strongly (no matter positively or negatively) correlated photons are optimal. We also found out that the results of our calculation may be very sensitive to the spectral widths of the photons produced by the SPDC source. In addition, we concluded that in realistic situation Alice and Bob would have to optimize their source over both the spectral widths of the generated photons and the type of spectral correlation in order to maximally extend the security distance.

The results of our work are, in particular, important for the QKD systems utilizing commercial telecom fibers populated by strong classical signals. In those systems temporal filtering

method can be used to reduce not only the dark counts registered by the detection system, but also the channel noise originating from the process of Raman scattering, which is the main factor limiting their performance.

10442-23, Session 2

Removing the post-selection loophole from energy-time Bell tests *(Invited Paper)*

Guilherme Barreto Xavier, Linköping Univ. (Sweden)

Fundamental tests of local realism, the so-called Bell tests, have been performed extensively over the past decades on a wide spectrum of physical systems. On a more practical aspect, they are a major component in the field of secure quantum communications. In this sense, Bell tests based on energy-time entanglement are particularly relevant due to their suitability to long-distance transmission over optical fibers. A long-standing loophole, due to the post-selection procedure in the standard adopted energy-time scheme, has been recently addressed with the geometrically modified "Hug" configuration. Here we will review recent experiments where the Hug configuration was used to perform a Bell inequality violation over optical fibers in the laboratory and over deployed optical networks. Finally, fresh results where a fully automated Bell test, based on the Hug configuration, was carried out for the first time will be presented.

10442-7, Session 3

Approaches to a global quantum key distribution network *(Invited Paper)*

Md Tanvirul Islam, Robert Bedington, Ctr. for Quantum Technologies (Singapore); Douglas K. Griffin, Russell Boyce, UNSW Canberra (Australia); Christian Kurtsiefer, Alexander Ling, Ctr. for Quantum Technologies (Singapore)

Progress in quantum computers and computational power threatens to weaken existing public key encryption. A global quantum key distribution (QKD) network can play a role in computational attack-resistant encryption. Such a network could use a constellation of airships and satellites as trusted nodes to facilitate QKD between any two points on the globe on demand. This requires both satellite-to-ground and inter-satellite links. However, the prohibitive cost of traditional satellite based development limits the experimental work demonstrating relevant technologies. To accelerate progress towards a global network, we use an emerging class of shoe-box sized spacecraft known as CubeSats. We have designed an entangled photon pair source that can operate on board CubeSats. The robustness and miniature form factor of the entanglement source makes it especially suitable for performing pathfinder missions. Using this design, we have performed a feasibility study for a satellite-to-satellite QKD demonstration mission in collaboration with the University of New South Wales; Canberra. This mission concept uses two 6U CubeSats in low Earth orbit and aims to demonstrate QKD between them over varying separations.

10442-8, Session 3

Enhancing implementation security of QKD *(Invited Paper)*

Kiyoshi Tamaki, Univ. of Toyama (Japan)

Quantum key distribution (QKD) is claimed to achieve information theoretical security, i.e., provable security against any possible eavesdropping. Unfortunately, however, such a high security can be obtained only in theory so far, and we have to make more efforts to guarantee implementation security of QKD, i.e., the security when we implement QKD in reality. Fortunately, thanks to the finding of the measurement device independent QKD, any security loopholes in measurement units in QKD apparatus have been closed, and the next step is securing sending devices.

In this talk, we introduce our recent results regarding with counter-measures against security loopholes in sending devices. It includes the loss-tolerant QKD, secure QKD in the presence of side-channel attacks, and their generalizations. We also present the security of QKD with iterative sifting.

Some results presented in this talk are based on joint works with Koji Azuma, Marcos Curty, Nobuyuki Imoto, Go Kato, Charles C. W. Lim, Hoi-Kwong Lo, Marco Lucamarini, and Akihiro Mizutani (in alphabetical order).

10442-9, Session 3

Continuous-Variable QKD implementation using pilot assisted synchronization

Lucian Corneliu Comandar, Hans H. Brunner, Fotini Karinou, Fred Fung, Stefano Bettelli, David Hillerkuss, Spiros Mikroulis, Qian Yi, Dawei Wang, Maxim Kuschnerov, Changsong Xie, Andreas Poppe, Momtchil Peev, Huawei Technologies Co., Ltd. (Germany)

Quantum key distribution (QKD) has been subject to constant development and research since its original proposal, particularly using discrete variable implementations [1]. This was enabled by advances in terms of detection techniques, protocols and security analyses resulting in breakthroughs in terms of both key rates and distance. Continuous variable (CV) QKD, even though less researched, is considered more resilient to noise caused by classical communication multiplexing [2]. Furthermore, experimental implementations of CV-QKD systems are realized using mature technologies developed for classical communication.

Traditionally, CV-QKD systems use a co-propagating laser signal that serves as local oscillator (LO) in Bob's receiver [3], which may open security loopholes as it allows the eavesdropper Eve to manipulate the LO intensity. Furthermore, the channel losses have to be compensated for the co-propagating LO, requiring large optical power on the transmitter side. Recently, more practical implementations using a separate laser as local LO in Bob's receiver synchronized using a pilot tone were proposed [4-6]. This removes the possibility for LO attacks and enables high local oscillator powers on the coherent detector.

Here, we present the development of a CV-QKD system using the pilot tone assisted scheme. Alice prepares weak coherent pulses that are modulated using QPSK at a repetition rate of 10 MHz. A pilot tone serves as frequency reference for Bob. The pilot tone has a power of 30 dB larger than the quantum signal and a frequency offset of 25 MHz with respect to the quantum signal. On Bob's side, signal and pilot are mixed with a strong LO (>6 dBm) before reaching a balanced detector with a shot noise to excess noise ratio exceeding 20 dB. The electrical signal is measured with a digitizer at a sampling rate of 200 MSa/s and 14 bit resolution. The frequency information obtained from the pilot tone is used to compensate for frequency drifts and laser phase noise. Subsequently, the QPSK signal is demodulated and the security analysis is applied [7]. We further study the effect of Raman scattering and four wave mixing in a multiplexing configuration with 20 classical channels, each with a launch power of -1 dBm, confirming the feasibility of distilling a usable secure key rate for co-propagation of classical signals with our CV-QKD signal over distances of several km.

[1] E. Diamanti, H.-K. Lo, B. Qi and Z. Yuan, "Practical challenges in quantum key distribution", Npj Quantum Information 2 16025 (2016);

[2] R. Kumar et al. "Coexistence of continuous variable QKD with intense DWDM classical channels", New J. Phys. 17 043027,

(2015);

[3] P. Jouguet, S. Kunz-Jacques, A. Leverrier, P. Grangier, E. Diamanti, "Experimental demonstration of long-distance continuous-variable

quantum key distribution", Nat. Photonics 7, 378 (2013);

[4] B. Qi, P. Lougovski, R. Pooser, W. Grice and M. Bobrek, "Generating the Local Oscillator "Locally" in Continuous-Variable Quantum Key Distribution Based on Coherent Detection", Phys. Rev. X 5, 041009 (2015);

[5] D. Huang, P. Huang, D. Lin, C. Wang and G. Zeng, "High-speed continuous-variable quantum key distribution without sending a local

Oscillator", Opt. Lett. 40, 3695 (2015).

[6] D. Soh, C. Brif, P. Coles, N. Lütkenhaus, R. Camacho, J. Urayama, and M. Sarovar, "Self-Referenced Continuous-Variable Quantum

Key Distribution Protocol," Phys. Rev. X 5, 041010 (2015).

[7] A. Leverrier et al. "Continuous-variable quantum-key-distribution protocols with a non-Gaussian modulation" Phys. Rev. A83, 042312 (2011).

10442-10, Session 3

Multimode entanglement assisted QKD through a free-space maritime channel

John Gariano, Ivan B. Djordjevic, The Univ. of Arizona (United States)

When using quantum key distribution (QKD), one of the tradeoffs for security is that the generation rate of a secrete key is typically very low. Recent works have shown that using a weak coherent source allows for higher secret key generation rates compared to an entangled photon source, when a channel with low loss is considered. In most cases, the system that is being studied is over a fiber-optic communication channel. Here a theoretical QKD system using the BB92 protocol and entangled photons over a free-space maritime channel with multiple spatial modes is presented. The entangled photons are generated from a spontaneous parametric down conversion (SPDC) source of type II. To employ multiple spatial modes, the transmit apparatus will contain multiple SPDC sources, all driven by the pump lasers assumed to have the same intensity. The receive apparatuses will contain avalanche photo diodes (APD), modeled based on the NuCrypt CPDS-1000 detector, and located at the focal point of the receive aperture lens. The transmitter is assumed to be located at Alice and Bob will be located 30 km away, implying no channel crosstalk will be introduced in the measurements at Alice's side due to turbulence. To help mitigate the effects of atmospheric turbulence, adaptive optics will be considered at the transmitter and the receiver. An eavesdropper, Eve, is located 15 km from Alice and has no control over the devices at Alice or Bob. Eve is performing the intercept resend attack and listening to the communication over the public channel. Additionally, it is assumed that Eve can correct any aberrations caused by the atmospheric turbulence to determine which source the photon was transmitted from. One, four and nine spatial modes are considered with and without applying adaptive optics and compared to one another.

10442-11, Session 4

Covert quantum communication *(Invited Paper)*

Juan Miguel Arrazola, Valerio Scarani, Ctr. for Quantum Technologies (Singapore)

Encryption is not enough when the sole fact that two parties are communicating can be incriminating to them. In such cases, we require methods for covert communication. In this work, we extend covert communication to the quantum regime by showing that covert quantum communication is possible over optical channels with noise arising either from the environment or from the sender's lab. In particular, we show that sequences of qubits can be transmitted covertly by using both a single photon and a coherent state encoding. We provide a simple protocol for covert quantum communication and derive analytical bounds on the probability that an adversary can detect the communication. We also analyze the performance of the protocol in a realistic setting with noise originating from background thermal radiation.

We study the possibility of performing covert quantum key distribution and show that positive key rates and covertness can be achieved simultaneously. Covert communication requires a secret key between sender and receiver, which raises the problem of how this key can be regenerated covertly. We show that covert QKD consumes more key than it can generate and propose instead a hybrid protocol for covert key regeneration that uses pseudorandom number generators (PRNGs) together with covert QKD to regenerate secret keys. The security of the new key is guaranteed by QKD while the security of the covert communication is at least as strong as the security of the PRNG.

10442-12, Session 4

Noise effects in quantum-limited optical communication with very low signal powers *(Invited Paper)*

Marcin Jarzyna, Piotr Kuszaj, Aleksandra Klimek, Victoria Lipinska, Michal Jachura, Wojciech Wasilewski, Konrad Banaszek, Univ. of Warsaw (Poland)

We discuss noise effects in strategies to reach the maximum transmission rate of a lossy narrowband optical channel under the constraint of a low mean photon number per time bin. When direct detection is used at the output, the ultimate capacity can be approached by optimizing pulse position modulation (PPM) or generalized on-off keying (GOOK) with respect to code parameters. We present an approximate analytical formula for the PPM and GOOK transmission rates, which quantifies the effects of photon statistics in terms of the g(2) normalized second-order intensity correlation function of the light source, and analyse effects of dark counts. The highly imbalanced instantaneous power distribution for PPM and GOOK encodings can be remedied by the use of binary phase shift keying (BPSK) with a joint detection receiver based e.g. on quantum memories. We show that for this scheme, the transmission rate in the presence of phase noise is equivalent to that of PPM and GOOK with super-Poissonian light statistics and dark counts, retaining the improvement over indvidual detection.

10442-13, Session 4

Satellite-Earth quantum channel with adaptive optics coupling to single-mode fibers

Michael B. Flanagan, Brett A. Sickmiller, Leidos, Inc. (United States); Mark T. Gruneisen, Air Force Research Lab. (United States)

Coupling of a free-space quantum channel to a single-mode optical fiber (SMF) has important implications to quantum network concepts involving SMF-coupled photon detectors and SMF-interfaces to atomic systems. Propagation through atmospheric turbulence however leads to wavefront errors that degrade mode-matching with SMFs. In a free-space quantum channel, this leads to photon losses in proportion to the severity of the aberration. This is particularly problematic for satellite-Earth quantum channels where atmospheric turbulence can lead to significant wavefront errors. This report considers optical wavefronts propagating from low-Earth orbit to a terrestrial ground station and evaluates the efficiency with which photons couple either through a circular field stop or

into a SMF situated in the focal plane of the optical receiver. The effects of propagation through atmospheric turbulence and a closed-loop adaptive optics (AO) system are calculated numerically.

10442-14, Session 4

Modeling and simulation framework in free space quantum link

Alex Duchane, Doug Hodson, Logan Mailloux, Air Force Institute of Technology (United States)

Quantum key distribution is a family of protocols that use optical pulses to generate shared random bit strings between two locations. If a high percentage of the optical pulses are comprised of single photons, then the statistical nature of light and information theory can be used to generate secure shared random bit strings which can then be converted to keys for encryption systems. When these keys are incorporated along with symmetric encryption techniques such as a one-time pad or the advanced encryption standard, then this method of key generation and encryption is resistant to future advances in quantum computing which will significantly degrade the effectiveness of current asymmetric key sharing techniques. This research first reviews the transition of quantum key distribution experiments from the laboratory environment to field experiments, and finally, ongoing space experiments. The methodology used to model the propagation of an optical pulse from low earth orbit to the ground and the effects of turbulence on the transmitted optical pulse will then be described. An adaptive optics system is modeled to correct for the aberrations caused by the atmosphere. The long-term point spread function of the completed low earth orbit to ground optical system will be described in the results section. Finally, the impact of this optical system and its point spread function on an overall quantum key distribution system as well as the future work necessary to show this impact will be described.

10442-15, Session 5

Quantum enhanced classical imaging and metrology *(Invited Paper)*

Bohumil Stoklasa, Jaroslav Rehacek, Zdenek Hradil, Martin Paur, Libor Motka, Palack? Univ. Olomouc (Czech Republic); Luis Lorenzo Sánchez-Soto, Univ. Complutense de Madrid (Spain)

The concepts of quantum detection and estimation theory can be of great help in the analysis of faint signals, which must be treated with extreme care due to the fragility and subtlety. But this is surely not the only domain, where the advanced concepts may be applied. Strong optical fields can be analyzed by similar techniques since by virtue of first quantization any optical wave plays role of a quantum state. More precisely, a classical mode of light can be given and alternative interpretation as a quantum state of the spatial degrees of freedom of a photon. Here the formulation of classical optics meets those of quantum information processing. The goal of the research is to optimize classical sensing schemes of strong signals in order to attain the best performance allowed by Nature. As examples of the approach, measurement of two point-like sources separation and full characterization of laser beams by a phase-space tomography will be discussed both theoretically and experimentally.

10442-16, Session 5

Adaptive quantum metrology under general Markovian dynamics *(Invited Paper)*

Rafal Demkowicz-Dobrzanski, Univ. of Warsaw (Poland); Pavel Sekatski, Univ. of Innsbruck (Austria); Jan Czajkowski, Univ. van Amsterdam (Netherlands)

We derive an explicit condition that determines whether in a noisy quantum frequency estimation problem the estimation precision of the most general adaptive quantum metrological protocol cannot reach the Heisenberg-like scaling. The condition is a simple algebraic statement on a relation between the Hamiltonian operator representing the unitary part of the dynamics and the noise operators appearing in the quantum Master equation, and does not require any finite-time integration of the dynamics. In particular these results allow us to understand when application of quantum error correction protocols in order to recover the Heisenberg scaling in quantum metrology is not possible. Additionally, we provide methods to obtain quantitative bounds on achievable precision in the most general adaptive quantum metrological models. Finally, we apply the newly developed tools to prove fundamental bounds in atomic interferometry with many-body effects such as many body losses as well as models involving many-body terms in the Hamiltonian part of the dynamics commonly referred to as non-linear quantum metrology.

10442-17, Session 6

Scalable platforms for integrated quantum photonics *(Invited Paper)*

Ryan M. Camacho, Brigham Young Univ. (United States)

Applications of distributed quantum information processing will require quantum networks at both the macro and micro scale. The primary technological need in both cases are scalable, deployable devices that can generate, process, and transfer quantum correlations. In this talk, I will discuss efforts to accomplish this using chipscale integrated photonics. In particular, I'll discuss the development of quantum key distribution using silicon photonics and entanglement distribution using diamond photonics.

10442-18, Session 6

Integrated photon sources for quantum information science applications

Michael L. Fanto, Air Force Research Lab. (United States)

No Abstract Available

10442-19, Session 6

Setting best practice criteria for self-differencing avalanche photodiodes in quantum key distribution

Alexander Koehler-Sidki, Univ. of Cambridge (United Kingdom) and Toshiba Research Europe Ltd. (United Kingdom); James F. Dynes, Marco Lucamarini, Toshiba Research Europe Ltd. (United Kingdom); George R. Roberts, Univ. of Cambridge (United Kingdom); Andrew W. Sharpe, Toshiba Research Europe Ltd. (United Kingdom); Seb J. Savory, Univ. of Cambridge (United Kingdom); Zhiliang L. Yuan, Andrew J. Shields, Toshiba Research Europe Ltd. (United Kingdom)

Quantum Key Distribution (QKD) allows a sender and a receiver (conventionally called Alice and Bob, respectively) to communicate securely over a channel that is controlled by an eavesdropper, Eve [1]. Whilst this is true in theory, in QKD implementation loopholes can arise due to deviations of components from their ideal behaviour [2]. One vital component is the single photon detectors used by Bob. Often

these are avalanche photodiodes (APDs), semiconductor devices which, when operated in Geiger mode, become sensitive to single photons. In order to increase the signal-to-noise ratio of APDs, a technique known as self-differencing (SD) was also developed [3]. SD-APDs are highly performant, leading to key rates in excess of 1 Mb/s if they run as expected [4]. To guarantee this behaviour against unwanted deviations, they need to be carefully characterised.

In this work, we aim to establish the appropriate steps to characterise and then operate SD-APDs, similarly to what has been done in [5] for gated APDs. We initially shine intense light from a CW laser onto the SD-APD and register the resulting counts. A difference in the outcome is found depending on the discrimination level set to detect the avalanches. It is good practice to set this level "just above" the noise floor so that only avalanches are detected. However there is currently no criterion to prescribe how much above the noise floor this should be. In some cases, higher discrimination levels could be useful to improve the signal to noise ratio. However, if Bob sets this level too high, even only by a few mV, the SD-APD count rate drops to zero, an effect previously observed for SD-APDs in [6] using a pulsed laser. Therefore we suggest to use this "blinding-avoidance criterion" to set the highest possible discrimination level for SD-APDs. We go on and discuss further measures to characterise and operate these devices in other regimes, with different light sources and with countermeasures similar to those already introduced for gated APDs [5,7].

[1] C. H. Bennett and G. Brassard, Proc. IEEE Int. Conf. Comp. Syst. Sig. Proc., Bangalore, India p. 175, (1984).

[2] V. Scarani, H. Bechmann-Pasquinicci, N. J. Cerf et al., Rev. Mod. Phys. 81, 1301, (2009).

[3] Z. L. Yuan, B. E. Kardynal, A. W. Sharpe et al., Appl. Phys. Lett. 91, 041114 (2007).

[4] A. R. Dixon, Z. L. Yuan, J. F. Dynes, A. W. Sharpe and A. J. Shields, Opt. Express 16, 18790 (2008).

[5] Z. L. Yuan, J. F. Dynes and A. J. Shields, Appl. Phys. Lett. 98, 231104, (2011).

[6] M.-S. Jiang, S.-H. Sun, G.-Z. Tang et al., Phys. Rev. A. 88, 062335 (2015).

[7] C. C. W. Lim, N. Walenta, M. Legré et al., IEEE J. Selec. Quant. Elec. 21, 6601305 (2015).

10442-20, Session 6

Nonlinear processes in lossy microring resonators

Paul M. Alsing, Air Force Research Lab. (United States); Edwin E. Hach, Rochester Institute of Technology (United States)

Microring resonators (mmr) are becoming a standard resource for highly efficient entangled photon pair generation [1]. We examine the nonlinear processes in mrr using an input-output formalism [2,3] that explicitly accounts for the contribution of the round trip circulation of the fields inside the mrr. This formalism reduces to the standard Langevin operator input-output formalism for cavities [4] in the high cavity Q limit, near cavity resonances. Our approach is more general, applicable for arbitrary internal and bus-ring coupling losses, and away from resonances. We compare/contrast these two formalisms, and apply our approach to the output quantum state resulting from spontaneous parametric down conversion and spontaneous four wave mixing within the mrr. We compare our results to similar calculations [5] employing the standard IO formalism, and note the role of the commutators of the noise operators on the undesired accidental singles rate.

[1] S. F. Preble, et al. "On-chip quantum interference from a single silicon ring resonator source," Phys. Rev. Appl. 4, 021001 (2015).

[2] M.G. Raymer and C.J. McKinstrie, "Quantum input-output theory for optical cavities with arbitrary coupling strength: Application to two-photon wave-packet shaping," Phys. Rev. A 88, 043819 (2013).

[3] P.M. Alsing, E. E. Hach III, C. Tison, and A. Smith, "A quantum optical description of losses in ring resonators based on field operator transformations," arxiv:1608.01280;

[4] D. F. Walls and G. J. Milburn, Quantum Optics, (Springer-Verlag, New York, 1994); M. Orszag, Quantum Optics, (Springer-Verlag, New York, 2000).

[5] M. Tsang, "Cavity quantum electro-optics II.'"Phys. Rev. A 84, 043845 (2011); M. Scholz, et al., "Analytical treatment of spectral properties and signal-idler intensity correlations for a double-resonant optical parametric oscillator for below threshold," Optics. Comm 282, 3518 (2009); Z. Vernon and J.E. Sipe, "Spontaneous four-wave mixing in lossy microring resonators" Rev. A 92, 033840 (2015).

10442-21, Session 6

GaN laser diodes for quantum technologies

Stephen Najda, P Perlin, T Suski, L Morona, S Stanczyk, M Leszczynski, P Wisniewski, R Czernecki, TopGaN Ltd. (Poland)

GaN laser diodes has the potential to be a key enabling technology for a range of quantum

technologies, including quantum computation, quantum communication and quantum sensing and timing, that have important implications for security and defence applications. Such quantum systems require a number of sophisticated and complex laser sources that can be potentially replaced by GaN laser diode technology thus providing a compact, rugged and reliable format, suitable for commercialisation.

Of direct interest are GaN laser diodes for cold-atom interferometry, quantum entanglement and single photons sources for a wide range of sensing and defence applications including optical atomic clocks for GPS navigation, quantum gravity sensors, accelerometers, gravimeters and magnetometers.

The advantage of GaN laser diode technology allows single mode, high power laser diodes to be fabricated over a wide wavelength range from the u.v., ~380nm to the visible ~530nm, by tuning the indium content of the laser GaInN quantum well. We have developed a range of GaN laser diodes (using the AlGaInN material system) targeted to meet the wavelength and power requirements suitable for optical clocks and atom interferometry systems. This includes the [5s2S1/2-5p2P1/2] cooling transition in strontium+ ion optical clocks at 422 nm, the [5s21S0-5p1P1] cooling transition in neutral strontium clocks at 461 nm and the [5s2s1/2 – 6p2P3/2] transition in rubidium at 420 nm.

Very narrow linewidths (<1MHz) are required for such applications, however in the present Fabry-Perot GaN LD's a broad mode comb is observed in spectral output. Ideally, a GaN DFB laser with an integrated etched grating to select and stabalise the longitudinal mode would be considered, however there are significant technical challenges to overcome before a 'conventional' buried DFB GaN laser can be realised. Alternatively, an extended cavity laser diode (ECLD) system can be considered to obtain very narrow linewidths suitable for quantum technology applications.

In addition, AlGaInN blue-green laser diode technology allows the possibility of visible light communications (VLC) that operate at very fast data rates (GHz) for quantum communications & quantum optics. We report GHz data transmission in free-space, underwater and in plastic optical fibre (POF).

10442-22, Session 6

Tapered waveguide high power AlGaInN laser diodes and amplifiers for optical integration and quantum technologies

Stephen Najda, TopGaN Ltd. (Poland)

The AlGaInN material system allows for laser diodes to be fabricated over a very wide range of wavelengths from u.v., ~380nm, to the visible ~530nm, by tuning the indium content of the laser GaInN quantum well. Catastropic optical mirror damage (COMD) limits the optical power of the GaN laser diode. A wider stripe GaN laser diode can be considered to increase the optical power, however, this leads to filamentation and poor optical beam profile.

We report our initial results with tapered GaN lasers to; i) increase the maximum optical power of the device and avoid COMD and ii) reduce filamentation and improve the beam profile. We also report the first results of a GaN tapered optical amplifier.

The combination of increased optical power with improved beam profile opens new possibilities for GaN laser diode technology in quantum technologies including quantum key & quantum networking applications.

SPIE. SECURITY+ DEFENCE
www.spie.org/sdinfo

SPIE. REMOTE SENSING
www.spie.org/rsinfo

Plan to attend

Two Meetings One Location 2018

Present your work at these two leading European meetings for satellite-based imaging systems and sensing, data/signal analysis technologies.

Mark your calendar for September 2018, in Berlin, Germany

Two symposia: **Security + Defence** and **Remote Sensing**